Understanding Complex Systems

Springer COMPLEXITY

Axel Pelster
Günter Wunner *Editors*

Selforganization in Complex Systems: The Past, Present, and Future of Synergetics

Proceedings of the International Symposium, Hanse Institute of Advanced Studies, Delmenhorst, Germany, November 13–16, 2012

Springer

Springer Complexity

Springer Complexity is an interdisciplinary program publishing the best research and academic-level teaching on both fundamental and applied aspects of complex systems—cutting across all traditional disciplines of the natural and life sciences, engineering, economics, medicine, neuroscience, social and computer science.

Complex Systems are systems that comprise many interacting parts with the ability to generate a new quality of macroscopic collective behavior the manifestations of which are the spontaneous formation of distinctive temporal, spatial or functional structures. Models of such systems can be successfully mapped onto quite diverse "real-life" situations like the climate, the coherent emission of light from lasers, chemical reaction–diffusion systems, biological cellular networks, the dynamics of stock markets and of the internet, earthquake statistics and prediction, freeway traffic, the human brain, or the formation of opinions in social systems, to name just some of the popular applications.

Although their scope and methodologies overlap somewhat, one can distinguish the following main concepts and tools: self-organization, nonlinear dynamics, synergetics, turbulence, dynamical systems, catastrophes, instabilities, stochastic processes, chaos, graphs and networks, cellular automata, adaptive systems, genetic algorithms and computational intelligence.

The three major book publication platforms of the Springer Complexity program are the monograph series "Understanding Complex Systems" focusing on the various applications of complexity, and the "Springer Series in Synergetics", which is devoted to the quantitative theoretical and methodological foundations, and the "SpringerBriefs in Complexity" which are concise and topical working reports, case-studies, surveys, essays and lecture notes of relevance to the field. In addition to the books in these two core series, the program also incorporates individual titles ranging from textbooks to major reference works.

Understanding Complex Systems

Founding Editor: Scott Kelso

Future scientific and technological developments in many fields will necessarily depend upon coming to grips with complex systems. Such systems are complex in both their composition—typically many different kinds of components interacting simultaneously and nonlinearly with each other and their environments on multiple levels—and in the rich diversity of behavior of which they are capable.

The Springer Series in Understanding Complex Systems series (UCS) promotes new strategies and paradigms for understanding and realizing applications of complex systems research in a wide variety of fields and endeavors. UCS is explicitly transdisciplinary. It has three main goals: First, to elaborate the concepts, methods and tools of complex systems at all levels of description and in all scientific fields, especially newly emerging areas within the life, social, behavioral, economic, neuro- and cognitive sciences (and derivatives thereof); second, to encourage novel applications of these ideas in various fields of engineering and computation such as robotics, nano-technology and informatics; third, to provide a single forum within which commonalities and differences in the workings of complex systems may be discerned, hence leading to deeper insight and understanding.

UCS will publish monographs, lecture notes and selected edited contributions aimed at communicating new findings to a large multidisciplinary audience.

More information about this series at http://www.springer.com/series/5394

Axel Pelster · Günter Wunner
Editors

Selforganization in Complex Systems: The Past, Present, and Future of Synergetics

Proceedings of the International Symposium, Hanse Institute of Advanced Studies, Delmenhorst, Germany, November 13–16, 2012

Springer

Editors
Axel Pelster
Fachbereich Physik
Forschungszentrum OPTIMAS
Technische Universität Kaiserslautern
Kaiserslautern
Germany

Günter Wunner
Institut für Theoret. Physik I
Universität Stuttgart
Stuttgart
Germany

ISSN 1860-0832 ISSN 1860-0840 (electronic)
Understanding Complex Systems
ISBN 978-3-319-27633-5 ISBN 978-3-319-27635-9 (eBook)
DOI 10.1007/978-3-319-27635-9

Library of Congress Control Number: 2015957036

Printed on acid-free paper

This Springer imprint is published by SpringerNature
The registered company is Springer International Publishing AG Switzerland

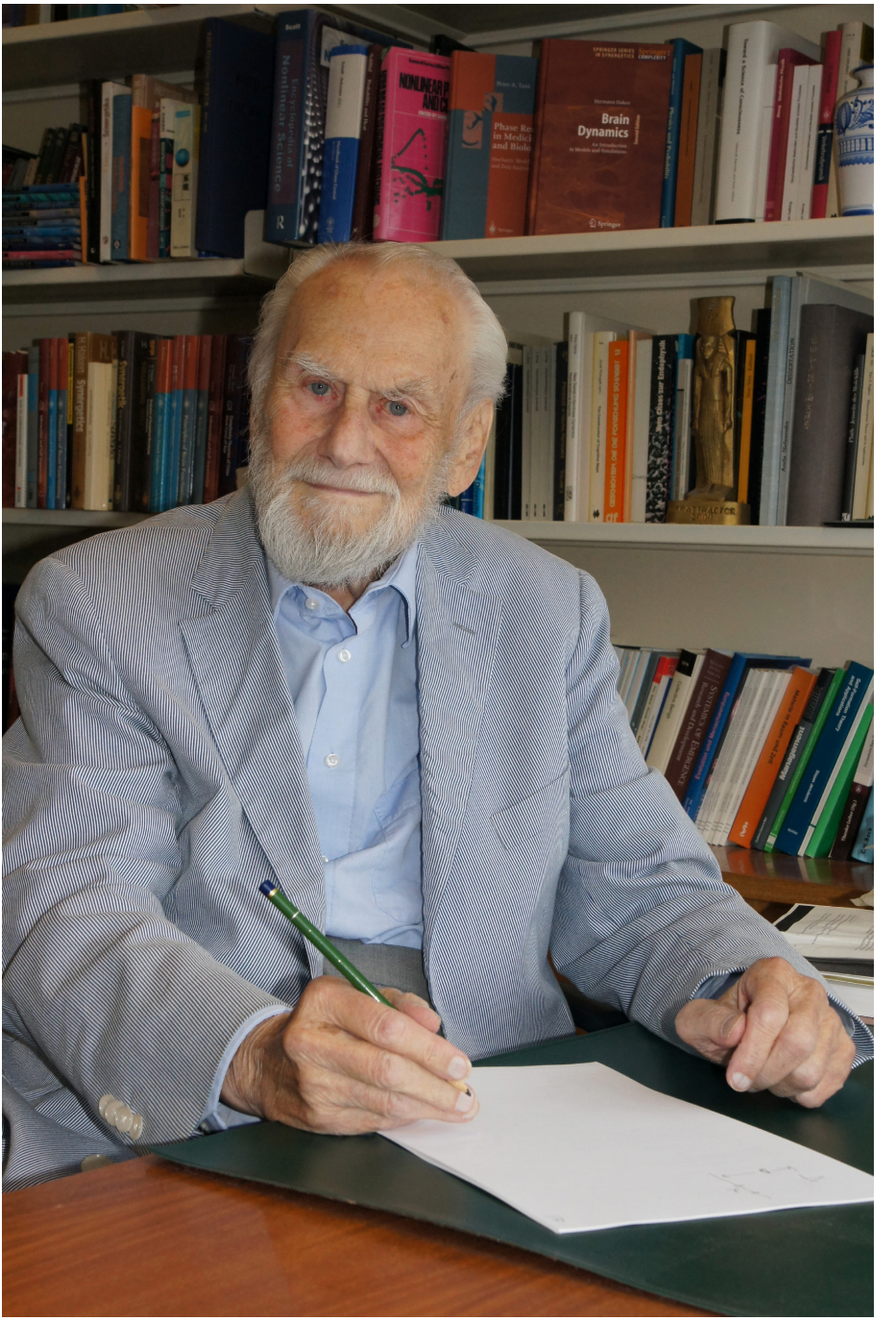

Hermann Haken, born July 12, 1927 in Leipzig (Germany) is physicist and professor emeritus in theoretical physics at the University of Stuttgart.

pelster@zedat.fu-berlin.de

Preface

In numerous systems of both living and nonliving nature complex spatio-temporal or functional patterns of self-organization processes are ubiquitous. They are extremely important in physics, chemistry, biology, medicine, as well as in the engineering, and even in the social sciences. Over the past several decades understanding such self-organization processes has not only changed physics, but has also led to improvements in our daily life. *Hermann Haken*, who celebrated his 85th birthday in 2012, is an internationally recognized pioneer in this respect, having laid the mathematical-physical basis for describing and analyzing self-organization processes with his fundamental theory of Synergetics. Haken successfully applied synergetic methods to investigate the laser and other physical systems, as well as in studies on the brain. Since it was founded, this truly interdisciplinary field has experienced a rapid growth, both in terms of the mathematical-physical methodology and the success that has been achieved by applying it to a diversity of different fields of research. On all length scales and in all areas of human life - from the quantum level right up to the spread of disease over air traffic junctions - self-organization and complex dynamics behaviour have turned out to play a key role. A more in-depth understanding of these processes will allow the development of diverse methods of control with which we can attempt to master the complexity of these systems. The potential of practical applications can certainly be enhanced if the different disciplines share their advanced and sophisticated methods, as well as their experiences with each other. Therefore, the International Symposium **Self-Organization in Complex Systems: The Past, Present, and Future of Synergetics** was organized at the Hanse-Wissenschaftskolleg, an Institute of Advanced Studies in Delmenhorst (Germany), in the period November 13-16, 2012. The Symposium covered the research field Synergetics as a whole, ranging from basic methods to concrete applications, by taking advantage of its interdisciplinary impact. Moreover, by combining a historical review with a present status report the Symposium gave young scientists an understanding of the allure and potency of this branch of research as well as its applicability in the future. In total the Symposium had 60 participants from, besides Germany, several European countries and the United States, among them 22 senior scientists delivering invited talks and 22 junior scientists presenting poster contributions. The present volume consists of the material of most of the invited talks as well as a selection from the posters at this meeting, and is published in the Series **Understanding Complex Systems** of the Springer Publishing Company. Additional information about the Symposium is available at the homepage

`http://www-user.rhrk.uni-kl.de/~apelster/Haken/index.html`

which contains, in particular, the booklet with abstracts of all contributions, the slides of the invited talks and a gallery with 260 pictures.

The quest for common and universal principles of self-organization in complex systems was clearly demonstrated by the wide range of interdisciplinary topics covered by the Symposium. At the beginning, complexity in the realm of classical physics was illustrated by the still open problem of turbulence in fluids which was presented both from an experimental and a theoretical point of view by *Joachim Peinke* and *Siegfried Grossmann*, respectively. While the former talk emphasized the present search for stochastic models to describe experimental data for turbulent and turbulence driven systems, the latter presentation informed about recent results regarding the flow organization in highly turbulent thermal convection. Another highlight was the investigation of nonlinear dynamical systems in general and the control of their bifurcations in particular via noise and time delays, which were covered by *Axel Hutt* and *Eckehard Schöll*. Here the impact of additive noise towards tuning the stability of nonlinear systems as well as the control of self-organizing complex systems and networks with time delay were analyzed in detail. This discussion was amplified by the treatment of statistical properties of time-dependent linear and nonlinear oscillators by *Marko Robnik*. A historical review of the widespread applications of Synergetics in the realm of chemical reactions was delivered by *Peter Plath*. There the phenomena of self-organization and pattern formation were crucial, for instance, for the successful description of oscillating chemical reactions and reactions with limit-cycle behaviour. Even more complex dynamics were presented by *Lisa Borland* who addressed the highly topical issue of the physics of finance. Following the spirit of Synergetics, she showed that time series of financial data exhibit highly nontrivial statistical properties which can be captured by more or less realistic models. They reveal cooperative effects of collective behaviour which turn out to lie at the root of many interesting phenomena of the financial markets.

Another branch of complexity was provided by a series of invited talks on quantum many-body systems. At first, quantum statistical problems were discussed in the talks by *Fritz Haake* on quantum chaotic equilibration in the absence of dissipation and by *Günter Mahler* on the emerging field of quantum thermodynamics. Whereas Haake compared the interdependence of classical and quantum dynamics by means of the concrete paradigmatic example of the Dicke model, where a large spin is coupled to an oscillator, Mahler focused on the general philosophical question how a qualitatively different type of behaviour may systematically emerge from the underlying quantum substrate. Afterwards, *Cun-Zheng Ning* reported on the trailblazer of Synergetics by discussing the spectacular properties of nanolasers and their experimental realization. In particular, the process of miniaturization recently led to the invention of many microcavity lasers such as photonic crystal lasers, distributed feedback lasers, and nanowire lasers with different properties. Another manifestation of light was introduced by *Martin Weitz* who reported on the spectacular recent experiment on the Bose-Einstein condensation of photons in a dye-filled microcavity at room temperature. The cavity mirrors provide both a confining potential and a non-vanishing effective photon mass, making the system formally equivalent to a two-dimensional gas of trapped, massive bosons. Inherently nonlinear mat-

ter waves were then the topics of the subsequent presentations on the theory of Bose-Einstein condensates. *Günter Wunner* reported about the possibility to realize parity-time-symmetric Bose-Einstein condensates in a double-well potential landscape. Despite the mutual presence of loss and gain stable condensates emerge which should be observable in an experiment. Quantum phase transitions of bosons in optical lattices were described by *Axel Pelster* within a Ginzburg-Landau theory. Here, the theoretical tools for analyzing non-equilibrium phase transitions in the realm of Synergetics turned out to be also applicable to the newly emerging field of phase transitions at zero temperature which are driven by quantum fluctuations.

An essential part of the Synergetics Symposium was devoted to the flourishing field of self-organization in neuroscience. Most prominently featured the talk by *Hermann Haken*, who discussed the brain both as a synergetic and a physical system. Despite the huge complexity of the brain due to the large number of neurons and their connections at the microsopic level, several enlightening neurophysiological experiments can be already understood at the macroscopic level with the choice of appropriate order parameters. Complementary to that approach *Gerhard Roth* described the psychological subject of personality development as a process of self-organization in terms of neurophysiology. Spectacular insights in treating brain diseases based on synergetic principles were described by *Peter Tass*. He demonstrated that coordinated reset neuromodulation allows unlearning pathological neuronal synchrony such as Parkinson's disease and tinnitus. Subsequently, *Günter Schiepek* demonstrated convincingly that Synergetics has now many indispensable applications in psychology. He reported about exciting progress in applying the physical concepts of phase transitions and critical instabilities to psychotherapeutic processes. Afterwards, functional properties of brain dynamics were modelled both in space and time by synergetic networks in the presentation by *Viktor Jirsa*. His workhorse was the connectivity matrix of the brain whose spatial components are defined by the underlying anatomical connections, whereas its temporal components are determined by the neural time delays. Afterwards, *Andreas Daffertshofer* discussed the related topic of the dynamics of synchrony and information processing in the nervous system. To this end he analyzed in detail within a Kuramoto-like network model how the phase dynamics of coupled neural oscillators depend on the corresponding amplitude changes. In contrast to that *Aneta Stefanovska* analyzed organic body functions with synergetic methods. To this end she introduced the new concept of a chronotaxic system as a model system far from thermodynamic equilibrium which adjusts its clocks. Finally, *Till Frank* transferred the fundamental concepts for the synergetic computer to the possible emergence of physical intelligence. He concluded with the statement that the synergetic computer defines a subclass of intelligent physical systems with many possible applications in the field of artificial intelligence.

All these invited talks about the present-day research status of Synergetics were completed by three historical contributions. At first *Hermann Haken* delivered obituaries for two of his former students and coworkers *Arne Wunderlin*

and *Rudolf Friedrich* who had died untimely in 2012. Furthermore, the evening lecture of *Bernd Kröger* highlighted the scientific life of Hermann Haken from different personal angles. Therein, the emphasis was to give special attention to the roadmap to Synergetics in the period from 1950 to 1983. Another impressive historical retrospect was provided by *Cun-Zheng Ning* who reflected upon personal memories how Synergetics was introduced in China. In particular, he concluded that the gradual spreading of ideas of self-organization in China at the beginning of the eighties in the last century definitely catalyzed and contributed to a gradual opening of the scientific China to the western world.

The organizers of the Symposium gratefully acknowledge generous financial support from the Volkswagen Foundation. In particular, we thank its program director *Ulrike Bischler* for her continuous moral support during all stages of the organization. The purpose of the Symposium to reveal future trends in the interdisciplinary research field of synergetics fitted perfectly into the general present-day guidelines of the Volkswagen Foundation. Furthermore, it should be recalled that the Volkswagen Foundation supported substantially Hermann Haken's outstanding research in the past. First, Synergetics was endorsed in its initial phase as an unconventional project by the Volkswagen Foundation from 1976 until 1980. Afterwards, Hermann Haken was asked by the Volkswagen Foundation to submit a proposal for a priority programme on Synergetics which was then funded from 1980 until 1990, final projects even expired only in 1991. With this the Volkswagen Foundation can claim to have contributed a large part of the financial foundations to the overwhelming scientific success of Synergetics in the different disciplines. The Symposium at the Hanse-Wissenschaftskolleg represented also for the Volkswagen Foundation a unique opportunity to reflect upon this past success more than 20 years after the synergetics funding ended, and to extrapolate them to future trends via a careful synopsis of the present research status. Also to this end the organizers of the Symposium publish the collected plenary lectures and selected poster contributions in form of the present Proceedings Book. We thank *Thomas Ditzinger* from the Springer Publishing Company for his kind assistance. Finally, we express our deepest gratitude to the Hanse-Wissenschaftskolleg in Delmenhorst (Germany) which provided a truly perfect and stimulating environment for such an international and interdisciplinary meeting. In particular, we thank the administrator *Christina Thiel* and the scientific manager *Wolfgang Stenzel* for their efficient assistance in all organizational matters.

Axel Pelster — Technische Universität Kaiserslautern (Germany), Fellow at the Hanse-Wissenschaftskolleg during the winter terms 2011-12 and 2012-13

Günter Wunner — Universität Stuttgart (Germany)

July 2014

Group photo of the participants of the International Symposium **Self-Organization in Complex Systems: The Past, Present, and Future of Synergetics**, Hanse Institute of Advanced Studies, Delmenhorst (Germany), November 13-16, 2012 (see list of participants on page 355).

Table of Contents

III Self-Organisation in Neuroscience

IV History

V Poster Contributions

Part I

Complexity in Classical Systems

Flow Organization in Highly Turbulent Thermal Convection

Siegfried Grossmann

Fachbereich Physik der Philipps-Universität
Renthof 6, D-35032 Marburg, Germany
grossmann@physik.uni-marburg.de
www.uni-marburg.de/fb13/personen/grossmann-siegfried/index_html

Dedication

Ladies and Gentlemen, dear colleagues and friends, it is with my greatest pleasure to address our Nestor and always stimulating academic advisor, Professor Hermann Haken, with my sincerest congratulations on the occasion of his 85th birthday. I wish to express my warmest thanks and appreciation for his leadership and his guidance.
Thank you, Hermann, for being our ideal over all the years, kindly accept all my, all our best wishes for you!

Abstract. Recent surprising results on very large Rayleigh-number thermal convection are presented and discussed. For Rayleigh numbers beyond about 10^{14} the scaling of the Nusselt number as well as the profiles are determined by turbulent boundary layers, though these are extremely thin. The theoretical interpretation is well consistent with the experimental data measured with the high pressure convection facility in Göttingen by Guenter Ahlers et al.

Keywords: Turbulence, Rayleigh-Bénard, thermal convection, log-layer, log-profiles, Nusselt-number, scaling

The results which I shall present have been obtained in close cooperation with the following colleagues: Detlef Lohse, Twente. – Experiment: Guenter Ahlers, Santa Barbara; Eberhard Bodenschatz, Göttingen; Denis Funfschilling, Nancy; Xiao-Zhou He, Göttingen; Ke-Qing Xia, Hong Kong; Quan Zhou, Shanghai. – Direct Numerical Simulation: Erwin van der Poel, Twente; Kazuyazu Sugiyama, Riken; Richard J. A. M. Stevens, Baltimore and Twente; Roberto Verzicco, Roma and Twente.

1 Introduction

Turbulent Rayleigh-Bénard convection has been the Drosophila of the physics of fluids for many decades, starting with the famous analytical calculation of

A. Pelster and G. Wunner (eds.), *Selforganization in Complex Systems: The Past, Present, and Future of Synergetics*, Understanding Complex Systems,
DOI: 10.1007/978-3-319-27635-9_1

the linear instability at the critical Rayleigh number $Ra_c = 1708$. The Rayleigh number is defined as usual, $Ra = g\beta_p L^3 \Delta/(\nu\kappa)$; g is the gravitational acceleration, β_p the isobaric expansion coefficient, L the height of the sample, and Δ the temperature difference between the hotter bottom and the colder top plates; ν and κ denote the kinematic viscosity and the temperature diffusivity, considered as temperature independent under present experimental conditions. Over the last decade experimental, theoretical, and numerical results have converged up to a Rayleigh number $Ra \sim 10^{12}$. – One of the quite unexpected findings is that even for such large Ra the boundary layers are still of Prandtl-Blasius, i. e., of laminar type, although time dependent. – In 2001 we had predicted that the transition to a turbulent boundary layer occurs around $Ra = 10^{14}$ (for gases), cf. [1]. Recently Ahlers et al. [2] indeed have experimentally found this laminar-turbulent transition at this very high Ra. Here due to a sufficiently large shear in the extremely thin boundary layers these eventually become turbulent, leading to a much stronger increase of the heat transfer with increasing Ra as in the laminar, the *classical* range below this turbulence onset. – In Grossmann and Lohse [3] we have calculated an effective scaling law $Nu \sim Ra^{0.38}$ for this ultimate regime by extending the unified scaling theory [4], [1], [5], [6], which determines the scaling behavior of the heat current Nu as well as the thermal wind amplitude Re as functions of the control parameters Rayleigh and Prandtl number Ra and Pr. Here the Prandtl number characterizes the fluid, $Pr = \nu/\kappa$, $Nu = Q/(\kappa\Delta L^{-1})$ describes the non-dimensionalized heat current density Q, and $Re = UL/\nu$ is the non-dimensionalized amplitude U of the convection (or wind) in the Rayleigh-Bénard container.

2 The Ultimate State of Thermal Convection for Very Large Rayleigh Numbers

Having explored strong thermal convection as described in the introduction we now also look at the local flow properties such as the (vertical) temperature profile. This turns out to show logarithmic dependence with distance z from the heated bottom and the cooled top plates [7]. This so called law of the wall and its properties as functions of the control parameters has been derived and analyzed in [8].

As a previously not yet studied surprise we have noticed the log-law in the classical regime below $O(10^{14})$ too, cf. above reference [7], apparently meaning that a turbulent bulk of thermal flow for Ra beyond the structure formation regime as observed at lower Ra, can well coexist with still laminar boundary layers. The notion *laminar* apparently has to be extended to time dependence on the gross convective time scale [9].

In the talk some of these self-organized flow structures in strongly driven thermal convection have been detailed together with some overview. The reader, who is interested in the development which lead to all the recent insight, is referred to reference [10]. A recent summarizing overview on the experimental details for the high pressure convection facility, known as the Göttingen Uboot, is provided

in [11]. The measurement of the wind amplitude U, non-dimensionalized as the Reynolds number $Re = UL/\nu$, the second important response of the Rayleigh-Bénard heat flow experiment besides the heat current Nu, is described in [12]. As an overview on Rayleigh-Bénard flow reference [13] is recommended.

Some more details of the talk are: As in most, if not all, laboratory fluid flows the boundary layers are of utmost importance also in thermal convection. Although the flow – in particular also in the boundary layers – is time dependent for not too small Rayleigh numbers Ra, we have learned meanwhile, cf. [9], the surprising lecture that nevertheless the boundary layers have profile features of laminar flow; laminar in the sense that they satisfy the Prandtl boundary layer equations. Thus *laminar* does *not* mean *time independent*!

The validity of the Prandtl boundary layer equations quantitatively means that the velocity ("kinetic") boundary layer thickness δ scales with the wind amplitude U or $Re = UL/\nu$ in the container as $\delta = a/\sqrt{Re}$. The empirical constant a in Rayleigh-Bénard flow in containers of width to height ratio (so called aspect ratio) of order 1 has been found as $a = 0.5$. Since the wind along the plates fluctuates locally and temporally in strength, so does δ fluctuate; but experiment as well as theory have confirmed that on the respective local δ-scale the profile is excellently of Prandtl-type.

The shear across the boundary layer can be quantified by a shear Reynolds number $Re_s = U\delta/\nu$. This then for laminar boundary layers is $Re_s = a\sqrt{Re}$. Now, if this boundary layer shear exceeds a certain range of size, say an interval around some Re_s^*, the boundary layer becomes turbulent. Re_s^* is not sharp, since onset of turbulence in shear flow depends on the type of disturbances. Empirical results for Re_s^* for various macroscopic flows give values in the range of about 320 to 420, meaning that Re has to exceed a $Re^* = (Re_s^*/a)^2 = 4.1 \times 10^5 - 7.1 \times 10^5$. The wind before transition according to [4] to [6] is $Re = 0.346 Ra^{4/9} Pr^{-2/3}$. Therefore the onset of turbulence in the boundary layers of thermal flow in gases, having $Pr = 0.84$, is expected (and has been predicted cf. [1] !) in the range $Ra^* = 3.7 \times 10^{13} - 1.3 \times 10^{14}$. This is well confirmed meanwhile by the Ahlers et al. experiments.

To give some numbers: The Prandtl boundary layer thickness at turbulence onset is (using above formulas) $\delta^*/L = 8 \times 10^{-4} - 6 \times 10^{-4}$, which in the Göttingen high pressure convection facility, the Uboot device, of $L = 2.24$ m height is $\delta^* = 1.8$ mm to 1.3 mm, very small indeed. Also after turbulence onset there is a linear layer in the immediate vicinity of the plates, known as the linear viscous sublayer, followed – after a transitional buffer range – by the log-law profile, called the "law of the wall". The viscous sublayer width $z_* = \nu/u_*$ is determined by the turbulent fluctuation amplitude u_*, defined (and measured) by the kinematic shear stress or drag at the wall (plate).

$$u_*^2 = \sigma_{xz}(0) = p_{xz}(0)/\rho = \nu \partial_z U_x(0) \ . \tag{1}$$

The turbulent fluctuation amplitude u_* is the key quantity for turbulent flows. E. g., u_*^2/U^2 is the friction coefficient; u_* also determines the turbulent transport coefficients $\nu_{turb} = \bar{\kappa} z u_*$ and $\kappa_{turb} = \bar{\kappa}_\theta z u_*$ as well as the local turbulent dissipation rate $\epsilon_u(z) = u_*^3/(\bar{\kappa} z)$. The empirical constant $\bar{\kappa}$ is called the von Kármán

constant, whose value in many flows is $\bar{\kappa} = 0.4$. – We have calculated u_* in [3] for a homogeneous plate to be the solution of the transcendental equation

$$\frac{u_*}{U} = \frac{\bar{\kappa}}{\ln(Re\frac{u_*}{U}\frac{1}{b})} \ . \tag{2}$$

Here $B_u = \bar{\kappa}^{-1}\ln(b^{-1})$ is called the profile constant of the log-law of the wall. – Calculating from this equation the thickness of the linear sublayer we obtain that z_*/L is of order 0.5×10^{-4} and thus an order of magnitude smaller than the laminar Prandtl width δ. In particular in the high Ra Uboot device it is $z_* \approx 0.11$mm.

The measured profile, see [7], i. e., the log-law of the wall, can be parametrized in the form

$$\frac{\langle T(z)\rangle - T_m}{\Delta} = A \cdot \ln\left(\frac{z}{L}\right) + B \ , \tag{3}$$

with T_m the arithmetic mean temperature between the bottom and top plates. This profile in vertical, z direction has been measured at about 10.1 cm off the side wall. Direct numerical simulations allow to calculate the profile also for all other wall distances but yet for smaller Ra, up to $\mathrm{O}(10^{13})$. In [8] we have succeeded to evaluate the parameters A and $B = \ln 2 \cdot A$ and find

$$A = -\frac{\kappa}{\bar{\kappa}_\theta}\frac{Nu}{u_* L} \approx -\frac{1}{2\bar{\kappa}}\frac{u_*}{U} \approx -0.038 \ . \tag{4}$$

A depends on Ra very weakly only, $A \propto Ra^{-0.043}$, and it depends on the distance r from the wall center, its magnitude $|A|$ increasing with distance r. We explain this by the decrease of the plate parallel velocity component $U \hat{=} U_x(r)$ with distance r from center; this interpretation is quantitatively well consistent with the experimental data.

All these theoretical results originate from a Reynolds stress plus mixing length ansatz in the time averaged Boussinesq equation, as detailed in [8]. The main issue is $\overline{\boldsymbol{u}'\theta'} \approx -\kappa_{turb}(z)\partial_z\theta$. Surprisingly enough the numerical values of the characteristic parameters as $\bar{\kappa}$ and B_u are rather near to those, which have been determined for flows along plates, in channels, and through pipes.

As I have demonstrated, there is quite a lot of exciting and surprising new insight into thermal convection at very large Rayleigh numbers Ra and its flow organization, but still much more has to be explored.

References

1. Grossmann, S., Lohse, D.: Thermal convection for large Prandtl numbers. Phys. Rev. Lett. **86**, 3316–3319 (2001)
2. Ahlers, G., Funfschilling, D., Bodenschatz, E.: Transitions in heat transport by turbulent convection. New J. Phys. **11**, 123001 (2009)
3. Grossmann, S., Lohse, D.: Multiple scaling in the ultimate regime of thermal convection. Phys. Fluids **23**, 045108 (2011)

4. Grossmann, S., Lohse, D.: Scaling in thermal convection: A unifying theory. J. Fluid Mech. **407**, 27–56 (2000)
5. Grossmann, S., Lohse, D.: Prandtl and Rayleigh number dependence of the Reynolds number in turbulent thermal convection. Phys. Rev. E **66**, 016305 (2002)
6. Grossmann, S., Lohse, D.: Fluctuations in turbulent Rayleigh-Bénard convection: the role of plumes. Phys. Fluids **16**, 4462–4472 (2004)
7. Ahlers, G., Bodenschatz, E., Funfschilling, D., Grossmann, S., He, X.-Z., Lohse, D., Stevens, R.J.A.M., Verzicco, R.: Logarithmic Temperature Profiles in Turbulent Rayleigh-Bénard Convection. Phys. Rev. Lett. **09**, 114501 (2012)
8. Grossmann, S., Lohse, D.: Logarithmic temperature profiles in the ultimate range of turbulent convection. Phys. Fluids **24**, 125103 (2012)
9. Zhou, Q., Sugiyama, K., Stevens, R.J.A.M., Grossmann, S., Lohse, D., Xia, K.-Q.: Horizontal Dependence of Velocity and Temperature Boundary-Layers in two-dimensional Numerical Turbulent Rayleigh-Bénard Convection. Phys. Fluids **23**, 125104 (2011)
10. Funfschilling, D., Bodenschatz, E., Ahlers, G.: Search for the ultimate state in turbulent Rayleigh-Bénard convection. Phys. Rev. Lett. **103**, 014503 (2009)
11. He, X.-Z., Funfschilling, D., Bodenschatz, E., Ahlers, G.: Heat transport by turbulent Rayleigh-Bénard convection for $Pr = 0.8$ and $4 \times 10^{11} < Ra < 2 \times 10^{14}$: Ultimate state transition for aspect ratio $\Gamma = 1.00$. New J. Phys. **14**, 063030 (2012)
12. He, X.-Z., Funfschilling, D., Nobach, H., Bodenschatz, E., Ahlers, G.: Transition to the Ultimate State of Turbulent Rayleigh-Bénard Convetion. Phys. Rev. Lett. **108**, 024502 (2012)
13. Ahlers, G., Grossmann, S., Lohse, D.: Heat Transfer and Large-Scale Dynamics in Turbulent Rayleigh-Bénard Convection. Review of Modern Physics **81**, 503–527 (2009)

Periodic External Input Tunes the Stability of Delayed Nonlinear Systems: From the Slaving Principle to Center Manifolds

Axel Hutt[1] and Jérémie Lefebvre[2]

[1] INRIA CR Nancy - Grand Est, 615 Rue du Jardin Botanique, 54602 Villers-les-Nancy, France
axel.hutt@inria.fr
http://www.loria.fr/~huttaxel

[2] Département des Neurosciences Fondamentales, Université de Genève, CMU, 1 rue Michel Servet, 1211 Genève 4, Switzerland

Abstract. The work illustrates a recent analysis technique that demonstrates that external periodic input affects the stability of the time-averaged nonlinear dynamics of a delayed system. At first, the article introduces the fundamental elements of delayed differential equations and then applies these to a nonlinear delayed problem close to a transcritical bifurcation. We observe a shift of stability in the system induced by the fast periodic driving.

Keywords: slaving principle, center manifold theorem, delay equations, bifurcation theory

1 Introduction

Self-interactions are one of the fundamental components of complex systems. The consideration of these reentrant contributions, oftentimes exhibiting some form of latency or delay, play an important role in numerous areas of research (lasers, machining, chemistry, control), especially in models of biological systems. As such, over the last decades, retarded dynamical systems have been used to successfully describe physiological systems like the eye light pupil reflex [1], blood circulation [2] or postural motor control [3]. The influence of time lags is also ubiquitous in neuroscience, where various feedback loops have been exposed throughout neural circuitry. It has indeed been shown that delays play many important functional roles in neural systems and constitute one of the main mechanism underlying network synchronization and spatio-temporal activity patterns [4–7]. Over the past years, the question as to how spatio-temporal forcing interacts with retarded dynamics has received a vivid interest. The exact function of delays in the integration of temporally fluctuating temporal signals is still unknown, mainly because of the lack of tools the dynamical systems theory provides for the study of the stability of non-homogeneous and/or non-autonomous problems.

A. Pelster and G. Wunner (eds.), *Selforganization in Complex Systems: The Past, Present, and Future of Synergetics*, Understanding Complex Systems,
DOI: 10.1007/978-3-319-27635-9_2

The center manifold theorem and the slaving principle have proven to be powerful tools in this task, and since then they have been successfully applied to many non-driven delayed problems [8–13]. The slaving principle may be seen as the physical equivalent, i.e. the representation in nature, of the major statement of the center manifold theorem. In this context, the center manifold theorem represents a promising candidate in the approach of the non-autonomous cases. However, the question whether the center manifold theorem may be extended to non-autonomous, i.e. forced, delayed problems is currently left poorly addressed. They are indeed indications that center manifolds do exist in infinite dimensional non-autonomous dynamical systems [14]. Furthermore, stochastic center manifold theory has been established in non-delayed noisy systems [15–17], and a similar approach has been used in the numerical analysis of non-linear ODEs, subject of time-dependent forcing, providing accurate results. However, as the need to analyse forced system arises, it is still unfortunately unclear how to apply and compute center manifolds for non-autonomous delayed feedback systems and to expose the underlying mechanism by which the unstable modes govern the dynamics. A solution to this problem would greatly enhance the possibilities of theoretical analysis of delayed systems, of prime importance in mathematical neuroscience and related fields.

In the following, we present a method that allows to compute center manifolds of delayed system with time-dependent driving. We first outline the fundamental elements of delay-differential equations and the corresponding center manifold reduction in delayed systems, summarizing the detailed discussions of [18, 10, 19–21]. We then present results for a periodically driven delayed model with quadratic non-linearity, and show that it describes accuratly the dynamics near a transcritical instability.

2 General treatment of autonomous DDEs

Consider the general autonomous scalar delay differential equation,

$$\dot{x}(t) = f(x(t), x(t-\tau)) = L(\{x(t), x(t-\tau)\}) + F(\{x(t), x(t-\tau)\}), \quad (1)$$

where L is a linear function with L(0)=0, and where F is a non linear and sufficiently smooth function, satisfying $F(0) = DF(0) = 0$. Both linear and non-linear parts of this system may contain delayed components. In the following, we will consider the control parameter ε and investigate the stability of Eq.(1) unfolded around the point $\varepsilon = 0$. It will prove convenient to work with the augmented system

$$\dot{x}(t) = f(x(t), x(t-\tau), \varepsilon) = L(x(t), x(t-\tau), \varepsilon) + F(x(t), x(t-\tau)\varepsilon). \quad (2)$$
$$\frac{d\varepsilon}{dt} = \qquad 0.$$

This allows to take immediately into account the role played by the parameters in subsequent derivations.

2.1 The embedding

In order to consider solutions $x(t)$ of Eq. (1) for $t \geq 0$, one needs a complete description of initial value problem, corresponding to the retarded dynamics into the interval $[-\tau, 0]$. This criterion implies that the map from the interval $[-\tau, 0]$ into $\mathbb{R}$ is not injective. Consequently, the system of Eq. (1) has ill-defined initial conditions, and uniqueness of solutions is not guaranteed [10]. It is therefore imperative to consider Eq. (1) in an appropriate phase space which would ensure its self-consistency. To take into account the continuous dependence of the flow $x(t)$ on the retarded dynamics, we introduce the parameter θ with $-\tau \leq \theta \leq 0$ and the new variable $z_t(\theta) \in \Re^2$, so that

$$z_t(\theta) \equiv (x(t+\theta), \varepsilon)^T. \tag{3}$$

Based on this definition, an appropriate phase space can be shown to be the Banach space of continuous maps $\mathcal{C} \equiv C([-\tau, 0], \mathbb{R} \times \mathbb{R})$ [10, 21]. Reformulating Eq.(1) to take into account the continuous dependence of the flow on θ, we formally obtain

$$[\frac{dx(t+\theta)}{dt}, \frac{d\varepsilon}{dt}]^T = \frac{d}{dt} z_t(\theta) \equiv \lim_{\delta t \to 0} \frac{(z_t(\theta + \delta t)) - z_t(\theta)}{\delta t}, \tag{4}$$

where we will distinguish instantaneous and retarded dynamics. For $-\tau \leq \theta < 0$, expanding around $\delta t = 0$ to first order yields [10]

$$\frac{d}{dt} z_t(\theta) = \lim_{\delta t \to 0} \frac{z_t(\theta) + \frac{\partial z_t(\theta)}{\partial(\theta)} \delta t - z_t(\theta)}{\delta t} = \frac{\partial z_t(\theta)}{\partial \theta}. \tag{5}$$

On the other hand, if $\theta = 0$, we simply get

$$\frac{d}{dt} z_t(0) = (\frac{dx(t)}{dt}, \frac{d\varepsilon}{dt})^T = (f(x(t), x(t-\tau)), 0)^T = (L[z_t] + F[z_t], 0)^T. \tag{6}$$

It is important to note that $L[z_t]$ and $F[z_t]$ are functionals. For instance, $L[z_t]$ may be written as [10]

$$L[z_t] = \int_{-\tau}^{0} z_t(\theta) \omega(\theta) z_t(\theta) d\theta = \int_{-\tau}^{0} d\eta[\theta] z_t(\theta), \tag{7}$$

with the density function $\omega(\theta)$. For the scalar DDE and a single parameter, $\omega(\theta)$ is a $2x2$-matrix.

We may conveniently summarize these specific cases by writing the system of Eq. (1) in $\mathcal{C}$ as a infinite dimensional ODE,

$$\frac{d}{dt} z_t(\theta) = \mathcal{A}(z_t(\theta)) + X_o F[z_t(\theta)], \tag{8}$$

where the *infinitesimal generator* $\mathcal{A}$ is defined by [10]

$$\mathcal{A}(z_t(\theta)) \equiv \frac{\partial z_t(\theta)}{\partial \theta} + X_o(L[z_t] - \frac{\partial z_t(\theta)}{\partial \theta}|_{\theta=0}]. \tag{9}$$

The connection function $X_o(\theta)$ allows the simultaneous treatment of the cases $\tau \leq \theta < 0$ and $\theta = 0$. It is defined *ad hoc* by

$$X_o(\theta) = \begin{cases} 0 & -\tau \leq \theta < 0 \\ \mathbb{I} & \theta = 0. \end{cases}$$

Hence, the dynamics of $(x(t+\theta), \varepsilon)^T = z_t(\theta)$ is governed by the infinite dimensional ODE in Eq. (8) appropriately defined in $\mathcal{C}$ and parameterized by θ.

2.2 Spectral analysis

Let us investigate the spectrum $\sigma(\mathcal{A})$ of the linear operator $\mathcal{A}$ taken from Eq.(9). To this end, we consider the linearized problem of Eq. (8)

$$\frac{d}{dt} z_t(\theta) = \mathcal{A}(z_t(\theta)). \tag{10}$$

Substituting the ansatz $z_t(\theta) = \phi(\theta) e^{\lambda t}$ at $\theta = 0$ yields the eigenvalue problem,

$$L[z_t] - \lambda z_t(0) = (L[z_t] - \lambda \mathbb{I})\phi(0) \equiv \Delta(\lambda)\phi(0) = 0. \tag{11}$$

Here $\phi(\theta)$ is the eigenvector associated with the Lyapunov exponent λ. The spectrum of $\mathcal{A}$ is defined by $\sigma(\mathcal{A}) = \{\lambda \in \mathbb{C} | \Delta(\lambda) = 0\}$. For $-\tau \leq \theta < 0$, we obtain an ODE on θ that defines the eigenvectors

$$\lambda \phi(\theta) e^{\lambda t} = \phi'(\theta) e^{\lambda t}, \tag{12}$$

where $\phi'(\theta)$ denotes the derivative of ϕ with respect to θ.

A solution of Eq.(12) is $\phi(\theta) = \phi(0) e^{\lambda \theta}$. Hence, for all the eigenvalues $\lambda_i \in \sigma(\mathcal{A})$, one finds an associated eigenvector $\phi_i(\theta)$, which constitutes a basis $\Phi(\theta) = [\phi_1(\theta), \phi_2(\theta), ...]$. This basis spans $\mathcal{C}$, and as such, we can choose to write any state vector $v \in \mathcal{C}$ in terms of the eigenbasis of $\mathcal{A}$.

However, it is possible that the basis Φ is neither orthogonal or normalized. Thus, consider the adjoint basis $\Psi^\dagger(s) = [\psi_1^\dagger(s), \psi_2^\dagger(s), ...]$ where $\psi_i^\dagger(s)$ are eigenvectors of the adjoint linear problem

$$\frac{d}{dt} y_t(s) = \mathcal{A}^\dagger(y_t)) = -A(y_t) = \begin{cases} -\frac{\partial y_t(s)}{\partial s} & 0 > s \geq \tau \\ -L[y_t] & s = 0. \end{cases} \tag{13}$$

Note that the adjoint problem of Eq.(10) is found to be the foward problem, with $t \to -t$ [18, 10]. To ensure the bi-orthonormality of the eigenbases of $\mathcal{A}$ and $\mathcal{A}^\dagger$, we further normalize the adjoint basis by

$$\Psi(\theta) = \big(\Psi^\dagger(\theta), \Phi(\theta)\big)^{-1} \Psi^\dagger(\theta), \tag{14}$$

where we introduce the bilinear form operator $(\ ,\ )$ in $\mathcal{C}$, defined by

$$\big(a(\theta), b(\theta)\big) \equiv a(0)b(0) - \int_0^\theta d\theta' \int_{-\xi}^0 d\xi [d\eta(\theta')] a(\xi - \theta') b(\xi), \tag{15}$$

with the measure $d\eta'(\theta)$ defined in Eq. (7). This bi-linear form is playing the role of the dot product in the space of functions. Normalizing the eigenbases provides

$$\big(\Psi, \Phi\big)(\theta) = \mathbb{I}.$$

Considering the previous results, an arbitrary state vector $v = v(\theta)$ can be expressed in terms of the eigenbasis of (10) as

$$v(\theta) = \Phi(\theta)(\Psi(\theta), v(\theta)).$$

2.3 Phase space decomposition and subspace dynamics

A well chosen decomposition of the spectrum can play a fundamental role characterizing instabilities of Eq. (8). Indeed, in the vicinity of an instability, we might assume, without loss of generality, that a finite number of Lyapunov exponents cross the imaginary axis while changing a control parameter and all other exponents are bounded to the left-hand plane. These bifurcating, or *unstable* exponents near the transition point introduce a very slow time scale, while the *stable* components relax much faster to their steady state. As a consequence, after a sufficiently long time, the dynamics of the system is essentially determined by the slow unstable modes: this is the essence of the slaving principle [12]. Indeed, one can choose $\sigma_{\mathcal{U}}(\mathcal{A}) \equiv \{\lambda \in \mathbb{C} | Re(\lambda) = 0\}$ which leads to $\mathcal{C} = \mathcal{U} + \mathcal{S}$, where $\mathcal{S} = \overline{\mathcal{U}}$. The space $\mathcal{U}$ is the eigenspace spanned by the eigenvectors associated with unstable Lyapunov exponents. These eigenvectors constitute a basis of $\mathcal{U}$, namely $\Phi_{\mathcal{U}}(\theta) \subset \Phi(\theta)$. This implies that there exists a complementary subspace $\mathcal{S}$, spanned by $\Phi_{\mathcal{S}}$, associated with stable Lyapunov exponents i.e. $\sigma_{\mathcal{S}}(A) \equiv \{\lambda \in \mathbb{C} | Re(\lambda) < 0\}$. Here, we label $\mathcal{U}$ the subspace spanned by the unstable eigenmodes i.e. for which the eigenvalue have a zero real part, which is analogous to the center subspace, but only the terminology differ. Following the discussion in the previous section, one can project the state vector $z_t(\theta)$ governed by (8) with respect to the unstable basis $\Phi_{\mathcal{U}}(\theta)$,

$$U_t(\theta) = \Phi_{\mathcal{U}}(\theta)\big(\Psi_{\mathcal{U}}(\theta), z_t(\theta)\big) = \Phi_{\mathcal{U}}(\theta)(u(t), \varepsilon)^T, \tag{16}$$

where $(u(t), \varepsilon)^T = \big(\Psi_{\mathcal{U}}(\theta), z_t(\theta)\big)$ is a vector containing the expansion amplitudes of $z_t(\theta)$ with respect to the unstable eigenbasis $\Phi_{\mathcal{U}}(\theta)$. According to this phase space decomposition, the state vector $z_t(\theta)$ may be separated into two disjoint elements, its stable and unstable components in $\mathcal{S}$ and $\mathcal{U}$, respectively. Consequently we can write $z_t(\theta) = U_t(\theta) + s_t(\theta)$, where

$$s_t(\theta) = z_t(\theta) - \Phi_{\mathcal{U}}(\theta)\big(\Psi_{\mathcal{U}}(\theta), z_t(\theta)\big) \equiv \Phi_{\mathcal{S}}(\theta)\big(\Psi_{\mathcal{S}}(\theta), z_t(\theta)\big). \tag{17}$$

Following this separation, we can project the dynamics of Eq.(3) in $\mathcal{S}$ and $\mathcal{U}$, by applying the projector (16) to Eq.(8), to obtain

$$\begin{aligned}\Phi_{\mathcal{U}}(\theta)\big(\Psi_{\mathcal{U}}(\theta), \frac{d}{dt}z_t(\theta)\big) &= \Phi_{\mathcal{U}}(\theta)\big(\Psi_{\mathcal{U}}(\theta), \mathcal{A}(z_t(\theta))\big) \\ &+ \Phi_{\mathcal{U}}(\theta)\big(\Psi_{\mathcal{U}}(\theta), X_o F[z_t]\big). \end{aligned} \tag{18}$$

Using the linearity of the bilinear form Eq.(15), the left hand side is just

$$\Phi_{\mathcal{U}}(\theta)\big(\Psi_{\mathcal{U}}(\theta), \frac{d}{dt}z_t(\theta)\big) = \frac{d}{dt}\Phi_{\mathcal{U}}(\theta)\big(\Psi_{\mathcal{U}}(\theta), z_t(\theta)\big) \tag{19}$$

$$\equiv \frac{d}{dt}U_t(\theta). \tag{20}$$

The projection of the linear operator $\mathcal{A}$ is simply

$$\Phi_{\mathcal{U}}(\theta)\big(\Psi_{\mathcal{U}}(\theta), \mathcal{A}(z_t(\theta))\big) = \Phi_{\mathcal{U}}(\theta)(\Psi_{\mathcal{U}}(\theta), \mathcal{A}(U_t(\theta))) + \Phi_{\mathcal{U}}(\theta)\big(\Psi_{\mathcal{U}}(\theta), \mathcal{A}(s_t(\theta))\big).$$

Then, we find with Eq.(11),

$$\Phi_{\mathcal{U}}(\theta)\big(\Psi_{\mathcal{U}}(\theta), \mathcal{A}(U_t(\theta))\big) = \Phi_{\mathcal{U}}(\theta)\big(\Psi_{\mathcal{U}}(\theta), \Lambda_{\mathcal{U}}U_t(\theta))\big), \tag{21}$$

where $\Lambda_{\mathcal{U}}$ is a diagonal matrix with entries being the elements of $\sigma_{\mathcal{U}}(A)$.

Computing the term $\Phi_{\mathcal{U}}(\theta)\big(\Psi_{\mathcal{U}}(\theta), \mathcal{A}(s_t(\theta))\big)$ uses the biorthonormality of the stable and unstable eigenbases. In the same spirit as in the case of the stable mode projection in equation Eq.(16), the stable component $s_t(\theta) \in \mathcal{S}$ of the state vector $z_t(\theta)$ may be written with respect to the eigenbasis of $\mathcal{S}$,

$$S_t(\theta) = \Phi_{\mathcal{S}}(\theta)\big(\Psi_{\mathcal{S}}(\theta), z_t(\theta)\big). \tag{22}$$

Using this fact, along with $\big(\Psi_{\mathcal{U}}, \Phi_{\mathcal{S}}\big) = 0$ yields

$$\Phi_{\mathcal{U}}(\theta)(\Psi_{\mathcal{U}}(\theta), \mathcal{A}(s_t(\theta))) = 0. \tag{23}$$

Thus, grouping the projection over the elements in $\mathcal{U}$ and $\mathcal{S}$ in Eq.(21) and Eq.(23) gives the projected linear component of Eq.(8)

$$\Phi_{\mathcal{U}}(\theta)\big(\Psi_{\mathcal{U}}(\theta), \mathcal{A}(z_t(\theta))\big) = \Phi_{\mathcal{U}}(\theta)\big(\Psi_{\mathcal{U}}(\theta), \Lambda_{\mathcal{U}}U_t(\theta))\big) = \Lambda_{\mathcal{U}}U_t(\theta). \tag{24}$$

The projection over the non-linear component $X_o F[z_t]$ of Eq.(8) is computed from Eq.(15), and reads

$$\Phi_{\mathcal{U}}(\theta)\big(\Psi_{\mathcal{U}}(\theta), X_o F[z_t]\big) = \Phi_{\mathcal{U}}(\theta)\Psi_{\mathcal{U}}(0)F[z_t]. \tag{25}$$

Thus, combining Eq. (24) and Eq. (25) for $z_t(\theta) = \Phi_{\mathcal{U}}(\theta)(u(t), \varepsilon)^T + s_t(\theta)$, yields the dynamics of the unstable modes of Eq. (3)

$$\begin{aligned}\mathcal{U} \ni \frac{du(t)}{dt} &= \Lambda_{\mathcal{U}}u(t) + \Psi_{\mathcal{U}}(0)F[\Phi_{\mathcal{U}}u(t) + s_t(\theta)] \\ \mathcal{U} \ni \frac{d\varepsilon}{dt} &= 0. \end{aligned} \tag{26}$$

Using the same approach, we apply the operator $(\mathbb{I} - \Phi_{\mathcal{U}}(\theta)(\Psi_{\mathcal{U}}(\theta), \ \cdot \ )$ to the state vector $z_t(\theta)$ of Eq. (8) to obtain the complementary dynamics of the stable modes in $\mathcal{S}$

$$\mathcal{S} \ni \frac{d}{dt} s_t(\theta) = \mathcal{A}(s_t(\theta)) + (X_o - \Phi_{\mathcal{U}}(\theta)\Psi_{\mathcal{U}}(0))F[\Phi_{\mathcal{U}} u(t) + s_t]. \tag{27}$$

2.4 The time-independent center manifold reduction

The manipulations described above can be seen as a procedure first identifying the stable and unstable manifolds, and secondly writing down the dynamics of Eq.(1) in $\mathcal{U}$ and $\mathcal{S}$ explicitly. The key idea behind this projection is first that one can reduce the dynamics of the infinite dimensional system in Eq. (8) onto the finite dimensional center eigenspace in Eq.(26) by applying the center manifold theorem, and second to get rid of delays. It provides a useful analysis platform on which one can investigate dynamic instabilities using the standard tools of linear analysis of ODEs.

Bifurcations are characterized by unstable Lyapunov exponents (i.e. exhibiting a zero-real part), or equivalently by a non-empty unstable eigenspace. The precise point in parameter space where $\sigma_{\mathcal{U}}(\mathcal{A}) \neq \emptyset$ is called the *instability threshold*, and can be quantitatively described by $\max_\varepsilon Re(\lambda) = 0 | \lambda \in \sigma(\mathcal{A})$. When this critical point is reached, the center manifold theorem applies, and the stable modes in $\mathcal{S}$ are slaved by the dynamics of the unstable modes in $\mathcal{U}$ [12]. Then

$$s_t(\theta) = h(\theta, u(t), \varepsilon), \tag{28}$$

holds true. Consequently, the unstable modes are further described by the *order parameter equation* (OPE)

$$\frac{du}{dt} = \Lambda_{\mathcal{U}} u + \Psi_{\mathcal{U}}(0) F[\Phi u + h(u)]. \tag{29}$$

While in the vicinity of an instability and given that the functional $h(u)$ is known, this system captures the dynamics of Eq.(1) entirely. Delayed components are not present anymore, and the dimensionality of this representation is finite, making the OPE very useful in the treatment of non linear DDEs. Most importantly, it is possible to reconstruct the flow $x(t)$ of the original delayed system of Eq.(1) solely from the unstable modes by

$$x^r(t) = \Phi_{\mathcal{U}}(0) u(t) + h(0, u(t), \varepsilon). \tag{30}$$

Although the center manifold theorem ensures that the functional $h(\theta, u(t), \varepsilon)$ exists, it is typically not unique and usually challenging to compute explicitly. Such a derivation is often realized using algebraic manipulation softwares, and other methods [20, 19].

The reconstructed flow of $x^r(t)$ converges to the original flow $x(t)$ as the manifold $h(\theta, u)$ gets closer to its exact form. Since $ds/dt = D_u h(u)(du(t)/dt)$ from Eq.(28), the center manifold satisfies the implicit relationship

$$D_u h(\theta, u, \varepsilon)[\Lambda u + \Psi_{\mathcal{U}}(0) F[\Phi u + h(u)] = \mathcal{A}(h(u)) + (X_o - \Phi_{\mathcal{U}}(\theta)\Psi_{\mathcal{U}}(0))\, F\left[\Phi_{\mathcal{U}} u + h(u)\right], \tag{31}$$

taking into account Eqs. (26) and (27). Here D_u denotes the partial derivative with respect to u.

A typical ansatz to compute $h(\theta, u, \varepsilon)$ is a polynomial expansion in powers of u and the control parameter ε. Then sorting the terms by orders of ε and u yields a set of first order linear differential equations in each of the polynomial coefficients for $-\tau \leq \theta < 0$. The initial conditions of these are fixed by solving Eq.(31) for $\theta = 0$. The dimensionality of the differential equations in each the coefficients is the same as the codimension of the bifurcation considered. With this ansatz, one can compute h up to any desired accuracy, by computing higher orders coefficients in the expansion and , hence, make $x^r(t)$ as close as desired to $x(t)$. However, for most applications an expansion to low order is sufficient.

2.5 The time-dependent center manifold reduction

Now consider the *non-autonomous* DDE

$$\dot{x}(t) = f(x(t), x(t-\tau), t) = L(\{x(t), x(t-\tau)\}) + F(\{x(t), x(t-\tau)\}) + I(t). \tag{32}$$

Equation (32) is a non-autonomous delay-differential equation and it is a challenging problem to find conditions for its stability. Close to a bifurcation point, the analysis of such DDEs has attracted increasing attention in the last years, e.g. considering more general [18, 22], deterministic [23, 24] or stochastic forces [25, 26]. The approach discussed in the previous sections cannot, formally, be used since the origin is no longer a fixed point and the eigenbases definition and associated phase space decomposition are not valid anymore. In addition, by virtue of the new time scales introduced by the external input, it is more difficult to identify separate time scales which is necessary in the center manifold technique.

However, when the driving $I(t)$ is small and fast compared to the relatively slow unstable modes, one may consider the fixed point of the autonomous system of Eq. (1) for the analysis of Eq. (32). This step is reasonable since previous studies on nonlinear delayed systems have shown that such driven delayed systems are stable under certain conditions in the sense of Input-to-state Stability [27]. One can then use the spectrum and subspace eigenbases from the autonomous

system to project the dynamics of the non-autonmous system of Eq. (32) and subsequently obtain the non-stationary version of Eqs. (26)-(27)

$$\mathcal{U} \ni \frac{du(t)}{dt} = \Lambda_{\mathcal{U}} u(t) + \Psi_{\mathcal{U}}(0) F(\Phi_{\mathcal{U}}(\theta) u(t) + s_t(\theta)) + \Psi_{\mathcal{U}}(0) I(t) \tag{33}$$

$$\mathcal{S} \ni \frac{d}{dt} s_t(\theta) = \mathcal{A} s_t(\theta) + (X_o - \Phi_{\mathcal{U}}(\theta)\Psi_{\mathcal{U}}(0))[F(\Phi_{\mathcal{U}}(\theta) u(t) + s_t(\theta)) + I(t)].$$

This result has been demonstrated formally in the case of linear non-autonomous delayed system [18]. Hence the approximation is reasonable since the amplitude of both the stable and unstable modes in the vicinity of an instability can be taken arbitrarily small by adjusting the control parameter, making the non-linear component F small enough. In other words, close to the origin, the nonlinear dynamics of the system is close to its linear dynamics.

To reduce the dimensionality of the system from infinity to few modes, we proceed with the asumption that the center manifold theorem still applies close to the instability and that the functional h exhibits an explicit time dependence now. This assumption has been considered successfully in non-delayed systems for quasi-periodic input [28]. Moreover the existence of time-dependent center manifolds in non-delayed systems has been proven for stochastic inputs $I(t)$ [15]. Accordingly we choose

$$s_t(\theta) = h(\theta, u(t), \varepsilon, t) \ . \tag{34}$$

As in the case of autonomous systems, the functional h has yet to be at least approximated, to be of any use in the analysis of Eq.(32). In particular, now the manifold $h(\theta, u, \varepsilon, t)$ satisfies

$$\begin{aligned} &D_u h(\theta, u, \varepsilon, t)[\Lambda u + \Psi_{\mathcal{U}}(0) F\left[\Phi_{\mathcal{U}} u(t) + h(u, \varepsilon, t)\right] + \Psi_{\mathcal{U}}(0) I(t)] + \frac{\partial h(\theta, u, \varepsilon, t)}{\partial t} \\ &= \mathcal{A}(h(u, \varepsilon, t)) + (X_o - \Phi_{\mathcal{U}}(\theta)\Psi_{\mathcal{U}}(0)) \left(F[\Phi_{\mathcal{U}} u(t) + h(u, \varepsilon, t)] + I(t)\right). \end{aligned} \tag{35}$$

As an ansatz, we add a time-dependent correction h_t to the expansion used in the autonomous case, such that the time-dependence in the center manifold takes the form of a fast additive perturbation

$$h(\theta, u, t, t') = h_n(\theta, \varepsilon, u) + h_t(\theta, t) + \mathcal{O}(m > n; u, \varepsilon, t), \tag{36}$$

where $\mathcal{O}(m; u, \varepsilon, t)$ denotes terms of order of magnitude m in u, ε and the time-dependent contribution. The ansatz of Eq. (36) assumes that the autonomous center manifold h_n of order n and the correction term h_t have similar order of magnitude. In the following we assume $\mathcal{O}(h_t) = 2$ and the order of h_n may be $n = 2$ or $n = 3$. This ansatz implies time-dependent corrections that are small compared to the amplitude of the unstable modes. This ansatz is analogous to the one used by [28] for forced non-linear ODEs, which proved to accurately reproduce the dynamics for various types of driving.

Moreover, Eq. (36) assumes that, to second order, the center manifold has a separable form in time t and modes u which facilitates the resolution of the resulting ODE system for $-\tau \leq \theta < 0$. Indeed, the substitution of this ansatz in Eq. (35) up to quadratic order, i.e. $n = 2$ leads to the same set of differential equations as the autonomous problem, with the notable exception of an additional slow equation in $h_t(\theta, t)$ of order 2. The terms in h_t are decoupled from the autonomous contribution $h_n(\theta, u)$ and obey

$$\frac{\partial h_t(\theta,t)}{\partial t} = \frac{\partial h_t(\theta,t)}{\partial \theta} - \Phi(\theta)\Psi(0)I(t) \ . \tag{37}$$

Here we chose $\mathcal{O}(I(t)) = 2$ Equation (37) is a linear first order non-homogeneous partial differential equation of the time correction coefficient h_t, which may be solved using the method of characteristics, given that $I(t)$ and the entries of the bases $\Phi(\theta)$ and $\Psi(\theta)$ are smooth enough. To solve Eq. (37), we have to distinguish the two cases:

- for $t + \theta \leq 0$, Eq. (37) is an intial value-problem with the history function $g(t)$, $-\tau \leq t \leq 0$, i.e. $h_t(\theta, 0) = g(\theta)$. Then the method of characteristics leads to

$$h_t(\theta,t) = -\int_0^t \Phi(t+\theta-s)\Psi(0)I(s)ds + H(\theta+t) \ , \ t+\theta < 0, \tag{38}$$

  with $H(\theta) = g(\theta)$. We point out that this solutins holds for the time interval $t \in [0; -\theta]$ only.
- for $t + \theta > 0$, Eq. (37) is a boundary value-problem at $\theta = 0$ and we find by the method of characteristics

$$h_t(\theta,t) = -\int_0^{-\theta} \Phi(-s)\Psi(0)I(t+\theta+s)ds + H(\theta+t) \ . \tag{39}$$

  Indeed, writing Eq.(35) for $\theta = 0$ yields

$$\frac{\partial h_t(0,t)}{\partial t} = L[h_t(t)] + (1 - \Phi(0)\Psi(0))\, I(t) \ . \tag{40}$$

  According to Eq.(39), we may write $h_t(\theta, t) = r(\theta, t) + H(t + \theta)$, where $r(\theta,t) = -\int_0^{-\theta} \Phi(-s)\Psi(0)I(t+\theta+s)ds$. Then inserting this expression into (40) leads to

$$\frac{\partial H(t)}{\partial t} = L[H(t)] + L[r(t)] + (1 - \Phi(0)\Psi(0))\, I(t) \ . \tag{41}$$

Recall that $L[H(t)]$ is a functional of $H(\theta + t)$ and thus $L[H(t)]$ may depend on $H(t)$ and $H(t - \tau)$. Similarly $L[r(t)]$ is a functional of $r(\theta, t)$. Given that the functional $r(\theta, t)$ is known and the linear term contains retarded terms, Eq.(41)

is a non-autonomous linear delay-differential equation in H which can be solved analytically [18, 29].

The approach illustrates the hypothesis that the non-autonomous case can be analyzed, in lowest order approximation, by a fast and small time-dependent correction on the center manifold. Higher degrees of accuracy than the second order could be achieved by proceeding to higher order terms in both modes and time dependent components of $h(\theta, u, \varepsilon, t)$ in Eq.(36). The time-mode separable form, i.e. the separation of the mode-dependent part h_a and the time-dependent part h_t, combined with the time-scale separation asumption allows to compute higher order terms in the modes expansion, while keeping the time-dependent component to second order. The subsequent section examines the hypotheses made and the corresponding results by applying the method to a specific example.

3 The asymmetrical transcritical bifurcation

To validate our approach, let us apply the procedure discussed in the previous sections to a non-autonomous delayed differential equation with quadratic nonlinearity near a codimension 1 instability. The system we consider reads

$$\frac{dx(t)}{dt} = -x(t) - R_1 x(t-\tau) - R_2 x^2(t-\tau) + I(t), \tag{42}$$

with the augmented system

$$\begin{aligned} \frac{dx(t)}{dt} &= -x(t) + x(t-\tau) - \varepsilon x(t-\tau) - R_2 x^2(t-\tau) + I(t) \\ \frac{d\varepsilon}{dt} &= 0, \end{aligned} \tag{43}$$

where we introduced the *control parameter* $\varepsilon \equiv R_1 + 1$. Applying the steps described in the previous section we obtain the reduced dynamics [30]

$$\begin{aligned} \frac{du(t)}{dt} &= \frac{1}{1+\tau} F[u(t) + s_t] + \frac{1}{1+\tau} I(t) \\ \frac{d\varepsilon(t)}{dt} &= 0 \\ \frac{d}{dt} s_t(\theta) &= \mathcal{A}(s_t) + \left(X_o - \frac{1}{1+\tau} \right) (F[u(t) + s_t] + I(t)). \end{aligned} \tag{44}$$

Now applying the center manifold theorem implies that the functional h depends on time explicitely and with the separation ansatz 36 h_t obeys

$$\frac{\partial h_t}{\partial t} = \frac{\partial h_t}{\partial \theta} - \frac{1}{1+\tau} I(t) \ . \tag{45}$$

Then Eqs.(38), (39) lead to the solutions

$$h_t(\theta,t) = -\frac{1}{1+\tau}\int_0^t I(s)ds + H(\theta+t) \quad , \quad t \le -\theta$$
$$h_t(\theta,t) = -\frac{1}{1+\tau}\int_0^{-\theta} I(t+\theta+s)ds + H(\theta+t) \quad , \quad t > -\theta, \tag{46}$$

with the initial condition $H(\theta) = g(\theta)$. Substituting these results into Eq.(41) yields the evolution equation of $H(t),\ t \ge 0$ for $\theta = 0$

$$\frac{dH}{dt} = -H(t) + H(t-\tau) - \frac{1}{1+\tau}\int_0^{\tau} I(t-\tau+s)ds + \frac{\tau}{1+\tau}I(t)\ . \tag{47}$$

We point out, that the last two terms may be viewed as an external driving and the linear terms are the same as the linear terms in the original system. By virtue of the spectrum of the linear operator the linear system in $H(t)$ in (47) is marginally stable close to the stability threshold (the maximum Lyapunov exponent is close to zero). The other Lyapunov exponents have negative real parts and their contribution vanish for large times.

To verify these results, let us consider the periodic driving $I(t) = I_o \sin(w_o t)$, whose amplitude I_o is small compared to the amplitude $u(t)$ and whose oscillation period is short compared to the slow evolution of $u(t)$. The autonomous components of the center manifold were found previously. The time-dependent correction is given by Eq.(46)

$$h_t(\theta,t) = H(t+\theta) + \frac{I_o}{w_o(1+\tau)}(\cos(w_o t) - 1) \quad , \quad t \le -\theta$$
$$h_t(\theta,t) = H(t+\theta) + \frac{I_o}{w_o(1+\tau)}(\cos(w_o t) - \cos(w_o(t+\theta))) \quad , \quad t > \theta\ . \tag{48}$$

Assuming the initial function $g(t) = 0,\ -\tau \le t \le 0$, and for large times $t \to \infty$, the solution of (47) reads

$$\begin{aligned} H(t) = &-\frac{I_o\tau}{(1+\tau)^2 w_o}(\cos(w_o t - 1)) \\ &+\frac{\tau I_o}{w_o^2(1+\tau)^2}\left(\sin(w_o t) - \sin(w_o(t-\tau)) - \sin(w_o\tau)\right) \\ &+R_1(I_o,w_o)\sin(w_o t) + R_2(I_o,w_o)\cos(w_o t). \end{aligned} \tag{49}$$

with constants $R_1(I_o,w_o)$ and $R_2(I_o,w_o)$ depending on the stimulus frequency w_o, the input strength I_o and the delay τ.
Taking into account the time-dependence of the center manifold gives access to more than just the good reconstruction of the systems dynamics. In general, non-autonomous components play a major role in the stability of dynamical systems,

especially in the vicinity of dynamic instabilities, i.e. in the presence of different time scales [17, 31]. Therefore, the study of time-corrected center manifolds yield details about input-induced bifurcations. Let us investigate the interaction of the input $I(t)$ with the transcritical bifurcation studied.

Based on the calculations in the previous section, we may write the order parameter equation as

$$\frac{du(t)}{dt} = \frac{1}{1+\tau}\left(-\varepsilon(u+h(-\tau,u,t)) - R_2(u+h(-\tau,u,t))^2 + I(t)\ \right), \qquad (50)$$

where we omitted the trivial dynamics of the control parameter ε. Over a finite time interval, we might time-average both sides of Eq.(50) to obtain

$$\begin{aligned}\left\langle \frac{du(t)}{dt} \right\rangle = \frac{1}{1+\tau}\big(&\langle I(t)\rangle - \varepsilon\langle u\rangle - \varepsilon\langle h(-\tau,u,t))\rangle \\ &-R_2\left\langle u^2\right\rangle - 2R_2\langle uh(-\tau,u,t))\rangle - R_2\left\langle h(-\tau,u,t)^2\right\rangle\big), \end{aligned} \qquad (51)$$

where the time averaging operator $\langle\cdot\rangle$ is defined over an interval T by

$$\langle\cdot\rangle = \frac{1}{T}\int_t^{t+T}(\ \cdot\ )dt.$$

Following the time scale separation issued by the center manifold theorem and the OPE, the input $I(t)$ is considered fast, compared to the unstable mode $u(t)$. Hence, for T sufficiently small, $u(t)$ is approximately constant, and we may consequently write $\langle u(t)\rangle \approx u(t)$. Thus, if the input is chosen such that $\langle I(t)\rangle = 0$, Eq.(51) may be written as

$$\begin{aligned}\left\langle \frac{du(t)}{dt} \right\rangle = -\frac{1}{1+\tau}R_2\Bigg(u^2 + \Bigg(\frac{\varepsilon}{R_2} + 2\langle h(-\tau,u,t)\rangle\Bigg)u \\ + \Bigg(\frac{\varepsilon}{R_2}\langle h(-\tau,u,t)\rangle + \left\langle h(-\tau,u,t)^2\right\rangle\Bigg)\Bigg)\ . \end{aligned} \qquad (52)$$

Because of the separation of the time scales, the fixed points of the averaged equation correspond to the fixed points of Eq.(50). Inserting the stable manifold $h(-\tau,u,t)$ with the terms in Eqs. (48) and (49) found in section 3, we gain the stationary states by setting $\left\langle \frac{du(t)}{dt} \right\rangle = 0$. In addition the focus to the solutions close to the origin, leads to the stationary states

$$\begin{aligned}u^o = \frac{1}{2A_0 + 2A_1\langle h_t\rangle}\Bigg(&-(B_0 + B_1\langle h_t\rangle) \\ &\pm\sqrt{(B_0+B_1\langle h_t\rangle)^2 - 4(A_0+A_1\langle h_t\rangle)\langle h_t^2,\rangle,}\Bigg) \end{aligned} \qquad (53)$$

with functions $A_0 = A_0(\varepsilon), A_1 = A_1(\varepsilon), B_0 = B_0(\varepsilon), B_1 = B_1(\varepsilon)$ and $h_t = h_t(-\tau,t)$. Since the external input can be viewed as a a linear superposition of

oscillations according to Fourier theory and hence h_t exhibits oscillations with the same frequencies, it is reasonable to assume that $\langle h_t \rangle \approx 0$. This assumption implies that the time-average window T is smaller than the period of the slowest Fourier component in the input. Then we find

$$u^o = \frac{1}{2A_0}\left(-B_0 \pm \sqrt{B_0^2 - 4A_0 \langle h_t^2 . \rangle}\right) \tag{54}$$

with $\left\langle h_t^2 \right\rangle \geq 0$. If $\left\langle h_t^2 \right\rangle = 0$, then $I(t) = 0$ and $u^o = 0,\ -B_0/A_0 \approx -\varepsilon \times const$ and the origin u^o is the only stationary solution for $\varepsilon = 0$. In contrast, if $\left\langle h_t^2 \right\rangle > 0$ for $I(t) \neq 0$ and the origin is not a stationary solution of the dynamics. New equilibria are moved to $\varepsilon_{min,1} > 0,\ \varepsilon_{min,2} < 0$. These solutions are roots of the polynomial $B_0^2(\varepsilon) - 4A_0(\varepsilon)\left\langle h_t^2 \right\rangle = 0$. These results demonstrate that the external input destroys stationary states, that existed without external input, and breaks the symmetry of the transcritical bifurcation: the external input changes the stability of the system.

To verify these analytical results, we choose the averaging interval as the period of one input cycle i.e. $T = 2\pi/w_o$ so that $\langle I(t) \rangle = 0$. Considering the full terms in Eq. (52) and by setting $\left\langle \frac{du(t)}{dt} \right\rangle = 0$, we may find the stationary states numerically, see Fig. 1. We immediately see that whenever $\left\langle h_t^2 \right\rangle > 0$, the symmetry of transcritical bifurcation is broken, and we obtain a imperfect bifurcation scenario. This symmetry breaking replaces the intersecting branches by two disjoint saddle-node curves. In order for the order parameter equation to capture this particular bifurcation diagram, the precision of the center manifold $h(\theta, t, u)$ is very important. The time-corrected center manifold brings a considerable amount of accuracy to the OPE, not only by adjusting the phase but also the amplitude of the system's response. Fig. 1 shows how the OPE with time-dependent center manifold reproduces the bifurcation diagram of the original DDE with an improved accuracy compared to the same problem but without any time-dependency on the center manifold.

4 Concluding Remarks

In this essay, we showed that the dynamics of a non-autonomous delayed feedback system could be captured by center manifold reduction. This is made possible by allowing an explicit time dependence of the manifold, taking the form of an additive time-dependent correction to the non-driven problem. We illustrated the approach by considering a scalar delay differential equation with quadratic non-linearity, driven by an additive time-periodic term, in the vicinity of a transcritical bifurcations. Numerical experiments are in good agreements with the analytical results. Higher degrees of accuracy could be reached by considering higher order terms in both time and mode dependent components of the center manifold.

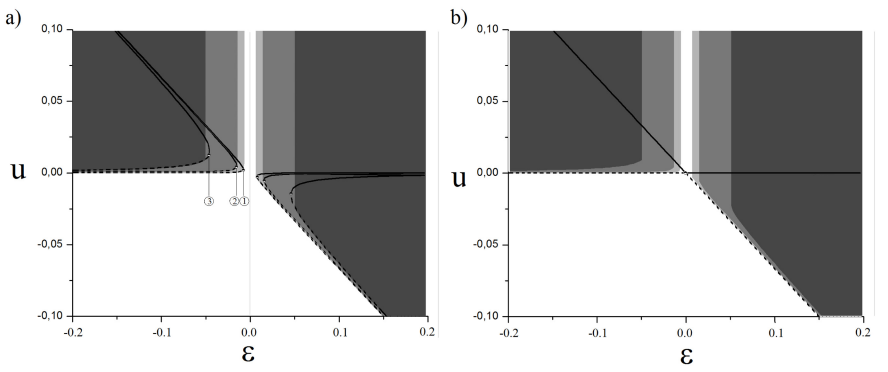

Fig. 1. Bifurcation diagram of the averaged order parameter equation. (a) Comparison of the basins of atttaction of the original DDE for different I_o with those predicted applying the proposed time-dependent center manifold reduction. The fixed point curves (solid and dashed lines) of the averaged OPE in Eq.(53) delimits the basins of attraction of the original system (42) shown in tones of shaded gray for different input amplitudes. The input amplitudes have been set to $I_o = 0.05$ (stationary solutions **1** and basin of attraction in light gray), $I_o = 0.1$ (stationary solutions **2** and basin of attraction in gray) and $I_o = 0.3$ (stationary solutions **2** and basin of attraction in dark gray). As the input amplitude increases i.e. $I_o > 0$, the basin of attraction of the stable fixed points splits and exhibit a band of unstable initial conditions, indicating that the input induces an imperfect transcritical bifurcation. In this case, the stable and unstable branches do not meet at $\varepsilon = 0$ as expected and are replaced by two saddle nodes bifurcations. (b) Plot of the fixed point curves predicted by the averaging of the original system (42) where a standard transcritical case is predicted. This result does not correspond to the dynamics of the original system. In contrast, the fixed point curves (53) of the averaged order parameter equation using time-dependent center manifold show saddle node bifurcations for different input amplitudes, delimiting the basins of attraction of the original system accurately for $I_o = 0.05$ and $I_o = 0.1$. For $I_o = 0.3$, the input amplitudes becomes large compared to the unstable mode amplitude. Additional parameters are $w_o = 15$, $\tau = 2.0$, $R_2 = 1.5$

It is still unclear how the initial conditions of the original DDE are mapped to those of the OPE. There appears to be discrepancy at $t = 0$ between the reconstructed and original flow of the system considered in this example, that we corrected manually to match the initial conditions of both the OPE and DDE. This deviations seems to be due to the yet unknown map from the interval $[-\tau, 0]$ to the initial value problem $x(0) = x_o$, induced by the projection onto stable and unstable subspaces. This discrepancy usually decays numerically with the transients. A tentative solution to this problem would require a consideration of the individual stable modes initial value problems, an information that appears to be lost with the application of the center manifold theorem and following approximations.

The time-dependent correction considered here is appropriate for additive driving only, as no time-mode mixing is present at lowest order. We might consequently expect that mutiplicative time-dependent forcing would require a different working ansatz, which would not allow a separation between autonomous and non-autonomous problems, as the example detailed here shows. This case would invariably lead to more involving calculations.

References

1. Longtin, A., Milton, J.G.: Modelling autonomous oscillations in the human pupil light reflex using nonlinear delay-differential equations. Bull. Math. Biol. **51**, 605–624 (1989)
2. Glass, L., Mackey, M.: From Clocks to Chaos: The Rhythms of Life. Princeton University Press, Princeton (1988)
3. Boulet, J., Balasubramaniam, R., Daffertshofer, A., Longtin, A.: Stochastic two delay-differential model of delayed visual feedback effects on postural dynamics. Phil. Trans. Royal Soc. A **368**, 423–438 (2010)
4. Hutt, A., Bestehorn, M., Wennekers, T.: Pattern formation in intracortical neuronal fields. Network: Comput. Neural Syst. **14**, 351–368 (2003)
5. Atay, F.M., Hutt, A.: Neural fields with distributed transmission speeds and constant feedback delays. SIAM J. Appl. Dyn. Syst. **5**, 670–698 (2006)
6. Coombes, S., Owen, M.: Bumps, breathers, and waves in a neural network with spike frequency adaptation. Phys. Rev. Lett. **94**, 148102 (2005)
7. Franovic, I., Todorovic, K., Vasovic, N., Buric, N.: Spontaneous formation of synchronization clusters in homogenous neuronal ensembles induced by noise and interaction delays. Phys. Rev. Lett. **108**, 094101 (2012)
8. Campbell, S.A.: Calculating center manifolds for delay differential equations using maple. In: Delay Differential Equations: Recent Advances and New Directions. Springer, Berlin (2008)
9. Redmond, B., LeBlanc, V., Longtin, A.: Bifurcation analysis of a class of first-order nonlinear delay-differential equations with reflectional symmetry. Physica D **166**, 131–146 (2002)
10. Wischert, W., Wunderlin, A., Pelster, A., Olivier, M., Groslambert, J.: Delay-induced instabilities in nonlinear feedback systems. Physical Review E **49**, 203–219 (1994)
11. Schanz, M., Pelster, A.: Synergetic system analysis for the delay-induced Hopf bifurcation in the Wright equation. SIAM J. Applied Dynamical Systems **2**, 277–296 (2003)
12. Haken, H.: Synergetics. Springer, Berlin (2004)
13. Schoener, G., Haken, H.: The slaving principle for Stratonovich stochastic differential equations. Z. Phys. B **63**, 493–504 (1986)
14. Chicone, C., Latushkin, Y.: Center manifolds for infinite dimensional nonautonomous differential equations. J. Diff. Eqs. **141**, 356–399 (1997)
15. Boxler, P.: A stochastic version of center manifold theory. Prob. Theory Relat. Fields **83**, 509 (1989)
16. Xu, C., Roberts, A.: On the low-dimensional modelling of Stratonovich stochastic differential equations. Physica A **225**, 62–80 (1996)

17. Hutt, A., Longtin, A., Schimansky-Geier, L.: Additive global noise delays turing bifurcations. Phys. Rev. Lett. **98**, 230601 (2007)
18. Hale, J., Lunel, S.: Introduction to functional differential equations. Springer, Berlin (1993)
19. Quesmi, R., Babram, M.A., Hbid, M.: A maple program for computing a terms of a center manifold, and element of bifurcations for a class of retarded functional differential equations with Hopf singularity. Appl. Math. Comp. **175**, 932–968 (2006)
20. Campbell, S.A., Belair, J.: Analytical and symbolically-assisted investigations of Hopf bifurcations in delay-differential equations. Can. Appl. Math. Quart. **3**, 137–154 (1995)
21. Faria, T., Magalhaes, L.: Normal forms for retarded functional differential equations with parameters and applications to Hopf bifurcation. J. Diff. Eqs. **122**, 281 (1995)
22. Asl, F., Ulsoy, A.: Analysis of a system of linear delay differential equations. J. Dyn. Syst. Meas. Cont. **125**, 215–223 (2003)
23. Li, J., Hansen, C.: Forced phase-locked response of a nonlinear system with time delay after Hopf bifurcation. Chaos Solit. Fract. **25**, 461–473 (2005)
24. Xu, J., Chung, K.: Effects of time delayed position feedback on a van der Pol–Duffing oscillator. Physica D **180**, 17–39 (2003)
25. Frank, T.D., Beek, P.J.: Stationary solutions of linear stochastic delay differential equations: Applications to biological systems. Phys. Rev. E **64**, 021917 (2001)
26. Guillouzic, S., L'Heureux, I., Longtin, A.: Small delay approximation of stochastic delay differential equation. Phys. Rev. E **59**, 3970 (1999)
27. Yeganefar, N., Pepe, P., Dambrine, M.: Input-to-state stability of time-delay systems: A link with exponential stability. IEEE Transactions On Automatic Control **53**, 1526–1531 (2008)
28. Cox, S., Roberts, A.: Center manifolds of forced dynamical systems. J. Austral. Math. Soc. Ser. B **32**, 401–436 (1991)
29. Amann, A., Schoell, E., Just, W.: Some basic remarks on eigenmode expansions of time-delay dynamics. Physica A **373**, 191–202 (2007)
30. Lefebvre, J., Hutt, A., LeBlanc, V.G., Longtin, A.: Reduced dynamics for delayed systems with harmonic or stochastic forcing. Chaos **22**, 043121 (2012)
31. Hutt, A., Longtin, A., Schimansky-Geier, L.: Additive noise-induced turing transitions in spatial systems with application to neural fields and the Swift-Hohenberg equation. Physica D **237**, 755–773 (2008)

Control of Desynchronization Transitions in Delay-Coupled Networks of Type-I and Type-II Excitable Systems

Eckehard Schöll[1], Judith Lehnert[1], Andrew Keane[1], Thomas Dahms[1], and Philipp Hövel[1,2]

[1] Technische Universität Berlin, Institut für Theoretische Physik
Hardenbergstr. 36, 10623 Berlin, Germany
[2] Bernstein Center for Computational Neuroscience, Humboldt-Universität zu Berlin
Philippstraße 13, 10115 Berlin, Germany
schoell@physik.tu-berlin.de
http://www.itp.tu-berlin.de/schoell

Abstract. We discuss synchronization and desynchronization transitions in networks of delay-coupled excitable systems. These transitions arise in response to varying the balance of excitatory and inhibitory couplings in a small-world topology. To describe the local dynamics, we use generic models for type-I excitability, which arises close to a saddle-node bifurcation on an invariant cycle (SNIC or SNIPER), and for type-II excitability, which occurs close to a Hopf bifurcation (FitzHugh-Nagumo model). For large delay times both type-I and type-II systems behave in a similar way. This is different for small delay times, where in case of type-I excitability we find novel multiple transitions between synchronization and desynchronization, when the fraction of inhibitory links is increased. In contrast, only a single desynchronization transition occurs for the FitzHugh-Nagumo model (type-II excitability) for all values of the delay time.

Keywords: complex networks, delayed coupling, synchronization, excitatory and inhibitory balancing, type-I and type-II excitability, small-world

1 Introduction

The control of the dynamics on complex networks has recently gained much interest within the interdisciplinary field of control of nonlinear dynamical systems [1]. Synchronization phenomena in networks are of great importance [2–5] in many areas ranging from physics and chemistry to biology and engineering. Chaos synchronization of lasers, for instance, may lead to new secure communication schemes [6–8]. The synchronization of neurons is believed to play a crucial role in the brain under normal conditions, for instance in the context of cognition, perception, and learning [9–12], and under pathological conditions such as epilepsy

A. Pelster and G. Wunner (eds.), *Selforganization in Complex Systems: The Past, Present, and Future of Synergetics*, Understanding Complex Systems,
DOI: 10.1007/978-3-319-27635-9_3

[13] and Parkinson's disease [14]. Time-delay effects are a key issue in realistic networks. For example, the finite propagation time of light between coupled semiconductor lasers [15–19] significantly influences the dynamics. Similar effects occur in neuronal [20–23] and biological [24, 25] networks. The importance of the effect of delay on synchronization in neural networks was already pointed out by Hermann Haken in his early pioneering work on brain dynamics [26, 9]. There exist different forms of synchronization, i.e., complete or isochronous (zero-lag) synchronization, generalized synchronization, cluster or group synchronization, and many other forms. Chimera states, where a network of identical oscillators splits into distinct coexisting domains of coherent (phase-locked) and incoherent (desynchronized) behavior, have gained much attention recently [27–34].

To determine the stability of a synchronized state in a network of identical units, a powerful method has been developed [35], i.e., the master stability function (MSF). This approach has been extended to networks with coupling delays [36–41], where the MSF depends non-trivially on delay times.

In this chapter we review recent work on synchronization and desynchronization transitions in delay-coupled networks and how they are influenced by the ratio between the number of excitatory and inhibitory links [42, 43]. The issue of balancing excitation and inhibition in neuronal networks has recently found great interest in the neurodynamics community [44–47]. In general, the stability of synchronization depends in a complicated way on the local dynamics of the nodes and the coupling topology. However, for large coupling delays synchronizability relates in a simple way to the spectral properties of the network topology, characterized by the eigenvalue spectrum of the coupling matrix. The MSF used to determine the stability of synchronous solutions has a universal structure in the limit of large delay: it is rotationally symmetric and increases monotonically with the radius in the complex plane. This allows for a universal classification of networks with respect to synchronization properties [39]. For smaller coupling delays the synchronization properties depend in a more subtle way upon the local dynamics, and the details of the network topology. Various cluster-synchronization states, where certain clusters inside the network show isochronous synchronization, can be realized by tuning the coupling parameters such as the coupling phase, coupling strength, and delay time [37, 41]. To find appropriate values of these control parameters, the speed-gradient method from control theory can be applied to achieve a desired state of generalized synchrony (*adaptive synchronization*) [48].

We consider two generic types of local dynamics of the nodes, namely type-I excitable dynamics (near a saddle-node bifurcation on an invariant cycle, or *saddle-node infinite period* (SNIPER) bifurcation), and type-II excitable dynamics (near a Hopf bifurcation, described, e.g., by the FitzHugh-Nagumo model). Transitions between synchronization and desynchronization can be induced by introducing inhibitory links into a regular excitatory network with a probability p, and by changing the balance between excitatory and inhibitory links [42, 43]. The type of network we primarily focus on in our investigations is the small-world (SW) network [49], which has a short average path distance between nodes, as

well as a large degree of clustering (in other words, many triangles in the network structure). These properties are found in many kinds of real-world structures, such as the collaboration between film actors, power grids, the World Wide Web and social relationships [49, 50, 3, 4]. In particular, large-scale cortical networks also show these properties [51, 52]. The brain has an architecture enabling both efficient global and local communication between neurons [53], which is captured well by the SW model.

Inhibition plays an important role in the nervous system [54]. Here, when constructing a network we begin with a regular ring network of excitatory links and, as in Ref. [42, 43], we add long-range inhibitory links into the network structure. This creates a SW network of the form proposed in Ref. [55].

In the following section, we introduce the model and the network topologies considered in the present study. In Sec. 3 we use the master stability function to investigate the stability of arbitrary synchronized networks with given coupling parameters (i.e. the coupling strength and the length of delay between coupled nodes). The MSF is calculated in Sec. 4 for networks coupled within a range of small delay time and coupling strength, which reveals the existence of synchronized states that have different stability conditions compared to coupling with larger delay times. The implications these results may have for specific complex networks are discussed in Sec. 5.

2 Models

In order to model excitability, the system must have a rest state, which corresponds to a stable fixed point. Small perturbations from the rest state can lead to a large excursion in the phase space, i.e., the emission of a spike (excited state), before returning to the rest state. In the context of neurodynamics, this is the firing state of the neuron [56].

Neurons can exhibit different excitability properties, depending upon the bifurcation scenario from the excitable to the oscillatory regime. In 1948, Hodgkin classified two types of neural excitability [57]:

Type-I neurons can generate action potentials of arbitrarily low frequency. This kind of behavior occurs near a saddle-node infinite period (SNIPER) bifurcation, also known as the SNIC bifurcation (saddle-node bifurcation on invariant cycle). The arbitrarily low frequency coincides with the period of the limit cycle going to infinity as the bifurcation parameter approaches a critical value, where the bifurcation occurs.

Type-II neurons are associated with a supercritical Hopf bifurcation. The frequencies of the action potentials remain within a certain non-zero range, while the amplitude of the limit cycle approaches zero with the bifurcation parameter.

As our model for type-I excitability we consider a generic normal form of a SNIPER bifurcation:

$$\mathbf{f}(\mathbf{x}) = \begin{pmatrix} \dot{x} \\ \dot{y} \end{pmatrix} = \begin{pmatrix} x(1-x^2-y^2)+y(x-b) \\ y(1-x^2-y^2)-x(x-b) \end{pmatrix}, \tag{1}$$

which reads in polar coordinates ($x = r\cos\varphi, y = r\sin\varphi$):

$$\dot{r} = r\left(1 - r^2\right) \tag{2}$$

$$\dot{\varphi} = b - r\cos\varphi. \tag{3}$$

$b > 0$ is the bifurcation parameter that influences the type of dynamics and determines where in the (x, y)-plane the fixed points are located, as discussed below. This model was used by Haken and coworkers [58, 59] for the first demonstration of coherence resonance [60], which occurs in excitable nonlinear systems if noise is added; it denotes the counterintuitive effect that the coherence of noise-induced oscillations is optimal for a certain finite noise intensity. Combining this effect with time-delayed feedback, the coherence resonance can be conveniently controlled [61, 62].

Here we focus on the deterministic dynamics of excitable elements (neurons) coupled with time delay τ in a network. We consider the dynamics of a network of N elements (labelled $i = 1, ..., N$) given by:

$$\dot{\mathbf{x}}_i = \mathbf{f}(\mathbf{x}_i) + \sigma \sum_{j=1}^{N} G_{ij}\mathbf{H}(\mathbf{x}_j(t-\tau) - \mathbf{x}_i(t)), \tag{4}$$

where $\mathbf{f}(\mathbf{x}_i)$ is the local dynamics as described by Eq. (1) for each element $\mathbf{x}_i = (x_i, y_i)$. G_{ij} determines the matrix $\mathbf{G}$ for the network structure, showing which elements are coupling together, and $\mathbf{H}$ is the coupling function. $\mathbf{H}$ is taken to be the 2×2 identity matrix; this means that the x-variable at time t is coupled with the x-variable at time $t - \tau$, the y-variable at time t is coupled with the y-variable at time $t - \tau$, but there is no cross-coupling between the x- and y-variable. The coupling parameters, which are identical for all connections, are the coupling strength σ and delay time τ.

For synchronous dynamics, the $2(N-1)$ constraints $\mathbf{x}_s \equiv \mathbf{x}_1 = \mathbf{x}_2 = \cdots = \mathbf{x}_N$ define a 2-dimensional synchronization manifold (SM) within the $2N$-dimensional phase space and the coupled system is reduced to an effective single system with feedback:

$$\dot{\mathbf{x}}_s = \mathbf{f}(\mathbf{x}_s) + \sigma\mathbf{H}(\mathbf{x}_s(t-\tau) - \mathbf{x}_s(t)), \tag{5}$$

with unity row sum $\sum_j G_{ij} = 1$, so that the nodes all receive the same level of input while they are synchronized. Any non-unity but constant row sum can be rescaled using the coupling strength σ.

Without delay, while the bifurcation parameter $b < 1$, there exists an unstable focus at the origin, as well as a saddle point and a stable node situated on the unit circle at $(x_i, y_i) = (b, \sqrt{1-b^2})$ and $(b, -\sqrt{1-b^2})$, respectively. At $b = 1$ the saddle point and stable node collide, so that for $b > 1$ a limit cycle exists along the unit circle. In the case of $b < 1$ (excitable regime), a perturbation which pushes the system from the stable node beyond the saddle point can result in a single oscillation along the unit circle. Delayed coupling can induce a homoclinic bifurcation, such that a limit cycle is produced that bypasses the

saddle point and stable node [61, 62]. Here, we will consider the excitable regime with $b = 0.95$ and investigate for which topologies the synchronized dynamics of complex networks is stable.

Next, as a paradigmatic model for type-II excitability we consider the Fitz-Hugh-Nagumo (FHN) model [63, 64], which exhibits a supercritical Hopf bifurcation:

$$\mathbf{f}(\mathbf{x}) = \begin{pmatrix} \epsilon\dot{x} \\ \dot{y} \end{pmatrix} = \begin{pmatrix} x_i - \frac{x_i^3}{3} - y_i \\ x_i + a \end{pmatrix}, \tag{6}$$

where x and y denote the activator and inhibitor variables, respectively. The parameter a determines the threshold of excitability. A single FHN oscillator is excitable for $a > 1$ and exhibits self-sustained periodic firing beyond the Hopf bifurcation at $a = 1$. Here, we will focus on the excitable regime with $a = 1.3$. The time-scale parameter ϵ is chosen as $\epsilon = 0.01$. The coupling function $\mathbf{H}$ is chosen with components $H_{11} = 1/\epsilon$ and zero otherwise.

In this chapter, complex small-world (SW) networks are considered, which we construct as a variation to the method proposed in Ref. [49], introduced in Refs. [55, 65]: (i) Each of the N nodes in a one-dimensional ring is given excitatory links to its k nearest neighbors on each side. Note that in terms of the matrix $\mathbf{G}$, an excitatory link between the i^{th} and j^{th} node means that $G_{ij} > 0$, while for an inhibitory link $G_{ij} < 0$. (ii) For each of the kN links we add with a probability of p another inhibitory link with strength -1 between two randomly chosen nodes (i.e. on average pkN randomly distributed inhibitory links). (iii) Self-coupling and multiple links between the same two nodes are not allowed. (iv) Finally, the entries in each row of $\mathbf{G}$ are normalized to ensure a unity row sum. If a row sum is equal to zero, then the network realization is discarded.

In the following, we determine the stability of the synchronized dynamics and compare the synchronization/desynchronization transitions for different local dynamics.

3 Stability of Synchronization

In the master stability approach [35], the stability of a synchronized state is determined by splitting the stability problem into a topological part, which is determined by the eigenvalues of the coupling matrix $\mathbf{G}$, and a dynamical part, which is given for an arbitrary network by the master stability equation

$$\delta\dot{\mathbf{x}}(t) = [D\mathbf{f}(\mathbf{x}_s) - \sigma\mathbf{H}]\delta\mathbf{x}(t) + (\alpha + i\beta)\mathbf{H}\delta\mathbf{x}(t - \tau), \tag{7}$$

which is found by linearizing Eq. (4) around Eq. (5) and is used to calculate the largest Lyapunov exponent $\Lambda(\alpha, \beta, \sigma, \tau)$, called the master stability function (MSF). Here $\delta\mathbf{x}$ is the perturbation of $\mathbf{x}$ away from the SM (i.e. $\mathbf{x} = \mathbf{x}_s + \delta\mathbf{x}$) and $D\mathbf{f}(\mathbf{x}_s)$ is the Jacobian matrix of Eq. (1) evaluated on the SM. Important for this approach is that, whereas one can calculate Lyapunov exponents for a specific network topology using the eigenvalues of the matrix $\mathbf{G}$, one considers here a continuous complex parameter $\alpha + i\beta$ representing the complex plane of

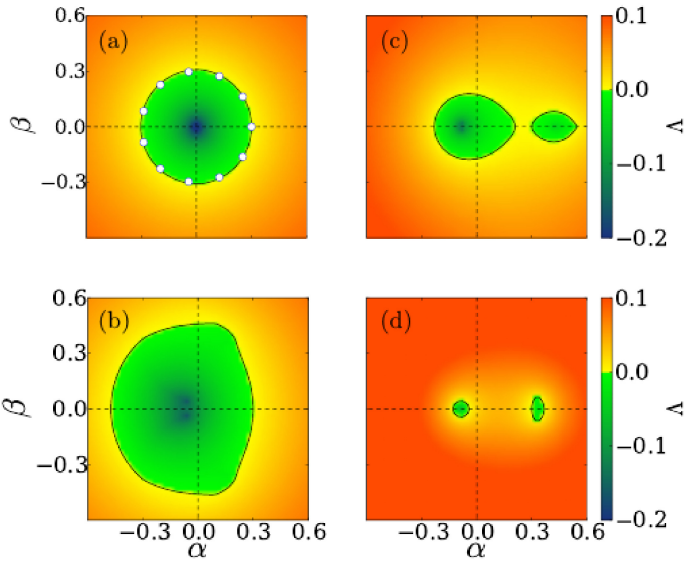

Fig. 1. MSF Λ for the SNIPER model (type-I excitability) for coupling parameters $\sigma = 0.3$ and (a) $\tau = 10$, (b) $\tau = 7$, (c) $\tau = 6.5$, and (d) $\tau = 6$. α and β are the real and imaginary parts of the scaled eigenvalues of the coupling matrix, $\sigma\nu_k$, respectively, and Λ is the largest Lyapunov exponent. White dots in panel (a) represent the scaled eigenvalues of a unidirectional ring of 11 nodes $(\sigma\nu_1, \ldots, \sigma\nu_{11})$. $b = 0.95$.

possible eigenvalues scaled by the coupling strength σ (i.e. $\alpha + i\beta$ is a continuous parametrization of $\sigma\nu_j$, where ν_j are the eigenvalues of $\mathbf{G}, j = 1, ..., N$). Thus, one can calculate the Lyapunov exponents for a region of the (α, β)-plane which gives sub-regions of stability, where $\Lambda < 0$, and instability, where $\Lambda > 0$. It is then easy to compare the synchronous stability of various networks by simply observing whether any of their eigenvalues fall inside an unstable region of the (α, β)-plane. If all the eigenvalues lie within stable regions, then perturbations away from the SM will decay exponentially.

Because of the unity row sum condition, $\mathbf{G}$ always has an eigenvalue $\nu_1 = 1$. This longitudinal eigenvalue (all others are called transversal) corresponds to perturbations within the SM and $\Lambda(\sigma\nu_1, 0, \sigma, \tau)$ is always zero because we are looking at periodic dynamics. As such, it is only the transversal eigenvalues that are important for determining the stability of synchronization.

Figure 1(a) shows the MSF of the SNIPER model (type-I excitability) with coupling parameters $\sigma = 0.3$ and $\tau = 10$. The white dots represent the eigenvalues of the matrix $\mathbf{G}$ for a unidirectional ring of 11 nodes. All eigenvalues are within the stable region of the MSF, thus the synchronization of all 11 nodes coupled with these parameters is stable.

According to Ref. [39], for τ in the order of the system's characteristic time scale (in this case, the period of the oscillations) and above, the MSF will always tend towards a rotational symmetry. Examples such as the one above in Fig. 1(a) confirm these general findings for the SNIPER model. When calculating MSFs for a large fixed τ while varying σ it becomes evident that the size of the stable region is scaled by σ, so that the stable region can be estimated very well by the circle $S((0,0),\sigma)$ (that is, a circle centered at the origin with a radius σ). Changes in large values of τ, however, despite influencing the Lyapunov exponents quantitatively, do not affect the shape of the stable region.

This rotational symmetry of the MSF was also found for type-II neurons, modelled as FitzHugh-Nagumo oscillators by Eq.(6) [42], see Fig. 2. In this case σ and τ do not affect whether the eigenvalues fit into the stable region of the MSF, so that only the topology of a network is important for the stability of its synchronization. Furthermore, because Gershgorin's circle theorem [66] guarantees that the eigenvalues of a network's coupling matrix with no self-coupling and purely excitatory coupling (i.e. $G_{ii} = 0$ and $G_{ij} \geq 0, 1 \leq i, j \leq N$) lie within the unit circle on the complex plane, the synchronization of such a network will always be stable. Finally, if additional inhibitory links are introduced with probability p to construct a SW network as described in Sec. 2, phase transitions from stable to unstable synchronization are found with increasing probability of inhibition p [42]. It should be noted from a comparison of Figs. 1 and 2 that all these results apply for the SNIPER neurons only with sufficiently large τ.

As an example, Fig. 3 shows two realizations of the SW coupling scheme with $N = 20$, $k = 2$, and $p = 0.05$ (panels (a) and (b)) and the corresponding eigenvalues of the coupling matrix depicted in the plot of the MSF in the complex (α, β)-plane (panels (c) and (d)). It can be seen that in panel (c) all eigenvalues lie in the stability domain, and hence synchronization is stable, whereas in panel (d) one eigenvalue lies outside the stability domain, leading to desynchronization. A statistical analysis for a large number of realizations can predict transitions from stable synchronization to desynchronization, as will be discussed in detail in Sec. 5 below.

4 Small delay times

If the delay time is not large enough, type-I excitability (SNIPER model) displays a distinctly different behavior than type-II excitability (FHN model): the rotational symmetry of the MSF no longer holds. In fact, while reducing τ one can witness how the rotational symmetry begins to break down. This is depicted in Fig. 1. For a constant coupling strength of $\sigma = 0.3$, the MSFs are numerically calculated for decreasing delay times. While at $\tau = 10$ the MSF still has its circular form (Fig. 1(a)), when decreasing τ, the stable (i.e. dark blue/green) region of the MSF begins to show signs of deformation. By $\tau = 7$ (see Fig. 1(b)) the stable region is clearly larger than the unit circle scaled by $\sigma = 0.3$ and has definitely lost its rotational symmetry. By $\tau = 6.5$ (see Fig. 1(c)) the stable region has already split into two disconnected regions. Letting τ decrease further,

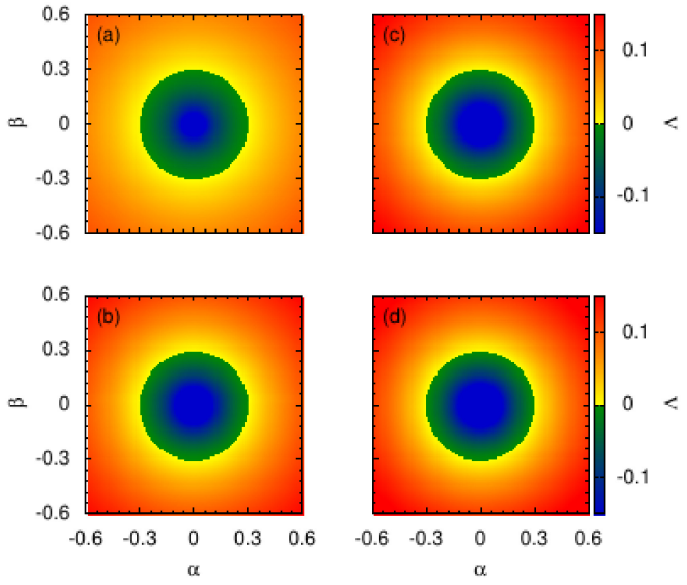

Fig. 2. Same as in Fig. 1 for the FitzHugh-Nagumo model (type-II excitability, $a = 1.3$, $\epsilon = 0.01$) for coupling parameters $\sigma = 0.3$ and (a) $\tau = 10$, (b) $\tau = 7$, (c) $\tau = 6.5$, and (d) $\tau = 6$.

the stable regions become increasingly smaller (see Fig. 1(d)). Note that the delay-induced limit cycle coexists alongside the stable fixed point and whether it is reached or not is therefore dependent on initial conditions. For τ less than about 4 (not shown here), the coupling is no longer able to induce the homoclinic bifurcation that creates the limit cycle at all (as discussed in Sec. 2), in other words, the neurons no longer oscillate. Instead, all solutions approach the stable fixed point.

It is now obvious that, in this regime of small delay, small changes in τ can have a great impact on the stability. The seemingly sudden change in the MSFs in Fig. 1 between $\tau = 7$ and $\tau = 6.5$ can be traced back to a qualitative change at a critical value τ_c, which will be discussed below. Except for this value, the boundary of stability evolves continuously with τ. This becomes clear by plotting the MSF versus the real part α of the eigenvalue (with $\beta = 0$) for varying τ. Taking this one slice of the eigenvalue plane gives a good indication of the growth and decay of the stable region in the MSF while changing τ. Figure 4 shows the MSF as a function of the real part α ($\beta = 0$) and the delay time τ, with fixed coupling strength 0.3. This produces a MSF on an (α, τ)-plane, which can be used for network topologies with a coupling matrix that yields real eigenvalues,

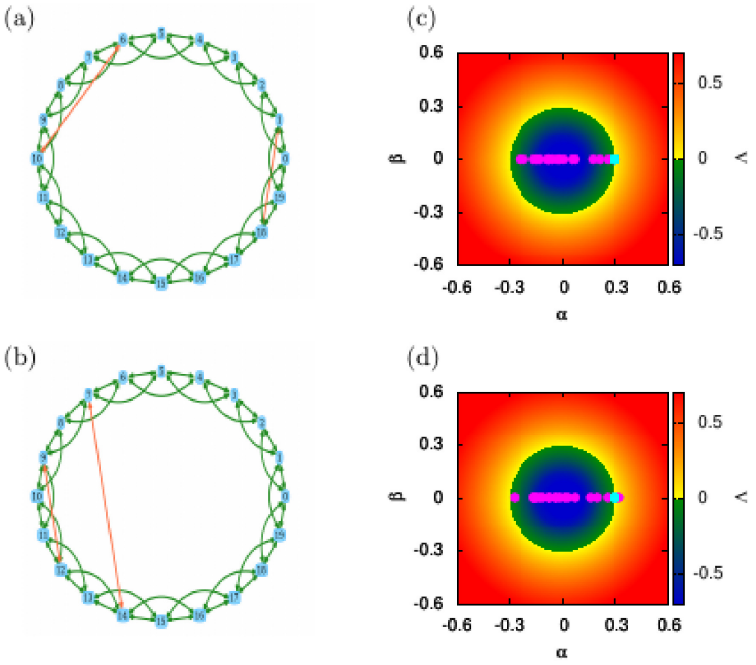

Fig. 3. Synchronization and desynchronization in a small-world network ($\sigma = 0.3$, $\tau = 1$): (a) and (b) are two different realizations with $N = 20$, $k = 2$, and $p = 0.005$. (c),(d): Master stability function Λ of the FitzHugh-Nagumo system ($a = 1.3$, $\epsilon = 0.01$). Dark gray (pink) circles in (c) and (d) mark transversal eigenvalues of the networks shown in panels (a) and (b), respectively; light gray (turquoise) circle: longitudinal eigenvalue.

e.g., symmetric matrices for undirected networks. In the following we restrict ourselves to undirected networks.

The stability depends on both σ and τ. In Fig. 4 the vertical boundary line at $\alpha = \sigma$, corresponding to the longitudinal eigenvalue (i.e. $\nu_1 = 1$, where $\Lambda = 0$), can be easily identified. It separates regimes of stable and unstable synchronization. Another characteristic is that the τ-dependent MSF has a critical delay time τ_c at which the stable region splits into two separate, disconnected regions. For values above τ_c the stable region is found to the left of the longitudinal eigenvalue; whereas for values below τ_c there may be one stable region to the right of the longitudinal eigenvalue and one to the left. τ_c seems to be an important value, because it marks the most significant τ-dependent qualitative change in the MSF. Ultimately, the MSF can be divided into three regimes of τ: (i) two or more smaller separate regions of stability exist when $\tau < \tau_c$; (ii) one large region of stability exists when $\tau > \tau_c$; (iii) the MSF has one rotationally sym-

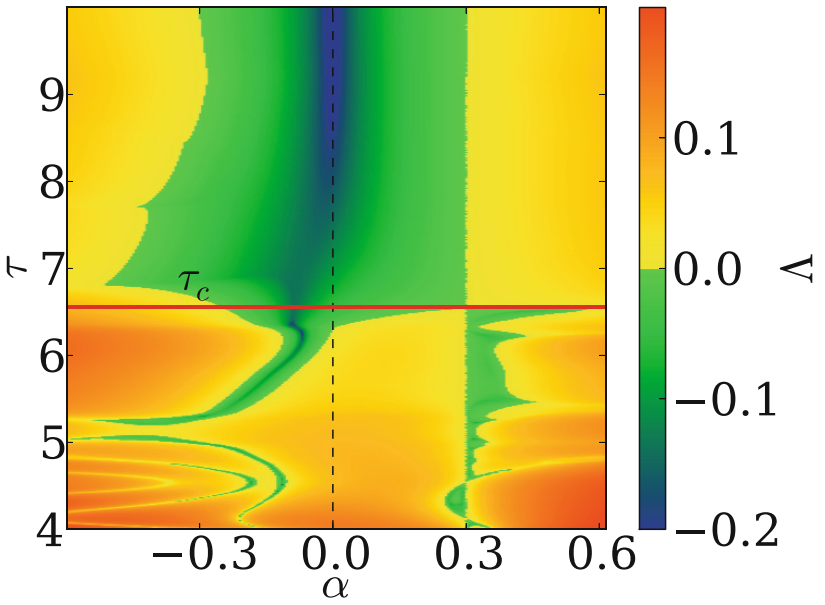

Fig. 4. MSF Λ of the SNIPER model ($b = 0.95$) for a fixed coupling strength $\sigma = 0.3$ in the plane of the real part α ($\beta = 0$) and the delay time τ. The horizontal red line shows the position of the critical delay time τ_c.

metric region of stability in the limit of $\tau \to \infty$ (which holds already in good approximation if τ is of the order of the intrinsic oscillation period or larger).

5 Multiple synchronization and desynchronization transitions

An obvious observation is that networks with purely excitatory coupling, which are always stable for large delay times as mentioned at the end of Sec. 3, may not show stable synchronization for $\tau < \tau_c$. It was explained in Sec. 3 that increasing the probability p of inhibitory links in the network can be a factor leading to unstable synchronization. This occurs because a larger probability of inhibition can push a part of the eigenvalue spectrum of any network beyond the longitudinal eigenvalue at $\alpha = \sigma$ (because Gershgorin's circle theorem no longer guarantees that all eigenvalues stay within the unit circle) and into the unstable region of the MSF. Now, in case of excitability of type-I for smaller τ, there may be a pocket of stability to the right of the longitudinal eigenvalue, so that increasing inhibition can make the otherwise unstable synchronization of a network stable.

This means that the transitions between stable and unstable synchronization as a function of the probability of inhibition p discussed in Ref. [42] are no

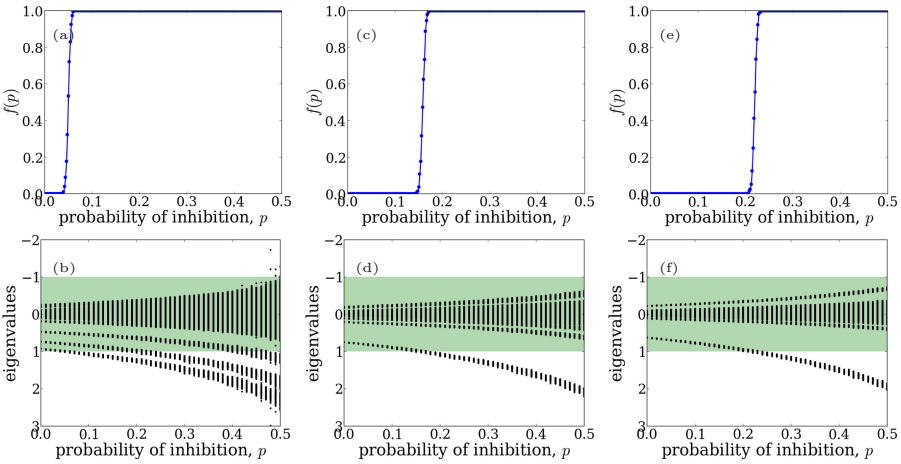

Fig. 5. Fraction of desynchronized networks f in dependence of the probability of additional inhibitory links p for 500 realizations of networks of $N = 200$ with (a) $k = 20$, (c) $k = 40$, and (e) $k = 50$. Corresponding eigenvalue spectra for (b) $k = 20$, (d) $k = 40$, and (f) $k = 50$ with 100 realizations for each p value. Here the green shaded regions represent the stable regions of the real part of the MSF typical for the SNIPER model for large delay and for the FitzHugh-Nagumo system for both small and large delay.

longer valid when τ is small in case of type-I excitability. The transitions are now sensitive to the coupling parameters, not just the network parameters N and k. Due to the multiple regions of stability, eigenvalues may wander in and out of stable regions, while increasing the probability of inhibition p. For large τ, or for any τ in case of type-II excitability, increasing p in the SW network model only results in one transition where the fraction of desynchronizing networks (i.e. networks with unstable synchronization) $f(p)$ switches from 0 to 1 (cf. Fig. 5).

For small τ, in case of excitability of type-I it is possible that $f(p)$ jumps back to 0, before increasing again to 1. This will occur if there is a separate region of stability to the right side in the MSF that is large enough that all the eigenvalues lying over there can fit inside.

The observation of multiple transitions between stable and unstable synchronization can be explained by looking at the eigenvalue spectra for SW networks for various p values. As discussed above in relation to the MSF method, each network topology has a coupling matrix $\mathbf{G}$, the eigenvalues from which can be used to determine the stability of the network's synchronized state. Because the "short-cuts" in the SW network are randomly introduced, each network with specific N, k and p values may have many realizations. By calculating the eigenvalues for a large number of realizations of the SW network with certain parameters (i.e. given N, k and p), one can find the bounds for the eigenvalue spectra.

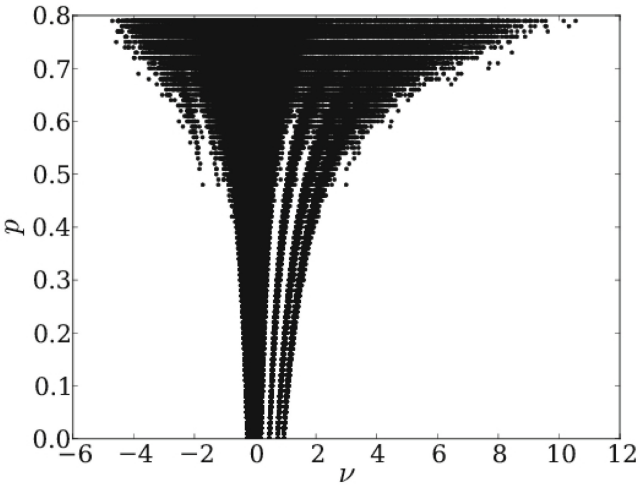

Fig. 6. Spectra of eigenvalues ν of undirected small-world networks with $N = 200$ and $k = 20$ and varying probability p of inhibitory links. 500 realizations of the eigenvalue spectrum are plotted for each value of p.

Figure 6 displays the superimposed eigenvalue spectra of 500 realizations for SW networks with parameters $N = 200$ and $k = 20$ (regular ring with excitatory coupling of k nearest neighbors on either side) in dependence on the probability of inhibition p. The longitudinal eigenvalues located at $\nu_1 = 1$ have been removed. One can see that the bounds for possible eigenvalues shift depending on the value of p. One can also see how the spectra begin to increasingly resemble the semicircular distribution [3] of a random network for larger p values, where the networks have lost their SW properties. The change of the eigenvalue spectrum with increasing p has been discussed in detail elsewhere [43].

The eigenvalue spectra bridge the gap between observations of the MSF (i.e. the dependence of the stability of synchronization on the eigenvalues) and what is seen in these transitions (i.e. the dependence of stability on the network topology). Increasing p allows isolated eigenvalues to increase in value and, in terms of the MSF, shift their locations further to the right in the (α, β)-plane. This is visualized in Fig. 7. Figures 7(b), (d) and (f) show the eigenvalue spectra for SW networks with $N = 200$ elements and $k = 20$, 40, and 50, respectively.

Figures 7(a), (c) and (e) show the corresponding fraction of desynchronized networks f in dependence on the probability of additional inhibitory links p. Consider, for instance, SW networks with parameters $N = 200$ and $k = 40$. In Fig. 7(c) $f(p)$ is shown for the exemplary coupling parameters $\sigma = 0.3$ and $\tau = 6.5$ with a corresponding plot of eigenvalues in Fig. 7(d). Note that the grey (green) shaded regions represent the stable regions of the line $\beta = 0$ on the (α, β)-plane of the MSF for $\sigma = 0.3$ and $\tau = 6.5$ (cf. Fig. 1(c)). For coupling parameters

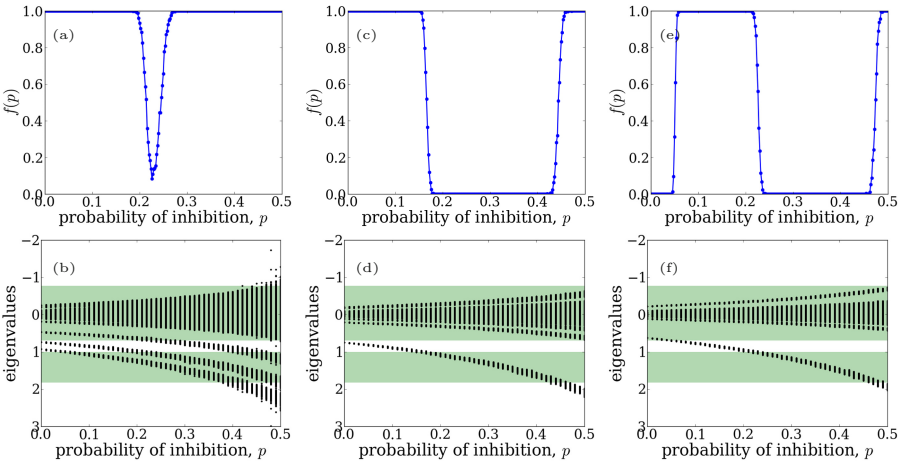

Fig. 7. Fraction of desynchronized networks f in dependence of the probability of additional inhibitory links p for 500 realizations of networks of $N = 200$ with (a) $k = 20$, (c) $k = 40$, and (e) $k = 50$ with $\sigma = 0.3$ and $\tau = 6.5$. Corresponding eigenvalue spectra for (b) $k = 20$, (d) $k = 40$, and (f) $k = 50$ with 100 realizations for each p value. Here the green shaded regions represent the stable regions of the real part of the MSF of the SNIPER model ($b = 0.95$).

where this region of stability is not large enough, f may briefly dip below 1 without decreasing to 0, because only some realizations may have eigenvalues that fit inside the stable region. In Fig. 7(a) where $k = 20$, f dips down to 0.14, because at most 14% of the realizations show stable synchronization (i.e. all the eigenvalues are inside the stable region). If the distance between the larger isolated eigenvalues matches the distance between stable regions (which is almost the case in Fig. 7(b)), then the transition curve only just touches the $f = 0$ axis at some value of p before increasing back to $f = 1$. Figure 7(e) is an example where a further transition is possible, because not only do all eigenvalues begin in stable regions at $p = 0$, but there is another regime of p where all eigenvalues fit inside stable regions. Note that further types of transitions can also occur for other network and coupling parameters.

The length of the transition from $f = 0$ to $f = 1$ is actually a measure of the variance of the isolated eigenvalues for an ensemble of realizations. For example, the variance of the isolated eigenvalues decreases as N is increased, so that the length of transition will be shorter in larger networks, and the transition becomes sharper.

When constructing a histogram of the eigenspectra for a particular value of p, the larger isolated eigenvalues seen to the right, e.g., in Fig. 7(b), result in small peaks of eigenvalues. See Fig. 8(a) for 1000 realizations of $p = 0.2$. For each realization of many SW networks there are isolated eigenvalues that are larger than most other eigenvalues in the spectrum. The small peaks of eigenvalues result from perturbations in isolated eigenvalues. For comparison, Fig. 8(b) shows

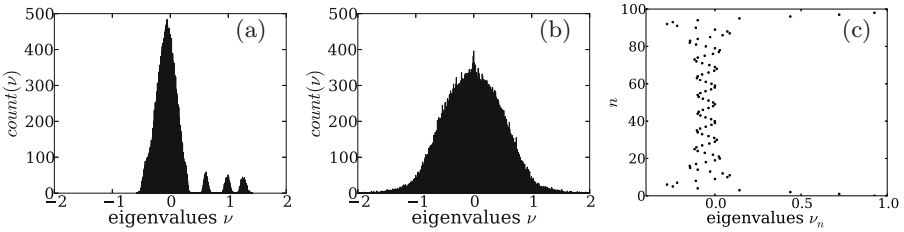

Fig. 8. (a), (b): Histograms (1000 bins) of eigenvalue spectra for 1000 realizations of (a) SW networks and (b) random networks with the same number of nodes, the same number of excitatory links and the same probability of inhibitory links ($N = 100$, $k = 10$, $p = 0.2$). (c): The eigenvalue spectrum for a regular network with $N = 100$ and $k = 10$. ν_n is the n^{th} eigenvalue, $n = 1, \ldots, N$.

the reference case of 1000 random networks with the same number of nodes and excitatory links and the same probability of inhibitory links as considered in Fig. 8(a).

The spectrum of a regular ring network, i.e., a SW network with $p = 0$, can be found analytically using the graph's symmetry operations [67] and is given by

$$\nu_l = \frac{1}{k}\sum_{j=1}^{k}\cos\left(2\pi j\frac{l}{N}\right) = \frac{1}{k}\left(\frac{\cos\left(k\pi\frac{l}{N}\right)\sin\left((k+1)\pi\frac{l}{N}\right)}{\sin\left(\pi\frac{l}{N}\right)} - 1\right), \qquad (8)$$

where $l = 1, ..., N-1$. Figure 8(c) shows this eigenspectrum for the $p = 0$ case. As p is increased these eigenvalues will be slightly perturbed (in a random manner) by the changing network structure, of which many realizations are possible. The isolated eigenvalues to the right-hand side in Fig. 8(c) eventually evolve into the smaller side peaks of eigenvalues in histograms for larger p as depicted in Fig. 8(a) for $p = 0.2$. These peaks show the distribution of the eigenvalue under the influence of the random nature of the SW "short-cuts" creation process – which is why the smaller eigenvalue peaks can be approximated by a normal distribution. To be precise, because the multiplicity of the above mentioned isolated eigenvalues at $p = 0$ is 2, the smaller eigenvalue peaks are two normal distributions that, at least for small p values, overlap each other to a large extent. This is furthermore the reason why the desynchronization transitions observed in Ref. [42] and Figs. 7(a), (c), and (e) look like the cumulative (integrated) distribution function. They reflect how an increase of p brings the area of the small eigenvalue peak accumulatively into the unstable region of the MSF.

To explain why the peaks wander with increasing p, consider not normalizing the rows of matrix $\mathbf{G}$, so that the row sums are not necessarily equal to 1. Then the location of the longitudinal eigenvalue decreases with p, because it is equal to the average row sum of $\mathbf{G}$ given by $2k(1-p)$. The locations of the other peaks increase slightly to maintain the eigenvalue sum of zero; a result of the trace of $\mathbf{G}$ being zero, since there is no self-feedback coupling. For large N this has only

a small effect. Thus, scaling the eigenvalues so that the longitudinal eigenvalue is always at 1 means that the transversal eigenvalues are multiplied by $\frac{1}{2k(1-p)}$. Accordingly they appear to increase with p, as seen in Figs. 7(b), (d) and (f).

6 Conclusion

We have investigated transitions between synchronization and desynchronization in complex networks of delay-coupled excitable elements of type I and type II, induced by varying the balance between excitatory and inhibitory couplings in a small-world topology. In our analysis we have used the master stability function approach. For large delay times it seems that both type-I neurons and type-II neurons must fulfill similar topological conditions in the network to allow for a stable synchronized state. This is different when considering small delay times. In case of the SNIPER model (type-I excitability), for a range of small coupling strengths and small delay times we have found novel multiple transitions between synchronization and desynchronization, when the fraction of inhibitory links is increased. This is different for the FitzHugh-Nagumo model (type-II excitability), where only a single transition from synchronization to desynchronization occurs for all values of the delay time. This can be explained by the different nature of the stability domains of the master stability function which consists of disconnected stability islands in case of type-I excitability for small τ. A small world model for complex networks with regular excitatory couplings and random inhibitory shortcuts has eigenvalue spectra with gaps between the larger eigenvalues, so that histograms of many realizations reveal isolated peaks of possible eigenvalues. Synchronization occurs whenever the domains of the eigenvalues fall onto the stability islands. It was shown that, because of this, small world networks can go through multiple transitions of synchronization and desynchronization in dependence on the probability of inhibitory short-cuts for the model of type-I excitability. Note that the same has also been shown for the Stuart-Landau model in Ref. [43], demonstrating that multiple transitions can also appear in networks of oscillatory nodes and are not limited to excitable systems.

Acknowledgments. This work was supported by the DFG in the framework of the SFB 910. PH acknowledges support by the BMBF (grant no. 01GQ1001B).

References

1. Schöll, E., Schuster, H.G. (eds.): Handbook of Chaos Control. Wiley-VCH, Weinheim (2008), second completely revised and enlarged edition
2. Pikovsky, A.S., Rosenblum, M.G., Kurths, J.: Synchronization. A Universal Concept in Nonlinear Sciences. Cambridge University Press, Cambridge (2001)
3. Albert, R., Barabási, A.-L.: Statistical mechanics of complex networks. Rev. Mod. Phys. **74**, 47 (2002)

4. Newman, M.E.J.: The structure and function of complex networks. SIAM Review **45**, 167 (2003)
5. Boccaletti, S., Latora, V., Moreno, Y., Chavez, M., Hwang, D.U.: Complex networks: Structure and dynamics. Physics Reports **424**, 175 (2006)
6. Cuomo, K.M., Oppenheim, A.V.: Circuit implementation of synchronized chaos with applications to communications. Phys. Rev. Lett. **71**, 65 (1993)
7. Boccaletti, S., Kurths, J., Osipov, G., Valladares, D.L., Zhou, C.S.: The synchronization of chaotic systems. Phys. Rep. **366**, 1 (2002)
8. Kanter, I., Kopelowitz, E., Kinzel, W.: Public channel cryptography: chaos synchronization and Hilbert's tenth problem. Phys. Rev. Lett. **101**, 84102 (2008)
9. Haken, H.: Brain Dynamics: Synchronization and Activity Patterns in Pulse-Coupled Neural Nets with Delays and Noise. Springer, Berlin (2007)
10. Singer, W.: Neuronal Synchrony: A Versatile Code Review for the Definition of Relations? Neuron **24**, 49 (1999)
11. Engel, A., Fries, P., Singer, W.: Dynamic predictions: Oscillations and synchrony in top-down processing. Nature Reviews Neuroscience **2**, 704 (2001)
12. Melloni, L., Molina, C., Pena, M., Torres, D., Singer, W., Rodriguez, E.: Synchronization of neural activity across cortical areas correlates with conscious perception. J. Neurosci. **27**, 2858 (2007)
13. Traub, R.D., Wong, R.K.: Cellular mechanism of neuronal synchronization in epilepsy. Science **216**, 745 (1982)
14. Tass, P.A., Rosenblum, M.G., Weule, J., Kurths, J., Pikovsky, A.S., Volkmann, J., Schnitzler, A., Freund, H.J.: Detection of n:m phase locking from noisy data: Application to magnetoencephalography. Phys. Rev. Lett. **81**, 3291 (1998)
15. Wünsche, H.J., Bauer, S., Kreissl, J., Ushakov, O., Korneyev, N., Henneberger, F., Wille, E., Erzgräber, H., Peil, M., Elsäßer, W., Fischer, I.: Synchronization of delay-coupled oscillators: A study of semiconductor lasers. Phys. Rev. Lett. **94**, 163901 (2005)
16. Carr, T.W., Schwartz, I.B., Kim, M.Y., Roy, R.: Delayed-mutual coupling dynamics of lasers: scaling laws and resonances. SIAM J. Appl. Dyn. Syst. **5**, 699 (2006)
17. Erzgräber, H., Krauskopf, B., Lenstra, D.: Compound laser modes of mutually delay-coupled lasers. SIAM J. Appl. Dyn. Syst. **5**, 30 (2006)
18. Fischer, I., Vicente, R., Buldú, J.M., Peil, M., Mirasso, C.R., Torrent, M.C., García-Ojalvo, J.: Zero-lag long-range synchronization via dynamical relaying. Phys. Rev. Lett. **97**, 123902 (2006)
19. D'Huys, O., Vicente, R., Erneux, T., Danckaert, J., Fischer, I.: Synchronization properties of network motifs: Influence of coupling delay and symmetry. Chaos **18**, 037116 (2008)
20. Timme, M., Wolf, F., Geisel, T.: Coexistence of regular and irregular dynamics in complex networks of pulse-coupled oscillators. Phys. Rev. Lett. **89**, 258701 (2002)
21. Rossoni, E., Chen, Y., Ding, M., Feng, J.: Stability of synchronous oscillations in a system of Hodgkin-Huxley neurons with delayed diffusive and pulsed coupling. Phys. Rev. E **71**, 061904 (2005)
22. Masoller, C., Torrent, M.C., García-Ojalvo, J.: Interplay of subthreshold activity, time-delayed feedback, and noise on neuronal firing patterns. Phys. Rev. E **78**, 041907 (2008)
23. Englert, A., Heiligenthal, S., Kinzel, W., Kanter, I.: Synchronization of chaotic networks with time-delayed couplings: An analytic study. Phys. Rev. E **83**, 046222 (2011)

24. Takamatsu, A., Tanaka, R., Yamada, H., Nakagaki, T., Fujii, T., Endo, I.: Spatiotemporal symmetry in rings of coupled biological oscillators of physarum plasmodial slime mold. Phys. Rev. Lett. **87**, 078102 (2001)
25. Tiana, G., Jensen, M.H.: The dynamics of genetic control in the cell: the good and bad of being late. Phil. Trans. R. Soc. (2013) (in print)
26. Haken, H.: Effect of delay on phase locking in a pulse coupled neural network. Eur. Phys. J. B **18**, 545 (2000)
27. Kuramoto, Y., Battogtokh, D.: Coexistence of Coherence and Incoherence in Nonlocally Coupled Phase Oscillators. Nonlin. Phen. in Complex Sys. **5**, 380 (2002)
28. Abrams, D.M., Strogatz, S.H.: Chimera states for coupled oscillators. Phys. Rev. Lett. **93**, 174102 (2004)
29. Martens, E.A., Laing, C.R., Strogatz, S.H.: Solvable model of spiral wave chimeras. Phys. Rev. Lett. **104**, 044101 (2010)
30. Motter, A.E.: Nonlinear dynamics: Spontaneous synchrony breaking. Nature Physics **6**, 164 (2010)
31. Omelchenko, I., Maistrenko, Y.L., Hövel, P., Schöll, E.: Loss of coherence in dynamical networks: spatial chaos and chimera states. Phys. Rev. Lett. **106**, 234102 (2011)
32. Omelchenko, I., Riemenschneider, B., Hövel, P., Maistrenko, Y.L., Schöll, E.: Transition from spatial coherence to incoherence in coupled chaotic systems. Phys. Rev. E **85**, 026212 (2012)
33. Hagerstrom, A., Murphy, T.E., Roy, R., Hövel, P., Omelchenko, I., Schöll, E.: Experimental observation of chimeras in coupled-map lattices. Nature Physics **8**, 658 (2012)
34. Tinsley, M.R., Nkomo, S., Showalter, K.: Chimera and phase cluster states in populations of coupled chemical oscillators. Nature Physics **8**, 662 (2012)
35. Pecora, L.M., Carroll, T.L.: Master stability functions for synchronized coupled systems. Phys. Rev. Lett. **80**, 2109 (1998)
36. Dhamala, M., Jirsa, V.K., Ding, M.: Enhancement of neural synchrony by time delay. Phys. Rev. Lett. **92**, 074104 (2004)
37. Choe, C.U., Dahms, T., Hövel, P., Schöll, E.: Controlling synchrony by delay coupling in networks: from in-phase to splay and cluster states. Phys. Rev. E **81**, 025205(R) (2010)
38. Kinzel, W., Englert, A., Reents, G., Zigzag, M., Kanter, I.: Synchronization of networks of chaotic units with time-delayed couplings. Phys. Rev. E **79**, 056207 (2009)
39. Flunkert, V., Yanchuk, S., Dahms, T., Schöll, E.: Synchronizing distant nodes: a universal classification of networks. Phys. Rev. Lett. **105**, 254101 (2010)
40. Heiligenthal, S., Dahms, T., Yanchuk, S., Jüngling, T., Flunkert, V., Kanter, I., Schöll, E., Kinzel, W.: Strong and weak chaos in nonlinear networks with time-delayed couplings. Phys. Rev. Lett. **107**, 234102 (2011)
41. Dahms, T., Lehnert, J., Schöll, E.: Cluster and group synchronization in delay-coupled networks. Phys. Rev. E **86**, 016202 (2012)
42. Lehnert, J., Dahms, T., Hövel, P., Schöll, E.: Loss of synchronization in complex neural networks with delay. Europhys. Lett. **96**, 60013 (2011)
43. Keane, A., Dahms, T., Lehnert, J., Suryanarayana, S.A., Hövel, P., Schöll, E.: Synchronisation in networks of delay-coupled type-I excitable systems. Eur. Phys. J. B **85**, 407 (2012)
44. Vogels, T.P., Abbott, L.F.: Gating multiple signals through detailed balance of excitation and inhibition in spiking networks. Nature Neurosci. **12**, 483 (2009)

45. Vogels, T.P., Sprekeler, H., Zenke, F., Clopath, C., Gerstner, W.: Inhibitory plasticity balances excitation and inhibition in sensory pathways and memory networks. Science **334**, 1569 (2011)
46. Ernst, U., Pawelzik, K.: Sensible balance. Science **334**, 1507 (2011)
47. Hennequin, G., Vogels, T.P., Gerstner, W.: Non-normal amplification in random balanced neuronal networks. Phys. Rev. E **86**, 011909 (2012)
48. Selivanov, A.A., Lehnert, J., Dahms, T., Hövel, P., Fradkov, A.L., Schöll, E.: Adaptive synchronization in delay-coupled networks of Stuart-Landau oscillators. Phys. Rev. E **85**, 016201 (2012)
49. Watts, D.J., Strogatz, S.H.: Collective dynamics of 'small-world' networks. Nature **393**, 440 (1998)
50. Adamic, L.A.: The small world web, vol. 1696/1999. Lecture Notes in Computer Science. Springer Berlin, Heidelberg (1999)
51. Sporns, O., Tononi, G., Edelman, G.M.: Theoretical Neuroanatomy: Relating Anatomical and Functional Connectivity in Graphs and Cortical Connection Matrices. Cereb. Cortex **10**, 127 (2000)
52. Sporns, O.: Small-world connectivity, motif composition, and complexity of fractal neuronal connections. Biosystems **85**, 55 (2006)
53. Latora, V., Marchiori, M.: Efficient behavior of small-world networks. Phys. Rev. Lett. **87**, 198701 (2001)
54. Haider, B., Duque, A., Hasenstaub, A.R., McCormick, D.A.: Neocortical network activity in vivo is generated through a dynamic balance of excitation and inhibition. J. Neurosci. **26**, 4535 (2006)
55. Newman, M.E.J., Watts, D.J.: Renormalization group analysis of the small-world network model. Phys. Lett. A **263**, 341 (1999)
56. Izhikevich, E.M.: Neural excitability, spiking and bursting. Int. J. Bifurcation Chaos **10**, 1171 (2000)
57. Hodgkin, A.L.: The local electric changes associated with repetitive action in a medullated axon. J. Physiol. **107**, 165 (1948)
58. Hu, G., Ditzinger, T., Ning, C.Z., Haken, H.: Stochastic resonance without external periodic force. Phys. Rev. Lett. **71**, 807 (1993)
59. Ditzinger, T., Ning, C.Z., Hu, G.: Resonancelike responses of autonomous nonlinear systems to white noise. Phys. Rev. E **50**, 3508 (1994)
60. Pikovsky, A.S., Kurths, J.: Coherence resonance in a noise-driven excitable system. Phys. Rev. Lett. **78**, 775 (1997)
61. Hizanidis, J., Aust, R., Schöll, E.: Delay-induced multistability near a global bifurcation. Int. J. Bifur. Chaos **18**, 1759 (2008)
62. Aust, R., Hövel, P., Hizanidis, J., Schöll, E.: Delay control of coherence resonance in type-I excitable dynamics. Eur. Phys. J. ST **187**, 77 (2010)
63. FitzHugh, R.: Impulses and physiological states in theoretical models of nerve membrane. Biophys. J. **1**, 445 (1961)
64. Nagumo, J., Arimoto, S., Yoshizawa, S.: An active pulse transmission line simulating nerve axon. Proc. IRE **50**, 2061 (1962)
65. Monasson, R.: Diffusion, localization and dispersion relations on"small-world" lattices. Eur. Phys. J. B **12**, 555 (1999)
66. Gerschgorin, S.A.: Über die Abgrenzung der Eigenwerte einer Matrix. Izv. Akad. Nauk. SSSR **7**, 749 (1931)
67. Farkas, I., Derenyi, I., Barabási, A.-L., Vicsek, T.: Spectra of real-world graph: Beyond the semicircle law. Phys. Rev. E **64**, 026704 (2001)

Adiabatic Invariants and Some Statistical Properties of the Time Dependent Linear and Nonlinear Oscillators

Marko Robnik

CAMTP - Center for Applied Mathematics and Theoretical Physics,
University of Maribor, Krekova 2, SI-2000 Maribor, Slovenia, European Union
Robnik@uni-mb.si
http://www.camtp.uni-mb.si

Abstract. We consider 1D time dependent Hamilton systems and the time evolution of initial microcanonical distributions. In linear oscillator (LO) the distribution of energy is *always* arcsine distribution, and the adiabatic invariant at the average energy (AIAE)(and thus the entropy) always increases. In nonlinear (quartic) oscillator there are regimes of slow driving where the AIAE can decrease, but increases for faster driving. Near the adiabatic regime the distribution is similar to arcsine distribution; in general it depends on the dynamical details. We also consider parametrically kicked systems. We prove for all homogeneous power-law potentials that in a single parametric kick the AIAE always increases. The approximation of one kick is good for times up to one oscillation period. In LO only, due to isochronicity, an initial kick disperses the microcanonical distribution, but an antikick at the right phase can restore it. The periodic parametric kicking is also studied. [1]

Keywords: Time-dependent linear and nonlinear Hamiltonian oscillators, adiabatic invariants, statistical properties of the energy

1 Introduction

In recent years the general interest in time dependent (nonautonomous) dynamical systems has increased a lot [1]. In this paper we consider time dependent Hamilton systems, where many interesting questions about their statistical behaviour can be studied [2–5]. Whilst the energy of the system is not conserved, the Liouville theorem of course still applies and thus the phase space volume is preserved by the phase flow. Since the energy is changing in time, we would like to have theoretical methods to calculate it for each particular initial condition. But in the context of statistical mechanics we are interested also in the behaviour of an ensemble of orbits, specified by - and emanating from - an ensemble of initial conditions. One of the most natural and fundamental ensembles

[1] It is my great pleasure to dedicate this work to Professor Hermann Haken on occasion of his 85th birthday.

A. Pelster and G. Wunner (eds.), *Selforganization in Complex Systems: The Past, Present, and Future of Synergetics*, Understanding Complex Systems,
DOI: 10.1007/978-3-319-27635-9_4

is the microcanonical ensemble of initial conditions, where the initial energy is sharply defined (Dirac delta function), but the distribution on the energy surface is uniform. Such an ensemble is particularly natural in fully chaotic, ergodic, systems. In case of full integrability of the initial (frozen) Hamiltonian system one could also assume that the initial conditions are uniformly distributed on an invariant torus, meaning that the canonical angles are uniformly distributed on a torus, whilst the mixed type cases are more complex to define.

In this paper we shall treat time dependent Hamilton systems with only one degree of freedom (1D), which (as frozen systems) are ergodic and integrable at the same time, but still very rich in behaviour. The microcanonical ensemble of initial conditions in this case is defined by the uniform distribution of the initial canonical angle (of the frozen initial Hamilton system at the starting time) on the interval $[0, 2\pi)$, on the initial torus (contour of constant energy). Thus, from the problem of a single dynamical system we come to the ensemble of (noninteracting) systems, whose statistical properties we would like to understand, for each particular preparation of the initial conditions, in our case the microcanonical distribution. Such a procedure is valid in deriving the thermodynamic properties of the macroscopic number of such noninteracting oscillators. For example, in case of a point particle in a one dimensional box with moving wall, we can derive the equilibrium ideal gas equation if we consider the adiabatic changes of the box. Clearly, as particles in ideal gas are not interacting at all, one particle is enough to derive the equation of state, by appropriate averaging over the ensemble of particles and/or over time. For other oscillators a similar approach is possible in general adiabatic and nonadiabatic (fast) changes, including *the parametric kicks* (discontinuous jumps of the system parameter), where the system and its transformations can be described statistically although far from equilibrium.

As the system evolves, we observe spreading of the energy distribution, due to the different dependence of the energy on the initial angle for each particular orbit. We seek the energy distribution at the later times, also in the asymptotic limit (if it exists) when time goes to infinity. In case of the linear oscillator we have the remarkable theorem, namely the distribution is universal for all time dependences and rigorously given by the *arcsine distribution* [6], as derived by Robnik and Romanovski with coworkers [7–11], and reviewed in the next section. The average energy, the variance and all the higher moments of the distribution function can be calculated analytically in closed form. In general nonlinear systems the distribution of the energy can be just anything, depending on the details of the system and its dynamics, and the analytical approach is very difficult.

In general nonlinear parametrically driven systems the two most important quantities are of course the average energy and the variance of the energy distribution. We allow for entirely arbitrary time dependence of the Hamilton system, through a parameter depending on time. This dependence could be adiabatic (infinitely slow) in one extreme, or a parametric kick in another extreme, or anything in between, including also the important special case of periodic dependence. The properties of the energy distribution are closely linked to the

question of the adiabatic invariants. In case of ideal adiabatic variation of the Hamiltonian the energy is sharply defined at all times (a Dirac delta distribution), with zero variance, but of course energy is changing in time, however in such a way, that the area inside the energy contour is preserved, which is precisely the adiabatic invariant of the system. See e.g. [2] for one dimensional systems. For the linear oscillator the adiabatic invariant was derived by Einstein in 1911 [12]. For multidimensional ergodic systems it has been proven by Paul Hertz [13] in 1910 and commented by Einstein [14], that the phase space volume inside the energy surface is the conserved quantity, the adiabatic invariant, which of course includes the one dimensional case.

If the parametric driving law is not ideally adiabatic, but proceeds with a finite speed, the energy distribution function spreads. The average energy and the variance of the energy are relevant for the (non)preservation of the adiabatic invariant. It is interesting from the point of view of the statistical mechanics to ask, what is the value of the adiabatic invariant at the average energy of the system as time goes on. The spread of the distribution of the adiabatic invariant is related to the variance of the energy distribution. In the case of the linear oscillator we have the remarkable theorem by Robnik and Romanovski [7–11] that the adiabatic invariant at the average energy always increases, for *any variation* of the frequency, except for the ideal adiabatic process, where it is preserved. Thus in any nonadiabatic process, up to the other extreme of parametric kick, we always find the increase of the adiabatic invariant. This is a kind of *irreversibility statement*: the adiabatic invariant is the phase space area inside the energy contour, thus proportional to the number of states in the sense of statistical mechanics. The entropy of the system is just the logarithm of the adiabatic invariant. Thus the entropy of the general parametrically driven linear oscillator is on the average always increasing, except for the ideal adiabatic changes where it is exactly preserved, and the process is reversible. We shall present this rigorous statement in the next section, when reviewing the case of the linear oscillator [11]. The linear oscillator is relatively easy to study in the above context, because the linear phase flow is explicitly known, and can be written down as a 2x2 matrix. Also, the flow map of the linear oscillator for any time variation can be expressed by the WKB method to all orders [15, 7–9, 11], and even just the leading order approximation works very well in the adiabatic limit. A similar method, but only in the leading order, can be used for certain nonlinear oscillators [16].

In nonlinear oscillators [17] the analysis is incomparably more difficult, just because we do not know the global phase flow. Therefore some studies must be performed numerically, which is still very difficult for accurate and long time integrations, whilst some others (like parametric kicking) can be done analytically. It is very interesting to observe, as we shall see, that in nonlinear oscillators the adiabatic invariant (and thus the entropy) of the initial microcanonical ensemble at the average final energy *can decrease* in relatively slow processes, just due to the nonlinearity. On the other hand, it nevertheless increases for sufficiently fast changes. We conjecture this in single parametric kicks [17], which can be inves-

tigated analytically and rigorously for a wide class of homogeneous power law kinetic energy and homogeneous power law potentials [18], including the quartic oscillator. The Conjecture is proven in this case.

The linear oscillator is characterized by the universal energy distribution, whilst in nonlinear oscillators the underlying distribution can be just anything, depending on the specific properties of the system. For example, in time periodic 1D systems we can find a wide spectrum of dynamical behaviour, from integrability to ergodicity, or the generic KAM scenario in between. The most important example is the kicked rotator (standard map), but there are many other time periodic systems [19, 4] which we will discuss. [2]

.

2 Review of the time dependent linear oscillator

2.1 The phase flow and the general considerations

We study 1D linear oscillator described by the Newton equation [3]

$$\ddot{q} + \omega^2(t)q = 0, \tag{1}$$

starting with the *microcanonical distribution of the initial conditions*, with initial energy E_0. Then we let the system evolve in time and calculate the probability distribution $P(E_1)$ of the final energy E_1. To describe $P(E_1)$ is in general a difficult problem, but for the 1D parametrically driven linear oscillator (1) the problem can be solved [7–9, 11]. [4] $P(E_1)$ is universal, as it does not depend on any special properties of $\omega(t)$, but depends only on the final average energy $\bar{E}_1$. It is the so-called arcsine distribution [6]

$$P(x) = \frac{1}{\pi\sqrt{2\mu^2 - x^2}}, \tag{2}$$

[2] Time periodic systems are interesting also from the point of view of the Fermi acceleration, that is unlimited growth of the energy, in 1D systems and higher dimensions, especially in time periodic (breathing) 2D billiard systems, which is a subject of very intense study in the past few years [20], especially in numerical calculations, where lots of interesting empirical material has accumulated, including the power law behaviours with universal scaling properties [22]. The first theoretical result on the conformally breathing fully chaotic 2D billiard systems has been recently obtained [20], where the acceleration exponent $\beta = 1/6$ has been derived, in perfect agreement with at least three different 2D time periodic and fully chaotic billiard systems [21].

[3] Given the general $\omega(t)$ the calculation of $q(t)$ in closed form is unsolvable problem. In the sense of mathematical physics (1) is exactly equivalent to the one-dimensional stationary Schrödinger equation: the coordinate q appears instead of the probability amplitude ψ, time t appears instead of the coordinate x and $\omega^2(t)$ plays the role of $\mathcal{E} - V(x) =$ energy – potential. If $\mathcal{E}$ is greater than any local maximum of $V(x)$ then the scattering problem is equivalent to our 1D harmonic oscillator problem.

[4] We do not consider the external forcing, but the details can be found in [10].

where $x = E_1 - \bar{E}_1$ and μ^2 is the variance.

We shall answer the questions as to when is the adiabatic invariant [14] $I = E(T)/\omega(T)$ conserved, and if it is not conserved, what is the variance μ^2 of the energy, and the higher moments etc. By T we denote the length of the time interval of the variation of the system parameter. We also introduce **the adiabatic parameter** $\epsilon = 1/T$. Then (the not sharply defined) ΔI in the literature is proportional to μ, namely $\Delta I \approx \mu/\omega$. We use the powerful WKB method [15] to calculate μ^2 (see also the review [11]). It gives exact leading asymptotic terms when $T \to \infty$, and moreover, generally and in principle we can do the expansion to all orders, exactly. Below we treat one exactly solvable case, namely the model of linear $\omega^2(t)$.

The Hamilton function $H = H(q, p, t)$, whose numerical value $E(t)$ at time t is precisely the total energy of the system at time t, is

$$H = \frac{p^2}{2M} + \frac{1}{2}M\omega^2(t)q^2, \tag{3}$$

where q, p, M, ω are the coordinate, the momentum, the mass and the frequency, respectively. The dynamics is linear in q, p, but the dependence of the variance μ^2 on $\omega(t)$ is nonlinear. By the index 0 and 1 we denote the initial ($t = t_0$) and final ($t = t_1$) value of the variables, and $T = t_1 - t_0$.

We consider the phase flow map

$$\Phi : \begin{pmatrix} q_0 \\ p_0 \end{pmatrix} \mapsto \begin{pmatrix} q_1 \\ p_1 \end{pmatrix} = \begin{pmatrix} a & b \\ c & d \end{pmatrix} \begin{pmatrix} q_0 \\ p_0 \end{pmatrix}. \tag{4}$$

Since the system is Hamiltonian, Φ is a linear area preserving map with $\det(\Phi) = ad - bc = 1$. Let $E_0 = H(q_0, p_0, t = t_0)$ be the initial energy and $E_1 = H(q_1, p_1, t = t_1)$ be the final energy, that is,

$$E_1 = \frac{1}{2}\left(\frac{(cq_0 + dp_0)^2}{M} + M\omega_1^2(aq_0 + bp_0)^2\right). \tag{5}$$

Introducing the new coordinates, namely the action $I = E/\omega$ and the angle ϕ,

$$q_0 = \sqrt{\frac{2E_0}{M\omega_0^2}}\cos\phi, \;\; p_0 = \sqrt{2ME_0}\sin\phi \tag{6}$$

from (5) we obtain

$$E_1 = E_0(\alpha\cos^2\phi + \beta\sin^2\phi + \gamma\sin 2\phi), \tag{7}$$

where

$$\alpha = \frac{c^2}{M^2\omega_0^2} + a^2\frac{\omega_1^2}{\omega_0^2}, \quad \beta = d^2 + \omega_1^2M^2b^2, \quad \gamma = \frac{cd}{M\omega_0} + abM\frac{\omega_1^2}{\omega_0}. \tag{8}$$

Given the uniform probability density of ϕ equal to $1/(2\pi)$, we can now calculate the averages. Thus

$$\bar{E}_1 = \frac{1}{2\pi}\oint E_1 d\phi = \frac{E_0}{2}(\alpha+\beta). \tag{9}$$

That yields $E_1 - \bar{E}_1 = E_0(\delta\cos 2\phi + \gamma \sin 2\phi)$ and

$$\mu^2 = \overline{(E_1-\bar{E}_1)^2} = \frac{E_0^2}{2}\left(\delta^2+\gamma^2\right) = \frac{E_0^2}{2}\left[\left(\frac{\bar{E}_1}{E_0}\right)^2 - \left(\frac{\omega_1}{\omega_0}\right)^2\right], \tag{10}$$

where we have denoted $\delta = (\alpha-\beta)/2$. As we shall see, in an ideal adiabatic process $\mu = 0$, and therefore $E_1 = \bar{E}_1 = \omega_1 E_0/\omega_0$, and consequently $P(E_1)$ is a delta function, $P(E_1) = \delta(E_1 - \omega_1 E_0/\omega_0)$. In such case the adiabatic invariant is preserved exactly, the final value of the adiabatic invariant $I_1 = E_1/\omega_1$ is equal to the initial one $I_0 = E_0/\omega_0$.

As shown in [7–9], for details see also [11], the odd moments of $P(E_1)$ (2) vanish exactly (due to the symmetry) whilst the even moments are just proportional to the powers of the variance μ^2.

Expression (10) is positive definite by definition and this leads to the important conclusion: In full generality (no restrictions on the function $\omega(t)$!) we have always $\bar{E}_1 \geq E_0\omega_1/\omega_0$ and therefore the final value of the adiabatic invariant (for the average energy!) $\bar{I}_1 = \bar{E}_1/\omega_1$ is always greater or equal to the initial value $I_0 = E_0/\omega_0$. In other words, *the value of the adiabatic invariant at the mean value of the energy never decreases*, which is a kind of irreversibility statement. Namely, the entropy of the system is just the logarithm of the phase space volume, in our case the latter one is $2\pi I$. Moreover, it is conserved only for infinitely slow processes $T = \infty$, which is an ideal adiabatic process, for which $\mu = 0$. For periodic processes $\omega_1 = \omega_0$ we see that sampling at the same phase of the period we always have $\bar{E}_1 \geq E_0$, so the mean energy never decreases. The other extreme opposite to $T = \infty$ is the instantaneous ($T = 0$) jump where ω_0 switches to ω_1 discontinuously, whilst q and p remain continuous, and this results in $a = d = 1$ and $b = c = 0$, and then we find

$$\bar{E}_1 = \frac{E_0}{2}\left(\frac{\omega_1^2}{\omega_0^2}+1\right), \qquad \mu^2 = \frac{E_0^2}{8}\left[\frac{\omega_1^2}{\omega_0^2}-1\right]^2. \tag{11}$$

Now we calculate the flow map (4), namely its matrix elements a, b, c, d. Starting from the Hamilton function (3) and its Newton equation (1) we consider two linearly independent solutions $\psi_1(t)$ and $\psi_2(t)$ and introduce the matrix

$$\Psi(t) = \begin{pmatrix} \psi_1(t) & \psi_2(t) \\ M\dot{\psi}_1(t) & M\dot{\psi}_2(t) \end{pmatrix}. \tag{12}$$

Proceeding in the familiar way we find the phase flow map Φ, namely

$$\Phi = \begin{pmatrix} a & b \\ c & d \end{pmatrix} = \Psi(t_1)\Psi^{-1}(t_0). \tag{13}$$

The derivation of the distribution function (2) in two different ways, namely first via the characteristic function using all the moments, and, second, calculating it directly algebraically, is given in [9, 11].

2.2 An example: linear $\omega^2(t)$

For the linear model (exactly solvable in terms of Airy functions) defined by

$$\omega^2(t) = \begin{cases} \omega_0^2 & \text{if } t \leq 0 \\ \omega_0^2 + \frac{(\omega_1^2 - \omega_0^2)}{T}\, t & \text{if } 0 < t < T \\ \omega_1^2 & \text{if } t \geq T \end{cases} \tag{14}$$

we can show [11], for the initial energy $E_0 = 1$, using the asymptotical properties of the Airy functions, or using the WKB theory to the leading order, that when $\epsilon \ll 1$ the variance is given by

$$\mu^2 = \overline{(E_1 - \bar{E}_1)^2} \approx \frac{\epsilon^2}{128}\left(9 - 4\sqrt{2}\,\cos(\frac{4 - 8\sqrt{2}}{3\,\epsilon})\right), \tag{15}$$

where $\epsilon = 1/T$. Note that μ^2 is oscillating faster and faster with ϵ going to zero, which is the adiabatic limit, but in the mean it vanishes quadratically with ϵ.

In nonlinear systems the theory must be reformulated entirely and is the subject of the next sections. [5]

3 Time dependent nonlinear 1D Hamilton oscillators: some generalities

As already announced, in the nonlinear 1D oscillators the universality of $P(E_1)$ for an initial microcanonical ensemble is lost. In fact, as we shall see, it can be just anything depending on the details in the phase space. The two main quantities are the mean energy $\bar{E}_1$ and the variance μ^2. The property of the non-negative change of the adiabatic invariant at the average energy $I(\bar{E}_1)$ upon the variation of the system parameter is lost, in general. It is remarkable that due to the nonlinearities for some slow processes the adiabatic invariant and - its logarithm (the entropy) - can decrease, in contradistinction to the linear oscillator case.

But the increase in the adiabatic invariant is definitely restored for sufficiently large value of the adiabatic parameter ϵ, that means for a sufficiently fast change, in particular in case of a parametric kick $\epsilon = \infty$. One example of a parametric kick was given above for the linear oscillator, see equation (11).

We now discuss some generalities. Let $H(q, p, t_0)$ be the initial Hamiltonian, also expressed in terms of its action-angle variables (I_0, θ_0), so that the frozen Hamiltonian H_0 can be supposed to be a function of I_0 alone, $H_0 = H_0(I_0, \theta_0) = H_0(I_0)$. Let K_0 be a contour of constant I_0 and therefore also of constant initial energy E_0. The initial conditions are uniformly distributed on K_0 w.r.t. θ_0, with the constant density $1/(2\pi)$. The area enclosed by K_0 is $\mathcal{A}_0 = 2\pi I_0$.

[5] For the case of a separatrix crossing some interesting numerical results have been obtained in [23], namely $P(E_1)$ there has a substantial structure and is by far not so simple as (2).

Now the Hamiltonian $H(q,p,t)$ is allowed to evolve in time, and with it we follow the evolution of the ensemble K_0, as governed by the Hamilton equations of motion. The final Hamiltonian at time t_1 is $H(q,p,t_1)$, whose action-angle variables (for the frozen Hamiltonian) are (I_1,θ_1), and we write $H_1 = H_1(I_1,\theta_1)$. Under this process the curve K_0 is mapped onto the curve K_1, which is no longer a curve of constant action I_1 and also not of constant energy E_1, but is enclosing the same area $\mathcal{A}_1 = \mathcal{A}_0$ as K_0, because the phase flow is area preserving, and also is topologically equivalent to a circle. The pointwise mapping is thus completely determined by the map $I_1 = I_1(\theta_0)$, $\theta_1 = \theta_1(\theta_0)$, both being periodic functions of θ_0, parameterized by the initial value of I_0, or by the initial energy $E_0 = E_0(I_0)$.

Therefore, due to the periodicity, (I_1,θ_1) can be Fourier expanded in terms of θ_0, as follows

$$I_1 = \sum_{-\infty}^{\infty} a_m e^{im\theta_0}, \quad \theta_1 = \theta_0 + \sum_{-\infty}^{\infty} b_m e^{im\theta_0}, \tag{16}$$

where the summation runs over all integers m, $i^2 = -1$, and since (I_1,θ_1) must be real valued, we have the condition for the I_0-dependent Fourier coefficients $a_m = a^*_{-m}$ and $b_m = b^*_{-m}$, where $*$ denotes the complex conjugation. If all b's vanish, we simply have the identity $\theta_1 = \theta_0$. Calculating the area $\mathcal{A}_1$ we have

$$\mathcal{A}_1 = \int I_1 \, d\theta_1 = 2\pi a_0 - 2\pi i \sum_{-\infty}^{\infty} a_m b_{-m} m = 2\pi I_0, \tag{17}$$

which is indeed a real quantity, as it can be easily checked. The equation (17) follows also from the symplectic condition (Poisson bracket), requiring that the two pairs of variables are canonical ones, which also is the Jacobian determinant of the mapping being equall to unity, as one can easily show. This condition implies further restrictions on the Fourier coefficients, but they are difficult to work out in general. Also, the single valuedness must be taken into account (the curve K_1 must have no self crossings). It seems that no general conclusions can be drawn in this picture for completely general mappings $(I_0,\theta_0) \to (I_1,\theta_1)$, Fourier represented in (16). Therefore we must conclude that in the general nonlinear systems the universality of the distribution function from the linear oscillator (2) is lost.

However, if the higher Fourier coefficients vanish, like in the case of the linear oscillator, or can be neglected in the first approximation due to weak nonlinearity or other reasons, keeping only the lowest two of them, we find the approximation $I_1 = a_0 + a_1 e^{i\theta_0} + a_{-1} e^{-i\theta_0}$. We see immediately that a_0 is the average final action $a_0 = \bar{I}_1$, and writing $a_1 = \Delta I e^{i\alpha}/2$, we find

$$I_1 = \bar{I}_1 + \Delta I \cos(\theta_0 + \alpha). \tag{18}$$

Assuming now that the angle θ_0 is uniformly distributed on the interval $(0, 2\pi)$ with the density $1/(2\pi)$, we derive the probability density distribution

$$P(I_1) = \frac{1}{\pi} \frac{1}{\sqrt{(\Delta I)^2 - (I_1 - \bar{I}_1)^2}}, \tag{19}$$

where the variance of I_1 is equal to $(\Delta I)^2/2$. This is indeed the universal distribution (2) found in the linear oscillator. The same distribution applies to the energy if the variance is small, because then locally I and E are linearly related. We conclude that in the nonlinear oscillators in the limit of small changes of the adiabatic invariant, which means in the adiabatic limit, or in the case of weak nonlinearity, the distribution of the final energies might be approximated by the arcsine distribution function (2). This is not true in general, for fast changes.

4 Numerical calculations for the quartic oscillator in the adiabatic regime

Due to the great theoretical difficulties in treating the general nonlinear systems we have to resort to the highly accurate numerical calculations for some model system, for which we choose the quartic oscillator defined by the Hamiltonian

$$H(q, p, t) = \frac{1}{2}p^2 + \frac{a(t)}{4}q^4, \tag{20}$$

where $\epsilon = 1/T$ (the adiabatic parameter) is so far an arbitrary positive number, and

$$a(t) = \begin{cases} 1 & \text{if } \ t \leq 0 \\ 1 + \epsilon t & \text{if } \ 0 < t < T \\ 2 & \text{if } \ t \geq T \end{cases}. \tag{21}$$

Although for some special families of $a(t)$ analytic results have been obtained [24, 25], the problem is in general not solvable. In order to solve the problem in a reliable way, especially in the long time limit (adiabatic limit $\epsilon \to 0$), we have implemented and tested the symplectic integrator (SI) of eighth order due to McLachlan [26] and MacLachlan and Quispel [27]. We have carefully tested and compared many other methods [17, 25]. In Fig. 1 we show the results of calculations. The energy distribution function is different from (2), but similar, as the system is close to the adiabatic regime.

The variance μ^2 as a function of ϵ behaves very similarly as in the linear oscillator, like in the example (15). The adiabatic invariant at the average energy for slow processes $\epsilon \leq 0.05$ can decrease as shown in Fig. 2. At larger ϵ it eventually increases [17].

5 Single parametric kick

From the adiabatic regime we now come to the opposite extreme, the instantaneous jump of the system parameter, the parametric kick. We state the Conjecture of Papamikos and Robnik[17] that the value of the adiabatic invariant at

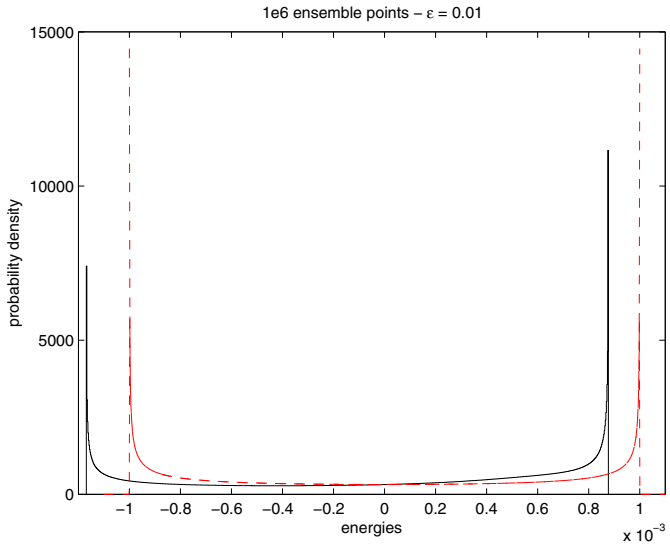

Fig. 1. The energy distribution function for the quartic oscillator for the adiabatic parameter $\epsilon = 0.01$. Linear $a(t)$ model. For comparison, the dashed curve is for the linear oscillator (2) with the same mean energy and the same variance μ^2.

the average energy always increases. We can prove this Conjecture for the special family of homogenenous power laws for the kinetic energy and the potential energy [17, 18], with the Hamilton function

$$H(q,p,a) = \frac{p^{2n}}{2n} + \frac{a}{2m}q^{2m}, \tag{22}$$

where a is the family parameter, and m, n are a positive integers. The parametric kick happens by the jump $a_0 \to a_1$. In a straightforward calculation we show that the average energy is equal to

$$\langle E_1 \rangle = E_0 \left(1 + \frac{n(a_1 - a_0)}{(m+n)a_0}\right). \tag{23}$$

Calculating the action at the average final energy $I_1(\langle E_1 \rangle) = I(\langle E_1 \rangle)$, taking $a = a_1$, and denoting $x = a_1/a_0$, we obtain $I_1(\langle E_1 \rangle) = I_0 f_m(x)$, where the universal function, indexed by m and n, is

$$f_{m,n}(x) = \frac{\left(1 + \frac{n}{m+n}(x-1)\right)^{\frac{m+n}{2m\,n}}}{x^{\frac{1}{2m}}}. \tag{24}$$

It has the minimum 1 at $x = 1$ (which means no change of the Hamiltonian at all), but is otherwise greater than one for all values of the ratio $x = a_1/a_0 \in (0, \infty)$. Therefore, the action at the average final energy upon a parametric kick

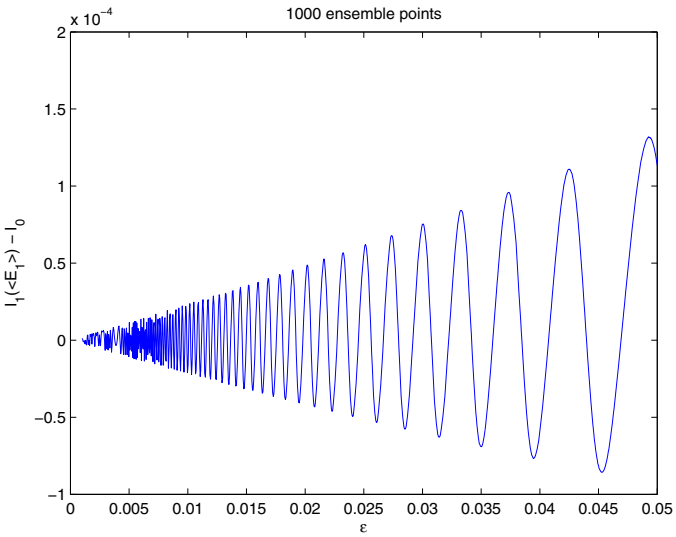

Fig. 2. The action difference $I_1(\bar{E}_1) - I_0$ for the quartic oscillator for the range $\epsilon \in [0, 0.05]$ for 1000 ensemble initial conditions at energy $E_0 = 1/4$. Linear $a(t)$ model.

in $2m$-oscillator always increases. In the limit $x \to \infty$ it goes as $f_{m,n}(x) \propto x^{\frac{1}{2n}}$. The special cases worth mentioning explicitly are the linear oscillator, $m = 1$, $n = 1$, $f_{1,1}(x) = \frac{x+1}{2\sqrt{x}}$, which is equivalent to equation (11), and the quartic oscillator $m = 2$,$n = 1$, $f_{2,1}(x) = (\frac{x}{3} + \frac{2}{3})^{\frac{3}{4}}/x^{\frac{1}{4}}$. In case $m = \infty$ we get a box potential and there is no time dependence at all, and consequently $f_{\infty,n}(x) = 1$. We have performed highly reliable and accurate numerical integrations using the 8th order SI for the various oscillators $m = 2, 3, 4$, $n = 1$, and found perfect agreement between the theory and numerics for a large value of the adiabatic parameters $\epsilon = 1/T$, where T is the time of linear variation of the parameter $a(t)$ defined in (21). The action jump formula (24) for the kicked system $\epsilon = \infty$ or $T = 0$ is exact only for the discontinuous jump, but it is surprising that it very well describes the behaviour of $I_1(\langle E_1 \rangle)$ at even finite values of ϵ, even down to the order of about $\epsilon \approx 1$, which means about one cycle of the oscillator. Thus we can conclude that qualitatively changes of the parameter on smaller or much smaller time scales than one period of the oscillator manifest themselves almost like a parametrically kicked system. This is demonstrated in Fig. 3. At $\epsilon = 10$ we get already perfect agreement. For details see [17].

Thus for the nonlinear oscillators (22) we have proven the Conjecture of positive jump of the action at the average final energy upon a single kick. The property means that the entropy in such systems upon a kick increases on the average, so we have some kind of irreversibility in the mean. The proof of the general Conjecture is difficult.

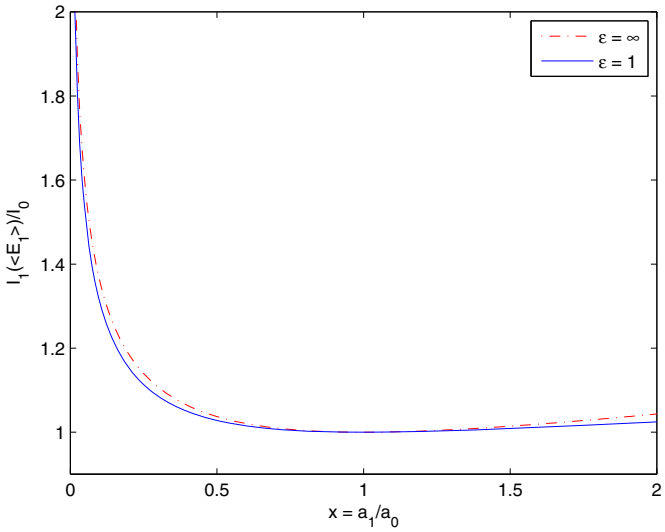

Fig. 3. The action ratio $I_1(\bar{E}_1)/I_0$ for the kicked quartic oscillator for $\epsilon = 1$ (linear model, numerical integration) versus $x = a_1/a_0$ for 1000 ensemble initial conditions at energy $E_0 = 1/4$ compared to $f_{2,1}(x)$.

6 Parametric kicking of the linear oscillator

6.1 The case of a kick and antikick

If the $\omega^2(t)$ is a piecewise constant function, namely equal to ω_0^2 up to time $t = 0$, where it jumps to ω_1^2, (kick) and at time T jumps back to ω_0^2 (antikick), we can explicitly calculate the variance μ^2

$$\mu^2 = \frac{E_0^2}{2}\left(\frac{1}{4}\left(\frac{\omega_1^2}{\omega_0^2} - \frac{\omega_0^2}{\omega_1^2}\right)^2 \sin^4\omega_1 T + \left(\frac{\omega_1}{\omega_0} - \frac{\omega_0}{\omega_1}\right)^2 \cos^2\omega_1 T \sin^2\omega_1 T\right). \quad (25)$$

In such case the variance μ^2 is periodic and vanishes whenever $\phi_1 = \omega_1 T = n\pi$, where n is any non-negative integer. This is a remarkable result: vanishing μ^2 means that the system is back to the microcanonical ensemble. Thus we conclude that the second kick, in this case antikick, can restore the original microcanonical distribution of the energies if the antikick happens at the right phase. Other details of double kicks can be found in [17].

6.2 The case of periodic kicking

The phase flow map $\Phi = \Phi_1^n$ (4) for n periods is a power of the maps for one period Φ_1. The determinant is always one, and thus everyhthing depends on the

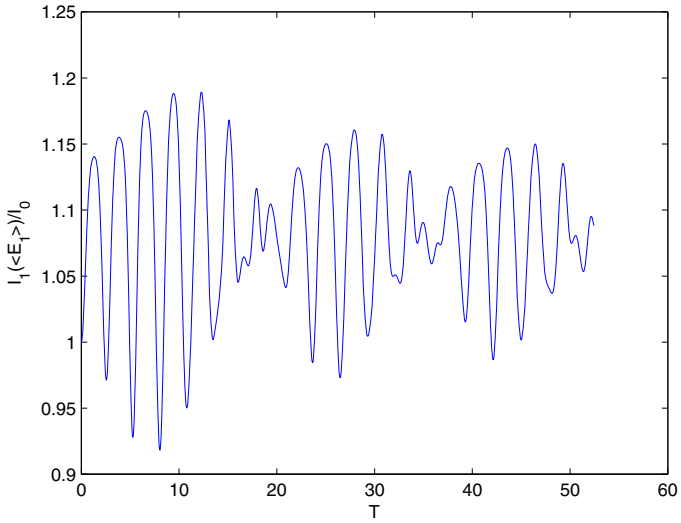

Fig. 4. The action ratio $I_1(\bar{E}_1)/I_0$ for the quartic oscillator for 1000 ensemble initial conditions at energy $E_0 = 1/4$, as a function of time T between the kick and antikick $a_0 = 1,\ a_1 = 2$. We observe oscillations below 1 for small T, showing that in nonlinear oscillators the action of the average final energy can decrease.

trace B of Φ_1. If $|B|$ is smaller or equal to 2 we have oscillatory behaviour, whilst in case of $|B| > 2$ we have the unstable case of exponential growth of the energy and also the adiabatic invariant: all matrix elements a, b, c and d grow as λ_1^n, where $\lambda_1 > 1$ is the larger solution of $\lambda^2 - B\lambda + 1 = 0$. Therefore, the mean energy $\bar{E}_1$ grows as $\propto \lambda_1^{2n}$ and the variance μ^2 grows as $\propto \lambda_1^{4n}$.

7 Parametric kicking of the quartic oscillator

7.1 The case of a kick and antikick

The system is as in (20) with $a = a_0$ for $t \leq 0$, $a = a_1$ for $0 \leq t \leq T$, and $a = a_0$ for $t \geq T$. Both, the action and μ^2 at final average energy are oscillatory functions of T, but not periodic. Moreover, the action is seen to decrease for some small T (Fig.4). The variance μ^2 (not shown) never gets down to $\mu^2 = 0$. Both properties are due to the nonisochronicity, due to nonlinearity [17].

7.2 The case of periodic kicking

Like in case of the periodic kicking of the linear oscillator we now assume for the quartic oscillator (20) that at time $t = 0$ we have a kick from $a_0 = 1$ to $a_1 = 2$, which at time $t = T$ jumps back to $a_0 = 1$, and at time $t = 2T$ back

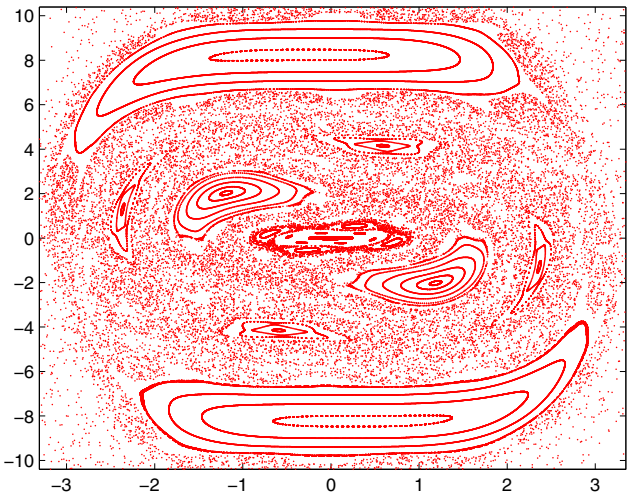

Fig. 5. The phase portrait of the phase space map Φ_1 for the periodically kicked quartic oscillator ($a_0 = 1,\ a_1 = 2,\ T = 1$).

to $a_1 = 2$, and this period is repeating itself ad infinitum. The flow map for the half period can be calculated analytically in terms of Jacobi elliptic functions [17], and the flow map for one period Φ_1 is just a product of the flow maps of the two half periods. Then, the flow map as a function of number n of periods is $\Phi_n = \Phi_1^n$, and it is area preserving. There is a scaling property of the flow map and as a consequence of that the topology of the phase portrait of such area preserving map $(q_1, p_1) = \Phi_n(q_0, p_0)$ is the same for all T. Thus it is enough to consider the case $T = 1$. The phase portrait of the map Φ_1 is shown in Fig. 5. We see the generic picture: some islands of stability and the surrounding chaotic sea. If the initial conditions are chosen entirely inside an island of stability, we shall see just the oscillatory regime. If the initial conditions are entirely or at least partially in the chaotic sea, we shall see unlimited energy growth (Fermi acceleration), because the chaotic sea is connected to infinity. But, of course, the microcanonical ensemble will be typically of the mixed type.

If we choose the initial conditions on a contour of $E_0 = 1/4$ for $a_0 = 1,\ a_1 = 2,\ T = 1$, we find that the average energy, the action and the variance are growing approximately linearly with n up to about $n \approx 200$, as shown for the energy in Fig. 6.

Piecewise linear periodic driving of the quartic oscillator has also been extensively studied [28] and it is of the mixed type again, but with a denser set of KAM invariant curves than in the periodic kicking, as the driving law has no discontinuities any more, only discontinuities of the first derivative. The energy distribution is then more like a Gaussian rather than arcsine.

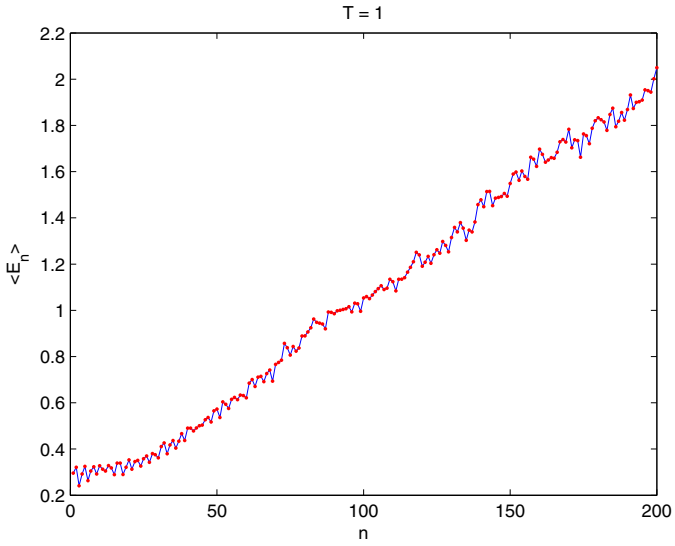

Fig. 6. The average energy $\bar{E}_1$ for the periodically kicked quartic oscillator for 1000 ensemble initial conditions at energy $E_0 = 1/4$, as a function of discrete time n (number of periods of the parameter a). The parameter values are $a_0 = 1,\ a_1 = 2,\ T = 1$. The data are dots and the line connecting them is just to guide the eye.

Acknowledgments. Financial support of the Slovenian Research Agency ARRS under the grants P1-0306 and J1-4004 is gratefully acknowledged.

References

1. Kloeden, P.E., Rasmussen, M.: Nonautonomous Dynamical Systems. American Mathematical Society, Providence (2011)
2. Arnold, V.I.: 1980 Mathematical Methods of Classical Mechanics. Springer-Verlag, New York (1980)
3. Lochak, P., Meunier, C.: Multiphase Averaging for Classical Systems. Springer-Verlag, New York (1988)
4. Zaslavsky, G.M.: The Physics of Chaos in Hamiltonian Systems. Imperial College Press, London (2007)
5. Ott, E.: Chaos in Dynamical Systems. Cambridge University Press, Cambridge (1993)
6. Feller, W.: Introduction to Probability Theory and its Applications, vol. II. Wiley, New York (1971)
7. Robnik, M., Romanovski, V.G.: Exact Analysis of Adiabatic Invariants in the Time-Dependent Harmonic Oscillators. J. Phys. A: Math. Gen **39**, L35–L41 (2006)
8. Robnik, M., Romanovski, V.G.: Energy Evolution in Time-Dependent Harmonic Oscillator. Open Syst. & Infor. Dyn. **13**, 197–222 (2006)

9. Robnik, M., Romanovski, V.G., Stöckmann, H.-J.: Exact Energy Distribution Function in a Time-Dependent Harmonic Oscillator. J. Phys. A: Math. Gen. **39**, L551–L554 (2006)
10. Kuzmin, A.V., Robnik, M.: Energy Evolution in Time-Dependent Harmonic Oscillator with Arbitrary External Forcing. Rep. on Math. Phys. **60**, 69–84 (2007)
11. Robnik, M., Romanovski, V.G.: Energy evolution and exact analysis of the adiabatic invariants in time-dependent linear oscillator. In: Robnik, M., Romanovski, V.G. (eds.) Proceedings of the 7th International Summer School/Conference on Let's Face Chaos through Nonlinear Dynamics, Maribor-Slovenia. Proc. of the AIP Conf., vol. 1076, pp. 185–212 (2008)
12. Einstein, A.: Bemerkungen zu den P. Hertzschen Arbeiten. Annalen der Physik **34**, 175–176 (1911)
13. Hertz, P.: Über die mechanischen Grundlagen der Thermodynamik. Annalen der Physik **33**, 225 and 537 (1910)
14. Einstein, A.: Inst. Intern. Phys. Solway, Rapports et Discussions **1**, 450 (1911)
15. Robnik, M., Romanovski, V.G.: Some Properties of WKB Series. J. Phys. A: Math. Gen. **33**, 5093–5104 (2000)
16. Papamikos, G., Robnik, M.: WKB Approach Applied to 1D Time-Dependent Nonlinear Hamiltonian Oscillators. J. Phys. A: Math. Theor. **45**, 015206+11 (2012)
17. Papamikos, G., Robnik, M.: Statistical Properties of 1D Time-Dependent Hamiltonian Systems: From the Adiabatic Limit to the Parametrically Kicked Systems. J. Phys. A: Math. Theor. **44**, 315102+29 (2011)
18. Andresas, D., Robnik, M.: (2012), to be submitted
19. Chirikov, B.V.: A Universal Instability of Many-Dimensional Oscillator Systems. Phys. Rep. **52**, 263–379 (1979)
20. Batistić, B., Robnik, M.: Fermi Acceleration in Time-Dependent Billiards: Theory of the Velocity Diffusion in Conformally Breathing Fully Chaotic Billiards. J. Phys. A: Math. Theor. **44**, 365101-1–365101-21 (2011)
21. Batistić, B., Robnik, M.: Dynamics of time-dependent conformally breathing billiards. In: Robnik, M., Romanovski, V.G. (eds.) Proceedings of the 8th International Summer School/Conference on Let's Face Chaos through Nonlinear Dynamics, Maribor-Slovenia. Proc. of the AIP Conf., vol. 1468, pp.27–37 (2012)
22. Leonel, E.D., McClintock, P.V.E., da Silva, J.K.L.: Fermi-Ulam Accelerator Model under Scaling Analysis. Phys. Rev. Lett. **93**, 014101 (2004)
23. Robnik, M., Wood, T.A.: Testing Adiabatic Invariance in Separatrix Crossing. Nonlinear Phenomena in Complex Systems (Minsk) **9**, 141–149 (2006)
24. Papamikos, G.: Lie and Noether Symmetries of a Class of Time-Dependent Anharmonic Oscillators. Nonlinear Phenomena in Complex Systems (Minsk) **14**(1), 49–59 (2011)
25. Papamikos, G.: PhD Thesis, CAMTP and Universityof Ljubljana (2011)
26. McLachlan, R.I.: On the Numerical Integration of Ordinary Differential Equations by Symmetric Composition Methods. SIAM J. Sci. Comput. **16**, 151–168 (1995)
27. McLachlan, R.I., Quispel, G.R.W.: Splitting Methods. Acta Numerica **11**, 341–434 (2002)
28. Papamikos, G., Sowden, B.C., Robnik, M.: Dynamical and Statistical Properties of Piecewise Linearly Periodically Modulated Quartic Oscillator. Nonlinear Phenomena in Complex Systems (Minsk) **15**, 227–240 (2012)

Synergetic Impact of Synergetics - Remembrances of a Chemist

Peter Plath

Fritz-Haber Institut der Max-Planck.Gesellschaft, Faradayweg 4-6, 14195 Berlin, Germany
peter_plath@t-online.de

Abstract. I review historical chemical experiments in which the phenomena of self-organisation and pattern formation were first observed. I then review theoretical models for the description of oscillating chemical reactions and reactions with limit-cycle behaviour. Finally I discuss a number of examples of chemical experiments for the explanation of which the concepts of synergetics were of paramount importance.

Keywords: self-organisation, pattern formation, chemical experiments, synergetics

1 Introduction

Hermann Haken who is among us fortunately (Fig. 1) can be called rightly so the father of synergetics. His powerful definition of synergetics can be summarized in the statement: "What we are looking for that is the action of many sub-systems in common, creating structures and new functions on a macroscopic scale" [1]. When explaining his ideas, he very often used the example of the Rayleigh-Bénard instability. For sufficiently small temperature gradients the Fourier law (1) governs the heat transport from the hot bottom of a vessel up to the cold surface of the fluid.

$$\frac{\partial T}{\partial t} = \kappa \nabla^2 T; \quad \kappa > 0 \, . \tag{1}$$

The subsystem of this randomly organized heat transport process consists of the molecules which undergo uncorrelated Brownian motion in the fluid. However, if the temperature gradient exceeds a critical value cooperative motion occurs among the molecules, forming the new subsystem of "droplets", the motion of which is caused by buoyant forces. In this way convection cells (Fig. 2) emerge in the fluid, organizing the heat transport more effectively than thermal conduction. For a chemist, it is really hard to gain an impression of this kind of movement in the fluid. Fortunately, S. Großmann et al. [2] published a photo taken by Yibing Do and Penger Tong which is of great visual impact illustrating the thermal flow within the fluid by liquid crystals of temperature depending colourings.

A. Pelster and G. Wunner (eds.), *Selforganization in Complex Systems: The Past, Present, and Future of Synergetics*, Understanding Complex Systems,
DOI: 10.1007/978-3-319-27635-9_5

Fig. 1. Hermann Haken Delmenhorst 2012.

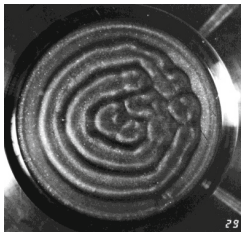

Fig. 2. Rayleigh-Bénard instability.

Fig. 3. Runge picture - pattern formation by front instabilities during chemical reactions in filter paper.

2 Historical Experiments

2.1 Runge Pictures

In chemistry there exists a lot of historical experiments on pattern formations, a long time before the idea of synergetics was developed by Hermann Haken. Let me briefly sketch some of these remarkable investigations. One of these experiments was carried out by the very successful industrial chemist F.F. Runge (1794 - 1867) in his "Chemische Produkte Fabrik" in Oranienburg, where he was its technical director since 1850. He was very much involved in the isolation of compounds which could be isolated from coal tar. In this way he detected phenol, quinoline, pyrrole, and aniline, which became fundamental substances for dye industry. This might be one of the reasons why he looked for inorganic mineral colours and their behaviour with respect to colouring of papers and clothes.

He investigated chemical reaction front instabilities while carrying out the reaction in the almost 2D space of filter papers. In contrast to grease or water spots in our clothes the spreading fronts are of fractal shape instead of almost cyclic form.

$$D(\alpha) = \frac{\ln \sum_{i=1}^{n} \sqrt{r_{i-1}^2 + r_i^2 - 2r_{i-1}r_i \cos s} - \ln k}{\ln(1/s)} \,. \tag{2}$$

Estimating the fractal dimension for the front in the Runge-picture shown above (Fig. 3) using eq. (2), one obtains $D(\alpha) = 0.933$. He published a series of reaction pictures in his very illustrative books: "Zur Farbenchemie - Musterbilder für Freunde des Schönen und zum Gebrauch für Zeichner, Maler, Verzierer und Zeugdrucker" (1850) and "Bildungstrieb der Stoffe - Veranschaulicht in selbständig gewachsenen Bildern" (1855) [3].

2.2 Liesegang Rings

At the end of the 19th century Raphael E. Liesegang (1896 - 1947) came forward with another exciting pattern formation process (1896) - he detected precipita-

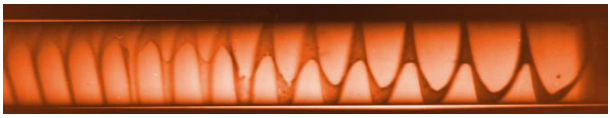

Fig. 4. Liesegang screw in Agar-Agar gel in a test tube (vertically oriented) [5].

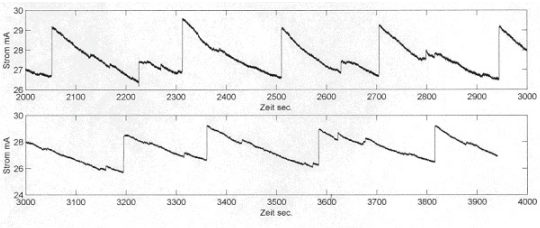

Fig. 5. Oscillating time-series of the dissolution of chromium in mineral acids (experiment by Th. Rabbow and P.J. Plath).

Fig. 6. Photograph of the first produced chromium pieces which Wi. Ostwald used for his experiments in 1899 and 1900 [5].

tion patterns of inorganic reactions in gels [3, 4]. He presented his findings as a working hypothesis for understanding standing waves in Crookes' gas discharge tubes (1879) (pattern formation in plasma instabilities) and called them "A-lines". Dousing a glass plate with a gelatin solution containing small amounts of potassium dichromate and putting some drops of silver-nitrate onto the stiff gel, he found that the silver ions diffuse into the gel, forming precipitation rings of silver-chromate. At that time he worked in the factory Ed. Liesegang OHG of his father as an industrial chemist studying the production of photographic layers. One can observe a lot of different patterns like spirals (Fig. 4) and rings while performing precipitation reactions, for example in gels or sandstones under various reaction conditions. The very small colloids of the precipitates which are formed if the concentration product of the corresponding ions exceeds its critical value are stabilized by the gel and can move for a short time without decomposition. If they collide they may form aggregates which stick in the gel. In this way precipitation patterns in the gel can be simulated effectively [6].

2.3 Oscillating dissolution of chromium

In 1900 Wilhelm Ostwald (1853 - 1932) published the first fundamental articles [7] on the oscillating dissolution of chromium in sulfuric acid (cf. Fig. 5). For his experiments he used the very first pieces of chromium (Fig. 6) which just had been produced. Moreover, he developed the first thermostat, and a recorder for documenting continuously and graphically his results. He was criticised very much for his results, especially because of the fact that he could not reproduce

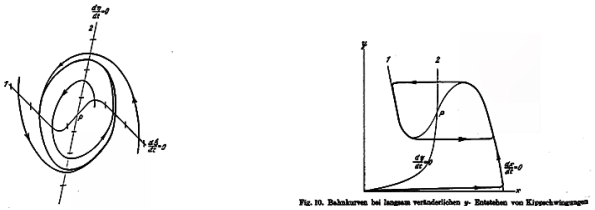

Fig. 7. Copy of the original drawings of K.F. Bonhoeffer.

them with a chromium piece produced later on. But he was totally right! We have reproduced his results with his original chromium pieces as well as with pure chromium manufactured our days.

2.4 Lotka Model

In 1910 A.J. Lotka (1880 - 1949) published his article "Zur Theorie der periodischen Reaktionen" in the same journal "Zeitschrift für physikalische Chemie", founded by Wilhelm Ostwald, in order to describe oscillating chemical reactions in homogeneous systems [8]:

$$\begin{aligned} A + X_1 &\xrightarrow{k_1} 2X_1 \\ X_1 + X_2 &\xrightarrow{k_2} 2X_2 \\ X_2 &\xrightarrow{k_3} F \\ A &\longrightarrow F \end{aligned} \qquad (3)$$

$$\begin{aligned} \frac{dc_1}{dt} &= k_1 c_a c_1 - k_2 c_1 c_2 \\ \frac{dc_2}{dt} &= k_2 c_1 c_2 - k_3 c_2 \end{aligned} \qquad (4)$$

He solved these equations. His set of coupled differential equations is well known in our days as Lotka-Volterra model.

2.5 K. F. Bonhoeffer - Electrochemical dissolution of iron

Working on the electrochemical dissolution of iron in nitric acid the physical-chemist Karl F. Bonhoeffer (1899 - 1957) - brother of Dietrich Bonhoeffer (1906 - 1945), the protestant theologian - observed electrochemical oscillations and described them by the zero isoclines of the well known system of differential equations (5) [9]. In this way he used the idea of limit cycle behaviour (Fig. 7) to describe periodic chemical reactions.

$$\begin{aligned} \frac{dx}{dt} &= -ax^3 + bx + c \\ \frac{dy}{dt} &= dx^2 + ex - f \end{aligned} \qquad (5)$$

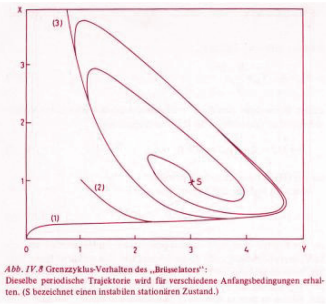

Fig. 8. Original drawing of the limit cycle behaviour of the Brusselator [14].

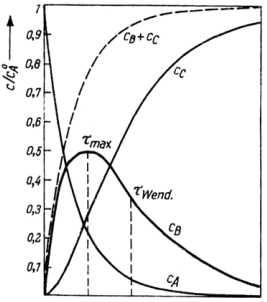

Fig. 9. Graphs of the consecutive reaction A → B → C [15].

2.6 Belousov - Zhabotinsky Reaction

All this and much more was known and had been published in famous journals when Boris P. Belousov (1893 - 1970) detected chemical oscillations during the cerium catalyzed bromation of citric acid in 1951 [10]. However, the study of pattern formation in chemical systems did not belong to the main stream research in chemistry, and therefore it is not astonishing that Belousov's results were not accepted in famous chemical journals in Russia until 1958, when Zhabotinsky published new results on this reaction replacing the catalyst cerium with ferroine and citric acid with malonic acid for better visualization. I have had similar experiences in Germany (FRG) in the late seventies when we tried to publish our first results on the oscillating Pd-catalysed methanol oxidation.

2.7 Ilya Prigogine - Brusselator

Working on the conflict between classical thermodynamics and real life evolution and pattern formation, Ilya Prigogine (1917 - 2003) [11, 12] developed the concept of the export of entropy from a system under consideration to its surrounding (1967/68). In this way, regarding open systems (6) and (7) (where A is an equal constant and E can grow without limitation), he developed in 1977 a set of kinetic equations which have an auto-catalytic reaction step: $2X + Y \rightarrow 3X$, in its corresponding set of chemical equations [13, 14]:

$$\begin{aligned} A &\rightarrow X \\ 2X + Y &\rightarrow 3X \\ B + X &\rightarrow Y + D \\ X &\rightarrow E \end{aligned} \qquad (6)$$

$$\begin{aligned} \frac{dX}{dt} &= A + X^2Y - BX - X \\ \frac{dY}{dt} &= BX - X^2Y \end{aligned} \qquad (7)$$

Such an auto-catalytic equation was very unusual for a chemist, who would never write: $2X + Y \rightarrow 3X$, but $Y \rightarrow X$. So it was very hard to understand

the chemical background of this model at those times. However, he introduced this description for constructing the non-linear ordinary differential equation (7), which he needed for creating a limit-cycle (Fig. 8). Nevertheless, in the eighties, his fruitful ansatz inspired a lot of chemists to look for similar auto-catalytic reactions.

2.8 Text-book knowledge in 1960 - 1970

However, looking into famous physical chemical textbooks of the early seventies, for example R. Brdička's "Basics of Physical Chemistry" [15], consecutive reactions of the type $A \to B \to C \to \cdots$ (cf. Fig. 9), were the most advanced descriptions of the kinetics of open chemical systems at this time. The Michaelis-Menten-kinetics of enzymatic reactions: $E + S \overrightarrow{\leftarrow} ES \to E + P$ with E = enzyme, S = substrate, and P = product, which is well known in bio-chemistry, is just a special simplification of the more general consecutive reactions.

3 The early days of Synergetics

Remembering all these convincing findings it is astonishing that it took about hundred years from their beginning that these ideas became united under one roof by Hermann Haken when he created "Synergetics" [16, 17] in the early seventies.

In April 1972 he organized the first international "Symposium on Synergetics" in Schloss Elmau, which is documented in the proceedings "Synergetics - Cooperative Phenomena in Multi-Component Systems" [18] which appeared 1973 with B.G. Teubner, Stuttgart. It needed some more years that this idea maturated in the scientific community.

In May 1977 Hermann Haken organized a second international workshop on synergetics at Schloss Elmau. There he stated "Synergetics is a rather new field of interdisciplinary research which studies the self-organized behaviour of systems leading to the formation of structures functionings" [19].

Summer 1977 was just the date, when N. Jaeger and me at the physical chemistry department of Bremen University became acquainted with the ideas of structure formation in irreversible processes by the small book of Werner Ebeling which had just appeared [20].

Two years later U.F. Franck and E. Wicke organized the first meeting of the Bunsen-Gesellschaft für Physikalische Chemie on chemical oscillations in Aachen (1979) (cf. Fig. 10) [21]. Meanwhile a lot of physical-chemists came up with ideas like chemical oscillations, structure formation in irreversible processes, etc., and they presented their first results on these topics to a wide spread auditorium. Among them there were P. Gray (England), A. Zhabotinsky (USSR), U.F. Franck, E. Wicke, and O.E. Rössler, who brought chaos to the chemists' mind at first (Fig. 11). He formulated the powerful idea: "Chaos can be realized in simple chemical systems" [22]. This was very stimulating and inspiring to look for chaos experimentally too.

Fig. 10. U.F. Frank (very left) and O.E. Rössler (left on top) at the Discussion Meeting "Kinetics of Physicochemical Oscillations" Aachen 1979.

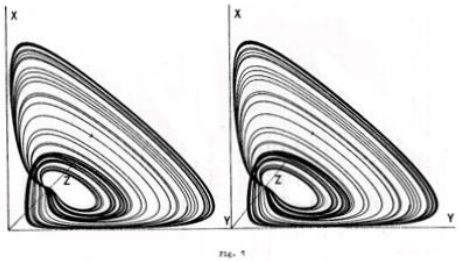

Fig. 11. Chaotic oscillations of Eq. (9). Stereoscopic display (two parallel projections). This is a copy of the original figure published by O.E. Rössler et al. [21].

$$\begin{aligned}
\dot{x} &= x(a_1 - k_{-1}x - z - y) + k_{-2}y^2 + a_1\,, \\
\dot{y} &= y(x - k_{-2}y - a_5) + a_2\,, \\
\dot{z} &= z(a_4 - x - k_5 x) + a_3\,. \qquad (8)
\end{aligned}$$

For this set of three non-linear kinetic equations (8) he offered a set of five chemical equations which can be interpreted conventionally by bi-molecular reactions.

Peter Gray from Leeds (Fig. 12) talked about the formation of "mushroom patterns" (Fig. 13) in the phase-space of chemical systems, while investigating auto-catalytic reactions. He called this: "classification of static instabilities". All these efforts are based upon the elementary approach to Thom's catastrophe-theory which also fills a whole chapter in Hermann Haken's "Introduction to Synergetics" [1].

Fig. 12. Peter Gray (right) [5].

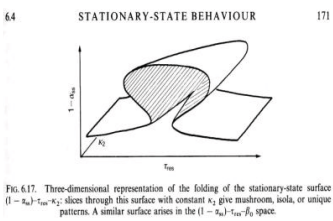

Fig. 13. Mushroom pattern in phase space [23].

4 Chemical experiments on synergetics

4.1 Heterogeneously catalysed methanol oxidation

We were very much fascinated by all these ideas! When we were working on the heterogeneously catalysed methanol oxidation with Pd-supported catalysts [24, 25], H. Haken's idea of synergetics described our observations by the cooperative action of subsystems, and fitted very much to our perception [26]. Moreover, we [27] observed sudden jumps in the temperature production during the long-time run of the exothermic methanol oxidation reaction (9)

$$\begin{aligned} 2CH_3OH + O_2 &\longrightarrow HCOOCH_3 + 2H_2O + \Delta H_1 \\ CH_3OH + 3/2O_2 &\longrightarrow CO_2 + H_2O + \Delta H_2\,. \end{aligned} \tag{9}$$

The catalytic reaction took place at the reactor temperature of about 80°C. The stepwise reduction of the flow rate of the gaseous educts from 90 to 40 ml/min diminished the heat production, and thus the temperature difference ΔT between the catalyst layer and the reactor temperature from 55°C down to about 35°C. After five hours we stopped this procedure and let the reaction go [27].

It took unbelievable 14 hours that the reaction system switched from the reaction channel of the total oxidation to CO_2 to the partial oxidation mechanism of formic acid methyl ester $HCOOCH_3$ accompanied by a sudden jump to lower temperature production, see Fig. 14.

Hours later we thought the system is over and will never be able to be activated again. This was an obvious error! Our traditionally trained chemical intuition misled us. A detailed inspection concerning the ideas of synergetics led to the hypothesis of a twofold cusp catastrophe, see Fig. 15. It was the bright diploma student Anna Haberditzl who carried out all the exciting experiments with unbelievable patience.

The other excellent student in our group at those times was Edith van Raaij. She detected the first oscillation of the catalytic methanol oxidation (cf. Fig. 16) and estimated experimentally the correlation between the time-series and underlying chemistry of the oscillations [24, 25].

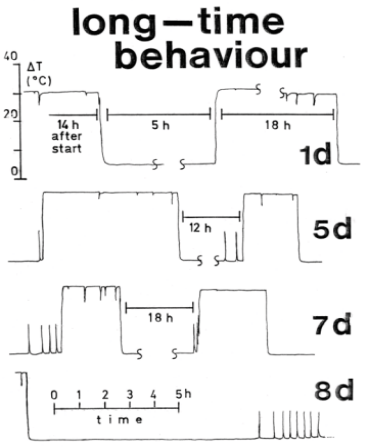

Fig. 14. Long-time behaviour of the Pd-catalysed methanol oxidation [27].

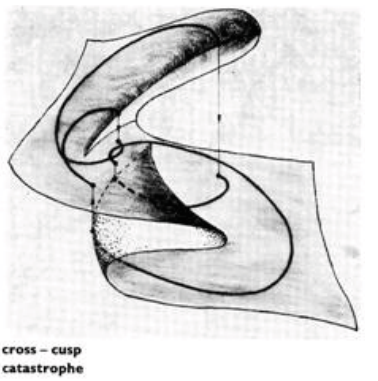

Fig. 15. Original sketch of the trajectory of the catalysed methanol oxidation onto a twofold folded 2D manifold [27].

These investigations were continued by Peter Svensson, who found toroidal oscillations [28] (Fig. 17) as well as experimental evidence of homoclinic chaos and type-II intermittency in the heterogeneously catalysed methanol oxidation [29]. At that time the phenomenology of this reaction was extremely fascinating, especially because of the fact that maps for the different basins of attraction were just discussed in synergetics. It was our aim to understand the possible structures of motion in the correlated control space of this reaction.

4.2 Fractals and fractal growth

In one of the Synergetics conferences at Schloss Elmau, Heinz-Otto Peitgen in 1984 [30, 31] presented his very illustrative work on Benoît Mandelbrot's idea of fractals [32]. Very soon it became clear that chaos and fractals belong to each other. Nevertheless, it was hard to combine these ideas with chemistry, up to the point that Kenneth Wilson [33] and Steven Wolfram [34] came up with their cellular automata [35]. Now, as chemists we could easily correlate figures of the two-dimensional electro-deposition of zinc between two immiscible solutions (see Fig. 18) with the fractal growth of mathematical dendrites [31]. A real burst of new investigations on the fractal pattern formation in various fields of physics [36] and chemistry [37] went off in the eighties. Surprisingly, this idea helped us several years later to understand the structure formation of beer foam [38], which resembles very much the construction of Apollonian circles and spheres (Fig. 19). Both examples are understandable intuitively for experimentally working chemists who are interested in fractals!

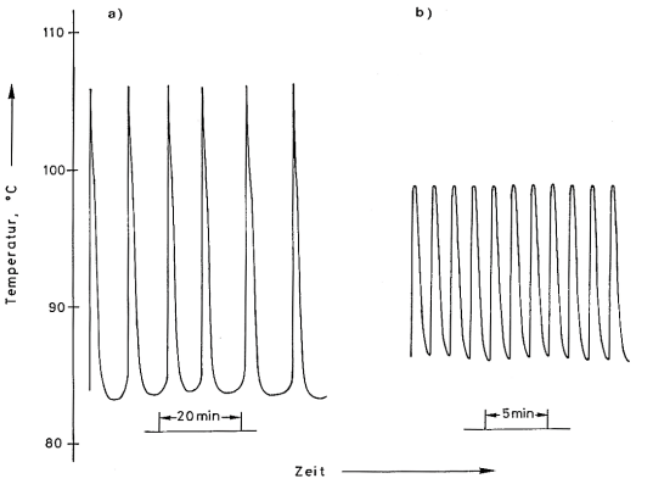

Fig. 16. Two periodic oscillations of the Pd-catalysed methanol oxidation. a) methanol 1,9 Vol % / oxygen; 41 ml/min; b) methanol 1,9 Vol % / air; 19 ml /min. These experiments have been carried out by Edith van Raaij [25].

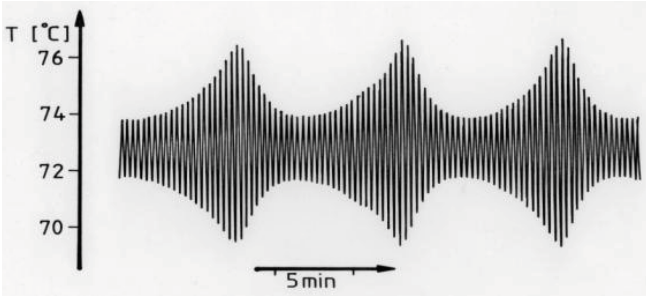

Fig. 17. Toroidal oscillations of the heterogeneously Pd-catalysed methanol oxidation [28].

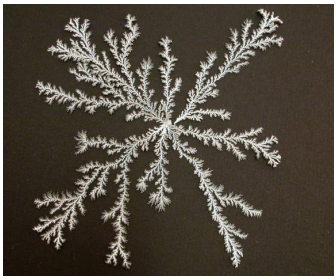

Fig. 18. Fractal pattern formation during electrochemical zinc deposition [5].

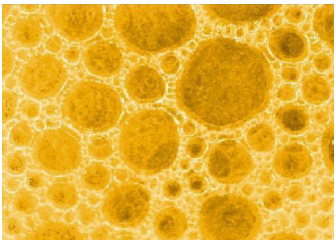

Fig. 19. Apollonian structure of bubbles in beer foam appears after the phase of drainage in the so called rearrangement phase [38].

Fig. 20. Solitary waves in the Belousov-Zhabotinsky reaction performed in a Petri dish. A single solitary wave, a target pattern and a rotating spiral is observable in different regions [5].

Fig. 21. Spirals during single crystal catalysis of CO-oxidation on Pt(110) [44].

4.3 Chemical waves in the BZ reaction

We remember the great potential of Fick's second law for structure formation if some critical values are exceeded. Now, combining Fick's second law with reaction equations a great variety of new structure formations should arise. Such reaction-diffusion equations (10) played a very import role in development of synergetics, since a local oscillation in an excitable chemical medium becomes a chemical wave by diffusion. The most exciting example for this kind of structure formation was the Belousov-Zhabotinsky reaction (BZR) [10]

$$\frac{\partial c_i}{\partial t} = f_i(c_1, c_2, \cdots, c_n) + D_i \nabla^2 c_i \,. \tag{10}$$

H. Haken used a picture of this kind of pattern formation in BZR for the cover of his famous and wide spread book "Erfolgsgeheimnisse der Natur" [16]. Self exciting cyclic waves, so-called target patterns, cyclic waves in excited media, and spiral waves can be observed, if one carries out this reaction in a thin layer, for example in a Petri dish (cf. Fig. 20). With enormous effort this reaction has been studied in all details theoretically as well as experimentally since decades. The waves in BZR became a key phenomenon for a huge variety of similar pattern formation processes [39, 40].

All these different patterns can be summarized by the idea of a solitary chemical wave. In earlier times they have been named auto-waves by V.I. Krinsky [39]. Such waves annihilate if they collide and they cannot be reflected if they touch a wall. Hans Meinhardt demonstrated the wide occurrence of chemical waves in his very illustrative book "The Algorithmic Beauty of Sea Shells" [41]. These waves have been simulated successfully by reaction-diffusion equations of the type of the activator-inhibitor model for example, but also by cellular automata models [42, 43]. However, the question remains what are the cooperative subsystems which lead to the observed patterns.

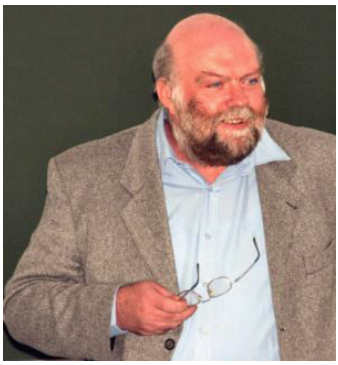

Fig. 22. Rudolf Friedrich 2007 during a talk in Bremen [46].

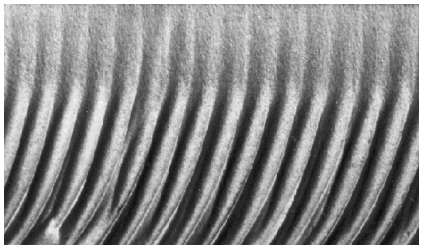

Fig. 23. Ripple formation in the side wall created by water-jet cutting. Original photo made by G. Radons and R. Friedrich [45].

G. Ertl and his group observed spiral waves on the surfaces of Pd single crystals during the catalytic oxidation of CO [44] (see Fig. 21). Although only a few atoms and molecules, respectively, are the acting subsystems, these processes could be modelled successfully by the reaction-diffusion systems which are based on the Langmuir-Hinshelwood mechanism, extended to surface sub-layers acting as storages for oxygen. In this way, we have an interesting situation: a homogeneous system which has been modelled in a continuous space by differential equations as well as by discrete mathematics via cellular automata, and we have a real discrete system in which pattern formation was modelled successfully by differential equations. As a consequence, synergetics cannot be reduced onto non-linear dynamics in terms of differential equations, which, however, obviously are powerful tool.

4.4 Cutting processes - ripple formation

Günter Radons and the late Rudolf Friedrich (Fig. 22) applied synergetics to the technical process of abrasive water-jet cutting [45], since ripple formation can be observed in the side walls of the cuts (Fig. 23). This inspired us to look for another technical process which was not well understood at the time: microstructuring by laser-jet-etching.

Thomas Rabbow investigated electrochemically the laser-jet-etching process [47]. Depending on the feeding rate of the work piece he also observed ripple formation in the trenches and their side walls (Fig. 24).

In this case electrochemical etching takes over the role of the abrasive material used in water-jet cutting processes. Because of such similarities Rudolf Friedrich insisted upon generalisation of these cutting processes in terms of synergetics. Together we organized the 16th Winter-Seminar at Zeinisjoch 2004 "Universelles Verhalten bei Schneidprozessen" (Universal behaviour in cutting processes), in order to discuss general principles of pattern formation in cutting processes.

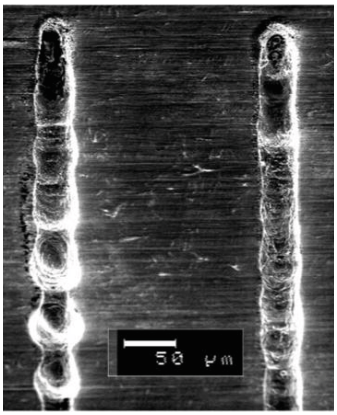

Fig. 24. Scanning electron microscope (SEM) - top view - image of a steel sample micro-structured by Laser-Jet Etched method revealing ripple formation in the side walls [47].

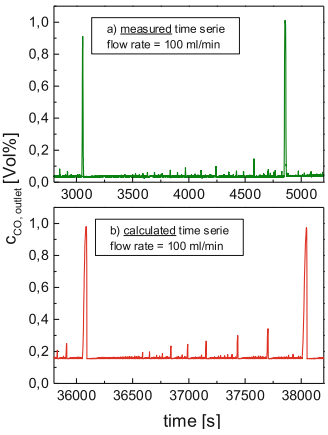

Fig. 25. Temporal fractal structure formation; Experiment: CO-oxidation in a micro-reactor; Model: 100 coupled elementary-reactors which are of about 10^{10} to 10^{11} Pd particles of almost the same size each of them [50].

4.5 Chaos in the catalytic CO-Oxidation

The brilliant physico-chemist Karin Möller worked on the chaotic behaviour of the heterogeneously catalysed CO-oxidation using Pd-loaded zeolites as support catalysts [26, 48]. Together with Nils Jaeger, it was our aim to figure out what are the acting subsystems which are responsible for the self-similar pattern formation of break-downs of conversion [49]. The palladium crystals, the Pd containing zeolite crystals, or even parts of the catalyst layer came into consideration as candidates for subsystems. Simulations were carried out carefully by Carsten Ballandis and compared with a huge amount of very exact new measurements (Fig. 25), leading to the surprising result that sets of Pd-particles of almost the same size form the cooperating subsystems which cause the self-similar temporal patterns of the time series [50]. This is due to the fact that the Pd-particles undergo phase transitions depending upon their size, which is characteristic of nano-particles. The exothermic CO-oxidation causes a heating up of the particles. The smaller the particles are, the higher is the resulting temperature of the particles. In this way they undergo the phase transition from palladium Pd to palladium oxide PdO earlier than the larger particles. The catalysis stops when the particle is in the PdO state where the particle cools down again. The coupling between all the particles of almost the same size is realized by the effective CO concentration in the catalyst layer or the reactor volume, respectively. In this way primitive elementary reactors are formed each of them containing about 10^{11} Pd-particles. These primitive elementary reactors take over the role of the cooperating units for the catalytic reaction in the sense of synergetics.

Groups of insignificantly larger primitive elementary reactors become entrained temporarily, forming elementary reactors. The fractal character of the time series results from the cooperation of these elementary reactors [49].

5 Conclusive remarks

Once, when we met during the "Winterseminar at Zeinisjoch", discussing chemical pattern formation, it was Arne Wunderlin who put forward the - for synergetics - fundamental request, namely, to look for the optimally cooperating subsystems which guarantee that the observed patterns can be described correctly. A fallback onto standard models like atoms, molecules, or the corresponding averaged concentrations might not be useful in any case. In chemistry, one also has to look for larger entities like droplets in Rayleigh-Bénard systems - we agreed on this. Chemically spoken, regions reacting synchronously might be the most suitable entities even for so-called homogeneous reaction systems, especially if they are not "well stirred". In case of the heterogeneously Pd-catalysed CO-oxidation we have provided the evidence of such synchronously acting particles, which together form the subsystems - the primitive elementary reactors - we looked for.

References

1. Haken, H.: Synergetics - An Introduction, Preface to first english edition, p. X. Springer-Verlag, Heidelberg (1990)
2. Ahlers, G., Großmann, S., Lohse, D.: Hochpräzision im Kochtopf - Neues zur turbulenten Wärmekonvektion. Physik Journal **1**, 31–37 (2002)
3. Kuhnert, L., Niedersen, U.: Selbstorganisation chemischer Strukturen. Ostwalds Klassiker der exakten Wissenschaften **272**, 63 (1987)
4. Liesegang, R.E.: Liesegangs Photographisches Archiv Nr. 801 Heft XXI. Düsseldorf (1896)
5. Photo: Plath, P
6. Sydow, U., Plath, P.J.: Structure formation during precipitation reaction in gels: New Liesegang patterns. Berichte der Bunsengesellschaft für Physikalische Chemie **102**, 1683–1688 (1998)
7. Ostwald, W.: Periodische Erscheinungen bei der Auflösung des Chroms in Säuren I and II. Z. Phys. Chemie **35**, 33–76 and 204–256 (1900)
8. Lotka, A.J.: Zur Theorie periodischer Reaktionen. Z. Phys. Chemie **72**, 508–511 (1910)
9. Bonhoeffer, K.F.: Zur Theorie der periodischen chemischen Reaktionen in erregbaren Medien. Ber. Verh. Sächs. Akad. Wiss. zu Leipzig, math.-nat. wiss. Klasse **95** (1943); S. Hirzel Verlag Leipzig, 58–70 (1944)
10. Winfree, A.T.: The prehistory of the Belousov-Zhabotinsky Oscillators. J. Chem. Educ. **61**, 661–663 (1984)
11. Prigogine, I., Nicolis, G.: On symmetry-breaking instabilities in dissipative systems. J. Chem. Phys. **46**, 3542–3550 (1967)

12. Prigogine, I., Lefever, R.: On symmetry-breaking instabilities in dissipative systems II. J. Chem. Phys. **48**, 1695–1700 (1968)
13. Prigogine, I.: Zeit, Struktur und Fluktuationen (Nobel-Lecture). Angew. Chem. **90**, 704–715 (1978)
14. Prigogine, I.: Vom Sein zum Werden. R. Piper & Co Verlag, München, Zürich (1979)
15. Brdička, R.: Grundlagen der Physikalischen Chemie, 10th edn. VEB Deutscher Verlag der Wissenschaften, Berlin (1971)
16. Haken, H.: Erfolgsgeheimnisse der Natur - Synergetik: die Lehre vom Zusammenwirken. Deutsche Verlags-Anstalt, Stuttgart (1981)
17. Haken, H.: Synergetik - Eine Einführung, p. 155. Springer-Verlag, Heidelberg (1990)
18. Haken, H.: Synergetics - Cooperative Phenomena in Multi-component Systems. B.G. Teubner, Stuttgart (1973)
19. Haken, H.: Synergetics - A Workshop, Preface. Springer Verlag, Heidelberg (1977)
20. Ebeling, W. Strukturbildung bei irreversiblen Prozessen. Mathem. Naturw. Bibliothek Bd. 60. BSB B.G. Teubner, Leipzig (1976)
21. Franck, U.F., Wicke, E.: Kinetic of Physicochemical Oscillations, vol. II Reprints of submitted papers. Fotodruck J. Mainz, Aachen (1979)
22. Willamowski, K.-D., Rössler, O. E.: Irregular oscillations in a realistic abstract quadratic mass action system. In: Proceedings of the Discussion Meeting - Kinetics of Physicochemical Oscillations in Aachen, pp. 505–513 (1979)
23. Gray, P., Scott, St.K.: Chemical Oscillations and Instabilities - Nonlinear Chemical Kinetics. Oxford Science Publications, Clarendon Press Oxford, p. 171 (1990)
24. Jaeger, N.I., Plath, P.J., van Raaij, E.: Modulated Catalytic Oscillations of the Oxidation of Methanol on Alumosilicate Catalysts Containing Pd. Heterogeneous Catalysis **2**, 15–20 (1979)
25. Jaeger, N.I., Plath, P.J., van Raaij, E.: Chemische Oszillationen bei der Methanoloxidation an einen Pd-Trägerkatalysator. Z. Naturforschung **36a**, 395–402 (1981)
26. Plath, P.J., Möller, K., Jaeger, N.I.: Cooperative Effects in Heterogenuous Catalysis Part II - Analysis and Modelling of the Temperature Dependence of the Oscillating Catalytic Oxidation of CO on a Pallydium Alumniumoxide supported Catalyst. J. Chem. Soc., Faraday Trans. I **84**(6), 1751–1771 (1988)
27. Haberditzl, A.Th., Jaeger, N.I., Plath, P.J.: Langzeitverhalten der bistabilen Oxidation des Methanols an Pd-Trägerkatalysatoren. Z. Phys. Chemie, Leipzig **265**, 449–463 (1984)
28. Jaeger, N.I., Plath, P.J., Svensson, P.: Toroidal Oscillations During the Oxidation of Methanol on Zeolite Supported Palladium. In: Rensin L., Jaeger N.I. (Eds), Temporal Order - Springer Series in Synergetics, vol. 29, pp. 101–102. Springer-Verlag, Heidelberg (1985)
29. Herzel, H., Plath, P., Svensson, P.: Experimental evidence of homolinic chaos and type-II intermittency during the oxidation of methanol. Physica D **48**, 340–352 (1991)
30. Peitgen, H.-O., Richter, P.: Harmonie in Chaos und Kosmos - Bilder aus der Theorie dynamischer Systeme. Die Sparkasse in Bremen, Bremen (1984)
31. Peitgen, H.O., Jürgens, H., Saupe, D.: Bausteine des Chaos: Fraktale, p. 440. Springer-Verlag und Klett-Cotta, Berlin, Heidelberg und Stuttgart (1992)
32. Mandelbrot, B.B.: Fractals - Form, Chance, and Dimension. W.H. Freeman and Company, San Francisco (1975)

33. Wilson, K.G.: Die Renormierungsguppe. Spektrum der Wissenschaften **10**, 67–82 (1979)
34. Wolfram, St.: Universality and Complexity in Cellular Automata. Physica D **10** vii–xii and 1–35 (1984)
35. Toffoli, T., Margolus, N.: Cellular Automata Machines A New Environment for Modeling. MIT Press, Cambridge (1986)
36. Pietronero, L., Tosatti, E.: Fractals in Physics. Noth-Holland, Elsevier Science Publishers B.V, Amsterdam, New York (1986)
37. Avnir, D.: The Fractal Approach to Heterogeneous Chemistry. John Wiley & Sons, New York (1989)
38. Plath, P., Sauerbrei, S.: Apollonische Umordnung des Schaums - wie zerfällt Bierschaum wirklich? Brauindustrie **20**(7), 20–23 (2004)
39. Krinsky, V.I.: Autowaves: results, problems, outlooks. In: Krinsky, V.I. (ed.) Self-Organization - Autowaves and Structures Far from Equilibrium. Springer Series in Synergetics, vol. 28, pp. 9–19. Springer-Verlag, Heidelberg (1984)
40. Winfree, A.T.: When Time Breaks Down - the Three-dimensional Dynamics of Electrochemical Waves and Cardiac Arrhythmias. Princeton University Press, Princeton (1987)
41. Meinhardt, H.: The Algorithmic Beauty of Sea Shells. Springer-Verlag (1998)
42. Gerhardt, M., Schuster, H., Tyson, J.J.: A Cellular Automaton Model of Excitable Media Including the Effect of Curvature and Dispersion. Science **247**, 1563–1566 (1990)
43. Markus, M., Krafczyk, M., Hess, B.: Randomized automata for isotropic modelling of two and three-dimensional waves and spatiotemporal chaos in excitable media. In: Holden, A.V., Markus, M., Othmer, H.G. (eds.) Nonlinear Wave Processes in Excitable Media. Plenum Press, New York (1991)
44. Nettesheim, S., von Oertzen, A., Rotermund, H.H., Ertl, G.: Reaction diffusion patterns in the catalytic CO-oxidation on Pt(110): Front propagation and spiral waves. J. Chem. Phys. **98**, 9977–9985 (1993)
45. Radons, G., Ditzinger, T., Friedrich, R., Henning, A., Kouzmichev, A., Westkämper, E.: Nonlinear dynamics and control of ripple formation in abrasive water-jet cutting. In: Radons, G., Neubauer, R. (eds.) Nonlinear Dynamics of Production Systems, pp. 391–410. Wiley-VCH Verlag GmbH & Co KGaA, Weinheim (2004)
46. Photo: Th. Rabbow
47. Mora, A., Haase, M., Rabbow, Th, Plath, P.J., Lehle, B.: Modelling laser-induced jet-chemical etching - discrete and continuous approaches. In: Plath, P.J., Haß, ECh. (eds.) Vernetzte Wissenschaften - Crosslinks in Natural and Social Sciences, pp. 137–152. Logos Verlag, Berlin (2008)
48. Jaeger, N.I., Möller, K., Plath, P.J.: Cooperative Effects in Heterogenuous Catalysis Part I - Phenomenology of the Dynamics of Carbon Monoxide Oxidation on Palladium Embedded in a Zeolite Matrix. J. Chem. Soc. Faraday Trans. I **82**, 3315–3330 (1986)
49. Plath, P.J.: Synergetic description of the catalytic CO-oxidation. In: Plath, P.J., Haß, ECh. (eds.) Vernetzte Wissenschaft - Crosslinks in Natural and Social Sciences, pp. 15–46. Logos Verlag, Berlin (2008)
50. Ballandis, C., Plath, P.J.: A New Discrete Model for the Non-Isothermic Dynamics of the Exothermic CO-Oxidation on Palladium Supported Catalyst. J. Non-Equilib. Thermodyn. **25**, 301–324 (2000)

The Physics of Finance: Collective Dynamics in a Complex World

Lisa Borland

Integral Development Corporation,
3400 Hillview Ave, Palo Alto, CA USA
lisa@evafunds.com

Abstract. Exploring the dynamics of financial time-series is an exciting and interesting challenge because of the many truly complex interactions that underly the price formation process. In this contribution we describe some of the anomalous statistical features of such time-series and review models of the price dynamics both across time and across the universe of stocks. In particular we discuss a non-Gaussian statistical feedback process of stock returns which we have developed over the past years with the particular application of option pricing. We then discuss a co-operative model for the correlations of stock dynamics which has its roots in the field of synergetics. In all cases numerical simulations and comparisons with real data are presented.

Keywords: finance, fat-tails, long-range memory, statistical feedback, correlation dynamics

1 Introduction

The field of finance is one with a rich history of its own. Yet in recent years it has attracted more and more people with scientific backgrounds, especially from the field of physics. This is not only due to the fact that physicists are particularly well-equipped to tackle many of the challenges of mathematical finance which provides alternative career paths on Wall Street, but also because vast amounts of financial data are now available. Nearly every transaction on a tick-by-tick basis for thousands of stocks and other financial instruments is being recorded electronically as we speak, resulting in something akin to a huge data-base of one of the most complex systems we can imagine. Hardly the result of a controlled experiment in a physics lab, the price formation process of a publicly traded asset is clearly the product of a multitude of evasive interactions. Individuals around the globe post orders to buy or sell a particular stock at a particular price. Transactions are cleared at a certain price at a given time, either by passing through the hands of a specialist on the trading floor, or automatically on the many electronic markets which have sprouted in recent years. Apart from fundamental properties of the company whose stock is being traded, factors such as supply and demand clearly must affect the price of stocks, as well as general trends in the particular industry in question. Stock specific events, such

A. Pelster and G. Wunner (eds.), *Selforganization in Complex Systems: The Past, Present, and Future of Synergetics*, Understanding Complex Systems,
DOI: 10.1007/978-3-319-27635-9_6

as mergers and acquisitions, have a big impact, as do world events, such as wars, terrorist attacks, and natural disasters. A recent example of this are the dramatic events seen in 2007 and 2008 which are perhaps due to fundamental flaws in our credit-based economy. The current European debt crisis is another example.

Stocks are traded for the most part on a central limit order book, such as the New York Stock Exchange. Modeling the intricate dynamics and microstructure of this order book is a field of study which has gotten some traction in recent years [1, 2]. When comparing to physics, that level of description can be seen as the microscopic level. However, it is often more tractable to use a mesoscopic description which aims at describing the price process as a stochastic Langevin equation where the key feature is how to capture the volatility, or noise, that drives the process. This is the most important effect since stock price changes (or returns) form moment to moment are essentially unpredictable so the deterministic part of the equation is less interesting (though of course, if you can predict it ever so slightly then you might become quite wealthy!)

For many years and in a large body of the financial literature, the random nature of price time-series was modeled by most as a simple Brownian motion. The first to propose such a model was Bachelier in his thesis in 1900, which lay largely undiscovered until much later when Black and Scholes wrote their famous paper in 1973 based on a very similar model. They made important contributions in particular to the pricing of options, for which they received the Nobel Price [3]. Options are traded instruments that give the right, not the obligation, to buy a stock at a later date at a certain price, called the strike price. In Black and Scholes work the log price is assumed to follow a Gaussian distribution and even today many trading assumptions and risk control notions are based off of that prior.

However, in more recent years there has been a large body of work which - in quite some detail and statistical accuracy due largely to the vast amount of observations available - has been able to document that the time-series of financial market data show some intriguing statistical properties, which deviate quite substantially from the Gaussian assumption. These features are referred to as stylized facts (cf [4, 5]). It is interesting to note that many of the stylized facts appear to be universal, in the sense that they are exhibited by a vast variety of financial instruments, as different as commodities like wheat, currencies such as the Euro-Dollar rate, and individual stocks. Some are also exhibited over various periods of history (and so can be seen as stationary), others are exhibited on a multiple of time-scales (and so can be seen as self-similar). Other interesting properties pertain to the dynamics and statistics of the cross-section of financial instruments. Ultimately, the goal is to comprehend and model the joint stochastic process of the price formation dynamics of the collection of stocks across time, so investigating various statistical properties both across time and across stocks is essential. The challenge then lies in coming up with a model that captures the dynamics inherent in the data. In addition, it is desirable that such a model is somewhat intuitive, parsimonious, and analytically tractable.

In this chapter we shall review a class of models that we have proposed in recent years, aimed at modeling the stock price dynamics in such a way as to capture as many of the statistical properties of real financial data as possible. We also show how these models could be used for important applications such as the pricing of options and other derivative instruments. In the first part we focus on financial time-series, and in the second part we look at cross-sectional dynamics across a universe of stocks. In all cases we shall see that notions of nonlinear cooperative feedback appear to be essential ingredients of this very complex real-world system.

2 Stylized Facts across Time

2.1 Returns

While a random walk with Gaussian noise will show fluctuations that are relatively constant over time, the case is quite different for a time-series of stock returns, usually defined as relative price changes or log price changes. As shown in Figure 1, there appear to be intermittent clusters of higher versus lower magnitude returns. This phenomenon is known as volatility clustering, and we will look at that in more detail further along. The probability distribution of these financial returns are typically fat-tailed. In fact, it has been shown that the distribution of both intra-day and daily returns can be very well fit by a power-law tail of about -3 (referred to by some as the cubic law of finance [6]). This tail index is consistent with that of a Tsallis distribution [7] with index q in the range 1.4-1.5, which fits very well to that of the returns (Figure 2). We shall work a lot with this class of distributions (which are equivalent to Student-t distributions), because this very same distribution fits to returns from a wide variety of financial instruments, such as stocks, currencies and commodities, with much the same q-index. Furthermore, this fat-tailed nature of returns holds for data from several different geographic regions such as North America, Japan and Europe. Because of this rather universal behavior, the non-Gaussian distribution is an important stylized fact. Clearly then, any model of financial data should try to capture at least this important feature. A related stylized fact is constituted by the observation that, as the time lag over which returns are calculated in increased, this power-law behavior of the distribution of returns persists for quite a while, decaying slowly to a Gaussian distribution as the lag increases, becoming indistinguishable from the Gaussian as the lag approaches something on the order of a few months [5].

2.2 Volatility

Volatility is typically defined as the square root of the squared variation of returns. Obviously, this definition is not unique because one can choose to calculate the squared variation over an arbitrary historical period. As it turns out, the statistical properties of volatility will not be too sensitive to this exact choice. What

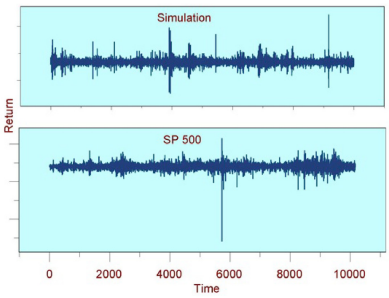

Fig. 1. Market Returns (bottom) and from our multi-time scale model (top)

do we know about volatility? Why do we care? In order to answer these questions, our view is to stand back a bit, and let the data speak. Are there consistent patterns in the statistical properties of the data? Are they universal? If financial data were Gaussian distributed, then the volatility would be the standard deviation of that distribution. In fact, this assumption is still made both by many practitioners and in many theoretical works in mathematical finance, although there is the increasing awareness of the shortfalls of such an assumption. In practice, for example, the devastating effects of the Gaussian assumption were seen in August of 2007 and October of 2008, when investors panicked claiming that 25-sigma events were wiping them out. In fact, these types of statements are only true if the underlying distribution is assumed to be Gaussian. If a heavy tailed distribution such as the Tsallis with q = 1.4 or 1.5 is assumed, then the behavior of the markets as we have seen them in recent years is to be expected, with a probability of about one or two extreme events per decade. Clearly it is extremely important for hedging and risk control purposes to have a richer understanding of volatility.

Data shows that time series of the volatility of the Dow Jones index for the past century exhibits clear periods of lower and higher volatility, typically clustered together. Note that while the distribution of returns is fat-tailed, volatility itself follows a close-to log-normal distribution. Interestingly, the same type of statistics is valid for volatility calculated every 5 minutes intra-day, implying a self-similar structure.The fact that volatility is self-similar on different timescales is a universal feature. The clustering feature that is observed is a signature that there is memory inherent in volatility; if volatility is high, it will persist for a while. This memory can be quantified by looking at the autocorrelation of volatility over increasing time lags. Such an analysis shows that there is a persistence which decays as a power law as the lag increases. There is also the feature of causality in the structure of volatility. In other words, some statistical properties of future volatility conditioned on past volatility are not invariant to reversing

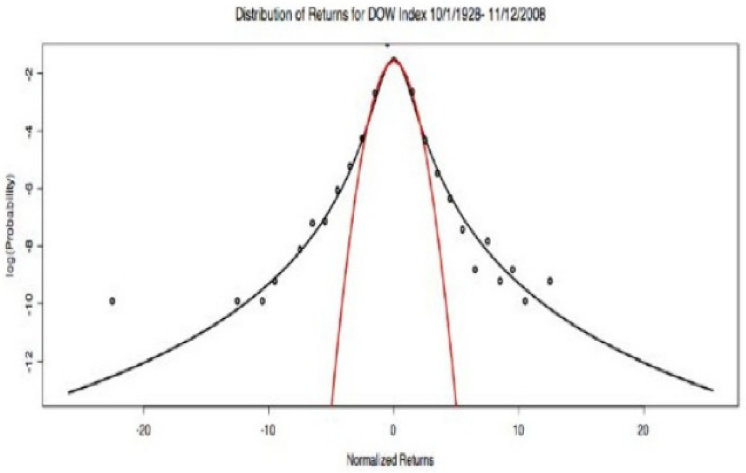

Fig. 2. The distribution of returns is well fit by a Tsallis distribution

the time order of a volatility time series. This reinforces the notion of memory and a dependency of volatility on its own past behavior. Another stylized fact of volatility that exhibits some asymmetry is the so-called leverage effect, which describes the positive correlation between negative returns and volatility; large negative price drops will give rise to subsequently higher volatility.

Some other interesting statistical features relate to the conditional volatility. Specifically, if you look at the probability of observing a volatility of a certain magnitude given that a volatility shock larger than some threshold was just observed, you will see something that translates into an Omori law for volatility. Just as earthquakes are followed by aftershocks, so are volatility shocks followed by other larger than normal shocks.

3 Stock Price Models

Several different models [8–10] have been proposed in an attempt to capture fat tails and volatility clustering which don't exist in the Gaussian Bachelier or Black-Scholes model. Popular approaches include Levy processes, which induce jumps and thus fat tails on short time- scales, but convolve too quickly to the Gaussian distribution as the time-scale increases. Stochastic volatility models, such as the Heston model where the volatility is assumed to follow its own mean-reverting stochastic process, reproduce fat tails, but not the long memory observed in the data. The same holds true for the simplest of Engle's Nobel prize

winning GARCH models in which the volatility is essentially an autoregressive function of past returns. Multifractal stochastic volatility models (similar to cascade models of turbulent flow) are another promising candidate [11], reproducing many of the stylized facts, lacking mainly in that they are strictly time reversal symmetric in contrast to empirical evidence. In addition, most of the above mentioned models are difficult if not impossible to deal with analytically. Analytic tractability is desirable for reasons such as efficiently calculating the fair price of options or other financial derivatives which in their own right are traded globally in high volumes and will be discussed in more detail later on. For now we focus on presenting a somewhat realistic model of stock returns themselves which we developed a few years ago [12–14]

3.1 A Non-Gaussian Model of Returns

The standard Black-Scholes stock price model reads

$$dS = \mu S dt + \sigma S d\omega \tag{1}$$

where $d\omega$ represents a zero mean Brownian random noise correlated in time t as

$$< d\omega(t) d\omega(t') >_F = \delta(t - t'), \tag{2}$$

Here, μ represents the rate of return and σ the volatility of log stock returns. This model implies that stock returns follow a lognormal distribution, which is only an approximate description of the actual situation. Furthermore, there is no memory in this process as it is purely Markovian. As already mentioned, it is observed that the power-law statistics of the distributions of real returns are very stable, well-fit by a Tsallis distribution of index $q = 1.4$ for returns taken over time-scales ranging from minutes to weeks, only slowly converging to Gaussian statistics for very long time-scales. Here we review a model of the underlying stock which is consistent with the returns distribution.

Our model bases on the non-Gaussian model [12, 13], where it was proposed that the fluctuations driving stock returns could be modeled by a statistical feedback process, namely:

$$dS = \mu S dt + \sigma S d\Omega \tag{3}$$

where

$$d\Omega = P(\Omega)^{\frac{1-q}{2}} d\omega. \tag{4}$$

In this equation, P corresponds to the probability distribution of Ω, which simultaneously evolves according to the corresponding nonlinear Fokker-Planck equation [15, 16]

$$\frac{\partial P}{\partial t} = \frac{\partial P^{2-q}}{\partial \Omega^2}. \tag{5}$$

The index q will be taken $q \geq 1$. It can be solved exactly yielding

$$P = \frac{1}{Z(t)} (1 - (1-q)\beta(t)\Omega(t))^{\frac{1}{1-q}} \tag{6}$$

The exact form of the coefficients Z and β are given in [13].

Eq. (6) recovers a Gaussian in the limit $q \to 1$ while exhibiting power law tails for $q > 1$. In that case, our model is exactly equivalent to the Black-Scholes model.

The statistical feedback term P can be seen as capturing the market sentiment. Intuitively, this means that if the market players observe unusually high deviations of Ω (which is essentially equal to the de-trended and normalized log stock price) from the mean, then the effective volatility will be high because in such cases $P(\Omega)$ is small, and the exponent $1-q$ a negative number. Conversely, traders will react more moderately if Ω is close to its more typical or less extreme values. As a result, the model exhibits intermittent behavior consistent with that observed in the effective volatility of markets. To incorporate the subtle effect of skew and the stylized fact known as the leverage effect, we further extend the stock price process as in [14].

4 Option Pricing

Once a model of stock price dynamics is proposed, it can be used for various applications such as estimating and managing risk, or for pricing derivative instruments, such as options. Options are financial derivatives which in their own right are traded globally in high volumes. They fill important financial functions with respect to hedging and risk control, as well as offer purely speculative opportunities. In short, options are financial instruments which depend in some contingent fashion on the underlying stock or other asset class. The simplest example is perhaps the European call option. This is the right (not obligation) to buy a stock at a certain price (called the strike K) at a certain time (called the expiration T) in the future.

Contracts similar to options were exploited already by the Romans and story has it that Thales the Greek mathematician used call options on olives to make a huge profit when he had reason to believe that the harvest would be particularly good. In Holland in the 1600s, tulip options were traded quite a bit by speculators prior to the famous tulip bubble. But it wasn't until 1974 that the fair price of options could be calculated somewhat reliably with the publication of the Nobel-prize winning Black-Scholes formula. This is still the most widely used option pricing model, not because of its accuracy (since it is based on a Gaussian model for stock returns which, as we discussed above, is unrealistic) but rather due to its mathematical tractability (which exists due to the same Gaussian assumptions). In fact, an impressive school of mathematical finance has been developed over the past three decades, and is based largely on notions stemming from the famous Black-Scholes paradigm.

Because real stock returns exhibit fat tails, yet the Black-Scholes pricing formula is based on a Gaussian distribution for returns, the probability that the stock price will expire at strikes far from its current price will be underestimated. Traders seem to correct for this intuitively; for the Black-Scholes model to match empirical option prices, higher volatilities must be used the

farther away the strike price is from the current stock price value. A plot of these Black-Scholes implied volatilities as a function of the strike price is thus not constant but instead most typically a convex shape, often referred to as the volatility smile. This way of representing option prices in terms of the Black-Scholes volatility is so widely used that prices are often quoted just in terms of this quantity, most often referred to simply as the vol.

The property that the Black-Scholes volatility exhibits a smile or skew shape that slowly flattens out as the time to expiration increases is the most important stylized fact of options. Many of the more realistic models convolve way too quickly to yield a Gaussian distribution although they might reproduce fat tails over a small time-scale. One of the nice properties of our statistical feedback models is just this slow convolution to a Gaussian. Hence, option pricing based on this model could be quite interesting. Another challenge with many models is related to notions pertaining to the definition of a unique equivalent martingale measure. Defining such a measure was the key ingredient in Black and Scholes seminal work, but many more complicated models that deviate from the Gaussian have often failed. Indeed, we were able to find such a unique equivalent Martingale measure for Eq(1), and this resulted in the ability to obtain closed-form solutions for pricing European call options. The price f of such an option is given by its expectation value in a risk-free (martingale) world as

$$f = E[e^{-rT} \max[S(T) - K, 0]] \tag{7}$$

where r is the risk-free rate. Assuming that S follows Eq(3) we obtain [13, 14]

$$f = S_0 \int_{d_1}^{d_2} \exp\left\{\sigma\Omega_T - \frac{\sigma^2}{2}[1 - (1-q)(\beta(T)\Omega_T^2)]\right\}$$
$$P_q(\Omega_T)d\Omega_T - e^{-rT}K \int_{d_1}^{d_2} P_q(\Omega_T)d\Omega_T \tag{8}$$

with P_q as in Eq. (6) and the explicit form of the coefficients given in [14]. These formulae are analytically tractable and converge to the Black-Scholes equation as $q \to 1$. However, for $q > 1$ they incorporate the effects of fatter tails. We also found option pricing formaulae for the generalized model with skew [14], and further work was done by [17]. Since a value of $q = 1.4$ nicely fits real returns over short to intermediate time horizons, this model is clearly more realistic than the standard Gaussian model. Using that particular value of q as calibrated from the historical returns distribution, fair prices of options can be calculated easily and compared with empirical traded option prices, exhibiting a very good agreement. In particular, while the Black-Scholes equation must use a different value of the volatility for each value of the option strike price in order to reproduce theoretical values which match empirical ones, the $q = 1.4$ model uses just one value of the volatility parameter across all strikes. One can calculate the Black-Scholes implied volatilities corresponding to the theoretical values based on the $q = 1.4$ model, and a comparison of this with the volatility smile observed in the market will reflect how closely the $q = 1.4$ model fits real

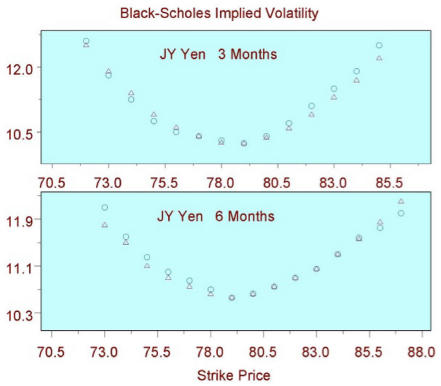

Fig. 3. Implied Black-Scholes volalities from the $q = 1.4$ model mactch extremely well to real traded values

prices. Excellent agreement over several expirations (time horizons) can be seen in Figure 3.

5 The Multi Time-Scale Model

Although very successful for pricing options, the statistical feedback model is still not entirely realistic. The main reason is that there is one single characteristic time in that model, and in particular the effective volatility at each time is related to the conditional probability of observing an outcome of the process at time t given what was observed at time $t = 0$. For option pricing this is perfectly reasonable because one is interested in the probability of the price reaching a certain value at some time in the future, based entirely on ones knowledge now. But this is a shortcoming as a model of real stock returns. In particular, in real markets, traders drive the price of the stock based on their own trading horizon. There are traders who react to each tick the stock makes, ranging to those reacting to what they believe is relevant on the horizon of a year or more, and of course, there is the entire spectrum in-between. Therefore, an optimal model of real price movements should attempt to capture this existence of multiple time-scales and long-range memory. We shall now show how we extend the above model to include multiple time-scales.

The effective volatility term $P^{1/(1-q)}$ in the statistical feedback model Eq(3) can be rewritten in the form

$$\sqrt{N'(1-(1-q)\beta'(\Omega(t)-\Omega(0))^2)} \tag{9}$$

by inserting the expression for P explicitly. where N' and β' are time-dependent constants. In this form it is clear that the volatility depends on the change in log-price at time t to the initial time t_0, since Ω is essentially the log of the price. A natural extension is to generalize to include feedback over not just one but

many time-scales, as discussed in [18]). The random return is constructed as the product of a time dependent volatility σ_i and a random variable ω_i of zero mean and unit variance:

$$dy_i = \mu dt + \sigma_i d\omega_i \tag{10}$$

where μ is the average drift, which we will set to zero in the sequel, meaning that we measure all returns relative to the average drift. The volatility is written to include feedback over multiple time-scales $(i - j)$.

$$\sigma_i^k = \sigma_0 \sqrt{1 + g \sum_{j=1}^{\infty} \frac{1}{(i-j)^\gamma} (y_i^k - y_j^k)^2} \tag{11}$$

where i corresponds to time. The parameter g is a coupling constant that controls the strength of the feedback, σ_0 is the baseline volatility and γ is a factor that determines the decay rate of memory in the system which can also be seen as the relative importance between short-term and long-term traders. This model is well-defined as soon as $\sum_{j=0}^{\infty} \frac{g}{i-j}^\gamma < 1$ or approximately that $\frac{g}{1-\gamma} < 1$ and $\gamma > 1$ [18]. The model can be calibrated to real stock data yielding $\gamma = 1.15$ and $g = 0.12$, and it is seen that all of the main stylized facts of stock returns are reproduced. Interestingly, the model also shows multi-fractal scaling akin to that seen in turbulent systems, although there is no explicit multi-fractality injected in the model. These results are discussed in [18]. In Figure(1) a simulation of that model is shown. The process describes real data very well, with obvious periods of lower and higher volatility clustering together.

6 Statistical Signatures across Stocks : Self-orgnaization of correlation

Up until now we have been focused on understanding and modeling the dynamics of stock returns across time. However, in order to grasp properties of the full joint stochastic process driving markets we turn our attention to the cross-sectional dynamics, across a universe of stocks at any given point in time. Along these lines, there have in recent years been several studies which focus on exploring the structure and dynamics of correlations across the different stocks that comprise the market [19–25]. In particular, these models and analysis explore correlations during market stress or times of bubbles, panic and crashes. This is important because it is under such extreme scenarios that investors are at most risk; their usual models and world-views might break down and the results could be devastating as seen in August 2007, October 2008, or during the so called Flash Crash of May 2010. Some of our contributions in this area [24, 25] has been to see if there are any particular cross-sectional statistical signatures in these periods of market panic. To get a grasp on the cross-sectional distribution of stock returns at a given time point, we can look at moments such as the mean, standard deviation, skew and kurtosis. We then look at these as a

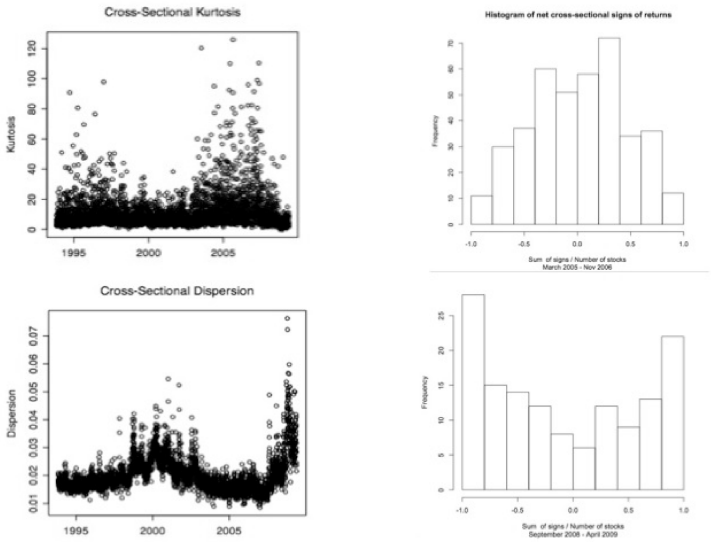

Fig. 4. Statistical signatures in normal and panic times

function of time. The standard deviation of returns is widely referred to as dispersion. Calculated across a universe of 1500 US stocks and plotted out for the time period 1993 - 2009, it is striking to see that the dispersion gets relatively big during the time periods defined as panic according to the discussion above. However, the more striking discovery is to plot out the cross-sectional kurtosis alongside the dispersion, or together with market returns (Figure (5)). Even by eye it is quite clear that there is a strong negative correlation between the two quantities, which is in fact about -25%. In times of panic, dispersion is high yet excess kurtosis practically vanishes. In more normal times, the dispersion is lower but the cross-sectional excess kurtosis is typically very high.

We want a model that can explain all of these findings, namely to preserve the fat-tailed time series properties of stocks, but which gives rise to the remarkable reduction in kurtosis and increase in correlations, cross-sectionally, that are characteristic of market panic. In such times, dispersion is high yet kurtosis is low, which implies that the data are more Gaussian in times of panic. This can be explained partially by the fact that the volatilities of the individual stocks are higher yet more alike in times of panic, a statement that is borne out by the data [24]. This might be one effect contributing to our findings, but we believe that the behavior of cross-sectional correlations is what drives the statistical signatures that we found. As a proxy for the collective behavior of all stocks in

the market, we define the following quantity

$$s = \frac{s_{up} - s_{down}}{s_{up} + s_{down}} \tag{12}$$

where s_{up} is the number of stocks that have positive returns over a given interval, and $s_{down}$is the number of stocks that have negative moves on that same interval (for example a day). If $s = 0$ then roughly the same number of stocks moved up as down, and the assumption is that the stocks had little co-movement and so were uncorrelated. If all stocks move together either up or down, though, the value of s will be +1 or -1 and the stocks will have high correlation. So, the following picture emerges: If $s = 0$ there is no correlation, and we are in a disordered state. However if $s \neq 0$ then there is correlation and we are in an ordered state. We will now make a leap and borrow some terminology from physics. We shall call s the order parameter. It is a macroscopic parameter that tells us whether there is order and correlation in the system, or not. In physics, in particular in the field of non-equilibrium thermodynamics and synergetics [26], the concept of the order parameter is often used to describe systems that exhibit spontaneous self-organization. Examples range from chemical kinetics to laser dynamics, from fluid dynamics to biological systems; from collective behavior in both the animal and human world to cloud formation. To illustrate the concept, let us look at an example which should be familiar and intuitive to most, namely magnetism.

In a ferromagnetic system, the total magnetic moment depends on the orientation of the individual magnetic spins comprising the system. It is proportional to the quantity

$$m = \frac{m_{up} - m_{down}}{m_{up} + m_{down}} \tag{13}$$

where m_{up} and m_{down} denote the number of spins lined up and down respectively. The distribution of possible outcomes of this macroscopic quantity is given by

$$P(m) = N \exp(F(m, T)) \tag{14}$$

where T is the temperature, N is a normalization factor and F is the free energy of the system. Depending on the value of T, the magnetic system will either be in an ordered or disorderd state. Assuming one can perform a Taylor expansion of F and invoking symmetry arguments, the corresponding Langevin equation takes the form

$$\frac{dm}{dt} = -\frac{a}{2}m - \frac{b}{4}m^3 + W_t \tag{15}$$

where W_t is thermal noise. The coefficient a can be written as

$$a = \alpha(T - T_c) \tag{16}$$

where T_c is the so-called critical temperature. One can envision these dynamics as motion in a potential well V given by $V(m) = -F(m)$. If $T > T_c$, the only minimum is the trivial one at $m = 0$. However, for $T < T_c$ there are two real roots appearing, yielding non-zero values of m. Clearly, m can be positive or

negative, depending on which minima is reached by the system. This is referred to as symmetry breaking. Due to the noise, the dynamics can also drive m from one minimum to the other. Because the value of T determines whether the system is in the disordered state ($m = 0$) or the ordered state ($m \neq 0$), it is called the control parameter. The probability distribution of the system in the disordered state will be a unimodal one, while the probability distribution of m in the ordered state will be bimodal. As T passes from above to below T_c, or vice-versa, there is clearly a phase transition: the state of the system is drastically altered. In this type of symmetric system, the phase transition is referred to as a second order one.

In the current setting, we make an analogy between the variable s and the magnetic moment m. We have observed rather drastic changes in the cross-sectional distribution of stocks in the times of panic versus more normal market conditions [24]. Histograms of s in both periods show that in normal times, s is unimodal, and in panic times we obtain a bimodal distribution consistent with the frame-work of a phase transition leading to self-organization in panic times (see Figure 4).

We postulate that the dynamics of s be given by

$$\frac{ds}{dt} = -\frac{a}{2}s - \frac{b}{4}s^3 + W_t. \tag{17}$$

We propose that

$$a = \sigma_c - \sigma_0 \tag{18}$$

where W_t is a Gaussian noise term and σ_0 corresponds to the baseline volatility level of stocks. This volatility is assumed constant across all instruments, and essentially measures the general uncertainty in the environment, so in this sense acts much as the temperature in the magnetic system. Note that it is the feedback effects in the system which induce stock-specific variations in volatility over time, and can largely explain most of the excess volatility observed in stock time-series, whereas the parameter σ_0 is not driving the stock-specific dynamics, but simply describes a "global" level of risk. The quantity σ_c would correspond to a critical level of uncertainty, below which the market is in a normal phase, and above which we have the onset of panic. Much as in the case of ferromagnetism, where the control parameter T can be tuned externally above or below the critical temperature, in our model the uncertainty level σ_0 captures the external environment. In a sense it represents the general perception of risk in the public mind. Our hypothesis is then that financial markets appear to exhibit a phase transition from the disordered to ordered state, after crossing a critical level of risk perception. Putting the dynamics together, we have the multi time-scale feedback process for each stock k

$$dy_i^k = \sigma_i^k d\omega_i^k \tag{19}$$

with $k = 1 \cdots N$, and the volatility of each stock k given by Eq(11) The random variables ω_i^k are drawn from a Gaussian distribution, uncorrelated in time such that $< \omega_i^k \omega_{i+\tau}^k >= \delta(i-(i+\tau))\tau$, yet amongst themselves at a given time point

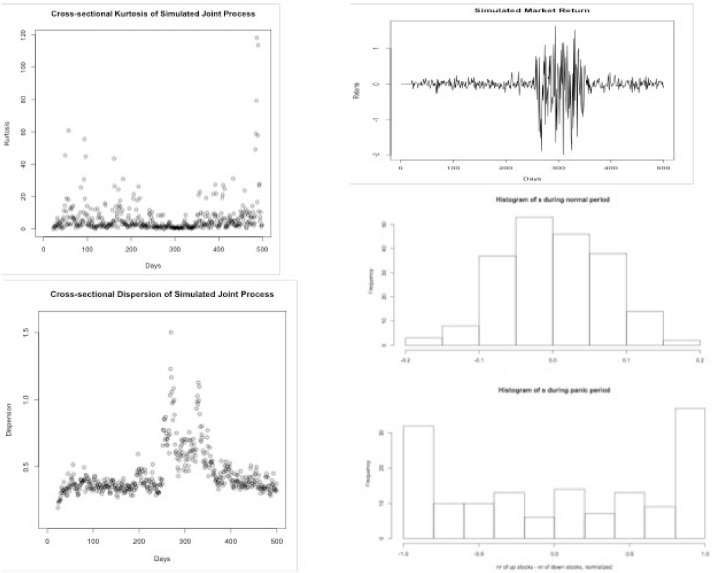

Fig. 5. Results of the simulation of the joint process

i across stocks k, they are correlated with correlation $|s|$. The macroscopic order parameter s is therefore just a signature of the cross-stock correlations, whose dynamic behavior manifests itself in the order parameter equation

$$\frac{ds}{dt} = -\frac{a}{2}s - \frac{b}{4}s^3 + W_t. \tag{20}$$

The coefficients must always be such that $|s| \leq 1$ which can be imposed by running the dynamics of s on a real valued variable $\hat{s}$ such that $s = \tanh(\hat{s})$.

What do we expect to see from this model? We have already seen that across time, it models very well many properties of real financial time-series. Across stocks, if $\sigma_0 < \sigma_c$, correlations fluctuate around $s = 0$ and we expect to see a unimodal distribution of s. The cross-sectional kurtosis should be rather high since there is no mechanism to cause either stocks or stock volatilities to have any co-movement at all, so at each time point it is as if the cross-sectional returns are drawn from a Gaussian process with stochastic volatility, yielding a fat-tailed distribution as the superposition. Then as the market crashes with $\sigma_0 > \sigma_c$, the system enters a phase transition. The order parameter s becomes $s \neq 0$ and the system enters the ordered phase with high co-movement. Because the random variables ω_i^k are now correlated across stocks, cross-sectional returns will be more similar and the distribution will have lower kurtosis. Additionally, due to the fact that the phase transition is triggered by an external shock in volatility, all stocks will tend to have higher volatilities and higher cross-sectional dispersion.

Simulations of this model for the joint stochastic process of stocks were performed and we refer the reader to [24] for details on the implimentation. Here we provide a summary. The baseline volatility was assumed to be $\sigma = 0.2$, and at a certain time a volatility shock $\sigma_{shock} = 0.6$ (consistent with levels observed in the VIX volatility index in late 2008) was applied to the system (see Figure 5). This induced the phase transition from the disordered state where correlation among stocks are relatively low, centered around zero, to a highly ordered state where the correlations are different from zero. We found that the main features of financial markets are captured within this framework. The order parameter s goes from 0 (the disordered state) to $s \approx 0.8$ (the ordered state) at the time of the volatility shock. When the shock subsides, it returns to the disordered state again. As expected, the market volatility rises when s is in the ordered state, which corresponds to the panic phase. In addition, the cross-sectional dispersion rises during the market panic, while the cross-sectional kurtosis drops close to zero. The correlation between the two quantities is in this example -17%, consistent with empirical observations that also showed a strong negative correlation. Histograms corresponding to the distribution of the order parameter s in the normal market phase as well as in the panic phase are in excellent agreement with the empirical observations of the real market data, namely unimodal in the normal phase, and clearly bimodal during the panic time. Encouraged by these findings we extended this joint stochastic model to include skew and explored its self-similar properties on different time-scales, as presented in [25]. Further studies of interest in a similar vein were done by others [19].

7 Conclusion

We have reviewed the anomalous features inherent in financial data across time and across stocks, which reflect the very complex and nonlinear interactions leading to price formation in financial markets. Our approach has been to propose models that intuitively capture the dynamics that could be at play, and to verify them in that they can reproduce the observed statistical signatures and stylized facts, also in derivative markets such as options. Common to all our studies is that cooperative effects, memory and nonlinear feedback appear at play, so many interesting techniques for the field of statistical physics and synergetics can be applied. Continuously evolving and changing, the field of finance will certainly continue to pose interesting challenges for scientists and practitioners alike for years to come.

References

1. Bouchaud, J.-P., Gefen, Y., Potters, M., Wyart, M.: Fluctuations and response in Financial markets: The subtle nature of random price changes. Quantitative Finance **4**(2), 176–190 (2004)
2. Farmer, J., Gerig, A., Lillo, F., Mike, S.: Market efficiency and the long-memory of supply and demand: Is price impact variable and permanent or fixed and temporary? Quantitative Finance **6**(2), 107–112 (2006)

3. Black, F., Scholes, M.: The Pricing of Options and Corporate Liabilities. Journal of Political Economy **81**, 637–659 (1973)
4. Bouchaud, J.-P., Potters, M.: Theory of Financial Risks and Derivative Pricing. Cambridge University Press (2004)
5. Gopikrishnan, P., Plerou, V., Nunes Amaral, L.A., Meyer, M., Stanley, H.E.: Scaling of the distribution of fluctuations of financial market indices. Phys. Rev. E **60**, 5305 (1999)
6. Gabaix, X., Gopikrishnan, P., Plerou, V., Stanley, H.E.: A theory of power-law distributions in Financial market Fluctuations. Nature **423**, 267 (2003)
7. Tsallis:, C.: J. Stat. Phys. **52**, 479 (1988); Curado, E.M.F., Tsallis, C.: J. Phys. A **24**, L69 (1991); **24**, 3187 (1991); **25**, 1019 (1992)
8. Heston, S.L.: A closed-form solution for options with stochastic volatility with applications to bond and currency options. Rev. of Fin. Studies **6**, 327–343 (1993)
9. Cont, R., Tankov, P.: Financial modelling with jump processes. CRC Press (2004)
10. Bollerslev, T., Engle, R.F., Nelson, D.B.: ARCH models. In: Engle, R.F., McFadden, D. (eds.) Handbook of Econometrics, vol. 4. Elsevier Science, Amsterdam (1994)
11. Muzy, J.-F., Delour, J., Bacry, E.: Modelling fluctuations of financial time series: from cascade process to stochastic volatility model. Eur. Phys. J. B **17**, 537–548 (2000)
12. Borland, L.: Option Pricing Formulas based on a non-Gaussian Stock Price Model. Phys. Rev. Lett. **89**(N9), 098701 (2002)
13. Borland, L.: A Theory of non-Gaussian Option Pricing. Quantitative Finance **2**, 415–431 (2002)
14. Borland, L., Bouchaud, J.-P.: A Non-Gaussian Option Pricing Model with Skew. Quantitative Finance **4**, 499–514 (2004)
15. Tsallis, C., Bukman, D.J.: Anomalous diffusion in the presence of external forces: Exact time-dependent solutions and their thermostatistical basis. Phys. Rev. E **54**, R2197 (1996)
16. Borland, L.: Microscopic dynamics of the nonlinear Fokker-Planck equation: a phenomenological model. Phys. Rev. E **57**, 6634 (1998)
17. Vellekoop, M.H., Nieuwenhuis, J.W.: On option pricing models in the presence of heavy tails. Quant. Finance **7**, 563–573 (2007)
18. Borland, L., Bouchaud, J.-P.: On a multi timescale statistical feedback model for volatility fluctuations. The Journal of Investment Strategies, 1–40 (2012)
19. Preis, T., Kenee, D., Stanley, H.E., Helbing, D., Ben-Jacob, W.E.: Quantifying the Behavior of Stock Correlations Under Market Stress. Nature, October 2012
20. Lillo, F., Mantegna, R.: Variety and volatility in financial markets. Phys. Rev. E **62**, 6126–6134 (2000)
21. Sornette, D.: Why stock markets crash: Critical Events in Complex Financial Systems. Princeton University Press (2002)
22. Kaizoji, T.: Power laws and market crashes. Prog. Theor. Phys. Suppl. **162**, 165–172 (2006)
23. Raffaelli, G., Marsili, M.: Dynamic instability in a phenomenological mode of correlated assets. J. Stat. Mech., 8001 (2006)
24. Borland, L.: Statistical Signatures in Times of Panic: Markets as a Self-Organizing System. Quant. Finance **12**(9), 1367–1379 (2012)
25. Borland, L., Hassid, Y.: Market Panic on Different Time-Scales. ArXiv e-prints 1010.4917 (2010)
26. Haken, H.: Synergetics: an introduction. Springer (1977)

Part II

Complexity in Quantum Systems

Quantum Thermodynamics: A Case Study for Emergent Behavior

Günter Mahler

Institut für Theoretische Physik I,
Universität Stuttgart, 70550 Stuttgart, Germany
mahler@itp1.uni-stuttgart.de
http://itp1.uni-stuttgart.de/institut/arbeitsgruppen/mahler

Abstract. Any attempt to provide a foundation of thermodynamics faces this central question: how come that a qualitatively different type of behavior emerges (as an effective description) from the underlying physical substrate?
Quantum thermodynamics is able to show that the partitioning of a closed quantum system into a smaller and a significantly larger part typically gives rise to thermal properties of the former, even though the system as a whole continues to exhibit unitary motion. Being based on entanglement, this feature may show up already in rather small total quantum systems, the dynamics of which can still be solved exactly. Furthermore, it allows for nano-thermodynamics, an entirely self-contradictory concept in the classical regime.
This picture differes substantially from the classical (statistical) description: It is not the system as such, which is thermal; rather it is made thermal by its environment. Thermal behavior is thus "apparent" only, i.e. dependent on the way the observer chooses to look. A much closer look would make the thermal properties disappear – just like a portrait will become unrecognizable after focusing on individual pixels. However, that very type of "looking" has to be included as part of the detailed modeling. Operational quantum thermodynamics establishes an intuitive link between the new quantum and the old classical description.

Keywords: Partitions, entanglement, typicality, Hilbert-space statistics, thermal attractor, quantum measurement

1 Introduction

1.1 Concepts

Compared to synergetics as a truely interdisciplinary field [1], quantum thermodynamics focusses on a much more restrictive theme – though fundamental in its own right.

Despite these obvious differences in scale a common set of concepts can be recognized to enter both fields: This set includes, in particular, hierarchical aspects (slow/fast variables, macro/micro-descriptions, relevant subspaces), interrelated

A. Pelster and G. Wunner (eds.), *Selforganization in Complex Systems: The Past, Present, and Future of Synergetics*, Understanding Complex Systems,
DOI: 10.1007/978-3-319-27635-9_7

with the extensive use of effective descriptions (coarse-graining, emergence, universality, control parameters).

It has long since been realized that physical phenomena are not just "out there" but depend on the approrpiate level of description. Simplifications (based on relevance concepts) and models (declaring certain constraints as given) are the tools for intuitive understanding. These effective theories [2] try to capture what is relevant in a given physical domain.

Effective theories are "closed", i.e., they do not require the explicit input of more detailed descriptions , except for the fit of some phenomenological parameters. This "closure" is quite remarkable and firther underlines the usefulness of approaches on different hierarchical levels.

"Brute force" numerical studies may establish valuable tests and help to find convincing effective descriptions, but cannot be a substitute for "qualitative modeling". In this context one may recall a comment by Picasso: "Art is a lie that helps us see the truth" [3].

1.2 Operationality

Information, quantum dynamics, and thermodynamics are the basic input for the study of quantum thermodynamic processes. Remarkably, these three fields are particularly suitable for for an operational approach. In fact, the concept of information can hardly be introduced without reference to communicating agents. Observational quantum mechanics with its focus on measurementand statistical features differs substantially from "abstract"(isolated) quantum mechanics. Thermodynamics can be seen as a control theory, its main laws as statements about what can be done by agents equipped with limited resources. And operations/descriptions eventually provide links between the three fields.

1.3 Contextuality

A common thread running through both synergetics and quantum thermodynamics is contextuality.

In quantum physics contextuality has a rather dramatic significance: The Kochen-Specker theorem [4] demonstrates that we arrive at a paradox (within the rules of quantum mechanics), if we assume that all possible experimentally answerable questions that can be asked about a given quantum system have definite yes/no answers. As a consequence the answer to a certain question depends on the context (of other questions having been posed).

A somewhat different type of contextuality is related to the choice of partitions. While also operational in nature, this choice has nothing to do with actual measurement results as such, but rather concerns the mere possibility for selecting global or local questions, respectively. A bi-partite scenario underlies the emergence of local thermal behavior [5].

2 Hilbert-space

The state space of quantum physics is a complex vector-space, the so-called Hilbert-space $\mathcal{H}$ (of dimension d). Each quantum system $\mu, \mu = A, B, \ldots$ contributes its own Hilbert-space, $\mathcal{H}(\mu)$. A vector ("pure state") in such a space is conveniently written in Dirac-notation as $\boldsymbol{\psi}(\mu) \rightarrow |\psi(\mu) >$ with the complex conjugate $\boldsymbol{\psi}^*(\mu) \rightarrow < \psi(\mu)|$. The vectors are taken to be normalized, i.e., $< \psi(\mu)|\psi(\mu) >= 1$. The Hilbert-space can be spanned by a set of orthogonal basis vectors, $|f^{(j)}(\mu) >, j = 1, 2, \ldots d(\mu)$. In order to specify such a set (for Hilbert-space μ) consider the eigen-equation of some properly chosen operator $\hat{F}(\mu)$ with

$$\hat{F}(\mu)|f^{(j)}(\mu) >= F_j(\mu)|f^{(j)}(\mu) > \ . \tag{1}$$

This is still entirely abstract; we postpone the specificatiom of model classes we have in mind.

2.1 Partitioning

A classical particle is described by $d = 6$ coordinates, 3 position and 3 momentum coordinates. For a composite system (N particles) the respective space is a direct sum, the so-called Γ-space. Its dimension is

$$D = \sum_{\mu=1}^{N} d(\mu) = 6N \ . \tag{2}$$

It scales linearly with N.

Definition 1 (Tensor space). *In quantum mechanics each subsystem μ brings its own Hilbert-space of dimension $d(\mu)$. For a composite system the total Hilbert-space is thus a direct product (or tensor-) space of dimension*

$$D = \prod_{\mu=1}^{N} d(\mu) \ . \tag{3}$$

For $d(\mu) = d$ one finds $D = d^N$, i.e., the total dimension scales exponentially with N. Typical Hilbert-spaces become incredibly huge indeed.

Definition 2 (Product representation). *A convenient set of basis vectors for a composite system are product states. For $N = 2$ and if $\hat{F}(A)$ and $\hat{F}(B)$ are complete operators within their respective subspace, A, B, the completeness relation reads*

$$\hat{1} = \hat{1}(A) \otimes \hat{1}(B) = \sum_{i=1}^{d(A)} \sum_{j=1}^{d(B)} |f^{(i)}(A), f^{(j)}(B) >< f^{(i)}(A), f^{(j)}(B)| \ . \tag{4}$$

Any pure state for such a bi-partite system can thus be represented in terms of those product-states, $|f^{(i)}(A)> \otimes |f^{(j)}(B)>= |f^{(i)}(A), f^{(j)}(B)>$*, as*

$$|\psi(A,B)> = \sum_{i=1}^{d(A)} \sum_{j=1}^{d(B)} |f^{(i)}(A), f^{(j)}(B)> \psi_{ij} \ ,$$
$$\psi_{ij} = < f^{(i)}(A), f^{(j)}(B)|\psi(A,B)> \ . \tag{5}$$

This is easily generalized to $N = 3, 4, \ldots$.

The opposite to composition is partitioning:

Definition 3 ("Virtual" partitioning). *Consider a total Hilbert-space of dimension d. If d is a prime number, the system is necessarily elementary. Otherwise it has a non-trivial prime-factorization[8]*

$$d = \prod_{j=1}^{r} q_j^{n_j} \ . \tag{6}$$

The number of such elementary subsystems, each of some prime-factor dimension q_j*, would be given by*

$$N_d = \sum_{j=1}^{r} n_j \ . \tag{7}$$

Definition 4 (Operationally accessible partitioning). *For a concrete system* $\hat{H}$ *living in such a product-Hilbert-space of dimension d only a fraction of those elementary subsystems will be "real", i.e. correspond to operationally well-defined and accessible subunits. Its number,* $N \leq N_d$*, and type is not an absolute property of the system but contextual. It defines a kind of reference frame. Each such unit is characterized by a (classical) index,* $\nu = A, B, C, \ldots$*. The index serves as a kind of address.*
For example, a Hilbert-space with $N_d = 3$ *may be described as a single system, N = 1, (ABC), as a bi-partite system, N=2, (A)(BC) or (AB)(C) or as* $N = N_d$*, (A)(B)(C). This is more than a formal aspect. While all these decompositions are formally equivalent, i.e., span the same total space, they give rise to different phenomena in terms of inter-subsystem correlations (entanglement). Different decompositions also lead to different notations for states:* $|k(ABC)>$ *or* $|k(A); m(BC)>$ *or* $|k(A); m(B); n(C)>$*, where the parameters* k, m, n *specify the respective (sub-) states.*

2.2 Typicality

We first note that the study of thermodynamic behavior is intimately related to typicality [6]: We are not so much concerned with specific models and specific states, but rather with typical models and typical states. Indeed, we know that thermal properties are not guaranteed; nevertheless, we want to argue that

under given (rather weak) constraints thermal behavior will be "likely". As a consequence, we do not need to run tests for each case in question (which would often be very hard to do) but instead base our judgement on mere probability of being correct (accepting occasional failures).

So what are "typical properties" of pure states? Underlying is subjective ignorance about the actual state, which is conveniently represented by an ensemble. Typical – in agreement with its colloquial meaning – are then properties, which occur for "almost all" ensemble members. In order to quantify such a behavior one needs to define a pure-state distribution function (cf. [5]). A convenient way to proceed is to introduce a specific parametrization for the pure states in question, with respect to a given basis set.

Definition 5 (Parametrization of pure states). *Any pure state* $|\phi>$ *in a given d-dimensional Hilbert-space (for the moment we suppress index* μ*) can be written in that basis* $|f^{(j)}>$ *as*

$$|\phi>=\sum_{j=1}^{d}(\eta_j+i\xi_j)|f^{(j)}> \ . \tag{8}$$

Here, η_j, ξ_j *are* $2d$ *real parameters. The normalization condition reads*

$$G(\eta_1,\xi_1,\eta_2,\xi_2,\ldots\eta_d,\xi_d)=\sum_{j=1}^{d}(\eta_j^2+\xi_j^2)=1 \ . \tag{9}$$

The corresponding pure state distribution does not relate to a concrete physical scenario like a thermal equilibrium state. There should be no bias, except symmetry (see below).

Definition 6 (Pure-state distribution w**).** *The distribution function parametrized as* $w(\eta_1,\xi_1,\ldots\eta_d,\xi_d,)$ *may now be considered a "prior" in the sense of Bayesian statistics. A simple way to arrive at this distribution is to apply the maximum entropy principle (MEP) subject to the single macro-constraint (norm)*

$$\overline{G}=\int d^d\eta d^d\xi w(\eta_1,\xi_1,\ldots\eta_d,\xi_d)\sum_{j=1}^{d}(\eta_j^2+\xi_j^2)=\text{const.} \tag{10}$$

This procedure immediately leads to the Gaussian [7]

$$\boxed{w(\eta_1,\xi_1,\ldots\eta_d,\xi_d)=\left(\frac{1}{\sqrt{\pi\gamma}}\right)^{2d}\exp\left(-G(\eta_1,\xi_1,\ldots\eta_d,\xi_d)/\gamma\right)} \tag{11}$$

We note that this distribution fulfills the normalization condition on average only. This deficiency can be cured in the asymptotic limit for large d*, if we set* $\gamma=1/d$*. In this limit the fluctuations of* G *become negligible.*

Alternatively, the above result can be obtained by requiring the distribution function $w(\eta_1, \xi_2, \ldots \eta_d, \xi_d)$ to be invariant under unitary transformations [5]. The choice of the underlying representation is arbitrqary should thus not matter.

According to eq.(11) an unbiased ensemble of pure states is characterized by the distribution function $w(\eta_1, \xi_1, \ldots \eta_d, \xi_d)$. This function allows us to define Hilbert-space averages of any function $h(|\phi>) = h(\eta_1, \xi_1, \ldots \eta_d, \xi_d)$ as an integral over the $2d$- dimensional parameter-space:

$$\overline{h} = \int w(\eta_1, \xi_1, \ldots \eta_d, \xi_d) h(\eta_1, \xi_1, \ldots \eta_d, \xi_d) d^d\eta d^d\xi \ . \tag{12}$$

Likewise one can define higher moments. Recall that this Hilbert-space statistics reflects subjective ignorance (an entirely classical concept); it has nothing to do with the statistical features of quantum mechanics proper.

3 Hilbert-space average method (HAM)

3.1 Landscapes

Proposition 1 (Hilbert-space average method (HAM)).
The function $h(|\phi>)$ can be visualized as a "landscape" over its $2d$-dimensional parameter-space. We can approximate

$$\boxed{h(|\phi>) = h(\eta_1, \xi_1, \ldots \eta_d, \xi_d) \approx \overline{h}} \tag{13}$$

provided that landscape of h is "flat" enough.

In particular let us consider some operator $\hat{Y}$ acting on the Hilbert-space $\mathcal{H}$. Its eigen-representation reads

$$\hat{Y} = \sum_k Y_k |y^{(k)}><y^{(k)}| \ . \tag{14}$$

We are free to take these eigenfunctions as the basis for the ensemble of pure states $|\phi>$ and their distribution w,

$$|\phi> = \sum_{j=1}^{d} (\eta_j + i\xi_j)|y^{(j)}> \ . \tag{15}$$

The expectation value of $\hat{Y}$ with resepct to $|\phi>$ is an example for $h(|\phi>)$; its Hilbert-space average is

$$\overline{h} = \overline{<\phi|\hat{Y}|\phi>} = \overline{<Y>} = \sum_j Y_j(\overline{\eta_j^2} + \overline{\xi_j^2}) = \frac{1}{d}\mathtt{Tr}\{\hat{Y}\} \ . \tag{16}$$

In the last step we have used that by symmetry and normalization $\overline{\eta_j^2} = \overline{\xi_j^2} = 1/(2d)$. Correspondingly one finds for

$$\overline{<Y>^2} = \frac{1}{d(d+1)} \left(\mathtt{Tr}\{\hat{Y}^2\} + \mathtt{Tr}\{\hat{Y}\}^2 \right) \tag{17}$$

(for details see [5]), which allows us to introduce the Hilbert-space variance

$$\Delta^2(< Y >) = \frac{1}{d+1}\left(\mathtt{Tr}\{\hat{Y}^2\}/d - \mathtt{Tr}\{\hat{Y}\}^2/d^2\right) . \tag{18}$$

HAM is thus justified for $\hat{Y}$, if

$$\Delta(< Y >) \ll \overline{< Y >} . \tag{19}$$

Definition 7 (Accessible region (AR)). *Unless the system is non-integrable, the Hilbert-space accessible from some initially prepared state may severely be constrained by various constants of motion. The system will never be able to leave the respective subspace.*

While the distinction between integrable and non-integrable models is often considered essential for the resulting statistical behavior, it is of minor concern here. We simply have to make sure that certain conditions of subsystem dimensions and weak inter-subsystem couplings are obeyed. The arguments in terms of HAM then go through.

3.2 Embedded system $A(B)$: thermalizing environment

We now turn to a bi-partite quantum system $A(B)$ with Hilbert-space dimension $d(A,B) = d_A d_B$. Here A is the embedded system of interest; to stress this functional asymmetry only B is written in parenthesis. Thermalizing environments B are the prime target of quantum thermodynamics: Here one is concerned with the question under which conditions an embedding quantum system is able to impart thermal properties on the embedded system A.

A simple argument can be based on Hilbert-space statistics (cf. [5]): Here we consider a closed bi-partite system $A(B)$ under energy-exchange; the subsystem A is taken to be a spin. We apply HAM for $\hat{Y} \to \hat{H}$, and accept that the Hamiltonian $\hat{H}$ is not complete: degeneracies will show up.

Example 1 (Equilibrium via energy exchange). We take system A to be a two-level system with energy-splitting ΔE and B to be a multi-level system with states $|j, k(B) >$, where k describes the degeneracies, $k = 1, 2, \ldots g_j$. (The degeneracy structure will turn out to be essential!) We single out two energy bands, j = 0 and j+1 = 1, and assume weak (resonant) interaction between A and B, $E_1 - E_0 = \Delta E$. The total energy of the system (A, B) is taken to be ΔE. Energy conservation then induces a correlation between allowed states in A and B, i.e., not all $d(A,B)$ states of the product-space are accessible. The accessible region AR can be projected out via the follwing two projectors,

$$\hat{P}_0 = |0(A) >< 0(A)| \otimes \sum_{k=1}^{g_1} |1, k(B) >< 1, k(B)| ,$$
$$\hat{P}_1 = |1(A) >< 1(A)| \otimes \sum_{m=1}^{g_0} |0, m(B) >< 0, m(B)| . \tag{20}$$

The accessible Hilbert-space has dimension $d_{acc}(A,B) = g_0 + g_1$. The respective occupation probabilities $< P_0 >, < P_1 >$, averaged according to HAM, eq.(16), are then found to be

$$\overline{< P_0 >} = \frac{\mathtt{Tr}\{\hat{P}_0\}}{d(B)} = \frac{g_1}{g_0 + g_1} \,, \tag{21}$$

$$\overline{< P_1 >} = \frac{\mathtt{Tr}\{\hat{P}_1\}}{d(B)} = \frac{g_0}{g_0 + g_1} \,. \tag{22}$$

The relative variance, $\Delta(< P_\mu >)/\overline{< P_\mu >}$ scales with $1/d_{acc}(B)$.

For $d_{acc}(B) \gg 1$ HAM is thus justified (i.e. the above properties are typical) and the expected equilibrium state of A reflects the degeneracy structure of the embedding subsystem B.

Definition 8 (Embedding temperature). *Even though the embedding system B is not a bath (i.e., is not in a stationary thermal state) the smaller subsystem A may be said to be in a thermal state with temperature $T(A)$,*

$$\frac{\Delta E}{k_B T(A)} = \ln\left(\frac{\overline{< P_0 >}}{\overline{< P_1 >}}\right) = \ln\left(\frac{g_1}{g_0}\right) . \tag{23}$$

This effective temperature will be called "embedding temperature", as it derives from the degeneracy structure of the quantum environment B with respect to the transition energy ΔE selected by A. In general, a different subsystem A (different transition energy) will have a different embedding temperature even within the same B.

On the other hand, different embeddings B will lead to different temperatures $T(A)$ for given A. In particular, for $g_0 = g_1$ one finds

$$\overline{< P_0 >} = \overline{< P_1 >} \approx 0,5 \,. \tag{24}$$

so that $T(A) = \infty$. For $g_0 = 1 \ll g_1$

$$\overline{< P_0 >} \approx 1 \,, \quad \overline{< P_1 >} \approx 0 \,. \tag{25}$$

This would imply $T(A) = 0$, apparently giving a simple route to zero temperature.

Remark 1 (Embedding temperature and third law). For the weak coupling condition to be valid in the limit $T(A) \to 0$, the interaction energy must be small compared to the energy of subsystem A, which approaches zero. As the thermal relaxation time depends on the interaction strength, this essentially means that the time to reach thermal equilibrium would go to infinity. In this sense the third law is saved: There is no efficient process to reach the absolute zero of temperature.

Remark 2 (Negative temperature). Negative embedding temperatures obtain for $g_1 < g_0$. Such a degeneracy structure can be realized by means of a cluster of non-interacting (identical) spins in the high energy regime. For $g_1 \to 1 \ll g_0$ one would get $T(A) \to -0$ (total inversion).

For such special Hamilton models (with bounded spectrum) embedding temperatures can be positive or negative: they both characterize possible equilibrium states.

Proposition 2 (Embedding temperature versus bath temperature). *Consider a more general environment B with discrete energy-spectrum $\{E_j, j = 1, 2, \dots\}$ and respective degeneracies g_j. Furthermore, let this system be in a thermal state with partition sum $Z(B)$ and temperature $\beta(B) = 1/k_B T(B)$,*

$$\hat{\rho}_{equ}(B) = \frac{1}{Z(B)} \sum_j \exp\left(-\beta(B) E_j\right) \sum_{k=1}^{g_j} |j, k(B) >< j, k(B)| \; . \tag{26}$$

Then consider a two-level system A in its excited state $|1(A) >$, which is weakly coupled to B. What will now be the effect of B on A?

Energy conservation implies that the initial pure state $|1(A); j, m(B) >$ with $1 \le m \le g_j$ would preferably be coupled to $|0(A); j+1, k(B) >$ with $1 \le k \le g_{j+1}$, so that – under HAM – the equilibrium state is expected to be

$$\overline{< P_0 >}_j = \frac{\mathtt{Tr}\{\hat{P}_0\}}{d_j(C)} = \frac{g_{j+1}}{g_j + g_{j+1}} \; , \tag{27}$$

$$\overline{< P_1 >}_j = \frac{\mathtt{Tr}\{\hat{P}_1\}}{d_j(C)} = \frac{g_j}{g_j + g_{j+1}} \; . \tag{28}$$

But in addition to taking the quantum expectation value and to apply the HAM we have now, in a third step, to perform a thermal averaging over the environmental states j:

$$\hat{\rho}_{equ}(A) = \frac{1}{Z(B)} \sum_j g_j \exp\left(-\beta(B) E_j\right) \times \\ \{\overline{< P_0 >}_j |0(A) >< 0(A)| + \overline{< P_1 >}_j |1(A) >< 1(A)|\} \; . \tag{29}$$

In general, this equation lacks a clear interpretation. For more transparent results specific models are needed about the environmental spectrum E_j and the degeneracy g_j.

For the following we assume for the environment B an equidistant spectrum,

$$E_j = j \Delta E \; . \tag{30}$$

All transitions between adjacent levels are thus resonant with the two-level system A. The following examples concern the degeneracy of B.

Example 2 (Exponential degeneracy). We assume

$$g_j = \exp\left(\gamma j \Delta E\right) , \tag{31}$$

γ is a real positive parameter. Then

$$\overline{< P_0 >} = \frac{1}{1 + \exp\left(-\gamma \Delta E\right)} , \tag{32}$$

$$\overline{< P_1 >} = \frac{1}{1 + \exp\left(\gamma \Delta E\right)} , \tag{33}$$

independent of j. The resulting temperature is $\Delta E / k_B T(A) = \gamma \neq \beta(B)$.

Example 3 (Binomial degeneracy).

$$g_j = \binom{n}{j} = \frac{n!}{(n-j)!j!} \tag{34}$$

Here, n is an integer > 0; for an intuitive realization we could think of an environment consisting of n non-interacting spins with identical energy splitting ΔE. One then finds,

$$\overline{< P_0 >}_j = \frac{n-j}{n+1} , \tag{35}$$

$$\overline{< P_1 >}_j = \frac{j+1}{n+1} . \tag{36}$$

Here we have made use of the identity

$$\binom{n}{k} + \binom{n}{k-1} = \binom{n+1}{k} . \tag{37}$$

After thermal averaging over the various bands j and with the partition sum

$$Z(B) = \sum_{j=0}^{n} \binom{n}{j} \exp\left(-\beta(B) j \Delta E\right) = \left(1 + \exp\left(-\beta(B) \Delta E\right)\right)^n \tag{38}$$

one gets in the thermodynamic limit, $n \to \infty$,

$$\beta(A) \approx \beta(B) . \tag{39}$$

In this case there is no conflict between embedding temperature and the bath temperature.

Both degeneracy models are idealized; deviations from the strict exponential form appear to be mandatory, though.

4 Observational quantum-thermodynamics

Quantum-thermodynamic settings do not include the observer: No means whatsoever are provided to transfer information to the outside world. In that sense the scenarios are similar to those studied in abstract quantum theory, i.e. based on isolated systems. It thus appears quite natural to add a section on observational quantum thermodynamics, just as we would have to add a section on observational quantum mechanics. In either case observation requires additional physical interactions: The act of observation tends to influence the observed.

In the following we will be concerned with a thermal system under permanent ("stroboscopic") supervision [9].

4.1 Periodic measurements

We will be concerned with the following bi-partite system

$$\hat{H}(AB) = \frac{\delta(A)}{2}\hat{\sigma}_3(A) + \hat{H}_0(B) + \hat{V}(BB) + \lambda\hat{V}(AB)\ . \tag{40}$$

The environment B consists of $n \gg 1$ spins. The corresponding product states

$$|\psi(B)>=|m(1), m(2), \ldots, m(n)> \quad m(\mu) = \mp 1\ , \tag{41}$$

are eigenfunctions to $\hat{H}_0(B)$ with eigenvalues $E_k(B) = \delta(B)k$, where k denotes the number of spins in state $m = 1$. For given band-index k all the states, $|n_k>, n_k = 1, 2, \ldots g_k$, have the same energy. Now focus on some index k_0, the "working point" in energy-space. For $n > k_0 \gg 1$ the binomial degeneracies (cf. Example 3) can be approximated by

$$g_k \approx g_0 \exp\left(\beta(k_0)E_k\right)\ , \tag{42}$$

$$\beta(k_0) \approx \frac{1}{\delta(B)} \ln\left(\frac{n}{k_0} - 1\right)\ . \tag{43}$$

Due to the weak interaction $\hat{V}(BB)$, each degenerate energy-level k becomes a band of width $\Delta\epsilon_k \ll \delta(B)$.

The interaction between subsystem A and B is scaled by the strength factor λ and given by

$$\hat{V}(AB) = \hat{\sigma}_1(A) \otimes \hat{I}(AB)\ , \tag{44}$$

$$\hat{I}(AB) = \sum_k \sum_{n_k, m_{k+1}} C_{k+1,k}(n_k, m_{k+1})|n_k>< m_{k+1}| + c.c.\ . \tag{45}$$

Here c.c. means complex conjugate term to be added. Only transitions between next neighbor bands are allowed. The coupling parameters $C_{k+1,k}(n_k, m_{k+1})$ form a set of hermitian matrices $C_{i,j}(a, b)$. The respective entries are taken from a Gaussian distribution normalized to $\overline{|C_{i,j}(a,b)|^2} = \sqrt{(g_i g_j)}$.

Note that this random-matrix model (for the subsystem-interaction) is an essential ingredient: in this way the Hamilton-model represents a whole class

of models rather than one given variant. Indeed, one can show that different realizations typically lead to the same desired behavior, eq.(50). (This does not exclude the existence of very special interaction types which would violate this simple picture.)

The total state will be written as

$$\hat{\rho}(AB) = \hat{\rho}(A) \otimes \hat{\rho}(B) - \hat{C}(AB) \; , \tag{46}$$

$$\hat{\rho}(A) = \mathtt{Tr}_B\{\hat{\rho}(AB)\} \quad \hat{\rho}(B) = \mathtt{Tr}_A\{\hat{\rho}(AB)\} \; . \tag{47}$$

Here $\hat{C}(AB)$ specifies the correlation between A and B, i.e., the deviation from product-form. Let the initial state at time t_0 have zero correlation; in particular, we start from the special product-state

$$\hat{\rho}(AB; t_0) = \hat{\rho}(A; t_0) \otimes \hat{\rho}(B; k_0) \; , \tag{48}$$

$$\hat{\rho}(B; k_0) \equiv \frac{1}{g_{k_0}} \sum_{n_{k_0}=1}^{g_{k_0}} |n_{k_0} >< n_{k_0}| \; . \tag{49}$$

Resonance will be assumed, i.e., $\delta(B) = \delta(A) = \delta$. Then the subsystem B acts as a thermalizing environment, correlation $\hat{C}(AB)$ builts up, and A relaxes to a state with temperature

$$\frac{1}{k_B T(A)} = \beta(A) = \beta(k_0) \; , \tag{50}$$

independent of the initial state of A. Up to this point this is just a typical scenario for quantum thermodynamics. The relaxation time scales with the interaction strength between system and environment.

Now we intend to retrieve information about A. This could be done in two different ways: Direct measurements on A or indirect measurements via B exploiting the correlation between A and B.

Measuring the energy of subsystem A directly would mean to find it in the ground- or excited state with probability $P_m(A)$ given by the thermal distribution. Immediately after measurement the subsystem would be found in the respective energy eigenstate $|m(A) >, m \mp 1$. This momentary state and the associated information gain would not last for long, though: With the embedding still present system A would again relax to its equilibrium state.

We switch now to the indirect measurement scenario. We restrict ourselves to the measurement of the band-index, k i.e., to an incomplete measurement. The projection by $\hat{P}_{k_1}(B)$ at time $t_1 = t_0 + \Delta t$ also influences subsystem A (co-jump, cf. [10]):

$$\hat{\rho}'(A; t_1) = \frac{\mathtt{Tr}_B\{\hat{P}_{k_1}(B)\hat{\rho}(AB; t_1\}}{\mathtt{Tr}_B\{\hat{P}_{k_1}(B)\hat{\rho}(B; t_1)\}} \tag{51}$$

$$= \hat{\rho}(A; t_1) + \frac{\mathtt{Tr}_B\{\hat{P}_{k_1}(B)\hat{C}(AB; t_1\}}{\mathtt{Tr}_B\{\hat{P}_{k_1}(B)\hat{\rho}(B; t_1)\}} \; . \tag{52}$$

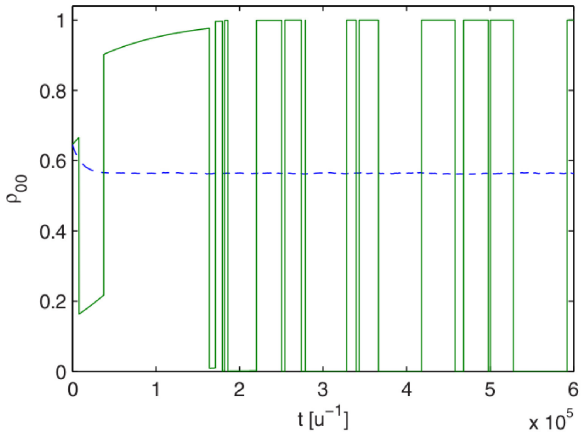

Fig. 1. Subsystem A subject to periodic measurements of the environment B [9]: single trajectory $\rho_{00}(t)$ (solid line) and ensemble avarage $\overline{\rho_{00}}(t)$ (broken line). Chosen parameters: $\delta = 0.8u$, $\beta = 0.75u^{-1}$, $\lambda = 4 \times 10^{-3}u$, $\Delta t = 2u^{-1}$, u = arbitrary energy unit. Initial state: unperturbed attractor.

After measurement we simplify the total state as the product state

$$\hat{\rho}(AB; t_1) \approx \hat{\rho}'(A; t_1) \otimes \hat{\rho}(B; k_1) \; . \tag{53}$$

This is an approximation as, due to the incomplete measurement, some correlations between A and B could still have survived. The whole process is now iterated: unitary evolution steps of duration Δt are interrupted by instantaneous measurement projections as described above. The result is a stochastic trajectory as shown in Fig. 1.

These trajectories correspond to the classical statistical idea that the thermal system is always in some well-defined state, but "fluctuates" between those such that the time-average is identical with the ensemble average. We now investigate the ensemble-average over such trajectories after a certain number of measurements (i.e. after the memory about the inital state has been lost). The result represents an attractor state, which can be expressed analytically as [9]

$$\overline{\rho}_{00}(\Delta t) = \frac{\exp\left(-\beta\delta/2\right)\sin^2\delta\Delta t + \exp\left(\beta\delta/2\right)\delta^2(\Delta t)^2}{2\cosh\beta\delta/2(\sin^2\delta\Delta t + \delta^2(\Delta t)^2)} \; . \tag{54}$$

The corresponding function is shown in Fig. 2.

This attractor state can alternatively be calculated as a time-average over a single trajectory; it has two remarkable bounds:

$$\lim_{\Delta t \to 0} \overline{\rho}_{00}(\Delta t) = 1/2 \; . \tag{55}$$

This lower bound means that for very rapid repetitions of measurements the system eventually heats up to $T(A) \to \infty$. Only apparently is this in conflict

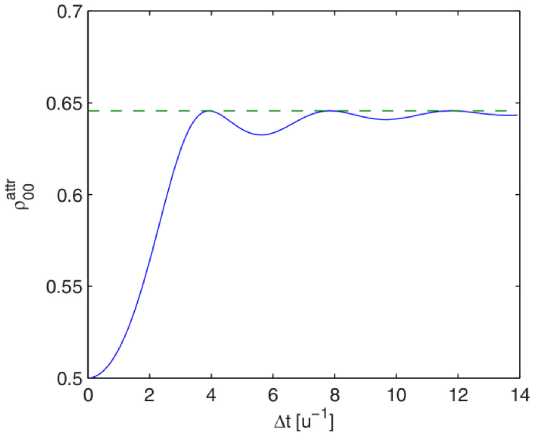

Fig. 2. Attractor for subsystem A depending on the time Δt between periodic measurements on B. Parameters as before. Broken line: upper bound and unperturbed attractor [9].

with the so-called Zeno effect, i.e. the freezing-in of the original state under "continuous" measurement: Indeed, for $\Delta t \to 0$ it would take infinitely long to reach that attractor state.

An upper bound for $\overline{\rho}_{00}$ is reached for

$$\Delta t = \frac{n\pi}{\delta} \quad n = 1, 2, \ldots \ . \tag{56}$$

This bound corresponds to $k_B T(A) = 1/\beta(k_0)$. Remarkably, this is the same temperature subsystem A would gain in the absence of any measurements. At these waiting times one finds a strict correlation between measuring the band-index k to have gone up by 1 (compared to its previous value) or down by 1 and the state of A: For "up" A is in the ground state, for "down" A is in the excited state. This is the strict "measurement logic". It guarantees that our information retrieval "makes sense".

For $\Delta t \to 0$, on the other hand, the correlation goes to zero: System B has no (useful) information about A. The measurements of the environment B only lead to an additional perturbation of A.

Observational quantum-thermodynamics thus provides an interesting link between the abstract thermal properties, which are stationary, and the measured thermal properties, which are fluctuating. The long-time average and the ensemble average of the latter agree with the former result, provided the measurement is run under optimal conditions, i.e. there is a clear measurement logic (in which case the information gained is "useful"). While measurement interactions mean perturbations – indeed, the observed local dynamics is stochastic, the unobserved dynamics stationary – the underlying thermal parameters turn out to be the same.

5 Summary

We have started from (abstract) Hilbert-space and used partitioning as a kind of external reference frame. This frame defines the notion of local versus global properties.

The parametrization of pure states (for the total system) allows to introduce functions on this parameter-space; examples are expectation-values of operators. These functions can be visualized as "landscapes". Flat landscapes may well be approximated by the respective average value, the so-called Hilbert-space average (HAM). This average is then "typical". Rarely will we find large deviations. A simple analogue would be the height within the Netherlands (average applicable) versus the height in Switzerland (average does not give a good predictor for one's actual height).

Typicality can be extended to composite quantum systems: For bi-partite systems in a pure state the local entropy of the smaller subsystem is found to be typically maximum (confirming entanglement as a typical feature).

These feartures do not depend on details of the Hamilton-model considered. Such details constrain the motion in Hilbert-space: In fact, the accessible region is, in general, much different from the total region (due to conservation laws).

It turns out that for weak coupling and for the environment B being sufficiently larger than the embedded system A, the latter exhibits thermal behavior (canonical distribution).

The effective dynamics for the embedded system shows irreversibility (relaxation into an equilibrium state), even though the total dynamics continues to be unitary. This underlines the fact that the thermal properties of A are emergent and contextual; they are absent from the point of view of the unpartitioned description.

The equilibrium state is quasi-stationary (temporal fluctuations occur as finite size effects) and characterized by a temperature.

Periodic observation of the environment allows to re-interprete the equilibrium state of the embedded system in terms of a time average over measurement results. Under ideal conditions this time-average approaches the ensemble-average (ergodicity); the resulting value is the same as obtained without observation. There is a "peaceful coexistence" between the classical and the quantum picture.

This coexistence has remarkable consequences: Without it a quasi-classical understanding of thermal phenomena would not have been possible, thus blocking scientific progress in this field at a time when quantum mechanics was unknown yet. On the other hand, the discussion of "quantum corrections" proper – based on quantum thermodynamics – will not be straight-forward but will require detailed analysis based on the formulation of pertinent quantum models.

Acknowledgments. I thank Hermann Haken for numerous and very valuable discussions.

References

1. Haken, H.: Synergetics. Springer, Berlin (1977)
2. Castellani, E.: Reductionism, emergence, and effective field theories (2000). http://philsci-archive.pitt.edu
3. cited in: Segel, L.A.: The infinite and the infinitesimal in models of natural phenomena. Rev. Mod. Phys. **63**, 225 (1991)
4. Kochen, S., Specker, E.P.: The problem of hidden variables in quantum mechanics. J. of Mathematics and Mechanics **17**, 59 (1967)
5. Gemmer, J., Michel, M., Mahler, G.: Quantum Thermodynamics, 2nd edn. Springer, Berlin (2009)
6. Lebowitz, J.L.: Boltzmann's Entropy and time's arrow. Physics Today **46**(9), 32 (1993)
7. Jaynes, E.T.: Information theory and statistical mechanics. Phys. Rev. **106**, 620 (1957)
8. Zanardi, P.: Virtual quantum subsystems. Phys. Rev. Lett. **87**, 077901 (2001)
9. Jahnke, Th, Mahler, G.: Quantum thermodynamics under observation: the influence of periodic quantum measurements. Eur. Phys. Lett. **90**, 50008 (2010)
10. Granzow, C.M., Mahler, G.: Quantum trajectories of interacting pseudo-spin networks. Appl. Phys. B **67**, 733 (1998)

Nanolasers: Current Status of The Trailblazer of Synergetics

Cun-Zheng Ning

School of Electrical, Computer and Energy Engineering, Arizona State University, Tempe, AZ 85287, USA
cning@asu.edu
http://nanophotonics.asu.edu

Abstract. The laser is a prototypical non-equilibrium and self-organizing system that led to the birth of synergetics, and thus considered the trailblazer of synergetics by Prof. Haken. The field of laser science and technology today is as active and exciting as it has ever been since the invention of lasers in 1960's and the trailblazing days in late 1970s. One of the constant themes of research in semiconductor lasers has been size miniaturization, which has led to the invention of many ever smaller lasers. But miniaturization using pure dielectric cavities encountered significant barriers due to the constraint of wavelength or the diffraction limit. To reduce the size of semiconductor lasers further into the nanoscale or deep sub-wavelength scale, metallic and surface-plasmon-polariton (SPP) waveguides were proposed and demonstrated experimentally in the last few years. Since then, such nanolasers have attracted a great deal of attention. Rapid progress has been made in various aspects of nanoscale lasers. After some brief introduction and personal reminiscences, this paper will discuss recent progress in experimental and theoretical studies of semiconductor nanolasers. We will first discuss various mechanisms of wave confinement at nanoscale. Major progress will be reviewed including the first experimental demonstration of continuous wave operation of sub-wavelength cavity lasers at room temperature. Future prospects of the further size reduction and remaining challenges will be discussed.

Keywords: Nanolasers, Semiconductor Lasers, Plasmonics, Waveguide, Surface Plasmon Polaritons

1 Introduction: The Laser, Synergetics and Personal Reminiscences

It is a great pleasure and honour for me to present a talk which resulted in this article at the Symposium celebrating the 85th birthday of Prof. Haken. In addition to the discussions about nanolasers, I would also use this opportunity to reminisce about my interactions with Prof. Haken and my time in Stuttgart to illustrate Prof. Haken's influences on me. This also gives me an opportunity to express my great appreciation and admiration of Prof. Haken for all the helps

A. Pelster and G. Wunner (eds.), *Selforganization in Complex Systems: The Past, Present, and Future of Synergetics*, Understanding Complex Systems,
DOI: 10.1007/978-3-319-27635-9_8

and support he provided to me, for being a mentor and a world-class scientist that has directly and indirectly influenced me and my scientific career. In 1980's when I entered my graduate study, the larger field around synergetics, self-organization, instabilities, chaos and nonlinear dynamics was a highly active area of research. I was fortunate enough to have met Prof. Haken in the right time of my career. I was a first year graduate student in 1982 at the Northwestern University (NWU) in Xi'an, China when Prof. Haken was invited there to give a series of lectures on synergetics. His trip was part of the overall plans of the Chinese Physical Society to introduce the most recent progress then in the world in the field of non-equilibrium statistical physics into China. The lectures were attended by researchers and graduate students across China. Since I was one of the only two graduate students in the area of non-equilibrium statistical physics from the host university, I had the unique opportunity to interact with Prof. Haken regularly during his two week stay in Xi'an. I benefited greatly from his lectures and decided to do a thesis on stability and non-equilibrium phase transitions in a two-mode laser with a saturable absorber as my master thesis. Later on, I was more than fortunate to travel for the first time in my life outside China when Prof. Haken invited me for a three-month visit to his Institute of Theoretical Physics and Synergetics in Stuttgart. The visit eventually led to my acceptance as one of his PhD students. That was more than a dream coming true, since I never before thought that I would get a chance to do a PhD. Now I was doing it in one of the best groups in the world. It was the freest time I enjoyed ever in my career so far, and I could work on almost any topics of my interest. Prof. Haken was always supportive. Guided by my interest in synergetics and lasers, my choice of research topics was mostly centered around instabilities and nonlinear dynamics of various lasers using the methods of synergetics. It was also one of the most productive periods and we were able to accomplished a few things and some of them have later attracted a great deal of interests, even till today. One of the first problems I encountered was how to deal with the arbitrary form of the order parameter (or Ginzburg-Landau) equations. While the Ginzburg-Landau equations for the Hopf-bifurcation typically takes the normal form for systems with a certain symmetry, they take a more arbitrary form for many systems without such symmetry or for spatial independent systems, after the application of the slaving principle [1, 2]. The general analysis of such non-normal form becomes difficult. Using a general nonlinear transformation due to Poincare, a nonlinear Ginzburg-Landau equation of quite general form can be transformed into the corresponding normal forms, depending on the type of instabilities or bifurcations. Such a combination of slaving-principle based reduction and subsequent nonlinear transformation turned out to be a powerful approach. I was able to apply this combination to carry out nonlinear analysis near various instabilities in different systems, including lasers with detuning and two-photon laser systems [3, 4].

The laser instability study, together with the great freedom I enjoyed in Prof. Haken's group also led to an interesting and unexpected development. The freedom allowed me to follow the new developments in other fields of study

that were not apparently related to my own research. In late 1980's and early 1990's, Berry's phase [5] was a topic of great interest. Berry's phase was initially discovered in a linear Hamiltonian system and was quickly extended to linear non-Hermitian systems. While studying the Hopf-bifurcation (or self-pulsing instability) in lasers, I realized that the phase behaviour of the laser field in the self-pulsing regime showed an anholonomic behaviour that is the hallmark of the Berry phase: In addition to a periodic part, the phase also contains a drift part. Thus when the intensity goes through a period in a pulsation, the phase does not come back to the starting value. The similarity to Berry's phase was not entirely surprising, since the U(1) gauge invariance in the laser field is the same as the phase arbitrariness in the wave functions of the Schroedinger equation. Despite the similarity in phenomenology, the mathematics that was used to describe the Berry's phase was not applicable to lasers in a self-pulsation mode. Fundamentally, the two types of the systems could not be more different: one being linear Hamiltonian systems, the other nonlinear open or synergetic systems showing periodic and chaotic attractors under sustained external pumping. The language used to describe the anholonomy was valid only for the conservative systems where the length of the vectors is conserved. Even though I was able to show all the phenomenological similarities to the Berry phase and to identify the type of dissipative systems that would show such phase anholonomy [6, 7],a more formal mathematical analogy was missing for almost two years. Convinced by the existence of a more profound link, I worked on and off for two years on this and was eventually able to show [8, 9] in a more general fashion that a geometric phase with all the properties of the Berry phase could be defined for a class of nonlinear dissipative systems with certain symmetries. These symmetries lead to the existence of what we called cyclic attractors in dissipative systems, for which geometric phases can be defined. Exactly as in the case of Hamiltonian systems, the total phase accumulated in a period of intensity pulsation can be decomposed into two parts, one determined by the system dynamics called dynamical phase, and the other given by a closed-loop line-integral along the trajectory or on an attractor, thus a pure geometrical quantity, called geometric phase. Independently but a bit later, similar mathematical structures for geometric phase were also studied by Landsberg [10] for dissipative systems. The theory of geometric phase in nonlinear dissipative systems is now sometimes known as Landsberg-Ning-Haken formalism [11]. Later, Rudolf Friedrich and I were able to generalize the existence of geometric phase to a more general situation of synergetic systems with continuous symmetries [9, 12]. Such geometric phases in dissipative systems later attracted significant interests and are still actively pursued [11]. During the process, I was to a large degree inspired by the spirit of synergetics and the work of Prof. Haken, who has explored the analogy and similarity of different systems to a masterful degree, especially in his generalization of phase transitions in equilibrium systems to non-equilibrium systems, the very essence of synergetics. In a sense, our generalization of the Berry phase from linear Hamiltonian systems to non-equilibrium and nonlinear systems displaying self-organization followed the very tradition of synergetics.

I finished my PhD in 1991 in a rather difficult time. Several historical world events "conspired" to make my next career move very difficult: the end of the cold war that led to the budget reduction for basic research in the west, the German reunification that required the shift of the research funding from the west to east as part of the "Aufbau Ost", the world-wide economical recession, and most importantly for me, the 1989 student event and the resulting unstable political situation in China. It was again Prof. Haken's great kindness and generosity that allowed me to continue my research in Stuttgart. Despite the unprecedented difficult funding situation also (or even) in his group, he was able to secure a position for me under the SFB project, then on-going in Stuttgart. While half-heartedly working on the optical switching of organic molecules for the SFB project, I was fascinated by the phenomenon of stochastic resonance and collaborated with Prof. Gang Hu on this topic for quite sometime. One of the major results of this collaboration was our realization of a new phenomenon [13], what we called then stochastic resonance without external force or signal. This phenomenon, later studied in 1997 under "coherence resonance" [14], has now become one of the most widely studied topics in the area of dynamical systems with noise, including in lasers.

The technical focus of this article is about the laser, a field of study that played a special role in Prof. Haken's distinguished career among a long list of fields, in which he has made pioneering and enduring contributions, as partly reflected in the other articles of this volume. When the laser was first invented in 1960s, engineers were busy searching for all possible new applications, while marvelled by the wonderful properties that the new kind of light possessed and promised. For physicists such as Hermann Haken, there were many fundamental questions to be answered. Chief among them was: what was the fundamental difference between this new type of light and the light from a regular lamp. In one of his earlier papers [19] (more generally see his famous monograph of Laser Theory [18]), he was able to show using the first-principle approach that the fundamental difference between a broadband thermal lamp and a laser source can be seen in the expectation value of the field operator, which was zero for the former and non-zero for the latter. The nonlinear Langevin equations they developed have since became the hallmark of the Stuttgart School. As a theoretical physicist, he quickly recognized further that the laser represented a new type of systems with special characters: The laser was an open system in the sense of thermodynamics where external pumping was essential and the interaction with the outside world in terms of various reservoirs were unavoidable. At the same time, both subsystems that interact with each other in a nonlinear way, the light field and the matter (atoms, molecules, or semiconductors)needed to be treated quantum mechanically. In other words, the laser represented a unique system where several important ingredients were present such as openness to the outside world and the presence of noise, in addition to being far away from equilibrium, non-linear, dissipative, and quantum mechanical. For such a system, proper theoretical tools and mathematical methods had to be developed. It was during this highly fruitful endeavour that Prof. Haken quickly established

the Stuttgart School as one of the key centres of laser research in the world. The efforts culminated to his first book as a volume in the celebrated Encyclopaedia of Physics [18], which has long become one of the standard texts on the quantum theory of lasers. It was also during this process that he realized that the physics, the general principles, and the mathematical methods they had developed were much more general than being only applicable to lasers. This more general pursuit that originated from the laser study has led to the establishment of the interdisciplinary science Synergetics [1, 2, 15, 16]. Thus the laser is considered as the trailblazer of synergetics by Prof. Haken [17].

One type of lasers that were studied in 1960s by Prof. Haken and his wife [20] and more extensively together with Prof. Haug [21] was semiconductor lasers. It was only natural that Prof. Haken wanted to develop a first principle theory for semiconductor lasers, since he had made a name for himself in developing quantum field theory for solids, especially through his work on polarons and excitons, prior to his arrival in Stuttgart and had developed the quantum theory for atomic and solid state lasers in the first few years of his time in Stuttgart. Right after the first experimental demonstration of semiconductor lasers [35–37] in 1962, they published their theory in the following year [20], where they determined the photon density and operating frequency of a semiconductor laser in the steady state, especially the dependence of frequency on Fermi levels (inversion). One of the important results from their free-carrier version of the quantum theory was what is now known as the linewidth enhancement factor. The paper by Haug and Haken [21] was the first to derive the linewidth of a semiconductor laser from the quantum Langevin equations. Even though they did not analyse more quantitatively the effective of such linewidth, the Hakens correctly pointed out the effects of carrier density on linewidth of semiconductor lasers, as the paper [20] explicitly states (directly translated from German): "The dependence of laser frequency on the inversion naturally leads to a finite linewidth as a result of Fermi level fluctuation". It was later realized by Henry [22] that such a linewidth enhancement is much larger than was first assumed as in the case of atomic lasers or in solid state lasers. Now this factor plays an important role in understanding the linewidth and other important properties of semiconductor lasers.

My experiences with laser physics and synergetics during my PhD research in Stuttgart and the "mandatory" study of Prof. Haken's book on the quantum field theory of solids [23] by all PhD students at Haken's Institute for their oral exam were of great help later when I took my first position in the US at the University of Arizona. At the time in Tucson, the microscopic theory of semiconductor lasers was further developed and applied to various semiconductor quantum structures, including various Coulomb interactions [24, 25]. During the almost 20 years since I left Stuttgart, I have been involved in the studies of various semiconductor nanostructures and lasers. Time and again, I found that the various earlier papers of Prof. Haken are of great relevance for my research. More directly, the experience and knowledge I gained in Stuttgart have been always important. One of the important topics at the frontier of semiconductor

laser research nowadays is nanolasers, or the study of the semiconductor laser miniaturization down to nanometer scale. This would be the focus of the my discussion in the remaining part of this article.

2 Nanolasers

Nanolasers [26] refer in general to lasers with sizes of sub-wavelengths in all three dimensions, or a total volume smaller than the wavelength cubed. The wavelengths here mean those in vacuum presently, even though wavelengths in media are more physically relevant. But the length scales at the vacuum wavelengths are the immediate goal of miniaturization to achieve. Such nanolasers are often only possible with semiconductors as the gain media, and thus the field is a natural evolution of the research on semiconductor lasers. One of the driving forces behind nanolaser research is the potential photonic integrated circuits (ICs) on a semiconductor chip for various information technology related applications, much similar to the IC technology in micro-electronics for our current computer chips. Such nano-photonic IC systems can potentially significantly expand the capability of electronic ICs in computing and communication. Current mainstream semiconductor lasers, while the smallest compared to other types of lasers such as gas or solid state lasers, are still too large for such nanophotonic ICs, and much larger compared to the sizes of the electronic devices. Thus further size reduction of semiconductor lasers can potentially impact photonics ICs in general, future information technology as well as other on-chip applications such as detection and sensing.

Research on nanolasers can be viewed as part of the overall trend of semiconductor laser miniaturization over the last 50 years since they were first demonstrated [35–37]. As we know, the radiative efficiency of a photonic device is proportional to the product of the photonic density of states (PDOS) and electronic density of states (EDOS). Thus tailoring the both densities of states has been an important part of research on quantum engineering from both electronic and photonic points of view. From the electronics point of view, tremendous progress in fabrication and crystal growth technologies over the last several decades have enabled dimensionality reduction from bulk semiconductors to quantum wells (2D), quantum wires (1D), and to quantum dots (0D). As shown in Fig. 1, such evolution allows the better tailoring of electronic states and positioning them in energy space where they are needed, thus avoiding the waster of charge carriers that would not be utilized in optical transitions. From the photonics point of view, the smaller size of laser cavities allows fewer modes within the optical gain spectrum, as shown in Fig. 2. Obviously, the ideal situation would be to align the single cavity mode in Fig. 2 with a single electronic state in Fig. 1, with both densities of states very sharply aligned, allowing the most efficient lasers to be made. Another manifestation of such cavity size reduction can be seen from the Purcell factor that expresses the enhancement of radiative process in a cavity relative to that in the free space:

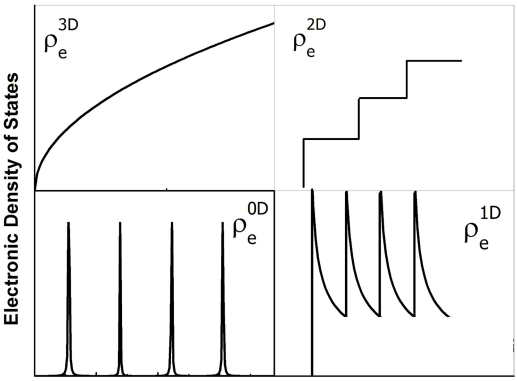

Fig. 1. Schematic of electronic density of states (EDOS)for the bulk (3D), quantum well (2D), quantum wire (1D) and quantum dot (0D) semiconductors.

$$F_p = \frac{\rho_{ph}^{cav}}{\rho_{ph}^{free}} = \frac{3}{4\pi^2}\frac{\lambda^3}{V_c}Q \tag{1}$$

where λ is the wavelength in the medium and Q and V_c are the cavity quality factor and volume, respectively. Obviously, the smaller the cavity volume is and the larger the cavity Q is, the stronger the Purcell enhancement is. Thus size reduction, in addition to benefiting the large scale integration of the photonic ICs, has an added advantage of making the radiative process more efficient. One of the important questions of current interest is: to what degree can a semiconductor laser be miniaturized or if there is an ultimate limit to such size reduction [26]. Wave confinement in a waveguide or cavity is achieved by the refractive index profile and the larger the index contrast is, the stronger the wave confinement and the smaller a cavity can be made. Thus one approach to nanolasers over the last 10 plus years has been to use semiconductor nanowires [27, 28] with a very large index contrast between that of a semiconductor and air. Strong wave confinement enables a nanowire of 100s nanometer in diameter to act as a laser gain medium and cavity at the same time. While this is still an active area of research, such pure dielectric or semiconductor structures can not support a lasing mode when the diameter becomes too small. It is easy to see that a pure semiconductor-based or semiconductor-dielectric laser structure would not allow much size reduction below the limit of half-wavelength (in the medium), the so-called diffraction limit. Thus alternative approach was needed.

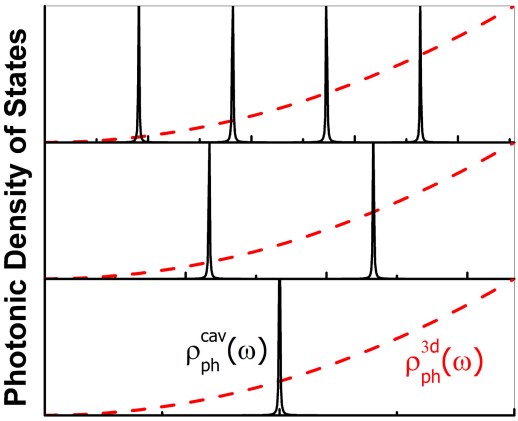

Fig. 2. Schematic of photonic density of states (PDOS)for a 3D cavity with reducing size from top to bottom. The PDOS for free space is also indicated by the parabolic curve in each panel for comparison.

3 Metallic or Plasmonic Structures as Nanolaser Cavities

While studying the means to improve the wave confinement with nanowires of small diameters [29, 30], we realized [31] that the plasmonic effect in metals such as silver can act as a means to strongly guide optical modes in a semiconductor-core metal-shell structure. Plasmonic effects had received great attention as a means for nanoscale focusing and confinement of light for sometime [53–56, 60, 57–59]. Most of such studies are concerned about the small confinement in metal-dielectric structures where the associated large loss is not addressed, with some more recent exceptions [31, 39, 65, 66], where plasmonic structures were considered together with semiconductor gain materials. One of the key questions for using plasmonic or metallic cavities for nanolasers is if it is possible to overcome the large metal loss by the gain in a semiconductor. Another is a feasible design integrating the semiconductor gain with metal confinement structures in a fabrication compatible manner. By using a semiconductor-core metal-shell structure as a model system, the possibility of over-compensating plasmonic loss in the metal shell by the optical gain in the semiconductor core was first studied [31] in a wide spectral range including plasmonic resonance. It was shown that such over-compensation is possible for a few modes near the "cut-off" frequencies, and especially near the surface plasmon resonance [42, 26], despite the large Joule loss in the metal. Independently, the similar structures were fabricated by Hill et al. [32], who demonstrated experimentally that such core-shell structure can indeed enable lasing with a core-diameter as small as 200 nm. This was the smallest semiconductor laser in this wavelength range at that time. Since then many variations have been investigated experimentally and theoretically [41, 43–47, 66, 48], and the core-shell structure has now been established

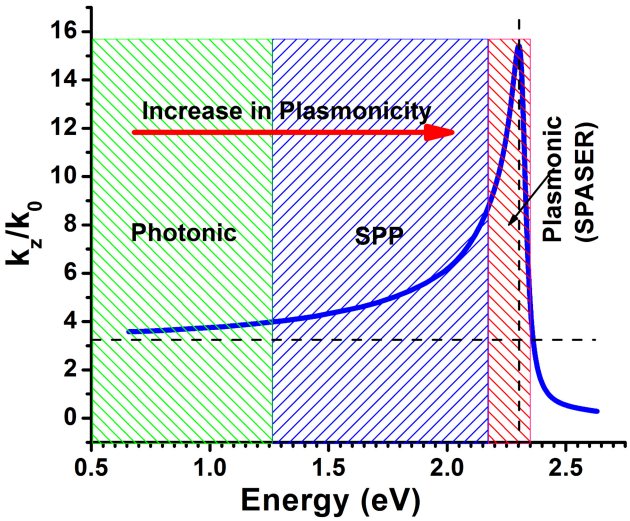

Fig. 3. Dispersion of wave-propagation at a semiconductor-silver interface (z-direction)with semiconductor dielectric constant taken to be 12. $k_0 = \omega/c$. Horizontal and vertical dashed lines indicate the wavevector in uniform semiconductor and the surface plasmon resonance, respectively

as a prototypical metallic cavity structure for nanolasers. Incidentally, it is interesting to note that prior to the publications of papers [31, 32] in 2007, all the micro- and nanolasers used pure semiconductor or dielectric cavities. After 2007, most, if not all, of the nanoscale lasers have metallic or plasmonic structures as the essential part of the cavities or main mechanisms for light confinement. The wide adoption of metallic or plasmonic cavities represents a paradigm shift in the development of semiconductor lasers towards dramatic size reduction. The basic idea of nanoscale confinement of optical modes by metallic structures can be seen from Fig. 3, where dispersion of wave propagation along a silver-semiconductor interface is plotted. The horizontal and vertical dashed lines indicate two limiting cases when the wave propagation is mostly dielectric, or plasmonic, respectively. In the first case, the metal plays the role of a perfect reflector and wave energy lies predominately outside the metal, while in the latter case, surface plasmons are fully excited and no photons are involved. As indicated by the arrow, the plasmonic effects, or "plasmonicity" thus increases from left to right as we approach the surface plasmon resonance. Thus we can roughly divide the frequency range below plasmon resonance into three regions as indicated in the figure: the low frequency region is a mostly dielectric regime, while near the surface plasmon resonance we have almost pure plasmonic excitation. In the intermediate regime, there is a wide region of different degrees

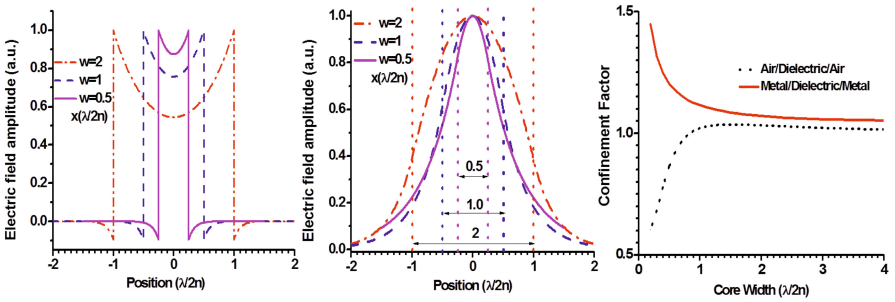

Fig. 4. Comparison of mode profiles in two types of slab wave-guides: Left: silver/semiconductor/silver with varying thickness of semiconductor core (dielectric constant 12); Middle: Similar to left but with silver replaced by air; Right: optical confinement factor that defines modal gain of the wave-guide, see [26, 34] for definition of the confinement factor. All thickness w is measured in the unit of $\lambda_0/2n$ where $\lambda_0 = 1.55\mu m$ and $n = 3.46$ is the refractive index of the semiconductor.

of mixture of photon and SP modes. Coherent oscillators in the regime near SP resonance has been termed SPASER [33]. The entire range of the dispersion relation can be explored for reducing wave guide beyond the diffraction limit, with different physics mechanisms, different degrees of confinement, and different amount of loss associated. The reason for reduced confinement near plasmon resonance can be illustrated by the rapid increase of k_z. A k_z roughly 15 times the wave vector in vacuum can be achieved near resonance. This increase in k_z can be viewed as a similar reduction of effective wavelengths, explaining the mechanism of size reduction. To illustrate the confinement in the case of dielectric approximation, or "photonic" regime in Fig. 3, we compare two slab waveguides: a) silver/semiconductor/silver sandwich structure and b) air/semiconductor/air structure. Fig. 4 shows the E-field profile across the waveguide a) (left) and waveguide b) (middle). As is clearly visible there, very good confinement can be always maintained in the case of metal cladding down to core width of $0.5\lambda_0/2n$, while the wave-guiding becomes quite poor in the case of air cladding (middle). To compare the two cases more quantitatively for the effective modal gain, we show in the right side of Fig. 4 the comparison of the confinement factor [26, 34], which determines the actual gain of a confined mode. It is interesting to see that as the core width decreases below $\lambda_0/2n$, the confinement factor for the waveguide with air cladding decreases rapidly, while the one with metal cladding increases significantly, due to the deteriorating transverse wave confinement in the first case, and the relative improvement of confinement in the case of metal cladding. Similar conclusions can be drawn also in the case of circular geometry. Fig. 5 shows the comparison of spatial patterns of a few modes around wavelength of $1.5\mu m$ for a cylindrical core-shell structure with silver or air cladding. As we see, the air cladding structure has very high Q when the core diameter is

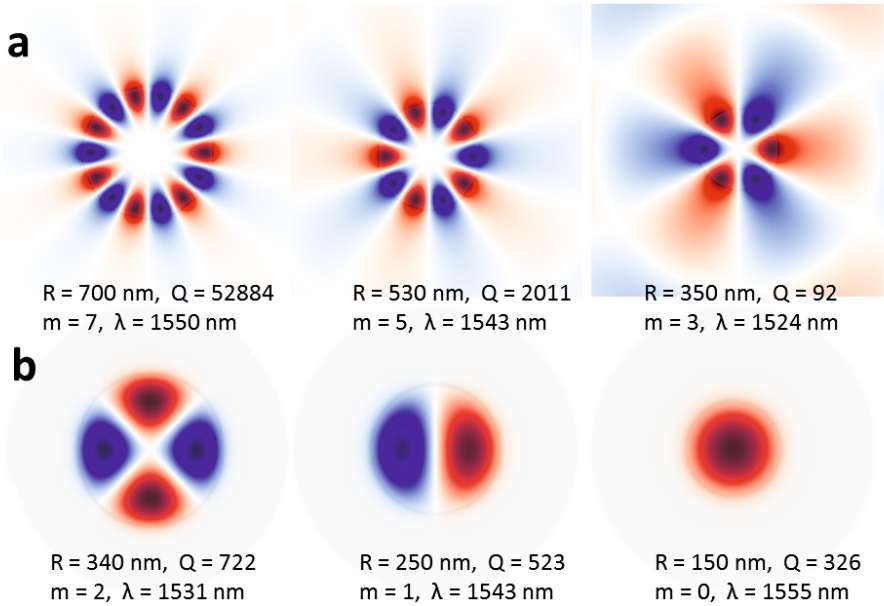

Fig. 5. Comparison of several modes at wavelengths around 1.5 μm. Top row: semiconductor (dielectric constant $\epsilon = 12$) disk surrounded by air. Bottom row: Semiconductor disk surrounded by silver. Despite significant loss at the near-infrared and smaller diameters, all silver-clad structures give larger cavity Q than high index contrast semiconductor-air structure with $R = 350nm$. R: radius of the semiconductor disk,m: mode index, λ: wavelength in vacuum.

large. However, with the reduction of core size, the Q factor for the air cladding decreases rapidly due to the increased radiative loss from the sides. For example, all the structures with metal cladding shown in Fig. 5(b) have core diameters smaller than that of the last one in the top row (with air cladding). But all those core-shell structures in (b) have much larger Q values than the last one in (a). In the cases of Fig. 5 and Fig. 4, the modes with metallic confinement are more dielectric modes or "photonic" as indicated in Fig. 3 (low energy regime). The advantages of such modes are the relatively low loss compared to the SPP regime or SPASER regime, but still with significant size reduction below the typically diffraction limit. The situations near SP resonance are described in several other papers [31, 26]. There is an interesting, but not yet completely resolved, issue of which regime is ultimately more beneficial for making smaller and more efficient nanolasers. The SPASER regime is extremely interesting, where coherent electronic motion could be potentially achieved through stimulated energy transfer between excited dipoles and oscillating plasmons [26] by optical means. Even though such spaser generation is in general dark, the dipole or multipole emissions of such stimulated oscillating plasmons could eventually emit photon

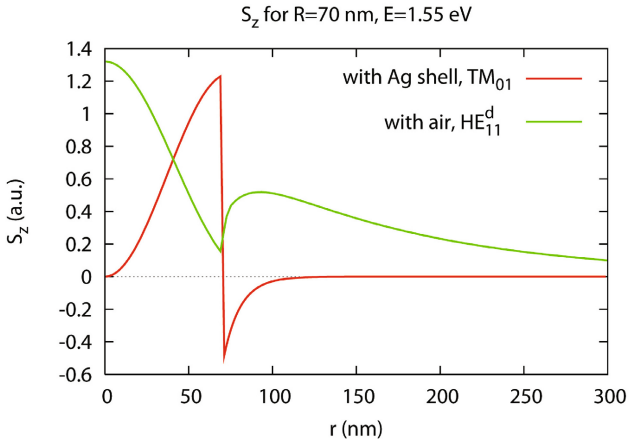

Fig. 6. Comparison of Poynting vectors (S_z) in core-shell structures with a semiconductor-metal or semiconductor-air [31, 26]. Dielectric constant of semiconductor is assumed to be ($\epsilon = 12$) and metal being silver. The fractions of the Poynting vector inside the core and metal are 1.28 and -0.28 respectively, while they are 0.09 inside and 0.91 outside the core, respectively, for the semiconductor-air structure.

fields to outside. Several experiments [47, 48] intended to demonstrate such a spaser and have shown interesting results. So far, coherent oscillation of a surface plasmon mode has not been measured directly, even though the associated photon modes were characterized. It is also interesting to establish the relationship between the properties of oscillating plasmons generated this way and the properties of photons emitted by such coherent plasmons.

For many applications that require conventional lasers but at nanoscale, the intermediate regime denoted by "SPP" in Fig. 3 is of great relevance. In this mixture-regime of SPPs, one can benefit from the much smaller confinement of plasmons, but can also detect the radiation of the photon waves at the same time. Fig. 6 shows transverse profile of the Poynting vector in a core-shell structure [31], similar to the situation shown in Fig. 5, but operating in the "SPP" regime. As can be seen, the profile with metal cladding shows localization at the core-shell interface. The overall confinement is much better than that with air cladding. This vast SPP regime of operating wavelengths has yet to be fully explored for nanolaser applications.

4 Recent Progress

Since the first feasibility study [31] and the initial demonstration of metallic cavity nanolases by Hill et al. [32], great progress has been made in a short period of 5 years. The initial demonstration used a cylindrical structure with a diameter of the core in the range of 240-280 nm. While this was an impressive small size, the core diameter is somewhat larger than the so-called diffraction limit of

$\lambda_0/2n_{eff} = 220nm$ or more accurately the minimum diameter of $\lambda_0/(\pi n_{eff}) = 146nm$ where $\lambda_0 = 1400nm$ is the wavelength of operation in vacuum and n_{eff} the effective index of refraction. To demonstrate the benefit and the irreplaceable role of metallic cavity and to beat the diffraction limit, a rectangular pillar structure was fabricated [40] such that the diffraction limit can be approached at least in one space direction, with the dimensions in other directions large enough to guarantee the existence of modes and the low enough threshold. The thinnest structure of this rectangular pillar has a thickness of 80-90 nm with a length of 6 micron. The total optical thickness of the device is: $90n_s+2\times20n_d+2\times20n_m nm$, where we assumed a metal layer penetration of 20 nm and include dielectric layers of 20 nm on either side of the semiconductor pillar. The effective indices of refraction for semiconductor (n_s), dielectrics (SiN,n_d), and metal (Ag, n_m) are assumed to be 3.1, 2.0 and 2.0, respectively. The total optical thickness of 400 nm is still smaller than the half-wavelength, 670 nm. This result has significance at several levels: 1) This was the first demonstration of a laser whose size in any dimension was below the half-wavelength (or diffraction) limit. 2) At the thickness of 80-90 nm, it is obvious that the structure is not enough to guide an optical mode to lase without metal cladding layers, thus demonstrating the necessity of metal cavity; 3)It is possible to over-compensate the metal loss to achieve lasing even with such thin semiconductor at the near infrared wavelength.

While such result was very encouraging, the operating temperature of these lasers was still too low (below 70 K)for such devices to have any practical applications. More importantly, there remained a more fundamental question: Is it possible for such nanolasers to ever operate at room temperature? This question is not only important for such nanolasers, it is also relevant for all the research activities around optical meta-materials where composite structures of metals and semiconductors are indispensable. The reason is that metal loss increases significantly with temperature due to increased phonon generation and the laser threshold will become too high to reach. The high injection level below threshold will also raise the temperature at device core, further decreasing the material gain and increasing the metal loss. It is therefore possible that such negative feedback would make such device impossible to work at room temperature. Thus it has been a challenge for the last few years to raise the operating temperature and to eventually achieve room temperature operation of sub-wavelength lasers.

In 2011, we were able to demonstrate several metallic-cavity lasers operating at 260 K [61]. Lasers with a total cavity volumes of $0.96\lambda_0^3$ or $0.78\lambda_0^3$ were shown lasing in continuous-wave (CW) mode under DC electrical injection up to 260 K. The laser linewidth was around 1-2 nm at the highest pumping level, representing a 3-7 times reduction of linewidth from the value below the lasing threshold. The device performance was further improved recently such that the operating at room temperature was demonstrated for several devices [50] with the smallest one having a volume of $0.42\lambda_0^3$. The linewidth of around 3-4 nm was however somewhat broad, considered too wider for such wavelength ranges. It was noted that overheating was the main reason that the devices could not operate at higher pumping, thus preventing better performances. A more sig-

nificant improvement of device performance was demonstrated more recently, [62–64] thanks to a modified design with somewhat thicker SiN insulating layer, improved surface treatment, better Ag deposition that led to large grain sizes on the order of device sizes. The most important indication of the performance improvement was the reduction of linewidth down to 0.5 nm at room temperature under continuous wave operation condition. This corresponds to a Q-factor under lasing condition of 3182, as compared to the Q of the empty cavity of 235. The device volume was $0.67\lambda_0^3$. This represents an unambiguous demonstration of the final goal of such sub-wavelength scale nanolasers. Such demonstration moves the nanolaser technology one step forward on the path of eventual applications. This might also have important implications to other meta-material related researches where metal-semiconductor composite structures are often used and where compensation of metal loss at room temperature is necessary.

5 Outlook

Nanolasers with sizes smaller than the operating wavelength in all three dimensions have attracted a great deal of attention over the last 6 years, since the proposal of the semiconductor-metal core-shell structures [31] and the first experimental realization [32]. Tremendous progress has been achieved in a short time span in theoretical understanding, device design, fabrication and characterization. Many design variations have been proposed and demonstrated. In the course of development of semiconductor lasers over the last 50 years, there have been a few paradigm shifts, the metallic cavity nanolaser being the most recent one. Such paradigm shifts have impacted significantly new design and development of better, smaller, and more efficient semiconductor lasers. Even though chip-scale integration and applications of semiconductor lasers have been proposed for a long time, the metallic cavity nanolasers represent a potential opportunity for such integration, since the smallest such nanolasers are already comparable with the modern day transistors in sizes. But before such chip-scale integrated nanophotonics becomes a reality, many challenges remain to be overcome. Chief among them are the followings:

- To achieve long lifetime operation: Even though the room temperature operation has been demonstrated, the lifetime is still too short due to high threshold and the associated severe heat generation. Further improvement in every step of the fabrication process is essential, from wafer growth, electron-beam lithography, various etching steps, interface and surface treatments, and deposition of dielectric and metallic layers, to achieve reduced threshold, reduced heat generation, and thus longer lifetime operation. Due to the small size of devices, any small error in fabrication would have a relatively large adverse effects on device performance. Thus perfection of fabrication is indispensable.
- To improve device efficiency: Currently the device efficiency is still too low and below 1% at low temperature and still lower at room temperature. Such

low efficiency is detrimental to on-chip applications due to wasted energy and heat generation. With improved fabrication and lower threshold, the efficiency will improve. New device design with better heat removal would further improve device efficiency. Even though the downsides associated with metals are known, but there are also upsides that have not been taken advantage of, such as the close proximity of metal layers to the active gain regions, which should facilitate more efficient heat removal. New designs taking advantage of such metal proximity should help improve the device efficiency. The replacement of poor thermal conducting dielectric materials by high quality semiconductor layers proposed recently [67] should improve many aspects of device performance.

- To further explore the siza reduction: Currently the smallest nanolaser of this type of design have volumes on the order of a fraction of in-vacuum wavelength cubed. Eventually it might be necessary to reduce the size even further to below the diffraction limit in all three dimensions. It is also interesting to see if there is a size limit to such down-scaling. Recently this was studied [67] with a more realistic design using a sandwich structure involving a single GaAs or InGaAs quantum well with AlGaAs barrier and sandwiched between two thin silver layer. It was shown that it is realistically possible to reduce the size down to as small as $1.5 \times 10^{-4}\lambda_0^3$, or with a physical size around 10^{-4} or $10^{-5}(\mu m)^3$. This would correspond to a few percent of the diffraction-limited volume $(\lambda_0/2n)^3$, where n is the index of refraction.
- To achieve efficient coupling and improve directionality: Even though such nanolasers are not intended for applications involving long distance free space coupling, far-field and near field patterns are important for short distance or direct near-field coupling. Due to the small size, the far-field emission angles can be as large as 90 degree [67]. Thus it is important to design structures that have small far-field lobes, or direct coupling through integration with a Si-waveguide [68] has to be adopted, as is shown recently through a simulation and design study.
- To reduce metal loss or to find alternative plasmonic structures: Metal loss remains one of the most important issues for such nanolasers, especially near the plasmonic resonance. Another related issue is that most of the metals are currently not grown with the typical epitaxial techniques used for growing semiconductors, even though some more recent research has demonstrated the usage of epitaxial metal [70]. Typical evaporation or sputtering techniques do not produce single crystal metals, thus exasperating the metal loss. A more preferred approach would be to use heavily doped semiconductors as plasmonic materials, as in the case of heavily doped InAs, which was studied recently [67]. There are several advantages of using such doped semiconductors including epitaxial compatibility with the growth of other semiconductors for gain regions, ability of growing the entire device in a single monolithic fashion, smaller plasmonic loss, and the tunability of plasmonic resonance after the fabrication of structure. All these advantages are expected to lead to smaller and better plasmonic or metallic nanolasers.

To conclude, it is fitting to point out the link of nanolaser with synergetics and an important consequence of the laser size reduction to nanoscale. As we mentioned, phase transition analogy between equilibrium and non-equilibrium systems has been an important aspect of synergetics. It is known that equilibrium phase transition requires a critical dimensionality and system size. While in the past such phase transition analogy has been mostly studied for large lasers, it is now possible to examine the phase transition properties more closely in the case of nanolasers. The relevant system size important for phase transition in the case of nanolasers seems to be the cavity size. The laser threshold is often characterized by a rapid super-linear increase of output intensity (L) as input current (I) is increased, or $L \propto I^s$, where the scaling index s is a measure of the sharpness of the transition. s changes from 20 to 1 when spontaneous emission factor changes from 0.001 for relatively large lasers to 1 [69] for extremely small lasers. It is known that the sharpness of the laser threshold transition is inversely proportional to spontaneous emission factor into lasing mode, which is in turn inversely proportional to the cavity size. Thus the sharpness of the threshold transition is proportional to the volume of the laser cavity. For nanolasers with ever decreasing cavity size, the spontaneous emission factor asymptotically approaches 1. In such a limit, $s \to 1$ and a nanolaser becomes a thresholdless device. The disappearance of a well-defined transition threshold in a nanolaser is again analogous to the situation in thermal equilibrium of a small size system. It is however, important to point out that such thresholdlessness does not mean that the laser threshold becomes zero, or thresholdless is not equal to threshold-zero. It simply means that a nanolaser in that limit is no longer a threshold device. The properties of light emission changes continuously as pumping is increased. The simple L-I curve is no longer enough to tell the change of the basic laser properties. More refined measurement, such as the second order correlation function is needed to characterize such continuous change of the laser properties [71]. It is therefore interesting to study how the results and conclusions of synergetics can be extended to nanoscale non-equilibrium systems, such as nanolasers.

Acknowledgements. The author thanks Alex Maslov, Kang Ding, and Martin Hill for their collaboration during different stages of the nanolaser research over the last 7 years. Kang Ding in addition prepared some of the figures. Different parts of the results reported here were obtained under the support of the Defense Advanced Research Project Agency (DARPA) program Nanoscale Architectures of Coherent Hyper-Optical Sources (NACHOS, W911-NF07-1-0314, managed by the late Henryk Temkin, Michael Haney, Scott Rodgers, and Michael Gerhold) and by the Air Force Office of Scientific Research (FA9550-10-1-0444, Gernot Pomrenke).

References

1. Haken, H.: Synergetics, An Introduction: Nonequilibrium Phase Transitions and Self-Organization in Physics, Chemistry, and Biology, 3rd edn. Springer, Berlin (1983)

2. Haken, H.: Advanced Synergetics: Instability Hierarchies of Self-Organizing Systems and Devices. Springer, Berlin (1993)
3. Ning, C.Z., Haken, H.: Detuned lasers and the complex Lorenz equations: sub- and supercritical Hopf bifurcations. Phys. Rev. A **41**, 3826 (1990)
4. Ning, C.Z., Haken, H.: Generalized Ginzburg-Landau equation for self- pulsing instability in a two-photon laser. Z. Phys. B **77**, 163 (1989)
5. Berry, M.V.: Quantal phase factors accompanying adiabatic changes. Proc. R. Soc. Lond. A **392**, 45–57 (1984)
6. Ning, C.Z., Haken, H.: Quasiperiodicity involving twin oscillations in the complex Lorenz equations describing a detuned laser. Z. Phys. B **81**, 457 (1990)
7. Ning, C.Z., Haken, H.: Phase anholonomy in dissipative optical systems with periodic oscillation. Phys. Rev. A **43**, 6410 (1991)
8. Ning, C.Z., Haken, H.: Geometrical phase and amplitude accumulations in dissipative systems with cyclic attractors. Phys. Rev. Lett. **68**, 2109 (1992)
9. Ning, C.Z., Haken, H.: The geometric phase in nonlinear dissipative systems (an invited review). Mod. Phys. Lett. B **6**, 1541 (1992)
10. Landsberg, A.S.: Geometrical phases and symmetries in dissipative systems. Phys. Rev. Lett. **69**, 865–868 (1992)
11. Sinitsyn, N.A.: The stochastic pump effect and geometric phases in dissipative and stochastic systems. J. Phys. A **42**, 193001 (2009)
12. Friedrich, R.: Higher instabilities in synergetic systems with continuou sysmmetries. Z. Phys. B **90**, 373–376 (1993)
13. Hu, G., Ditzinger, T., Ning, C.Z., Haken, H.: Stochastic resonance without external signal. Phys. Rev. Lett. **71**, 807 (1993)
14. Neiman, A.: Coherence resonance. Scholarpedia **2**, 1442 (2007). `http://www.scholarpedia.org/article/Coherence\_resonance`
15. Haken, H., Graham, R.: Synergetik. Die Lehre vom Zusammenwirken. Umschau **6**, 191 (1971)
16. Haken, H.: Cooperative phenomena in systems far from thermal equilibrium and in nonphysical systems. Rev. Mod. Phys. **47**, 67–121 (1975)
17. Haken, H.: Light II. Laser Light Dynamics. North Holland, Amsterdam (1986)
18. Haken, H.: Laser Theory. vol. XXV/2c, Encyclopedia of Physics. Springer, Berlin (1970)
19. Haken, H.: Theory of coherence of laser light. Phys. Rev. Lett. **13**, 329–331 (1964)
20. Haken, E., Haken, H.: Zur Theorie des Halbleiter-Lasers. Z. Phys. **176**, 421–428 (1963)
21. Haug, H., Haken, H.: Theory of noise in semiconductor laser emission. Z. Phys. **204**, 262–275 (1967)
22. Henry, C.: Theory of the linewidth of semiconductor lasers. IEEE J. Quantum Electron. **18**, 259–264 (1982)
23. Haken, H.: Quantenfeldtheorie des Festkrpers, 2nd edn. Teubner, Stuttgart (1993)
24. Haug, H., Koch, S.W.: Quantum Theory of the Optical and Electronic Properties of Semiconductors. World Scientific, Singapore (2004)
25. Chow, W.W., Koch, S.W., Sargent, M.: Semiconductor-Laser Physics. Springer, Berlin (1994)
26. Ning, C.Z.: Semiconductor Nanolasers (Tutorial). Phys. Stat. Sol. B **247**, 774–788 (2010)
27. Huang, M.H., Mao, S., Feick, H., Yan, H., Wu, Y., Kind, H., Weber, E., Russo, R., Yang, P.: Room-Temperature Ultraviolet Nanowire Nanolasers. Science **292**, 1897–1899 (2001)

28. Ning, C.Z.: Semiconductor nanowire lasers. In: Coleman, J.J., Bryce, A.C., Jagadish, C. (eds.) Advances in Semiconductor Lasers. Semiconductors and Semimetals, vol. 86, pp. 455–486. Academic Press, Burlington (2012)
29. Maslov, A.V., Ning, C.Z.: Reflection of guided modes in a semiconductor nanowire laser. Appl. Phys. Lett. **83**, 1237 (2003)
30. Chin, A., Vaddiraju, S., Maslov, A., Ning, C.Z., Sunkara, M., Meyyappan, M.: Near Infrared Sub-wavelength-wire lasing. Appl. Phys. Lett. **88**, 163115 (2006)
31. Maslov, A.V., Ning, C.Z.: Size reduction of a semiconductor nanowire laser using metal coating. SPIE Proceed. **6468**, 64680I (2007)
32. Hill, M.T., Oei, Y.S., Smalbrugge, B., Zhu, Y.C., Veries, T.D., Veldhoven, P.J.V., et al.: Lasing in metallic-coated nanocavities. Nat. Photon. **1**, 589–594 (2007)
33. Bergman, D., Stockman, M.: Surface plasmon amplification by stimulated emission of radiation: quantum generation of coherent surface plasmons in nanosystems. Phys. Rev. Lett. **90**, 027402 (2003)
34. Li, D.B., Ning, C.Z.: Peculiar features of confinement factors in a metal-semiconductor waveguide. Appl. Phys. Lett. **96**, 181109 (2010)
35. Hall, R.N., Fenner, G.E., Kingsley, J.D., Soltys, T.J., Carlson, R.O.: Coherent light emission from GaAs junctions. Phys. Rev. Lett. **9**, 366–386 (1962)
36. Nathan, M.I., Dumke, W.P., Burns, G., Dill, F.H., Lasher, G.: Stimulated emission of radiation from GaAs p-n junctions. Appl. Phys. Lett. **1**, 62–64 (1962)
37. Holonyak, N., Bevacqua, S.F.: Coherent visible light emission from Ga(AsP) junctions. Appl. Phys. Lett. **1**, 82 (1962)
38. Nezhad, M.P., Tetz, K., Fainman, Y.: Gain assisted propagation of surface Plasmon polaritons on planar metallic waveguides. Opt. Express **12**, 4072–4079 (2004)
39. Maier, S.A.: Gain-assisted propagation of electromagnetic energy in subwavelength surface plasmon polariton gap waveguides. Opt. Commun. **258**, 295–299 (2006)
40. Hill, M.T., Marell, M., Leong, E.S.P., Smalbrugge, B., Zhu, Y.C., Sun, M.H., van Veldhoven, P.J., Geluk, E.J., Karouta, F., Oei, Y.S., Ntzel, R., Ning, C.Z., Smit, M.K.: Lasing in metal-insulator-metal sub-wavelength plasmonic waveguides. Opt. Express **17**, 11107–11112 (2009)
41. Nezhad, M.P., Simic, A., Bondarenko, O., Slutsky, B., Mizrahi, A., Feng, L., et al.: Room-temperature subwavelength metallo-dielectric lasers. Nat. Photon. **4**, 395–399 (2010)
42. Li, D.B., Ning, C.Z.: Giant modal gain, amplified surface plasmon-polariton propagation, and slowing down of energy velocity in a metal-semiconductor-metal structure. Phys. Rev. B **80**, 153304 (2009)
43. Yu, K., Lakhani, A., Wu, M.C.: Subwavelength metal-optic semiconductor nanopatch lasers. Opt. Express **18**, 8790–8799 (2010)
44. Perahia, R., Mayer, T.P., Safavi-Naeini, A.H., Painter, O.: Suface-plasmon mode hybridization in subwavelength microdisk lasers. Appl. Phys. Lett. **95**, 201114–201116 (2009)
45. Kwon, S.H., Kang, J.H., Seassal, C., Kim, S.K., Regreny, P., Lee, Y.H., et al.: Subwavelength plasmonic lasing from a semiconductor nanodisk with silver nanopan cavity. Nano Lett. **10**, 3679–3683 (2010)
46. Lu, C.Y., Chang, S.W., Chuang, S.L., Germann, T.D., Bimberg, D.: Metal-cavity surface-emitting microlaser at room temperature. Appl. Phys. Lett. **96**, 251101–251103 (2010)
47. Oulton, R.F., Sorger, V.J., Zentgraf, T., Ma, R.M., Gladden, C., Dai, L., et al.: Plasmon lasers at deep subwavelength scale. Nature **461**, 629–632 (2009)

48. Noginov, M.A., Zhu, G., Belgrave, A.M., Bakker, R., Shalaev, V.M., Narimanov, E.E., et al.: Demonstration of a spacer-based nanolaser. Nature **460**, 1110–1112 (2009)
49. Li, D.B., Ning, C.Z.: Giant modal gain, amplified surface plasmon-polariton propagation, and slowing down of energy velocity in a metal-semiconductor-metal structure. Phys. Rev. B **80**, 153304–153307 (2009)
50. Ding, K., Liu, Z.C., Yin, L.J., Hill, M.T., Marell, M.J.H., Veldhoven, P.J.V., Netzel, R., Ning, C.Z.: Room-temperature continuous wave lasing in deep-subwavelength metallic cavities under electrical injection. Phys. Rev. B **85**, 041301–041305 (2012)
51. Park, H.G., Kim, S.H., Kwon, S.H., Ju, Y.G., Yang, J.K., Baek, J.H., et al.: Electrically driven single-cell photonic crystal laser. Science **305**, 1444–1447 (2004)
52. Altug, H., Englund, D., Vuckovic, J.: Ultrafast photonics crystal nanocavity laser. Nat. Phys. **2**, 485–488 (2006)
53. Zia, R., Selker, M.D., Catrysse, P.B., Brongersma, M.L.: Geometries and materials for subwavelength surface plasmon modes. J. Opt. Soc. Am. A **21**, 2442–2446 (2004)
54. Kusunoki, F., Yotsuya, T., Takahara, J., Kobayashi, T.: Propagation properties of guided waves in index-guided two-dimensional optical waveguides. Appl. Phys. Lett. **86**, 211101–211103 (2005)
55. Tanaka, K., Tanaka, M.: Simulations of nanometric optical circuits based on surface plasmon polariton gap waveguide. Appl. Phys. Lett. **82**, 1158–1160 (2003)
56. Feng, N.N., Brongersma, M.L., Negro, L.D.: Metal-dielectric slot-waveguide structures for the propagation of surface plasmon polaritons at 1.55 m. IEEE J. Quan. Electron. **43**, 479–485 (2007)
57. Feigenbaum, E., Orenstein, M.: Optical 3D cavity modes below the diffraction-limit using slow-wave surface-plasmon-polaritons. Opt. Expr. **15**, 2607–2612 (2007)
58. Miyazaki, H.T., Kurokawa, Y.: Squeezing visible light waves into a 3-nm-thick and 55-nm-long plasmon cavity. Phys. Rev. Lett. **96**, 097401–097404 (2006)
59. Kaminow, I.P., Mammel, W.L., Weber, H.P.: Metal-clad optical waveguides: analytical and experimental study. Appl. Optics **13**, 396–405 (1974)
60. Dionne, J.A., Sweatlock, L.A., Atwater, H.A., Polman, A.: Plasmon slot waveguides: Towards chip-scale propagation with subwavelength-scale localization. Phys. Rev. B **73**, 035407 (2006)
61. Ding, K., Liu, Z.C., Yin, L.J., Wang, H., Liu, R.B., Hill, M.T., Marell, M.J.H., van Veldhoven, P.J., Notzel, R., Ning, C.Z.: Electrical injection, continuous wave operation of subwavelength-metallic cavity lasers at 260 K. Appl. Phys. Lett. **98**, 231108–231110 (2011)
62. Ding, K., Hill, M., Liu, Z., Yin, L., Sahin, D., van Veldhoven, P., Geluk, E., Vries, T.D., Ning, C.Z.: Record performance of a CW metallic subwavelength-cavity laser at room temperature. In: Conference on Lasers and Electro-Optics (CLEO), San Jose, CA, May 6–11, 2012
63. Ding, K., Hill, M.T., Liu, Z.C., Yin, L.J., van Veldhoven, P.J., Ning, C.Z.: Unambiguous demonstration of room temperature CW operation of a subwavelength metallic cavity laser. In: 23rd International Semiconductor Laser Conference (ISLC), pp. 145–146. IEEE, San Diego, October 7–10, 2012. 10.1109/ISLC.2012.6348376
64. Ding, K., Hill, M.T., Liu, Z.C., Yin, L.J., Veldhoven, P.J.V., Ning, C.Z.: Record performance of electrical injection sub-wavelength metallic-cavity semiconductor lasers at room temperature. Opt. Express **21**, 4728–4733 (2013)

65. Rana, F., Manolatou, C.: Subwavelength Nanopatch cavities for semiconductor plasmon lasers. IEEE J. Quan. Electron. **44**, 435–447 (2008)
66. Oulton, R.F., Sorger, V.J., Genov, D., Pile, D.F.P., Zhang, X.: A hybrid plasmonic waveguide for subwavelength confinement and long-range propagation. Nat. Photon. **2**, 496–500 (2008)
67. Li, D.B., Ning, C.Z.: Interplay of various loss mechanisms and ultimate size limit of a surface plasmon polariton semiconductor nanolaser. Opt. Express **20**, 16348–16357 (2012)
68. Ding, K., Ning, C.Z.: Metallic subwavelength-cavity semiconductor nanolasers. Light: Science and Applications **1**, e20 (2012)
69. Ning, C.Z.: What is a laser threshold? IEEE J. Sel. Top. Quant. Electr. **19**, 1503604 (2013)
70. Lu, Y.-J., Kim, J., Chen, H.-Y., Wu, C., Dabidian, N., Sanders, C.E., Wang, C.-Y., Lu, M.Y., Li, B.-H., Qiu, X., Chang, W.-H., Chen, L.-J., Shvets, G., Shih, C.-K., Gwo, S.: Plasmonic Nanolaser Using Epitaxially Grown Silver Film. Science **337**, 450–453 (2012)
71. Gies, C., Wiersig, J., Lorke, M., Jahnke, F.: Semiconductor model for quantum dot based microcavity lasers. Phys. Rev. A **75**, 013803 (2007)

Description of Bose-Einstein Condensates in $\mathcal{PT}$-Symmetric Double Wells

Dennis Dast, Daniel Haag, Holger Cartarius, Günter Wunner,
Rüdiger Eichler, and Jörg Main

Institut für Theoretische Physik 1, Universität Stuttgart, Pfaffenwaldring 57,
70550 Stuttgart, Germany
{dennis.dast,daniel.haag,holger.cartarius,wunner,
ruediger.eichler,main}@itp1.uni-stuttgart.de
http://itp1.uni-stuttgart.de/institut/arbeitsgruppen/wunner

Abstract. The Gross-Pitaevskii equation for a Bose-Einstein condensate in a $\mathcal{PT}$-symmetric double-well potential is investigated theoretically. An in- and outcoupling of atoms is modelled by an antisymmetric imaginary potential rendering the Hamiltonian non-Hermitian. Stationary states with real energies and $\mathcal{PT}$-symmetric wave functions are found, which proves that Bose-Einstein condensates are a good candidate for a first experimental verification of a $\mathcal{PT}$-symmetric quantum system. Time-resolved calculations demonstrate typical effects only observable in $\mathcal{PT}$-symmetric potentials, viz. an oscillation of the condensate's probability density between these wells with an oscillation frequency critically depending on the strength of the in- and outcoupling. $\mathcal{PT}$-broken eigenstates with complex energy eigenvalues are also solutions of the time-independent Gross-Pitaevskii equation but are not true stationary states of its time-dependent counterpart. The comparison of a one-dimensional and a three-dimensional calculation shows that it is possible to extract highly precise quantitative results for a fully three-dimensional physical setup from a simple one-dimensional description.

Keywords: Bose-Einstein condensates, $\mathcal{PT}$ symmetry, Gross-Pitaevskii equation, stationary states, dynamics

1 Introduction

Mainly due to the experimental accessibility, which became possible very recently [1, 2], non-Hermitian $\mathcal{PT}$-symmetric quantum mechanics has gained an increasing attention over the last years [1–17]. It describes physical systems governed by a complex Hamiltonian which is not Hermitian but fulfils parity-time symmetry. This means that the Hamiltonian remains invariant under the combined action of the parity ($\mathcal{P}$) and time reversal ($\mathcal{T}$) operators, i.e. $[\mathcal{PT}, H] = 0$, with

$$\mathcal{P}x = -x\,, \qquad \mathcal{P}p = -p \tag{1a}$$

$$\mathcal{T}x = x\,, \qquad \mathcal{T}p = -p\,, \qquad \mathcal{T}\mathrm{i} = -\mathrm{i}\,. \tag{1b}$$

A. Pelster and G. Wunner (eds.), *Selforganization in Complex Systems: The Past, Present, and Future of Synergetics*, Understanding Complex Systems,
DOI: 10.1007/978-3-319-27635-9_9

In spite of their non-Hermiticity these Hamiltonians possess real energy spectra for properly chosen physical parameters. Besides the emergence of real energy eigenvalues, phenomena are observable which are only possible in non-Hermitian systems and not known in Hermitian quantum mechanics describing the spectra of bound states. The most striking effects are connected with so-called exceptional points [18], i.e. isolated points in the physical parameter space at which two or even more solutions pass through a branch point singularity, where both the energies *and* the wave functions of the two states become identical.

Bender and Boettcher introduced a simple and instructive model that covers all interesting features of a $\mathcal{PT}$-symmetric quantum system [3]. It consists of the Hamiltonian

$$H = p^2 - (\mathrm{i}x)^N \ , \tag{2}$$

where N is allowed to assume the value of any real number. In a very simple calculation it can be confirmed that $[\mathcal{PT}, H] = 0$, i.e. this Hamiltonian is $\mathcal{PT}$ symmetric. Evidently, $N = 2$ represents the harmonic oscillator, of which we know that its spectrum is real and positive. Bender and Boettcher found that this fact remains true for all $N \geq 2$, however, if N is reduced below 2 one observes that successively one pair of consecutive eigenvalues after the other passes through a branch point singularity. Beyond the branch point both eigenvalues become complex and complex conjugate. This eigenvalue structure already describes the typical behaviour of parameter-dependent $\mathcal{PT}$-symmetric Hamiltonians.

In the wake of the discovery of Bender and Boettcher, a large number of systems with $\mathcal{PT}$-symmetric Hamiltonians have become the subject of theoretical and experimental studies. It is no surprise that the most sophisticated experimental progress in the investigation of $\mathcal{PT}$-symmetric physical systems has been achieved in optics [5, 7, 9, 12, 15, 16, 19]. The gain and loss contributions required to set up a non-Hermitian $\mathcal{PT}$-symmetric system can be implemented, e.g. with optical pumping (gain) and absorptive media (loss), i.e. by exploiting well established techniques.

Due to the well known analogy that the wave equation for the transverse electric field mode is formally equivalent to a one-dimensional Schrödinger equation these optical systems can be considered as a simulation of the motion of a quantum particle in a potential of the form $V(x) = -k^2 n^2(x)$, where n is the (complex) refractive index. However, these studies cannot completely substitute studies of quantum systems, and the verification of $\mathcal{PT}$ symmetry in a true quantum system is highly desirable. Klaiman et al. [9] proposed a quantum analogue to the optical experiments consisting of a Bose-Einstein condensate in a double-well potential. The gain and loss terms could be realised by coherently removing atoms from one well and injecting atoms into the other.

At sufficiently low temperatures one may assume that *all* atoms of a dilute gas of weakly interacting Bosons trapped in an optical potential are in their ground state. Then the system can be well described by the Gross-Pitaevskii equation [20, 21], i.e. the Hartree approximation of the corresponding many-particle equation, where all single-particle orbitals are given by the same state. In a particle number scaled form and in appropriate units the Gross-Pitaevskii

equation reads

$$\mathrm{i}\dot{\psi}(\boldsymbol{x},t) = \left(-\Delta + V(\boldsymbol{x}) - g|\psi(\boldsymbol{x},t)|^2\right)\psi(\boldsymbol{x},t)\ . \tag{3}$$

The trapping potential for the atoms is described by $V(\boldsymbol{x})$. Additionally, the atoms interact via the short-range van der Waals force, of which a description with an s-wave scattering process is sufficient in the dilute gas. Its strength g is determined by the scattering length.

It is the scattering term $-g|\psi(\boldsymbol{x},t)|^2$ which needs a further consideration since it leads to a crucial modification of the Schrödinger equation. The Gross-Pitaevskii equation (3) is nonlinear in the wave function. This has direct consequences for the $\mathcal{PT}$ symmetry of the system. For a $\mathcal{PT}$-symmetric system we require, as mentioned above, $[\mathcal{PT}, H] = 0$. Since the kinetic energy term in the Hamiltonian is always $\mathcal{PT}$ symmetric one directly obtains the necessary condition for the potential,

$$V^*(-\boldsymbol{x}) = V(\boldsymbol{x})\ . \tag{4}$$

This has also to be fulfilled by the scattering term. Thus, for the total Hamiltonian to be $\mathcal{PT}$ symmetric the square modulus of the wave function which is the solution of the Gross-Pitaevskii equation has to be a symmetric function of $\boldsymbol{x}$.

In previous studies of $\mathcal{PT}$-symmetric systems with nonlinearity it was found that the nonlinearity not necessarily destroys the appearance of real eigenvalues in the spectrum or their coalescence in branch point singularities. Indeed, $\mathcal{PT}$-symmetric eigenstates with real energies have been found for a non-Hermitian Bose-Hubbard model [10, 11, 22], quantum mechanical model potentials [8], optical waveguide structures [7, 15], and for Bose-Einstein condensate in an idealised double-δ trap [23, 24], or in a spatially extended double well [25].

In this article we will solve the Gross-Pitaevskii equation for a Bose-Einstein condensate in a double well with antisymmetric imaginary potential contributions describing effectively gain and loss processes. We show that it exhibits $\mathcal{PT}$-symmetric solutions, which is important because $\mathcal{PT}$-symmetric wave functions always have a square modulus which is a symmetric function of the coordinate x. A Bose-Einstein condensate is a fully three-dimensional object, however, for the investigation of the $\mathcal{PT}$ symmetry only a gain-loss profile in one spatial direction is required. Thus, one may assume that it is sufficient to reduce the theoretical description to one dimension without losing any relevant information. We will demonstrate that this is exactly the case. But the correspondence of the one- and three-dimensional solutions we obtain is even stronger. We show that the solution of a Gross-Pitaevskii equation with adequately rescaled nonlinearity is capable of providing quantitatively correct predictions for the fully three-dimensional treatment. By the variation of the trap frequencies it will always be possible to realise a regime in which the influence of the two additional dimensions can be obtained without any explicit calculation. Furthermore, we show that a stable dynamics of condensate wave functions is possible in the system with gain and loss. This will be crucial for an experimental observability.

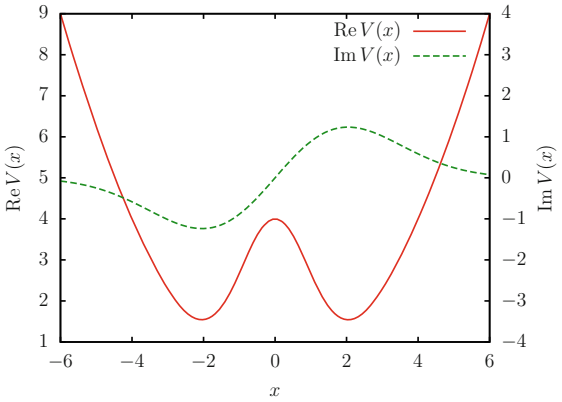

Fig. 1. Visualisation of the $\mathcal{PT}$-symmetric external potential in x direction. The real part (solid line) defines the confinement of the condensed atom cloud, and the imaginary part (dashed line) describes the in-/outcoupling of atoms.

In Sect. 2 we present the system and the corresponding Gross-Pitaevskii equation. Additionally, we introduce two numerical methods for the calculation of the stationary states. Then we discuss the numerical results for the energy eigenvalues and investigate quantitatively the quality of one-dimensional model calculations for the fully three-dimensional condensate in Sect. 3. Finally, we study the stability of the condensate with numerically accurate dynamical computations in Sect. 4. Conclusions are drawn in Sect. 5.

2 Theoretical description of the Bose-Einstein condensate in the double well

2.1 Gross-Pitaevskii equation

The Bose-Einstein condensate of atoms with mass m is, in the mean-field limit, described by the Gross-Pitaevskii equation (3), where we assume a potential of the form

$$V(\boldsymbol{x}) = \frac{m}{2}\omega_x^2 x^2 + \frac{m}{2}\omega_{y,z}^2(y^2+z^2) + v_0 e^{-\sigma x^2} + \mathrm{i}\Gamma x \mathrm{e}^{-\rho x^2} \,. \tag{5}$$

It consists of a three-dimensional harmonic trap with trapping frequencies ω_x for the x direction and $\omega_{y,z}$ for the two remaining spatial coordinates. To form a double well it is superimposed with a Gaussian barrier in x direction. This results in the one-dimensional projection of the potential as shown in Fig. 1. It is obvious that the barrier has its maximum at $x = 0$. Its height is v_0 and the width of the Gaussian is given by σ. The imaginary contribution of strength Γ is an effective description of a gain or loss of atoms. As can be confirmed by a simple calculation the external potential (5) is $\mathcal{PT}$ symmetric.

The coherent addition and removal of atoms proposed by Klaiman et al. [9] can in principle be achieved by several methods. For example, appropriate laser setups forming Bragg beams may be exploited to actively transport atoms from a reservoir to one of the wells and to eject atoms from the other [26, 27]. The reservoir can be a third well or a completely independent trap geometry. One may also imagine a geometry with multiple wells in a row. If these wells are close enough such that the condensate's probability density may tunnel from one well to its neighbouring well a flow of particles with a defined direction could be generated by different potential offsets for the single wells. However, in this article we concentrate on the effects of the $\mathcal{PT}$-symmetric external potential and will keep the equations as simple as possible. Thus, we adopt the formalism used for the optical systems [5, 7, 9, 12, 15, 16, 19], where a complex refractive index was used, and simulate an outcoupling of atoms with a negative imaginary potential contribution in the left well, whereas a positive imaginary part in the right well reflects in incoupling of atoms. Since the potential affects the probability amplitude of the whole condensate the physical interpretation is a *coherent* coupling, which is in agreement with our physical interpretation of the process since we do not consider individual atoms but a macroscopic wave function of the condensed phase.

With the length scale $a_0 = \sqrt{\hbar/2m\omega_x}$ defined by the trap frequency in the direction of the double well and the unit of energy $E_0 = \hbar^2/2ma_0^2$ the dimensionless potential assumes the form

$$V(\boldsymbol{x}) = \frac{1}{4}x^2 + \frac{1}{4}\omega_{y,z}^2(y^2+z^2) + v_0 e^{-\sigma x^2} + \mathrm{i}\Gamma x \mathrm{e}^{-\rho x^2} \ . \tag{6}$$

Then the dynamics is governed by the time-dependent Gross-Pitaevskii equation (3). To obtain stationary solutions we solve its time-independent variant, viz.

$$\left(-\Delta + V(\boldsymbol{x}) - g|\phi(\boldsymbol{x})|^2\right)\phi(\boldsymbol{x}) = \mu\phi(\boldsymbol{x}) \ , \tag{7}$$

where the chemical potential μ has been introduced with the usual ansatz $\psi(\boldsymbol{x},t) = \phi(\boldsymbol{x})\mathrm{e}^{-\mathrm{i}\mu t}$. For all calculations we keep the parameters $v_0 = 4$ and $\sigma = 0.5$ fixed. The width parameter ρ of the imaginary gain-loss potential is chosen to be

$$\rho = \frac{\sigma}{2\ln(4v_0\sigma)} \ . \tag{8}$$

This choice guarantees that the extrema of the real and imaginary potential parts coincide, as is illustrated in Fig. 1. A one-dimensional description is obtained with the potential

$$V(x) = \frac{1}{4}x^2 + v_0 e^{-\sigma x^2} + \mathrm{i}\Gamma x \mathrm{e}^{-\rho x^2} \ , \tag{9}$$

in which only the x direction is considered and all y and z terms are removed. Obviously it contains all the relevant information about the $\mathcal{PT}$ symmetry.

2.2 Numerical methods

We apply two independent methods to solve the time-dependent and time-independent Gross-Pitaevskii equations (3) and (7). Our first method is a Gaussian variational approach [28, 29] based on the idea to restrict the wave function to a Gaussian form, viz.

$$\psi(\boldsymbol{z},\boldsymbol{x}) = \sum_{k=1}^{N_\mathrm{G}} \mathrm{e}^{-\left[A_x^k (x-q_x^k)^2 + A_{y,z}^k (y^2+z^2)\right]} \mathrm{e}^{\mathrm{i}p_x^k (x-q_x^k) - \varphi^k} \ . \tag{10}$$

Within this approach the dynamics is described by the small set of variational parameters

$$\boldsymbol{z}(t) = \left\{ A_x^k(t), A_{y,z}^k(t), q_x^k(t), p_x^k(t), \varphi^k \right\} \ . \tag{11}$$

The most simple ansatz is a superposition of two Gaussian wave functions, each of them located in one of the wells, i.e. $N_\mathrm{G} = 2$ in (10). Then the real coordinates q_x^1, q_x^2, p_x^1 and p_x^2 determine the positions and momenta of the Gaussians. The widths of the Gaussians are given by the complex parameters A_x^1, A_x^2, $A_{y,z}^1$ and $A_{y,z}^2$, where we chose identical widths for the y and z directions, in agreement with the symmetry of the external potential (5). Finally, the complex quantities φ^1 and φ^2 determine the amplitudes and phases.

The application of the McLachlan time-dependent variational principle [30],

$$\delta I = \delta || i\chi(\boldsymbol{z}(t),\boldsymbol{x}) - H\psi(\boldsymbol{z}(t),\boldsymbol{x}) ||^2 \stackrel{!}{=} 0 \ , \tag{12}$$

leads to a set of ordinary differential equations for the parameters (11) after the variation with respect to χ and the subsequent replacement $\dot{\psi} \equiv \chi$. Stationary states or solutions of the time-independent Gross-Pitaevskii equation (7) are found if the conditions $\dot{A}_x^k = \dot{A}_{y,z}^k = \dot{q}_x^k = \dot{p}_x^k = 0$, and $\dot{\varphi}^1 = \dot{\varphi}^2$ are fulfilled. A detailed explanation of the procedure can be found in reference [25].

The advantage of the Gaussian variational method is its high scalability, i.e. the difference of the numerical costs between the one- and three-dimensional descriptions is very moderate. Nevertheless, it provides highly precise solutions [31–33]. However, since in this analysis of $\mathcal{PT}$-symmetric Bose-Einstein condensates the method is applied for the first time to nonlinear complex potentials we compare its results to numerically exact solutions of the Gross-Pitaevskii equation in one dimension. To obtain the numerically exact stationary states the wave functions are integrated outward from $x = 0$ in positive and negative direction using a Runge-Kutta algorithm. The initial values $\mathrm{Re}\,\psi(0), \psi'(0) \in \mathbb{C}$, and $\mu \in \mathbb{C}$ are chosen such that the wave functions are square integrable ($\psi(\infty) \to 0, \quad \psi(-\infty) \to 0$) and normalised $||\psi|| = 1$. For numerically exact dynamical calculations we apply the split-operator method.

3 Stationary states

3.1 General behaviour of the solutions

Fig. 2 shows the results of the solution of the Gross-Pitaevskii equation (7). Let

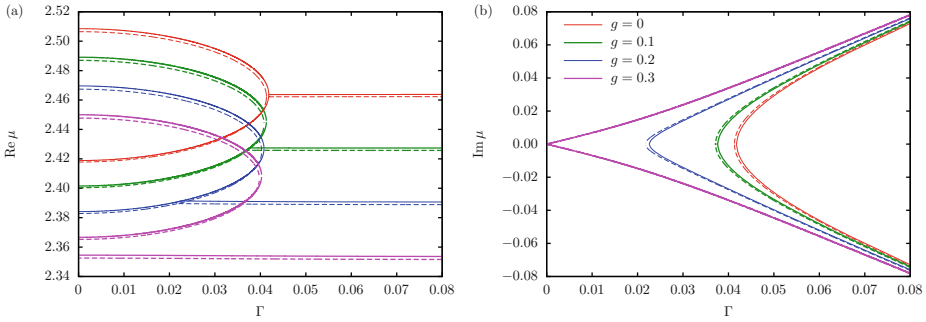

Fig. 2. Real and imaginary parts of the energy eigenvalues μ of the stationary Gross-Pitaevskii equation (7) as a function of the the gain-loss parameter Γ. The Gaussian approximation (solid lines) and the numerically exact solutions (dashed lines) show an excellent agreement. In the left panel, g increases from top to bottom, in the right panel from right to left.

us first concentrate on the linear case $g = 0$, which exhibits the typical behaviour known from other $\mathcal{PT}$-symmetric systems (top curve in the left panel and rightmost curve in the right panel). Below a critical value $\Gamma_{\mathrm{EP}} \approx 0.04$ of the gain-loss parameter Γ we find two real eigenvalues, corresponding to a ground state with completely symmetric wave function for $\Gamma = 0$ and an excited state, of which the wave function is completely antisymmetric for $\Gamma = 0$. At $\Gamma_{\mathrm{EP}} \approx 0.04$ the two solutions merge in an exceptional point, where we have confirmed that indeed the wave functions become identical. Increasing Γ further we obtain two complex conjugate solutions. One also notes that the agreement between the Gaussian approximation and the numerically exact solution is excellent.

Obviously the real eigenvalues do not vanish in the case $g \neq 0$. This is an important result since it indicates a persistence of the $\mathcal{PT}$ symmetry in the nonlinear quantum system. Non-decaying states are present. However, if we want to be sure about the symmetry we have to look at the wave functions. As mentioned in the introduction the $\mathcal{PT}$ symmetry of the Gross-Pitaevskii equation (7) depends on its solution, or, to be more precise, on the shape of the wave function's square modulus. It has to be a symmetric function of x. Is this the case? The answer to this question is given in Figs. 3(a) and (b), which show the wave functions belonging to both real eigenvalues for $g = 0.2$ and $\Gamma = 0.03$. The square moduli are symmetric functions of x. This confirms that the case of exact $\mathcal{PT}$ symmetry is fulfilled.

There are also, as in the linear case, states with complex eigenvalues. From linear $\mathcal{PT}$-symmetric models we know that these complex eigenvalue solutions belong to $\mathcal{PT}$-broken wave functions. This behaviour is also found in our case, cf. Figs. 3(c) and (d). This has crucial impact on the nonlinear Gross-Pitaevskii equation. Since the square moduli of the wave functions are not symmetric functions of x the $\mathcal{PT}$ symmetry of the *Hamiltonian* is destroyed.

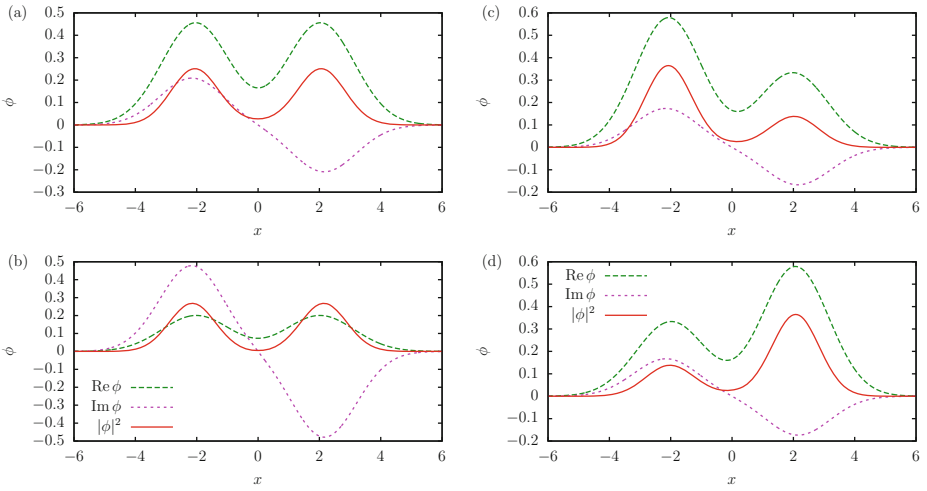

Fig. 3. The wave functions of the ground (a) and the excited (b) eigenstates with real eigenvalues possess symmetric square moduli, and thus correspond to the case of exact $\mathcal{PT}$ symmetry. By contrast, the wave functions of the complex eigenvalue solutions with negative (c) and positive (d) imaginary part do not have symmetric square moduli. All wave functions are shown for $g = 0.2$ and $\Gamma = 0.03$. Since there are almost no visible differences between the variational Gaussian and the numerically exact solutions only the variational wave functions are drawn.

In Fig. 2 we observe a further crucial difference between the linear and the nonlinear system. In the linear case $g = 0$ the two complex eigenvalue solutions emerge exactly at the value Γ_{EP} at which the non-decaying eigenstates with real eigenvalues vanish. This does not hold for the nonlinear system, i.e. for $g \neq 0$. In the latter case the complex eigenvalue solutions are born at a value $\Gamma_{\mathrm{c}} < \Gamma_{\mathrm{EP}}$. At the exceptional point Γ_{EP} only the real eigenvalue states vanish and new complex solutions do not appear. It is known that this unusual bifurcation scenario has its origin in the non-analyticity of the Gross-Pitaevskii equation [25, 34], which is a topic of ongoing research.

3.2 Importance of the one-dimensional solutions

Since only the x coordinate is relevant for the $\mathcal{PT}$ symmetry of the potential (5) it is not surprising that the one-dimensional calculations considered so far already cover qualitatively all relevant effects. However, we want to go one step further and ask whether the one-dimensional calculations are also capable of providing precise quantitative predictions for a completely three-dimensional setup. To do so, we investigate simple but plausible assumptions on the two remaining directions and their influence on the energy eigenvalues.

The first effect of the two additional directions is clearly the interaction of the atoms in the condensate with the trapping potentials defined by the trap frequency $\omega_{y,z}$ in (6). If we assume that only the ground state of the corresponding

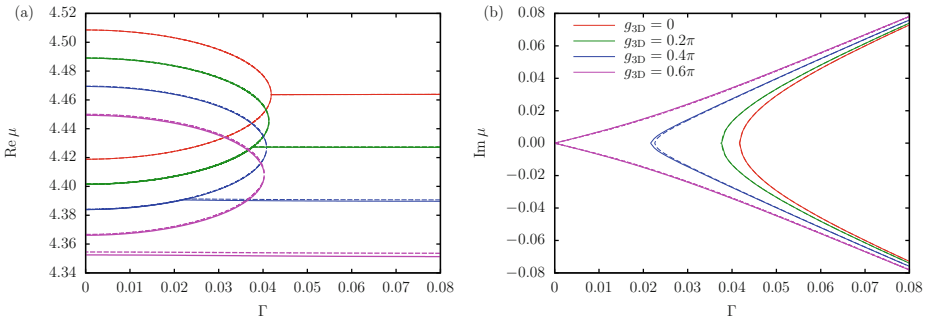

Fig. 4. The real (a) and nonvanishing imaginary (b) parts of the energy eigenvalues of the one-dimensional model (dashed lines) are compared with the fully three-dimensional calculations (solid lines). One observes a very good quantitative description by the simple one-dimensional treatment of the system. The differences can hardly be seen in the graph. Again, in the left panel, g increases from top to bottom, and in the right panel from right to left.

oscillators is occupied, which is reasonable in the condensed phase, we obtain an energy shift by a value of $\Delta\mu = \omega_{y,z} = 2$ in the units introduced in Sect. 2.1.

Since the Gross-Pitaevskii equation (7) contains also the nonlinear scattering term we have to take into account the normalisation integral for the energy contribution of the s-wave contact interaction. An estimate of the difference between the one- and three-dimensional contact energies can be extracted from its expectation value. We wish to describe the three-dimensional setup by an equivalent one-dimensional model, and thus we demand that the expectation values of both contact energies are identical, viz.

$$\int_{\mathbb{R}^3} dx\, dy\, dz\, g_{3D} |\psi_{3D}(\boldsymbol{x})|^4 \stackrel{!}{=} \int_{\mathbb{R}} dx\, g_{1D} |\psi_{1D}(x)|^4 \,. \tag{13}$$

This leads to the relation

$$g_{3D} = \frac{4\pi}{\omega_{y,z}} g_{1D} \tag{14}$$

between the value g_{1D} which has to be used in the one-dimensional model in order that it results in the same contact energy as a three-dimensional wave function with g_{3D}. Again, we assumed that the harmonic oscillator ground state with its wave function ψ_0 is a good approximation for the directions y and z. Furthermore, we used the product ansatz

$$\psi_{3D}(\boldsymbol{x}) \approx \psi_{1D}(x)\psi_0(y)\psi_0(z) \,. \tag{15}$$

Of course, these simple considerations are only correct in the linear form of the Gross-Pitaevskii equation (7), with $g = 0$. However, in Fig. 4 we observe a remarkable agreement between the one-dimensional results based on the simple assumptions and the results of the fully three-dimensional calculations even

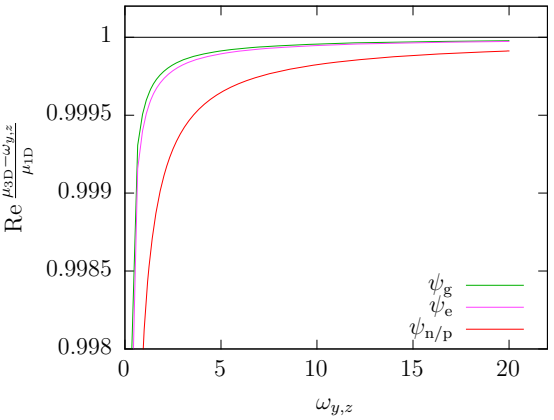

Fig. 5. Real part of the ratio (16) as a function of $\omega_{y,z}$ for the ground state ψ_g, the excited state ψ_e, and the $\mathcal{PT}$-broken states $\psi_{n/p}$. All calculations are carried out for a nonlinearity of $g_{3D} = 1.2\pi/\omega_{y,z}$, i.e. $g_{1D} = 0.3$. For higher values of $\omega_{y,z}$ the ratio converges to unity, i. e. the agreement between the solutions in one and three dimensions becomes better and better. The $\mathcal{PT}$-symmetric solutions converge faster than the $\mathcal{PT}$-broken solutions.

for nonlinearities as large as $g_{1D} \approx 0.3$. It is almost impossible to identify the differences.

In a further step one may assume that the one-dimensional description even becomes better when the geometry of the setup is designed to favour the spatial extension in only the x direction. The previous calculations for the three-dimensional potential were carried out with a constant trapping frequency of $\omega_{y,z} = 2$. The trapping frequencies influence the condensate's shape, and thus it is expected that they have an impact on how precise the stationary solutions in one dimension can be transferred to solutions in three dimensions. The limit $\omega_{y,z} \to \infty$ effectively describes the one-dimensional potential because the widths of the wave function in y and z directions must vanish. Therefore the behaviour in the three-dimensional potential can be predicted more accurately by the one-dimensional solutions for higher values of $\omega_{y,z}$. Figure 5 confirms the convergence of the energy eigenvalues in the three-dimensional potential to the solutions in one dimension with increasing $\omega_{y,z}$. What is shown is the value of the ratio

$$\frac{\mu_{3D} - \Delta\mu}{\mu_{1D}} = \frac{\mu_{3D} - \omega_{y,z}}{\mu_{1D}}. \tag{16}$$

If the solutions in three dimensions are exactly described by the product ansatz (15) the ratio will be equal to one. Indeed, we observe convergence to unity for increasing values of $\omega_{y,z}$.

The convergence in the limit $\omega_{y,z} \to \infty$ is expected. What is, however, of greater interest is, at which values of the trapping frequencies the one-dimensional model becomes sufficiently accurate. We see from Figure 5 that in particular for

the stationary solutions with real eigenvalues, i.e. the $\mathcal{PT}$-symmetric states, one has rapid convergence. To achieve a good agreement between the solutions in one and three dimensions it is obviously sufficient to choose a trapping frequency $\omega_{y,z}$ which is larger than that for the x direction, i.e. in the units used for our calculation $\omega_{y,z} > 1$. This is remarkable since this does by far not mean that we are investigating a quasi one-dimensional setup. The spatial extension in y and z directions may be comparable to that in x direction and it is still possible to extract quantitatively correct values from a simple and numerically less expensive one-dimensional calculation.

4 Dynamics of the condensate

Before we investigate the temporal evolution of the wave functions we have to note an important consequence of the nonlinear system with gain and loss. In Sect. 3.1 we observed $\mathcal{PT}$-broken solutions with complex energy eigenvalues and called them stationary states. From the point of view of the time-dependent Gross-Pitaevskii equation (3) this is not correct. The consequence of the imaginary parts of the energies is a decay or growth of the state's probability amplitude. This affects the scattering term $-g|\psi|^2$, and introduces an explicit time dependence into the nonlinear Hamiltonian. Thus, these states cannot be considered to be true stationary solutions of the time-dependent Gross-Pitaevskii equation. Strictly speaking, they lose their physical relevance. We will see, however, that they still have important consequences for the dynamics of the whole system.

If we prepare the condensate in a state close to the stationary real eigenvalue solutions for values of Γ below the appearance of the $\mathcal{PT}$-broken states their influence is supposed to be negligible. This can be confirmed in a numerically exact propagation of such initial states using the split-operator method. Since we have demonstrated in Sect. 3.2 that a fully three-dimensional calculation is not necessary we restrict our calculations to the one-dimensional model which is more illustrative.

In Figs. 6(a), (b), and (c) we visualise the evolution of the probability amplitude of an initial wave packet

$$\psi(x, t = 0) = \frac{1}{\sqrt{2}} \left(\phi_{\mathrm{g}}(x) + \mathrm{e}^{\mathrm{i}\varphi} \phi_{\mathrm{e}}(x) \right) , \tag{17}$$

where $\phi_{\mathrm{g}}(x)$ and $\phi_{\mathrm{e}}(x)$ are the ground and excited state, respectively, and $\varphi = \pi/2$ was chosen. We observe the same behaviour as it appears already in linear systems [9]. An oscillation of the probability amplitude between the two wells sets in, and the oscillation frequency decreases with increasing Γ. Close to the exceptional point at $\Gamma \approx 0.04$ the oscillation period tends to infinity. A detailed quantitative analysis reveals that the influence of the nonlinearity is only a slightly higher oscillation frequency as compared to the linear case $\Gamma = 0$.

A drastic qualitative change of the wave function's behaviour is observed in Fig. 6(d), where the phase was chosen to be $\varphi = \pi$ and the gain-loss parameter

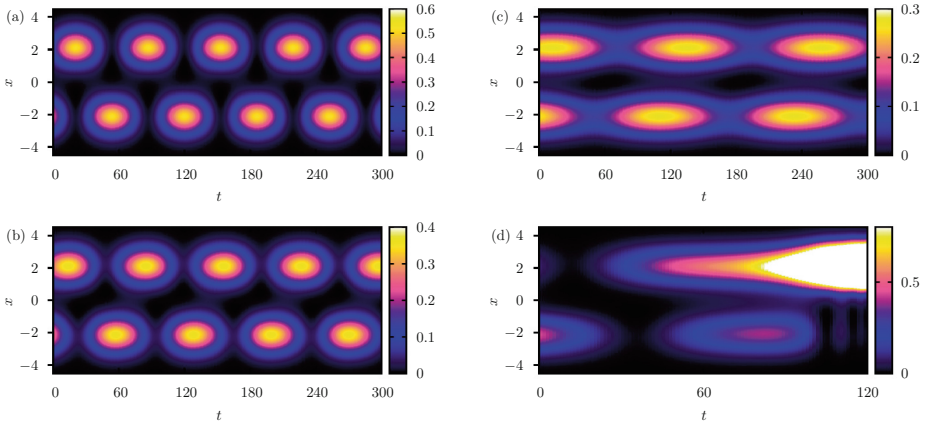

Fig. 6. Visualisation of the probability amplitude's spatial distribution as a function of time. The initial wave packet is defined by (17). In all calculations $g = 0.2$ was chosen. For the choice $\varphi = \pi/2$ stable oscillations are observable in the cases $\Gamma = 0$ (a), $\Gamma = 0.02$ (b), and $\Gamma = 0.04$ (c). For $\Gamma = 0.03$ and $\varphi = \pi$ we observe an explosion of the wave packet (d).

$\Gamma = 0.03$ is in a regime in which the additional $\mathcal{PT}$-broken states are present for $g = 0.2$, cf. Fig. 2. The condensate does not oscillate between the wells. The probability amplitude tunnels into the well with gain ($x > 0$) which leads immediately to an "explosion" of the wave function, i.e. it grows beyond all limits. Of course this is only correct in our description of the gain and loss effects with imaginary potentials which correspond to infinitely large reservoirs. In a realistic situation this description will break down at some point.

There is a simple explanation for the exploding behaviour. The two $\mathcal{PT}$-broken solutions with complex eigenvalues exist and they possess a considerable overlap with the time-evolved wave function (17). In this case the eigenstate with positive imaginary part of the energy can dominate the long-time behaviour since it grows. This can also happen close to the ground state, which does not need to be stable in the nonlinear system with gain and loss. In fact, a detailed stability analysis by solving the Bogoliubov-de Gennes equations confirms that the ground state becomes unstable as soon as the complex eigenvalue solutions emerge at a critical value Γ_c [25].

As we have seen in Fig. 6(c) the instability of the ground state does not necessarily lead immediately to a destruction of the oscillation. For the value $\Gamma = 0.04$, i.e. very close to the exceptional point also the $\mathcal{PT}$-broken solutions exist. However, the probability amplitude almost pulsates in both wells with a low frequency as it is known from linear $\mathcal{PT}$-symmetric systems, and does not seem to be disturbed by the growing and decaying complex eigenvalue solutions. An extensive study of the initial conditions reveals that the phase φ in (17) critically influences the fate of the initial wave packet.

5 Conclusion

The most important result of this work is the verification of the existence of $\mathcal{PT}$-symmetric eigenstates of the Gross-Pitaevskii equation for a Bose-Einstein condensate in an external $\mathcal{PT}$-symmetric potential. Due to an incoupling and outcoupling of atoms in the two wells, which can be described by imaginary potential contributions, the Hamiltonian is complex and non-Hermitian. It does not necessarily need to support true stationary states. However, the $\mathcal{PT}$-symmetric solutions possess real energy eigenvalues, and thus demonstrate that stationary eigenstates that do not decay or grow exist even though a gain and loss of atoms is always present. This behaviour is known from linear $\mathcal{PT}$-symmetric quantum systems, but its appearance in the mean-field description of Bose-Einstein condensates is a nontrivial finding since the Hamiltonian of the Gross-Pitaevskii equation is nonlinear. Thus, the solution has an effect on the Hamiltonian's symmetry, i.e. only after the wave functions have been found one can be sure that the system fulfils any symmetry. In other words, one may conclude that the Hamiltonian picks as real eigenvalue solutions exactly those states which render itself $\mathcal{PT}$ symmetric.

The real energy eigenvalues are the only true stationary states of the system. It is also possible to find solutions of the time-independent Gross-Pitaevskii equation with complex energy eigenvalues. However, they cannot be considered to be physical. Due to the decay or growth enforced by the imaginary energy contributions these states introduce an explicit time dependence into the nonlinear Hamiltonian, and thus are not stationary solutions of the time-dependent Gross-Pitaevskii equation. As is known from linear systems the complex energies found for the time-independent Gross-Pitaevskii equation belong to wave functions with broken $\mathcal{PT}$ symmetry. Since their square moduli are not symmetric functions of the spatial coordinates they destroy also the Hamiltonian's $\mathcal{PT}$ symmetry. A striking difference between linear and nonlinear systems is the point of emergence of the states with broken $\mathcal{PT}$ symmetry. In linear systems they are born exactly at the critical parameter value Γ_{EP} at which the two real eigenvalue states vanish in an exceptional point. For a nonvanishing nonlinearity g we observe that the complex eigenvalue solutions bifurcate from the ground state at a lower gain-loss parameter Γ_c.

It is remarkable that the effects of the $\mathcal{PT}$-symmetric double well can be excellently described by one-dimensional calculations. Of course, one can immediately see that it is possible to construct a one-dimensional $\mathcal{PT}$-symmetric potential. Then one does not expect to lose any qualitative information when one reduces a fully three-dimensional physical system to a one-dimensional description. Our calculations showed that for Bose-Einstein condensates in a double well the correspondence between three- and one-dimensional calculations is even stronger. Highly precise quantitative predictions for the energy eigenvalues of the physical condensate wave function can be obtained from simple one-dimensional considerations. This fact holds for condensate geometries which by far cannot be called one-dimensional.

The time evolution of the wave functions revealed that for low enough gain-loss parameters Γ the condensate behaves as waves in linear $\mathcal{PT}$-symmetric systems. The probability amplitude oscillates between the wells, where the oscillation frequency decreases for increasing Γ and tends to zero close to the exceptional point at which the real eigenvalues solutions merge. As soon as Γ is strong enough for the appearance of the $\mathcal{PT}$-broken complex energy states the temporal evolution of the condensate can become unstable and lead to an infinite growth of the probability amplitude in the well with gain. This effect depends critically on the preparation of the initial state. For an experimental realisation the most important finding is the existence of a stable dynamics.

The present work shows that Bose-Einstein condensates are good candidates for the first experimental observation of a $\mathcal{PT}$-symmetric quantum system. However, there are still some questions which have to be answered. So far, we introduced the coherent in- and outcoupling of atoms only via complex potentials. A topic of ongoing research are several setups with additional wells acting as reservoirs of atoms. These setups are based on the idea that one has a closed system in which the double well is embedded. We wish to investigate how it is possible to drive a coherent flow of atoms between the reservoir and the two wells such that the double well alone can *effectively* be described by the imaginary potential presented in this article.

From the theoretical point of view it would be desirable to understand how a coherent in- or outcoupling of atoms can be understood on a microscopic level. This will require considerations beyond the mean-field limit but will certainly provide more insight into the physical processes. The systems also revealed a number of mathematical challenges. The unusual bifurcation scenario with the $\mathcal{PT}$-symmetric solutions bifurcating from the ground state has its origin in the non-analyticity of the Gross-Pitaevskii equation. The investigation of the nature of these bifurcation points requires a proper analytic extension.

References

1. Guo, A., Salamo, G.J., Duchesne, D., Morandotti, R., Volatier-Ravat, M., Aimez, V., Siviloglou, G.A., Christodoulides, D.N.: Observation of $\mathcal{PT}$-symmetry breaking in complex optical potentials. Phys. Rev. Lett. **103**, 093902 (2009)
2. Rüter, C.E., Makris, K.G., El-Ganainy, R., Christodoulides, D.N., Segev, M., Kip, D.: Observation of parity-time symmetry in optics. Nat. Phys. **6**, 192 (2010)
3. Bender, C.M., Boettcher, S.: Real spectra in non-Hermitian Hamiltonians having $\mathcal{PT}$ symmetry. Phys. Rev. Lett. **80**, 5243 (1998)
4. Jakubský, V., Znojil, M.: An explicitly solvable model of the spontaneous $\mathcal{PT}$-symmetry breaking. Czech. J. Phys. **55**, 1113–1116 (2005)
5. Ruschhaupt, A., Delgado, F., Muga, J.G.: Physical realization of $\mathcal{PT}$-symmetric potential scattering in a planar slab waveguide. J. Phys. A **38**, L171 (2005)
6. Mostafazadeh, A.: Delta-function potential with a complex coupling. J. Phys. A **39**, 13495 (2006)
7. Musslimani, Z., Makris, K.G., El-Ganainy, R., Christodoulides, D.N.: Optical solitons in $\mathcal{PT}$ periodic potentials. Phys. Rev. Lett. **100**, 30402 (2008)

8. Musslimani, Z.H., Makris, K.G., El-Ganainy, R., Christodoulides, D.N.: Analytical solutions to a class of nonlinear Schrödinger equations with $\mathcal{PT}$-like potentials. J. Phys. A **41**, 244019 (2008)
9. Klaiman, S., Günther, U., Moiseyev, N.: Visualization of branch points in $\mathcal{PT}$-symmetric waveguides. Phys. Rev. Lett. **101**, 080402 (2008)
10. Graefe, E.M., Günther, U., Korsch, H.J., Niederle, A.E.: A non-Hermitian $\mathcal{PT}$ symmetric Bose-Hubbard model: eigenvalue rings from unfolding higher-order exceptional points. J. Phys. A **41**, 255206 (2008)
11. Graefe, E.M., Korsch, H.J., Niederle, A.E.: Mean-field dynamics of a non-Hermitian Bose-Hubbard dimer. Phys. Rev. Lett. **101**, 150408 (2008)
12. Makris, K.G., El-Ganainy, R., Christodoulides, D.N., Musslimani, Z.H.: Beam dynamics in $\mathcal{PT}$ symmetric optical lattices. Phys. Rev. Lett. **100**, 103904 (2008)
13. Jones, H.F.: Interface between Hermitian and non-Hermitian Hamiltonians in a model calculation. Phys. Rev. D **78**, 065032 (2008)
14. Mostafazadeh, A., Mehri-Dehnavi, H.: Spectral singularities, biorthonormal systems and a two-parameter family of complex point interactions. J. Phys. A **42**, 125303 (2009)
15. Ramezani, H., Kottos, T., El-Ganainy, R., Christodoulides, D.N.: Unidirectional nonlinear $\mathcal{PT}$-symmetric optical structures. Phys. Rev. A **82**, 043803 (2010)
16. Makris, K.G., El-Ganainy, R., Christodoulides, D.N., Musslimani, Z.H.: $\mathcal{PT}$-symmetric optical lattices. Phys. Rev. A **81**, 063807 (2010)
17. Mehri-Dehnavi, H., Mostafazadeh, A., Batal, A.: Application of pseudo-Hermitian quantum mechanics to a complex scattering potential with point interactions. J. Phys. A **43**, 145301 (2010)
18. Moiseyev, N.: Non-Hermitian Quantum Mechanics. Cambridge University Press, Cambridge (2011)
19. El-Ganainy, R., Makris, K.G., Christodoulides, D.N., Musslimani, Z.H.: Theory of coupled optical $\mathcal{PT}$-symmetric structures. Opt. Lett. **32**, 2632 (2007)
20. Gross, E.P.: Structure of a quantized vortex in Boson systems. Nuovo Cimento **20**, 454 (1961)
21. Pitaevskii, L.P.: Vortex lines in an imperfect Bose gas. Sov. Phys. JETP **13**, 451 (1961)
22. Graefe, E.M., Korsch, H.J., Niederle, A.E.: Quantum-classical correspondence for a non-Hermitian Bose-Hubbard dimer. Phys. Rev. A **82**, 013629 (2010)
23. Cartarius, H., Wunner, G.: Model of a $\mathcal{PT}$-symmetric Bose-Einstein condensate in a δ-function double-well potential. Phys. Rev. A **86**, 013612 (2012)
24. Cartarius, H., Haag, D., Dast, D., Wunner, G.: Nonlinear Schrödinger equation for a $\mathcal{PT}$-symmetric delta-function double well. Journal of Physics A **45**, 444008 (2012)
25. Dast, D., Haag, D., Cartarius, H., Wunner, G., Eichler, R., Main, J.: A Bose-Einstein condensate in a $\mathcal{PT}$ symmetric double well. Fortschritte der Physik **61**, 124–139 (2013)
26. Shin, Y., Jo, G.B., Saba, M., Pasquini, T.A., Ketterle, W., Pritchard, D.E.: Optical weak link between two spatially separated Bose-Einstein condensates. Phys. Rev. Lett. **95**, 170402 (2005)
27. Gati, R., Albiez, M., Fölling, J., Hemmerling, B., Oberthaler, M.: Realization of a single Josephson junction for Bose-Einstein condensates. Appl. Phys. B **82**, 207 (2006)
28. Heller, E.J.: Classical S-matrix limit of wave packet dynamics. J. Chem. Phys. **65**, 4979 (1976)

29. Heller, E.J.: Frozen Gaussians: A very simple semiclassical approximation. J. Chem. Phys. **75**, 2923 (1981)
30. McLachlan, A.D.: A variational solution of the time-dependent Schrödinger equation. Mol. Phys. **8**, 39 (1964)
31. Rau, S., Main, J., Köberle, P., Wunner, G.: Pitchfork bifurcations in blood-cell-shaped dipolar Bose-Einstein condensates. Phys. Rev. A **81**, 031605(R) (2010)
32. Rau, S., Main, J., Wunner, G.: Variational methods with coupled Gaussian functions for Bose-Einstein condensates with long-range interactions. I. General Concept. Phys. Rev. A **82**, 023610 (2010)
33. Rau, S., Main, J., Cartarius, H., Köberle, P., Wunner, G.: Variational methods with coupled Gaussian functions for Bose-Einstein condensates with long-range interactions. II. Applications. Phys. Rev. A **82**, 023611 (2010)
34. Graefe, E.M.: Stationary states of a $\mathcal{PT}$ symmetric two-mode Bose-Einstein condensate. J. Phys. A **45**, 444015 (2012)

Part III

Self-Organisation in Neuroscience

The Brain as a Synergetic and Physical System

Hermann Haken

Center of Synergetics, Institut für Theoretische Physik 1, Universität Stuttgart,
Pfaffenwaldring 57, 70550 Stuttgart, Germany
cos@itp1.uni-stuttgart.de
http://itp1.uni-stuttgart.de/institut/arbeitsgruppen/haken

Abstract. This paper presents an outline of our brain theory that we have developed over the past 30 years. Some remarks on the early stages of Synergetics that I initiated some 40 years ago are included. Using basic concepts of Synergetics such as order parameters and the slaving principle, brain functions are modeled both at the macroscopic (order parameter) and the microscopic (neuronal) levels. I deal with movement coordination, psychophysics (ambiguous figures), pattern recognition by the synergetic computer, my "light house model" of a neural net, and give some hints at applications to psychology and psychotherapy ("principle of indirect steering"). Finally, I discuss relations between Synergetics and Complexity Science.

1 The human brain

Our brain is the most complex system we know. It consists of about 100 billion neurons, where a single neuron can be connected with up to 10000 other neurons. This "system" enables our recognition of faces and objects, movement patterns, it serves movement control of our limbs, it produces our thoughts and allows us to express them by speech and gestures, it homes our feelings, just to mention a few characteristic features. But who or what steers the neurons so to produce all these marvelous processes? The famous neurophysiologist Sir John Eccles suggested that the brain is a computer and the mind its programmer. Indeed, the "computer" metaphor is still present in numerous publications (with the "mind" exorcised). In contrast to this picture, some thirty years (in 1982) ago I suggested to treat the brain as a "synergetic" system and jointly with E. Basar, H. Flohr, and A.J. Mandell (Basar et al. [1]), I organized a meeting entitled: "Synergetics of the brain". According to this suggestion, the brain is a self-organizing system, which can be theoretically treated by basic concepts and results of Synergetics.

2 Synergetics: Two examples from physics and a historical remark

I initiated this kind of study by a lecture, jointly with my then coworker Robert Graham in the winter term 1969/70, and continued it in the summer term 1970 (cf. also Haken, Graham [2]). To explain the incentive of our endeavor, I briefly recall my favorate subject of my research at that time:

A. Pelster and G. Wunner (eds.), *Selforganization in Complex Systems: The Past, Present, and Future of Synergetics*, Understanding Complex Systems,
DOI: 10.1007/978-3-319-27635-9_10

2.1 The laser paradigm

A typical example is the ruby laser (first realized by Maiman in 1960 [3]). In a crystal (Al_2O_3) rod, impurity atoms (Cr^+) are embedded. When excited by a "pump" lamp from the outside, the impurity atoms emit light which lends the ruby crystal its typical red color. Two mirrors (one semitransparent) mounted at the rod's end faces serve for a reflection of light waves, emitted in axial direction, so that they can intensely interact with the atoms. By means of stimulated emission (first introduced by Einstein to derive Planck's law of black body radiation), light waves are amplified and, eventually, leave the laser rod in axial direction. What happens, when we increase the pump power of the outer light source? First, light waves (or photons) are spontaneously emitted, which is an entirely *random process*. Even when the waves are enhanced by stimulated emission, which is expressed by the acronym laser (light emission by stimulated emission of radiation) this *randomness* ("Gaussian noise") persists (while the linewidth decreases with increasing pump strength). In the physics community, this line narrowing was considered as *the typical* feature of laser light (besides its high intensity and directionality). In 1964 I showed theoretically, that at a critical pump strength laser light undergoes a dramatic qualitative change (Haken [4]): the noisy output is replaced by a single highly ordered ("coherent") wave. This was the first example of an open (quantum) system far from equilibrium which shows a disorder-order transition actually in close analogy to phase-transitions of systems in thermal quilibrium, based on the Landau theory, as we elaborated later (Graham, Haken 1968,70; also de Giorgio, Scully 1970). But still more important: Here we had an explicit example of a process of *self-organization*!

2.2 A fluid heated from below

In order to bring out some typical features of self-organization which can be clearly visualized ("demonstrare ad oculos") I quote some experimental results (Fig. 1).

In a circular pan, a thin fluid layer (e.g. oil) is heated from below and cooled from above. If the temperature difference Δ between the lower and upper surface is small, heat is conducted microscopically: macroscopically the fluid is at rest. Beyond a critical Δ, a *macroscopic pattern* emerges: a honey comb structure (Bénard [5]). In spite of a completely *homogenous* heating and cooling, a highly ordered structure appears! When, in addition, also the border of the pan is heated uniformly, the structure changes qualitatively: the hexagons are replaced by a spiral (which can be one-or multi-armed) (Bodenschatz et al., experiments [6]; Bestehorn et al., theory [7]).

2.3 A historical remark

While the *laser* provides us with a quantum system away from thermal equilibrium that shows *temporal order*, the fluid exemplifies the formation of *spatially ordered patterns* in a classical non-equilibrium system.

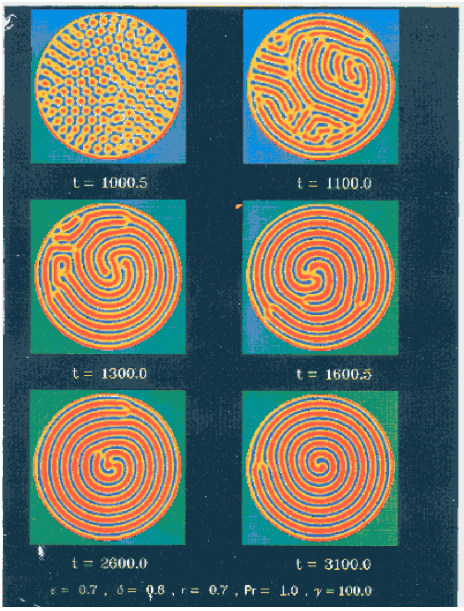

Fig. 1. Fluid layer heated from below.: l.h.s.: formation of hexagons, r.h.s.: formation of spirals when the border is heated in addition. (From Bestehorn, M., Fantz, M., Friedrich, R., Haken, H. [7].)

Are these two cases just two strange singular events (which even seemed to contradict the second law of thermodynamics) or are they just two manifestations of an important new class of phenomena? The attempt to answer such a question lies at the heart of my "Synergetics" endeavor. Historically, the incentive for my approach was – besides the laser paradigm – not the just mentioned example of fluid dynamics, but two phenomena of "phase transitions" in quite other fields, namely Sociology and biological evolution. In 1968 my close colleague Wolfgang Weidlich developed his theory on phase-transitions in the formation of public opinion (Weidlich 1971 [8]), and I learned of Manfred Eigen's work on the evolution of molecular species (Eigen [9]) (see also Eigen, Schuster [10], Weidlich [11]). So my conclusion at that time was: phase-transition-like phenomena must be ubiquitous.

To put this new insight into a broader context, in 1972 I organized a symposium on Synergetics (cf. its proceedings (Haken [12])).

My introduction started with the words "In many disciplines of science we deal with systems composed of many subsystems ... Very often the properties of the large system cannot be explained by a mere random superposition of actions of the subsystems. Quite on the contrary the subsystems behave in a well organized manner, so that the total system is in an ordered state or shows actions which one might even call purposeful. Furthermore one often observes abrupt changes between disorder and order or transitions between different states

of order. Thus the question arises, who are the mysterious demons who tell the subsystems in which way to behave so to create order, or, in a more scientific language, which are the principles by which order is created." And I concluded my introduction with the statement ... "that in spite of the completely different nature of the systems, their behavior is governed, at a well defined level of consideration, by a few very general principles which offers an explanation of the often amazingly similar performance of such systems."

3 Synergetics: Goal

This interdisciplinary field of research, Synergetics (S.), deals with systems composed of many parts, elements etc. S. distinguishes between the *macroscopic* level and the *microscopic* level by length- and/or time-scale separation. S. studies the spontaneous formation of temporal, spatial, functional structures, i.e. the emergence of new qualities via *self-organization*. S. focusses its attention on *open* systems, i.e. systems subject to an in – and outflow of energy, matter and/or information. The central goal of S. is: *to unearth general principles (or laws) underlying self-organization irrespective of the nature of the individual parts of the considered systems*.

Thus the parts may be, e.g., atoms, photons, molecules, but also neurons or people in society. "It hardly needs to be mentioned that once such common principles are established, they are of an enormous stimulus and help for future research" (quotation from my preface to the proceedings of our first Synergetics meeting in 1972 (Haken [12])).

An important feature of Synergetics has always been to make contact with experiments as closely as possible. For more details cf. Haken [13–16] and the Springer Series in Synergetics.

In the present paper I don't present the theoretical approaches but rather their verbalization. For lack of space, I must also refrain from discussing the various relationships between S. and general system theory (in the sense of L. von Bertalanffi [17, 18] dynamic systems theory including bifurcation theory, center and inertial manifold theory (e.g. Pliss [19], Kelley [20]), Robinson [21]), Landau theory of phase transitions (Landau, Lifshitz [22]), thermodynamics, statistical physics, quantum field theory, cybernetics and possibly other fields. (In my opinion, the work of myself and my coworkers has given substantial new insights into several of these fields).

4 Synergetics: Basic concepts

4.1 Control parameters

They qualitatively describe the input of energy, matter, information into the considered system. Examples are: power input into the laser, temperature difference in convection experiments.

In brain dynamics: Coffein (blocks Serotonin receptors), Haldol (blocks Dopamin2 receptors), neurotransmitters, neuromodulators, hormones (e.g. oxytocine); the latter acting as internal control parameters.

4.2 Instability

At a critical control parameter value the state of a system tends to disappear and to be replaced by a new one. Critical fluctuations may occur that drive the system into its new state.

4.3 Order parameters

occur close to the instability point. They are new collective variables that serve as macroscopic *descriptors*. They are in general few and obey low dimensional nonlinear dynamics subject to fluctuations.

4.4 Slaving principle

The order parameters determine the behavior of the individual parts (like a puppeteer who lets the puppets dance).

4.5 Circular causality

In contrast to the "puppeteer" metaphor, the puppets – through their cooperation – determine the behavior of the order parameters. This raises far reaching ontological questions. (catchword: mind-body problem) that I will not discuss here.

At any rate: This concept allows us to treat a synergetic (self-organizing) system at two levels:

- macroscopic: order parameters
- microscopic: "consensualization" between parts (elements)

While the second approach requires very many data, the former requires few data ("information compression"). In the following I will elaborate on this distinction in the context of brain dynamics.

5 The phenomenological level I Movement coordination and order parameters

In 1981 Scott Kelso published his experimental results on human movement coordination (Kelso [23]). He instructed subjects to move their index fingers in parallel at a given frequency, ω. While at low frequency the subjects could perform this movement, at an increased, critical frequency ω_c, the movement switched involuntarily to a *symmetric* coordination (Fig. 2). This transition was

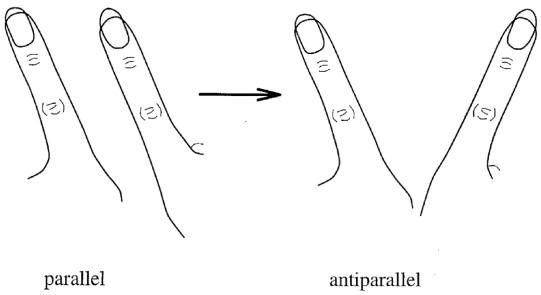

Fig. 2. Kelso Experiment: Change of relative phase in index finger movement

modeled by Haken, Kelso, Bunz (HKB) [24] in the spirit of Synergetics: The pronounced change of the movement pattern occurs at a critical frequency, ω_c. Thus the frequency ω serves as *control parameter*.

The relative position of the index fingers can be mathematically captured by a relative phase ϕ. Because ϕ changes at $\omega = \omega_c$, it may serve as *order parameter*.

As had been elaborated previously in Synergetics, the order parameter dynamics can be modeled by an equation of the form

$$\frac{d\phi}{dt} = \frac{\partial V(\phi)}{\partial \phi} + F(t) \; , \tag{1}$$

where V is a "potential" and $F(t)$ a stochastic force. The crux was to find a suitable $V(\phi)$. Our model V is depicted in Fig. 3. Initially (upper valley) the movement state is characterized by $\phi = \pi$. With increasing ω, the corresponding potential minimum flattens and disappears: The state $\phi = \pi$ undergoes an *instability* and changes into $\phi = 0$.

Now, again in the spirit of Synergetics, a number of important conclusions can be drawn:

1. *hysteresis*: When lowering ω, the "system" will not return from $\phi = 0$ to $\phi = \pi$.
2. a flat potential implies *critical slowing* down and
3. *critical fluctuation* (see Fig. 4).

Kelso and his co-workers were able to experimentally (even quantitatively) verify our predictions. These results lead us to conclude that the brain does not act according to a computer motor program. Rather the features 1-3 are characteristic of self-organization. This is a strong hint at our interpretation that *the brain is a self-organizing system.*

Further beautiful experiments on this issue were performed by Kelso and his group, while theory was carried further by L. Borland, A. Daffertshofer, T. Frank, A. Fuchs, G. Schöner and others, both at Stuttgart and Boca Raton, FA. (For reviews cf. e.g. Kelso [26], Haken [27]). A general conclusion based on these experiments and related ones is: Humans (as well as animals, e.g. quadrupeds)

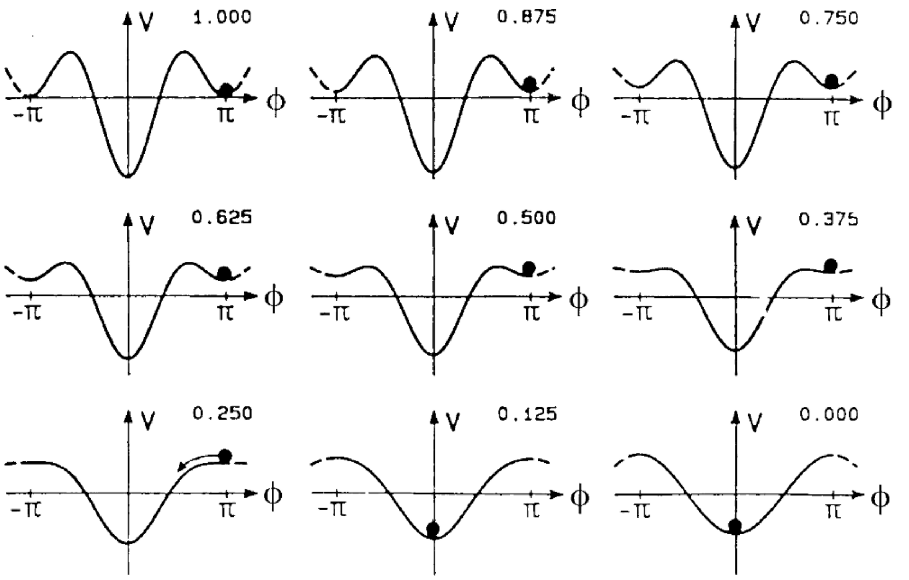

Fig. 3. Change of potential V when frequency ω is increased. Read Fig. from upper left to lower right corner (Haken et al. [24]).

realize only specific movement patterns depending on control parameters, e.g. prescribed speed of performance.

6 The phenomenological level II Psychophysics and order parameters

Our starting point is a typical relation between order parameters and the enslaved parts: While order parameters react to external influences ("perturbations") slowly, parts act on a faster time-scale (time-scale separation). This invites us to the following analogy with brain processes:

While percepts are processed on time scales of 1/10 sec or still longer, neurons function on a time scale of milliseconds.

These facts suggest to establish an analogy (for a review cf. Haken [27])

$$\text{percepts} \leftrightarrow \text{orderparameters}$$
$$\text{neurons} \leftrightarrow \text{parts(elements)}$$

Note the ontological question that lurks behind this analogy!

Nevertheless, let us study a few typical cases of order parameter dynamics with respect to perception. A typical order parameter potential has two valleys indicating two different stable order parameter values, i.e. *bistability.* Which is actually happening in perception (Fig. 5). Do you perceive Einstein's face or?

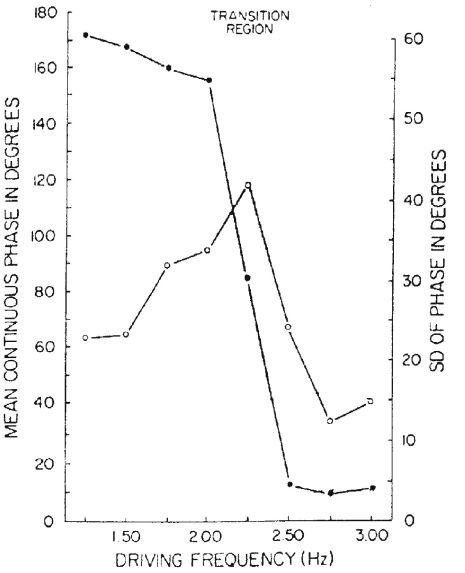

Fig. 4. Fluctuations of relative phase (open circles) and mean phase (solid dots) versus driving frequency (Kelso et al. [25])

Thus, the same picture "induces" two quite different percepts, i.e. "bistability" in perception. Strictly speaking over a somewhat longer time span, oscillations occur (see below). I owe Michael Stadler (Bremen) the hint to oscillations in perception.

A further example is hysteresis, we already came across above in a different context. Hysteresis means that the state of a system depends on history. Fig. 6 provides us with an example from perception: The switching from the perception of a man's face (upper left corner) to that of a kneeling woman (lower right corner) depends on the sequence in which we look at this series of pictures.

In the case of two order parameters, oscillations may occur (limit cycles in the sense of dynamical system theory). In perception such oscillations may be observed when looking at ambiguous figures (Fig. 7). Old or young lady? The dynamics was mathematically modelled under the assumption that each percept is controlled by an "attention" parameter that fades away after that the percept is recognized. As I learned later, Gestaltpsychologist Wolfgang Köhler had made the same suggestion in 1920 [29] (though he didn't model it mathematically). Our model allowed us to establish several relationships between first recognition time, bias, recognition times etc. (Ditzinger, Haken [30]), and to make contact with experimental results (Borsellini et al. [31, 32]).

Fig. 5. Bistability in perception: Einstein's face or three bathing girls?

7 Down to the microscopic level: models Pattern recognition by the synergetic computer

Here, I exploit an analogy between pattern *formation* and pattern *recognition*. This analogy is based on the concepts of order parameters, on the slaving principle, and on circular causality (for a review cf. Haken [33]).

In *pattern formation*, let initially a part of the total system be in an ordered state. This part calls on, in general, several order parameters which then compete among each other. The initially stronger order parameter wins this competition ("principle of winner takes all") and, eventually enslaves the total system, i.e. it establishes a fully ordered pattern. (An example: in the convection instability, initially a single roll is prescribed. Then, by the just described mechanism, a complete system of parallel rolls is formed.)

In pattern *recognition*, the individual parts are features, e.g. grey values of pixels into which a pattern is decomposed. Consider as a concrete example face recognition. Then only some features, e.g. that of a nose, may be given. Those features call upon order parameters which compete among each other, the initially strongest wins and, again via the slaving principle, restores the whole pattern, e.g. face. Cf. Fig. 8: example of stored prototype patterns, and Fig. 9: recognition process, based on the following algorithm, which I formulate, quite in the spirit of Synergetics, both at the microscopic (feature) level and at the macroscopic (order parameter) level.

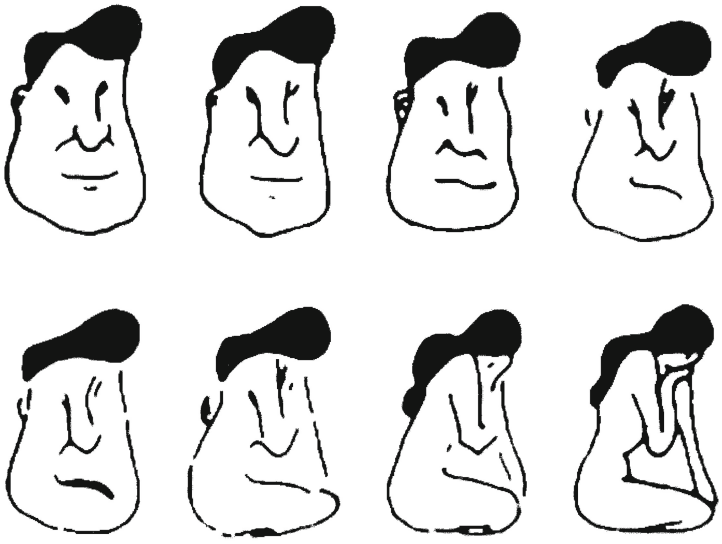

Fig. 6. Hysteresis in perception (cf. text)

At the microscopic level, each pixel $l, l = 1, ...L$, is represented by its grey value q_l, which is mapped onto a neutral net so that q_l is also the excitation level of the model neuron l. Then I introduced evolution equations for the state vector $q = (q_1, ..., q_L)$,

$$\dot{q}(t) = -\text{grad}_q V(q, c) \; , \tag{2}$$

where V is a polynominal of q up to fourth order with coefficients $c = (c_{ll'}, \dots)$ that can be interpreted as synaptic strengths. V describes a hilly landscape which I constructed in such a way that each of its valleys corresponds to one and only one of the prototype patterns: The corresponding values of c can be either inserted "by hand" into the computer or, more importantly, learned by the rule

$$\langle V(q, c) \rangle_q = \min \; ! \; , \tag{3}$$

where the average $\langle \; \rangle$ refers to a sequence of partially incomplete patterns whose "idealization" is thus achieved. My algorithm was implemented by my former co-worker Armin Fuchs on a serial computer (cf. Figs. 8, 9) (Fuchs, Haken [34]), where recognition has been made invariant against displacements, rotation and scaling. Using attention parameters and their fading away (cf. Sect. 6) our approach was also able to recognize faces in a complex scene. An example is given by Fig. 10. The transition to the macroscopic (order parameter) level is achieved by the transformation of the pixel vector q

$$q(t) = \sum_k \xi_k(t) \nu_k + \text{rest} \; , \quad k = 1, \dots, k \leq L \tag{4}$$

Fig. 7. Oscillations in perception (cf. text)

where $\xi_k(t)$ is the order parameter associated with the prototype pattern vector

$$\nu_k = (\nu_{k1}, \ldots, \nu_{k,L}) \; . \tag{5}$$

The resulting order parameter equations are

$$\dot{\xi}_k = \xi_k \left(\lambda_k + a\xi_k^2 - b \sum_m \xi_m^2 \right) \; , \tag{6}$$

wih $\lambda_k \geq 0$ the attention parameters, and $a, b > 0$.

A comparison with the vast body of pattern recognition procedures developed by other authors can be only sketched.

My procedure belongs to the class of recurrent neural attractor networks. The probably best known example is the Hopfield net (Hopfield [35]). Its disadvantage is the large number of spurious attractor states. To let the dynamical system escape from these unwanted attractors, the laborious procedure of simulated annealing has to be applied. The Grossberg/Carpenter procedure rests on Lyapunov functions (Carpenter, Grossberg [36]) which are less precise than our potential function, however.

8 Down to the physical level of the brain: Coping with the dynamics of "real" neurons

This problem has been dealt with by several members of my former institute, including A. Daffertshofer, T. Frank, V. Jirsa, P. Tass. Of course, there are also approaches by other authors. Here I present my own "light house model" (cf. Haken [37]) which starts from some well known experimental findings. A typical

Fig. 8. Example of stored prototype patterns (after Fuchs, Haken [34])

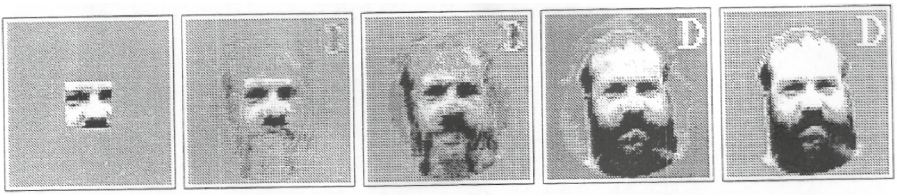

Fig. 9. Example of recognition process (after Fuchs, Haken [34])

neuron emits spike trains into its axon which branches making contact to other neurons. The contact is achieved by synapses which convert spikes into electric currents to the soma of the neuron, which sums them up, and "fires" beyond a threshold, i.e. it emits a spike train. The basic equations of the light house model are:

1. Electric current ψ_m of dendrite m is generated by an axonal pulse from neuron k:
$$\left(\frac{d}{dt}+\gamma\right)^{\alpha}\psi_m = a_{mk}P_k \ . \tag{7}$$
Here, γ is a damping constant, exponent α with $1 < \alpha < 2$ is a fraction in accordance with experiments, a_{mk} is an experimentally determined transformation rate. (A more general formulation contains a sum over k on the r.h.s.)
2. Pulse production by neuron k, light house analogy:
When the rotating light beam emitted from a light house hits an observer, he or she will notice a series of light flashes ("spikes"). Their time intervals depend on the rotation speed of the beam.
The direction of the beam is described by an angle ϕ. If the beam hits the observer at $\phi = 0$, then (s)he will be hit again and again at times $t_n, n = 1, 2, \ldots$, where $\phi(tn) = 2\pi n$.

Fig. 10. Recognition of a complex scene (after Fuchs, Haken [34])

Thus the rotation speed $\dot{\phi}$ determines the spike emission rate, which, in the case of a neuron, is determined by the incoming dendritic currents. I model this effect by means of the equation

$$\dot{\phi}_k(t) + \Gamma\phi_k(t) \bmod 2\pi = \sum_m C_{km}\psi_m(t) + \sum_{ml} d_{kml}\psi_m(t)\psi_l(t) + p_k \ , \quad (8)$$

where p_k is the incoming signal. I have treated these equations rather extensively (including also time-delays and noise). Here I mention only two special cases: In the case of dense pulse sequence I was able to derive the equations of the synergetic computer [33, 38] so that my equations allow pattern recognition. Under different conditions, my equations describe spike train synchronization where contact can be made with experiments by Gray and Singer [39] as well as by Eckhorn et al. [40] and their respective groups.

9 Further down to the molecular level

In the foregoing I have given a brief sketch of how I had applied basic concepts of Synergetics to different levels of brain functions. In this approach, neurons (somata), axons and dendrites are treated as entities. But these "devices" are, by themselves, complicated systems, composed of molecules. Among the numerous phenomena at this level, the following intrigues me particularly (cf. Alberts et al. [41] for a review).

In an axon, there are microtubuli enbedded, which are long fibers. Along them, biomolecules called kinesin may move by means of movable "heads" (or better "legs"). The kinesin molecules can transport organels that are larger than the kinesin. Powered by ATP, kinesin is an open system – to be treated as a quantum system.

In our recently (September 2012) published book: Haken/Levi: Synergetic Agents [42] we have started to deal with such processes. In a first step we

treated a related problem: muscle contraction based on the propagation of myosin molecules on actin fibers by using methods of quantum field theory and quantum statistics of systems far from equilibrium.

10 Back to the phenomenological level: Psychology and psychotherapy

Interestingly, Synergetics, originally quite unexpected, has made its way into psychology and psychotherapy (cf. also the contribution by Günter Schiepek to these proceedings, as well as Haken and Schiepek [43]). Clearly in the present context, a few remarks must suffice here.

Behavioral patterns may be conceived as order parameters. Thus changes of behavioral patterns can be interpreted as phase transitions, often with their typical features, e.g. critical fluctuations. Research in Synergetics has revealed the important role of the *principle of indirect steering*.

This means, the change of a *control parameter* can induce the evolution of a new (behavioral) pattern by means of self-organization. This has fired a discussion on appropriate control parameters in psychotherapy: specific verbal interventions, or specific drugs? Or both?

Eventually, Synergetics cannot escape to try an answer to the eternal mind-body problem (on which I am presently having fascinating discussions with Harald Atmanspacher and Wolfgang Tschacher).

My suggestion is the analogy

$$\begin{aligned} &\text{body} && \leftrightarrow \text{parts} \\ &\text{mind} \leftrightarrow && \text{orderparameters} \end{aligned}$$

Thus in view of the principle of "circular causality" mind and body are just two sides of the same coin. As I had learned in the meantime, this is just the opinion of Spinoza. Just to conclude this section with a burning question: Will the problem of *qualia* remain an eternal enigma?

11 Concluding remarks and outlook

Out of the vast field of Synergetics with its relations to many scientific disciplines, I have presented a small section.

I have chosen the example of our attempts to model some aspects of brain function to elucidate how basic concepts of Synergetics can be applied to this fascinating field. As our studies (seem to) suggest, the human brain manages to compress the complexity of perception and action time and again into low dimensional dynamics of a rather small number of – in each case appropriately established – order parameters.

Critics may object that this is a too narrow view based on a "Synergetic bias". On the other hand, our brain manages to compress the complexity of our world all the time: e.g. by categorization as witnessed by language. Thus I think

that the Synergetics approach may be a useful tool to cut one's way through the jungle of the brain's complexity.

At any rate, this issue brings me to discuss the relation between *Synergetics* and the presently flourishing field of *Complexity Science*. Synergetics is surely one (or even the) forerunner of Complexity Science, both of which share their emphasis on *interdisciplinarity*. But there are also differences that are best explained by looking at the different styles of scientific work:

1. Production of new data (information production)
2. Formulation of principles, laws etc. (information compression)

When I defined the scope of Synergetics I strongly emphasized 2.

Searching for common principles still remains an important goal which has to go along also with 1. This is clearly demonstrated by the various presentations at the Delmenhorst meeting (cf. these proceedings).

Readers interested in Synergetics/Complexity Science are referred to the monograph series edited by H. Haken and S. Kelso (cf. references [14], [28]).

References

1. Basar, E., Flohr, H., Haken, H., Mandell, A.J.: Synergetics of the Brain. Springer Verlag, Berlin (1983)
2. Haken, H., Graham, R.: Synergetik, die Lehre vom Zusammenwirken. Umschau **6**, 191–195 (1971)
3. Maiman, T.H.: Stimulated optical radiation in ruby. Nature **187**, 493–494 (1960)
4. Haken, H.: A Nonlinear Theory of Laser Noise and Coherence. 1. Zeitschrift für Physik **181**, 96–124 (1964)
5. Bénard, H.: Rev. Gen. Sci. Pures Appl. **11** 1261, 1309 (1900)
6. Bodenschatz, E., Cannell, D.S., de Bruyn, J.R., Ecke, R., Hu, Y.-C., Lerman, K., Ahlers, G.: Experiments on three systems with non-variational aspects. Physica D **61**, 77–93 (1992)
7. Bestehorn, M., Fantz, M., Friedrich, R., Haken, H.: Hexagonal and spiral patterns of thermal convection. Phys. Lett. A **174**, 48–52 (1993)
8. Weidlich, W.: The statistical description of polarization phenomena in society. Brit. J. Math. Stat. **24**, 251–266 (1951)
9. Eigen, M.: The self-organization of matter and the evolution of biological macromolecules. Naturwissenschaften **58**, 465–523 (1971)
10. Eigen, M., Schuster, P.: The Hypercycle: A Principle of Natural Self-Organization. Springer, New York (1979)
11. Weidlich, W.: Sociodynamics: A Systematic Approach to Mathematical Modelling in the Social Sciences. Harwood Academic Publishers, Amsterdam (2000)
12. Haken, H. (ed.): Synergetics. Cooperative Phenomena in Multi-Component Systems. B.G. Teubner, Stuttgart (1973)
13. Haken, H.: Synergetics. An Introduction. Nonequilibrium Phase Transitions and Self-Organization in Physics, Chemistry and Biology. Springer, Berlin (1977)
14. Haken, H. (ed.): Springer Series in Synergetics, founded in 1977, now part of the Springer Complexity Program. Springer, Berlin
15. Haken, H.: Advanced Synergetics. Instability Hierarchies of Self-Organizing Systems and Devices. Springer, Berlin (1983)

16. Haken, H.: Synergetics. Introduction and Advanced Topics. Springer, Berlin (2004)
17. Von Bertalanffi, L.: The theory of open systems in physics and biology. Science **111**, 23–29 (1950)
18. Von Bertalanffi, L.: Biophysik des Fließgleichgewichts. Vieweg, Braunschweig (1953)
19. Pliss, V.A.: A reduction principle in the theory of stability of motion. IZV. Akad. Nauk SSSR., Mat. Ser. **28**, 1297 (1964)
20. Kelley, A.: In: Abraham, R., Robbin, J. (eds.) Transversal Mappings and Flows. Benjamin, New York (1967)
21. Robinson, J.C.: Finite-dimensional behavior in dissipative partial differential equations. Chaos **5**, 330–345 (1985)
22. Landau, L.D., Lifshitz, I.M.: Course of Theoretical Physics, vol. 5. Statistical Physics. Pergamon-Press, London (1959)
23. Kelso, J.A.S.: On the oscillatory basis of movements. Bulletin of Psychonomic Society **18**, 63 (1981)
24. Haken, H., Kelso, J.A.S., Bunz, H.: A Theoretical model of phase transitions in human movements. Biol. Cybernetics **51**, 347–356 (1985)
25. Kelso, J.A.S., Scholz, J.P., Schöner, G.: Non-equilibrium phase transitions in coordinated biological motion: Critical fluctuations. Physics Letters A **118**, 279–284 (1986)
26. Kelso, J.A.S.: Dynamic patterns: The self-organization of brain and behavior. MIT Press, Boston (1995)
27. Haken, H.: Principles of Brain Functioning. A Synergetic approach to Brain Activity, Behavior and Cognition. Springer, Berlin (1996)
28. Kelso, S. (ed.), Monograph Series: Understanding Complex Systems, as part of the Springer Complexity Program. Springer, Berlin
29. Köhler, W.: Die physischen Gestalten in Ruhe und im stationären Zustand. Vieweg, Braunschweig (1920)
30. Ditzinger, T., Haken, H.: Oscillations in the perception of ambiguous patterns. Biol. Cybern. **61**, 279–287 (1989)
31. Borsellino, A., deMarco, A., Allazetta, A., Rinesi, S., Bartollini, B.: Reversal time distribution in the perception of visual ambiguous stimuli. Kybernetik **10**, 139–144 (1972)
32. Borsellino, A., Carlini, R., Riani, M., Tuccio, M.T., deMarco, A., Penengo, P., Trabucco, A.: Effects of visual angle on perspective reversal for ambiguous patterns. Perception **11**, 263–273 (1982)
33. Haken, H.: Synergetic computers and cognition. Springer, Berlin (1991)
34. Fuchs, A., Haken, H.: Pattern recognition and associative memory as dynamical process in a synergetic system I+II, Erratum. Biol. Cybern. **60**, 17–22, 107–109, 476 (1988)
35. Hopfield, J.J.: Neural networks andphysical systems with emergent collective computational abilities. Proc. Natl. Acad. Sci. **79**, 2554–2558 (1982)
36. Carpenter, C., Grossberg, S.: The art of adaptive pattern recognition by a self-organizing neural network. Computer, 77–87, March 1980
37. Haken, H.: Brain Dynamics. An Introduction to Models and Simulations. Springer, Berlin (2002/2007)
38. Haken, H.: Synergetic computers for pattern recognition and associative memory. In: Haken, H. (ed.) Computational Systems, Natural and Artificial, pp. 2–22. Springer, Berlin (1987)
39. Gray, C.M., Singer, W.: Stimulus specific neuronal oscillations in orientation columns of cat visual cortex. Proc. Natl. Acad. Sci. USA **86**, 1698–1702 (1987)

40. Eckhorn, R., Bauer, R., Jordan, W., Brosch, M., Kruse, W., Munk, M., Reitblöck, H.J.: Coherent oscillations: a mechanism of feature linking in the visual cortex? Multiple electrode and correlation analyses in the cat. Biol. Cybern. **60**, 121–130 (1988)
41. Alberts, B., Johnson, A., Lewis, J., Raff, M., Roberts, K., Walter, P.: Molecular Biology of the Cell, 5th edn., Garland Science, Part of Taylor and Francis Group LLC (2008)
42. Haken, H., Levi, P.: Synergetic agents. From multi-robot systems to molecular robotics. Wiley, Weinheim (2012)
43. Haken, H., Schiepek, G.: Synergetik in der Psychologie. Hogrefe, Göttingen (2006)

Neurobiological Principles of Mental Development in the Child

Gerhard Roth

Brain Research Institute, University of Bremen, 28359 Bremen, Germany
gerhard.roth@uni-bremen.de
http://www.ifh.uni-bremen.de/roth

Abstract. The mental development of a child is closely linked to the development of the brain. This does not mean that this development can be understood to be purely neurobiological. Rather, the brain is the organ of feeling, thinking, and action planning, where a number of factors concur and interact with each other in complex ways. These include (1) genetic predispositions and characteristics of individual brain development, (2) early attachment experience, (3) psychosocial and imprinting experience during infancy, and (4) education and training in later childhood, adolescence, and adulthood.
These factors act at different times upon the individual development and thus enter brain development, i.e. genetic predisposition and brain development conditions show an early influence on the structuring of the personality, followed by the early bonding experience and early psychosocial experience in childhood. For both factors it is very difficult to determine their individual effect, as they sometimes interact intensely before birth. Taken together they deeply influence most certainly the development of personality. Education and training in adolescence and adulthood have, by contrast, a lesser impact on the shaping of the individual and social personality.

Keywords: neurobiology, mental development

1 Early brain development

The brain shapes very early its basic structure in the development of an embryo, which is common for all mammals and consists of a paired end brain (telencephalon) and an unpaired interbrain (diencephalon), midbrain (mesencephalon), bridge (pons) and extended mark (medulla oblongata) as well as a cerebellum [1]. The resulting brain parts slide against each other, bend down, or one part overgrows the other as happens in the human brain. The relative sequence of the parts of the brain remains strictly intact. During brain growth the formation of nerve cells is extremely high and amounts throughout pregnancy to about 250,000 neurons per minute with a maximum of 500,000 per minute. Whereas the cell division in the human brain is largely completed in the twentieth week of pregnancy, cell migration continues long after the birth.

A. Pelster and G. Wunner (eds.), *Selforganization in Complex Systems: The Past, Present, and Future of Synergetics*, Understanding Complex Systems,
DOI: 10.1007/978-3-319-27635-9_11

Important for the function of the brain as a system of information processing is not only the formation of nerve cells, which is substantially completed in humans at birth with local exceptions, but also the formation of cell contacts (synapses) in cell bodies, dendrites and axons, called synaptogenesis [2, 3]. Axonal projections are already formed from the nerve cells during their migration, while dendrites usually develop only after the cells have reached their final destination. The formation of dendrites and synapses as points of contact between axons and dendrites, or between dendrites of different neurons starts to a large extent with the fifth month of pregnancy, but increases after birth again massively together with the formation of dendrites. However, this happens differently in different parts of the brain. In the visual cortex, for example, a doubling of the synaptic density takes place between the second and fourth month after birth and the maximum number is approximately reached within one year. Subsequently, the number of synapses drops, and the adult level is reached at about eleven years. In the frontal cortex, the maximum synaptic density is likewise achieved within a year, but the number of synapses is twice as high as in the visual cortex; synapse reduction begins here only with five to seven years and does not come to a certain stop before an age of eighteen years.

The main principle of the development of specific neuronal connections, formed in the brain, is that initially far more synapses are formed than are needed later on. This means that at first an overproduction of synapses, and then a dramatic reduction occurs. It is believed that among the billions and billions of synapses a local competition takes place, which is essentially conducted about nutrients and growth substances (called trophic factors) as well as about to ensure a minimum of neuronal excitation. In fact, does a synapse receive too little of everything, then it dies. As a consequence first diffuse, i.e. nonspecific synaptic links are installed, then they are reduced selectively and adaptively due to the competition between synapses. Thereby, the respective network is made more efficient [4]. In the provision of adequate neuronal excitation both internally generated stimuli and those derived from the environment play a major role.

Another important factor in the structural and functional maturation of the brain is the myelination of nerve fibers. To this end a so-called myelin sheath is formed around an axon. The myelination of an axonal extension allows a much (in some cases hundreds of times) faster propagation of action potentials through the axons than in unmyelinated fibers. Without a massive myelination in the brain excitation processes would run much slower, this would severely impair the cerebral cortex with its trillions of axonal connections and would make many complex cognitive performances impossible. Therefore, the process of myelination of the cerebral cortex is an important component in the development of higher cognitive and psychological benefits [5].

The myelination of axons in the brain begins after completion of cell migration and finishes gradually until they reach adulthood. Thereby, there is a clear gradient. Before birth, the axons of cells are myelinated in the spinal cord and the medulla oblongata and immediately after birth the axons of cells in

the mesencephalon and cerebellum. In the first and second year follow axons in the thalamus and in limbic centers of the end-brain and in the basal ganglia and then those in the primary sensory and motor areas of the cerebral cortex. Subsequently, the secondary sensory and motor areas are myelinated. Still later myelination takes place in the associative areas of the cortex. Here the fibers of the prefrontal and particularly the orbitofrontal cortex are myelinated at last; this may drag on until the age of 20. The growth of dendrites, the death of synapses, and the myelination are accompanied by a parcellation of the brain into structural units, namely into nuclei outside the cortex and later into cortical areas. The final step in the differentiation is the fine wiring in these structures. Thereby, the neurochemical specificity of neurons develops, i.e. the equipment with specific excitatory, inhibitory and modulating neurotransmitters and neuropeptides.

The aforementioned brain centers develop in the vertebrate brain in a very specific sequence [6]. At first, the hypothalamus and the amygdala as well as the tracks connected with the brainstem are developed very early, namely, around the fifth and sixth week of pregnancy, followed by the nucleus accumbens, the septum, and the limbic main communication routes in the sixth and seventh week. Already in the third month of pregnancy one can differentiate the various nuclei of the amygdala. The basal ganglia begin their development in the seventh and eighth week as well as the deep cerebellar nuclei and parts of the vestibulo- and spinocerebellum and parts of the limbic cortex (e.g. the insular cortex). However, although only little is known about the process of fine wiring within these centers, one can assume that it begins very early. At least, the main centers and the limbic connecting tracts are available well before birth. The hippocampus begins to bend in the middle third of the embryonic development in a characteristic "sea horse-like" manner and the connections of the three parts of the hippocampus (ammon's horn, subiculum, gyrus dentatus) among each other and with the adjacent entorhinal cortex form starting with the twentieth week. The first links of the hippocampus formation with the isocortex do not occur prior to the twenty-second week.

The actual training of the isocortex with its convolutions and fissures, which represent signs of increased cell formation, begins to a significant extent in the fourteenth to the seventeenth week in the cingulate cortex and in the occipital cortex as well as in the adjacent parietal lobe. Then the central groove and the upper temporal sulcus follow in the eighteenth to the twenty-first week of pregnancy, followed by further sulci and gyri in the parietal, temporal and occipital lobes. In the twenty-sixth to the twenty-ninth week both sulci and gyri of the frontal lobe are added. The formation of secondary temporal, frontal and orbital sulci and gyri marks the end between the 30th and 37th week, i.e. just before birth. The sequence of cognitive, mental and motor development of a child corresponds very closely to the first occurrence of the sensory, motor, cognitive and executive functions of the cerebral cortex.

The brain of the newborn has all the sulci and gyri of the mature brain. It weighs 300 to 400 grams and already contains the final number of neurons

(except those born postnatally in the hyppocampus), which, however, are still relatively immature. The subsequent massive increase in mass of the brain to an average of 1300 to 1400 grams in adults is primarily due to the length growth of dentrites and the myelination of axons as well as the increase in glial cells and brain blood vessels. The fine wiring of the cerebral cortex is thus taking place essentially after birth [3].

According to the anatomical development of the brain the sensory systems mature at different times. The sense of balance develops first; it is formed up to the end of the 5th month of pregnancy, followed by olfaction and the sense of taste. The visual system is also developing prenatally. From the 5th month the first visual synapses form, a strong growth takes place between the 14th und and 28th week of pregnancy. However, the highlight of this development lies in the first postnatal age, as already described. Like seeing, hearing takes place even before birth, but this happens apparently subcortical, because the auditory cortex develops only in the first two years after birth. The gross motor skills are present along with the sense of balance well before birth, also specific forms of arm and hand movements, such as thumb-sucking. Targeted access occurs from the 4th month, the fine motor skills between the eighth and the eleventh month, the release of a grasped object starting with the 13th month. Upright walking takes place at the end of the first year, that is when the motor cortical fields are mature enough for leg movements. This relatively late maturing is explained by the fact that the myelination and the fine wiring of these cortical fields progresses from head to foot.

From the second half of the first year, the areas of the frontal lobe slowly start working. Clearly the number of synapses is increased, and this comes along for an infant with nuanced perceptions and feelings from the 10th month on. With two and a half years a further maturation of the prefrontal cortex occurs in terms of the dendritic length and growth as well as the synaptic fine connection, especially as far as the prefrontal cortex and the Broca area are concerned. This is viewed to be the basis for the formation of conscious thought and other higher cognitive functions, the syntactic-grammatical language and self-consciousness. Apparently at this very time, i.e. at an age between two and three years, the development begins when the human child leaves behind both cognitively and communicatively his nonhuman contemporaries, see Ref. [7].

The development of language begins with the sensibility for the affective and emotional tone of language and intonation. This already happens before birth in the right hemisphere, which dominates in the first months after birth. Only then the left hemisphere begins to become active with the temporal region, i.e. with the later Wernicke area. The right frontal area, which is opposite to the Broca area, is developed in advance in its neuronal fine structure, e.g. the dendrite length, until the 12th month. Between the twelfth and fifteenth month the dendrite length increases faster at the left hemisphere, but between the twenty-fourth and thirty-sixth month after birth both right and left frontal areas develop at the same rate. Between three and six years, however, the left frontal

area dominates, i.e. the Broca area. This is consistent with the fast development of a syntactic language, which takes place afterwards.

In summary, the limbic system and the subcortical system of behavioral control, i.e. the basal ganglia, are formed early prenatally and well before the hippo campo-cortical system form, i.e. as early as the fifth embryonic week. The cortical system as the site of the conscious ego matures, however, only after birth, and this maturation process is completed not before the end of puberty. Until recently little was known on the development of the brain during adolescence. But meanwhile we know that, during this important stage of life, new connections are made in many parts of the brain, among others stimulated by sex hormones, which are then selectively degraded. The word of the "construction site of the adolescent brain" does apply, in particular to the frontal and the temporal lobe.

2 The structure of the "psychic apparatus"

The shaping of the human psyche is largely determined by subcortical and limbic cortical centers and areas of the brain, which interact with cognitive and motor centers in a characteristic way, see Refs. [6, 8]. Thus, large parts of the brain are involved in the constitution of the personality of a person. Though there is some overlap, one can differentiate four levels of the brain, which run on personality-related processes. At each level there are again several to many centers, which interact among each other and with other centers. In this respect, the level structure shown below should not be viewed selective.

The lowest level is the autonomic-affective level. It is represented by the limbic-autonomic main axis of the brain, which include parts of the septal and hypothalamic region, the central amygdala, the central gray matter and the autonomic-visceral centers of the brain stem (midbrain, pons, medulla oblongata). These areas of the brain secure our biological existence via controlling the metabolic balance, circulation and blood pressure, temperature regulation, the digestive and endocrine system as well as nutrition and fluid intake, waking and sleeping. Deficits in these regulation systems can lead to severe physical impairment. This level also controls our most fundamental affective behaviors and sensations such as offensive and defensive behavior, flight and freezing, aggressiveness, anger and sexual behavior. These drives and emotional states are in their way largely genetically determined - we share them with other mammals and especially primates - and are therefore only slightly influenced by experience and voluntary control. In particular, they run completely unconscious; they are aware only via excitations which travel from there to the cortex.

In their individual shaping these centers set the properties of the temperament, with which the people come into the world, i.e. whether a person is curious, daredevil or careful, communicative or taciturn, brave or timid, etc. This layer is formed in the brain already during the first few weeks of pregnancy. Here one finds also innate mechanisms of the interaction of the later infant with his mother, in particular the an attachment behavior, and his other close environment, see below.

The second level arranged above is that of emotional conditioning and emotional learning. To this end the corticale, mediale und basolaterale amygdala, the mesolimbic system (nucleus accumbens, ventral tegmental area and substantia nigra) are involved. The basolateral amygdala is the site of conditioned linkage of emotionally relevant, mostly negative or surprising, but also positive events with the basic feelings of fear, anxiety, defense and surprise. This includes the recognition of the importance of emotional and communicative signals such as facial expressions, gestures, voice intonation and posture. The medial and cortical amygdala handles smell and taste preferences as well as social smell signals called pheromones which play an important role for the individual likes and dislikes. These preferences are partly genetically determined and partly experience-dependent.

Interaction partner and simultaneously "opponent" of the amygdala is the mesolimbic system. It dominates during the registration and processing of natural reward events ("this has gone well" and "that was fun") and represents the cerebral reward system via the release of pleasure-producing substances of the brain (the so-called endogenous opioids). This means that everything which produces lust, joy, satisfaction etc. in us is bound to the distribution of certain substances in the brain. On the other hand, it is the basic motivation system which "promises" a reward via the distribution of the neuromodulator dopamine and, thus, "motivates" our behavior, as we shall see. The activity of dopaminergic neurons in the nucleus accumbens depends on the prediction of rewards [9].

This middle limbic level arises somewhat later than the lower level, but also before birth, and develops primarily in the early days after birth. It shapes the unconscious parts of the self, due to early childhood experiences, especially early attachment experiences. This produces in a recursive way the basic structures of the relationship to ourselves (self-image) and to others (empathy) as well as the basic categories of what is considered to be good or bad from an "infantile" way. Although these basic structures and categories result partly from unconscious and partly from conscious learning processes, they solidify step by step, and thus become "angel" or "vicious" circle in the sense of Papusek [10], i.e. experiences are selectively made in order to confirm anticipations and preferences. At this central limbic level it is determined what we seek out or have to repeat as it is connected with gratification and pleasure and what we have to avoid, as it is associated with an increase in the needs, pain and aversion. It is thus crucial for the mental level, both in terms of a normal and an abnormal development.

The third level is that of conscious, predominantly socially mediated emotions and motives. It includes the limbic parts of the cerebral cortex. These include the insular, the cingulate and the orbitofrontal cortex, which interact in turn partly parallel and partly hierarchically with each other. The insular cortex is the processing site of affective sensations, including the affective pain perception, i.e. it determines when and how a body injury hurts, and is also the place of the affective-emotional visceral perception of the famous "gut feelings". The anterior cingulate cortex with its lower, ventral part is related to risk perception and risk

assessment and with the affective tone of pain sensations, especially with pain expectation, whereas the dorsal part is concerned with cognitive attention and error monitoring.

The orbitofrontal cortex (OFC), i.e. the lower frontal lobe, which is located above the eye sockets (orbita), and the adjacent ventromedial frontal cortex (VMC, with transitions to the anterior cingular cortex, ACC) are in a certain sense the "highest" limbic cortex. Lesions in OFC and VMC lead to the inability to capture the social communicative context, for example the importance of scene representations or the expressions of faces. The OFC is the seat of networks, which represent the rules for moral and ethical behavior, i.e. those behaviors that are appropriate to preserve us the support and appreciation of our fellow human beings in the narrow sense and the society in the broader sense. It is that part of the brain, which needs the longest maturity and is reasonably "mature" not until the age of 18-20 years. Both OFC and VMC play a major role in the control of the affective limbic level and of the selfish-infantile drive from the centers of limbic middle level, the amygdala and the mesolimbic system, on the basis of socially mediated experience. It is the site of development of the components of the conscious itself and the affective-emotional, also socially mediated ego, and here elements of morality and ethics are formed, which as described by Sigmund Freud as the superego.

These three limbic levels contrast with the cognitive-linguistic level, which forms inside the cerebral cortex in the stricter sense, the six-layeredisocortex. It includes executive, i.e. preparatory treatment areas, in particular the dorsolateral prefrontal cortex (PFC). In the left PFC also resides the Broca speech area that represents the neural basis of the human syntactic-grammatical language. The dorsolateral PFC is part of working memory and, thus, of intelligence and mind. It is related with the spatio-temperal structuring of sensory perceptions, with tactical and contextual acting and speaking as well with the development of goals.

This is the level of the cognitive-linguistic ego and of grammatical-syntactical communication. On the one hand it is examined "which side one's bread is buttered on", and on the other hand it is about problem solving and purpose-rational action planning. Finally, this is the level of rational or pseudo-rational representation and justification of the conscious ego in front of oneself and of others. This level is closely connnected with the sensory (i.e. visual, auditory and tactile) areas as well as with the motoric centers of the cerebral cortex, but it has only few links to those limbic centers, including the OFC and VMC. This means that the upper frontal lobe, as the seat of intelligence and understanding, hardly interacts with the lower frontal lobe as an instance of moral-ethical control, risk assessment and control feeling.

The presented "four-layer model" of psyche and personality explains well the complexity of personality. There are largely genetically or prenatally fixed portions of temperament, above resides probably the most important limbic level of emotional conditioning in early childhood. Both together make up the core of our self-centered personality, which works largely unconsciously or cannot be

recalled (Freud's "infantile amnesia"). The development of this core of our personality is largely finished with 5-6 years. At about four years the development of the third limbic level begins at which we socialize through early childhood attachment experience through our extended family, i.e. father, siblings, grandparents, uncles, aunts as well as playmates and classmates. Here we learn how to behave, such that others like us and help us when necessary. We do this not necessarily out of pure human love, but because of the experience acquired early in life, that the others (apart from our parents) do not help us, if we do not help them, i.e. if we do not develop "reciprocal altruism". This socialization takes a long time and is largely completeled not before twenty years when the personality is more or less "consolidated".

The fourth level of intelligence, mind and language develops roughly in parallel to the upper limbic level, but largely independent of it. This fact is of great importance for the school, because here you will often find that boys and girls are "highly intelligent", but their personalities are not sufficiently developed (which is a problem when skipping classes). The opposite can also happen that someone is relatively "mature" of his or her personality, i.e. reveals a good social conduct, but remains somewhat slow in his/her cognitive abilities.

3 Neuromodulators and personality

In first approximation one can identify six neurobiological-psychological basic systems which are characterized by the specific interaction of neuroactive substances in the above mentioned limbic and cognitive centers of the brain. These basic systems also arise partly at different times in cooperation of genetic and environmental factors.

The first neurobiological-psychological system is the stress management system, which is also called the stress axis. Its function is to direct the organism towards coping with physical and psychological stress and strains. It emerges quite early in the development of the brain, that is already in the first weeks of pregnancy, but is functioning well only at the end of the first postnatal year of life. This system is activated by the limbic centers, which are responsible for detecting potentially threatening or negative events (e.g. the amygdala), and reacts hereupon in two steps. The first and fast stress response is based on the activation of neuromodulators adrenaline (epinephrine) in the adrenal medulla and noradrenaline in the locus coeruleus ("blue core") of the brain stem. The release of adrenaline into the blood stream and then into the body and of noradrenaline in the autonomic centers of the brain lead in a matter of seconds to an increase in muscle tone, responsiveness and attention. Adrenaline and noradrenaline in turn trigger the second and slower stress reaction [11]. This begins with the release of corticotropin releasing factor (CRF) in cells of the hypothalamus, which then migrates to the anterior part of the pituitary gland. There it effects both the production and the release of the adrenocorticotropic hormone (ACTH). ACTH travels through the blood stream to the adrenal cortex, where it stimulates the formation of glucocorticoids, in humans mainly cortisol. Cortisol in turn moves

through the blood stream into the body and the brain, where it triggers a variety of effects. It mobilizes our metabolism by increasing glucose and fatty acid levels in the blood and, thus, puts the body in a position to accomplish demanding achievements.

In the brain cortisol acts on two different receptors, especially in the amygdala, the hippocampus and the orbitofrontal cortex, namely the mineralocorticoid and the glucocorticoid receptors. Low doses of cortisol and mild stress activate primarily the mineralocorticoid, stronger stress the glucocorticoid receptors. Due to the latter the activation of those brain centers is increased which control the reactions for eliminating the threat or stress, for instance, escape, defense, fight or more complex countermeasures. The effect of this stress hormone is slower and more long-lasting than that of adrenaline and noradrenaline [12]. Simultaneously cortisol controls directly via the glucocorticoid receptors or indirectly via the hippocampus and the orbitofrontal cortex the release of CRF and ACTH in the hypothalamus or in the pituitary. Thus, there exists a negative feedback between cortisol on the one hand and CRF and ACTH on the other hand, which should prevent that too much CRF, ACTH and cortisol are produced at a stress reaction [11]. A special role in this negative feedback of the CRF-ACTH-cortisol system plays the hippocampus, which has a particularly large number of corticosteroid receptors and, therefore, reacts particularly sensitive to severe stress. The reduction of the stress-related cxcitement is enhanced by the simultaneous release of endogenous opioids and other "primary brain drugs" and of serotonin, which has a sedative and anxiety-dampening effect in this context.

Mild stress is necessary in order to prepare body and brain for dealing with and addressing problems and dangers, and high stress can temporarily lead to a release of unsuspected forces. Chronic high levels of stress on the other hand leads to physical and mental decline in performance, insomnia, over-excitement, depression, stomach aches and headaches, forgetfulness and a strong decrease of sexual activity. Here it is the failure of the aforementioned negative feedback of the stress axis and, correspondingly, an ongoing overproduction of CRF, ACTH and cortisol, called "hypercortisolism", which damages in particular the hippocampus (although mostly reversible). During the course of the stress response one speaks of an "inverted U" shape. People strongly differ in the way they deal with stress, i.e. it belongs to the personality of a person, how much stress he or she can withstand, i.e. "stress resilience", determining how quickly and effectively potentially negative and threatening events are recognized, how fast the stress axis "boots up" body and brain and how quickly the excitement may be "shut down". Some people can tolerate a lot of stress and under stress reach a "top form", while others are very sensitive to stress and barely tolerate some stress or excitement. Some are excited and calm down quickly, others are slowly excited and have trouble to calm down later on.

The just mentioned U-shaped pattern of stress response can therefore turn out to be highly individual. This is supported by the highly individual production rates of CRF, ACTH, and cortisol, by the distribution pattern, by the number

of glucocorticoid receptors, and by the effect of soothing substances (endogenous opioids, serotonin, etc.), and all this is determined partly genetically and partly environmentally. High levels of stress can cause great damage for an unborn child via the mother, or after birth directly on the infant, because the stress axis is yet unfinished and especially vulnerable [13–15]. But also in the later life severe acute stress (a serious accident, physical abuse, great mental suffering) may cause a psychological trauma and may lead to the formation of post-traumatic stress disorder (PTSD), which is associated with structural and functional deficits, especially in the hippocampus and the frontal cortex [16].

The second neurobiological-psychological system is the self-calming system. It develops partly before birth and partly postnatally. It is mainly determined by the meuromodulator serotonin (5-hydroxytryptamine, abbreviated 5-HT) Serotonin is produced in the nuclei, which sit on the midline (the "seam", greek and latin "raphe") of the lower brain stem and, therefore, are called "raphe nuclei". From here serotonin is spread via different nerve fiber tracts in the brain, especially in limbic centers such as the amygdala, hypothalamus, mesolimbic system, hippocampus, basal ganglia, orbitofrontal, cingulate, and insular cortex. Serotonin acts there, but also directly at its place of origin, the raphe nuclei, on a variety of receptors, which may have very different effects on their support cells. A group of receptors, the so-called 5-HT-1A receptors, are involved in the regulation of food intake, of sleep and of temperature; psychologically they cause a damping and calming-down and are significantly involved in the oppression of harmful activity stimuli (see below). A deficiency in serotonin production and increase, a deterioration of its effect via the so-called serotonin transporter as well as an activation of 5-HT-2A receptors initiates insomnia, depression, anxiety, risk aversion, reactive aggression and impulsivity. Such people typically interpret the world as threatening and feel constantly worried which manifests itself - most often in men - in "reactive" physical violence ("you have to fight after all!"), in women more in self-harm ("I am myself to blame for everything") and in both sexes in depression.

Human personality is characterized by their ability, how to deal with stress, and more significantly by the degree of confidence or anxiety, balance or inner serenity, frustration tolerance and sense of threat; and all this is essentially determined by the functional state of the serotonergic system, which closely interacts with the stress system and with substances such as the endogenous opioids and the "attachment hormone" oxytocin (see below). The management of acute high stress therefore depends also strongly on the effectiveness of the self-calming system, while, conversely, humans with deficiencies in this system, which show a high degree of anxiety and risk aversion, also show strong deficits in coping with stress. Just as the stress processing system, the performance of the self-calming system is partly genetically determined and partly influenced by environmental factors. Severe stress and strong psychological trauma in early childhood, for instance in form of physical or psychological abuse or neglect, and sexual abuse, lead to a sustainable, partly irreversible damage to the self-calming system [13, 17].

The third neurobiological-psychological system is the internal evaluation system. This system essentially comprises the activity of the amygdala and the mesolimbic system, which rate - metaphorically speaking - everything what a person experiences and is doing, according to the consequences for one's own welfare and draw conclusions for the further behavior. The recording of positive events is connected with the release of brain's own opioids through centers of the hypothalamus, which act upon receptors in the mesolimbic system, mainly in the nucleus accumbens, but also in the amygdala and in the orbitofrontal, cingulate, and insular limbic cortex, and which are linked with the feeling of reward and, thus, with joy, pleasure and desire. The recording of negative events is related to the release of substance P ("P" for "pain"), arginine vasopressin, and cholecystokinin and generates feelings of aversion, pain, and threat up to panic. Closely connected to this are also a serotonin deficit as well as an increased production of the stress factors CRF, ACTH, and cortisol. In addition comes the effect of noradrenaline associated with stress, fear, anxiety, the increase of the general awareness and the sense of threat and the consolidation of negative aversive memories. This positive-negative rating develops very early, no later than the first birthday, and determines how strong a person responds to reward and punishment, and whether one is more reward receptive ("extraverted") or punishment receptive ("neuroticistic").

The evaluation system forms the basis of the motivation system, by establishing that things and actions leading to reward should be repeated, whereas things and actions leading to pain or punishment should be avoided. The repetition tendency is based on the conscious or unconscious assumption that the reward will return upon repetition, i.e. it is driven by the expectation of reward. In the brain, this is achieved by the dopamine system, see Ref. [9]. Dopamine is primarily produced in the substantia nigra and the ventral tegmental area of the brain stem and acts upon many limbic brain centers, mainly the nucleus accumbens, the amygdala, the hippocampus and the orbitofrontal prefrontal and anterior cingulate cortex. Different types of dopamine-producing and dopamine-affected neurons register type, intensity and probability of occurrence of rewards and store it in the reward memory, which becomes the basis for reward expectancy and prediction. Still other dopaminergic nerve cells register, whether and to what extent an expected reward has actually occurred, and, thus, act - metaphorically speaking - as "confirmation" or "disappointment" neurons; their activity naturally influences the reward memory.

A pulse-like increase of the dopamine level is associated with the drive to seek or perform a reward-promising object or action. Accordingly an elevated dopamine level is connected with mental activation, reward expectation, sensation seeking and increased creativity, a lack of dopamine leads to a lack of ideas and imagination, lack of motivation and depression. A strong and sustainable increase of the dopamine level leads to a desire for adventure and variety, mental restlessness, impulsiveness, aggressiveness, flight of ideas and delusions.

The same applies for the registration of adverse events, in particular pain and punishment and for the memory of punishment, which defines what should be

avoided. It is connected with the activity of neurons in the amygdala, the nucleus accumbens and the orbitofrontal cortex, which are sensitive to serotonin, substance P and arginine-vasopressine. A low level of serotonin may be congenital-constitutive, but may also be caused, as already mentioned, by strongly negative early childhood experiences such as neglect, physical and sexual violence or inconsistent education. This leads to a preponderance of the punishment memory in the child and, thus, to avoidance behavior up to total inaction or, in women, to a tendency to self-harm, and in men to increased levels of aggression and violence or other anti-social behavior.

These three systems (or four systems if one considers the dopaminergic motivational system as a system of its own) form together predominantly on the lower and middle limbic level the core of our self-centered personality by defining how we handle stress, deal with frustrations, how we respond to rewards and punishments and what motives us. They also form the basis of three other psychological basic systems that develop subsequently and add a socially mediated part to the self-centered core of our personality.

This includes the impulse inhibition system. The behavior of infants and young children is usually impulsive and does not tolerate delayed gratification ("I want everything, and immediately"). Inhibition and tolerance for delayed gratification or postponement of elimination of negative things start developing from the first year until adulthood. Responsible for this on the brain side is the maturation of the lower and inner frontal lobe, i.e. the orbitofrontal, anterior and ventromedial cingulate cortex, as the upper limbic level, see above. They form inhibitory pathways to the subcortical limbic centers of the lower and middle limbic level (hypothalamus, amygdala, mesolimbic system), which in turn are designed for impulsive reactions and immediate gratification of egocentric motives [18]. The impulsive system is driven by the just described motivational dopamine system, inhibition essentially takes place via the serotonin system [19–21]. The bottom and medial frontal lobe contains many serotonin receptors, and an activation of the frontal lobe via these receptors increases over the descending pathways the inhibition of the mentioned subcortical limbic centers via their inhibitory neurons. This applies both to appetitive as aversive reactions, i.e. the urge for immediate reward as well as the tendency to immediate escape, defense or immediate attack. This explains why the lack of serotonin and, thus, a sub-activity of the frontal cortex usually occurs with anxiety disorders and violent antisocial behavior, as well as with experience with addiction, gambling addiction and high-risk behavior [22].

The next system is the attachment and empathy system. In its primary stage as an attachment system it is developing in a few weeks after birth, when the infant begins to smile at his mother or other primary attachment person and interacts with her increasingly complex ways. It is believed that this strenghens the emotional coupling between infant and attachment person and increases the differentiation of the emotional world of infants and small children, and is coined in the emotion of the mother. Accordingly, a depressive mother will strengthen the negative feelings of her child and, apart from disseminating depression pro-

moting genes, reinforces the tendency to depression of a child in non-genetic ways.

An essential role in this binding plays the neuropeptide oxytocin, which is produced in the hypothalamus and promotes the uterus contractions and milk flow. In mammals including humans, it occurs as a "attachment hormone" in mother-child and also in adult couple relationships and sexual behavior, but also generally in trusting social contacts [23, 24]. This effect of oxytocin is reinforced by the release of endogenous opioids and serotonin, which enhance the sense of well being during intense social relationships. Disturbances in social behavior, for example autism, Asperger's syndrome, antisocial personality disorder and psychopathy, are associated with deficits in the oxytocin budget.

These disorders are associated with deficits in the empathy system, which develop from the attachment system. Empathy includes the ability to "read" thoughts and intentions of others, which is also called "theory of mind". One has to add the ability to show "compassion", i.e. empathy in the strict sense. The former may well occur without the latter, for example, psychopaths who can superbly read and take advantage of the thoughts, desires and fears of other people, but act ruthlessly [25, 26].

The human empathy system encompasses both subcortical limbic centers such as the mesolimbic system and the amygdala (especially when recognizing the facial expression) and cortical limbic centers, especially the anterior orbitofrontal, cingulate and insular cortex for the perception of "pain" in others, as well as areas of the parietal and temporal lobes, which are involved in the recognition of faces and gestures. Unfortunately, this system is often referred to as cortical "mirror neuron system" on the basis of "mirror neurons" which were discovered and closely examined in macaque monkeys, see Refs. [27, 28]. The one is completely unrelated to the other, because in macaques the mirror neurons are not involved in empathy or imitation (macaques show neither the one nor the other) and are found in a premotor and not in a limbic or a cognitive region of the cortex as in humans [29].

The last neurobiological-physiological system is the system of sense of reality and the perception of risk. It develops after the age of three, when the cognitive abilities of the brain develop gradually, in particular in terms of attention and memory skills. This system is primarily bound to the neurotransmitter and neuromodulator acetylcholine, which is mainly formed in the so-called basal forebrain. The basal forebrain affects massively the cognitive areas of the cortex via the release of acetylcholine, in particular the frontal lobes as well as the hippocampus wich is central to learning and memory. Acetylcholine increases both attention and concentration by "focusing" neuronal activity in the frontal lobes and in the selective retrieval memory contents; a disturbance of the basal forebrain (e.g. in case of Alzheimer's desease) and thus a reduction of the acetylcholine level cause a lack of concentration and a reduced memory performance up to dementia. The states of the attention and concentration is also supported by the release of noradrenaline in the locus coeruleus, which causes either a

general arousal or a specific task-related response via a tonic or phasic effect, respectively.

The features of this system also include the ability to recognize risks of a particular situation and, thus, potential negative consequences of our actions. Here, mainly the activity of the dorsal portion of the anterior cingulate cortex plays a role, which has a close relationship with the adjacent dorsolateral prefrontal cortex. It is believed that the anterior cingulate cortex "recognizes" the risks and sends corresponding signals to the prefrontal (cognitive) and orbitofrontal (emotional and ethic) cortex, which results in certain global strategies of action (see above). Persons with deficits in the anterior cingulate and prefrontal cortex fail to detect risks, whereas people with deficits in the orbitofrontal cortex are able to do high-risk things, even if they know these risks [30].

This rational-cognitive system of the prefrontal and dorsal cingulate cortex is the one which together with the orbitofrontal system of social control develops slowest and is more or less mature only at the beginning of adult life - i.e. the attainment of adulthood is characterized by the fact that young people slowly come "to reason and understanding" and have learned simultaneously "how to behave".

4 Final remarks

During the past years, neuroscientists, together with psychologists of personality and psychiatrists, have studied intensively the relationship between neuroanatomical, neurophysiological and neuropharmacological properties of the brain and personality traits, including their individual characteristics and diseases [31]. Therefore, it becomes increasingly better to relate the prevailing classifications of personality, for instance after the "Big Five" of Costa and McGrae, with these brain properties and to explain why the basic features used in these classifications (neuroticism, extraversion, openness, conscientiousness, and compatibility) are not truely selective, because the underlying psychological basic systems interact pharmacologically and functionally both positively and negatively. This could be addressed here only in a very superficial way.

The emotional and cognitive development of the child is determined by a sequential maturation of limbic structures at the three limbic levels plus the cognitive-linguistic level and the corresponding maturation of the neuropharmacological systems which drives the interaction between the levels. The most important finding here is that both maturation processes are based on a complex interaction between genetic-epigenetic and environmental processes, in which early attachment experience during early childhood play a major role. To explain all this in more detail has to be left to future publications.

References

1. O'Rahilly, R., Müller, F.: The Embryonic Human Brain. An Atlas of Developmental Stages, 2nd edn. Wiley-Liss, New York (1999)

2. Huttenlocher, P.R., Dabholkar, A.S.: Regional differences in synaptogenesis in human cerebral cortex. Journal of Comparative Neurology **387**, 167–178 (1997)
3. Eliot, L.: (2001): Was geht da drinnen vor? Die Gehirnentwicklung in den ersten fünf Lebensjahren. Berlin Verlag, Berlin (2010)
4. Raff, M.C., Barres, B.A., Burne, J.F., Coles, H.S., Ishizak, Y., Jacobson, M.D.: Programmed cell death and the control of cell survival: Lessons from the nervous system. Science **262**, 695–700 (1993)
5. Toga, A.W., Thompson, P.M., Sowell, E.R.: Mapping brain maturation. Trends in Neurosciences **29**, 148–159 (2006)
6. Roth, G.: Fühlen, Denken, Handeln. Wie das Gehirn unser Verhalten steuert. Suhrkamp, Frankfurt (2003)
7. Tomasello, M.: Die kulturelle Entwicklung des menschlichen Denkens. Suhrkamp, Frankfurt (2002)
8. Roth, G., Dicke, U.: Funktionelle neuroanatomie des limbischen systems. In: Förstl, H., Hautzinger, M., Roth, G. (Hrsg.) Neurobiologie Psychischer Störungen, pp. 1–74. Springer, Heidelberg (2006)
9. Schultz, W.: Multiple dopamine functions at different dime courses. Ann. Rev. Neurosci. **30**, 259–288 (2007)
10. Papoušek, M., Hofacker. N.: Klammern, trotzen, toben – störungen der emotionalen verhaltensregulation des späten säuglingsalters und kleinkindalters. In: Papoušek, M., Schieche, M., Wurmser, H. (Hrsg.) Regulationsstörungen der frühen Kindheit. Huber, Bern, pp. 201–232 (2004)
11. Gunnar, M.R., Quevedo, K.: The neurobiology of stress and development. Annual Review of Psychology **58**, 145–173 (2007)
12. Sapolsky, R.M., Romero, M., Munck, A.U.: How do glucocorticoids influence stress responses? Integrating permissive, suppressive, stimulatory, and preparative actions. Endocrine Reviews **21**, 55–89 (2000)
13. Caspi, A., Sugden, K., Moffitt, T.E., Taylor, A., Craig, I.W., Harrington, H., McClay, J., Mill, J., Martin, J., Braithwaite, A., Poulton, R.: Influence of life stress on depression: moderation by a polymorphism in the 5-HTT gene. Science **301**, 386–389 (2003)
14. Davis, E.P., Glynn, L.M., Dunkel-Schetter, C., Hobel, C., Chicz-Demet, A., Sandman, C.A.: Corticotropin-releasing hormone during pregnancy is associated with infant temperament. Developmental Neuroscience **27**, 299–305 (2005)
15. Lupien, S.J., McEwen, B.S., Gunnar, M.R., Heim, C.: Effects of stress throughout the lifespan on the brain, behaviour and cognition. Nature Reviews Neuroscience **10**, 434–445 (2009)
16. Loman, M.M., Gunnar, M.R.: Early experience and the development of stress reactivity and regulation in children. Neuroscience and Biobehavioral Reviews **34**, 867–876 (2010)
17. Canli, T., Lesch, K.-P.: Long story short: the serotonin transporter in emotion regulation and social cognition. Nature Neuroscience **10**, 1103–1109 (2007)
18. Kringelbach, M.L., Rolls, E.T.: The functional neuroanatomy of the human orbitofrontal cortex: Evidence from neuroimaging and neuropsychology. Progress in Neurobiology **72**, 341–372 (2004)
19. Cools, R., Roberts, A.C., Robbins, T.W.: Serotonergic regulation of emotional and behavioural control processes. Trends Cogn. Sci. **12**, 31–40 (2008)
20. Dayan, P., Huys, Q.J.M.: Serotonin in affective control. Ann. Rev. Neurosci. **32**, 95–126 (2009)
21. Berger, M., Gray, J.A., Roth, B.L.: The expanded biology of serotonin. Ann. Rev. Med. **60**, 355–366 (2009)

22. Brown, S.M., Manuck, S.B., Flory, J.D., Hariri, A.R.: Neural basis of individual differences in impulsivity: Contributions of corticolimbic circuits for behavioral arousal and control. Emotion **6**, 239–245 (2006)
23. Campbell, A.: Attachment, aggression and affiliation: The role of oxytocin in female social behavior. Biological Psychology **77**, 1–10 (2008)
24. Ross, H.E., Young, L.J.: Oxytocin and the neural mechanisms regulating social cognition and affiliative behavior. Frontiers in Neuroendocrinology **30**, 534–547 (2009)
25. Blair, R.J.R.: Responding to the emotions of others: Dissociating forms of empathy through the study of typical and psychiatric populations. Consciousness and Cognition **14**, 698–718 (2005)
26. Blair, R.J.R., Peschardt, K.S., Budhani, S., Mitchell, D.G.V., Pine, D.S.: The development of psychopathy. Journal of Child Psychology and Psychiatry **47**, 262–276 (2006)
27. Rizzolatti, G., Craighero, L.: The Mirror-Neuron System. Annual. Rev. Neurosci. **27**, 169–192 (2004)
28. Rizzolatti, G., Fabbri-Destro, M.: The mirror system and its role in social cognition. Curr. Opinion Neurobiol. **18**, 179–184 (2008)
29. Fecteau, S., Pascual-Leone, A., Théoret, H.: Psychopathy and the mirror neuron system: Preliminary findings from a non-psychiatric sample. Psychiatry Research **160**, 137–144 (2008)
30. Anderson, S.W., Bechara, A., Damasio, H., Tranel, D., Damasio, A.R.: Impairment of social and moral behavior related to early damage in human prefrontal cortex. Nature Neuroscience **2**, 1032–1037 (1999)
31. Hariri, A.R.: The neurobiology of individual differences in complex behavioral traits. Ann. Rev. Neurosci. **32**, 225–247 (2009)

Synergetics in Psychology: Patterns and Pattern Transitions in Human Change Processes

Günter Schiepek[1], Stephan Heinzel[2], Susanne Karch[3], Martin Plöderl[1], Guido Strunk[4]

[1] Institute of Synergetics and Psychotherapy Research, Paracelsus Medical University and Christian Doppler University Hospital, Ignaz Harrer Str. 79, 5020 Salzburg, Austria
guenter.schiepek@ccsys.de
http://www.pmu.ac.at/forschung/forschungsinstitutionen-und-programme/synergetik-und-psychotherapieforschung.html
[2] Department of Psychology, Humboldt University, Berlin, Germany
[3] Department of Psychiatry and Psychotherapy, Ludwig-Maximilians-University Munich, Germany
[4] Technical University Dortmund, Faculty of Economics and Social Sciences, Dortmund, Germany

Abstract. Synergetics has arrived in psychology. More than this – it has proven to be an inspiring research paradigm for investigating and modelling complexity and dynamics of mental, behavioural, and social phenomena. The evolution of human systems is characterized by features as circular causality, the emergence and dynamics of order parameters, order transitions, and critical instabilities. Psychotherapy research was one of the most productive fields for empirical research on self-organization in psychology. Referring to several studies on psychotherapy processes we will demonstrate that human development and learning generate some kind of order. They are chaotic in a strict sense, i.e., they can be characterized by low-dimensional, complex, and changing dynamics. Empirical studies used different data sources, coding methods, and time scales and focused on synchronization, non-stationarity, and local instabilities of psychotherapeutic processes. Referring to the concept of order transitions, synergetics offers an explanation to what is called "sudden changes" in psychotherapy. Empirical evidence also exists for coordinated order transitions in the dynamics of subjective experiences and brain activity, measured by repeated fMRI scans. During the treatment of patients with obsessive-compulsive disorder (OCD), transitions started by the destabilization of current patterns and hence by critical fluctuations. The most important change rates of neuronal activity in different brain areas occurred during cognitive-affective order transitions.

Keywords: Synergetics, psychology, order transitions, psychotherapy research, brain dynamics

A. Pelster and G. Wunner (eds.), *Selforganization in Complex Systems: The Past, Present, and Future of Synergetics*, Understanding Complex Systems,
DOI: 10.1007/978-3-319-27635-9_12

1 Introduction

Synergetics describes, measures, and explains processes of pattern formation and pattern transition in complex nonlinear systems. Although Hermann Haken developed it in the field of quantum optics (laser physics) and applied it firstly to other physical phenomena like the emergence of convection patterns in fluids, he noticed quite early that its principles and the mechanisms of self-organization hold for true independently of the matter of the systems they occur in [1]. Synergetics is thus not only a theory of pattern formation in physics; it is a general theory of structures and a conceptualizing module for modelling and thinking in quite different disciplines. Its general concepts, equations, and mathematical formalisms successfully founded the perhaps most important transdisciplinary framework and connecting pattern of modern science.

In terms of the structuralistic concept of theories and theory dynamics [2], synergetics provides a theory kernel which applies successfully to many phenomena in the natural sciences and the humanities [3]. Beginning from models of pattern formation in physics, chemistry, and biology, Hermann Haken early applied it also to brain dynamics (e.g., [4, 5]). He thereby gave rise to the insight that the brain is perhaps the most interesting example of a complex, self-organizing system. More than 10^{11} nonlinear interconnected neurons create a dynamic meganetwork of neuronal networks with emerging and submerging synchronizations, nearly instantaneous adaptability and flexibility with ever changing pattern formation working "at the edge of chaos", and realizing combined (activating and inhibiting) feedback mechanisms following the principles set forth by synergetics [6, 7].

In contrast to early presentations of synergetics, when the listing of examples synergetics was applied to jumped from biological structures and brain dynamics to macro-sociology (where synergetics modelled the change of opinions and attitudes of large populations by the master equation, [8]), later on mental and behavioural phenomena were introduced into the set of examples, too [9, 10]. It became evident that the paradigm of self-organization would be a very promising approach to psychology. The laws and principles of synergetics helped for a deeper understanding of neural, mental, and behavioural processes. Fruitful interdisciplinary cooperation in modern psychology was underpinned by the unifying terminology, formalism, and modelling tools of synergetics.

When taking a closer look at psychological phenomena like perception, learning, decision making, thinking, feeling, or social interaction and behaviour coordination in dyads or groups, we can appreciate that they are dynamic in nature and characterized by specific "Gestalts". They can be described by synergetic features such as

- order and order parameters, in many cases also hierarchies of order parameters,
- enslaving of system components by order parameters,
- coordination (competition or cooperation) of order parameters,
- order transitions (non-equilibrium phase transitions) with symmetry breaking,

- critical instabilities and fluctuations during the emergence of new or changed patterns,
- multistability,
- hysteresis,
- circular causalities between the components of a system, and
- circular causality from the bottom (relative micro-level of a system) to the top (relative macro-level of a system) and from the top to the bottom.

In consequence, synergetics has successfully been applied to many topics in psychology:

General psychology

- motoric coordination (e.g. [11–14])
- perception (e.g., [15, 16])
- decision making (e.g., [3, 17])
- memory (ekphorisation as a spontaneous self-organizing process of neural networks triggered by internal and external stimuli, former system states, and boundary conditions, e.g., [33, 18])
- learning (e.g., [9, 19, 20])
- intentionality of cognition and action processes (e.g., [21, 22])
- dynamics of emotions (e.g., [3, 23])
- creativity and innovation (e.g., [24])
- speech recognition and speech acquisition (e.g., [25])
- the emergence of phenomenal consciousness (e.g., [3])
- the dynamics of the ,,self“ (e.g., [3, 26])

Developmental Psychology

- child development (e.g., [23, 27])
- assimilation and accommodation of schemata (e.g., [27])

Social psychology

- dyadic interaction (patient-therapist, mother-child) (e.g. [28, 29])
- attitude change (e.g., [8, 30])
- group dynamics (e.g., [3, 31–33])
- stability and instability of collective behaviour (e.g., [30, 34])

Clinical psychology

- etiology of mental disorders (e.g., [35, 36]),
- mental disorders as dynamical diseases (e.g., [35, 37–39]),
- psychotherapy (process-outcome-research, feedback and monitoring) (e.g., [3, 40–43])

Management / organizational psychology (e.g., [3, 44]).

Looking back to the last three decades, synergetics gave some important inspirations to modern academic psychology: First, it introduced a “thinking

in complexity" [45] on mental and social phenomena. Since after World War II positivism and linear causality had become the dominating paradigm, complexity had been ruled out from psychological modelling. Second, concepts of time and dynamics were integrated into psychological thinking. Even though it seems quite obvious that things evolve in time and that they are not "being" but "becoming", the important tools for thinking in dynamics and for nonlinear time series analysis had to be imported to psychology from the outside – from the theory of self-organization and dynamic systems. Third, synergetics introduced a fruitful research paradigm to psychology by consequently relating models to empirical testing. The complexity of hypotheses increased noticeable, since not only differences between experimental conditions or pre-post-differences were in the focus of interest, but specific dynamic patterns, emerging dynamics, and contra-intuitive phenomena. Fourth, synergetics gave rise to a specific ,,imago hominis" accentuating the autonomy of individuals (in contrast to focussing on their dependency of external input) but without forgetting the social context of interpersonal synchronization and cooperation. Finally, synergetics turned psychology back to its own history by connecting it to its roots in "Gestalt psychology" and other traditional approaches.

The Gestalt psychology of the early 20^{th} century was concerned with patterns ("Gestalts") of perception, thinking, behaviour, and interaction (e.g., group dynamics, [46]). Psychologists like Wolfgang Köhler (e.g., [47]), Wolfgang Metzger (e.g., [48]), Max Wertheimer, Kurt Lewin (e.g., [46]) and others can be seen as predecessors of modern complexity research in psychology [49] . Another precursor of self-organization theory is Jean Piaget's equilibration theory of action-cognition patterns (schemata) describing assimilation-accomodation-cycles of schemata [50] by using input from the inner and outer environment as disturbing stimulation. Another historical line – anthropological medicine – accentuated concepts of circular causality. The "Gestaltkreis" integrates feedback loops between sensorial and actional systems on the one side, and individual and environmental systems on the other side (ecosystemic approach) [51] .

2 Dynamic Patterns in Psychotherapy

One of the prominent topics of applied synergetics in psychology is human development during psychotherapy, which has become an important field of research similar as laser physics did in the early steps of synergetics. One of the reasons is that psychotherapy is an intensive learning and development process integrating cognitive, affective, and behavioural systems. Stable, dysfunctional patterns of processing are destabilized in order to give rise to new patterns and the deformation of potential landscapes and thereby creating changed mental attractors. In such a way, self-organizing processes can very well be studied in psychotherapy research.

One of the basic questions is whether therapy-related dynamics of behaviour, cognition, and emotion manifest some kind of order or not. If this is not the case, we would expect irregularity or white noise. But if psychotherapy was a

self-organizing process, one would expect some kind of complex dynamic order – in other words: deterministic chaos. The term "deterministic chaos" refers to complex dynamic structures in time signals generated in "real world systems" by deterministic or – more realistic – by combined deterministic and stochastic processes [52–54]. The term "chaos" covers a large spectrum of dynamic patterns between irregularity on the one hand and regularity and order on the other hand. One consequence with specific relevance to psychotherapy is a fundamental limitation of predictability and of linear controllability of processes. Another consequence is the distinctive individuality of processes; any notion of superposition of dynamics within or between individuals (systems) cannot be maintained meaning that concepts like "standard tracks" or "normative processes" are inappropriate to describe psychological phenomena.

2.1 Patients and Measurement Procedure

To investigate the hypothesis of ordered dynamics in psychotherapeutic change processes we used the data from daily self-assessments of 149 patients (average age: 34.3 years, 92 female, 57 male) during in-patient psychotherapy in a psychiatric hospital. The self-ratings were collected through an Internet-based device, the so called Synergetic Navigation System (SNS, [42]). In the last years, Internet-based real-time methods like the SNS were successfully used in research and practice for process monitoring and ambulatory assessment [55, 56]. Real-time monitoring allows for the optimization of therapy processes [57, 58] and offer detailed insights into process-related patterns. Every day, patients completed the Therapy-Process Questionnaire (TPQ) provided by the SNS. The TPQ is a self-assessment tool for patients undergoing in-patient or out-patient psychotherapeutic treatment. The study described here made use of the in-patient version with 23 items, grouped into 5 scales [59].

Most of the patients were categorized to three ICD-10 diagnostic groups: F30 (affective disorders), F40 (neurotic stress-related and somatoform disorders), and F60 (specific disorders of personality, esp. F60.3, emotionally unstable personality disorder, referred to as borderline type in other classification systems). On average, the TPQ was completed by patients during 97 days (SD: 50.3). The number of days defines the length of the time series and roughly corresponds to the days of hospital treatment. 5.1% of the entries were missing; the missing values were restored by a cubic spline function implanted in the SNS. Figure 1 gives an example of the 5 time series of a patient, corresponding to the 5 subscales of the TPQ.

The measurement series of all 149 patients were joined together, resulting in 5 artificial time series with a length of n = 14,425 points (one time series for each subscale of the TPQ). Different durations of hospital stay were not counterbalanced, i.e., patients with longer treatments hold a greater fraction of the resulting artificial time series.

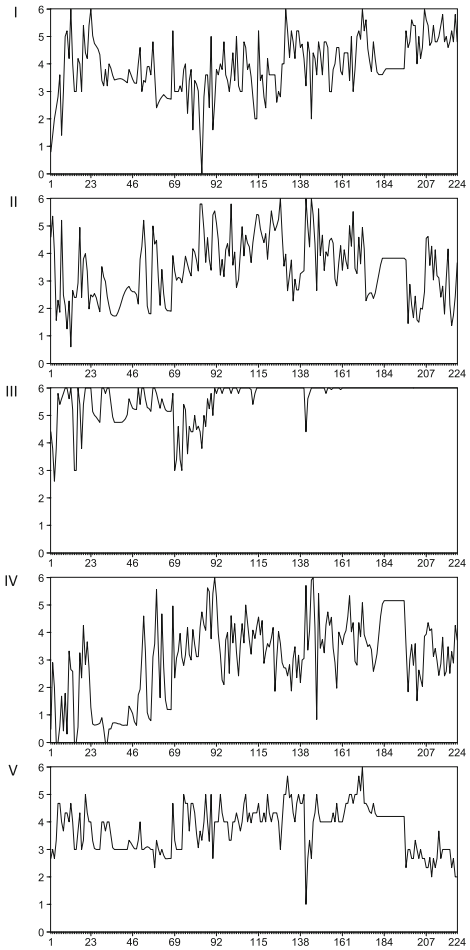

Fig. 1. Example of time series from TPQ scales (factors). Factor I: Therapy progress; Factor II: Complaints and problem pressure; Factor III: Relationship quality and trust in therapists; Factor IV: Dysphoric affects; Factor V: Relationship with fellow patients / ward atmosphere. All scales were normalized to a range from 0 to 6. (Female patient, 25 years old; diagnosis: F33.10 major depressive disorder, recurrent; 224 measurement points = days).

2.2 D2 and Pointwise D2 (PD2)

Fractal dimensionality of a time series estimates the number of independent system components or subsystems whose interaction creates the system dynamics. The dimensionality of an attractor corresponds to the degrees of freedom of the generating system and can be seen as an indicator of its complexity.

There are several definitions and methods for calculating fractal dimensionality. A well known method for empirical time series is the D2 algorithm, which

is based on the embedding of a time series in a reconstructed phase space whose dimensions were created by time-delay coordinates [60]. The method calculates a correlation integral [61, 62] by a counting algorithm over all Euclidean distances between vector points within the phase space. The estimate of the D2 correlation dimension results from a diagram which plots D2 against increasing numbers of embedding dimensions. In case of saturation, D2 estimates converge to a fixed value with increasing embedding dimensions (for details see [3] pp. 484-489, [54] pp. 208-214). While D2 provides a complexity estimation of the attractor of the whole process, the pointwise D2 (PD2) portrays the possible changes of dimensional complexity over time (non-stationarity). D2-estimates are taken from vector point to vector point and can be portrayed in a PD2 to time diagram [63, 64].

2.3 Surrogate Data Analysis

When there is no saturation of D2 estimates for increasing time-delay embedding dimensions, this theoretically means that the process under consideration does not entail systematic order. In practice, however, the hidden dynamic order of the data has to correspond to the resolution of the measurement scale and to the length of the time series. If the scale is too coarse grained and by this, the corresponding m-dimensional phase space doesn't include a sufficient number of m-dimensional voxels, even ordered time series will cover the phase space and fail any D2 convergence. On the other hand, time series without sufficient measurement points n (n $\ll$ number of available voxels in the phase space) cannot cover the phase space, even if they result from pure randomness (white noise). Here, the pseudo-evidence of saturation would erroneously reject the null-hypothesis of no existing dynamic structure. In both cases the procedure fails to differentiate between randomness and order.

A random series only covers the entire phase space (resulting in no D2 saturation with increasing numbers of embedding dimensions) if the time series is long enough. In a 10-dimensional embedding space, only 10 levels of a measurement scale result in 10^{10} possible voxels or data constellations within the phase space. If a diced time series wanted to cover the entire phase space, the series would have to include at least the same number of measurement points. If the time series is too short for covering the phase space, it is possible to calculate finite correlation dimensions even for randomness. Safely backing up D2 or PD2 analyses therefore requires surrogate data testing [65] which tests for nonlinearity or chaos in a given time series [66] .

Surrogate time series preserve some characteristics of the original time series while others are changed. A simple surrogate can result from shuffling the values of the series, leading to a random surrogate. The dynamic structure vanishes but the series maintains distribution characteristics as mean, median, or variance. In applying complexity estimates, the surrogate differs from the original time series. If not, the original itself seems to be only a random arrangement of values. Generally, surrogate data sets are created by different procedures in order to obtain or destroy specific statistic distributions and dynamic features

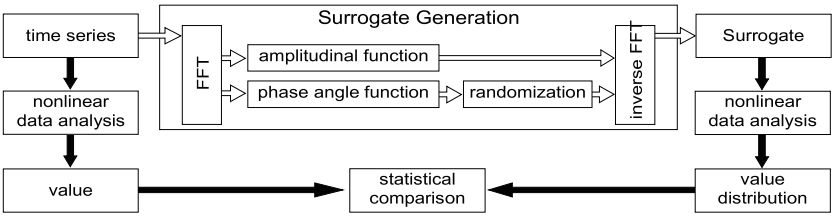

Fig. 2. Procedures of surrogate data analysis, based on statistical comparisons of dynamic features resulting from nonlinear time-series analysis (e.g., fractal dimensionality). The distribution of the features of a large number of surrogates is compared against the feature of the original time series. In case of FFT surrogates, linear autocorrelations and the frequency spectrum of the time series are retained in the surrogates while nonlinear features are destroyed by the procedure of phase angle randomization. Surrogate data tests will thus be indicative for nonlinearity. Depending on the null hypothesis under consideration, surrogates can be generated by quite different methods.

of the data. A surrogate corresponds to a specific null-hypothesis. Eliminating nonlinear qualities should result in the effect that the nonlinearity and chaoticity of the original is discarded. By this, the crucial part in surrogate data testing is the algorithm for surrogate generation.

More sophisticated than random surrogates is the surrogate production by applying a Fast Fourier Transformation (FFT) [66–71]. The time series is submitted to a Fourier-analysis with randomization of the resulting function phase angles. When the spectral density function and the randomized phase angle function are subsequently used to generate a surrogate via Fourier synthesis, the surrogate retains the frequency spectrum of the original time series but has lost its nonlinear features. It seems to be the result of a linear stochastic process. Linear correlations within the data are preserved, whereas nonlinear qualities are lost. A surrogate data test using such kind of surrogates tests for nonlinearity, which is a prerequisite for chaotic dynamics (Figure 2). Calculations were performed with GChaos 19.0 (www.complexity-research.com), a nonlinear analysis program written by one of the authors (G. Strunk).

2.4 PD2 of TPQ Factor Dynamics and D2-Differences Between Original Time Series and FFT-Surrogates

The time series of the factors of the TPQ were analyzed by the PD2 algorithm. We adopted Skinner's [63] criterion of at least 75% valid measurement points for the calculation and interpretation of the PD2 for all 5 factors (Table 1). This implies that the majority of the processes is suitable for interpretation as ordered dynamics instead of being a stochastic processes.

The arithmetic means of the PD2 range from 0.947 to 5.187 and are indicative for low-dimensional chaotic processes. Large standard deviations (as compared to the means of PD2) result from the variability in the PD2 dynamics which

I Therapy Progress	% valid time points in PD2	88.72%	
	PD2 AM±SD	0.947	±2.263
	surrogate data test D2: t (p)	113.070	(<0.001)
II Complaints and Problem Pressures	% valid time points in PD2	77.49%	
	PD2 AM±SD	2.650	±3.662
	surrogate data test D2: t (p)	89.103	(<0.001)
III Relationship Quality and Trust in Therapists	% valid time points in PD2	87.80%	
	PD2 AM±SD	3.239	±2.940
	surrogate data test D2: t (p)	54.681	(<0.001)
IV Dysphoric Affect	% valid time points in PD2	90.61%	
	PD2 AM±SD	1.114	±2.420
	surrogate data test D2: t (p)	100.368	(<0,001)
V Relationship with Fellow Patients	% valid time points in PD2	81.70%	
	PD2 AM±SD	5.187	±2,803
	surrogate data test D2: t (p)	42.043	(<0,001)

Table 1. PD2 of TPQ factor time series and surrogate data test of D2 using FFT surrogates of TPQ factor time series (see Figure 1; TPQ: Therapy Process Questionnaire). The time series of the 5 factors of 149 patients were joined together, resulting in 5 artificial time series with a length of n = 14,425 points. 30 FFT surrogate time series were generated for each factor dynamics to produce a distribution of D2 estimates. Maximum embedding dimension was 15. The table presents the percentage (%) of valid PD2 values, the arithmetic mean (AM) and the standard deviation (SD) of the PD2s of the 5 empirical (original) time series, and the t- and p- values of the surrogate data tests.

refer to different levels of fractal dimensionality between patients, but also to the nonstationarity of the dynamics and hence to phase transitions during treatment.

FFT surrogates from the time series of TPQ factors were used for a comparison to the original time series. Since the PD2 scaling range was not sufficiently large for surrogates (which results in insufficient valid measurement points), the surrogate test is based on the D2 algorithm. 30 FFT surrogate time series were generated per TPQ factor to obtain statistical distributions of the D2 values, which served as a reference for comparison with the original time series by t-tests. The greatest number of embedding dimensions in the time-delay phase space was 15. For surrogate time series lacking D2 saturation, the average D2 estimates were used to compare embedding dimensions from 10 to 15. For results see Table 1.

When nonlinear dynamic structures are destroyed by producing FFT surrogates, one expects significantly increased fractal complexity of the surrogates. This hypothesis could be confirmed: all t-tests were highly significant ($p < 0.001$). The data represent a nonlinear dynamic structure.

The hypothesis of chaoticity and nonlinearity of psychotherapeutic processes was corroborated once again. Calculating fractal dimensionality via PD2 results in saturation of the mean PD2 estimates in low-dimensional ranges. The PD2's

high standard deviation is an indicator of non-stationary processes (phase transitions). The crucial point is validation through FFT surrogate testing which is methodically rigorous and discriminating, because it not only contains means and variances of the surrogate time series used for comparison but also their frequency spectrums. Only nonlinear characteristics are removed, providing the basis for statistically significant D2 complexity differences.

3 Order Transitions in Human Dynamics

3.1 Patient-Therapist Interaction

In psychotherapy research there has been a rapid rise in interest in the study of patterns of change. In the sense of synergetics, these patterns correspond to the order parameter dynamics of the process. If the prerequsites for self-organized order transitions are given, they should occur with only small external driving forces or even without any additional input. Indeed, discontinuous transitions of dynamic patterns were found in the social dynamics of psychotherapies and in the social dynamics of groups.

In a study on the dynamics of the therapeutic relationship [28, 72] we used the method of Sequential Plan Analysis, which is a development of the hierarchical plan analysis proposed by Grawe and Caspar [73] . By "plans" here one understands more or less conscious and verbally or non-verbally communicated intentions and/or self-presentations in a social situation. Patient's and therapist's interactional behavior was analysed on the basis of video recordings. The construction of a hierarchical plan analysis leads to an idiographic categorical system for the observation of the patient-therapist interaction. Two complete therapies (13 and 9 therapy sessions, resp.) were encoded with a sampling rate of 10 seconds. At this measuring frequency, a psychotherapy process of 13 sessions was represented by multiple time series of about 3,800 measurement points, and a therapy of 9 sessions by time series of about 2,900 points.

Nonlinearity was proven by surrogate data tests [65] using random surrogates and FFT-based phase-randomized surrogates. Then the time series were analysed by methods which are sensitive to the nonlinearity as well as the non-stationarity of processes. The methods of PD2 [64] and of the Local Largest Lyapunov Exponents [74] were used to identify phase-transition like discontinuities. Following the evolution of PD2 dimensionalities, both therapies realized non-stationarities, and both therapies showed periods of strongly synchronized (with correlations from 0.80 to 1.00) and anti-synchronized PD2-processes (with correlations from -.80 to -1.00) between patient and therapist (Figure 3). Quite similar and even more pronounced dynamical jumps could be identified in the development of the Local Largest Lyapunov Exponents (LLLE) (Figure 4), representing changes in the chaoticity of a time signal [28]. Most of the discontinuities of the LLLE were exactly synchronized between patient and therapist. Obviously both persons create a dynamic self-organizing communication system, which enables and triggers the individual change processes of the patient.

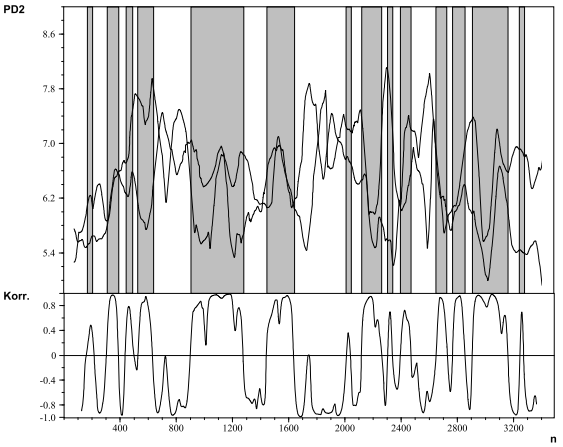

Fig. 3. Dynamics of PD2 of patient and therapist from one of the two therapies under consideration (13 sessions, 3,800 measurement points). A smoothing was realized by a gliding window of 100 PD2 values. The lower part of the figure represents the correlation between the two PD2 dynamics, with correlations calculated in a gliding window of 100 points. Periods of strong positive correlations are marked by a grey background, periods of strong negative correlations are marked by a white background.

These results receive support from nonlinear coupling measures between the time series of the interaction partners. Pointwise Transinformation as well as Pointwise Coupling Conditional Divergence [75, 76] were applied to the data, and both indicate changing and time-dependent coupling strengths between the time series of the interacting persons. There is no priority of the therapist's influence on the patient, or vice versa. Constituting the circular causality of psychotherapeutic self-organization, this finding contradicts the classical opinion where the input from the therapist supposedly determines the patient's output.

The converging results corroborate the hypothesis of (i) nonlinearity and deterministic chaos realized in therapeutic change dynamics and interaction, (ii) spontaneous order transitions in these processes, and (iii) synchronization and synchronized order transitions between patient and therapist. Furthermore there are some studies that focus on self-organized synchronization between patient and therapist at different time scales and with different methods [29, 77–79].

3.2 Group Dynamics

The method of Sequential Plan Analysis was not only applied to patient-therapist interaction, but also to the microdynamics of group interaction [3]. In a group of five persons a creativity and problem solving task was to be solved within 2 $\frac{1}{2}$ hours (creation of ideas, rules, and physical handicraft realisation of a prototype board game from different materials). Similar to the psychotherapy study the sampling rate was 10 seconds. The superordinate plans which could be identified

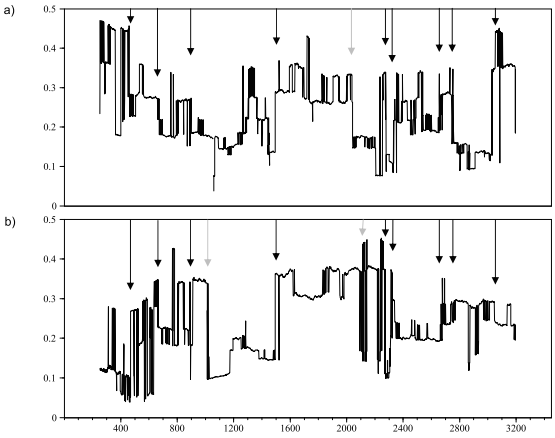

Fig. 4. Synchronized jumps in the dynamics of Local Largest Lyapunov Exponents (black arrows) during a therapy of 13 sessions (3,800 measurement points). Grey arrows indicate not clearly synchronized changes. (a) therapist, (b) patient. For the patient, the embedding was realized in a 6-dimensional phase space, constructed by 3 plans (time series) at the top of the plan hierarchy with each time series represented by two time delay coordinates, $x(t)$ and $x(t-\tau)$. For the therapist, the embedding was realized in a 8-dimensional phase space, constructed by 4 plans (time series) at the top of the plan hierarchy with each time series represented by two time delay coordinates, $x(t)$ and $x(t-\tau)$. LLLE estimates were calculated in a gliding window of 500 points by the algorithm of Rosenstein et al. [74].

for all five persons were (1) spontaneity and emotional engagement vs. shyness, restricted behaviour, and orientation to social norms, (2) engagement in the group interaction and in positive social climate, (3) task orientation. Length of time series was about 810 coding points. D2 as well as mean PD2 estimates saturated at a fractal dimensionality of about 5 for all categories. The embedding of the time series was realized by two ways: (1) The phase space was constituted by the three dimensions of superordinated plans with five trajectories representing the five group members, or (2) the phase space was constituted by the five persons with three trajectories representing the time course of the three plans (additional embedding dimensions result from time delay coordinates). In both cases PD2 results show an evolving pattern of quasi-attractors with changing complexity, and LLLEs (algorithm from [74]) portray chaoto-chaotic phase-transitions with clear-cut interpersonal jumps – similar to the dyadic interaction of the psychotherapy study.

3.3 Sudden Changes Reflect Order Transitions in Psychotherapy

Phase-transition-like phenomena characterize the short-term as well as the long-term evolution of cognitive, affective, and social systems. In psychotherapy, sudden changes seem to be a universal and robust phenomenon. A substantial per-

centage of patients experience discontinuously shaped changes. Sudden gains, especially if they occur early in the therapy process, uphold until the end of treatment or seem to be a necessary prerequisite for successful treatment [77, 80–82]. However, the mechanisms underlying such discontinuous shapes of symptom severity and other change markers are still not well understood challenging classical views of linear input-output-functions or dose-to-effect-relations. It is an anomaly of conventional psychotherapy science which postulates that specific factors of treatment cause the therapeutic effect in a linear way (or in a damped function related to the dose). Consequently, explanations tried to provide evidence for changes in relevant factors occurring before symptom changes, such as cognitive restructuring in the pre-gain-sessions of cognitive therapy [82]. Others have disputed this interpretation and have argued on behalf of common factors such as positive expectations, induction of hope, or positive therapeutic relationship [83, 84]. Kelly et al. [80] did not find any factors, such as changes in self-esteem, attribution style, concurrent psychological treatment or psychotropic medication to precede sudden treatment gains.

Actually, in psychotherapy research there are no adequate theoretical models explaining discontinuously shaped transitions in a fundamental way, still employing the idea of being uniquely reactive to external input like instructions, (minor) interventions, or therapeutic techniques. Synergetics, on the contrary, provides a model predicting that once system dynamics has reached an instability point, phase transitions are likely to occur. There are specific prerequisites for self-organized pattern transitions, such as (i) the existence of a system with nonlinearly interacting components or subsystems, (ii) the existence of one or several control parameters driving the system out of the actual stability state, and (iii) relatively stable boundary conditions. If the conditions for self-organized order transitions are met – that is to say, the instability point draws closer – a nonlinear shift-like change will be the consequence of the slightest additional external input. One of the predictions of the model is the occurrence of critical fluctuations just before a system undergoes such qualitative changes of pattern formation.

To investigate the above mentioned phase-transition-like phenomena in psychotherapy, we used the data from daily self-assessments of 18 patients with obsessive-compulsive disorder (OCD; ICD diagnosis: F42; average age: 32.2 years, SD = 9.6; 9 female, 9 male). The therapies were realized in a day-treatment center at Munich. Mean duration of treatment was 61 days (SD = 12.5, range from 37 to 88 days). Exposure with response prevention (ERP) was the principal cognitive-behavioural intervention of the therapy. ERP is a therapeutic procedure in the treatment of OCD, where patients are confronted with symptom provoking stimuli but abstain from performing compulsive rituals (e.g., cleaning).

Similar to the study we reported in chapter 2, the self-ratings were done by the Synergetic Navigation System (SNS, [42]). Every day, patients completed the Therapy-Process Questionnaire (TPQ) provided by the SNS. Two times per week, patients filled out the Yale-Brown Obsessive Compulsive Scale (Y-BOCS)

provided by the SNS. The Y-BOCS is a self-assessment scale for obsessions and compulsions [85]. In order to compare individual change dynamics to ERP we related the individual symptom severity trajectories to the onset of ERP.

Building on the earlier finding that phase transitions (here referred to as order transitions) in self-organizing systems are introduced by critical fluctuations and instabilities [3, 86], a measure of dynamic complexity was calculated on the time series resulting from daily self-ratings in order to identify non-stationarity and critical instabilities in short time series. In contrast to statistical variance, this complexity measure identifies jumps, volatility and pattern complexity of signals. It is used for the analysis of discrete time series data with a known data range (for the algorithm see [87]). Dynamic complexity combines a fluctuation measure and a distribution measure in a multiplicative way. The fluctuation measure is sensitive to the amplitude and frequency of changes in a time signal, and the distribution measure scans the scattering of values – or system states – realized within the theoretical range of possible values – or system states. In order to identify nonstationarity, the dynamic complexity is calculated within a window of 7 data points (= 7 days) moving over the time series of each patient.

The processes of each patient (see Figure 5 for an example) are evidence for increased dynamic complexity of the subscales and most of the items of the TPQ just before or during sudden changes, which are characterized by the steepest gradient (decrease) of the Y-BOCS curve. Significant decrease of symptom severity (Y-BOCS) takes place before (!) the most important therapeutic intervention – exposure with response prevention (ERP) – of the treatment process was started, a result in line with the theory of synergetics and findings across several disciplines.

Figure 6 aggregates the dynamics of all 18 patients. For each patient, the individual ERP-onset was defined at $t = 0$, and the trajectories of the total Y-BOCS scores were related to this event. In 72% of the 18 cases, the steepest gradient of symptom change was located before ERP-onset. Figure 6 illustrates that the mean trajectory of the z-transformed individual total scores of the Y-BOCS has its steepest change gradient before ERP starts (t = -4 days), and symptom severity reaches a significantly reduced level at the day of ERP onset at $t = 0$ ($T(17) = 3.07$; $p = 0.007$).

The same procedure was accomplished with the mean dynamic complexity signal of all items of the TPQ, calculated within a moving window of 7 data points. This complexity signal was related to ERP-onset as well. Figure 6 illustrates the mean z-transformed complexity signal of the change processes of the 18 subjects. Besides a complexity peak at the beginning of treatment, which may be interpreted as an initial instability period representing individual doubts and varying degrees of working intensity at the start of the treatment process, the most important peak occurred three days before the steepest gradient of symptom reduction was realized and about 7 days before ERP-onset ($T(17) = 2.48$, $p = 0.026$). In terms of synergetics, this corresponds to the assumed critical instabilities accompanying order transitions of a self-organizing system.

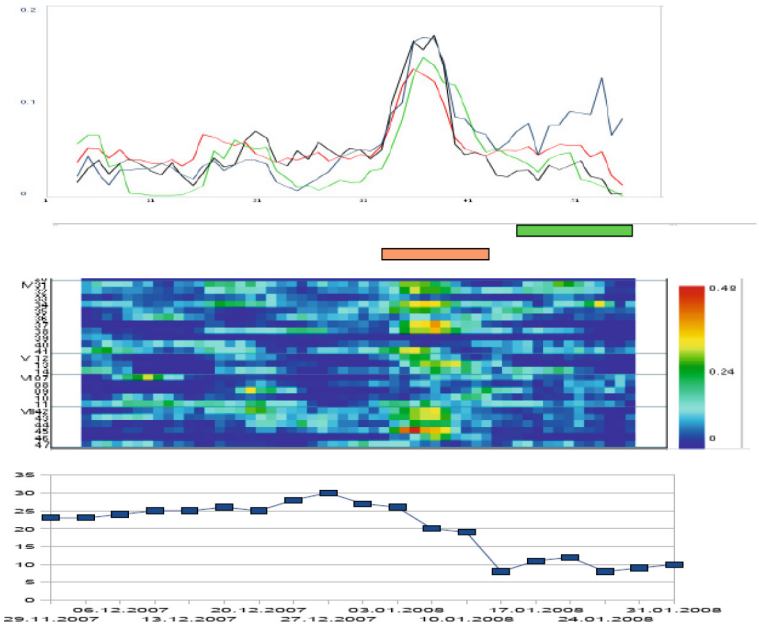

Fig. 5. Order transition in the therapy process of a patient with OCD (64 days = measurement points). Brown bar: critical instability (period of statistical significance of increased dynamic complexity). Green bar: Period of ERP. The curves at the top of the diagram represent the dynamic complexity of factors of the TPQ: Factor I: Therapy progress (blue), Factor II: Complaints and problem pressure (black), Factor IV: Dysphoric affects (red), and "getting new insights and perspectives", which is a factor from a former factor analysis. Below the complexity-resonance-diagram where the intensity of dynamic complexity is translated into colours. Yellow, orange, and red correspond to high complexity values. The lower part of the diagram represents the course of the Y-BOCS which was completed two times per week. The steepest gradient of symptom reduction was realized during the period of critical instability.

4 The Self-organizing Brain

The human brain is one of the most fascinating complex systems. Since function corresponds to structure and vice versa, structural changes can be understood as functional self-organization of neural populations. Changes of synaptic coupling strengths and network configurations (re-wiring patterns) follow the synchronized co-activity of neurons. Perception, action and transition of action patterns, decision making, and cognitive, behavioural, as well as emotional learning are generated by principles of self-organization [3, 6, 7, 86]. At a neuronal level they correspond to and are based on nonlinear brain dynamics. The emergence of order parameters and the occurrence of phase transitions can be described and measured on psychological as well as on neuronal levels.

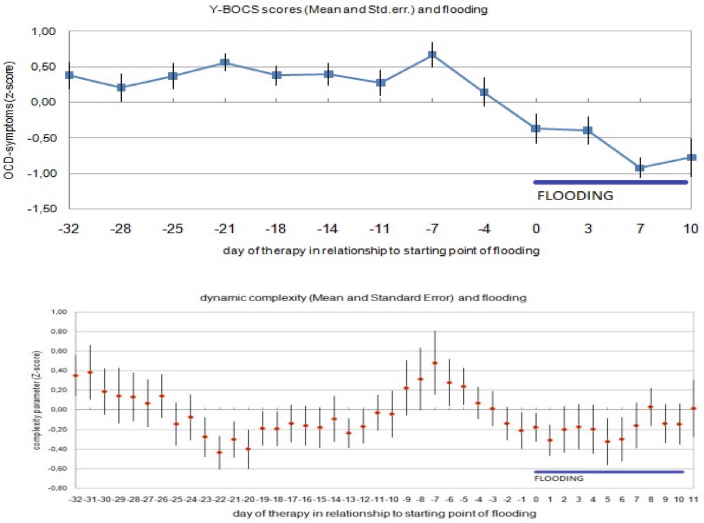

Fig. 6. Mean course of symptom severity (Y-BOCS, z-transformed) (upper part), and mean course of dynamic complexity (z-transformed), normalized in relation to the beginning of ERP during the behavior therapy of 18 OCD patients (day treatment center Munich). Vertical bars: standard error.

4.1 Brain Correlates of Gestalt Perception

One of the phenomena modelled by synergetics is Gestalt perception – the emergence of percepts and the switching of ambiguous visual patterns (e.g., Necker cube or stroboscopic alternative motion). These processes of Gestalt perception constitute the link between Gestalt psychology and actual mathematical modelling in synergetics [88]. The binding of different perceptual features or components to coherent structures or "qualia" seems to be due to synchronization processes of extended brain regions and converging integrative areas [89]. "Pattern perception is pattern formation" – as Hermann Haken puts it into pointed words.

Tallon-Baudry et al. [90, 91] measured enhanced gamma-band activity (30-50 Hz) in the EEG of the primary and secondary visual cortex while subjects identified a triangle from the offered stimulus material. This could be a fingerprint of corresponding neuronal synchronization processes. The activity occurred when subjects saw a real object (triangle) or a figural illusion of the object (Kanizsa-triangle), but not if the same geometrical components could not be composed to a true Gestalt. The research group of Basar-Eroglu and Stadler [92] measured increased gamma-band activity in EEG during states of perceptual switching triggered by stroboscopic alternative motions. To summarize: Perception of multistability is one of the multifold cognitive processes giving rise to 40 Hz enhancement in the cortex, and coherent oscillations reflect an important mechanism of

feature binding in the visual cortex which corresponds to the emergence of a neuronal order parameter. Changing order parameter dynamics during different cognitive activities was shown by Schupp et al. [93]. Mental imagery of an object could be differentiated from its concrete perception. The dimensional complexity of prefrontal EEG was increased during sensory imagery compared to the real perception of the same object [94].

4.2 Neuronal Activity During Motoric Instability and Motoric Order Transitions

The well-known movement coordination paradigm modelled by Haken, Kelso, and Bunz [12] was used to demonstrate neuronal correlates of instability and symmetry breaking processes in the motoric brain. The order parameter in this finger movement experiment is the relative phase of the index fingers of both hands. Metronome-pacing – with movement frequency as the control parameter – triggers the system from parallel (out-of-phase) to mirror (in-phase) movement. Meyer-Lindenberg et al. [95] showed that the emergence of patterns in open, non-equilibrium systems like the brain is governed by their (in-)stability in response to small disturbances. Transitions could be elicited by interference at the neuronal level. Functional neuroimaging (PET) identified premotor (PMA) and supplementary motor (SMA) cortices as having neuronal activity linked to the degree of behavioural instability, induced by increasing frequency of the finger movement. These regions then were transiently disturbed by transcranial magnetic stimulation (TMS) of different intensity, which caused sustained and macroscopic behavioural transitions from the less stable out-of-phase to the stable in-phase movement, whereas the stable pattern could not be affected. Moreover, the intensity of the disturbance needed (a measure of neuronal stability) was correlated to the degree of the control parameter (movement frequency) and thereby to the behavioural stability of the system.

4.3 Coordinated Order Transitions of Mental and Brain Dynamics

A fMRI-study[5] investigated order transitions of brain activity related to subjective experiences of patients during their psychotherapy process [41, 96]. Repeated fMRI scans were related to the degree of stability or instability of the ongoing dynamics (measured by the dynamic complexity of daily TPQ-ratings). The time series of dynamic complexity were averaged over the items of the TPQ,

[5] Multi-center study of the Ludwig-Maximilians-University Munich, University Hospital of Psychiatry (PD Dr. O. Pogarell, Dr. S. Karch, Dr. Ch. Mulert), Hospital of Psychosomatic Medicine Windach/Ammersee and Day Treatment Center Munich/Westend (Dr. I. Tominschek, Dipl. Psych. S. Heinzel, Prof. Dr. M. Zaudig), University Hospital Vienna/Astria, Clinic of Psychiatry (Prof. Dr. M. Aigner, Prof. Dr. G. Lenz, Dr. M. Dold, Dr. A. Unger), MR Centre of Excellence, Medical University Vienna/Austria (Prof. Dr. E. Moser, PD Dr. Ch. Windischberger). The study was coordinated by G. Schiepek.

and the maxima of these dynamics were used as an indicator of the most intensive fluctuation periods and the discontinuous transition(s) during the therapies. Real-time monitoring by the Synergetic Navigation System allows for the identification of stable or unstable periods and by this for a decision on the appropriate moments of fMRI acquisitions. Wherever possible, fMRI measurements were realized shortly before or after these transitions.

3 or 4 scans were realized during each of the psychotherapy processes of 9 patients and compared to the scans of 9 healthy controls without therapy. The study included patients with obsessive-compulsive disorder (OCD) of the washing/contamination fear subtype (DSM IV: 300.3), without co-morbid psychiatric or somatic diagnoses. All patients except for one were drug naïve. Patients were matched to healthy controls.

OCD seems to be an appropriate model system for synergetic studies in clinical psychology, since the pathological order parameter is quite evident, the disease has an obvious and often stable time course, and therapeutic order transitions – if they do occur at all – are easy to be observed. OCD-specific functional neuroanatomy is partially known. It includes an integrated network of cortico-striato-thalamo-cortical feedback-loops and limbic structures (amygdala, hippocampus, insular cortex, anterior cingulate cortex) [97, 98].

The visual stimulation paradigm of the study used symptom provoking, disgust provoking, and neutral pictures. The disgust and the neutral pictures were taken from the International Affective Picture System, whereas the OCD-related pictures were photographed in the home setting of the patients, showing specific and individual symptom provoking stimuli [41, 96]. Here we refer on the contrast of individualized symptom provoking pictures vs. neutral pictures.

Results from a Single Case. For illustrative purposes we report on the results of a single case. It is a female patient, whose fMRI scans were taken three times during the 59 days of their hospital stay at days 9, 30, and 57. The matched healthy control was also scanned three times at identical time intervals as the patient. The second acquisition was done after an intensive period of critical instability of the TPQ-based time series, but just before ERP started. The instability maximum of the patient's process was the precursor of an important personal decision to divorce from her husband. (Her OCD symptoms had developed in the context of a long-lasting marital conflict.) This decision was the essential order transition of the therapy.

Indeed, the most pronounced changes in brain activity occurred from the first to the second fMRI scan, whereas BOLD response differences from the second to the third session were only slight. The changes from the first to the second scan perhaps represent the neuronal correlates of her personal order transition (decision to divorce) related to the resolution of a severe personal conflict. Not only these changes occurred before the ERP procedure was introduced but also a marked symptom reduction took place (measured by the Y-BOCS) (Figure 7).

The alternations of brain activity during this period involved widespread areas, e.g. medial frontal brain regions including anterior cingulate cortex, superior

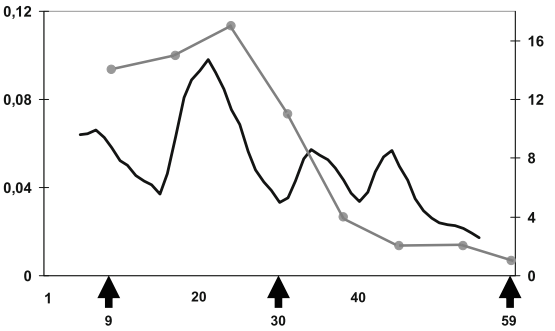

Fig. 7. The course of the Y-BOCS of a female patient (completed once per week; grey line). The steep gradient of symptom reduction in the middle of the hospital stay is preceeded by an intensive period of critical instability of therapy-related self-ratings. Black curve: Mean dynamic complexity of the items of the TPQ. Black arrays indicate the days when fMRI scans were realized. ERP started 2 days after the second fMRI scan.

and middle frontal gyrus, inferior frontal and precentral gyrus, superior temporal gyrus, superior parietal lobe, cuneus, thalamus, caudate nucleus in both hemispheres, as well as the right fusiform gyrus (Figure 8). The OCD-associated BOLD responses of the second and third session revealed only small differences (Figure 8). Slightly enhanced responses were found during the second session compared to the third session in the precuneus and the inferior parietal lobe. The middle frontal gyrus, the left inferior parietal lobe, the cuneus, the superior and middle frontal gyrus, and the cingulate gyrus responded slightly stronger during the third session compared to the second session. In the healthy control to the patient, no such changes of brain activity took place between the scans.

Thalamic and basal ganglia activation is part of the dorsolateral-caudate-striatum-thalamus circuitry of OCD. Especially the caudate nucleus takes a role within the executive dysfunction model of compulsions [99], and its activity has been found to be reduced after treatment (e.g., [100]).

The function of the anterior cingulate cortex is interesting with regard to synergetics. The cingulate cortex comprises various functions like somatosensoric integration, mediation of affective and cognitive processes, control of attention, and processing of painful stimuli. Additionally, it plays an important role as conflict monitoring system: it is sensitive to ambiguous or conflicting information [101, 102], is involved in decision making [103, 104], and its activation is predictive to treatment outcome in depression [105]. This is true especially for the dorsal (cognitive) structures of the ACC. By this, its activity could be an indicator of symmetry states of brain functioning, which are characterized by two or more dynamic patterns or attractors in competition. In the present case, the ACC activation at the beginning of the therapy could be either part of the pathology or could be indicative for the critical instability of the cognitive-affective system of the patient, preparing her important decision. The second

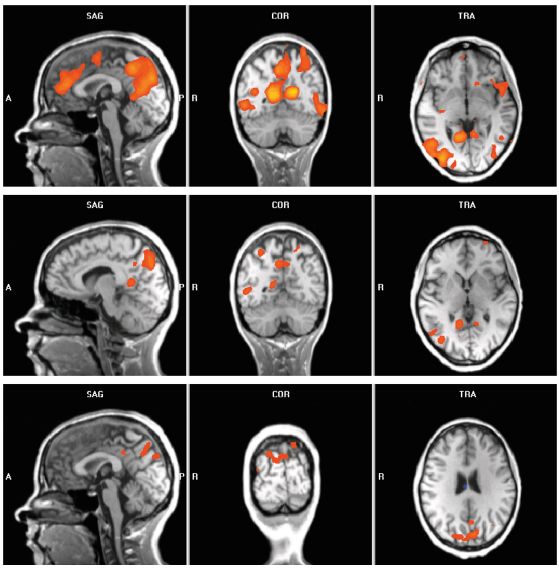

Fig. 8. Brain activation patterns of a patient with OCD (washing/contamination fear) during psychotherapy. BOLD signals from a 1.5 Tesla fMRT scanner. Top: first scan (9^{th} day of hospital stay; $x = 0$, $y = -55$, $z = -2$; p(uncorr) < 0.001). Middle: second scan (30^{th} day of hospital stay; $x = 8$, $y = -54$, $z = -5$; p(uncorr) < 0.001). Bottom: third scan (57^{th} day of hospital stay; $x = 0$, $y = -85$, $z = 26$; p(uncorr) < 0.001). Activations during the presentation of individual symptom provoking pictures contrasted to activations during the presentation of standard neutral pictures. The brain activations before the order transition (first scan) (medial frontal brain regions including anterior cingulate cortex, superior and middle frontal gyrus, inferior frontal and precentral gyrus, superior temporal gyrus, superior parietal lobe, cuneus, thalamus, caudate nucleus, right fusiform gyrus) are markedly reduced at the second and third scan.

fMRI measure was conducted during a local minimum of critical fluctuations. Whether the impressive change in cingulate activation could be attributed to a changed critical symmetry state of the neuronal self-organization before vs. after the phase transition or to changes in symptom severity cannot be decided within a single case study, but seems to be an interesting question for further research.

Results from the Sample of OCD-Patients. Similar results were to be seen in the whole sample of all 9 patients [96]. In order to quantify the changes of neuronal activity over the fMRI scans, 8 brain regions were identified that are important in OCD-related neuronal processing: the anterior and medial cingulate cortex as well as the supplementary motor area (CC/SMA), the dorsolateral prefrontal cortex (DLPFC) right and left, the insula right and left, the parietal cortex right and left, and the cuneus.

When interscan-intervals including order transitions (OT) were compared to intervals without order transitions (NOT), the changes of the number of signifi-

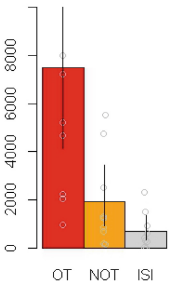

Fig. 9. Differences in order transition intervals for patients (OT: order transitions, red), non-order-transitions for patients (NOT: non-order-transitions, yellow) and inter-scan-intervals (ISI) for healthy controls (grey). Y-axis: mean voxel number differences between scans. 95%-confidence intervals of the means were bootstrapped with R's boot.ci function using 10,000 resamples and the "bca" type of confidence intervals.

cant voxels for the contrast between individualized symptom provoking pictures and neutral pictures show increased BOLD responses during OT in all relevant brain regions. The healthy controls received no therapy so that any distinction between intervals with and without order transitions has no importance. By this, in healthy subjects functional changes were averaged across all inter-scan-intervals (ISI). Figure 9 illustrates the changes in significant voxels averaged for the 8 brain areas of OT and NOT (patients), and ISI (controls). Activation rates and change rates were significantly higher for patients compared to controls.

The differences between order transition intervals (OT) of the patients (mean voxel number difference: 7480, SD: 6835) and non-order-transition intervals (NOT) of patients (mean voxel number difference: 1900, SD: 1968) reached significance. In addition, the number of activated voxels differenced significantly between order transition intervals of patients and the inter-scan-intervals (ISI) of the controls, whereas the differences between the NOT intervals of patients and the inter-scan-intervals (ISI) of the controls were quite similar. For each of the 8 brain regions we identified, pronounced differences occurred between OT and NOT and even more clearly for OT vs. ISI, but not for NOT vs. ISI. The most pronounced differences were realized in the CC/SMA, the DLPFC left, DLPFC right and insula right. The differences in the area of the cuneus and the left parietal cortex did not reach significance because of the NOTs' wide confidence intervals. The high individual variability is partly the result of distinctly differing change patterns in patients as well as therapy processes.

An additional result concerns the intercorrelations of the involved brain areas. When comparing correlations before and after order transitions, the difference is striking, independent of where the order transitions were located in the course

of therapy. The mean intercorrelation of the brain areas changed from 0.73 (SD: 0.09) to 0.33 (SD: 0.33) (p of the difference < 0.001). In addition to the decline in correlation, a differentiation of intercorrelations occurred which is reflected in an increase in variation (standard deviation of the intercorrelations increased from 0.09 to 0.33). This could be taken as an indicator of a decreased network-synchronization of OCD-specific brain areas before and after order transitions.

To conclude: Most patients showed clearly recognizable order transitions in different brain areas. Changes in the activity of brain areas outside of order transitions were considerably weaker, similar to the differences between fMRI scans of the healthy controls which did not undergo psychotherapy and by this did not experience any dynamic changes. The strong connection between cognitive-affective order transitions and BOLD responses reversely validate the operationalization of order transitions by the maximum of dynamic complexity of the time series gained from daily self-assessments by the Synergetic Navigation System.

5 Perspectives

Order or phase transitions indicate the spontaneous emergence of collective patterns or qualitative pattern shifts in complex non-equilibrium systems. Based on an empirically sound transfer of this and other concepts from synergetics to human systems functioning, psychotherapy can now be interpreted as the procedural creation of conditions conducive to biological, mental, and social self-organization processes [3]. This opens new perspectives for basic and applied research, but also for the treatment of mental disorders. New developments in the real-time monitoring of human change processes by internet-based devices with integrated nonlinear analysis methods like the Synergetic Navigation System offer effective means of therapy feedback and therapy control [57, 106].

Other encouraging developments concern invasive and non-invasive brain stimulation which applies to neurological diseases as Parkinsonian or essential tremor, chronic tonal Tinnitus, but hopefully also to psychiatric disorders as OCD or mayor depression [107]. The difference between new technologies of stochastic phase resetting applying mathematical tools and concepts of synergetics at the one hand and high frequency stimulation at the other is that high stimulation frequencies mimic tissue lesions by a blocking effect on the stimulated target. However, learning and un-learning needs the activity of neuronal cell populations. New technologies are demand-controlled and are activated only during certain stimulation intervals. Its effect is a desynchronization of pathologically synchronized populations of neurons, using multi-site coordinated reset (CR) stimulation [107] or nonlinear delayed feedback stimulation [108]. Both methods counteract abnormal interactions and detune the macroscopic frequency of the collective oscillators – that is the abnormally established order parameters of neuronal synchronization. Thereby they restore the naturally varying frequencies of the individual oscillatory units. Neurons get in the range of physiological functioning and can engage in changing and varying synchronization patterns. In consequence, the coupling strengths connecting synapses (synaptic weights)

are changed and a long term rewiring of neuronal networks is reached. Changed function triggers the emergence of healthy attractors and by this changes the structure of neuronal networks. For therapeutic effects on chronic Tinnitus see [109].

In the future technologies of non-invasive brain stimulation could be combined with a SNS-based psychotherapy for the optimization of self-organizing changes in therapeutic processes.

References

1. Haken, H.: Synergetics. An Introduction. Nonequilibrium Phase Transitions in Physics, Chemistry, and Biology. Springer, Heidelberg (1977). 2nd edn., 1983, 3rd edn., 1990
2. Stegmüller, W.: Theorie und Erfahrung. Zweiter Halbband: Theorienstrukturen und Theoriendynamik. Springer, Heidelberg (1973)
3. Haken, H., Schiepek, G.: Synergetik in der Psychologie (Synergetics in Psychology). Hogrefe, Göttingen (2006). 2nd edn., 2010
4. Haken, H.: Synopsis and introduction. In: Basar, E., Flor, H., Haken, H., Mandell, A.J. (eds.) Synergetics of the Brain. Springer Series in Synergetics, vol. 23, pp. 3–25. Springer, Heidelberg (1983)
5. Basar, E., Flor, H., Haken, H., Mandell, A.J. (eds.): Synergetics of the Brain. Springer Series in Synergetics, vol. 23. Springer, Heidelberg (1983)
6. Haken, H.: Principles of Brain Functioning. A Synergetic Approach to Brain Activity, Behavior, and Cognition. Springer, Heidelberg (1996)
7. Haken, H.: Brain Dynamics. Springer, Heidelberg (2002)
8. Weidlich, W., Haag, G.: Concepts and Models of a Quantitative Sociology. Springer, Heidelberg (1983)
9. Haken, H., Stadler, M. (eds.): Synergetics of Cognition. Springer, Heidelberg (1990)
10. Tschacher, W., Schiepek, G., Brunner, E.J. (eds.): Self-Organization and Clinical Psychology. Springer, Heidelberg (1992)
11. Kelso, J.A.S.: Coordination dynamics in human brain and behaviour. In: Friedrich, R., Wunderlin, A. (eds.) Evolution of Dynamical Structures in Complex Systems, pp. 223–234. Springer, Heidelberg (1992)
12. Haken, H., Kelso, J.A.S., Bunz, H.: A theoretical model of phase transition in human hand movements. Biol. Cybern. **51**, 347–356 (1985)
13. Kelso, J.A.S.: Dynamic Patterns. The Self-Organization of Brain and Behavior. MIT Press, Cambridge (1995)
14. Kelso, J.A.S., Scholz, J.P., Schöner, G.: Non-equilibrium phase transitions in coordinated biological motion: critical fluctuations. Physics Lett. A **118**, 279–284 (1986)
15. Haken, H.: Pattern formation and pattern recognition - an attempt at a synthesis. In: Haken, H. (ed.) Pattern Formation by Dynamic Systems and Pattern Recognition, pp. 2–13. Springer, Heidelberg (1979)
16. Haken, H.: Synergetic Computers and Cognition. Springer, Heidelberg (1991). 2nd edn., 2004
17. Haken, H.: An application of synergetics. Decision making as pattern recognition. Z. Wissenschaftsforschung 9/10, pp. 45–72 (1996)

18. Bestehorn, M., Haken, H.: Associative memory of a dynamical system: the example of the convection instability. Z. Physik B **82**, 305–308 (1991)
19. Vetter, G., Stadler, M., Haynes, J.D.: Phase transitions in learning. J. Mind Behav. **18**, 335–350 (1997)
20. Tschacher, W., Dauwalder, J.-P. (eds.): The Dynamical Systems Approach to Cognition. World Scientific, Singapore (2003)
21. Tschacher, W., Haken, H.: Intentionality in non-equilibrium systems? The functional aspects of self-organized pattern formation. New Ideas Psychol. **25**, 1–5 (2007)
22. Haken, H., Tschacher, W.: A theoretical model of intentionality with an application to neural dynamics. Mind and Matter **8**, 7–18 (2010)
23. Lewis, M.D., Granic, I. (eds.): Emotion, Development, and Self-Organisation. Dynamic Systems Approaches to Emotional Development. Cambridge University Press, Cambridge (2002)
24. Broekstra, G.: A synergetics approach to disruptive innovation. Kybernetes **31**, 1249–1259 (2002)
25. Tolkien, B., Wagner, T., Böbel, F.G.: Using a synergetic computer in speech recognition and identification of persons. In: Proceedings of the 1st International Conference on Applied Synergetics and Synergetic Engineering. Fraunhofer ISS, Erlangen (1994)
26. Marks-Tarlow, T.: The self as a dynamical system. Nonlin. Dyn. Psychol. Life Sci. **3**, 311–345 (1999)
27. Thelen, E., Smith, L. (eds.): A Dynamic Systems Approach to the Development of Cognition and Action. MIT Press/Bradford Books, Cambridge (1996)
28. Kowalik, Z.J., Schiepek, G., Kumpf, K., Roberts, L.E., Elbert, T.: Psychotherapy as a chaotic process II. The application of nonlinear analysis methods on quasi time series of the client-therapist-interaction: a nonstationary approach. Psychother. Res. **7**, 197–218 (1997)
29. Ramseyer, F., Tschacher, W.: Synchronisation in dyadic psychotherapy sessions. In: Vrobel, S., Rössler, O.E., Marks-Tarlow, T. (eds.) Simulataneity: Temporal Structures and Observer Perspectives, pp. 329–347. World Scientific, Singapore (2008)
30. Weidlich, W.: Sociodynamics. A Systematic Approach to Mathematical Modelling in the Social Sciences. Harwood, Amsterdam (2000)
31. Vallacher, R.R., Nowak, A. (eds.): Dynamical Systems in Social Psychology. Academic Press, San Diego (1994)
32. Nowak, A., Vallacher, R.R.: Dynamical Social Psychology. Guilford Press, New York (1998)
33. Langthaler, W., Schiepek, G. (Hrsg.): Selbstorganisation und Dynamik in Gruppen. LIT-Verlag, Münster (1998)
34. Nachtigall, C.: Selbstorganisation und Gewalt. Waxmann, Münster (1998)
35. Schiepek, G., Schoppek, W., Tretter, F.: Synergetics in psychiatry: simulation of evolutionary patterns of schizophrenia on the basis of nonlinear difference equations. In: Tschacher, W., Schiepek, G., Brunner, E.J. (eds.) Self-Organization and Clinical Psychology, pp. 163–194. Springer, Heidelberg (1992)
36. Kruse, P., Carmesin, H.O., Stadler, M.: Schizophrenie als korrespondenzproblem plastischer neuronaler netze. In: Schiepek, G., Tschacher, W. (Hrsg.) Selbstorganisation in Psychologie und Psychiatrie, pp. 171–190. Vieweg, Braunschweig (1997)

37. Mackey, M.C., an der Heiden, U.: Dynamical diseases and bifurcations: understanding functional disorders in physiological systems. Funkt. Biol. Med. **1**, 156–164 (1982)
38. Belair, J., Glass, L., an der Heiden, U., Milton, J.: Dynamical disease: identification, temporal aspects, and treatment strategies of human illness. Chaos **5**, 1–7 (1995)
39. an der Heiden, U.: Dynamische krankheiten: neue perspektiven der medizin. In: Mainzer, K. (Hrsg.) Komplexe Systeme und Nichtlineare Dynamik in Natur und Gesellschaft, pp. 247–264. Springer, Heidelberg (1999)
40. Schiepek, G., Perlitz, V.: Self-organization in clinical psychology. In: Meyers, R.A. (ed.) Encyclopedia of Complexity and Systems Science, pp. 7991–8009. Springer, Heidelberg (2009). doi:10.1007/978-0-387-30440-3_472
41. Schiepek, G., Tominschek, I., Karch, S., Lutz, J., Mulert, C., Meindl, T., Pogarell, O.: A controlled single case study with repeated fMRI measures during the treatment of a patient with obsessive-compulsive disorder: testing the nonlinear dynamics approach to psychotherapy. World J. Biol. Psychiatry **10**, 658–668 (2009)
42. Schiepek, G., Aichhorn, W.: Real-Time Monitoring in der Psychotherapie (Real-time monitoring in psychotherapy). Psychother. Psych. Med. **63**, 39–47 (2013)
43. Tschacher, W., Scheier, C., Grawe, K.: Order and pattern formation in psychotherapy. Nonlin. Dyn. Psychol. Life Sci. **2**, 195–215 (1998)
44. Beisel, R.: Synergetik und Organisationsentwicklung. Hampp, München (1994)
45. Mainzer, K.: Thinking in Complexity. The Complex Dynamics of Matter, Mind, and Mankind, 3rd edn. Springer, Heidelberg (1997)
46. Lewin, K.: Field Theory in Social Psychology. Harper, New York (1951)
47. Köhler, W.: Die physischen Gestalten in Ruhe und im stationären Zustand. Vieweg, Braunschweig (1920)
48. Metzger, W.: Psychologie. Steinkopff, Darmstadt (1940). 3. Aufl., 1963
49. Stadler, M., Kruse, P.: The self-organization perspective in cognition research. historical remarks and new experimental approaches. In: Haken, H., Stadler, M. (eds.) Synergetics of Cognition, pp. 32–52. Springer, Heidelberg (1990)
50. Piaget, J.: Die Äquilibration der kognitiven Strukturen. Klett-Cotta, Stuttgart (1976)
51. von Uexküll, T., Wesiack, W.: Wissenschaftstheorie: ein bio-psycho-soziales modell. In: Adler, R.H., Herrmann, J.M., Köhle, K., Schonecke, O.W., von Uexküll, T., Wesiack, W. (Hrsg.) Thure von Uexküll. Psychosomatische Medizin, pp. 13–52. Urban & Schwarzenberg, München (1996)
52. Ott, E.: Chaos in Dynamical Systems. Cambridge University Press, Cambridge (1993)
53. Schuster, H.G.: Deterministic Chaos. An Introduction. VCH, Weinheim (1989)
54. Strunk, G., Schiepek, G.: Systemische Psychologie. Einführung in die komplexen Grundlagen menschlichen Verhaltens. Spektrum Akademischer Verlag, Heidelberg (2006)
55. Bussmann, J., Ebner-Priemer, U., Fahrenberg, J.: Ambulatory activity monitoring. Europ. Psychologist **14**, 142–152 (2009)
56. Ebner-Priemer, U., Trull, T.: Ecological momentary assessment of mood disorders and mood dysregulation. Psychol. Assessment **21**, 463–475 (2009)
57. Lambert, M.J.: Yes, it is time for clinicians to routinely monitor treatment outcome. In: Duncan, B., Miller, S., Wampold, B., Hubble, M. (eds.) The Heart and Soul of Change, 2nd edn., pp. 237–266. American Psychological Association, Washington (2010)

58. Schiepek, G.: Complexity and nonlinear dynamics in psychotherapy. Europ. Rev. **17**, 331–356 (2009)
59. Schiepek, G., Aichhorn, W., Strunk, G.: Der Therapie-Prozessbogen (TPB). Faktorenstruktur und psychometrische Daten. Z. Psychosom. Med. Psychother. **58**, 257–265 (2012)
60. Fraser, A.M., Swinney, H.: Independent coordinates from strange attractors from Mutual Information. Phys. Rev. A **33**, 1134–1140 (1986)
61. Grassberger, P., Procaccia, I.: On the characterization of strange attractors. Phys. Rev. Lett. **50**, 346–356 (1983)
62. Grassberger, P., Procaccia, I.: Measuring the strangeness of strange attractors. Physica D **9**, 189–208 (1983)
63. Skinner, J.E.: The Point-D2 Algorithm. Baylor College of Medicine, Houston (1992)
64. Skinner, J.E., Molnar, M., Tomberg, C.: The point correlation dimension: performance with nonstationary surrogate data and noise. Int. Physiol. Behav. Sci. **29**, 217–234 (1994)
65. Rapp, P.E., Albano, M.E., Zimmerman, I.D., et al.: Phase-randomized surrogates can produce spurious identifications of non-random structure. Phys. Lett. A **192**, 27–33 (1994)
66. Theiler, J., Eubank, S., Longtin, A., Galdrikian, B., Farmer, J.D.: Testing for nonlinearity in time series: the method of surrogate data. Physica D **58**, 77–94 (1992)
67. Prichard, D., Theiler, J.: Generating surrogate data for time series with several simultaneously measured variables. Phys. Rev. Lett. **73**, 951–954 (1994)
68. Schreiber, T.: Interdisciplinary application of nonlinear time series methods. Phys. Report **308**, 1–64 (1999)
69. Schreiber, T., Schmitz, A.: Improved surrogate data for nonlinearity tests. Phys. Rev. Lett. **77**, 635–638 (1996)
70. Schreiber, T., Schmitz, A.: Surrogate time series. Physica D **142**, 346–382 (2000)
71. Small, M., Judd, K.: Detecting nonlinearity in experimental data. Int. J. Bifurc. Chaos **8**, 1231–1244 (1998)
72. Schiepek, G., Kowalik, Z.J., Schütz, A., Köhler, M., Richter, K., Strunk, G., Mühlnickel, W., Elbert, T.: Psychotherapy as a chaotic process I. Coding the client-therapist-interaction by means of sequential plan analysis and the search for chaos: a stationary approach. Psychother. Res. **7**, 173–194 (1997)
73. Caspar, F.: Beziehungen und Probleme verstehen. Eine Einführung in die psychotherapeutische Plananalyse. Huber, Bern (1996)
74. Rosenstein, M.T., Collins, J.J., de Luca, C.J.: A practical method for calculating Largest Lyapunov Exponents from small data sets. Physica D **65**, 117–134 (1993)
75. Vandenhouten, R.: Analyse instationärer Zeitreihen komplexer Systeme und Anwendungen in der Physiologie. Shaker Verlag, Aachen (1998)
76. Lambertz, M., Vandenhouten, R., Langhorst, P.: Transiente kopplungen von hirnstammneuronen mit atmung, herzkreislaufsystem und EEG: ihre bedeutung für ordnungsübergänge in der psychotherapie. In: Schiepek, G. (Hrsg.) Neurobiologie der Psychotherapie, pp. 302–324. Schattauer, Stuttgart (2003)
77. Gumz, A., Bauer, K., Brähler, E.: Corresponding instability of patient and therapist process ratings in psychodynamic psychotherapies. Psychother. Res. **22**, 26–39 (2012)
78. Walter, S., Schiepek, G., Schneider, S., Strunk, G., Kaimer, P., Mergenthaler, E.: The synchronization of plan activations and emotion-abstraction-patterns in the

psychotherapeutic process - a single case study. Psychother. Res. **20**, 214–223 (2010)
79. Rockstroh, B., Watzl, H., Kowalik, Z.J., Cohen, R., Sterr, A., Müller, M., Elbert, T.: Dynamical aspects of the EEG in different psychopathological states in an interview situation. A pilot study. Schizophrenia Res. **28**, 77–85 (1997)
80. Kelly, M., Roberts, J., Ciesla, J.: Sudden gains in cognitive behavioral treatment for depression: when do they occur and do they matter? Behav. Res. Ther. **43**, 703–714 (2005)
81. Stiles, W., Leach, C., Barkham, M., Lucock, M., Iveson, S., Shapiro, D., Iveson, M., Hardy, G.: Early sudden gains in psychotherapy under routine clinic conditions: practice-based evidence. J. Consult. Clin. Psychol. **71**, 14–21 (2003)
82. Tang, T., DeRubeis, R.: Sudden gains and critical sessions in Cognitive-Behavioral Therapy for depression. J. Consult. Clin. Psychol. **67**, 894–904 (1999)
83. Ilardi, S.S., Craighead, W.E.: The role of non-specific factors in cognitive-behavior therapy for depression. Clin. Psychol. Res. Prac. **1**, 138–156 (1994)
84. Ilardy, S.S., Craighead, W.E.: Rapid early response, cognitive modification, and nonspecific factors in cognitive-behavior therapy for depression: a reply to Tang and DeRubeis. Clin. Psychol. Sci. Pract. **6**, 295–299 (1999)
85. Goodman, W.K., Price, L.H., Rasmussen, S.A., Mazure, C., Fleischmann, R.L., Hill, C.L., Heninger, G.R., Charney, D.S.: The Yale-Brown obsessive compulsive scale. I. Development, use, and reliability. Arch. Gen. Psychiatry **46**, 1006–1011 (1989)
86. Haken, H.: Synergetics. Introduction and Advanced Topics. Springer, Heidelberg (2004)
87. Schiepek, G., Strunk, G.: The identification of critical fluctuations and phase transitions in short term and coarse-grained time series - a method for the real-time monitoring of human change processes. Biol. Cybern. **102**, 197–207 (2010)
88. Haken, H.: Synergetics as a tool for the conceptualization and mathematization of cognition and behavior - how far can we go? In: Haken, H., Stadler, M. (eds.) Synergetics of Cognition, pp. 2–31. Springer, Heidelberg (1990)
89. Singer, W., Gray, C.M.: Visual feature integration and the temporal correlation hypothesis. Ann. Rev. Neurosci. **18**, 555–586 (1995)
90. Tallon-Baudry, C., Bertrand, O., Wienbruch, C., Ross, B., Pantev, C.: Combined EEG and MEG recordings of visual 40 Hz resonates to illusory triangles in human. Neuroreport **8**, 1103–1107 (1997)
91. Tallon-Baudry, C., Bertrand, O.: Oscillatory gamma activity in humans and its role in object representation. Trends Cog. Sci. **3**, 151–162 (1999)
92. Basar-Eroglu, C., Strüber, D., Kruse, P., Basar, E., Stadler, M.: Frontal gamma-band enhancement during multistable visual perception. Int. J. Psychophysiology **24**, 113–125 (1996)
93. Schupp, H.A.T., Lutzenberger, W., Birbaumer, N., Miltner, W., Braun, C.: Neurophysiological differences between perception and imagery. Cog. Brain Res. **2**, 77–86 (1994)
94. Lutzenberger, W., Elbert, T., Birbaumer, N., Ray, W.J., Schupp, H.: The scalp distribution of the fractal dimension of the EEG and its variation with mental tasks. Brain Topography **5**, 27–34 (1992)
95. Meyer-Lindenberg, A., Ziemann, U., Hajak, G., Cohen, L., Faith Berman, K.: Transitions between dynamical states of differing stability in the human brain. Proc. Nat. Acad. Sci. USA **99**, 10948–10953 (2002)

96. Schiepek, G., Tominschek, I., Heinzel, S., Aigner, M., Dold, M., Unger, A., Lenz, G., Windischberger, C., Moser, E., Plöderl, M., Lutz, J., Meindl, T., Zaudig, M., Pogarell, O., Karch, S.: Discontinuous patterns of brain activation in the psychotherapy process of obsessive compulsive disorder: converging results from repeated fMRI and daily self-reports (2013, submitted)
97. Kwon, J.S., Jang, J.H., Choi, J.S., Kang, D.H.: Neuroimaging in obsessive compulsive disorder. Expert Rev. Neurother. **9**, 255–269 (2009)
98. Menzies, L., Chamberlain, S.R., Laird, A.R., Thelen, S.M., Sahakian, B.J., Bullmore, E.T.: Integrating evidence from neuroimaging and neuropsychological studies of obsessive-compulsive disorder: the orbitofronto-striatal model revisited. Neurosci. Biobehav. Rev. **32**, 525–549 (2008)
99. Friedlander, L., Desrocher, M.: Neuroimaging studies of obsessive-compulsive disorder in adults and children. Clin. Psychol. Rev. **26**, 32–49 (2006)
100. Nakao, T., Nakagawa, A., Yoshiura, T., Nakatani, E., Nabeyama, M., Yoshizato, C., Kudoh, A., Tada, K., Yoshioka, K., Kawamoto, M., Togao, O., Kanba, S.: Brain activation of patients with obsessive-compulsive disorder during neuropsychological and symptom provocation tasks before and after symptom improvement: a functional magnetic resonance imaging study. Biol. Psychiatry **57**, 901–910 (2006)
101. van Veen, V., Carter, C.C.: The anterior cingulate as a conflict monitor: fMRI and ERP studies. Physiol. Behav. **77**, 477–482 (2002)
102. van Veen, V., Carter, C.C.: The timing of action-monitoring processes in the anterior cingulate cortex. J. Cog. Neurosci. **14**, 593–602 (2002)
103. Sanfey, A.G., Rilling, J.K., Aronson, J.A., Nystrom, L.E., Cohen, J.D.: The neural basis of economic decision-making in the Ultimatum Game. Science **300**, 1755–1758 (2003)
104. King-Casas, B., Tomlin, D., Anen, C., Camerer, C.F., Quartz, S.R., Montague, P.R.: Getting to know you: reputation and trust in a two-person economic exchange. Science **308**, 78–83 (2005)
105. Mayberg, H.S., Brannan, S.K., Mahurin, R.K., Jerabek, P.A., Brickman, J.S., Tekell, J.L., Silva, J.A., McGinnis, S., Glass, T.G., Martin, C.C., Fox, P.T.: Cingulate function in depression: a potential predictor of treatment response. Neuroreport **8**, 1057–1061 (1997)
106. Schiepek, G., Eckert, H., Kravanja, B.: Grundlagen systemischer Therapie und Beratung. Systemische Praxis, Band 1. Hogrefe, Göttingen (2013, in press)
107. Tass, P.A., Hauptmann, C.: Therapeutic modulation of synaptic connectivity with desynchronizing brain stimulation. Int. J. Psychophysiology **64**, 53–61 (2007)
108. Popovych, O.V., Hauptmann, C., Tass, P.A.: Control of neural synchrony by nonlinear delayed feedback. Biol. Cybern. **95**, 69–85 (2006)
109. Tass, P.A., Adamchic, I., Freund, H.J., von Stackelberg, T., Hauptmann, C.: Counteracting tinnitus by acoustic coordinated reset neuromodulation. Restor. Neurol. Neurosci. **30**, 137–159 (2012)

Auditory Streaming as a Paradigm of Synergetic Pattern Formation in Brain and Behavior

Viktor Jirsa[1⋆], Felix V. Almonte[2], Ajay S. Pillai[3], and Betty Tuller[4]

[1] Institut de Neuroscience des Systemes UMR1106 Inserm,
Aix-Marseille Universite, 13005 Marseille, France
http://ins.univ-amu.fr/research-teams/theoretical-neurosciences-group
[2] Center for Complex Systems & Brain Sciences,
Florida Atlantic University, Boca Raton, FL 33431, USA
[3] Human Motor Control Section, National Institutes of Health,
10 Center Drive, Rm 7D42, Bethesda, Maryland 20892, USA
[4] National Science Foundation, 4201 Wilson Blvd., Arlington VA 22230, USA

Abstract. Synergetics has established a well-known top-down approach to the modeling of perceptual phenomena in psychology and cognitive sciences. This phenomenological approach is deply rooted in the theory of pattern formation and offers a formal justification that in the proximity of transitions from one pattern to another a low-dimensional description via canonical models is permissible. We exploit this thinking in the context of auditory scene analysis, specifically auditory streaming, where the brain network integrates or segregates sounds that arise from two or more distinct sources. We interpret the process of integration and segregation as a pattern formation process and demonstrate through mathematical modeling, behavioral experiments and functional magnetic resonance imaging (fMRI) that selected networks in the brain get differentially activated as a function of the percept. We propose a functional architeture composed of brain areas with tonotopic organization (auditory cortex) and non-tonotopic organization (various parietal areas including right superior parietal lobule and precuneus). The dynamics of this functional architecture extends beyond auditory streaming and suggests the existence of informational convergence zones in the brain that get selectively activated in a nonlinear all-or-none fashion. This dynamics is reminiscent of phase transitions as discussed in synergetics and generalizes concepts well established in multisensory integration.

Keywords: auditory streaming, synergetics, perception, emergence, fMRI, BOLD signal

1 Introduction

Synergetics is an interdisciplinary field of research founded by Hermann Haken [1] and explains how macroscopic self-organized pattern formation occurs in open

⋆ Corresponding author: viktor.jirsa@univ-amu.fr

A. Pelster and G. Wunner (eds.), *Selforganization in Complex Systems: The Past, Present, and Future of Synergetics*, Understanding Complex Systems,
DOI: 10.1007/978-3-319-27635-9_13

systems operating away from equilibrium. Examples of such pattern formation range from the formation of Rayleigh-Bénard convection rolls in liquids to various chemical instabilities and morphogenesis in biological systems [2]. Though synergetics has its roots in physical systems, its concepts and mathematical apparatus generalize to other disciplines describing the collective self-organizing dynamics of multi-component systems.

One of the more recent applications of synergetics is found in the psychological sciences. In particular, perceptual phenomena related to state transitions are amenable to synergetic analysis. In this context, we will discuss the phenomenon of auditory scene analysis, particularly auditory streaming. Auditory stream segregation, or streaming, has been used as a model for how the auditory system integrates or segregates sounds that arise from two or more distinct sources. For example, when listening to bass and soprano vocalists singing simultaneously, the two voices are perceived as separate from each other but each voice is simultaneously perceived as an integrated perceptual event. In the laboratory, a similar effect can be created using sequences of tones. In a typical streaming experiment, two sequences are created using alternating high and low tones. Sequences vary in the frequency difference between the tones and presentation rate. In general, when the frequency separation is relatively small and/or the rate is relatively slow, listeners perceive a single integrated melody (or stream) and can accurately report the ordering of the tones. But when the frequency separation is relatively large and/or the rate relatively fast, listeners report hearing two auditory streams, one with higher pitch than the other. They can easily attend selectively to one or the other stream but they are unable to hear the tones as a single integrated stream and cannot report the relative order of individual events between the two streams. In this sense, streaming may be regarded as a pattern formation process, where the perceptual patterns emerge dependent on the details of the input sequences. The parameters characterizing the input sequence serve as unspecific control parameters, equivalent to the control parameters in a physical system. This is in stark contrast to response-driven approaches where the specific characteristics of the input signal determine the time course of the driven system. Prevailing models from auditory streaming studies focussed on the examination of auditory cortex responses and posit that streaming will be evoked whenever the tones of the input excite non-overlapping populations of neurons. Parametric variations of stimulations or stimulus features could produce neural activity patterns, which vary linearly with the sigmoidal firing rate of neural populations. While such patterns have been widely reported in vision, only limited evidence for such a mechanism exists in the auditory system. More importantly, such mechanisms rely heavily on the tonotopic organization of the auditory cortex. Yet evidence from neural recordings in humans suggests that activations during auditory streaming paradigms are significantly more widespread, involving brain areas outside of the auditory cortex that have no tonotopic organization [3, 4]. This suggests that the large network activated during the formation of streaming-related percepts results in the emergence of

brain pattern dynamics.

In this chapter we will remind the reader of our model of auditory streaming [5], which predicted that widespread brain networks with mixed organization (tonotopic and non-tonotopic) would be involved in auditory streaming. Next we provide behavioral evidence for a particular prediction of this architecture, namely, the phenomenon of amplitude streaming, in which tone sequences that differ only in the amplitude of consecutive tones can form integrated or segregated streams. This distinguishing feature poses a particular challenge to functional architectures comprised of only tonotopically organized networks. Through functional Magnetic Resonance Imaging (fMRI), we tested the neuroarchitectural predictions of our auditory streaming model and report the findings in the final section of this chapter.

1.1 Auditory stream segregation

Auditory stream segregation has long been a focus of psychophysical research (e.g., [6]). The phenomenon has proven to be robust and may be fundamentally related to other integration and segregation phenomena in perception. Related studies have been conducted in humans (e.g., [6–15]), monkeys [16], and bats [17], and several theories have been proposed to account for the phenomenon. In Gestalt theory, streaming is viewed as arising from fundamental principles inherent in the input patterns, such as proximity (of the tone frequencies), similarity, and spatiotemporal cohesion [18–25]. Bregman (1990) appeals to Gestalt principles in explaining auditory grouping mechanisms, and auditory scene analysis in general, but recruits other explanatory concepts such as integrative schemas when Gestalt principles fail. Other general theories invoked to explain auditory streaming include filter, or channel models, e.g., [26], that hold that streaming is based on selective attention to a single perceptual dimension such as pitch. Nevertheless, spectral separation and other differences in power spectrum are not necessary conditions for perceptual stream segregation (e.g., [14, 15]). Streaming also occurs in sequences of amplitude modulated, harmonically complex tones (e.g., Joris, Schreiner, and Rees; 2004). Moreover, channel models fail to accommodate streaming effects that are dependent on relationships among tones, such as quality, higher-order frequency relationships [27] and timbre [28]. Others (e.g., [7, 29]) propose that listeners attend to frequency motions in perceiving auditory streams. In fact, some researchers claim that Gestalt principles are generally inadequate explanations for entire classes of acoustic and visual grouping, for example in speech perception [30] and vision [22]. Although in nature there are many kinds of gestalten, that is organized patterns of perception or behavior, the means by which those patterns arise is as yet unclear.

Other work has highlighted the dynamic nature of streaming phenomena by demonstrating the importance of initial percept (van Noorden, 1975) and longer-term temporal effects [31, 32]. In one influential series of experiments, van Noorden presented tones with two different pitches in the order low-high-low-low-high-low (ABAABAABA). Tones were of equal amplitude and duration and

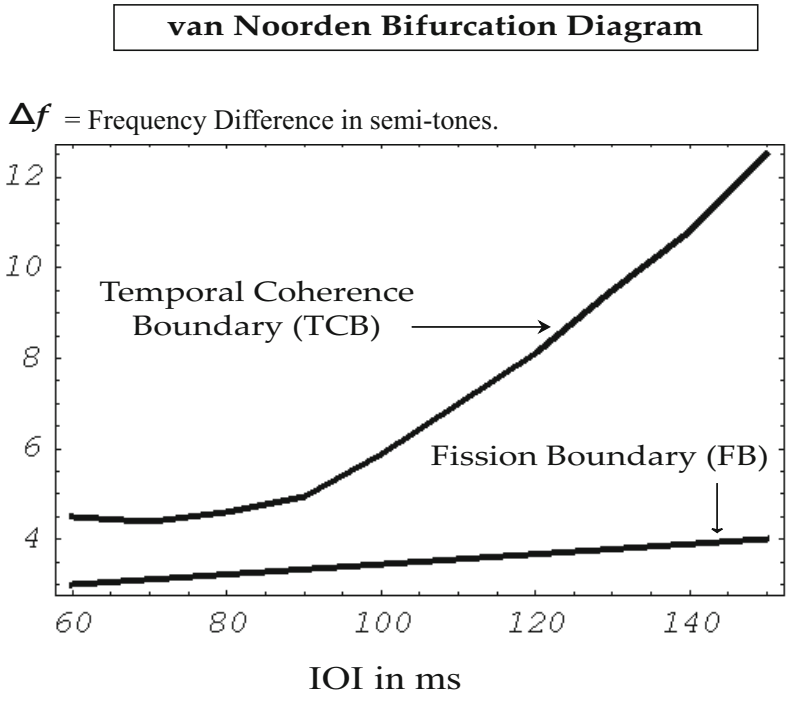

Fig. 1. *Stimulus sequences.* Variations of frequency difference or interstimulus intervals (ISI) are used as control parameters to manipulate the emergence of a particular percept.

the onset interval between successive tones was identical. Van Noorden presented listeners with tone sequences in which the frequency difference between the A and B tones was small and asked them to follow the gallop rhythm formed (so that perception was of an integrated tone sequence). He also presented tone sequences in which the frequency difference between the A and B tones was much larger and asked the listeners to focus their attention on the string of low tones (so that two segregated sequences of different frequency tones were perceived). See Figure 1 for example stimulus sequences, which were used in the experiments reported in this chapter. van Noorden (1975) then manipulated the frequency difference between A and B tones and their interstimulus-onset-interval (IOI) toward the other sequence type (integrated or segregated) and mapped the perceptual changes (see Figure 2). He found (1) a frequency-time boundary beneath which all sequences were heard as integrated, regardless of instructions (the Fission Boundary, FB) and (2) a frequency-time boundary above which all sequences were heard as segregated, regardless of instructions (the Temporal Coherence Boundary, TCB). In the bistable region between these two boundaries, a sequence could be heard as either integrated or segregated

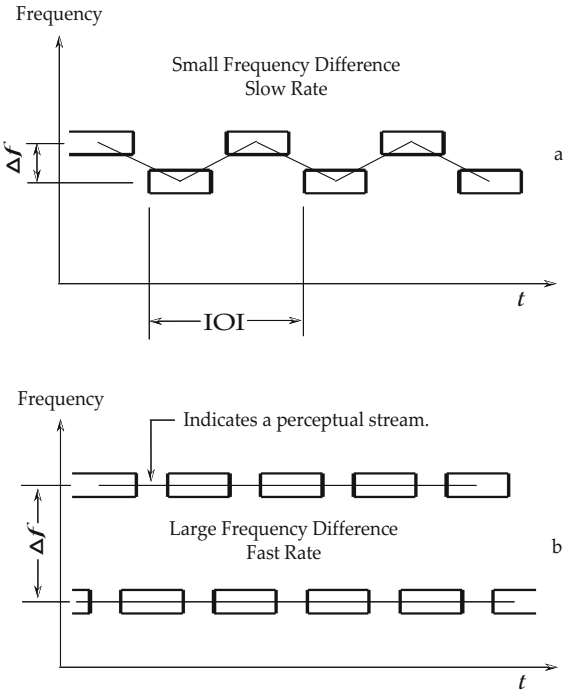

Fig. 2. *van Noorden's bifurcation diagram.* Variations of two control parameters, the frequency difference of tones and their interstimulus interval (ISI), allow to span a two-dimensional parameter space. The parameter space is partitioned into three regimes, one region with the percept one stream, another region with the percept two streams and a region in between which permits both.

depending upon initial instructions, with hysteresis phenomena observed when traversing the bistable regime.

1.2 Physiological correlates of auditory streaming

Complementary to the psychophysical approaches to the integration and segregation of sounds, there are currently two predominant neurophysiological theories of how the nervous system integrates environmental signals. The first theory is referred to as the binding theory and assumes that an integrated percept arises when activity in cortical areas becomes synchronized [33]. The second theory is grounded in the field of multisensory integration and assumes the existence of informational convergence zones. These convergence zones are made of cortical and subcortical networks such as the network consisting of the superior colliculi, the inferior parietal areas and the insula which is activated during the integration of speech and vision [34] among other behaviors. Both sources of neurophysiological evidence suggest that activations of larger networks are relevant for perceptual integration. Importantly, they also involve neural areas with

no known tonotopic architecture. For example, the left inferior parietal cortex has been hypothesized to be involved in the integration of visual-acoustic information to a common percept parametrized by temporal disparity [35]. Other researchers have found similar networks to be involved in the spatiotemporal integration of visual cues during collision judgments [36]. In the more related, but also more complex situation of speech perception, Hickock and Poeppel [37] argued that the left inferior parietal cortex is also involved in the integration of auditory-motor processes. Recruitment of these higher areas is largely non-specific to the modalities involved, which implies a general mechanism for the integration of signals to a coherent percept.

Specific to the phenomenon of auditory streaming, work by Snyder and colleagues (2008, 2009) confirms the presence of hysteresis in that perception and Event Related Potential (ERP) magnitude during an auditory streaming task depend on whether the prior sequence was perceived as integrated or segregated. Cusack [4] reported increased BOLD activity in the anterior intraparietal sulcus during two versus one-stream percepts, but did not find differences in the auditory cortex based on percept or frequency separation. The latter is in contrast to findings by Gutschalk and colleagues [38] who found covariations in magnetoencephalographic (MEG) signals with both frequency separation and percept. In event-related fMRI experiments of auditory streaming, Kondo and Kashino [39] found activations in auditory cortex, posterior insula, medial geniculate body, and supra-marginal gyrus but no contrasts were carried out regarding effects of perceptual organization or frequency separation. These results underline the need for further examination of the neurophysiological basis of auditory streaming, in particular the involvement of brain areas outside of the auditory cortex.

2 The Almonte et al. model of auditory streaming

The functional architecture proposed by Almonte and colleagues [5] was inspired by the large literature on integration phenomena across sensory modalities, in which multisensory convergence zones (represented by certain brain areas such as the insula) integrate information from different sensory modalities through an increased activation covariant with the percept of multisensory integration [40]. Almonte and colleagues explored the possibility of a homeomorphic architecture for auditory streaming comprising two layers. One layer, a neural field [41–44], is tonotopically organized such that the frequency of the acoustic stimulus maps onto a location in neural space. The second layer is a non-tonotopically organized subsystem and classifies the spatiotemporal neural field dynamics along very much the same lines as convergence zones in multisensory paradigms. The classification itself is not just a measurement (else the application of a simple measure to the neural field would suffice) but is itself a dynamic integrating process. In fact, bistability and hysteresis are properties of the classification dynamics rather than properties of the neural field dynamics. From the view point of synergetics, the second subsystem defines the order parameter of the percep-

tual pattern forming system, whereas the first subsystem performs a form of preprocessing of the input stimulus sequence.

The dynamics of the neural field $\mu(x,t)$ are given by the Jirsa-Haken wave equation [44] accommodating auditory inputs $s(x,t)$ as follows:

$$\left[\frac{1}{\gamma^2}\frac{\partial^2}{\partial t^2}+\frac{2}{\gamma}\frac{\partial}{\partial t}+1-r^2\nabla^2\right]\mu_v=\left(1+\frac{1}{\gamma}\frac{\partial}{\partial t}\right)\varsigma(\mu_v+s(x,t)), \tag{1}$$

where, as a reminder, $\gamma = c/r$, c is the speed of spike propagation and r parameterizes the spatial decay of lateral interactions. The external input or stimulus to the neural sheet is $s(x,t) : \mathbf{R}^2 \to \mathbf{R}$, which contains all the spatiotemporal characteristics of the auditory input stream. Periodic boundary conditions, $\mu(0,t) = \mu(L,t), \quad t \geq 0$, are used. The second subsystem is not tonotopically organized, hence its spatial dimension is of no relevance, when we consider only the competition of two streams. In fact, the ability to show multistable pattern formation is the only relevant property of this subsystem. A simple multistable subsystem with its scalar state variable $y(t)$ is given by the equation

$$\dot{y} = \varepsilon y - y^3 - I_0 + I(t), \tag{2}$$

where ε is a constant that captures all linear contributions. I_0 contains all constant contributions given rise to the rest state activity. The functional $I(t)$ is specified as

$$I(t)=\int_0^L h(\mu(x,t))dx \qquad h(n)=\left\{\begin{array}{ll}0, & n\leq\Omega\\ n, & n>\Omega\end{array}\right\}, \tag{3}$$

where Ω is a neural activity threshold. The equations (1), (2) and (3) define the dynamics of a stream classification model in one of its simplest forms. Figure 3 illustrates the architecture of the model.

To understand van Noorden's results, we parametrize a sequence of consecutive tones by their frequency difference, Δf, and their inter-onset interval, IOI. As the neural field evolves, it is integrated across space and time yielding the time dependent, but scalar, activity $I(t)$ driving the second system. $I(t)$ represents the relevant "information" from the neural field μ as a spatiotemporally integrated activity measure, which depends on the amount of dispersion over space and time. The greater the dispersion, the greater will be the value of $I(t)$ at a given time point. Figure 4 shows the contour lines of neural field activity over space x and time t for the bistable situation.

The final state reached by the second system defined in Eq. (2) with activity y will depend on $I(t)$ and its own intrinsic dynamics. For an intermediate value of $I(t)$, there is a bistable regime in which y can assume either one of the fixed points. The negative fixed point is identified with perceiving one stream and the positive fixed point with perceiving two streams. The time series for y are shown in Figure 5 for several different initial conditions of the activity y. After a transient the activity becomes stationary, displaying three possible scenarios (see Figure 5 from top to bottom): one stream only, or the bistable situation, in

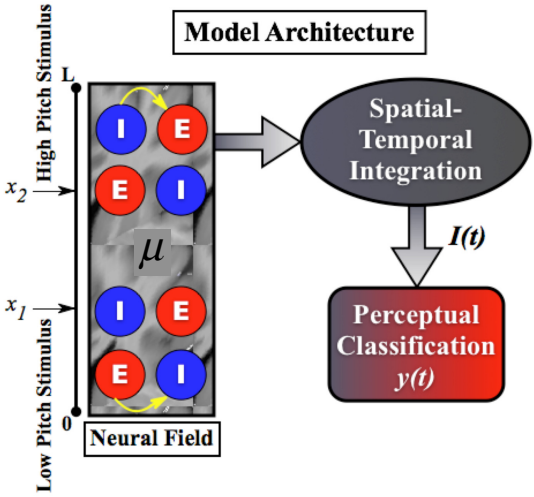

Fig. 3. *Cortical architecture of the model.* The neural field is illustrated by the rectangular box showing the neural activity $\mu(x,t)$ composed of inhibitory and excitatory neurons. The input $s(x,t)$ is provided at locations x_i via the Gaussian localization function $e^{-(x-x_i)^2/\delta_i}$ with width $\sqrt{\delta_i}$. The explicit model parameters used in the simulations are given in Almonte et al (2005).

which either one integrated stream or two separate streams may be perceived, or finally two streams only. For each choice of Δf and IOI, the model equations (1) and (2) are solved numerically and their stationary states determined. The results are plotted in the two-dimensional parameter space shown previously in Figure 1.

3 A novel paradigm: amplitude streaming

Do the mechanisms leading to the emergence of auditory streaming need to be explained through tonotopically structured networks? Or may there be a crucial role to be played within the functional architecture by subsystems with no tonotopic organization? In what follows, we study specifically whether auditory streaming involves interacting neural subnetworks, some tonotopic but others non-tonotopically organized and acting as information convergence zones for the classification of the perceptual world. To this end, we first show that perceptual streaming occurs for sequences of pure tones with constant frequency but systematic amplitude modulation across tones. This demonstration is a necessary step because our model does not depend on the system being organized

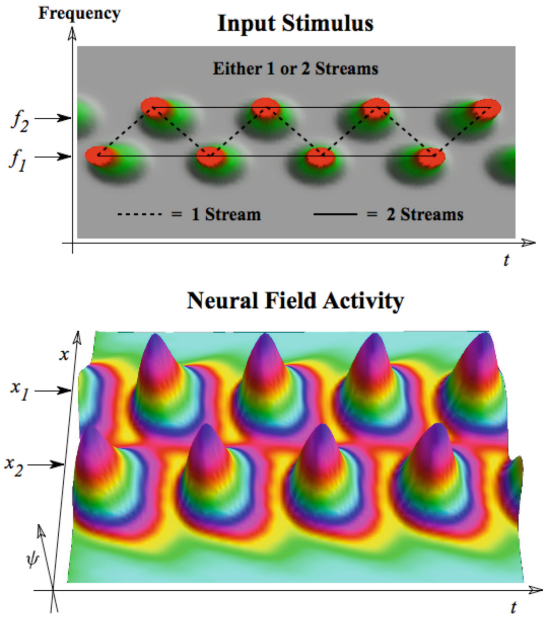

Fig. 4. *Bistable regime of auditory streaming.* The stimulus sequences (top) and its resulting neural field dynamics (bottom).

tonotopically. We then, in the next section, examine the BOLD responses from listeners who perceive auditory streaming 1) on the basis of frequency differences among equal amplitude tones and 2) on the basis of amplitude differences of same-frequency tones.

In order to assess perceptual streaming on the basis of amplitude differences alone, we constructed sequences containing 40 sinusoidal tones of constant frequency (600 Hz) and duration (100ms) and an inter-onset interval (IOI) of 110ms (i.e., an interstimulus interval of 10ms). The only parameter varied across sequences was the amplitude ratio (AR) between adjacent tones (T1 and T2). AR was kept constant within each of the 20 T1-T2 pairs in a sequence. Values of AR relative to the highest amplitude tone were 0.2, 0.3, 0.4, 0.5, 0.6, 0.7, 0.8, and 1 (AR = 1 denotes equal amplitude of T1 and T2). Amplitude was linearly ramped over the first and last 10ms of each tone.

Pairs of 40-tone sequences were presented 5 times to subjects in random order, with 500ms between members of each sequence pair. The subject's task was to judge which of the two sequences in a pair sounded slower. When tone sequences of the type used here are perceived as two streams, they are perceived to be slower than sequences perceived as a single stream. Subjects responded by pressing one of three labeled keys on a keypad: Pressing the number 1 meant that the first sequence was perceived as slower; pressing 2 meant that the second sequence was perceived as slower; and pressing = meant that the two sequences

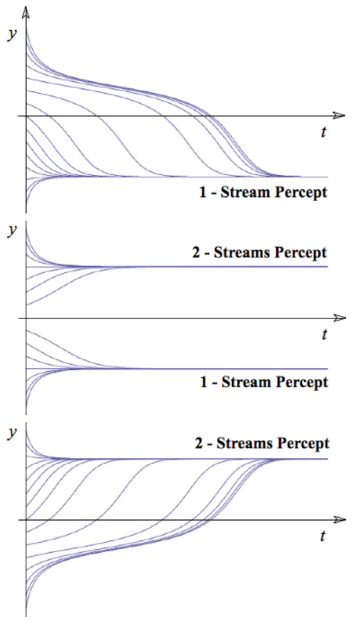

Fig. 5. *Percept formation.* For multiple initial conditions the time series of $y(t)$ are plotted for the three regimes, one stream only (top), bistable (middle) and two streams only (bottom).

were perceived as equal in rate. All combinations of sequences were included, with the exception of sequences having AR = 0.3, AR = 0.5, and AR = 0.7 paired with itself, for a total of 230 sequence pairs. Order of sequence presentation for each pair was counterbalanced.

A control condition was included in which each trial consisted of three short tone sequences presented with 500ms ISI between sequences. Each sequence was either 1) a T1-T2 sequence with AR = 0.2 and IOI = 110ms, or 2) a sequence with T1=1 and IOI = 220ms, i.e., T2 was omitted. Triad orders were sequences (a) 1, 2, 1; (b) 2, 1, 1; (c) 1, 2, 2; and (d) 2, 1, 2. Sequence 1 contained 12 tones. Sequence 2 contained 6 tones, with double the IOI of sequence 1, in order to verify that subjects reliably heard the lowest amplitude tones. The procedure was an ABX, forced-choice task in which subjects judged whether the rate of the third tone sequence (X) was more like the first sequence (A) in the triad or more like the second sequence (B) in the triad. Subjects responded by pressing one of two labeled keys on a keypad: Pressing the number 1 meant that the rate of the third (test) sequence was more like the first sequence. Pressing 2 indicated that the rate of the third sequence was more like the second sequence.

All subjects (N=11) had normal hearing according to self-report and were naive to the purpose of the experiment. They were told that there were no right

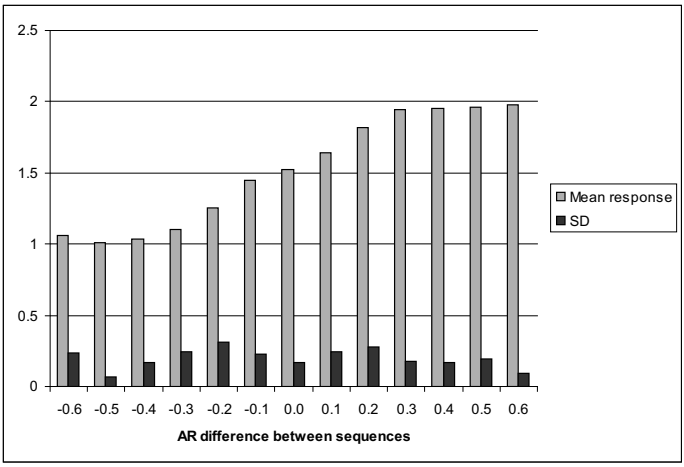

Fig. 6. *Amplitude Streaming.* Behavioral results are shown based on amplitude variation of consecutive tones.

or wrong answers and that our interest was purely in how they perceived the tone sequences.

Responses from the control condition were examined to verify that all subjects were able to hear the lowest amplitude tone reliably. All subjects responded with at least 85% accuracy (9 of the 11 responded with 95% accuracy or better). Thus, the low amplitude tone was indeed perceived and contributed to the perception of a faster rate sequence.

Figure 6 shows the means and standard deviations of the responses across subjects for the perception of streaming in sequences of amplitude-modulated pure tones. The x-axis represents the AR difference between the two sequences in each pair. When the difference is negative, the amplitude difference between successive tones within a sequence is greater in the first sequence than the second. In this case, subjects judge the first sequence to be slower than the second, indicating that streaming has occurred in the first sequence but not in the second. When the AR difference is positive, the amplitude difference between successive tones within a sequence is greater in the second sequence than the first. In this case, subjects judge the second sequence to be slower than the first, indicating that streaming has occurred only in the second sequence. For small AR differences, subjects judge the rates of the sequences to be equal, indicating that streaming occurred in both sequences (denoted on the y-axis by 1.5 in Figure 6). Moreover, there is no order effect. AR differences of -0.6, for example, are equivalent to AR differences of 0.6. The lack of an order effect was confirmed statistically by a 2-way repeated measures ANOVA with order and AR difference as factors. For order, $F(1, 5) = 2.67$, $p > 0.1$ and the interaction of order and AR difference was similarly not significant, $F(5, 5) = 1.88$, $p > 0.1$.

Amplitude Streaming (AS)		
Condition: Name	f_1, f_2 **in Hz**	A_1, A_2
1: AS	1000, 1000	0.2, 1
3: Control	1000, 1000	1, 1
4: Control	1000, 0	1, 0
5: Control	1000, 1000	0.2, 0.2
6: Control	1000, 1000	0.2, 0
Frequency Streaming (FS)		
Condition: Name	f_1, f_2 **in Hz**	A_1, A_2
2: FS	500, 1000	1, 1
3: Control	1000, 1000	1, 1
4: Control	1000, 0	1, 0
7: Control	500, 500	1, 1
8: Control	500, 0	1, 0

Table 1. Parameter values for experimental conditions consisting of tone sequences *ABAB...AB*. Conditions 3 & 4 function as controls for both amplitude and frequency streaming. In order to examine the neural effects of auditory streaming, several control conditions needed to be built into the experimental design. Condition 1 is the condition most likely to result in amplitude streaming, since the tones are of the same frequency but with very different amplitudes. Condition 2 is most likely to result in frequency streaming. Conditions 3 and 5 were used to eliminate rate effects as the only cause of a significant amount of neural activation in amplitude streaming (condition 1). Conditions 4 and 6 were used to eliminate amplitude effects as the only cause of a significant amount of neural activation in amplitude streaming (condition 1). Control conditions 3 and 7 were used to eliminate rate effects as the only cause of a significant amount of neural activation in frequency streaming (Condition 2). Conditions 4 and 6 were used to eliminate amplitude effects as the only cause of a significant amount of neural activation in frequency streaming (condition 2).

In summary, in spite of the fact that all tones were of equal frequency and IOI was constant across sequences, amplitude difference alone was sufficient to cause the pure-tone sequences to split into two perceptual streams. This is in agreement with the model's prediction of the possibility of perceiving one or two streams depending on the AR of the tone sequences.

4 Amplitude streaming and its associated BOLD responses

Next we consider the BOLD responses from listeners who perceive auditory streaming 1) on the basis of frequency differences among equal amplitude tones and 2) on the basis of amplitude differences of same-frequency tones. Eight subjects (4 females and 4 males) between 23 and 42 years of age participated in the fMRI experiment. All subjects were in good health with normal hearing (by self-report) and no past history of psychiatric or neurological disease. Informed

consent was collected from each subject prior to the experiment and the study was approved by the Florida Atlantic University Institutional Review Board.

Because scanner noise is a primary concern when using fMRI for auditory perceptual experiments, we used a sparse sampling (or clustered volume) scanning technique [3]. The long TRs used by this technique directly influence the possible experimental design, especially, experiment duration, which affects the number of trials that can be collected for each experimental run. Auditory stimuli were presented to the subjects in 12-second on-blocks followed by 12 seconds of silence. The on-blocks consisted of pure tone sequences. The only parameters that were varied were the frequency difference between adjacent tones, the silent gaps between tones, and the amplitude ratio of adjacent tones. Tone durations were always 50ms with 5ms amplitude ramping at the beginning and end of each tone. Interstimulus silent intervals were either 100ms or 250ms, depending on the condition (see Table 1). Each on-block contained the maximum number of [tone, silentgap] pairs that fit in the 12-second interval; any remaining time was divided into two equal durations of silence at the beginning and end of each tone sequence. fMRI scans lasted 2sec and began 2sec before the end of each block, so that the tone stimuli were still present during the scanning period. Each of the eight conditions was repeated twenty times during the experiment for a total run time of 64 minutes. The order of stimulus presentation was randomized across presentation blocks and conditions, but not across subjects, with the constraint that no condition was repeated consecutively.

Before the beginning of the experiment, subjects went through a short training session with sequences from Conditions 1 and 2, each repeated 3 times in random order. The purpose of the training session was to allow the subjects to become familiar with the stimulus sequences and to determine via verbal report whether they perceived 1) amplitude-based streaming in Condition 1 (equal frequency tones of different amplitude) and 2) frequency-based streaming in Condition 2 (different frequency tones with equal amplitude). A General Electric (GE) 3T Signa scanner was used to acquire T1-weighted structural images and functional EPI images for the measurement of the blood oxygenation level-dependent (BOLD) effect. The acquisition scheme and parameters used for the functional scans were as follows: echo-planar imaging (EPI), gradient recalled echo, TR = 12 s, TE = 35 ms, flip angle = 90 degrees, 64 x 64 matrix, 30 axial slices per scan each of thickness 5 mm acquired parallel to anterior-posterior commissural line. The data was preprocessed and analyzed using Statistical Parametric Mapping software [10] (SPM2 from Wellcome Department of Cognitive Neurology, London, UK). Motion correction to the first functional scan was performed within subject using a six-parameter rigid-body transformation. The 8 subjects had less than 7mm of translation in all directions and less than 6.0 degrees of rotation about the three axes. The mean of the motion-corrected images was then coregistered to the individual 30-slice structural image using a 12-parameter affine transformation. The images were then spatially normalized to the Montreal Neurological Institute (McGill University, Canada, http://www.bic.mni.mcgill.ca/) template brain by applying a 12-parameter affine transformation, followed by

a nonlinear warping using basis functions. These normalized images were interpolated to 2 mm isotropic voxels and subsequently smoothed with a 4 mm isotropic Gaussian kernel. A random-effects, model-based, statistical analysis was performed with SPM2 [10] in a two level procedure. The first level consists of estimating a General Linear Model (GLM) [11] of the form: $Y = Xv + e$ for each subject where X is a (m x n) experimental design (basis) matrix (m = 320 = Total number of stimulus presentations and n = 8 = Number of conditions), and v is a constant vector representing weights for each basis vector of X. Each column vector of X consists of a series of entries of zeros for the off-blocks and ones for the on-blocks and represents different stimulus conditions in each functional run and six motion parameters obtained from the realignment. v is estimated using the method of least squares and minimizing the error e. Individual contrast images were created by correlating the brain response with the aforementioned covariates for each subject. Global differences among subjects were controlled by proportional scaling. The individual contrast images were then entered into a second-level analysis, using a separate one-sample t-test for each term in the general linear model. The summary statistical maps were thresholded at $p < 0.05$ (uncorrected for multiple comparisons). These maps were overlaid on a high-resolution structural image in the Montreal Neurological Institute (MNI) orientation.

In previous work, no explicit contrasts were carried out to test for effects of perceptual organization or frequency separation (such as [39]) reinforcing the need for further examination of the involvement of areas outside the auditory cortex in streaming. Here we develop a set of constraints based on set theoretical operations allowing us to address differential effects related to streaming or streaming in combination with amplitude, frequency, or rate changes. Figure 7 shows voxels which correlate with streaming percepts. The voxels in panels A (amplitude streaming), B (frequency streaming), & C (the intersection of amplitude and frequency streaming) are related only to streaming percepts. Anatomical areas activated by amplitude streaming (panel A in Figure 7) include primary auditory areas as well as parietal areas (right superior parietal lobule (SPL) and precuneus). Similarly, for frequency streaming (panel B) there are activations in primary auditory areas and beyond, including the left inferior parietal lobule (IPL), supramarginal gyrus (SG), precuneus, parietal lobe subgyral (Brodmann area 40), right inferior and superior parietal lobule, and middle and superior temporal gyri. The implication of the right parietal cortex is consistent with related findings in which intraparietal sulcus (IPS) showed greater activity when two streams were perceived rather than one [4] and reports that right parietal cortex influences the auditory perceptual scene - more specifically, sound movement (Griffiths et al. [9]). The findings are also consistent with the results of Bushara and colleagues [45] who found that the hierarchical organization of the auditory system extends beyond the temporal lobe to include areas in the posterior parietal and prefrontal regions, especially for auditory spatial processing.

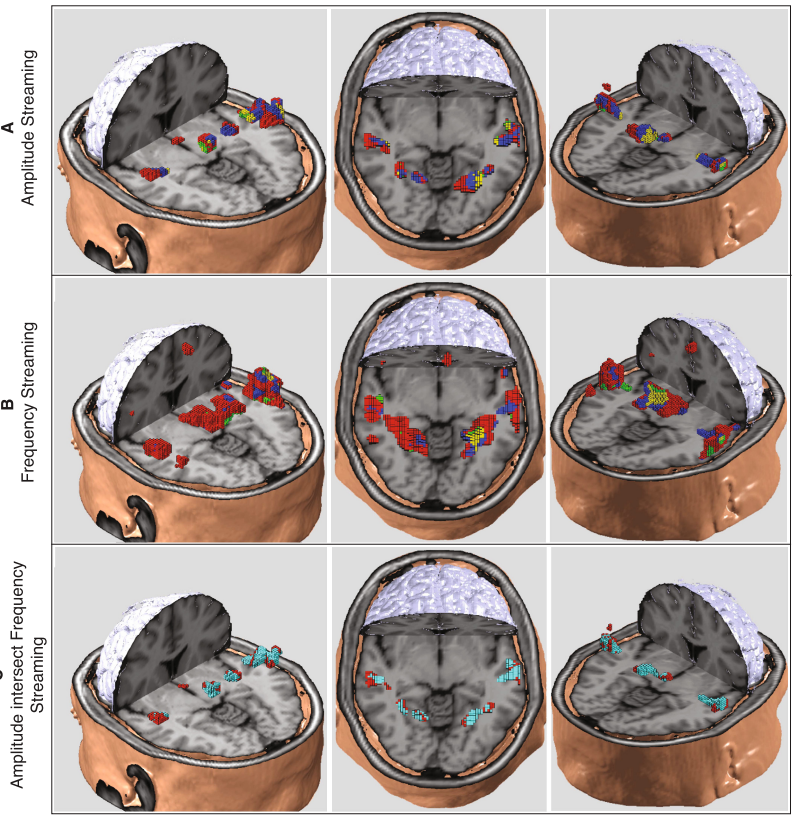

Fig. 7. *Streaming results in the BOLD response.* Three different activation patterns are shown. Active voxels related to the percept of amplitude and frequency streaming and their intersection at $p < 0.05$. The voxels are color coded to show contributions due only to the streaming percept (red voxels) and any other effects not related to amplitude, frequency, and rate changes in the stimuli. Whereas the blue, cyan, green, and yellow voxels are related to amplitude, frequency, or rate changes in the stimuli.

Panels A and B in Figure 7 show areas of significant BOLD increases for amplitude and frequency streaming. In contrast, there are relatively few voxels with significant activity that are common to both amplitude and frequency streaming (panel C). There is ∼44% overlap among the voxels of panels A and C and ∼8% overlap among voxels of panels B and C. The non-empty intersection shown in panel C defines the necessary condition for the existence of convergence zones that influence the perception of both amplitude and frequency streaming. If we subtract (voxel by voxel) these common networks from the voxels in panels A and B we obtain specific networks corresponding only to amplitude and frequency streaming percepts respectively. The networks represented by the voxels in panels A, B, and C are independent of the changes in the control parameters since the effects of these parameter changes were subtracted out. Complemen-

tary to this conclusion, there also exist specific neural networks that influence the perception of either amplitude or frequency streaming but not both since there exist voxels in panels A and B complementary to the intersection shown in Panel C.

5 Conclusions

We have shown in the auditory domain that by specifying primary experimental stimulus conditions (amplitude and frequency modulation, in our case), together with appropriate controls, we can identify convergence zones related to the percepts induced by the primary stimulus conditions. Convergence zones were determined by subtracting effects present in individual control conditions using contrasts dependent on relationships among the primary conditions and controls (see Felix Almonte's PhD thesis, Florida Atlantic University 2006, for details). Convergence zones were found mainly within the right parietal areas. Thus, even though parietal areas may be multimodal, they still account for unimodal auditory temporal integration. Convergence zones are interpreted as networks that integrate higher order information leading to specific perceptual states, thus making them plausible representational candidates for the neural substrates of awareness. From the synergetic view point, convergence zones basically track the perceptual dynamics as we propose here, but they also participate in a widespread brain network responsible for the overall brain pattern formation. Hence, when convergence zones change their activation dynamics, it corresponds to a larger spatiotemporal reorganization of the brain patterns as described by phase transitions in synergetic systems. From a more traditional neuroscience perspective, convergence zones form dominant parts of cell assemblies in a neural representational strategy, for instance as proposed by Singer, relying on the dynamic association of feature-specific cells into functionally coherent cell assemblies. The cell assemblies represent the constellation of features defining a particular perceptual object. These possibilities combined with our experimental results provide support for theoretical models of perception that employ the idea of convergence zones as mediators for the organization of percepts.

Acknowledgements. The research reported here was supported by the Brain Network Recovery Group through the James S. McDonnell Foundation and the FP7-ICT BrainScales. Any opinion, finding, and conclusions or recommendations expressed in this material are those of the authors and do not necessarily reflect the views of the National Science Foundation.

References

1. Haken, H.: Synergetics. An Introduction. Springer, Berlin (1983)
2. Cross, M.C., Hohenberg, P.C.: Pattern formation outside of equilibrium. Rev. Mod. Phys. **65**, 851–1112 (1993)

3. Dykstra, A.R., Halgren, E., Thesen, T., Carlson, C.E., Doyle, W., Madsen, J.R., Eskandar, E.N., Cash, S.S.: Widespread brain areas engaged during a classical auditory streaming task revealed by intracranial EEG. Frontiers in Human Neuroscience **5**, 74 (2011)
4. Cusack, R.: The intraparietal sulcus and perceptual organization. J. Cogn. Neuroscience **17**, 641–651 (2005)
5. Almonte, F., Jirsa, V.K., Large, E.W., Tuller, B.: Integration and segregation in auditory streaming. Physica D **212**, 137–159 (2005)
6. Miller, G.A., Heise, G.A.: The trill threshold. The Journal of the Acoustical Society of America **22**, 637–638 (1950)
7. van Noorden, L.P.A.S.: Temporal coherence in the perception of tone sequences. Ph.D. thesis, Eindhoven University of Technology (1975)
8. Bregman, A.S.: Auditory streaming: Competition among alternative organizations. Perception and Psychophysics **23**, 391–398 (1978)
9. Bregman, A.S.: Auditory Scene Analysis: The perceptual organization of sound. MIT Press (1990)
10. Lackner, J.R., Goldstein, L.M.: Primary auditory segregation of repeated consonant-vowel sequences. The Journal of the Acoustical Society of America **56**, 1651–1652 (1974)
11. Neisser, U.: Cognitive Psychology. Appleton-Century-Croft (1967)
12. Warren, R.M., Warren, R.P.: Auditory illusions and confusions. Scientific American **223**, 30–36 (1970)
13. Helenius, P., Uutela, K., Hari, R.: Auditory stream segregation in dyslexic adults. Brain **122**, 907–913 (1999)
14. Grimault, N., Bacon, S.P., Micheyl, C.: Auditory stream segregation on the basis of amplitude-modulation rate. The Journal of the Acoustical Society of America **111**, 1340–1348 (2002)
15. Vliegen, J.V., Oxenham, A.J.: Sequential stream segregation in the absence of spectral cues. The Journal of the Acoustical Society of America **105**, 339–346 (1999)
16. Izumi, A.: Auditory stream segregation in japanese monkeys. Cognition **82**, B113–B122 (2002)
17. Moss, C.F., Surlykke, A.: Auditory scene analysis by echolocation in bats. The Journal of the Acoustical Society of America **110**, 2207–2226 (2001)
18. Wertheimer, M.: Gestalt theory. Social Research **11** (1924). Translation of lecture at the Kant Society, Berlin
19. Koffka, K.: Principles of Gestalt Psychology. Harcourt, Brace and Company, Inc. (1935)
20. Köhler, K.: Gestalt Psychology. Liveright (1947)
21. Hartmann, G.W.: Gestalt Psychology. The Ronald Press Company (1935)
22. Kubovy, M., Pomerantz, J.R. (eds.): Perceptual Organization. Lawrence Erlbaum Associates, Inc., Publishers (1981)
23. Gobar, A.: Philosophic Foundations of Genetic Psychology and Gestalt Psychology. Martinus Nijhoff, The Hague, The Netherlands (1968)
24. Gordon, I.E.: Theories of Visual Perception. John Wiley & Sons (1989)
25. Lewin, K.: Principles of Topological Psychology. McGraw-Hill Book Company (1936)
26. Broadbent, D.: Perception and Communication. Pergamon Press (1958)
27. Idson, W.L., Massaro, D.W.: Cross-octave masking of single tones and musical sequences: The effects of structure on auditory recognition. Perception and Psychophysics **19**, 155–175 (1976)

28. Singh, G.P., Bregman, A.S.: The influence of different timbre attributes on the perceptual segregation of complex tone sequences. The Journal of the Acoustical Society of America **102**, 1943–1952 (1997)
29. Jones, M.: Time, our lost dimension: Toward a new theory of perception, attention, and memory. Psychological Review **83**, 323–355 (1976)
30. Remez, R.E., Rubin, P.E., Berns, S.M., Pardo, J.S., Lang, J.M.: On the perceptual organization of speech. Psychological Review **101**, 129–156 (1994)
31. Snyder, J.S., Carter, O.L., Lee, S.K., Hannon, E.E., Alain, C.: Effects of context on auditory stream segregation. J. Exp. Psychol. Hum. Percept. Perform. **34**, 1007–1016 (2008)
32. Snyder, J.S., Holder, W.T., Weintraub, D.M., Carter, O.L., Alain, C.: Effects of prior stimulus and prior perception on neural correlates of auditory stream segregation. Psychophysiology **46**, 1208–1215 (2009)
33. Engel, A.K., Fries, P., Singer, W.: Dynamic predictions: Oscillations and synchrony in topdown processing. Nature Reviews: Neuroscience **2**, 704–716 (2001)
34. Calvert, G.A.: Crossmodal processing in the human brain: Insights from functional neuroimaging studies. Cerebral Cortex **11**, 1110–1123 (2001)
35. Bushara, K.O., Grafman, J., Hallett, M.: Neural correlates of auditory-visual stimulus onset asynchrony detection. The Journal of Neuroscience **21**, 300–304 (2001)
36. Assmus, A., Marshall, J.C., Ritzl, A., Noth, J., Zilles, K., Fink, G.R.: Left inferior parietal cortex integrates time and space during collision judgments. NeuroImage **20**, S82–S88 (2003)
37. Hickok, G., Poeppel, D.: Towards a functional neuroanatomy of speech perception. Trends in Cognitive Sciences **4**, 131–138 (2000)
38. Gutschalk, A., Micheyl, C., Melcher, J.R., Rupp, A., Scherg, M., Oxenham, A.J.: Neuromagnetic correlates of streaming in human auditory cortex. J. Neuroscience **25**, 5382–5388 (2005)
39. Kondo, H.M., Kashino, M.: Involvement of the thalamocortical loop in the spontaneous switching of percepts in auditory streaming. J. Neuroscience **29**, 12695–12701 (2009)
40. Calvert, G.A., Spence, C., Stein, B.E. (eds.): The Handbook Of Multisensory Processes. MIT Press (2004)
41. Amari, S.: Biomathematics: Current Status and Future Perspectives, chap. A Mathematical Theory of Self-Organizing Nerve Systems, pp. 159–177. North-Holland (1982)
42. Wilson, H.R., Cowan, J.D.: A mathematical theory of the functional dynamics of cortical and thalamic nervous tissue. Kybernetik **13**, 55–80 (1973)
43. Jirsa, V.K., Haken, H.: Field theory of electromagnetic brain activity. Phys. Rev. Lett. **77**, 960–963 (1996a)
44. Jirsa, V.K., Haken, H.: Derivation of a field equation of brain activity. J. Biol. Phys. **22**, 101–112 (1996b)
45. Bushara, K.O., Weeks, R.A., Ishii, K., Catalan, M.J., Tian, B., Rauschecker, J.P., Hallett, M.: Modality-specific frontal and parietal areas for auditory and visual spatial localization in humans. Nat. Neuroscience **2**, 759–766 (1999)

Introduction to Chronotaxic Systems – Systems far from Thermodynamics Equilibrium that Adjust Their Clocks

Aneta Stefanovska, Philip T. Clemson, and Yevhen F. Suprunenko

Department of Physics, Lancaster University, Lancaster, UK
anetalancaster.ac.uk
http://www.physics.lancs.ac.uk/people/aneta-stefanovska

Abstract. The complex, fluctuating dynamics that abounds in nature is now easily monitored and analysed, applying either stochastic or deterministic methods. It has been demonstrated that complex systems far from thermodynamic equilibrium, especially living systems, often exhibit time-varying dynamics. To date they have been usually treated as stochastic. Here we focus on the non-autonomous properties of complex systems and propose a new class of dynamical systems. Namely, we assume that a basic dynamical unit which inherently possesses an internal source of energy, is continuously perturbed by the environment and maintains its stability by adjusting the rate of exchange of energy and matter with the environment. We provide a mathematical formalism for such systems, combining the recent theory of pullback attractors with the theory of self-sustained oscillators. We name the new class of systems as *chronotaxic* and, based on measured data, show that the heart possesses properties characteristic of chronotaxic systems. This means that its dynamics is largely deterministic, which opens new possibilities for diagnosis and prediction. We expect that many complex systems will be identified as chronotaxic and that their models will become much simpler and more realistic.

Keywords: non-autonomous systems, time-varying dynamics, coupled oscillators, chronotaxic systems, biological oscillations

1 Introduction

Complex dynamical systems are a significant challenge for theoretical modelling and for the inverse problem approach [1]. Specifically, we face the problem of understanding how the dynamics is generated when three components are unknown. These are the dynamics of the internal system, the environment and the interaction between them two. The separation of these components is in general an unsolved problem. Nonetheless, as we show in this chapter, such a separation is now possible for a certain class of systems. Such systems naturally resist disorder when exposed to a strong external influence. These features are

A. Pelster and G. Wunner (eds.), *Selforganization in Complex Systems: The Past, Present, and Future of Synergetics*, Understanding Complex Systems,
DOI: 10.1007/978-3-319-27635-9_14

typically found in biological systems such as the cardiovascular system [2, 3], mitochondrial oscillations [4, 5] and the brain [6, 7]. Similar behaviour is also observed among certain low-temperature systems with simpler dynamics, e.g. surface state electrons on liquid helium [8]. Attempts have also been made to apply the properties of limit cycle systems in robotics [9].

Another important aspect of complex systems are ensembles and networks of oscillatory units. These include the dynamics of thin liquid films, cellular networks, brain dynamics and the cardiovascular system as well as social dynamics and social networks. Theories and models, such as the various Kuramoto models, have been developed to describe the temporal and spatiotemporal behaviour of these complex systems [10–13]. This traditional approach involves building an autonomous model of this ensembles, and then including the influence of the environment via time-dependent parameters or weak perturbations [9, 14]. Here, we present a new class of non-autonomous systems that inherently possess a source of internal energy, are continuously perturbed by external perturbations and are able to maintain stability while perturbed, resulting in their oscillatory behaviour with time-variable characteristic frequencies.

In the next section we present our motivation for proposing this new class of non-autonomous dynamical systems and summarise the background of the work leading to the proposal. In Sec. 3 we introduce chronotaxic systems and in Sec. 4 we provide their mathematical formulation. In Sec. 5 we discuss methods of data analysis that are suitable for reconstructing their dynamics from measured data. Finally, in Sec. 6 we summarise this chapter.

2 Motivation and Background

In nature, and especially for living systems, it is often the case that not all parts of the system can be observed. The system may, for example, be comprised of subsystems, many of which might be inaccessible. An example of such a situation is provided in Fig. 2(a), where different signals related to the cardiovascular system (respiration, ECG, blood pressure and skin microvascular blood flow in wrist and ankle) are simultaneously recorded. Several oscillatory processes can be seen already in the time domain propagated through the system and recorded by different sensors. The instantaneous frequency of the heart, also known as heart rate variability (HRV), derived from the R-peaks in the ECG, is also shown. It is obvious that it is not constant, but rather varies in time and the nature of this variation – stochastic or deterministic, or both – has been a subject of intensive research in the past decades. Many studies have shown that these oscillatory processes originate from certain physiological functions (beating of the heart, expansion and contractions of the lungs with breathing, movements of the smooth muscles in the vascular walls, cyclical activation of sympathetic nerves and oscillatory processes across the endothelial cells that form the inner layer of the entire vascular system), and that they influence each other (e.g. [2, 15–17]). In such cases, if only one signal is observed, the variation in its dynamics can be mistakenly classed as stochastic or chaotic. In modelling there is often

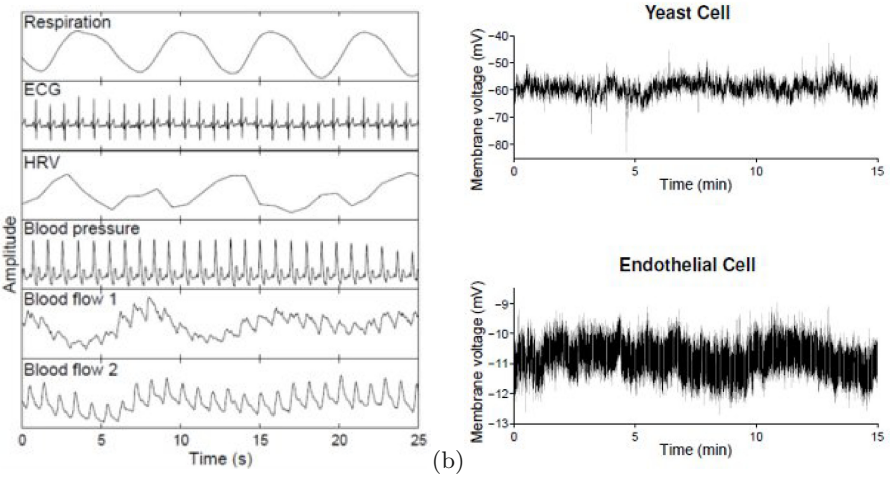

Fig. 1. Examples of systems with inherent time variability. (a) Simultaneous recordings of signals related to the function of the cardiovascular system. The instantaneous frequency of the heart, known as HRV, derived from R-peaks in the ECG signal, is also shown indicating that the frequency of the heart beat is not constant, but rather varies with time. The nature of this variation has been a subject of intensive research over the past decades and to date there is no commonly accepted opinion whether it originates from a stochastic or a deterministic source. Figure modified from [2]. (b) The membrane potential of two types of non-excitable cells as recorded using the whole-cell configuration of the patch clamp technique [18].

not enough information about what to include in the description of the system; for example, what is considered to be environment can be a part of the system. As a result of a lack of information, the model of the resulting complex dynamics of the observed system can be overcomplicated, and its deterministic component can be well hidden. Here we argue that the traditional approach to modelling is not realistic and does not provide a simple way of studying such systems.

Another example of such systems is the cell. Its membrane potential also exhibits time-varying dynamics. Fig. 1(b) and 2-right show the time-evolution of the resting membrane potential recorded in non-excitable cells by the whole-cell patch clamp technique. Information in the subtle fluctuations of the membrane potential of such cells has been left unexplored. Mitochondrial oscillations, Fig. 2-left, have also been shown to exhibit complex time-dependent dynamics [4, 5] with similar frequency as that seen in the cell membrane potential, Fig. 2-right.

The most challenging features of these systems is the inherent time-variability of their dynamics, which has often been overlooked by standard analytical and "inverse problem" approaches [19]. Consequently, using conventional approaches, the dynamics of these systems looks too complex, which prevents any detailed

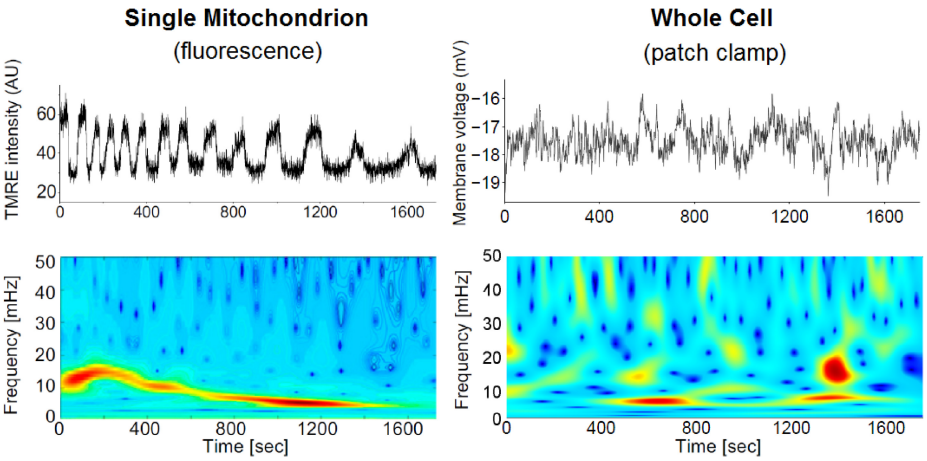

Fig. 2. Mitochondrial oscillations viewed in the time domain and in the wavelet transform. (Left) Oscillations in a single mitochondrion using a fluorescent dye which is sensitive to the membrane potential. Figure modified from [4]. (Right) Intermittent oscillations are observed at a similar frequency in the wavelet transform of the membrane potential of an endothelial cell, recorded using the patch clamp technique [18].

understanding. This furthermore leads to the system being misrepresented as stochastic and/or chaotic despite exhibiting dynamics that is both deterministic and stable with respect to perturbations and variations in initial conditions. It is obvious that the explicit time-dependence, which originates from the non-autonomous nature of the dynamics, should be taken into account.

The mathematical theory of non-autonomous dynamical systems was introduced to tackle the problem of systems under external influence [20, 21]. The problem of characterising complex systems under stochastic influence was investigated almost in parallel within the theory of random dynamical systems [22, 23]. The latter approaches were mainly motivated by practical applications including climate [24, 25], neuroscience [26, 27] and evolutionary science [28]. In climate science efforts have been made to define statistically the effective complexity of time-varying systems [24], and a theory of non-autonomous dynamical systems has brought new physical information about a system using concepts of random attractors and time-dependent invariant measures [25]. In neurophysiology, the dynamics of the brain has been modelled as a set of interactions between separate simple systems, rather than as a single complex or chaotic system [27]. In addition, some of the most relevant work has been applied to measured brain data where it was found that the attractor of the system is time-dependent [26]. Random dynamical systems were used to establish that a variational free energy minimization provides a sufficient account of self-organised behavior in biological systems [7]. Meanwhile in evolutionary science, the importance of separating the various interacting species into distinct open systems has also been identified and

used to explain how nature maintains diversity [28]. Further development has also led to the concept of pullback attractors [20], which generalise the notion of attractors within the theory of non-autonomous dynamical systems, including random [22] and snapshot [23] attractors.

In parallel with the development of the mathematical theories mentioned above, practical applications stimulated the development of novel data analysis methods for the inverse problem approach. In particular, several methods that provide time-localised analyses of dynamical systems were proposed. In studies of cardiovascular and brain dynamics, the wavelet transform was applied [15] to cope with the inherent time variability of such systems as seen in Figs. 1 and 2. Wavelet-based [29, 30], phase coherence [30, 31] and recently Bayesian-based inference [32, 33] methods have since been introduced to deal with the properties of systems with inherently time-varying parameters.

Despite these achievements we are still left with the problem of separating the components of the dynamics. The conditions for when this problem is solvable have not been strictly defined. In our work [34] we make progress by formulating the new class of non-autonomous dynamical oscillatory systems that we introduce in the next section.

3 Introduction of Chronotaxic Systems

We define chronotaxic systems through a unification of two concepts: the concept of self-sustained limit cycle oscillations [10, 35], and the concept of time-dependent attractors [20]. The first concept determines the oscillatory dynamics, and the second one provides the conditions for stable motion along the limit cycle. As a result, such systems resist external perturbations because all dynamical variables have stable time-dependent values due to oscillatory dynamics of a point attractor. As we will see below such properties allow a reduction in the complexity of the full dynamics of these systems. This is made possible because the motion of the point attractor can be separated from the weak perturbations acting on it. In order to illustrate the characteristics of the new class of systems and the importance of it being distinguishably classified as such, we provide examples of a theoretical model.

3.1 Autonomous Self-sustained Oscillatory Systems

First, we consider a very important class of oscillatory systems which are defined by processes which can sustain their oscillatory dynamics and which can resist external perturbations. In the case of autonomous dynamical systems such processes are modeled by self-sustained autonomous oscillatory systems [10, 35, 36]. We review briefly the main properties of these systems in order to provide the background for the extension of the theory of self-sustained oscillations to the case of non-autonomous systems.

Since its introduction [36] the theory of self-sustained oscillations has been proven to be useful in the description of various phenomena [10, 35]. The main

property of self-sustained oscillations is that they do not depend on the initial conditions of the system – a system starting from any initial state (allowed within a model) approaches the regime of stable oscillations. Once the stable oscillations are established, they do not decay or change in time. In phase space, such behavior is described by the presence of an asymptotically stable, isolated closed curve – a limit cycle Γ_0. All of the system's trajectories in phase space converge to the limit cycle. The motion on the limit cycle is strictly periodic: thus if the $N-$dimensional autonomous dynamical system with a state vector $\mathbf{x} \in R^m$ is located on a limit cycle at time t, $\mathbf{x}(t) \in \Gamma_0$, then after a period T the system returns to its previous state $\mathbf{x}(t+T) = \mathbf{x}(t)$. The limit cycle has an important property: the phase space coordinate which is tangent to the limit cycle has a zero Lyapunov exponent, in contrast to all other coordinates which have negative Lyapunov exponents. Such a coordinate is called a phase, denoted as α. So perturbations to the phase neither decay nor grow in time. As a result, when a limit cycle oscillation interacts with another limit cycle oscillation, synchronization between their phases and frequencies is possible. The ability to synchronize is used as a criterion to identify limit cycle oscillations.

3.2 Chronotaxic Systems as Non-autonomous Self-sustained Oscillatory Systems

In the case of non-autonomous systems a variety of oscillations resembling autonomous self-sustained oscillations are possible. Thus, for example, the limit cycle can be time-dependent and it can change its shape and position, or the frequency of oscillations can be time-dependent. For the time being we focus on the latter case, i.e. we assume that the motion along the limit cycle is time-dependent. The period of oscillations therefore changes in time. By having the phase introduced as a coordinate on the limit cycle it is possible to characterize such oscillations by an instantaneous angular velocity $\dot{\alpha}$, which can be considered as an instantaneous oscillation frequency on the limit cycle. Such dynamics can be described by a model of limit cycle oscillations with time-dependent frequencies; but the phase in this model again has a zero Lyapunov exponent. Under external perturbations the instantaneous frequencies can be changed easily because there is no restoring force.

There is, however, an important class of stable oscillatory systems for which the oscillations have a determined frequency. The frequency of oscillations of such systems cannot easily be changed by external perturbations. Such dynamical systems can be described as non-autonomous because, in contrast to autonomous systems, it is possible to consider "limit cycle"-type oscillatory systems where all dynamical variables (including the phase) have time-dependent steady states. We propose to consider such systems as a new class [34]. These systems are non-autonomous, oscillatory and have a stable amplitude dynamics similarly to the self-sustained limit cycle, but additionally the frequency of the oscillations is stable against external perturbations. The main feature of these systems, apart from the presence of an attracting limit cycle, is that the phase has a negative Lyapunov exponent. This is provided by a point attractor which moves along

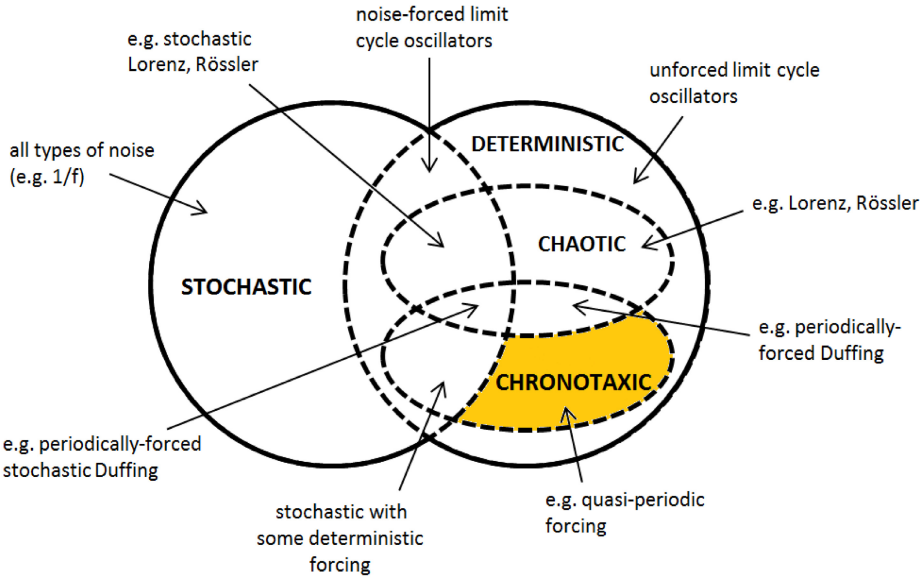

Fig. 3. Relationship between chronotaxic systems and other dynamical systems. Chronotaxic systems are innately non-stochastic and non-chaotic, being purely deterministic in nature. But they can become both stochastic, and/or chaotic, if perturbed by stochastic or chaotic influences.

the limit cycle. The attractor determines the time-dependent phase of the system. External perturbations cause the system to deviate from this phase but the frequency stays the same for a certain range of external perturbations. Thus the frequency is not easily perturbed, but it resists external perturbations. The system therefore maintains the initial unperturbed dynamics. We name these systems *chronotaxic* (*chronos* – time, *taxis* – order) [34] to emphasise their defining property which is the ability to resist perturbations and to maintain their unperturbed dynamics. Below we define these systems theoretically, analyze their properties and discuss how they can be identified.

In general, chronotaxic systems are explicitly time-dependent, non-chaotic and deterministic. They should possess the following properties: 1) Time-dependent perturbations of a self-sustained oscillatory system result in complex dynamics. 2) Under such perturbations the stability evident in the unperturbed limit cycle may be lost. Yet, chronotaxic systems are able to retain their stability through the time dependent adjustments of the initial limit cycle.

Before providing the theoretical formulation of chronotaxic systems, let us point out the position of chronotaxic systems among other dynamical systems. Fig. 3 illustrates how chronotaxic systems relate to the existing categories (e.g. deterministic, non-autonomous, dynamical systems); they possess certain features which allow us to put them in a separate class.

4 Mathematical Definition of Chronotaxic Systems

The definition of chronotaxic systems is based on non-autonomous systems. These are defined by a skew-product flow [20, 37, 38] generated by the autonomous system of unidirectionally coupled differential equations (which are also called the master-slave configuration [1], or drive and response systems [39]):

$$\begin{cases} \dot{\mathbf{p}} = \mathbf{f}(\mathbf{p}) \ , \\ \dot{\mathbf{x}} = \mathbf{g}(\mathbf{x}, \mathbf{p}) \ , \end{cases} \tag{1}$$

where $\mathbf{p} \in R^n$, $\mathbf{x} \in R^m$. The dynamics of the system $\mathbf{x}$ is non-autonomous in the sense that $\dot{\mathbf{x}} = \mathbf{g}(\mathbf{x}, \mathbf{p}(t))$. Assuming we have a solution $\mathbf{p}(t)$, the dynamics of $\mathbf{x}$ can be expressed in terms of solutions $\mathbf{x}(t, t_0, \mathbf{x_0})$, i.e. it can be reformulated as a process. Mathematically the process means a continuous mapping $(t, t_0, \mathbf{x_0}) \longmapsto \mathbf{x}(t, t_0, \mathbf{x_0}) \in R^m$ for all $(t, t_0, \mathbf{x_0}) \in R \times R \times R^m$ which satisfies the initial condition $\mathbf{x}(t_0, t_0, \mathbf{x}_0) = \mathbf{x}_0$ and the cocycle property $\mathbf{x}(t_2, t_0, \mathbf{x}_0) = \mathbf{x}(t_2, t_1, \mathbf{x}(t_1, t_0, \mathbf{x}_0))$.

The steady oscillatory dynamics of chronotaxic systems is provided by an asymptotically attracting closed isolated trajectory $\tilde{\Gamma}_0$ – a non-autonomous analog of the limit cycle – and by a steady state $\mathbf{x}^A(t)$ which moves along $\tilde{\Gamma}_0$ trajectory. By the non-autonomous analog $\tilde{\Gamma}_0$ of the limit cycle we understand a closed isolated trajectory $\tilde{\Gamma}_0$ which attracts all points in the phase space. Points move along the cycle $\tilde{\Gamma}_0$ thus representing the oscillating dynamics of the system. All coordinates of the system not tangent to the cycle $\tilde{\Gamma}_0$ are required to have a negative Lyapunov exponent. A phase α, a coordinate which is tangent to the cycle $\tilde{\Gamma}_0$, can now be introduced. However, because the system is non-autonomous, the condition that the phase α has zero Lyapunov exponent is not necessary. Thus $\tilde{\Gamma}_0$ effectively has all properties of a limit cycle in autonomous systems except that the phase on $\tilde{\Gamma}_0$ no longer has a zero Lyapunov exponent. Next, it is required that the influence from the system $\mathbf{p}$ on the system $\mathbf{x}$ results in a unique steady state $\mathbf{x}^A(t)$ which moves along $\tilde{\Gamma}_0$ trajectory. Hence, $\mathbf{x}^A(t) \in \tilde{\Gamma}_0$ for any moment of time t. Therefore, the phase of the system on the $\tilde{\Gamma}_0$ has negative Lyapunov exponent. Similarly, starting from any initial points on the limit cycle a system is attracted to a time-dependent point $\mathbf{x}^A(t)$ at time t.

Attraction at a given moment of time t rather than in the infinite future is characterised by so called pullback attraction [40, 20]: all trajectories which start at initial time $t_0 \in R$ and $\mathbf{x}_0 \in R^m$, are attracted to $\mathbf{x}^A(t)$ if one considers the limit $t_0 \to -\infty$,

$$\lim_{t_0 \to -\infty} \left| \mathbf{x}(t, t_0, \mathbf{x}_0) - \mathbf{x}^A(t) \right| = 0 \ . \tag{2}$$

Moreover, the point $\mathbf{x}^A(t)$ satisfies the condition of invariance

$$\mathbf{x}(t, t_0, \mathbf{x}^A(t_0)) = \mathbf{x}^A(t) \ . \tag{3}$$

According to properties (2) and (3) the point $\mathbf{x}^A(t)$ is the time-dependent pullback attractor. Hence, the system $\mathbf{x}$ defined in this section is chronotaxic. The motion of the point attractor $x^A(t)$ along $\tilde{\Gamma}_0$ features as a special kind of limit cycle for non-autonomous systems – a *chronotaxic limit cycle*.

Furthermore, we assume that equations (1) describe a system $\mathbf{x}$ which approaches its point attractor and moves together with it. The motion of the point attractor is defined by the system $\mathbf{p}$. Thus, it is possible to consider the system $\mathbf{p}$ as part of a bigger system $(\mathbf{x}, \mathbf{p})$, where we do not have information about $\mathbf{p}$ or it is impossible to measure it. Deviations of the system $\mathbf{x}$ from the attractor will therefore occur if its dynamics is influenced by processes external to (1).

Having formulated chronotaxic systems in mathematical terms we now summarise their properties. The fact that a limit cycle exists means that the amplitude of a chronotaxic system is sustained at a stable value in the face of external perturbations. Physically this means that the system is both thermodynamically open and has an internal source of energy. Chronotaxic systems are thus dissipative dynamical systems. In contrast to autonomous limit-cycle oscillators, the phase of oscillations can resist external perturbations within a certain range due to a point attractor which moves along the limit cycle. This also means that the frequency of oscillations is stable and cannot be substantially changed by external perturbations. The observed part of the system is also intrinsically non-autonomous, which means that its motion depends on the initial time as well as on the actual time, even when external environment is stationary. Below we provide two examples illustrating the implications of these properties.

4.1 Examples of Chronotaxic Systems

Phase dynamics Generally, the point attractor moves along the attracting time-dependent cycle $\tilde{\Gamma}_0(t)$ instead of the limit cycle $\tilde{\Gamma}_0$. For now, we restrict the discussion to the case of a stationary Γ_0. If the deviations of $\mathbf{x}$ from the limit cycle $\tilde{\Gamma}_0$ are negligible, we can focus only on phase dynamics [10]. The phase of $\mathbf{x}$ on $\tilde{\Gamma}_0$ is given by an unwrapped phase $\alpha_{\mathbf{x}}$. Its value increases by 2π after each full cycle around $\tilde{\Gamma}_0$. The phase $\alpha_{\mathbf{x}}(t, t_0, \alpha_{\mathbf{x}0})$ is defined mathematically as a mapping $\alpha_{\mathbf{x}} : R \times R \times S^1 \to R$, which satisfies the initial condition $\alpha_{\mathbf{x}}(t_0, t_0, \alpha_{\mathbf{x}0}) = \alpha_{\mathbf{x}0}$, $\alpha_{\mathbf{x}0} \in (0, 2\pi)$, and the cocycle property $\alpha_{\mathbf{x}}(t_2, t_0, \alpha_{\mathbf{x}0}) = \alpha_{\mathbf{x}}(t_2, t_1, \arg\exp[i\alpha_{\mathbf{x}}(t_1, t_0, \alpha_{\mathbf{x}0})])$, where we wrap the phase $\alpha_{\mathbf{x}}(t_1, t_0, \alpha_{\mathbf{x}0})$ on the interval $(0, 2\pi)$. The phase of the point attractor $\mathbf{x}^A$ denoted as $\alpha^A_{\mathbf{x}} \in S^1$ is an attractor for the phase $\alpha_{\mathbf{x}}$ wrapped on the interval $(0, 2\pi)$.

The description of the dynamics of the phase of $\mathbf{x}$, $\alpha_{\mathbf{x}}(t)$, which has the attractor $\alpha^A_{\mathbf{x}}$, can be simplified via the coupling of $\alpha_{\mathbf{x}}$ to a single time-dependent phase $\alpha_{\mathbf{p}}(t)$,

$$\dot{\alpha}_{\mathbf{x}} = g(\alpha_{\mathbf{x}}, \alpha_{\mathbf{p}}(t)) \,, \tag{4}$$

where $g : R \times R \to R$, and $\alpha_{\mathbf{p}} \in R$ has as angular velocity $\omega_0(t) = \dot{\alpha}_{\mathbf{p}}(t)$. We assume that the motion of the attractor $\alpha^A_{\mathbf{x}}$ is completely described by the function $\omega_0(t)$ and by a coupling function g. It is important that phase slips between $\alpha_{\mathbf{p}}$ and $\alpha_{\mathbf{x}}$ do not occur, i.e. the difference $|\alpha_{\mathbf{p}} - \alpha_{\mathbf{x}}|$ lies within a constant interval of width 2π. Then the value of $\dot{\alpha}^A_{\mathbf{x}}$ deviates slightly from $\omega_0(t)$ as $\omega_0(t)$ varies. These deviations decay when $\omega_0(t)$ is constant.

The stability of the dynamics due to a point attractor moving along a limit cycle is demonstrated in the following example. Consider only the phase dynam-

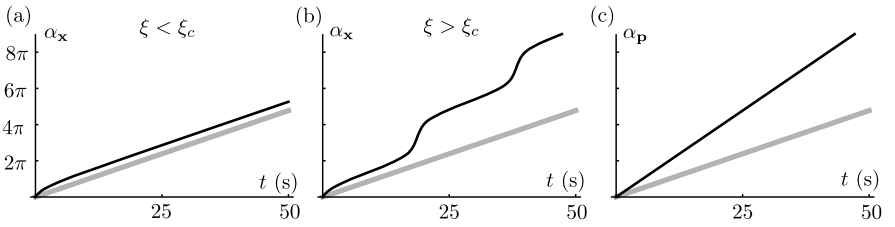

Fig. 4. The phase with unperturbed frequency $\omega_0 = 0.3$ (grey lines) and with frequency perturbed by $\xi > 0$ (black line) of three systems: (a) the chronotaxic system (5) with weak perturbations $\xi < \xi_c$, $\xi_c = 1.3$ (perturbations do not change frequencies), (b) the chronotaxic system (5) with strong perturbations $\xi > \xi_c$ (perturbations cause phase slips, $\xi = 1.35$), (c) a limit cycle self-sustained oscillator $\dot{\alpha}_{\mathbf{p}} = \omega + \xi$, $\xi = 0.3$, where frequency can easily change.

ics of a chronotaxic system described by a phase $\alpha_{\mathbf{x}}$:

$$\dot{\alpha}_{\mathbf{x}} = -\sin(\alpha_{\mathbf{x}} - \alpha_{\mathbf{p}}(t)) + \xi \,, \tag{5}$$

where $\alpha_{\mathbf{p}}(t) = \omega_0 t$, and ξ is the external perturbation. In the general case the phase $\alpha_{\mathbf{p}}(t)$ can have a more complex than linear dependence on time, and the external perturbation ξ can be time-dependent too. When $|\xi - \omega_0| < 1$ the point attractor $\alpha^A_{\mathbf{x}}(t)$ for a phase $\alpha_{\mathbf{x}}$ exists and can be found analytically: $\alpha^A_{\mathbf{x}}(t) = \alpha_{\mathbf{p}}(t) - \arcsin(\omega_0 - \xi)$. Considering for simplicity $\omega_0 > 0$, and $\xi > 0$, the point attractor exists for $\xi < \xi_c$, where $\xi_c = \omega_0 + 1$. For this case, when $\xi < \xi_c$, as is shown in Fig. 4(a), the frequency $\alpha_{\mathbf{x}}$ is not changed by external perturbations, and the phase is only slightly shifted from the unperturbed time-dependent phase. When ξ is bigger than ξ_c, phase slips occur, and the frequency is no longer stable. However when ξ is close to ξ_c, there could be a long time interval between phase slips when the perturbed frequency only slightly deviates from its unperturbed value. Such a case is shown in Fig. 4(b), where the frequencies of the perturbed and unperturbed systems are given by the gradients of the black and grey lines respectively. In Fig. 4(b) time intervals can be clearly seen where the gradient of the two lines is similar, i.e. the frequencies of the two systems are similar. These time intervals are separated by phase slips. When phase slips occur the frequency of the perturbed system changes rapidly during a short time. After a phase slip, the frequency of the perturbed system, shown in Fig. 4(b), returns to a value that is close to the frequency of the unperturbed system. When the self-sustained limit cycle oscillator without a point attractor is considered, with a phase $\alpha_{\mathbf{p}}$,

$$\dot{\alpha}_{\mathbf{p}} = \omega_0 + \xi \,, \tag{6}$$

any non-zero perturbations ξ do shift in frequency and cause the phase to drift, as is shown in Fig. 4(c).

In general ξ can represent a time-dependent perturbation $\xi(t)$. In such a case the observed behavior will be similar to that shown in Fig. 4(a) – the chronotaxic systems will resist external perturbations and the phase of the chronotaxic system will be characterized by a time-dependent attractor $\alpha^A_{\mathbf{x}}(t)$.

5 Chronotaxic Systems in Inverse Problems

In applying the theoretical aspects from the previous section to the real world an important question must be posed: how can we detect a chronotaxic system from observations? The following will detail the procedure for detecting chronotaxicity in a single time series from an observed system, as well as the restrictions for when this can be used. Later, this framework will be demonstrated by applying it to data a numerically-generated and a real-world system.

5.1 Time Series Analysis of Chronotaxic Systems

Background One of the most important issues in the analysis of any non-autonomous system is that many of the common time-independent analytical methods do not give useful information. In most cases the frequency distribution of the system is nonstationary, which means the Fourier transform contains a mixture of the power spectra at different times that becomes difficult to interpret. In addition, other representations such as probability distributions and phase space embeddings give a time-averaged view of the system that makes it appear high-dimensional and stochastic [41, 19].

The usual way of dealing with nonstationary data is to perform the same analyses but only on part of the time series by using a moving time window. This creates a number of issues, however, the first of which is that the window cannot be made infinitesimally small for discrete data. This means that it is not possible to obtain an instantaneous measure of the system localised exactly at each point. In the case of the Fourier transform a smaller window size also reduces the frequency resolution of the Fourier spectrum, which has a huge impact on the detection of low-frequency oscillations (an effect known as the Gabor limit [42]). In phase space, the system may be unable to explore all parts of the attractor and in non-autonomous systems the amount explored is time-dependent, causing distortions in the reconstructed attractor.

Fortunately, a solution to the problems of the windowed Fourier transform can be found in the wavelet transform [43],

$$W(s,t) = \int_{-L/2}^{L/2} \Psi(s, u-t)x(u)du, \tag{7}$$

where $x(t)$ is a time series of length L and $\Psi(s,t)$ is a *wavelet* stretched according to the scale s. This method calculates each frequency component using a different sized window; shorter for high-frequencies and longer for low-frequencies. Consequently, the wavelet transform is always optimised to give the best time-frequency resolution possible given the Gabor limit.

In the case of phase space analysis there is, however, no methodology to reconstruct a time-dependent attractor without some sort of "blurring", which actually occurs in two forms. The first is the simple fact that the data used in the embedding is taken from some time interval, where data at the beginning of the interval correspond to the attractor at a different time from that derived from data at the end of the interval. The second effect is more subtle as it is related to the parameters used in the time delay embedding theorem of Takens and Mañé [44, 45]. In particular, the time delay used ensures that the phase space dimensions are independent and the parameter is constant for the entire embedding. When the attractor is non-autonomous, and since the parameter is not adaptive, this means that the dependence of the dimensions may change in time, resulting in an attractor that is more blurred (time-dependent) than it actually is. At present it is therefore best that phase space should be avoided in the analysis of potentially chronotaxic systems.

Separation of Phase and Amplitude One of the requirements for chronotaxic systems is that they possess a limit cycle. The existence of a limit cycle means that the system can be transformed to polar coordinates where a phase and amplitude can be defined, which correspond respectively to the angular direction and radial distance from a reference point.

In the time-frequency domain the transformation to polar coordinates is fairly trivial. The amplitude of the system's oscillations in time is known, while the phase can be found by using a complex basis such as the Morlet wavelet. Even without a complex basis the phase can be obtained automatically from the integral of the frequency, which is known for every point in time; but all this assumes that the system oscillates at one continuous frequency in time. Rapid jumps in frequency cannot be tracked due to the time-frequency resolution limit, although this is already a condition for the existence of a point attractor in chronotaxic systems. The other restriction is that no two oscillatory components should be present at any one time as, otherwise, each oscillation requires a separate transformation to polar coordinates. The only exception to this is when the oscillations are in fact harmonics caused by nonlinearities in the system but corresponding to the same limit cycle oscillation. In this case the harmonics can actually be used to help extract the phase and amplitude in the time-frequency domain [46].

It is fairly straightforward to calculate the frequency and amplitude of a limit cycle oscillation for every point in time using the wavelet transform. This also means that the phase can be found as well since it is simply the frequency integrated over time. Doing this provides the phase dynamics, but to calculate the actual Fourier phase one must use the complex Morlet wavelets,

$$\Psi(s,t) = \frac{1}{\sqrt[4]{\pi}} \left(e^{\frac{2\pi i \omega_o t}{s}} - e^{-\frac{2\pi\omega_o^2}{2}} \right) e^{-\frac{t^2}{2s^2}}. \tag{8}$$

The phase is then $\arg(W(s,t))$.

By separating the phase and amplitude dynamics, one can test to see whether the oscillations have the properties of a chronotaxic system. In particular, the

amplitude dynamics corresponds to convergence of the system to the limit cycle, which is influenced only by a negative Lyapunov exponent and external perturbations. On the other hand the phase dynamics corresponds to convergence to the point attractor, which is also influenced by a negative Lyapunov exponent and external perturbations, but also by the motion of the point attractor itself.

Direction of Coupling Another important property of chronotaxic systems is that they can be decomposed into two parts: the driving part $\mathbf{p}$ and the driven part $\mathbf{x}$. The time-dependent dynamics of the system results from the coupling between these two parts. Unfortunately, it is usually impossible to obtain the dynamics corresponding to $\mathbf{p}$ from the phase $\alpha_{\mathbf{x}}$ while the system is perturbed. This information must instead come from another time series which contains only the dynamics of the point attractor and is not influenced by the rest of the system.

Once the phases α_{x} and α_{p} have been extracted, the next stage is to determine how they are coupled. In chronotaxic systems, the dynamics of α_{x} are influenced by a coupling to α_{p}. Because α_{p} is not dependent on any variable related to α_{x}, there should be little or no coupling in the direction from α_{x} to α_{p}. If there was a strong enough coupling in both directions then the distinction between the internal system and its environment would become uncertain.

One way of detecting couplings is to calculate the conditional mutual information (CMI) between α_{x} and α_{p} and applying the principle of Granger causality to find the information flow in each direction [29, 47–49]. However, there is always some baseline information between even two completely unrelated time series, which means surrogate data must be used to test for significance [50, 16, 19]. There is also no contraint on the form and strength of coupling in a chronotaxic system being constant in time, but the method for calculating CMI assumes that the time series is stationary. As before, the immediate solution is to perform the same analyses using a moving time window but this reduces the accuracy of the CMI, which means that even very strong couplings may not pass the significance test given by the surrogate data.

Nonetheless, in a similar way to the wavelet transform, methods can be constructed to precisely track changes in the couplings in time. Bayesian inference [51–53] can be applied to detect the change in the coupling functions between the phases of two oscillations in time [32, 33]. It assumes that the phase dynamics is described by

$$\dot{\alpha}_i = \omega_i + f_i(\alpha_i) + g_i(\alpha_i, \alpha_j) + \xi_i(t), \tag{9}$$

where ω_i is the natural frequency of the oscillation, $f_i(\alpha_i)$ is the self-coupling of the phase, $g_i(\alpha_i, \alpha_j)$ are the cross-couplings and $\xi_i(t)$ is white Gaussian noise. The coupling terms are modelled using a Fourier basis [32, 33]. The most likely combination of parameters for this basis is inferred by locating the stationary point in the negative log-likelihood function, known as maximum likelihood estimation. For inferring the coupling parameters for two phases $\alpha_{1,2}$, this function

is defined as [32]

$$S = \frac{N}{2}\ln|E| + \frac{h}{2}\sum_{n=1}^{N}(c_k^{(l)}\frac{\partial\Phi_{l,k}(\alpha_{(1,2),n})}{\partial\alpha_l} + \left[\dot{\alpha}_{i,n} - c_k^{(i)}\Phi_{i,k}(\alpha^*_{(1,2),n})\right](E^{-1})_{ij}\left[\dot{\alpha}_{j,n} - c_k^{(j)}\Phi_{j,k}(\alpha^*_{(1,2),n})\right]), \tag{10}$$

where Φ is the Fourier basis, c_k are the parameters (Fourier coefficients) of the basis, E is the correlation matrix for the noise in the two phases ($\langle\xi_i(t)\xi_j(\tau)\rangle = \delta(t-\tau)E_{ij}$). The parameters c_k are calculated from a covariance matrix Ξ and can be used to calculate the directionality index d [32]. The Bayesian theorem is applied by taking Ξ from the previous time window, known as the *posterior*, and using it as the starting point for inferring parameters for the next window, known as the *prior*. This allows information to propagate between windows, causing the inferred parameters to become more accurate with time.

Note that, up to this stage, the method still only applies to the case where the parameters are not time-varying. To account for changes in the values of the parameters, the prior must take the form of a convolution between the posterior of the previous window and a diffusion matrix which describes the change in c_k [32, 33]. The standard deviation corresponding to the diffusion of the parameters is assumed to be a known fraction of the parameters themselves, $\sigma_k = pc_k$, where p is known as the propagation constant. This modification allows the method to track the change in the couplings over time.

5.2 Application

The above methodology is now applied to the time series data of two different chronotaxic systems.

The first is a phase oscillator, which is already simulated in polar coordinates so that separation of phase and amplitude is not needed. However, the effect of noise in the system means that the oscillator does not stay on the point attractor, so identification of chronotaxic properties is nontrivial.

The second involves real data recorded from the human cardiovascular system. In this case the phases are unknown and so the analysis is performed primarily in the time-frequency domain.

Phase Oscillator Consider the chronotaxic system

$$\begin{cases}\dot{\alpha}_{\mathbf{p}} = \omega_0(t),\\ \dot{\alpha}_{\mathbf{x}} = \varepsilon\omega_0(t)\sin(\alpha_{\mathbf{x}} - \alpha_{\mathbf{p}}) + \xi\eta(t),\end{cases} \tag{11}$$

where the coupling function $\varepsilon\omega_0(t)\sin(\alpha_{\mathbf{x}}-\alpha_{\mathbf{p}})$ explicitly depends on time, while the coupling strength ε is constant. The function $\eta(t)$ is normalised white Gaussian noise with intensity D, where $\xi = \sqrt{2D} = 1.5$. When $\xi(t) = 0$, $|\varepsilon| \geq 1$ and $\omega_0(t) > 0$, a time-dependent pullback attractor $\alpha^*_{\mathbf{x}}(t)$ can be found analytically: $\alpha^*_{\mathbf{x}}(t) = \alpha_{\mathbf{p}}(t) - \arcsin(1/|\varepsilon|) + 0.5\pi(1+\mathrm{sign}(\varepsilon)) + 2\pi k$, where k is an arbitrary

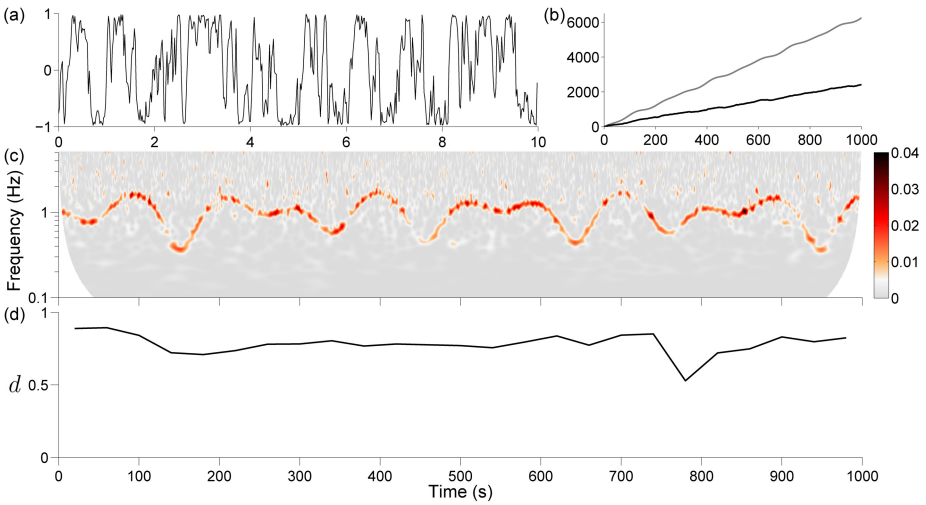

Fig. 5. Trajectory of the system (11) when under strong influence from noise ($\sigma = 5$) in relation to its time-dependent point attractor. Phase slips and perturbations due to noise for the time series $\sin(\phi)$ are shown in (a). In (b) the phase ϕ (black) is shown against the phase of the point attractor (grey). The Morlet wavelet transform power spectrum of $\sin(\phi)$ is shown in (c), revealing a continuous time-dependent frequency corresponding to the motion of the point attractor. The direction of coupling found using Bayesian inference is shown in (d) with the directionality index d taking values from -1 to 1, where positive values indicate coupling from the attractor to the oscillator and negative values indicate coupling in the opposite direction.

integer. Assuming the function $\sin(\alpha_{\mathbf{x}})$ as an observed signal from the system, we analyse its time series and present results in Fig. 5 using $\varepsilon = 1.2$ and

$$\omega_0(t) = \omega_1 \left[1 - \frac{\cos(\omega_2 t)}{3} + \frac{\cos(\omega_3 t)}{3} \right], \tag{12}$$

with $\omega_1 = 2\pi$ rad s^{-1}, $\omega_2 = 0.002$ rad s^{-1} and $\omega_3 = 0.001\ \pi$ rad s^{-1}.

Figure 5 (a) shows a sample of the complex dynamics seen in the time series $\sin(\alpha_{\mathbf{x}})$. The strength of the noise is such that the oscillator undergoes phase slips and it is not clear from Figure 5(b) that the phase is in any way coupled to the phase of the unperturbed system (i.e. $\alpha^A_{\mathbf{x}}$). Figure 5(c) provides evidence that some underlying deterministic dynamics exist in the system, where a fairly continuous line can be observed in the time-frequency domain. From the data in figure 5(d) it is clear that there is a strong coupling in the direction from the oscillator to the point attractor.

Cardiorespiratory System Time series analogous to the previous example of a coupled phase oscillator can be generated from the cardiorespiratory system.

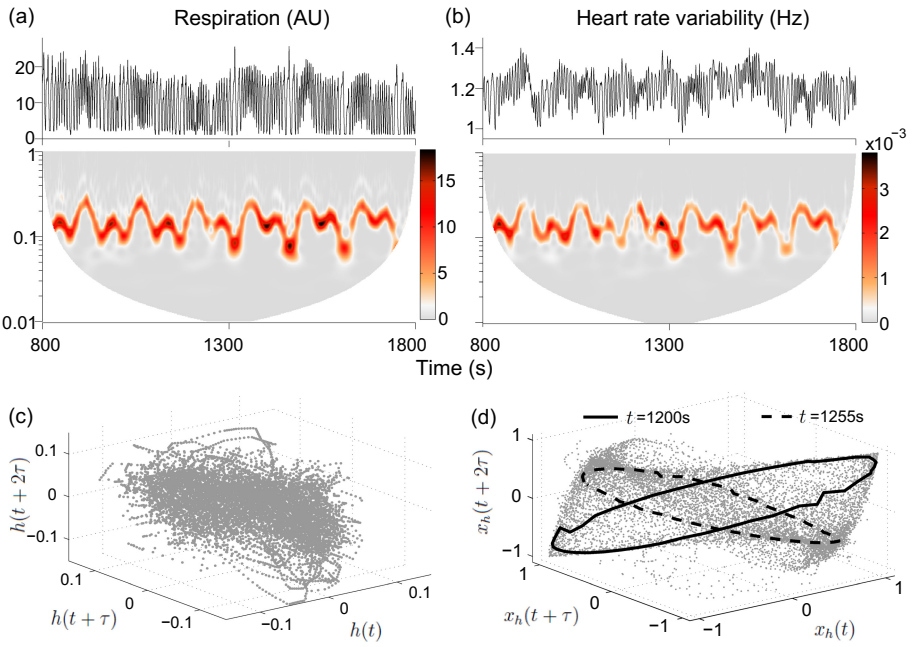

Fig. 6. Analysis of (a) respiration and (b) HRV time series of a subject whose breathing was paced quasi-periodically. In the time domain (top) the influence of the respiration can be seen as oscillations of variable amplitude and frequency. The wavelet transforms (bottom) show that these oscillations closely follow the respiration frequency. The phase space plots (c) and (d) show the time delay embedded time series of (c) detrended HRV, $h(t)$, with time delay $\tau = 1.9$ s, and (d) $x_h(t) = \cos(\alpha_h(t))$ with time delay $\tau = 1.5$ s, where $\alpha_h(t)$ is a phase of $h(t)$ which was reconstructed using nonlinear mode decomposition [46]. In (d) small parts of the embedded trajectory during time intervals $(t,\, t + 2\pi/\omega_0(t))$ reveal a time-dependent cycle. Figure modified from [34].

The electrocardiogram and respiration (measured using a stretch-sensitive belt around the chest) of a human subject were recorded for 30 minutes while they lay in a supine position. During the recording the respiration was modulated using the same function as (12) but with $\omega_1 = 0.3\pi$ rad s^{-1}, $\omega_2 = 0.0275\pi$ rad s^{-1} and $\omega_3 = 0.01325\pi$ rad s^{-1}.

Fig. 6 shows the analysis of the time series in the time-frequency domain. The wavelet transform of the heart rate variability shows the strong influence of the respiration frequency. More important, however, is that the line observed in the wavelet transform is discontinuous where some of these gaps correspond to phase slips. These would not be expected to occur if the phase of the heart rate variability did not contain an attracting point. The phase space embeddings show further evidence of chronotaxic dynamics. While the standard embedding in (c) appears to show a very complex and noisy system, the embedding after

phase and amplitude separation in (d) reveals an attractor which corresponds to a stable but time-dependent cycle.

5.3 Conclusion

Chronotaxic systems appear to be among the most challenging to analyse and interpret effectively in inverse problems. Many common forms of analysis can cause these systems to appear high-dimensional or even stochastic because the methods in question do not track time-dependent dynamics. Instead, methods such as the wavelet transform are required to separate the phase and amplitude dynamics from the time-frequency domain, allowing further analysis by methods based on Bayesian inference to extract the nature of the interactions within the system. Now that we have formulated them as a specific class of systems and defined their distinguishing properties, we expect new methods to be proposed and generally that their properties easier to identify from measured data.

6 Summary

We have introduced a new class of systems and named it chronotaxic [34] to encompass their defining properties – the ability to sustain stability in the amplitude and the time-dependent frequencies of oscillation under continuous perturbation. These systems are non-autonomous and oscillatory. We have presented a theoretical description of such systems and formulated their defining properties. We have shown how their ability to sustain stable oscillatory dynamics against external perturbation is generated by a time-dependent point attractor with oscillatory motion.

Chronotaxic systems have many potential applications. Among these are the modelling of complex systems, networks and ensembles of oscillators when not all parts of the dynamics are directly observed. The idea of chronotaxic systems was primarily motivated by the analysis of living systems, where inherently stable but time-varying characteristic frequencies were identified, and we expect them to be essential for their effective modelling.

In addition, chronotaxic systems provide a new mechanism for obtaining complex dynamics from stable deterministic dynamics. Instead of the traditional view of this type of dynamics as being stochastic, we now propose this new class of systems that categorizes them as deterministic. While the dynamics under external perturbation may look stochastic, we have demonstrated that the underlying deterministic motion of the point attractor can be extracted. Thus the complexity in the description of chronotaxic systems can be reduced, which we have illustrated using inverse problem methods. The introduction of chronotaxic systems is therefore changing the perception of what is seen as the deterministic universe. Hence, we expect many chronotaxic systems to be discovered in nature, leading to an improved understanding of their dynamical behavior.

Acknowledgements A.S. would like to warmly thank Hermann Haken for many inspiring discussions over the past two decades. Her frequent visits to the Institute of Theoretical Physics at the University of Stuttgart in the nineties were when the problem of the origin of time-varying dynamics began to be formulated and it took another decade to propose the new class of dynamical systems presented in this chapter. A.S. is also grateful to numerous collaborators and colleagues for useful discussions on time-varying, non-autonomous dynamics, too many to name them all. The work has been financially supported by various grants from the Slovenian Research Agency, UK Research Councils and the EU, and is currently supported by the Engineering and Physical Sciences Research Council (UK) [Grant No. EP/100999X1].

References

1. Haken, H.: Synergetics: An introduction and advanced topics. Springer, Berlin (2004)
2. Stefanovska, A., Bračič, M.: Physics of the human cardiovascular system. Contemp. Phys. **40**, 31–55 (1999)
3. Stefanovska, A., Lotrič M.B. Strle, S., Haken, H.: The cardiovascular system as coupled oscillators? Phisiol. Meas. **22**, 535–550 (2001)
4. Kurz, F.T., Aon, M.A., O'Rourke, B., Armoundas, A.A.: Spatio-temporal oscillations of individual mitochondria in cardiac myocytes reveal modulation of synchronized mitochondrial clusters. PNAS **107**, 14315–14320 (2010)
5. Kurz, F.T., Aon, M.A., O'Rourke, B., Armoundas, A.A.: Wavelet analysis reveals heterogeneous time-dependent oscillations of individual mitochondria. Am. J. Physiol. **299**, H1736–H1740 (2010)
6. Rudrauf, D., Douiri, A., Kovach, C., Lachaux, J.P., Cosmelli, D., Chavez, M., Adam, C., Renault, B., Martinerie, J., Van Quyen, M.L.: Frequency flows and the time-frequency dynamics of multivariate phase synchronization in brain signals. Neuroimage **31**, 209–227 (2006)
7. Friston, K.: A free energy principle for biological systems. Phys. Rep. **14**, 2100–2121 (2012)
8. Konstantinov, D., Chepelianskii, A.D., Kono, K.: Resonant Photovoltaic Effect in Surface State Electrons on Liquid Helium. J. Phys. Soc. Jpn. **81**, 093601 (2012)
9. Buchli, J., Righetti, L., Ijspeert, A.J.: Engineering entrainment and adaptation in limit cycle systems - From biological inspiration to applications in robotics. Biol. Cybern. **95**, 645–664 (2006)
10. Kuramoto, Y.: Chemical Oscillations, Waves, and Turbulence. Springer-Verlag, Berlin (1984)
11. Acebron, J.A., Bonilla, L.L., Vicente, C.J.P., Ritort, F., Spigler, R.: The Kuramoto model: A simple paradigm for synchronization phenomena. Rev. Mod. Phys. **77**, 137–185 (2005)
12. Craster, R.V., Matar, O.K.: Dynamics and stability of thin liquid films. Rev. Mod. Phys. **81**, 1131–1198 (2009)
13. Breakspear, M., Heitmann, S., Daffertshofer, A.: Generative models of cortical oscillations: neurobiological implications of the Kuramoto model. Front. Hum. Neurosci. **4**, 190 (2010)
14. Petkoski, S., Stefanovska, A.: Kuramoto model with time-varying parameters. Phys. Rev. E **86**, 046212 (2012)

15. Stefanovska, A., Bračič, M., Kvernmo, H.D.: Wavelet analysis of oscillations in the peripheral blood circulation measured by laser Doppler technique. IEEE Trans. Bio. Med. Eng. **46**, 1230–1239 (1999)
16. Shiogai, Y., Stefanovska, A., McClintock, P.V.E.: Nonlinear dynamics of cardiovascular ageing. Phys. Rep. **488**, 51–110 (2010)
17. Iatsenko, D., Bernjak, A., Stankovski, T., Shiogai, Y., Owen-Lynch, P.J., Clarkson, P.B.M., McClintock, P.V.E., Stefanovska, A.: Evolution of cardiorespiratory interactions with age. Phil. Trans. R. Soc. A **371**, 20110622 (2013)
18. Clemson, P. Roberts, S., Owen-Lynch, J., McClintock, P.V.E., Stefanovska, A.: Oscillations in endothelial cells and ion channel dynamics. In: Proc. ESGCO 2010, Berlin (2010)
19. Clemson, P.T., Stefanovska, A.: The dynamical systems approach to turbulence as an inverse problem. sumbitted to Phys. Rep. (2013)
20. Kloeden, P.E., Rasmussen, M.: Nonautonomous Dynamical Systems. American Mathematical Soc., Providence (2011)
21. Vishik, M.I., Chepyzhov, V.V.: Filter banks allowing perfect reconstruction. Math. Notes **51**, 622–624 (1992)
22. Crauel, H., Flandoli, F.: Attractors for random dynamical systems. Prob. Theory Rel. Fields **100**, 365–393 (1994)
23. Romeiras, F., Grebogi, C., Ott, E.: Multifractal properties of snapshot attractors of random maps. Phys. Rev. A **41**, 784–799 (1990)
24. Bretherton, C.S., Widmann, M., Dymnikov, V.P., Wallace, J.M., Blade, I.: The effective number of spatial degrees of freedom of a time-varying field. J. Climate **12**, 1990–2009 (1999)
25. Chekroun, M.D., Simonnet, E., Ghil, M.: Stochastic climate dynamics: Random attractors and time-dependent invariant measures. Physica D **240**, 1685–1700 (2011)
26. Saermark, K., Ashkenazy, Y., Levitan, J., Lewkowicz, M.: The necessity for a time local dimension in systems with time-varying attractors. Physica A **236**, 363–375 (1997)
27. Stam, C.J.: Nonlinear dynamical analysis of EEG and MEG: Review of an emerging field. Clin. Neurophysiol. **116**, 2266–2301 (2005)
28. de Oliveira, P.M.C.: Why do evolutionary systems stick to the edge of chaos. Theory Biosci. **120**, 1–19 (2001)
29. Jamšek, J., Paluš, M., Stefanovska, A.: Detecting couplings between interacting oscillators with time-varying basic frequencies: Instantaneous wavelet bispectrum and information theoretic approach. Phys. Rev. E **81**, 036207 (2010)
30. Sheppard, L.W., Stefanovska, A., McClintock, P.V.E.: Detecting the harmonics of oscillations with time-variable frequencies. Phys. Rev. E **83**, 016206 (2011)
31. Sheppard, L.W., Stefanovska, A., McClintock, P.V.E.: Testing for time-localised coherence in bivariate data. Phys. Rev. E **85**, 046205 (2012)
32. Stankovski, T., Duggento, A., McClintock, P.V.E., Stefanovska, A.: Inference of time-evolving coupled dynamical systems in the presence of noise. Phys. Rev. Lett. **109**, 024101 (2012)
33. Duggento, A., Stankovski, T., McClintock, P.V.E., Stefanovska, A.: Dynamical Bayesian inference of time-evolving interactions: From a pair of coupled oscillators to networks of oscillators. Phys. Rev. E **86**, 061126 (2012)
34. Suprunenko, Y.F., Clemson, P.T., Stefanovska, A.: Chronotaxic systems: A new class of self-sustained non-autonomous oscillators. Phys. Rev. Lett. **111**, 024101 (2013)
35. Pikovsky, A., Rosenblum, M., Kurths, J.: Synchronization - A Universal Concept in Nonlinear Sciences. Cambridge University Press, Cambridge (2001)

36. Andronov, A.A., Vitt, A.A., Khaikin, S.E.: The Theory of Oscillators. Pergamon Press, Oxford (1966)
37. Kloeden, P.E., Kozyakin, V.S.: The perturbation of attractors of skew-product flows with a shadowing driving system. Dis. Cont. Dyn. Sys. **7**, 883–893 (2001)
38. Kloeden, P.E., Lorenz, T.: Mean-square random dynamical systems. J. Diff. Eqns. **253**, 1422–1438 (2012)
39. Kocarev, L., Parlitz, U.: Generalized synchronization, predictability, and equivalence of unidirectionally coupled dynamical systems. Phys. Rev. Lett. **76**, 1816–1819 (1996)
40. Kloeden, P.E.: Pullback attractors in nonautonomous difference equations. J. Difference Eqns. Appl. **7**, 883–893 (2001)
41. Clemson, P., Stefanovska, A.: Time series analysis of turbulent and nonautonomous systems. In: AIP Conf. Proc. 1468, Let's Face Chaos Through Nonlinear Dynamics: 8th International Summer School/Conference, pp. 69–81. AIP, Melville (2012)
42. Gabor, D.: Theory of communication. J. IEEE **93**, 429–457 (1946)
43. Kaiser, G.: A Friendly Guide to Wavelets. Birkhäuser, Boston (1994)
44. Takens, F.: Detecting strange attractors in turbulence. In: Rand, D.A., Young, L.S. (eds.) Lecture notes in Mathematics, vol. 898, pp. 366–381. Springer, New York (1981)
45. Mãńe, R.: On the dimension of the compact invariant sets of certain non-linear maps. In: Rand, D.A., Young, L.S. (eds.) Lecture notes in Mathematics, vol. 898, pp. 230–242. Springer, New York (1981)
46. Iatsenko, D., Stefanovska, A., McClintock, P.V.E.: Nonlinear mode decomposition: a noise-robust, adaptive, decomposition method based on the synchrosqueezed wavelet transform. arXiv:1207.5567 [math.NA] (2013)
47. Paluš, M., Stefanovska, A.: Direction of coupling from phases of interacting oscillators: An information-theoretic approach. Phys. Rev. E **67**, 055201 (2003)
48. Paluš, M.: From nonlinearity to causality: statistical testing and inference of physical mechanisms underlying complex dynamics. Contemp. Phys. **48**, 307–348 (2007)
49. Vejmelka, M., Paluš, M.: Inferring the directionality of coupling with conditional mutual information. Phys. Rev. E. **77**, 026214 (2008)
50. Paluš, M.: Detecting phase synchronization in noisy systems. Phys. Lett. A **235**, 341–351 (1997)
51. Smelyanskiy, V.N., Luchinsky, D.G., Stefanovska, A., McClintock, P.V.E.: Inference of a nonlinear stochastic model of the cardiorespiratory interaction Phis. Rev. Lett. **94**, 098101 (2005)
52. Luchinsky, D.G., Smelyanskiy, V.N., Duggento, A., McClintock, P.V.E.: Inferential framework for nonstationary dynamics. I. Theory. Phys. Rev. E **77**, 061105 (2008)
53. Duggento, A., Luchinsky, D.G., Smelyanskiy, V.N., Khovanov, I., McClintock, P.V.E.: Inferential framework for nonstationary dynamics. II. Application to a model of physiological signaling. Phys. Rev. E **77**, 061106 (2008)

Coarse-Grained Order Parameter Dynamics of the Synergetic Computer and Multistable Perception in Schizophrenia

Till D. Frank and Dobromir G. Dotov

Department of Psychology, Center for the Ecological Study of Perception and Action, University of Connecticut, 406 Babbidge Road, Storrs, CT, 06269, USA
till.frank@uconn.edu
http://psych.uconn.edu/faculty/frank.php

Abstract. The synergetic computer that has originally been developed as an algorithm for pattern recognition has also been used in the life sciences as a model for various self-organizing perceptual processes. Coarse-graining of the order parameter equations of the synergetic computer is discussed for sets of to-be-perceived patterns that vary in the degree to which they can be distinguished from each other. Coarse-gaining is exploited to conduct a model-based analysis on literature data of multistable perception under schizophrenia as tested in motion-induced blindness (MIB) experiments. The analysis not only supports earlier suggestions that schizophrenia reduces the occurrence frequency of the MIB effect but also suggests that the perceptual system of schizophrenia patients is characterized by a greater degree of asymmetry.

Keywords: multistable perception, schizophrenia, synergetic computer, motion-induced blindness

1 Introduction

The synergetic computer is an algorithm for pattern recognition [1]. The algorithm is based on self-organization principles and has been developed within the framework of synergetics [2]. Although the algorithm has been developed to solve pattern recognition problems [1, 3–7], it has been generalized and applied in various related, interdisciplinary fields. In particular, the algorithm has been generalized to allow for hierarchical pattern recognition processes [8]. Economic and industrial applications in the field of settlement dynamics [9, 10], job assignment problems and robotics [11–17], and signal transmission via message buffer [18] have been addressed. Although the synergetic computer describes an artifical associative memory or decision-making system, due to its roots in synergetics and the theory of self-organization, the synergetic computer has also been regarded as a benchmark model for self-organizing psychological processes and self-organizing motor control system. In this context, oscillatory phenomenon induced by certain perceptual [19, 20], and auditory [21, 22] stimuli have been

A. Pelster and G. Wunner (eds.), *Selforganization in Complex Systems: The Past, Present, and Future of Synergetics*, Understanding Complex Systems,
DOI: 10.1007/978-3-319-27635-9_15

discussed and application to priming [23, 24], grasping [25, 26], and motor development during infancy [27, 28] can be found in the literature.

The pattern recognition algorithm is a winner-takes-all system that for a given initial stimulus pattern converges to a fixed point solution indicating the perception of a stored prototype pattern. The algorithm can be discussed from the perspective of the to-be-perceived and stored patterns. Alternatively, the algorithm can be studied from the perspective of the pattern amplitudes. In line with the fact that the synergetic computer is considered as a computational or artificial self-organizing system mimicking natural self-organizing systems, the amplitudes have typically been considered as order parameters [1, 29, 30].

Let ξ_k denote the order parameters of $k = 1, \ldots, N$ patterns. We consider the order-parameter dynamics of the synergetic computer in the following form [1]

$$\frac{\mathrm{d}}{\mathrm{d}t}\xi_k = \xi_k \left(\lambda - B \sum_{m \neq k, m=1}^{N} \xi_m^2 - C \sum_{m=1}^{N} \xi_m^2 \right) \tag{1}$$

with $\lambda, B, C > 0$. Equation (1) can be cast into a form that is convenient for conducting a stability analysis of fixed points in the generalized case that will be considered in Section 3 when the attention parameter λ depends on the pattern index [7, 23–27]. Accordingly, Eq. (1) can equivalently be expressed by $\mathrm{d}\xi_k/\mathrm{d}t = \xi_k(\lambda - g\, C \sum_{m \neq k, m=1}^{N} \xi_m^2 - C\xi_k^2)$, where we have introduced the coupling parameter $g = 1 + B/C > 1$. The parameter C can be put to $C = 1$ without loss of generality such that

$$\frac{\mathrm{d}}{\mathrm{d}t}\xi_k = \xi_k \left(\lambda - g \sum_{m \neq k, m=1}^{N} \xi_m^2 - \xi_k^2 \right) . \tag{2}$$

Alternatively, the parameter λ and the order parameters ξ_k may be rescaled by $\sqrt{C}$ and the rescaled equations are considered [26]. Solutions of Eq. (2) under initial conditions $\xi_k(0) \geq 0$ will be considered, which implies that all order parameters remain semi-positive definite for all times (i.e., $\xi_k(t) > 0 \; \forall t \geq 0$).

In what follows, we will derive order parameter equations on several levels of coarse-graining. The ideas that will be developed below are closely related to the ideas developed in earlier studies on hierarchical generalizations of the order parameter equations of the synergetic computer [8].

2 Approximative coarse-grained order parameter dynamics

In Section 2.1, we will consider first a special case that will be used in Section 3 in the application for multistable perception of schizophrenia. Subsequently, in section 2.2, the general case will be discussed.

2.1 Special case

In this section, it is assumed that all patterns $k = 2, \ldots, N$ possess a common feature that is not present in the 'default' pattern $k = 1$. In this special case, we consider the course-grained order parameter U defined by

$$U = \sqrt{\sum_{s \in I_U} \xi_s^2} \tag{3}$$

with the index set $I_U = \{2, \ldots, N\}$. Due to the 'winner-takes-all' property of the synergetic computer (see Section 1) it follows that if one of the order parameters ξ_k^* with $k^* \in I_U$ becomes finite in the stationary case, then $U = \xi_k^* > 0$. If the order parameter ξ_1 of the default pattern becomes finite in the stationary case, then $U = 0$.

Before exploiting the definition (3), it is useful to cast the order parameter equations (2) of the synergetic computer in yet another form. Eq. (2) can be written like

$$\frac{\mathrm{d}}{\mathrm{d}t}\xi_k = \xi_k \left(\lambda - g \sum_{m=1}^{N} \xi_m^2 - (1-g)\xi_k^2 \right) , \tag{4}$$

where the mixed term contains the sum of all squared order parameters. Note that in Eq. (4) the cubic term ξ_k^3 actually has a positive coefficient because of $g > 1$ (or since $-(1-g) = B > 0$ holds using $C = 1$ again). Substituting the definition (3) into Eq. (4), we obtain

$$\begin{aligned} \frac{\mathrm{d}}{\mathrm{d}t}\xi_1 &= \xi_1 \left(\lambda - g[U + \xi_1^2] - (1-g)\xi_1^2 \right) , \\ \frac{\mathrm{d}}{\mathrm{d}t}U &= U \left(\lambda - g[U + \xi_1^2] \right) - (1-g)\frac{1}{U} \sum_{s \in I_U} \xi_s^4 . \end{aligned} \tag{5}$$

In the stationary case, we have either $U = \xi_k^* > 0$ and $\xi_{j \neq k^*} = 0$ if a pattern $k^* \in I_U$ is selected or $U = 0$, $\xi_{k \in I_U} = 0$, $\xi_1 > 0$. In both cases, the dynamical system (5) for ξ_1 and U exhibits the same stationary fixed points as the coupled dynamical system

$$\begin{aligned} \frac{\mathrm{d}}{\mathrm{d}t}\xi_{1,a} &= \xi_{1,a} \left(\lambda - g[U_a + \xi_{1,a}^2] - (1-g)\xi_{1,a}^2 \right) , \\ \frac{\mathrm{d}}{\mathrm{d}t}U_a &= U_a \left(\lambda - g[U_a + \xi_{1,a}^2] - (1-g)U_a^2 \right) \end{aligned} \tag{6}$$

for the variables $\xi_{1,a}$ and U_a. Note that Eq. (6) assumes the form of the order parameter equations of the synergetic computer again. The question arises to what extent the variables $\xi_{1,a}$ and U_a can be regarded as useful approximations to the order parameter ξ_1 and the coarse-grained order parameter U.

In this context, we first note that the expression U^4 reads

$$U^4 = \left[\sum_{s \in I_U} \xi_s^2 \right]^2 = \sum_{s \in I_U} \xi_s^4 + \text{mixed terms of the form } \left(\xi_i^2 \xi_{j \neq i}^2 \right)_{i,j \in I_U} . \tag{7}$$

Consequently, Eq. (5) reads

$$\frac{\mathrm{d}}{\mathrm{d}t}\xi_1 = \xi_1\left(\lambda - g[U+\xi_1^2] - (1-g)\xi_1^2\right) \ ,$$
$$\frac{\mathrm{d}}{\mathrm{d}t}U = U\left(\lambda - g[U+\xi_1^2] - (1-g)U^2\right)$$
$$+\text{mixed 3rd order terms of the form } \frac{1}{U}\left(\xi_i^2\xi_{j\neq i}^2\right)_{i,j\in I_U} \ . \qquad (8)$$

As indicated the mixed terms are considered third order terms because the products of order 4 are divided with the variable U that depends linearly on the scales of the variables $\xi_{k\in I_U}$.

The dynamical systems (6) and (8) differ by the mixed terms occurring in the U-dynamics of the model (8). In order to assess the relevance of these terms, we apply a concept from psychophysics: the 'just noticeable difference' (JND) of sensations [31]. We assume that all patterns under consideration differ from each other by a distance measure D that will not be specified in detailed. For a human observer the patterns under consideration differ such that they can be distinguished from each other. In this sense, for all pairs of patterns the distance measure D is larger than a certain threshold that corresponds to the JND.

Mathematically speaking, we assume that the initial conditions are such that the order parameters ξ_k differ at $t=0$ by a certain amount that reflects the distance D between the patterns and accounts for the aforementioned requirement that the sensation patterns (stimuli) under consideration differ at least by the JND. We distinguish between two cases.

Case I: It is assumed that patterns with a JND induce relative large differences between the initial values $\xi_k(0)$ of the order parameters. Accordingly, we assume that

$$\exists k^* \ : \ \forall j \neq k^* \ : \ \xi_{k^*}(0) \gg \xi_j(0) \ . \qquad (9)$$

In this case, the order parameter ξ_k^* of the pattern k^* will not only win the selection process defined by Eq. (4) but the mixed terms in the U-dynamics of Eq. (8) will be negligibly small at all times relative to the U^3 term:

$$\forall t \geq 0 \ : \ U^3(t) \gg \text{mixed 3rd order terms of the form } \frac{1}{U(t)}\left(\xi_i^2(t)\xi_{j\neq i}^2(t)\right)_{i,j\in I_U} \ .$$

If Eqs. (10) holds, then the dynamical systems (6) and (8) exhibit approximately the same transient and stationary solutions. Consequently, the model (6) involving the variable U_a is a good approximative model for the original order parameter model (4) of the synergetic computer. In particular, in the limiting case $\xi_{j\neq k*}(0)/\xi_k^*(0) \to 0$ a point-wise convergence $\xi_{1,a}(t) \to \xi_1(t)$ and $U_a(t) \to U(t)$ holds at any time point t provided that we use the consistent initial conditions $\xi_{1,a}(0) = \xi_1(0)$ and $U_a(0) = U(0)$. An illustration is shown in Fig. 1AB.

Case II: It is assumed that patterns with a JND induce differences between order parameters $\xi_k(0)$ that are scaled to the size of the set of patterns and are at least of the magnitude $\sqrt{N-1}$. More precisely, we assume that

$$\exists k^* \ : \ \forall j \neq k^* \ : \ \xi_{k^*}(0) > \xi_j(0)\sqrt{N-1} \ . \qquad (10)$$

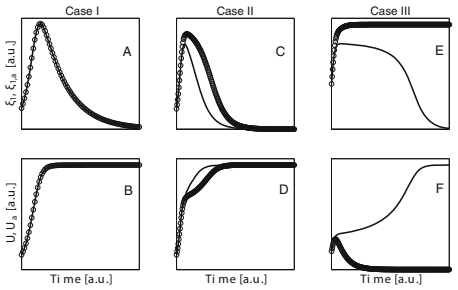

Fig. 1. Illustrations of solutions for case I (A,B), II (C,D), III (E,F) initial conditions. Solutions of Eq. (4) (solid lines) and Eq. (6) (circles) are shown under consistent initial condition: $\xi_{1,a}(0) = \xi_1(0)$, $U_a(0) = U(0)$. See text for details. Parameters: $N = 10$, $\lambda = 2.0$, $g = 1.3$. Case I initial conditions: $\xi_5(0) = 0.2$, $\xi_{j\neq 5}(0) = 0.2/\sqrt{(N-1)}/10/(1+0.1\epsilon)$. Case II: $\xi_5(0) = 0.2$, $\xi_{j\neq 5}(0) = 0.2/\sqrt{(N-1)}/(1+0.2\epsilon)$. Case III: $\xi_1(0) = 0.25$, $\xi_{j\neq 1}(0) = 0.2 + 0.01\epsilon$. In all cases, ϵ was uniformly distributed in $[0, 1]$.

Let us distinguish between the two sub-cases that $k^* \in I_U$ and $k^* \notin I_U$ (i.e., $k^* = 1$). If $k^* \in I_U$ then the original order parameter dynamics will converge to a fixed point with $\xi_{k^*} > 0$ such that in the stationary case $U(st) = \xi_{k^*}(st)$ holds. Moreover, it follows that $U(0) > \xi_{k^*}(0) > \xi_1(0)$. Consequently, if the dynamical system (6) is considered under consistent initial conditions (i.e., $\xi_{1,a}(0) = \xi_1(0)$ and $U_a(0) = U(0)$), then U_a converges to the finite stationary value $U_a(st) = U(st) = \xi_{k^*}(st) > 0$ of the original dynamical system (4) and $x_{1,a}(t)$ converges to zero consistent with the stationary behavior of ξ_1: $\xi_{1,a}(st) = \xi_1(st) = 0$. In contrast, if $k^* = 1$ then the original selection equation dynamics (4) converges to the fixed point with $\xi_1 > 0$ and $U = 0$. In addition, it follows that

$$U^2(0) = \sum_{s\in I_U} \xi_s^2(0) < \sum_{s\in I_U} \frac{\xi_1^2(0)}{N-1} = \xi_1^2(0) \;\Rightarrow U(0) < \xi_1(0)\;. \tag{11}$$

If, again, the dynamical system (6) is considered under consistent initial conditions (i.e., $\xi_{1,a}(0) = \xi_1(0)$ and $U_a(0) = U(0)$), then U_a converges to the stationary value $U_a(st) = U(st) = 0$ and $x_{1,a}(t)$ converges to its finite fixed point value consistent with the stationary behavior of ξ_1: $\xi_{1,a}(st) = \xi_1(st) > 0$. In summary, if condition (10) is satisfied, then the dynamical system (6) involving the variable U_a exhibits the same stationary behavior than the original selection equation model (4) provided that both dynamical systems are considered under consistent initial conditions. Figure 1CD exemplifies solutions of the dynamical systems (4) and (6) for this case.

In view of the fact that in the two aforementioned cases the performance of the dynamical model (6) is consistent in the stationary case with the original order parameter equation model (4) and given that both models exhibit formally the same mathematical structure, we will consider in what follows the coupled differential equations (6) involving the variables $\xi_{1,a}$ and U_a as the (approxima-

tive) coarse-grained order parameter equation model of the original synergetic computer model (4) (or (1)) involving the variables $\xi_1, \ldots, \xi_N$.

Finally, let us consider the general case in which neither of the two conditions described above are satisfied.

Case III: If the conditions considered in cases I and II are not satisfied, then the dynamical model (6) may exhibit solutions that are inconsistent with the order parameter dynamics (4) even if both dynamical models are solved under consistent initial conditions. Let us prove this statement by an example. Let $\xi_1(0) = b > 0$ and $\xi_{k \in I_U}(0) = a > 0$ with $b > a$. For these initial conditions the original pattern recognition algorithm (4) converges to a fixed point with $\xi_1(st) > 0$ and $\xi_k = 0$ for $k \in I_U$ indicating that the default pattern $k = 1$ is recognized. Next, we consider the special case in which the distance D between the default pattern $k = 1$ and the other patterns $k \geq 2$ is not that large such that if the default pattern is presented we have $b > a$ but $b^2 < (N-1)a^2$. That is, the condition of case II is violated. From $b^2 < (N-1)a^2$ it follows that $U(0)^2 = (N-1)a^2 > a^2 = \xi_1^2(0)$. In other words, although for $b > a$ and $b^2 < (N-1)a^2$ the condition $\xi_1(0) > \xi_k(0)$ holds for any $k \neq 1$, we have $U(0) > \xi_1(0)$. Consequently, if we solve the coarse-grained selection equations (6) under consistent initial conditions ($\xi_{1,a}(0) = \xi_1(0)$ and $U_a(0) = U(0)$), then $U_a(t)$ converges to a finite stationary value $U_a(st) > 0$ and $x_{1,a}(t)$ converges to zero in the stationary case. The coarse-grained dynamical model (6) indicates that one of the patterns $k \geq 2$ was recognized, which is in contradiction with the recognition process described by the original selection equations (4). Figure 1EF illustrates this case.

In summary, we have considered the special case in which the set of N patterns under considerations exhibits a distinct default pattern and $N-1$ patterns that constitute a class of non-default patterns. On a coarse-grained level, we considered the order parameters x_1 and U that describe whether a pattern is recognized as the default pattern ($\xi_1(st) > 0$) or as a pattern belonging to the class of non-default patterns ($U(st) > 0$). It was shown that for this special case a dynamical model for the variables $\xi_{1,a}$ and U_a can be derived (see Eq. (6)) that under certain circumstances behave approximatively in the same way as ξ_1 and U, respectively. More precisely, if patterns are considered that differ at least by a JND that induces (i) a relative large gap or (ii) at least a gap of $\sqrt{N-1}$ in the spectrum of initial amplitudes $\xi_k(0)$, then in the stationary case the coarse-grained order parameter dynamics involving $\xi_{1,a}$ and U_a yields consistent results with the fine-grained dynamics of $\xi_1, \ldots, \xi_N$. This implies that the pattern selection made by the two dynamical systems is consistent. Under the condition (i) the two dynamical models exhibit also approximatively the same transient solutions. If neither of the two gap conditions (i) and (ii) are satisfied, then the two models may yield inconsistent results. These considerations are summarized schematically in Table 1.

Importantly, the two dynamical models for the approximative coarse-grained order parameters $\xi_{1,a}$ and U_a and for the fine-grained order parameters $\xi_1, \ldots, \xi_N$ exhibit formally the same mathematical structure.

Table 1. Correspondence of fine- and coarse grained dynamics

Case	'JND' impact	Initial conditions	Fine- & coarse-grained
I	Large gap	$\exists k^* : \forall j \neq k^* :$ $\xi_{k^*}(0) \gg \xi_j(0)$	Consistent transient and stationary solutions
II	Moderate gap	$\exists k^* : \forall j \neq k^* :$ $\xi_{k^*}(0) > \sqrt{N-1}\,\xi_j(0)$	Consistent stationary solutions
III	Gap conditions I and II not satisfied		Stationary solutions may or may not be consistent

2.2 General case

Let us consider M levels of coarse-graining $L \in \{1, .., M\}$. The first level ($L = 1$) contains N_1 patterns. To each pattern an order parameter $\xi_{k,1}$ is assigned that is used to indicate whether the pattern is recognized. On the second level, patterns are grouped together such that there are $N_2 < N_1$ pattern classes. To each pattern class a coarse-grained order parameter $\xi_{k,2}$ is assigned that is used to indicate whether a pattern out of the class is recognized. In general, each level exhibits N_L pattern classes (with $N_1 > N_2 > \cdots > N_M$) that are described by N_L coarse-grained order parameters $\xi_{k,L}$. For the sake of simplicity, the patterns of level $L = 1$ and the corresponding amplitudes $\xi_{k,1}$ will be treated as if they were pattern classes and pattern class amplitudes, respectively.

At this stage, it is useful to introduce the index sets $I_{k,L+1} \subset \{1, \ldots, N_L\}$. The index set $I_{k,L+1}$ contains all the pattern class indices j from the coarse-grained level L that are grouped together to the class k of the level $L + 1$. For example, the index set I_U discussed in Section 2.1 becomes $I_{k=2,L=2} = \{2, \ldots, N\}$. The sets satisfy $\forall k \neq j\ ,\ k, j \in \{1, \ldots, N_{L+1}\}\ :\ I_{k,L+1} \cap I_{j,L+1} = \emptyset$ and $\cup_{k=1}^{N_{L+1}} I_{k,L+1} = \{1, \ldots, N_L\}$. In words, all sets belonging to a particular level of coarse-graining are mutually disjunct and the unification of all sets of a coarse-graining level $L + 1$ gives the index set of all pattern classes of the previous level L. In analogy to Eq. (3), coarse-grained order parameters $\xi_{k,L+1}$ are defined iteratively by

$$\xi_{k,L+1} = \sqrt{\sum_{s \in I_{k,L+1}} \xi_{s,L}^2}\ . \tag{12}$$

Let us assume that for a particular level L of coarse-graining the selection equations for $\xi_{k,L}$ assume the form of the order parameter equations of the synergetic computer. In analogy to Eq. (4), we consider the selection equations

$$\frac{\mathrm{d}}{\mathrm{d}t}\xi_{k,L} = \xi_{k,L}\left(\lambda - g\sum_{m=1}^{N_L}\xi_{m,L}^2 - (1-g)\xi_{k,L}^2\right) \tag{13}$$

for $k \in \{1, \ldots, N_L\}$. Proceeding as in Section 2.1, we use

$$\sum_{m=1}^{N_L} \xi_{m,L}^2 = \sum_{k=1}^{N_{L+1}} \left(\sum_{s \in I_{k,L+1}} \xi_{s,L}^2 \right) = \sum_{m=1}^{N_{L+1}} \xi_{m,L+1}^2 \, . \tag{14}$$

Differentiating Eq. (12) with respect to time t and substituting Eqs. (13) and (14) into the resulting equation, we obtain in analogy to Eq. (5) the following result

$$\frac{\mathrm{d}}{\mathrm{d}t}\xi_{k,L+1} = \xi_{k,L+1} \left(\lambda - g \sum_{m=1}^{N_{L+1}} \xi_{m,L+1}^2 \right) - (1-g) \frac{1}{\xi_{k,L+1}} \sum_{s \in I_{k,L+1}} \xi_{s,L}^4 \tag{15}$$

for $k \in \{1, \ldots, N_{L+1}\}$. Using the same line of arguments as in Section 2.1, the most right standing term in Eq. (15) can be expressed in terms of $\xi_{k,L+1}$ and mixed terms of the form $\xi_{i,L}^2 \xi_{j,L}^2$ with $i \neq j$. Consequently, in analogy to Eq. (8), Eq. (15) can be cast into the form

$$\begin{aligned} \frac{\mathrm{d}}{\mathrm{d}t}\xi_{k,L+1} = \xi_{k,L+1} & \left(\lambda - g \sum_{m=1}^{N_{L+1}} \xi_{m,L+1}^2 - (1-g)\xi_{k,L+1}^2 \right) \\ & + \text{mixed 3rd order terms } \frac{1}{\xi_{k,L+1}} \left(\xi_{i,L}^2 \xi_{j \neq i,L}^2 \right)_{i,j \in I_{k,L+1}} \, . \end{aligned} \tag{16}$$

Neglecting the third order mixed terms, we obtain a coupled set of approximate selection equations of the coarse-grained level $L+1$ that read

$$\frac{\mathrm{d}}{\mathrm{d}t}\xi_{k,L+1} = \xi_{k,L+1} \left(\lambda - g \sum_{m=1}^{N_{L+1}} \xi_{m,L+1}^2 - (1-g)\xi_{k,L+1}^2 \right) \tag{17}$$

and just assumes the form of the order parameter equations of the previous level L, see Eq. (13).

Finally, we assume that the patterns under consideration exhibit a JND that induces gap conditions as discussed in cases I and II of Section 2.1 for the initial amplitudes $\xi_{k,L}(0)$ on all coarse-grained levels L. Under these conditions, the mixed third order terms in Eq. (16) can be neglected (Case I) or affect the transient dynamics only to a relatively small degree which implies that the approximate selection equations (17) of the level $L+1$ yield consistent results with the selection equations (13) of the level L (Case II).

Let us exemplify the relationship between the selection equations (13) and (17) on subsequent levels L and $L+1$ of coarse-graining. For illustration purposes it is sufficient to consider just two levels $M = 2$ and a set of $N_1 = 4$ patterns on $L = 1$ that is reduced to $N_2 = 2$ pattern classes on the level $L = 2$. Furthermore, the patterns $k = 1, 2$ and $k = 3, 4$ on $L = 1$ are assumed to constitute the pattern classes $k = 1$ and $k = 2$ on $L = 2$. That is, we have $I_{1,2} = \{1, 2\}$ and $I_{2,2} = \{3, 4\}$.

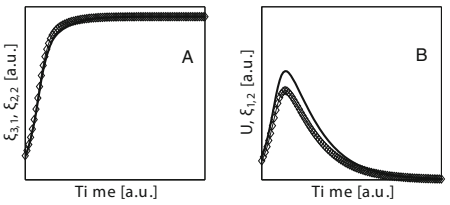

Fig. 2. $\xi_{1,2}$ (panel A) and $\xi_{2,2}$ (panel B) computed from Eqs. (18) and (19) (solid lines) and Eq. (20) (circles) for consistent Case II conditions with $\xi_{3,1}(0) = 0.2$, $\xi_{j\neq 3}(0) = 0.2/\sqrt{(N-1)}/(1+0.2\epsilon)$, ϵ uniformly distributed in $[0,1]$, and $N = 4$, $\lambda = 2$, $g = 1.3$.

For $L = 1$ the order parameter equations for $\xi_{k,1}$ with $k = 1, 2, 3, 4$ read

$$\frac{\mathrm{d}}{\mathrm{d}t}\xi_{k,1} = \xi_{k,1}\left(\lambda - g\sum_{m=1}^{N_L}\xi_{m,L}^2 - (1-g)\xi_{k,1}^2\right) \tag{18}$$

and the coarse-grained order parameters on the level $L = 2$ are defined by

$$\xi_{1,2} = \sqrt{\xi_{1,1}^2 + \xi_{2,1}^2}\ , \quad \xi_{2,2} = \sqrt{\xi_{3,1}^2 + \xi_{4,1}^2}\ . \tag{19}$$

Under Case I and II initial conditions, the coarse-grained order parameters on level $L = 2$ satisfy at least approximately the selection equations

$$\begin{aligned}\frac{\mathrm{d}}{\mathrm{d}t}\xi_{1,2} &= \xi_{1,2}\left(\lambda - g[\xi_{1,2}^2 + \xi_{2,2}^2] - (1-g)\xi_{1,2}^2\right)\ ,\\ \frac{\mathrm{d}}{\mathrm{d}t}\xi_{2,2} &= \xi_{2,2}\left(\lambda - g[\xi_{1,2}^2 + \xi_{2,2}^2] - (1-g)\xi_{2,2}^2\right)\ .\end{aligned} \tag{20}$$

Under case I initial conditions $\exists\, k^* \ :\ \xi_{k^*,1}(0) \gg \xi_{j\neq k^*,1}(0)$ the solutions of the coarse-grained differential equations (20) are good approximations to the exact solutions calculated from Eqs. (18) and (19) provided consistent initial conditions $\xi_{2,1}(0) = \sqrt{\xi_{1,1}^2(0) + \xi_{2,1}^2(0)}$ and $\xi_{2,2}(0) = \sqrt{\xi_{3,1}^2(0) + \xi_{4,1}^2(0)}$ are used. In order to illustrate this correspondence, we solved Eqs. (18), (19), and (20) numerically, see Figure 2.

3 Motion-induced blindness and schizophrenia

Motion-induced blindness is an optical illusion produced by a visual stimulus composed of a fixed stationary foreground pattern and a rotating background pattern. Typically, the foreground pattern consists of three yellow dots arranged in a triangle, whereas the background pattern is a rotating array (or grid) of blue dots. A human observer exposed to the MIB stimulus typically reports that some of the target dots disappear for a while. In this sense, the motion of the background pattern induces a temporary blindness with respect to the target pattern [32].

3.1 Modeling of fine- and coarse-grained order parameter dynamics

We distinguish between 8 spatio-temporal patterns on the level $L = 1$ that fall into two classes on the coarse-grained level $L = 2$. There is one perceptual pattern not subjected to a MIB effect (i.e., the three yellow target dots are perceived), which is regarded as the default pattern indexed by $k = 1$ on $L = 1$. The default pattern constitutes its own class on $L = 2$ Moreover, there are 7 different patterns that are subjected to a MIB effect (i.e., at least one dot is perceived as being absent). They are indexed by $k = 2, \ldots, 8$ on $L = 1$. and constitute the class of 'incomplete patterns' on $L = 2$. On $L = 2$ the default pattern is index by $k = 1$ and the incomplete patter class is index by $k = 2$. Following earlier work on selective attention phenomena [1, 4], certain oscillatory phenomena of the perceptual [19, 20] and auditory system [21, 22], priming [23, 24], grasping [25, 26], and child development [27, 28], we assume that in general the attention parameters of the two classes are different from each other. In this case, the evolution equations for $L = 1$ and $L = 2$ read

$$\frac{\mathrm{d}}{\mathrm{d}t}\xi_{k,1} = \xi_{k,1}\left(\lambda_{k,1} - g\sum_{m=1,m\neq k}^{N}\xi_{m,1}^2 - \xi_{k,1}^2\right) \quad , \quad k = 1, \ldots, 8 \tag{21}$$

and

$$\frac{\mathrm{d}}{\mathrm{d}t}\xi_{1,2} = \xi_{1,2}\left(\lambda_{1,2} - g\,U^2 - \xi_{1,2}^2\right) \ , \ \frac{\mathrm{d}}{\mathrm{d}t}U = U\left(\lambda_U - g\,\xi_{1,2}^2 - U^2\right) \tag{22}$$

with $\lambda_{1,1} = \lambda_{1,2}$ and $\lambda_{k,2} = \lambda_U$ for $k = 2, \ldots, 8$. The coarse-grained order parameter variables $\xi_{1,2}$ and U are related to the fine-grained order parameters $\xi_{1,1}, \ldots, \xi_{8,1}$ as discussed in the Section 2 with $\xi_{1,2} \leftrightarrow \xi_{1,1}$ and $U \leftrightarrow \sqrt{\sum_{k=2}^{8}\xi_{k,1}^2}$.

The stability of the winner-takes-all fixed points $\xi_{k^*,1} = \sqrt{\lambda_{k*,1}} \wedge \xi_{j\neq k^*,1} = 0$ of Eq. (21) and $(\xi_{1,2} = \sqrt{\lambda_{1,2}}\ ,\ U = 0)$, $(\xi_{1,2} = 0\ ,\ U = \sqrt{\lambda_U})$ for Eq. (22) depend on the attention parameter spectrum. The stability of fixed points of the synergetic computer in the case of an inhomogeneous attention parameter spectrum has been discussed in detail in a series of studies [7, 23–27]. From these studies it follows that for the default pattern the stability depends on $\lambda_{1,2}$, λ_U, and g like

$$\left.\begin{array}{l}\xi_{1,1} = \sqrt{\lambda_{1,2}} \ \wedge \ \xi_{k\geq 2,1} = 0 \\ \xi_{1,2} = \sqrt{\lambda_{1,2}} \ \wedge \ U = 0\end{array}\right\} = \begin{cases}\text{stable} & \text{if } \lambda_{1,2} > \lambda_U/g \\ \text{unstable} & \text{if } \lambda_{1,2} < \lambda_U/g\end{cases} . \tag{23}$$

By analogy, for the incomplete patterns we have

$$\left.\begin{array}{l}\exists\, k^* \geq 2 \ : \ \xi_{k^*,1} = \sqrt{\lambda_U} \ \wedge \ \xi_{j\neq k^*,1} = 0 \\ \xi_{1,2} = 0 \ \wedge \ U = \sqrt{\lambda_U}\end{array}\right\} = \begin{cases}\text{stable} & \text{if } \lambda_U > \lambda_{1,2}/g \\ \text{unstable} & \text{if } \lambda_U < \lambda_{1,2}/g\end{cases} . \tag{24}$$

In what follows, we will primarily focus on the coarse-grained model. The oscillatory switching between the default pattern and a pattern out of the class of incomplete patterns can be modeled by assuming that the attention parameters

$\lambda_{1,2}$ and λ_U vary in time [18–22]. More precisely, we assume that if the default pattern is perceived then $\lambda_{1,2}$ decays gradually until the critical ratio $\lambda_{1,2} = \lambda_U/g$ is reached at which the percept becomes unstable, see Eq. (23). Consequently, the perceptual dynamics is subjected to a bifurcation and the perceptual experience of the default pattern is replaced by the percept of one of the incomplete patterns. However, the percept is assumed to induce again a decay in the corresponding attention parameter. That is, λ_U is assumed to decay gradually, while $\lambda_{1,2}$ relaxes back to a 'rest level of attention'. Among various possible dynamical systems that are able to capture these mechanisms, we will use the following evolution equations for the attention parameter dynamics:

$$\frac{\mathrm{d}}{\mathrm{d}t}\lambda_{1,2} = -\frac{1}{\tau}(\lambda_{1,2}(t) - b_{1,2}) \ , \quad \frac{\mathrm{d}}{\mathrm{d}t}\lambda_U = -\frac{1}{\tau}(\lambda_U(t) - b_U) \tag{25}$$

with

$$\begin{aligned} b_{1,2} = 0 \ \wedge \ b_U = b_0 \ \text{ if } \ \xi_{1,2} = \sqrt{\lambda_{1,2}} \ \wedge \ U = 0 \\ b_{1,2} = b_0 \ \wedge \ b_U = 0 \ \text{ if } \ \xi_{1,2} = 0 \ \wedge \ U = \sqrt{\lambda_U} \ , \end{aligned} \tag{26}$$

where b_0 denotes the aforementioned rest level and $\tau > 0$ is a time constant.

Our aim is to investigate the oscillatory dynamics (22), (25), (26) in a special case which allows for a semi-analytical approach. To this end, we note that the parameter τ defines the characteristic time scale of the attention parameter dynamics. Likewise, $1/\lambda_{1,2}$ and $1/\lambda_U$ define the characteristic time scale of the dynamics of $\xi_{1,2}$ and U. Let $\lambda_{c,low}$ and $\lambda_{c,high}$ with $\lambda_{c,low} > \lambda_{c,high} = g\lambda_{c,low}$ denote the critical attention parameters at which percept-switching occurs. Then $\lambda_{1,2}$ and λ_U oscillate between these levels. Consequently, $\xi_{1,2}(t)$ and $U(t)$ evolve on a time scale at least as fast as given by $1/\lambda_{c,low}$. If $\lambda_{c,low}$ is chosen large enough (the value of $\lambda_{c,low}$ depends on the model parameters b and g) such that $1/\lambda_{c,low}$ is much shorter than τ, then the $\xi_{1,2}(t)$ and $U(t)$ are fast evolve variables, whereas the attention parameters $\lambda_{1,2}(t)$ and $\lambda_U(t)$ are slowly evolving variables. Figure 3 illustrates this case. In this case, the oscillation period can be calculated from the attention parameter dynamics alone. Moreover, differences in the transient behavior of the fine- and coarse-grained dynamics become irrelevant as long as both levels of consideration yield consistent results in the stationary case (case II, see Table 1).

In order to derive an expression for the oscillation period, we consider the case in which λ_U decays from $\lambda_{c,high}$ towards zero and $\lambda_{1,2}$ relaxes back towards b_0:

$$\begin{aligned} \lambda_{1,2} &= \lambda_{c,low} \exp\left\{-\frac{t}{\tau}\right\} + b_0 \left(1 - \exp\left\{-\frac{t}{\tau}\right\}\right) \ , \\ \lambda_U &= \lambda_{c,high} \exp\left\{-\frac{t}{\tau}\right\} \ . \end{aligned} \tag{27}$$

This phase will be terminated when $\lambda_{1,2} = \lambda_{c,high}$ and $\lambda_U = \lambda_{c,low}$. The duration of the phase corresponds to half of the oscillation period. Therefore, at $t = T/2$

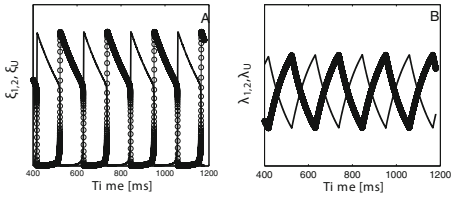

Fig. 3. Oscillatory behavior of the order parameters (panel A) $\xi_{1,2}$ (solid), ξ_U (circles) and attention parameters (panel B) $\lambda_{1,2}$ (solid), λ_U (circles) for $\tau = 100$ms, $g = \exp\{1\}$, $b_0 = g + 1$ as computed from Eqs. (22), (25), (26). Note that the observed period is $T \approx 2\tau$ as expected.

we have

$$\lambda_{c,high} = \lambda_{c,low} \exp\left\{-\frac{T}{2\tau}\right\} + b_0 \left(1 - \exp\left\{-\frac{T}{2\tau}\right\}\right) ,$$
$$\lambda_{c,low} = \lambda_{c,high} \exp\left\{-\frac{T}{2\tau}\right\} . \tag{28}$$

Substituting $\lambda_{c,high} = g\lambda_{c,low}$ into the second relation of Eq. (28), we can determine T as a function of g and τ like $T = 2\tau \ln(g)$. Substituting $\lambda_{c,high} = g\lambda_{c,low}$ into the first relation of Eq. (28), we then obtain a relationship between the parameters b_0 and g:

$$b_0 = g + 1 . \tag{29}$$

This relation tells us that the scenario described above can not be realized for any arbitrary values of g and b_0. Rather, the model parameters must satisfy the matching condition (29). Eliminating b_0 by means of Eq. (29), the model defined by Eqs. (22), (25), (26) involves two unknown parameters g and τ. If we fix one of the two parameters, then the remaining parameter can be estimated from the experimentally observed oscillation period T_{obs}. In this context, a particular simple model can be constructed if we put $g = e$ (where $e = \exp\{1\}$). In this case, we have $T = 2\tau$, and the model parameter τ can be estimated from the observed oscillation period T_{obs} like $\tau_{estim} = T_{obs}/2$.

Let us generalize the model in order to account for the fact that in MIB experiments the default percept and the incomplete percepts are not necessarily perceived for the same amount of time. That is, in general, the MIB paradigm involves perceptual oscillations composed of two phases with unequal durations. In order to introduce two phases with different phase durations, we include a bias in the dynamical model defined by Eqs. (22), (25), (26). To this end, Eq. (22) is replaced by

$$\frac{\mathrm{d}\xi_{1,2}}{\mathrm{d}t} = \xi_{1,2}\left(\lambda_{1,2} + \frac{\delta}{2} - g\,U^2 - \xi_{1,2}^2\right) , \quad \frac{\mathrm{d}U}{\mathrm{d}t} = U\left(\lambda_U - \frac{\delta}{2} - g\,\xi_{1,2}^2 - U^2\right) . \tag{30}$$

For $\delta > 0$ the duration of the phase with $\xi_{1,2} > 0$ and $U = 0$ becomes longer than the duration of the phase with $\xi_{1,2} = 0$ and $U > 0$. According to our

interpretation of the model, we say that for $\delta > 0$ there is a bias towards perceiving the default pattern. Likewise, for $\delta < 0$ the model reflects a perceptual systems exhibiting a bias towards the perception of an incomplete pattern. If we consider the parsimony model defined by Eqs. (25), (26), and (30) with fixed parameters $g = \exp\{1\}$ and $b_0 = g + 1$, then we have two parameters τ and δ at our disposal to model experimentally observed durations of the phase of default pattern perception and the phase of incomplete pattern perception.

3.2 Schizophrenia patients data versus controls

Schizophrenia patients frequently show deficits in the perceptual processing of visual stimuli. In particular, perceptual processes are affected that involve higher cognitive functions such as feature binding [33–36]. On the other hand, there is evidence that the MIB phenomenon involves such higher cognitive processes and does not arise from low hierarchical processes like retinal suppression. For example, visual aftereffects that are assumed to emerge on a relative low hierarchical level of sensory processes are induced by the target dots of the MIB stimulus although these dots are not perceived by the observers [37, 38]. In other words, there is experimental evidence that when a target dot is not perceived by an observer then the sensory stimuli of the target dot is still processed in low hierarchical levels of the perceptual system but it is not processed ('correctly') on higher cognitive levels involved in consciousness and sensory experiences that are explicit to the observer. This point of view is also supported by experimental studies that point out the similarity between the MIB phenomenon and other Gestalt theoretical phenomena such as perceptual filling-in [39]. In summary, higher cognitive functions are relevant both for the MIB phenomenon and our understanding of schizophrenia, which makes the MIB phenomenon a promising paradigm to investigate schizophrenia [40].

In a study by Tschacher et al. [40] controls and schizophrenia patients were tested on the MIB phenomenon. Both groups were exposed to three trials of 60 seconds. On the average, the number of total MIB experiences within these three minutes was about 42 for controls and 29 for patients (see Table 3 in [40]). In what follows we distinguish between total and single event durations. The total durations of the MIB experiences was about 42 seconds for controls and 33 seconds for patients. From these data we can obtain a crude measure for the duration of a single MIB event. For controls we obtain a single MIB duration of about $T_{\mathrm{MIB}} = 1.0$s (i.e., 42sec/42). For patients we obtain a single MIB event duration duration of about $T_{\mathrm{MIB}} = 1.1$s (i.e., 33sec/29). Likewise, we can calculate a crude measure for how long on average the perception of a default pattern was experience before it became unstable (single event duration). Controls perceived the default pattern on the average for a total period of 138 seconds. Assuming (in line with our simplified model) that there were on average 42 switches to the default percept, we obtain an estimated single event duration of $T_{\mathrm{default}} = 3.3$s (i.e., 138sec/42). Likewise, for patients we obtain a single event duration of the default pattern of about $T_{\mathrm{default}} = 4.5$s (i.e., 147sec/33). In view of Eq. (30), we anticipate that a model-based analysis of the data should reveal that the

Table 2. Descriptive experimental data and model parameters

	Data		Model	
Group	T_{default} [ms]	T_{MIB} [ms]	τ [ms]	δ [1/ms]
Controls	3300	1000	1500	1.6
Patients	4500	1100	1700	1.8

parameter δ is larger for schizophrenia patients because the asymmetry of the durations of the MIB and non-MIB phases is more pronounced.

We fitted the model parameters δ and τ to reproduce the duration data T_{MIB} and T_{default} for controls and patients. To this end, τ was varied in the interval $[T_{\text{default}}, T_{\text{MIB}}]$ in steps of 100 ms, while δ was varied in the interval $[0, 2.0]$ 1/ms in steps of 0.1. The results of this fitting procedure are summarized in Table 2. As expected, we found that the asymmetry parameter δ is larger for schizophrenia patients than for controls.

4 Discussion

We studied coarse-graining of order parameter equations of the synergetic computer and followed in part earlier studies on hierarchical generalizations of the synergetic computer concept [8]. In particular, we showed that under certain conditions the coarse-grained order parameter equations exhibit the same mathematical structure as the corresponding fine-grained order parameter equations. In this sense, self-organizing artificial and natural systems, whose dynamics can be described (at least to some approximation) by the synergetic computer equations, exhibit a scale free system dynamics. A model-based analysis of literature data on multistable perception of schizophrenia patients tested in an MIB experiment was carried out. The observation that the frequency of MIB experiences is lower for schizophrenia patients than for controls corresponds in the model to a time scale parameter τ that is larger for schizophrenia patients than for controls. In addition, the model-based analysis highlights a second perceptual characteristics of schizophrenia patients that has so far received only little attention. The two different perceptual phases in MIB experiments seem to be less symmetric in duration under schizophrenia. This shows up as a symmetry breaking parameter δ which is larger for schizophrenia patients than for controls.

References

1. Haken, H.: Synergetic computers and cognition. Springer, Berlin (1991)
2. Haken, H.: Synergetics: Introduction and advanced topics. Springer, Berlin (2004)

3. Haken, H.: Nonequilibrium phase transitions in pattern recognition and associative memory. Z. Physik B **70**, 121–123 (1988)
4. Fuchs, A., Haken, H.: Pattern recognition and associative memory as dynamical processes in a synergetic system. I. Translational invariance, selective attention and decomposition of scene. Biol. Cybern. **60**, 17–22 (1988)
5. Fuchs, A., Haken, H.: Pattern recognition and associative memory as dynamical processes in a synergetic system. II. Decomposition of complex scenes, simultaneous invariance with respect to translation, rotation, and scaling. Biol. Cybern. **60**, 107–109 (1988)
6. Daffertshofer, A., Haken, H.: A new approach to recognition of deformed patterns. Pattern Recognition **27**, 1697–1705 (1994)
7. Frank, T.D.: New perspectives on pattern recognition algorithm based on Haken's synergetic computer network. In: Fournier, M.D. (ed.) Perspective on Pattern Recognition, chap. 7, pp. 153–172. Nova Publ., New York (2011)
8. Daffertshofer, A., Haken, H.: Adaptive hierarchical structures. In: Mira, J., Sandoval, F. (eds.) From Natural to Artifical Neural Computation. Lecture Notes in Computer Science, vol. 930, pp. 76–84. Springer, Berlin (1995)
9. Daffertshofer, A., Haken, H., Portugali, J.: Self-organized settlements. Environ. Plann. B **28**, 89–102 (2001)
10. Daffertshofer, A.: How do ensembles occupy space? Eur. Phys. J. Special Topics **157**, 79–91 (2008)
11. Starke, J., Schanz, M., Haken, H.: Treatment of combinatorial optimization problems using selection equations with cost terms. Part II. Physica D **134**, 242–252 (1999)
12. Starke, J., Kaga, T., Schanz, M., Fukuda, T.: Experimental study on self-organized and error resistant control of distributed autonomous robotic systems. Int. J. Robotics Research **24**, 465–486 (2005)
13. Starke, J., Schanz, M.: Dynamical system approaches to combinatorial optimization. In: Du, D.Z., Pardalos, P. (eds.) Handbook of Combinatorial Optimization, vol. 2, pp. 471–524. Kluwer Academic Publisher, Dordrecht (1998)
14. Starke, J., Ellsaessar, C., Fukuda, T.: Self-organized control in cooperative robots using a pattern formation principle. Phys. Lett. A **375**, 2094–2098 (2011)
15. Haken, H.: Decision making and optimization in regional planning. In: Beckmann, M., Hohannsson, B., Snickars, F., Thord, R. (eds.) Knowledge and Networks in a Dynamic Economy, pp. 25–40. Springer, Berlin (1998)
16. Haken, H., Schanz, M., Starke, J.: Treatment of combinatorial optimization problems using selection equations with cost terms. Part I. Physica D **134**, 227–241 (1999)
17. Frank, T.D.: Multistable selection equations of pattern formation type in the case of inhomogeneous growth rates: with applications to two-dimensional assignment problems. Phys. Lett. A **375**, 1465–1469 (2011)
18. Frank, T.D.: Rate of entropy production as a physical selection principle for mode-mode transitions in non-equilibrium systems: with an application to a non-algorithmic dynamic message buffer. European Journal of Scientific Research **54**, 59–74 (2011)
19. Ditzinger, T., Haken, H.: Oscillations in the perception of ambigious patterns: a model based on synergetics. Biol. Cybern. **61**, 279–287 (1989)
20. Ditzinger, T., Haken, H.: Impact of fluctuations on the recognition of ambiguous patterns. Biol. Cybern. **63**, 453–456 (1990)
21. Ditzinger, T., Tuller, B., Kelso, J.A.S.: Temporal patterning in an auditory illusion: the verbal transformation effect. Biol. Cybern. **77**, 23–30 (1997)

22. Ditzinger, T., Tuller, B., Haken, H., Kelso, J.A.S.: A synergetic model for the verbal transformation effect. Biol. Cybern. **77**, 31–40 (1997)
23. Frank, T.D.: On a multistable competitive network model in the case of an inhomogeneous growth rate spectrum with an application to priming. Phys. Lett. A **373**, 4127–4133 (2009)
24. Frank, T.D.: Psycho-thermodynamics of priming, recognition latencies, retrieval-induced forgetting, priming-induced recognition failures and psychopathological perception. In: Hsu, N., Schütt, Z. (eds.) Psychology of Priming, chap. 9, pp. 175–204. Nova Publ., New York (2012)
25. Frank, T.D., Richardson, M.J., Lopresti-Goodman, S.M., Turvey, M.T.: Order parameter dynamics of body-scaled hysteresis and mode transitions in grasping behavior. J. Biol. Phys. **35**, 127–147 (2009)
26. Lopresti-Goodman, S.M., Turvey, M.T., Frank, T.D.: Behavioral dynamics of the affordance "graspable". Attention, Perception, and Psychophysics **73**, 1948–1965 (2011)
27. Frank, T.D., van der Kamp, J., Savelsbergh, G.J.P.: On a multistable dynamic model of behavioral and perceptual infant development. Dev. Psychobiol. **52**, 352–371 (2010)
28. Frank, T.D.: Motor development during infancy: a nonlinear physics approach to emergence, multistability, and simulation. In: Columbus, A.M. (ed.) Advances in Psychology Research, vol. 83, chap. 9, pp. 143–160. Nova Publ., New York (2011)
29. Bestehorn, M., Haken, H.: Associative memory of a dynamical system: an example of the convection instability. Z. Physik B **82**, 305–308 (1991)
30. Frank, T.D.: Multistable pattern formation systems: candidates for physical intelligence. Ecological Psychology **24**, 220–240 (2012)
31. Smeets, J.B.J., Brenner, E.: Grasping Weber's law. Current Biology **18**, R1089–R1090 (2008)
32. Bonneh, Y.S., Cooperman, A., Sagi, D.: Motion-induced blindness in normal observers. Nature **411**, 798–801 (2001)
33. Rabinowicz, E.M., Opler, L.A., Owen, D.R., Knight, R.A.: Dot enumeration perceptual organization task (DEPOT): evidence for a short-term visual memory deficit in schizophrenia. J. Abnormal Psychology **105**, 336–348 (1996)
34. Uhlhaas, P.J., Silverstein, S.M.: The continuing relevance of Gestalt psychology for an understanding of schizophrenia. Gestalt Theory: An International Multidisciplinary Journal **25**, 256–279 (2003)
35. Uhlhaas, P.J., Silverstein, S.M.: Perceptual organization in schizophrenia spectrum disorders: empirical research and theoretical implications. Psychological Bulletin **131**, 618–632 (2005)
36. Tschacher, W.: How specific is the Gestalt-informed approach to schizophrenia. Gestalt Theory: An International Multidisciplinary Journal **26**, 335–344 (2004)
37. Hofstoetter, C., Koch, C., Kiper, D.C.: Motion-induced blindness does not affect the formation of negative afterimages. Consciousness and Cognition **13**, 691–708 (2004)
38. Montaser-Kouhsari, L., Moradi, F., Zandvakili, A., Esteky, H.: Orientation-selective adaptation during motion-induced blindness. Perception **33**, 249–254 (2004)
39. Hsu, L.C., Yeh, S.L., Kramer, P.: Linking motion-induced blindness to perceptual filling-in. Vision Research **44**, 2857–2866 (2004)
40. Tschacher, W., Schuler, D., Junghan, U.: Reduced perception of the motion-induced blindness illusion in schizophrenia. Schizophrenia Research **81**, 261–267 (2006)

Part IV

History

Hermann Haken – His Roadmap to Synergetics

Bernd Kröger

Im Schönblick 13, 72076 Tübingen, Germany
drberndkroeger@t-online.de

Abstract. During the last sixty years Hermann Haken has made numerous contributions to the scientific endeavor, not only to physics. We focus on the time from 1950 to 1983. This includes his early years at Erlangen University, where Haken was concentrating on solid-state physics. Then he developed the quantum-mechanical theory of the laser with the members of his "Stuttgart School" during the years 1962 to 1967.
At the end of this period he and his student Robert Graham could show that the laser is an example of a nonlinear system far from thermal equilibrium that shows a phase transition-like behavior. This led to the formulation of Synergetics in 1970. Influenced by his tremendous knowledge of the laser and the role of fluctuations in systems far from thermal equilibrium Haken then developed the mathematical tools for Synergetics, especially the generalized Ginzburg-Landau equations and the slaving principle.

Keywords: Haken biography, synergetics history, self-organization, laser, non-equilibrium phase transition, Elmau conferences, Versailles conferences

Hermann Haken was born on the 12th July 1927 in Leipzig. The place was by chance because his parents lived in the nearby town of Halle where Hermann later on also went to school in the "Oberschule der Francke'schen Stiftungen". Due to a long lasting chronical illness he was not recruited by the army and studied mathematics at the University of Halle in the period 1946 – 1948. It was the time following the Second World War and the city of Halle was part of the Soviet occupation zone. So, after his first examinations passed, his parents decided that Hermann should move to relatives living in Nuremberg, which was part of the American occupation zone and continue his studies at the nearby University of Erlangen. In 1951 he finished his PhD in mathematics [1] and in 1952 got a position at the Institute of Theoretical Physics.

Experimental physics at Erlangen was focused on what is now called solid-state physics. There existed a close connection to the researchers of the SIEMENS AG and its nearby research laboratory at Pretzfeld. Here, the famous physicist Walter Schottky and his colleague Eberhard Spenke worked since the time when the laboratory had been moved from Berlin during the war in 1943. Spenke wanted to write a book about semiconductors and asked Hermann Haken to help him with the theoretical quantum mechanical part [2]. Haken especially

A. Pelster and G. Wunner (eds.), *Selforganization in Complex Systems: The Past, Present, and Future of Synergetics*, Understanding Complex Systems,
DOI: 10.1007/978-3-319-27635-9_16

studied the work of Vladimir Fock about the second quantization and, as he remembers, *"I learned the whole methodology of the so called quantum field theory. And by that I was one of the first physicists that applied this method to problems of solid state and semiconductor physics"* [3]. His own research concentrated on the theory of electron-hole pairs, the so called excitons. Here Haken learned the fundamentals from the famous book of Herbert Fröhlich "Elektronentheorie der Metalle" [4]. Fröhlich, a German theoretical physicist with Jewish roots, was assistant of Arnold Sommerfeld and had to flee from Germany in 1933. Since 1948 he occupied the chair of theoretical physics at the University of Liverpool. After finishing his postdoctoral thesis [5] and writing several papers on the exciton theory Haken got an invitation from Herbert Fröhlich for a three-months visit at his institute in Liverpool. This was the beginning of a lifelong friendship. Fröhlich visited Haken regularly at the University of Stuttgart as guest professor during the 1960s and 1970s and was essential for Haken's participation at the first Versailles conferences (see later).

Back home in Erlangen an invitation from Cornell University as guest professor for the winter term 1959/60 dropped in. Being in the United States Haken again received an invitation, this time from the famous Bell Telephone Laboratories in Murray Hill. This is why Hermann Haken went there in spring 1960, where he met his friend and colleague Wolfgang Kaiser. He introduced him to the then hot debated topic about the possible realization of a laser. But before the publication of Theodore Maiman appeared in August [6], Haken had to go back to Germany. He had been offered the chair of theoretical physics at the Technische Hochschule Stuttgart, which he finally accepted in November 1960. His knowledge of the quantum mechanical field theory played a decisive role in his appointment:

"Dr. Haken is one of the leading young theoretical physicists working in the field of solid-state physics. He has achieved international recognition for his work on excitons in nonmetallic crystals. He is the only German theoretician who, in problems of solid-state physics, successfully applies the general methods of quantum-mechanical field theory."[1]

In Stuttgart Hermann Haken immediately concentrated on the theoretical investigation of the new phenomenon of the laser[2]. Together with one of his first students, Herwig Sauermann, he developed a semi-classical approach of the Laser theory in 1963. Only some months later, in a seminal paper submitted in July 1964 [7] he formulated a nonlinear quantum mechanical version of the theory. The main purpose of this paper was

"to bridge the gap between linear and nonlinear theories of laser action. As we have shown linear theories represent a very good approximation at small in-

[1] Cited from "Antrag des Berufungsausschusses (Nachfolge Prof. Fues) an den Großen Senat der Technische Hochschule Stuttgart vom 12. Januar 1960" (Personalakte Haken, Universitätsarchiv Stuttgart) (translation by the author).

[2] An account of the race to the theoretical understanding of the laser between Hermann Haken and his Stuttgart School and the American researchers Willis Lamb, Marvin Scully and Melvin Lax is given in another paper of the author (to be published).

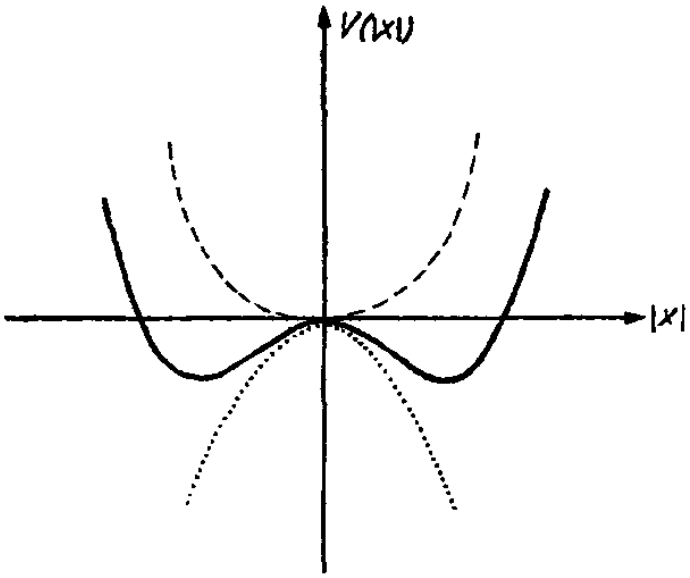

Fig. 1. Plot of "potential energy" versus light amplitude. Dashed curve below threshold (linear and nonlinear theory); dotted curve above threshold, linear theory leads to instability; solid curve above threshold, nonlinear theory [7].

version. On the other hand there is a marked threshold beyond which the system behaves qualitatively very differently from below threshold, its amplitude oscillating around a stable value".

For the first time Haken could show that the laser light changes its quality at the threshold. Below threshold it consists of numerous different single light waves, whereas above threshold a single nearly indefinitely long coherent wave is obtained.

"In contrast to linear theories there exists a marked threshold. Below it the amplitude decreases after each excitation exponentially and the linewidth turns out to be identical with those of previous authors. [. . .] Above the threshold the light amplitude converges towards a stable value, whereas the phase undergoes some kind of undamped diffusion process".

Only in a nonlinear theory, where also the effects of the heatbath to which the laser is coupled are taken into account, the different behavior of the light shows up. Haken used the picture of a potential plot to visualize the difference, see Fig. 1. The linear theory only shows an unstable value for the light amplitude above threshold whereas in the nonlinear treatment a symmetry-breaking occurs (leading to a bifurcation) and two stable attractors arise. Looking back to this paper Haken states [8]

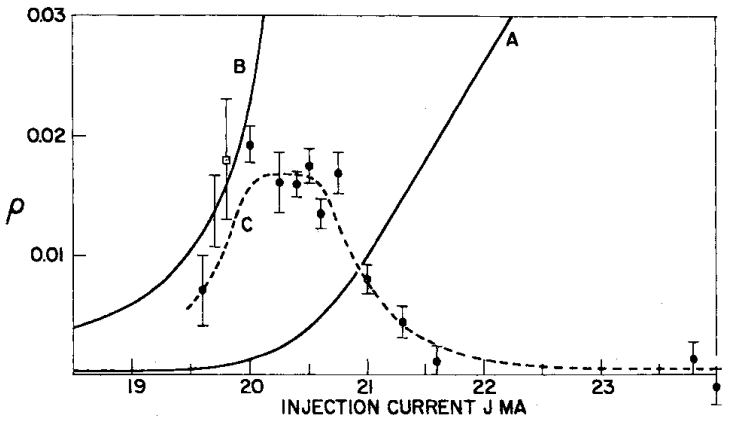

Fig. 2. Intensity fluctuation for the leading mode versus injection current (dashed line: theory prediction) [9].

"in this paper I introduced noise. Before, noise has only been calculated for the [electromagnetic] field, but noise for the atoms occurred for the first time. The other novelty has been the operator method according to Heisenberg's second quantisation formalism. First of all the elimination procedure: the adiabatic method was known, but it was new that you are able to do it also with quantum mechanical operators. And the Ansatz for the field operator. To split the operator into a classical and a quantum mechanical part, that was also new."[3]

In this work Haken did not only show the different quality of the light emission below and above the transition point but he also predicted the reduction of the intensity fluctuations with increasing "pump" strength, see Fig. 2. This was confirmed in a paper by American experimentalists only one year later [9].

The development of the full nonlinear quantized laser equations with its different applications and including noise took about three years. Mathematically there are three different ways to deal with the problems: The Langevin picture (Heisenberg treatment), the master equation Ansatz (Schrödinger picture) and the Fokker-Planck approach. Hermann Haken had a couple of high profile co-workers. We have to mention Hannes Risken, Wolfgang Weidlich, Robert Graham and Fritz Haake. This group of theoreticians together with their students were called the Stuttgart School and pursued all three ways. Risken, his first assistant, who became professor of theoretical physics at the University of Ulm in 1971, was a specialist of the Fokker-Planck equation. Wolfgang Weidlich, joining Haken in 1963 and receiving the chair of the second theoretical physics institute of the Technische Hochschule Stuttgart in 1966, was a master of the master equation and worked with Fritz Haake. Hermann Haken and his stu-

[3] Translation by the author.

dent Robert Graham preferred the Langevin approach. From 1964 to 1970 the Stuttgart School published more than fifty papers on the subject. As early as 1965 Hermann Haken took the task of writing a monograph about laser theory in the famous Handbuch der Physik [10]. Working extremely hard, he finally fell ill in autumn 1966 and had to take a time out for some months. He recovered soon and in April 1968 together with Robert Graham published an article on the "Quantum Theory of Light Propagation in a Fluctuating Laser-Active Medium" [11]. For the first time, they stated an analogy between the laser and a superconductor at threshold:

"The connection between laser theory and the theory of condensation also shows up in this solution where, e.g. the threshold condition is obtained as the condition for the occurrence of off-diagonal-long-range order in the light field (ODLRO). The solution well above threshold is discussed in connection with some concepts of phase transition theory, such as order parameters, broken symmetry and symmetry restoring elementary excitations."[4]

This idea was then worked out and two years later Graham and Haken published their paper "Laserlight – First Example of a Second-Order Phase Transition Far Away from Thermal Equilibrium" [13][5]. Here they state very clearly that *"the laser threshold appears as a second-order phase transition in all details. It is indicated that our theory provides a new formalism also for the Ginzburg-Landau theory"*. The very important point is that this theory holds not only for systems in thermal equilibrium but also for systems far away from this equilibrium state. They also conclude *"that the concept of a phase transition is much more general than usually thought of."* The mathematical correspondence of the laser theory and the Ginzburg-Landau theory of superconductivity is shown in Fig. 3.

In a talk delivered at the Spring Conference 1970 of the German Physical Society in Freudenstadt (a town in the Black Forest) Hermann Haken presented the results found by Graham and himself and then asked [15]:

"Is the laser a sole example for a phase transition far away from thermal equilibrium or are there other classes of corresponding phenomena? One can show that there are, indeed, corresponding phenomena in nonlinear optics, for instance the parametric oscillator. And, we believe, that our methods can also be applied to other problems, i.e. the Gunn-effect. [...] Finally a totally different field may be mentioned, namely biology. Fröhlich mentioned some time ago that in biological systems certain collective oscillations, that are highly excited above thermal equilibrium, may play an important role [...]"[6].

It is interesting that Haken drew the conclusion: *"Our above considerations have shown that by increasing the energy the properties of a system may change not only quantitatively but also qualitatively, so that an application of our re-*

[4] In a footnote they state that "analogies between laser theory and the theory of superfluidity have been discussed by Ref. [12]".

[5] At about the same time, Marvin Scully and V. de Giorgio also found this analogy [14].

[6] Translated from German by the author.

Laser equation:

$$f = N \exp\left(-\frac{B}{Q}\right)$$

$$B = \int \left\{ \alpha \left|E(x)\right|^2 + \beta \left|E(x)\right|^4 + \gamma \left| \left(\frac{d}{dx} - i \frac{\omega_0}{c} \right) E(x) \right|^2 \right\} dx$$

Ginzburg-Landau theory of superconductivity:

$$f = N \exp\left(-\frac{F}{k_B T}\right)$$

$$F = \int \left\{ \alpha \left|\psi(\mathbf{x})\right|^2 + \beta \left|\psi(\mathbf{x})\right|^4 + \frac{1}{2m} \left| \left(\boldsymbol{\nabla} - \frac{2ei}{c} \mathbf{A} \right) \psi(\mathbf{x}) \right|^2 \right\} d^3x$$

Fig. 3. Analogy between laser theory and Ginzburg-Landau theory of superconductivity [15].

sults on biological questions may be of interest." The above citation of Herbert Fröhlichs article is especially interesting. It was delivered as the opening speech of the first international conference "From Theoretical Physics to Biology" held in Paris, 1967.

These conferences, "From Theoretical Physics to Biology" took place at Versailles every second year, starting in June 1967. They had the goal to offer a platform for biologists, physicists and chemists to discuss the question, whether life could be explained from the laws of physics or if there must be other explanations be taken into account. This old philosophical question had been revived through the book of Erwin Schrödinger "What is Life?" [16]. The answer given by Schrödinger that life could be explained by the laws of physics and chemistry alone was questioned by the noted physicist Eugene P. Wigner. In an article titled "The probability of the existence of a self-reproducing unit" [17] he came to the conclusion that the probability was infinitely small that the many parts needed for the task would find together spontaneously. This was the background of the conferences. The so called Versailles conferences had great influence on the development of the theory of self-organization that took place in the late sixties and seventies of the 20th century. The ten conferences that were organized between 1967 and 1988 attracted many leading scientist and Nobel Prize winners. Among them were Manfred Eigen, a physico-chemist from Göttingen and Ilya Prigogine from Brussels. Hermann Haken attended nine out of the ten conferences and got in close contact to Eigen and Prigogine. Eigen remembers [18]

"I got to know [Haken] in Paris first. [...] I had to give a talk after his presentation and was a little bit late ... and then I spoke about my findings and

Autocatalytic reaction ("Hypercycle ansatz"), Manfred Eigen, 1971:

$$\dot{n}_j = k_j \cdot n_A \cdot n_j - \gamma_j \cdot n_j$$
$$n_A = n_0 - \sum_j n_j$$

n_j = number of molecules in state j; k_j = gain-coefficient; n_A = number of molecules of type A; γ_j = loss-coefficient; n_0 = start concentration of molecules A.

Single-mode laser ansatz, Hermann Haken, 1964:

$$\dot{n}_\lambda = n_\lambda \cdot \omega_\lambda \cdot D - 2\kappa_\lambda \cdot n_\lambda$$
$$D = \sum_\mu \sigma_\mu \approx D_0 - (2D_c/\gamma_\perp) \sum_\lambda \omega_\lambda n_\lambda$$

n_λ = number of photons of mode λ; D_c = critical inversion number of all atoms at threshold.

Fig. 4. Analogy between the self-organization ansatz by Manfred Eigen (The Hypercycle) and the single-mode laser equations derived by Hermann Haken [20].

wanted to write my equations onto the blackboard. But, I said "they are already there, how did they get there? [Interviewer: The rate equations?] Yes, in fact the ones from Haken, but they were very similar, namely the autocatalytic term."[7].

At that time Eigen was working on his famous Hypercycle Theory about the first steps in the development of life [19]. It was a year before that Hermann Haken had heard about this model of self-organization of macromolecules at a talk by Eigen in Göttingen. Shortly afterwards Haken was able to show a strong analogy between the reaction formalism by Eigen and his own equation for the single-mode laser, see Fig. 4.

The analogies of the laser equations to superconductivity and to the Hypercycle theory of Eigen convinced Hermann Haken that there must be common roots in these phenomena of self-organization. Already in 1970 he gave a lecture at the University of Stuttgart (as it was now called since 1967) entitled "Fließgleichgewichte, Phasenübergänge und Fluktuationen in Quantensystemen weit weg vom thermischen Gleichgewicht"[8]. In this lecture Haken used the word "Synergetik" for the first time. The word comes from the Greek word $\sigma\upsilon\nu\epsilon\rho\gamma\iota\alpha$ and has the meaning of "[parts] working together".

To test his hypothesis Haken together with Graham published an article titled "Synergetik – Die Lehre vom Zusammenwirken"[9] in the March issue 1971 of the popular German Science magazine Umschau [21]. Here they stated that complex

[7] Translated by the author from German.

[8] Flow equilibrium, phase transitions and fluctuations in quantum systems far away from thermal equilibrium. The handwritten plan of the lecture was found in the Haken papers (Archiv Haken).

[9] "Synergetics – the science of working together".

systems made up of many subsystems may be looked at and analyzed from a common perspective. The systems they mentioned were the laser, the structure of a forest, the production of an enzyme, the creation of life or the development of a language. The theory of phase transitions allows for this common perspective and they finished their article with the words:

"In summary, it can be said that a variety of quite different phenomena can be dealt with with the help of only a few concepts. The mysterious order principles governing the cooperation of the parts of a large system turn out to be feedback control systems created by the subsystems. Surprisingly abrupt changes in these order principles are generated by phase transitions. A way for the mathematical treatment of these phenomena therefore seems possible."

But to Haken's astonishment there was no reaction of the scientific community. This may be due to the fact that the Umschau was not the favorite German scientific magazine to be read by scientists. This would have been the journal "Naturwissenschaften" where Haken later on published several articles.

In the meantime Haken, Graham, and Weidlich were analyzing the reason for the similarity between phase transitions in equilibrium systems and those far away from thermal equilibrium. Guiding line was of course the laser theory. In a series of papers in 1970 and 1971 [22–24] they looked for the common principle that was valid for the laser (far away from thermal equilibrium) as well as for the Landau theory of superconductors (thermal equilibrium). They detected it in the existence of the famous "potential condition" that is central to the application of the Landau theory. The solution presented was simple but unexpected:

"Recently, we found the unexpectedly simple answer to this question: Within the framework of a Fokker-Planck equation the potential conditions in their most general form are equivalent to the condition of detailed balance."

Under this condition it is possible to describe systems far from thermal equilibrium using some of the methods of classical equilibrium thermodynamics. At this point of the development Hermann Haken knew what to look for: phase transitions in systems far from thermal equilibrium that are in the state of detailed balance.

Phase transition theory was a central topic of theoretical physics at that time and played an important part for instance at the meetings of the German Physical Society. At the spring meeting 1969 Siegfried Grossmann from Marburg gave a talk on "Analytische Eigenschaften thermodynamischer Funktionen und Phasenübergänge"[10] and at the annual convention of in Salzburg that year H. Thomas delivered a plenary talk about phase transitions, too.

The emergence of order was also on the agenda at the early Versailles conferences that Hermann Haken attended. We find headlines like "Self-Organization, emergence of order in systems, physical aspects of order in biological systems and questions of information in biological and physical systems" on the list of topics of the Versailles conferences in 1969 and 1971 [25, 26]. At the third conference in June 1971 Haken delivered a talk on "Cooperative Phenomena far from

[10] "Analytical properties of thermodynamical functions and phase transitions".

thermal Equilibrium". Even now, after the publication of the Umschau article, he did not use or mention the word Synergetics.

Now the time had come for Haken to organize his first conference on Synergetics that took place in April 1972 at the Bavarian resort of Elmau [27]. He remembered that his motive for this conference had been threefold: a) to look for more specific examples of analog behavior in systems far from equilibrium (and not only in thermal equilibrium), b) to get leading international scientists interested in Synergetics, and c) to promote Synergetics to a wider scientific audience[11]. The conference topics were "Mathematical and Physical Concepts for Cooperative Systems, Instabilities and Phase Transition-Like Phenomena in Physical Systems far from thermal Equilibrium, Biochemical Kinetics and Population Dynamics, Biological Structures and General Structures". Some of these topics were also dealt with at the first three Versailles conferences, but the scope of Hakens Ansatz was new, much broader, concentrated on systems far from thermal equilibrium and went far beyond biological questions. How much influence his participation at the first three Versailles conferences had on his thinking at that time is hard to say, but seven of the speakers present at Elmau (out of 23) had also been participants in Versailles. There were three other groups of attendees: speakers of the late German Physical Society meetings, Japanese solid-state physicists that had worked on statistical multicomponent systems and scientists that had published on phase transitions and, of course, members of the Stuttgart School. In his opening talk Haken brought into focus the order parameter concept that makes it possible to abstract from the largely different properties of the subsystems like electrons, molecules or neurons and to concentrate on the one or few order parameters that describe the macroscopic behavior of the system. Then he dealt with two other systems from biology and chemistry that show oscillatory behavior: The Lotka-Volterra rules of population dynamics and the Belousov-Zhabotinsky reaction. And finally, after once again explaining the laser, he pointed to the great importance of symmetry breaking in different phase transition-like phenomena.

The conference in Elmau had been a great success for Hermann Haken. Even years later, one of the participants, Rolf Landauer, an eminent physicist working at IBM, who has been very influential in computer information theory, remembered [28]:

"Hermann Haken in 1972 had the first interdisciplinary meeting [...] Probably not everything presented at Hakens session in 1972 has stood up, but all of it was serious and represented real intellectual depth and effort. Participation was a breath-taking experience for me; for the first time I found myself among people with comparable interests and a comparable sense of values. I was no longer an orphan! And the meeting had another earmark of a good conference: The conference had broad representation in its selection of speakers; it was not dominated by the organizer and his close associates."

The next time, where we find the word Synergetics, is in the Festschrift "Cooperative Phenomena" on the occasion of Herbert Fröhlich's retirement in the

[11] Hermann Haken: personal communication to the author.

following year 1973 [29]. A subchapter has the heading "Synergetics" and along with his own contribution contains also articles of Ilya Prigogine, B. Holland and others. Haken's paper was only a slight modified version of the Elmau article, but with one addition. Having in mind the influential book of Jacques Monod "Le hazard et la nécessité" [30] he looked at the equation for the order parameter of the single-mode laser. This equation consists of two terms. The first one deals with the interaction of the lightfield with the electrons of the laser medium and is deterministic. The second term describes the spontaneous emission by excited electrons due to quantum mechanical effects. So he came to the conclusion [31]:

[This equation] "is one of the simplest examples, but very instructive of the interplay between fluctuating forces [. . .] and systematic forces [. . .] or, in Monods words, of the interplay between "chance and necessity"."

Deterministic forces that are "triggered" by fluctuations at the transition points are one key element of the ordering phenomena of self-organization.

The reader should not be misled and get the impression that during the years 1971 – 1974 Hermann Haken only would have been occupied with phase transition phenomena and Synergetics. This was not the case. During this time he published no less than seventeen papers in solid-state physics as author or co-author and from 1971 to 1977 he supervised eleven diploma thesis and dissertations of his students. In 1973 he also published his textbook on "Quantum field theory of solid-state physics". So it seems fair to say that Synergetics during these years did not play a central role in the activities of the institute. It was a special activity of Hermann Haken.

The physics of cooperative systems and phase transitions in equilibrium and non-equilibrium systems were discussed on many occasions during 1974 and 1975. Finally, Hermann Haken was asked to summarize the knowledge on these topics in a fundamental paper that appeared in the January edition of the Review of Modern Physics [32]. In this widely read publication this article drew a lot of interest as it is shown in the more than 650 citations it got[12]. While working on the Review of Modern Physics paper Haken also dealt with the so called Brusselator, a chemical reaction scheme that shows oscillations and can be compared with the Belousov-Zhabotinsky reaction. The Brusselator was the main research model of Prigogine and his co-workers Nicolis and Leféver. Only weeks after the publication of the Review article Haken submitted a paper to the Zeitschrift für Physik entitled "Statistical Physics of Bifurcation, Spatial Structures and Fluctuations of Chemical Reactions" [33], where he could present a mathematical solution for the Brusselator model and for the Bénard reaction. The mathematical tools he used were the advanced Ginzburg-Landau equations that he had developed and refined during the recent months. This fundamental work for Synergetics was then published only weeks later under the title "Generalized Ginzburg-Landau-Equations for Phase Transition like Phenomena in Lasers, Non-Linear Optics, Hydrodynamics and Chemical Reactions" [34]. The far reaching scope of his results was very clear to him. He wrote

[12] Science Citation Index, as of 8th June 2011.

Lorenz equations	**Laser equations**
$\dot{\xi} = \sigma\eta - \sigma\xi$	$\dot{E} = \kappa P - \kappa E$
$\dot{\eta} = \xi\zeta - \eta$	$\dot{P} = \gamma E D - \gamma P$
$\dot{\zeta} = b(r-\zeta) - \xi\eta$	$\dot{D} = \gamma_{\parallel}(\lambda+1) - \gamma_{\parallel} D - \gamma_{\parallel}\lambda E P$

Identity conditions:

$t \to t'\sigma/\kappa\,, \quad E \to \alpha\xi\,, \quad$ with $\alpha = [b(r-1)]^{-1/2}\,,\ r > 1$

$P \to \alpha\eta\,, \quad D \to \zeta\,, \quad \gamma_{\parallel} = \kappa b/\sigma\,, \quad \gamma = \kappa/\sigma\,, \quad \lambda = r - 1$

Fig. 5. Analogy between the Lorenz equations of hydrodynamics and the single-mode laser equations [35].

"Our procedure has immediate applications to the Taylor instability, to various chemical reaction models, to the parametric oscillator in nonlinear optics and to some biological models. Furthermore, it allows us to treat analytically the onset of laser pulses, higher instabilities in the Bénard and Taylor problems and chemical oscillations including fluctuations."

In a footnote to the paper he mentioned the formal identity of his single-mode laser equations with the Lorenz equations of atmospheric physics. Again only four weeks later he submitted his results to the journal Physics Letters, where the article appeared on May 19th, see Fig. 5. Haken was one of the first scientists to "rediscover" the work of Edward Lorenz. The Lorenz equations became the fundamental paradigm of what was later known as chaos theory. Haken saw that particular result [35]

"The most important result is that spiking occurs randomly though the equations are completely deterministic".

So 1975 was a very successful year for Hermann Haken. He also got a first grant from the Volkswagenwerk Foundation for Synergetics that run as an "unusual project". Equipped with a sabbatical term from the university and the money from the foundation he started two projects. The first one was writing a book about Synergetics and then planning for the second Elmau conference.

The seminal book entitled "Synergetics An Introduction, Nonequilibrium Phase Transitions and Self-Organization in Physics, Chemistry and Biology" appeared in 1977 but was finished already in November 1976 [36]. It sold out quickly and within one year a second edition was necessary. Here Haken included a chapter of the rising chaos theory. To go into the details of this fundamental work is beyond the scope of this article. Therefore we will only mention the influence of chance and necessity (reminiscent of the work of Jacques Monod) that Haken expressed in the layout of the book, see Fig. 6.

Now the word Synergetics was "out" and Haken was going to promote it. The next step was the planning and realization of the second Elmau conference in May 1977. Under the Heading "Synergetics – A workshop" we find the following items: "General Concepts (including Catastrophe Theory); Bifurcation Theory, Instabilities in Fluid Dynamics; Solitons; Non-equilibrium Phase Transitions in

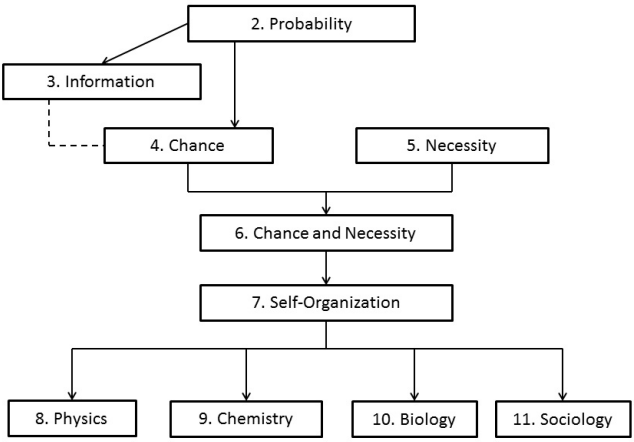

Fig. 6. Logical organization of the chapters in Hermann Haken's book "Synergetics" from 1977 [36].

Chemical Reactions; Chemical Waves and Turbulence (including a talk on Chaos by O. Rössler); Morphogenesis and Biological Structures". Hermann Haken's intention was to spread the word Synergetics beyond the scientific community he had cooperated with during the last years. So he invited many new scientists he had not met before. Nobel Prize Winner Alfred Kastler and the "Father" of catastrophe theory René Thom were among them.

Only one month later Haken used his talk at the 4th Rochester conference on Quantum Optics to present his thoughts about Synergetics to the international, especially American physicist community. The title of his speech fitted the topic perfectly "The Laser Trailblazer of Synergetics". In his talk he also highlighted the role of the laser with respect to the now widely discussed Lorenz equations [37]:

"The Laser when pumped high enough is the first realistic system obeying the Lorenz equations."

In November 1977 a conference on bifurcation theory and its applications in scientific disciplines was held in New York. One of the organizers, Otto Rössler from Tübingen, has been a participant at the second Elmau conference in May and knew the ideas of Hermann Haken very well. If one compares the contents of both meetings the similarity of topics is striking [38]. In his talk "Synergetics and Bifurcation Theory" Haken presented the laser as a model system for an exact computable bifurcation hierarchy. In 1978 and early 1979 Haken then got a

Conference Date	Topic
30.04.-06.05.1972	Synergetics:
	Cooperative Phenomena in Multi-Component Systems
02.05.-07.05.1977	Synergetics - A Workshop
30.04.-05.05.1979	Pattern Formation by Dynamic Systems
	and Pattern Recognition
27.04.-02.05.1981	Chaos and Order in Nature
26.04.-01.05.1982	Evolution of Order and Chaos
02.05.-07.05.1983	Synergetics of the Brain
06.05.-11.05.1985	Complex Systems - Operational Approaches
	in Neurobiology, Physics and Computers
04.05.-09.05.1987	Computational Systems - Natural and Artificial
13.06.-17.06.1988	Neural and Synergetic Computers
04.06.-08.06.1989	Synergetics of Cognition
22.10.-25.10.1990	Rhythms in Physiological Systems

Fig. 7. Dates and topics of the 11 Elmau Conferences on Synergetics.

research grant to write a textbook on laser theory for students. He used this time also to promote Synergetics at at least four international conferences [39–42].

At the end of 1978 the first term for the grant of the Volkswagen Foundation was about to expire and Haken came in for a prolongation. He was astonished and pleased to hear that the Foundation asked him to give Synergetics a broader scope. The "unusual project" should apply for a full "priority program" that was finally granted in spring 1980. There were two decisive arguments in favor of the priority program. The first one was its broad scope: according to the referees Synergetics comprised the following scientific fields [43]

- **Mathematics:** Bifurcation Theory, Theory of Singularities, Stochastic;
- **Physics:** Laser, nonlinear optics, Hydrodynamics, Turbulence Theory, electric current instabilities;
- **Chemistry:** chemical oscillators, dissipative structures;
- **Biology:** Population Dynamics, Morphogenesis, neural networks;
- **Engineering:** nonlinear continuum mechanics, fluid mechanics;
- **Informatics:** self-organization of computer and computer networks[13].

[13] Translated by the author.

(1973) Synergetics – Cooperative Phenomena	(1983) Advanced Synergetics
Physics: • Laser • Superconduction • Ferromagnetism	Physics: • Laser • Bénard Effect • Hydrodynamics • Plasmaphysics • Solid-State Physics
Chemistry: • Bénard Effect	Chemistry: • Belousov-Zhabotinsky • Brusselator • Oregenator
Biology: • Hypercycle (Eigen)	Biology: • Biological Clocks • coordinated muscle operation • Morphogenesis • Evolution • Immunsystem
	Computer: • Pattern recognition • Self-Organization (parallel computing) • Reliable systems from unreliable components
	Economy
	Engineering Sciences
	Ecology: Phase transitions
Sociology: • Opinion Formation	Sociology: • Opinion formation

Fig. 8. Comparison of scientific fields dealt within the two books on Synergetics from 1973 [27] and 1983 [45].

The second reason was the awarding of the Nobel Prize for Chemistry to Ilya Prigogine in autumn 1977. This has made the word "dissipative systems" known to a broader public and hence nonlinear systems theory far from equilibrium [44]. The priority program lasted ten years from 1980 to 1990 and in total 115 different projects were supported. In this way Synergetics got a boost and Hermann Haken used three ways to promote his activities. The Elmau conferences got a regular schedule, i.e. they took place every second year, the book series "Springer Series in Synergetics" was created and the theoretical work at the institute in Stuttgart could be intensified. The best way of exchanging new ideas had been the Elmau conferences. A look at the topics shows quite clearly how the ideas of Synergetics spread to ever new fields, see Fig. 7.

In 1982, after implementing the program, Hermann Haken wrote his second important book "Advanced Synergetics" [45]. In this work he presented in a systematic form the mathematical results that he had developed mainly with his co-worker Arne Wunderlin during the last five years. The topics comprised stability theory, order parameter theory and the full methods of the slaving principle. In Hakens words *"these concepts represent the "hard core" of synergetics in its present form"*.

If we compare the road Synergetics has taken during the ten years from 1972 with the first Elmau Conference "Synergetics – Cooperative Phenomena" [27] to the "Advanced Synergetics" book published in 1983 [45] one can clearly observe the broad development of the field, see Fig. 8. It is fair to say that with the publication of his book "Advanced Synergetics" the first phase of the history of Synergetics ended. During the following years the methods of Synergetics coping with large systems were applied to numerous fields. Working in this field, many researchers were often reminded of the words of Hermann Haken in this book

"The basic concepts of synergetics can be explained rather simply, but the application of these concepts to real systems calls for considerable technical (i.e. mathematical) know-how."

References

1. Haken, H.: Zum Identitätsproblem bei Gruppen. Math. Z. **56**, 335–362 (1952)
2. Haken, H.: Interview from 21.09.2010, p. 11. Archive of Universität Stuttgart (Archiv Haken)
3. Haken, H.: Nel senso della sinergetica. Di Renzo, Rome (2005)
4. Fröhlich, H.: Elektronentheorie der Metalle. Springer, Berlin (1936)
5. Haken, H.: Zur Quantentheorie des Mehrelektronensystems im schwingenden Gitter. Teil 1. Z. Phys. **146**, 527–554 (1956)
6. Maiman, T.: Stimulated Optical Radiation in Ruby. Nature **187**, 493–494 (1960)
7. Haken, H.: Nonlinear Theory of Laser Noise and Coherence I. Z. Phys. **181**, 96–124 (1964)
8. Haken, H.: Interview from 09.10.2012, p. 8. Archive of Universität Stuttgart (Archiv Haken)
9. Armstrong, J.A., Smith, A.W.: Intensity Fluctuations in a GaAs Laser. Phys. Rev. Lett. **14**, 68–70 (1965)
10. Haken, H.: Laser theory. In: Flügge, S. (ed.) Handbuch der Physik, Band XXV/2c. Springer, Berlin (1970)
11. Graham, R., Haken, H.: Quantum Theory of Light Propagation in a Fluctuating Laser-Active Medium. Z. Phys. **213**, 420–450 (1968)
12. Cummings, F.W., Johnston, J.R.: Theory of Superfluidity. Phys. Rev. **151**, 105–112 (1966)
13. Graham, R., Haken, H.: Laserlight - First Example of a Second-Order Transition Far Away from Thermal Equilibrium. Z. Phys. **237**, 31–46 (1970)
14. Scully, M., deGiorgio, V.: Analogy between the Laser Threshold Region and a Second-Order Phase Transition. Phys. Rev. A **2**, 1170–1177 (1970)
15. Haken, H.: Laserlicht - ein neues Beispiel für eine Phasenumwandlung? In: Schottky, W. (ed.) Festkörperprobleme, vol. X, pp. 351–365. Vieweg, Braunschweig (1970)

16. Schrödinger, E.: What is life?. Cambridge University Press, Cambridge (1944)
17. Wigner, E.P.: The probability of the existence of a self-reproducing unit. In: The Logic of Personal Knowledge: Essays Presented to Michael Polany on his Seventieth Birthday, pp. 231–238. Routledge & Kegan Paul, London (1961)
18. Eigen, M., Winkler-Oswatitsch, R.: Interview from 24.05.2011 in Göttingen. Archive of Universität Stuttgart (Archiv Haken)
19. Eigen, M.: Selforganization of matter and the evolution of biological macromolecules. Naturwisssenschaften **58**, 465–523 (1971)
20. Haken, H.: Cooperative phenomena in systems far from thermal equilibrium. In: Marois, M. (ed.) Proc. of the 3rd Int. Conference on From Theoretical Physics to Biology, Versailles, 1971, pp. 35–49. Karger, Basel (1973)
21. Haken, H., Graham, R.: Synergetik - die Lehre vom Zusammenwirken. Umschau **6**, 191–195 (1971)
22. Graham, R., Haken, H.: Fluctuations and Stability of Stationary Non-Equilibrium Systems in Detailed Balance. Z. Phys. **245**, 141–153 (1971)
23. Graham, R., Haken, H.: Generalized Thermodynamic Potential for Markoff Systems in Detailed Balance and Far from Thermal Equilibrium. Z. Phys. **243**, 289–302 (1971)
24. Graham, R., Haken, H., Weidlich, W.: Flux Equilibria in Quantum Systems Far Away from Thermal Equilibrium. Phys. Lett. A **32**, 129 (1970)
25. Marois, M. (ed.): Proc. of the Second Conference on From Theoretical Physics to Biology, June 30–July 5, 1969. Editions CNRS, Paris (1971)
26. Marois, M. (ed.): Proc. of the Third Conference on From Theoretical Physics to Biology, June 21–June 26, 1971. Karger, Basel (1973)
27. Haken, H. (ed.): Synergetics – Cooperative Phenomena in Multi-Component Systems. Proceedings of the Symposium on Synergetics from April 30 to May 6, 1972, Schloß Elmau. Teubner, Stuttgart (1973)
28. Landauer, R.: Poor Signal to Noise Ratio in Science Dynamic Patterns in Complex Systems. World Scientific, Singapore (1988)
29. Haken, H., Wagner, M. (eds.): Cooperative Phenomena. Festschrift Herbert Fröhlich. Springer, Berlin (1973)
30. Monod, J.: Le hasard et la nécessité. Ed. du Seuil, Paris (1970)
31. Haken, H.: Synergetics - towards a new discipline. In: Haken, H., Wagner, M. (eds.) Cooperative Phenomena. Festschrift Herbert Fröhlich, pp. 363–373. Springer, Berlin (1973)
32. Haken, H.: Cooperative phenomena in systems far from thermal equilibrium and in nonphysical systems. Rev. Mod. Phys. **47**, 67–121 (1975)
33. Haken, H.: Statistical Physics of Bifurcation, Spatial Structures and Fluctuations of Chemical Reactions. Z. Phys. B **20**, 413–420 (1975)
34. Haken, H.: Generalized Ginzburg-Landau Equations for Phase Transition-Like Phenomena in Lasers, Nonlinear Optics, Hydrodynamics and Chemical-Reactions. Z. Phys. B **21**, 105–114 (1975)
35. Haken, H.: Analogy between Higher Instabilities in Fluids and Lasers. Phys. Lett. A **53**, 77–78 (1975)
36. Haken, H.: Synergetics - An Introduction: Nonequilibrium Phase Transitions and Self-Organization in Physics, Chemistry, and Biology. Springer, Berlin (1977)
37. Haken, H.: The laser - trailblazer of synergetics. In: Mandel, L., Wolf, E. (eds.) Proc. of the 4th Rochester Conference on Coherence and Quantum Optics, pp. 49–62. Plenum Press, New York (1978)
38. Gurel, O., Rössler, O.: Bifurcation theory and its applications in scientific disciplines. New York Academy of Sciences, New York (1979)

39. Haken, H.: Nonequilibrium phase transitions and instability hierarchy of the laser, an example from synergetics. In: Pacault, A., Vidal, C. (eds.) Synergetics far from Equilibrium, pp. 22–33. Springer, Berlin (1978)
40. Haken, H.: Synergetics - Some Recent Trends and Developments. Suppl. Progr. Theor. Phys. **64**, 21–34 (1978)
41. Haken, H.: Synergetics and a new approach to bifurcation theory. In: Güttinger, W., Eikemeier, E. (eds.) Structural Stability in Physics, pp. 31–40. Springer, Berlin (1979)
42. Haken, H.: Synergetic computers - an alternative to neurocomputers. In: Garrido, L. (ed.) Proceedings of the XIth Sitges Conference on Statistical Mechanics of Neural Networks, Sitges, Barcelona, Spain, June 3–7, 1990, pp. 331–340. Springer, Berlin (1990)
43. Volkswagen, S.: Kuratoriumsunterlage Nr. 1404/62 vom 6. Juni 1979. Hannover
44. Volkswagenwerk, S.: Bericht - Stiftung Volkswagenwerk, 1980. Vandenhoek & Ruprecht, Göttingen (1981)
45. Haken, H.: Advanced Synergetics. Instabilitiy Hierarchies of Self-Organizing Systems and Devices. Springer, Berlin (1983)

Obituaries

Hermann Haken

Center of Synergetics, Institut für Theoretische Physik 1, Universität Stuttgart,
Pfaffenwaldring 57, 70550 Stuttgart, Germany
cos@itp1.uni-stuttgart.de
http://itp1.uni-stuttgart.de/institut/arbeitsgruppen/haken

In 2012 two very sad news reached the physics community and – frankly speaking – shocked me. Two of my former students and coworkers, Arne Wunderlin and Rudolf Friedrich had untimely died.

Arne Wunderlin (1947 – 2012)

Arne studied physics at the University of Stuttgart from 1966 till 1971. His diploma thesis was entitled "Behandlung von elektronischen Kollektivanregungen im Festkörper mit Hilfe von Quasiwahrscheinlichkeiten" [Treatment of electronic collective excitations in a solid by means of quasi-probabilities]. His Ph.D. thesis (1975) had the title "Über statistische Methoden und ihre Anwendung auf Gleichgewichts- und Nichtgleichgewichtssysteme" [On statistical methods and their application to equilibrium- and nonequilibrium systems]. The topic of his "habilitation" (1985) was "Mathematische Methoden der Synergetik und ihre Anwendungen auf den Laser" [Mathematical methods of synergetics and their applications to the laser]. In 1992 Arne Wunderlin was nominated apl. Professor at the University of Stuttgart and in the summer term 1995 he served as visiting professor at the University of Potsdam.

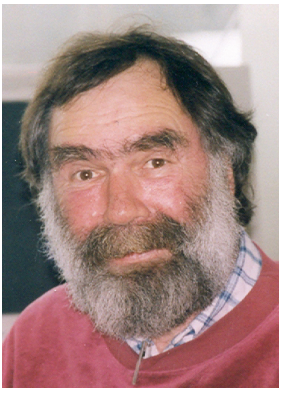

Arne Wunderlin

The research areas of Arne were widespread. Here I can name only the most important.

1. In solid state physics, he developed new mathematical methods to deal with superconductivity, including nonequilibrium states.
2. He dealt with excitons of high density as well as with the convection instability of fluid dynamics.
3. His contributions to the development of Synergetics were quite substantial. Arne dealt with nonlinear partial stochastic differential equations at instabilities. In particular he had the idea of how to extend my "slaving principle" to arbitrary order.
4. Then his research activities turned to a newly developing field: delay differential equations at instability points.

A. Pelster and G. Wunner (eds.), *Selforganization in Complex Systems: The Past, Present, and Future of Synergetics*, Understanding Complex Systems,
DOI: 10.1007/978-3-319-27635-9_17

5. Arne dealt, jointly with Axel Pelster, also with highly abstract problems such as nonintegrable space-time-transformations.
6. Finally, Arne's widespread interests are witnessed by his contribution to the theory of elasticity: general solution of incompability problems of 3-dim. linear anisotropic media.

Arne published (jointly with me) a book (1990): "Die Selbststrukturierung der Materie" It is a pity that we never have tried to translate this book into English. (Probably a title could have been: How matter forms its structure) He also edited the book Evolution of Dynamical Structures in Complex Systems, 1992, (jointly with Rudolf Friedrich) and also the book Lasers and Synergetics (jointly with Robert Graham and me).

Arne was a dedicated academic teacher whose lectures were highly esteemed by his students. His lectures comprised both the regular courses in theoretical physics as well as special courses on turbulence, synergetics, relativistic quantum field theory, light and matter, to mention a few of them.

Arne was all the time willing to discuss problems with my diploma and Ph.D. students. He was of an enormous help to all of us. We appreciated him highly also because of his great kindness. Arne was married and had three children. We will keep him in good memory.

Rudolf Friedrich (1956 – 2012)

Rudolf studied physics at the University of Stuttgart from 1975 till 1982. His diploma thesis (1982) was devoted to "Höhere Instabilitäten beim Taylor Problem der Flüssigkeitsdynamik" [Higher Instabilities of the Taylor problem of fluid dynamics]. In his Ph.D. thesis (1986) he dealt with "Stationäre, wellenartige und chaotische Konvektion in Geometrien mit Kugelsymmetrie" [Stationary, wave-like, and chaotic convection in geometries with spherical geometry]. The topic of his "habilitation" (1992) was: "Dynamische Strukturen in synergetischen Systemen" [Dynamical structures in synergetic systems]. In 1999, Rudolf Friedrich was nominated apl. professor at the University of Stuttgart, and in 2001 he became professor of theoretical physics and director of the institute of theoretical physics of the University of Münster.

Rudolf Friedrich

The research areas of Rudolf Friedrich were very broad. His work was not only characterized by its depth, but also by its close connection with experiments.

1. In fluid dynamics, he dealt with a variety of instabilities, i.e. changes of one spatio-temperal structure into another one, where he took different geometries (e.g. cylindrical, spherical) into account.
2. He dealt with analogies between pattern formation and pattern recognition.

3. In brain research, he developed a spatio-temporal analysis of multi-channel Alpha EEG (electro encephalogram) map series. Here the goal was to demonstrate that the underlying dynamics is governed by few order parameters. In particular, Rudolf was able to show that in the case of "petit mal" epilepsy the dynamics is that of Shilnikov Chaos. A beautiful result!
4. A good deal of Rudolf's research activities in Münster was devoted to various aspects of turbulence. Here I can mention only a few examples:
   Derivation of a Fokker-Planck-equation, statistics of Lagrangian velocities, spiral turbulence, time series analysis, magnetic fields in turbulent fluids. Rudolf introduced fractional substantial derivatives, and dealt with anomalous transport.
5. His interest in practical problems in engineering is witnessed by his work on the effects of water jets on metal cutting.

Rudolf Friedrich edited the book Evolution of Dynamical Structures in Complex Systems, 1992 (jointly with Arne Wunderlin). Rudolf was a dedicated academic teacher giving courses and seminars on theoretical physics. Since 2008 he had been member of the "Dynamics and Statistics" section of DFG (German Science Foundation). He was speaker of the center for nonlinear science of the University of Münster, a member of the board of German-Chinese Sonderforschungsbereich Transregio 61 (special research section), and director of research, Sonderforschungsbereich 458.

During his time at my institute, I got to know Rudolf as a very helpful and humorous student and colleague. Rudolf was married and had three children. His son is just about to finish his physics study, and I wish him heartfully to be able to carry on the fundamental work of his father.

Quite obviously, my obituaries can hardly do justice to the wonderful personalities of Rudolf Friedrich and Arne Wunderlin, and their important scientific work. But nevertheless, I hope my remarks will contribute to keep both of them in our minds.

Part V

Poster Contributions

Mean-Field Theory for Extended Bose-Hubbard Model with Hard-Core Bosons

Nicolas Gheeraert[1], Shai Chester[2], Mathias May[3], Sebastian Eggert[4], and Axel Pelster[4,5]

[1]University of Edinburgh, School of Physics and Astronomy, James Clerk Maxwell Building, Mayfield Road, Edinburgh, EH9 3JZ, Scotland
[2]Columbia University, Department of Physics, 538 W. 120th St, NY 10027, New York, USA
[3]Institut für Theoretische Physik, Freie Universität Berlin, Arnimallee 14, 14195 Berlin, Germany
[4]Fachbereich Physik, Technische Universität Kaiserslautern, Erwin-Schrödinger-Straße, 67663 Kaiserslautern, Germany
[5]Hanse-Wissenschaftskolleg, Lehmkuhlenbusch 4, 27753 Delmenhorst, Germany
axel.pelster@physik.uni-kl.de
www-user.physik.uni-kl.de/axel.pelster/index.html

Abstract. Here we analyze the extended Bose-Hubbard model for hard-core bosons in both a quadratic and a triangular lattice within a mean-field approximation. Especially interesting is the appearance of the supersolid phase for certain parameter values of the triangular lattice. We find analytical results for energies, condensate densities as well as phase boundaries except for the supersolid phase, for which just the density wave to supersolid boundary is derived analytically. The resulting quantum phase diagram for the triangular lattice coincides with a mathematically equivalent fermion model and agrees qualitatively with a recent Monte Carlo simulation.

Keywords: extended Bose-Hubbard model, hard-core bosons, Mott insulator, density wave, superfluid, supersolid

1 Introduction

Ultracold bosons in optical lattices are highly controllable and accurately observable quantum systems, which can be used as ideal quantum simulators to investigate open questions such as about intricate macroscopic quantum phenomena [1]. One prominent example is the elusive phenomenon of supersolidity, which amounts to a spontaneous breaking of both $U(1)$ and translational symmetry. Although initial experiments to observe supersolidity in helium turned out to be unsuccessful [2, 3], it has recently been proposed to realize a supersolid with dipolar bosons in a triangular optical lattice (see, for instance, Ref. [4] and references therein).

A. Pelster and G. Wunner (eds.), *Selforganization in Complex Systems: The Past, Present, and Future of Synergetics*, Understanding Complex Systems,
DOI: 10.1007/978-3-319-27635-9_18

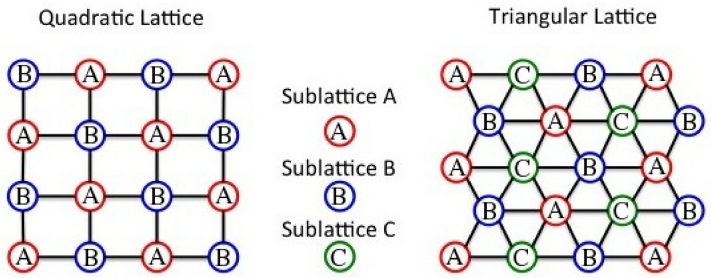

Fig. 1. The checkerboard pattern on the quadratic lattice (*left*) and a pattern with three sites in the unit cell on the triangular lattice (*right*).

Therefore, we analyze in the following a lattice potential close to absolute zero filled with bosons, where the dipoles are either of magnetic atomic or electric molecular origin. We consider hard-core bosons, i.e. bosons with such a strong contact interaction that two or more of them can not be at the same place at the same time. This is experimentally achieved by increasing the scattering length to a high value close to a Feshbach resonance using an external magnetic field [5]. Due to the additional dipolar interaction the interaction between next-neighbor bosons can be attractive or repulsive.

The Hamiltonian for the resulting extended Bose-Hubbard model reads:

$$\hat{H} = -J \sum_{<i,j>} \hat{a}_i^\dagger \hat{a}_j + \frac{V}{2} \sum_{<i,j>} \hat{n}_i \hat{n}_j - \mu \sum_i \hat{n}_i \,, \tag{1}$$

where $\hat{a}_i$ and $\hat{a}_i^\dagger$ are the bosonic annihilation and creation operators, whereas $\hat{n}_i = \hat{a}_i^\dagger \hat{a}_i$ denotes the bosonic number operator on the lattice site i. The symbol $< i, j >$ stands for next-neighbor combinations of sites i and j. The first term in Eq. (1) describes the hopping of bosons from site to site with the hopping energy J, the second describes the next-neighbor interaction with its strength V, and the third describes the dependency on the chemical potential μ within a grand-canonical description.

In this model we determine the ground-state quantum phase diagram by analyzing the mean-field approximation of the Hamiltonian (1) for a periodic distribution of bosons on the lattice like the checkerboard pattern and a pattern with three sites in the unit cell, which are both illustrated in Fig. 1. The quadratic lattice is not frustrated, i.e. the lattice geometry allows a density distribution, in which sites with density 1 have only sites with density 0 as next neighbors and vice versa. In the triangular lattice this is not possible, so it is called frustrated. In the following it will turn out that this frustration seems to be correlated to the appearance of the supersolid phase.

1.1 Mean-field approximation

It is not possible to determine the eigenvalues of the Hamiltonian in Eq. (1) exactly due to the presence of bilocal operators, i.e. a product of two operators at neighboring lattice sites. Using the mean-field (MF) approximation (see, for instance, Ref. [6]), however, we can rewrite the bilocal operators of the Hamiltonian approximately as

$$\hat{a}_i^\dagger \hat{a}_j \approx \psi_i^* \hat{a}_j + \psi_j \hat{a}_i^\dagger - \psi_i^* \psi_j \tag{2}$$

$$\hat{n}_i \hat{n}_j \approx \varrho_i \hat{n}_j + \varrho_j \hat{n}_i - \varrho_i \varrho_j \ , \tag{3}$$

where $\psi_i := \langle \hat{a}_i \rangle$ denotes the condensate density and $\varrho_i := \langle \hat{n}_i \rangle$ represents the boson density at lattice site i.

With Eqs. (2) and (3) the extended Bose-Hubbard Hamiltonian (1) is approximated according to

$$\hat{H} \overset{\text{MF}}{\approx} \sum_i \hat{h}_{\text{MF},i} \ , \tag{4}$$

where the local Hamiltonian reads

$$\hat{h}_{\text{MF},i} := -J \left(\hat{a}_i \Psi_i^* + \hat{a}_i^\dagger \Psi_i - \psi_i^* \Psi_i \right) + \frac{V}{2} \left(2 \hat{n}_i R_i - \varrho_i R_i \right) - \mu \hat{n}_i \ . \tag{5}$$

Here the mean fields

$$\Psi_i := \sum_{j \in NN_i} \psi_j, \qquad R_i := \sum_{j \in NN_i} \varrho_j \tag{6}$$

represent sums over expectation values on nearest neighboring sites, which have to be determined self-consistently. To this end we consider now periodic patterns in the distribution of ψ_i and ϱ_i over the lattice like the checkerboard pattern for the quadratic lattice or the pattern with three sites in the unit cell for the triangular lattice (see Fig. 1). Such a symmetry reduces the mean-field Hamiltonian for the whole lattice to the following Hamiltonian for one unit cell (UC):

$$\hat{h}_{\text{MF,UC}} = \left(J \Psi - \frac{V}{2} R \right) - J \sum_X \left(\hat{a}_X \Psi_X^* + \hat{a}_X^\dagger \Psi_X \right) + 2 \sum_X \hat{n}_X \left(\frac{V}{2} R_X - \frac{\mu}{2} \right) \tag{7}$$

with the abbreviation

$$\Psi := \sum_X \psi_X^* \Psi_X, \qquad R := \sum_X \varrho_X R_X \ , \tag{8}$$

where the sum has a finite number of summands $X \in \{A, B, \ldots\}$ named by capital letters corresponding to Fig. 1.

1.2 Finding the ground state

After having calculated the energy eigenvalues E_i of the Hamiltonian (7) for different patterns, we have to describe the ground state at zero temperature for this system. Therefore the values of the mean-field parameters on each sublattice are determined by extremizing the energy eigenvalues:

$$\partial_{\varrho_X} E_i = 0 \quad \forall X\,, \qquad \partial_{\psi_X} E_i = 0 \quad \forall X\,. \tag{9}$$

In principle we have to consider each pattern and find out, which has the lowest ground-state energy. But here we will just discuss the special patterns shown in Fig. 1. An example for a pattern, which we do not describe, is a stripe pattern with $\Psi_A = \Psi_B = 2\psi_A + 2\psi_B$ on the quadratic lattice, which is not a special case of the checkerboard. Its energies can be calculated, but it turns out not to appear in the ground state.

1.3 Possible phases

The simplest non-superfluid phase, which occurs, is the Mott insulator (MI). All bosons are localized at lattice sites, i.e. the condensate density vanishes at all sites according to $\psi_X = \psi_Y = 0 \quad \forall X, Y$, and all are distributed homogeneously, thus $\varrho_X = \varrho_Y \quad \forall X, Y$. There are just two cases for hard-core bosons - the empty lattice with $\varrho_X = \varrho_Y = 0 \quad \forall X, Y$ and the full lattice with $\varrho_X = \varrho_Y = 1 \quad \forall X, Y$. In the second non-superfluid class of phases - the density wave phase (DW) - all bosons are localized, too, but the density distribution is not homogeneous, i.e. $\exists X, Y \quad \varrho_X \neq \varrho_Y$.

For non-vanishing condensate densities two classes of phases are defined. When the density distribution is homogeneous, i.e. $\varrho_X = \varrho_Y \quad \forall X, Y$, but the bosons are not localized, i.e. $\psi_X = \psi_Y \neq 0 \quad \forall X, Y$, then the phase is called superfluid (SF). The remaining possible phases are called supersolid (SS), i.e. the density distribution is not homogeneous, thus $\exists X, Y \quad \varrho_X \neq \varrho_Y$ and at least two condensate densities are unequal, so $\exists X, Y \quad \psi_X \neq \psi_Y$.

2 Quadratic lattice

The checkerboard pattern is described by the two sites A, B in the unit cell. To find the Hamiltonian for this pattern, we have to express Ψ_A, Ψ_B, R_A, and R_B in terms of ψ_A, ψ_B, ϱ_A, and ϱ_B according to Eq. (6), which is $\Psi_A = 4\psi_B$, $\Psi_B = 4\psi_A$, $R_A = 4\varrho_B$ and $R_B = 4\varrho_A$, since the next neighbors of every site are always four of the other kind (see Fig. 1).

We can now write the Hamiltonian in the two-site basis

$$\mathcal{B} = \{|0,0\rangle\,, |1,0\rangle\,, |0,1\rangle\,, |1,1\rangle\}\ , \tag{10}$$

where $|n_A, n_B\rangle$ denotes the state of the unit cell with n_X bosons on site X. Thus the Hamiltonian becomes

$$\left(\hat{h}_{\mathrm{MF,UC}}\right)_{\mathcal{B}} = \\ = \begin{pmatrix} E_0 & -4J\psi_A^* & -4J\psi_B^* & 0 \\ -4J\psi_A & E_0 + 4V\varrho_A - \mu & 0 & -4J\psi_B^* \\ -4J\psi_B & 0 & E_0 + 4V\varrho_B - \mu & -4J\psi_A^* \\ 0 & -4J\psi_B & -4J\psi_A & E_0 + 4V\left(\varrho_A + \varrho_B\right) - 2\mu \end{pmatrix} \quad (11)$$

with the abbreviation $E_0 := J\Psi - VR/2 = 4J\left(\psi_A^*\psi_B + \psi_B^*\psi_A\right) - 4V\varrho_A\varrho_B$.

Determining the mean-field parameters via (9) leads to simple solutions for $\psi_A = \psi_B = 0$, which are the non-superfluid phases - Mott insulator (MI) and density wave (DW):

ϱ_A	ϱ_B	$\psi_A = \psi_B$	$\frac{E}{V}$	domain of J, μ	phase
0		0	0	$\mathbb{R}$	MI
0	1		$-\frac{\mu}{V}$		DW
1	0				
1			$4 - 2\frac{\mu}{V}$		MI

So in the density wave phase we find a checkerboard density distribution with zero or one boson localized at the respective lattice sites.

For the superfluid phase, i.e. $\psi_X = \psi_Y \neq 0 \quad \forall X, Y$, the Hamiltonian is not diagonal, but the energy eigenvalues and the mean-field parameters can be calculated analytically:

$\varrho_A = \varrho_B$	$\psi_A = \psi_B$	$\frac{E}{V}$	domain of J, μ	phase
$\frac{\frac{\mu}{V}+4\frac{J}{V}}{4+8\frac{J}{V}}$	$\frac{\sqrt{\frac{\mu}{V}+4\frac{J}{V}}\sqrt{4+4\frac{J}{V}-\frac{\mu}{V}}}{\left\lvert 4+8\frac{J}{V}\right\rvert}$	$-\frac{\left(\frac{\mu}{V}+4\frac{J}{V}\right)^2}{4+8\frac{J}{V}}$	$0 \leq \frac{\mu}{V} + 4\frac{J}{V}$ $0 \leq 4 + 4\frac{J}{V} - \frac{\mu}{V}$	SF

We find conditions here, under which these formulas are valid, because outside of the domain for J and μ (see previous table) the density $\varrho_A = \varrho_B$ could not be between 0 and 1, which is a necessary condition for hard-core bosons. Note that the self-consistency equations (9) turn out to not allow a supersolid phase in the quadratic lattice.

Since we know now the energies of all phases, we can calculate, which energy becomes the smallest one for certain parameter values J and μ, yielding the quantum phase diagram shown in Fig. 2. The phase boundaries can be expressed analytically in the following way:

DW-MI	$\frac{\mu}{V} = -4\frac{J}{V}$	second-order transition
DW-MI	$\frac{\mu}{V} = 4\frac{J}{V} + 4$	second-order transition
DW-SF	$2 < \frac{\mu}{V}: \quad \frac{\mu}{V} = 2 + 2\sqrt{1 - 4\left(\frac{J}{V}\right)^2}$ $\frac{\mu}{V} < 2: \quad \frac{\mu}{V} = 2 - 2\sqrt{1 - 4\left(\frac{J}{V}\right)^2}$	first-order transition

The order of the phase transitions describes, whether the order parameters ψ and ϱ change continuously or discontinuously with J and μ (see Fig. 3).

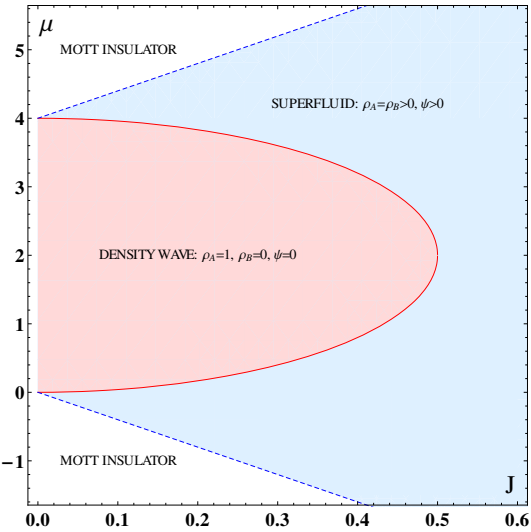

Fig. 2. Phase diagram of the quadratic lattice with continuous (*dashed*) and discontinuous (*solid*) phase transitions (J and μ in units of V).

3 Triangular lattice

The considered pattern from Fig. 1 for the triangular lattice of three sites A, B, C in the unit cell yields according to Eq. (6) the mean fields $\Psi_A = 3\psi_B + 3\psi_C$, $\Psi_B = 3\psi_A + 3\psi_C$, $\Psi_C = 3\psi_A + 3\psi_B$, $R_A = 3\varrho_B + 3\varrho_C$, $R_B = 3\varrho_A + 3\varrho_C$ and $R_C = 3\varrho_A + 3\varrho_B$. The Hamiltonian for one unit cell turns out to be a 8×8-matrix, which we omit here for the sake of simplicity. Analyzing the corresponding self-consistency equations (9), we find the non-superfluid states, i.e. $\psi_X = \psi_Y = 0 \quad \forall X, Y$, which are the empty lattice (MI), the full lattice (MI) and, additionally, two density wave phases with average densities of 1/3 and 2/3 and degenerated energies:

ϱ_A	ϱ_B	ϱ_C	$\psi_A = \psi_B = \psi_C$	$\frac{E}{V}$	domain of J, μ	phases
0			0	0	$\mathbb{R}$	MI
0	0	1		$-\frac{\mu}{V}$		DW
0	1	0				
1	0	0				
1	1	0		$3 - 2\frac{\mu}{V}$		
1	0	1				
0	1	1				
1				$9 - 3\frac{\mu}{V}$		MI

The superfluid phase with $\psi_X = \psi_Y \neq 0 \quad \forall X, Y$ is here quite similar to the quadratic lattice, just a few constants have changed, and again, we find certain conditions for the domain of J and μ:

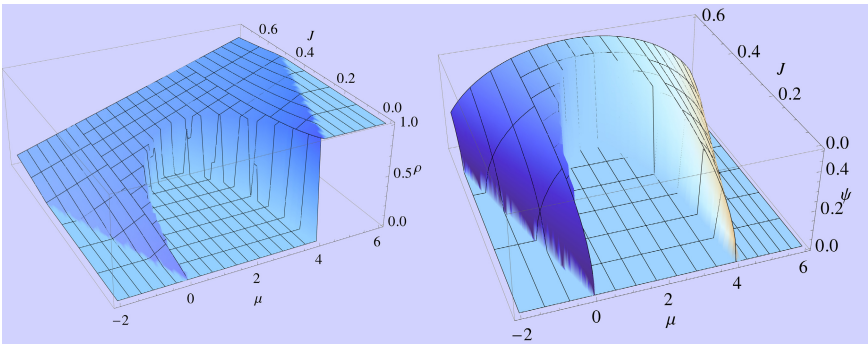

Fig. 3. Order parameters ϱ (*left*) and ψ (*right*) over J and μ. In the density wave region ϱ is chosen to be zero. In the other regions we have $\varrho_A = \varrho_B = \varrho$ (J and μ in units of V).

$\varrho_A = \varrho_B = \varrho_C$	$\psi_A = \psi_B = \psi_C$	$\frac{E}{V}$	domain of J, μ	phases
$\frac{\frac{\mu}{V}+6\frac{J}{V}}{6+12\frac{J}{V}}$	$\frac{\sqrt{\frac{\mu}{V}+6\frac{J}{V}}\sqrt{6+6\frac{J}{V}-\frac{\mu}{V}}}{\left\lvert 6+12\frac{J}{V}\right\rvert}$	$-\frac{\left(6\frac{J}{V}+\frac{\mu}{V}\right)^2}{4+8\frac{J}{V}}$	$0 \leq \frac{\mu}{V}+6\frac{J}{V}$ $0 \leq 6+6\frac{J}{V}-\frac{\mu}{V}$	SF

For the supersolid case with $0 \neq \psi_A = \psi_B \neq \psi_C \neq 0$ we can still diagonalize the Hamiltonian and find a universal minimal energy E_{SS}, which turns out to be too complicated for an exact extremalization.

Finding the phase transitions is simple for the SF-DW and SF-MI transition using the above mentioned analytical expressions for the energies. The DW-SS transition is of second order, so we can insert the DW-parameters into the extremalization equation $\partial E_{\mathrm{SS}}/\partial \psi_A = 0$ to find it. The resulting phase boundary makes the density wave region asymmetric (see Fig. 4). For the SS-SF transition we can not use this method, because this transition is of first order and the analytic expression for the energy of the supersolid is unknown, thus no analytical curve has been found. However, a numeric simulation shows, that this curve is simply a straight line. That fits to the results found in Ref. [7] for a mathematically equivalent fermion model.

Furthermore we compare in Fig. 4 the mean-field results with the recent Monte Carlo simulations of Ref. [4], where the J-axis is dilated by a factor of 2. The comparison shows, that quantum fluctuations cause the superfluid to shrink or, equivalently, the density waves to grow and the SS-SF transition is no longer a straight line in the Monte Carlo simulation. Thus, we conclude, that the mean-field approximation produces qualitatively correct results, but quantitatively it is not that accurate. The mean-field approximation could, in principle, be improved by interpreting the mean fields as variational parameters and by taking into account quantum fluctuations systematically as has been shown for the Bose-Hubbard model in Ref. [8].

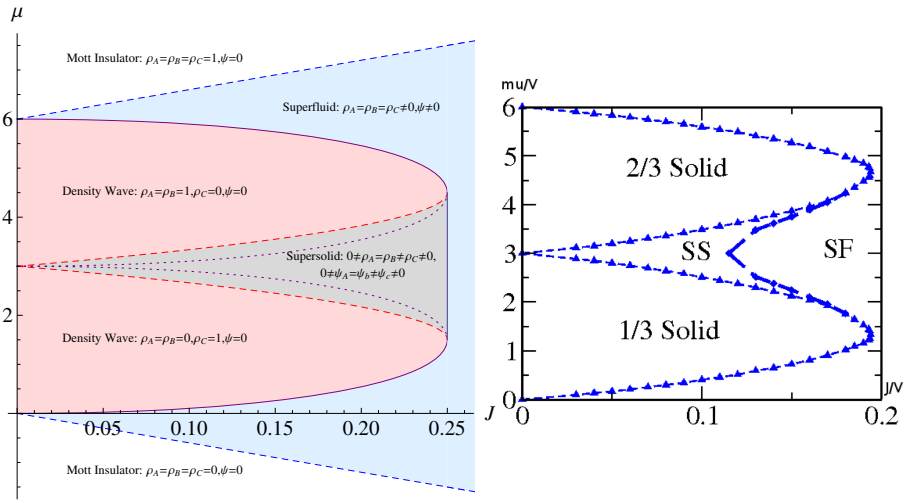

Fig. 4. *left*: Mean-field phase diagram of the triangular lattice with continuous (*dashed*) and discontinuous (*solid*) phase transitions. The *dotted* lines in comparison with the DW-SS transition illustrate the asymmetry of the DW region (J and μ in units of V). *right*: Exact phase diagram found using Monte Carlo methods [4]. Note that the J-axis is dilated by a factor of 2 in comparison with the mean-field results on the *left*.

4 Acknowledgement

This project was supported by the German Academic Exchange Service (DAAD) within the program Research Internships in Science and Engineering (RISE) and by the German Research Foundation (DFG) via the Collaborative Research Center SFB/TR 49.

References

1. Bloch, I.: Ultracold quantum gases in optical lattices. Nature Physics **1**, 23–30 (2005)
2. Kim, E., Chan, M.H.W.: Probable observation of a supersolid helium phase. Nature **427**, 225–227 (2004)
3. Kim, D.Y., Chan, M.H.W.: Absence of Supersolidity in Solid Helium in Porous Vycor Glass. Phys. Rev. Lett. **109**, 155301 (2012)
4. Zhang, X.-F., Dillenschneider, R., Yu, Y., Eggert, S.: Supersolid phase transitions for hard-core bosons on a triangular lattice. Phys. Rev. B **84**, 174515 (2011)
5. Chin, C., Grimm, R., Julienne, P., Tiesinga, E.: Feshbach resonances in ultracold gases. Rev. Mod. Phys. **82**, 1225–1286 (2010)
6. Kurdestany, J.M., Pai, R.V., Pandit, R.: The inhomogeneous extended Bose-Hubbard model: Mean-Field theory. Ann. Phys. **524**, 234–244 (2012)
7. Murthy, G., Arovas, D., Auerbach, A.: Superfluids and supersolids on frustrated two-dimensional lattices. Phys. Rev. B **55**, 3104 (1996)
8. dos Santos, F.E.A., Pelster, A.: Quantum phase diagram of bosons in optical lattices. Phys. Rev. A **79**, 013614 (2009)

Bose-Einstein Condensates in Compact Astrophysical Objects

Christine Gruber[1†] and Axel Pelster[2,3‡]

[1] Department of Physics, Freie Universität Berlin, Germany
[2] Department of Physics, Technische Universität Kaiserslautern, Germany
[3] Hanse-Wissenschaftskolleg, Delmenhorst, Germany
[†]chrisigruber@fu-berlin.de [‡]axel.pelster@physik.uni-kl.de
www-user.physik.uni-kl.de/axel.pelster/index.html

Abstract. We explore two possible applications of the theory of Bose-Einstein condensates in astrophysical contexts, one being white dwarfs and neutron stars, the other being Bose-Einstein condensates of dark matter. There is a general consensus that the conditions in these astrophysical environments allow for the formation of a Bose-Einstein condensate and thus the investigation of such scenarios are important for the determination of the physical properties of these astrophysical objects.

Keywords: Bose-Einstein condensation, astrophysics, white dwarf, neutron star, dark matter

1 Introduction

The earliest work on neutron stars has been performed by Tolman [1], as well as Oppenheimer and Volkoff [2]. They considered neutrons with an equation of state determined by Fermi statistics in a general relativistic setting and calculated the resulting stable equilibrium configuration, see also Ref. [3]. The gravitational collapse of a cloud of neutrons is counteracted by the neutron degeneracy pressure due to the Pauli exclusion principle, which leads to a prediction for the maximum masses of neutron stars of about $0.7\,M_\odot$. Observations however proved the existence of neutron stars with up to $2\,M_\odot$ [4], which is in contradiction with the limit predicted by Refs. [1, 2]. Currently there exists an abundance of different models trying to explain the observed masses of neutron stars, most of them predicting the existence of other kinds of matter in the core of a neutron star. Explanations reach from hyperons, i.e. strange baryons, over kaons and pions, both heavy mesons, to quark matter in the core, while the outer layers and crusts are supposed to be dominated by neutrons and electrons [5]. There is the general consensus that the neutrons in neutron stars are in a superfluid phase [6], i.e. they are bound in states of two neutrons, so-called Cooper pairs, and can thus effectively be treated as bosons. Investigations of typical temperatures and densities in neutron stars show that these bosons, with an effective mass of $m = 2m_n$, are in a regime in which Bose-Einstein condensation (BEC) can occur. Thus it is reasonable to investigate whether the maximum mass or

A. Pelster and G. Wunner (eds.), *Selforganization in Complex Systems: The Past, Present, and Future of Synergetics*, Understanding Complex Systems,
DOI: 10.1007/978-3-319-27635-9_19

other properties like the equation of state of the neutron star change under the assumption of Bose-Einstein condensated neutron pairs. This theory is known as BCS-BEC-crossover [7], and has been proven to exist in laboratory experiments on dilute ultracold quantum gases [8], but was never addressed in astrophysical settings. A second field of application for BECs in astrophysics are boson stars - either denoting the abstract concept of a star purely consisting of generic bosons [9], or using objects like white dwarfs, which contain in principle several species of particles, but are dominated by one bosonic species, like e.g. ^{4}He white dwarfs [10, 11]. Results can be compared to an abundance of existing theories on neutron stars and white dwarfs, explaining observations with varying success. Finally, some theories suggest dark matter to be bosonic and present in the form of a Bose-Einstein condensate [12–14]. This could explain some of the puzzles observed in galactic dynamics, like the rotation curves of visible matter around the center of a galaxy. Due to the completely unknown nature of dark matter, the application of BEC is yet unspecified. However, it is assumed that the conditions in dark matter halos are in principle suitable for superfluid or Bose-Einstein condensated phases of the constituent particles for some models of dark matter [15].

In the following we review the idea of applying the theory of Bose-Einstein condensation, a phenomenon occurring in cold dilute quantum gases, in the context of astrophysical compact objects. To this end we compare in Section 2 different theoretical treatments of interacting bosons in astrophysical contexts. In Section 3 we then investigate the implications in the cases of neutron stars (NSs), white dwarfs (WDs), and dark matter (DM).

2 Theoretical treatment of interacting bosons

There have been plenty of calculations in the field of Bose-Einstein condensates in astrophysical contexts, for generic boson stars as well as white dwarfs and even neutron stars. All kinds of scenarios have been considered, from Newtonian gravity to general relativistic treatments, and from non-relativistic to relativistic particle dispersions [16–18]. In the following we will introduce three approaches which differ in the assumed conditions for the investigated system.

2.1 Non-relativistic bosons in Newtonian gravity

Non-relativistic bosons are described by a condensate wave function which obeys the Gross-Pitaevskii equation, i.e. a non-linear Schrödinger type equation [16],

$$i\hbar\frac{\partial}{\partial t}\psi(\mathbf{x},t) = \left[-\frac{\hbar^2}{2m}\nabla^2 + \int d^3r'\, U(\mathbf{x},\mathbf{x}')\,|\psi(\mathbf{x}',t)|^2\right]\psi(\mathbf{x},t)\,, \tag{1}$$

using contact interaction and Newtonian gravitational interaction,

$$U(\mathbf{x},\mathbf{x}') = g_0\,\delta(\mathbf{x}-\mathbf{x}') - \frac{Gm^2}{|\mathbf{x}-\mathbf{x}'|}\,, \tag{2}$$

where m denotes the particle mass, and $g = 4\pi\hbar^2 a/m$ represents the strength of the contact interaction depending on the s-wave scattering length a.
Choosing the Madelung representation of the condensate wave function, i.e. splitting it into an amplitude and a phase according to

$$\psi(\mathbf{x},t) = \sqrt{n(\mathbf{x},t)}\; e^{iS(\mathbf{x},t)}\,, \tag{3}$$

transforms the Gross-Pitaevskii equation Eq. (1) into two coupled hydrodynamic equations for the mass density $\rho(\mathbf{x},t) = m\,n(\mathbf{x},t)$, namely the continuity equation and the Euler equation for the velocity field $\mathbf{v} = \hbar\nabla S/m$ of the fluid,

$$\frac{\partial\rho}{\partial t} + \nabla\cdot(\rho\,\mathbf{v}) = 0\,, \tag{4a}$$

$$\rho\left[\frac{d\mathbf{v}}{dt} + (\mathbf{v}\cdot\nabla)\,\mathbf{v}\right] = -\nabla P(\rho) - \rho\,\nabla\Phi(\mathbf{x},t) - \nabla\cdot\sigma_Q\,. \tag{4b}$$

Here, the Newtonian gravitational potential $\Phi(\mathbf{x},t)$ is defined as

$$\Phi(\mathbf{x},t) = -\int d^3x'\frac{Gm}{|\mathbf{x}-\mathbf{x}'|}\,\rho(\mathbf{x}',t)\,, \tag{5}$$

fulfilling Poisson's equation

$$\nabla^2\Phi(\mathbf{x},t) = 4\pi G\,\rho(\mathbf{x},t)\,. \tag{6}$$

Furthermore,

$$\sigma_{ij}^{Q} = \frac{\hbar^2}{4m^2}\,\rho\,\nabla_i\nabla_j\ln\frac{\rho}{m} \tag{7}$$

denotes the so-called quantum stress tensor, which has the dimension of a pressure and represents a quantum contribution stemming from the kinetic term in the Gross-Pitaevskii equation. From the form of the equations above, the pressure can be read off as

$$P(\rho) = \frac{g}{2m^2}\,\rho^2\,, \tag{8}$$

which corresponds to a polytropic equation of state of the form $P = K\,\rho^{1+1/n}$, with the polytropic index $n = 1$.
Henceforth we will apply the Thomas-Fermi approximation in the scenario, which is justified for a system with a very large particle number and a uniform distribution of particles. Mathematically this corresponds to neglecting the quantum pressure term σ_Q. Moreover, we will assume a static configuration, and thus neglect time derivatives as well as all velocity terms. Using the identification of the pressure in Eq. (8), Eq. (4b) turns out to be

$$\nabla P = -\rho\,\nabla\Phi\,. \tag{9}$$

Here it is suitable to introduce spherical coordinates as, due to the symmetry of the problem, the angular coordinates do not occur in the calculations any more.

Combining Eq. (6) and Eq. (9) leads, with appropriate units for radial coordinate and density, to the so-called Lane-Emden equation,

$$\frac{1}{r^2}\frac{d}{dr}\left(r^2\,\frac{d\rho}{dr}\right) = -\rho^n\,, \tag{10}$$

describing the density profile of the condensate $\rho(r)$. From this, quantities like the maximum mass of stable configurations can be calculated. Solving for the density and subsequently integrating up to the first zero of the function yields the maximum mass, which depends on the yet unspecified s-wave scattering length a of the particles [16]:

$$M_{\max} \simeq \frac{\pi}{2}\frac{\hbar c^2\sqrt{a}}{(Gm)^{3/2}}\,. \tag{11}$$

2.2 Non-relativistic neutrons in general relativistic setting

Instead of Newtonian gravity, we can also consider the laws of General Relativity [16]. With a spherically symmetric ansatz for the metric,

$$ds^2 = -e^{-\nu(r)}dt^2 + e^{\mu(r)}dr^2 + r^2 d\Omega^2\,, \tag{12}$$

and the following assumptions for the metric functions,

$$\frac{d\nu(r)}{dr} = -\left[\frac{2}{P(r)+\rho(r)c^2}\right]\frac{dP(r)}{dr}\,, \tag{13}$$

$$e^{\mu(r)} = \left[1-\frac{2GM(r)}{r}\right]^{-1}\,, \tag{14}$$

Einsteins field equations are transformed into the Tolman-Oppenheimer-Volkoff form [1, 2],

$$\frac{dP(r)}{dr} = -\frac{G\left[\rho(r)+\frac{P(r)}{c^2}\right]\left[\frac{4\pi P(r) r^3}{c^2}+M(r)\right]}{r^2\left[1-\frac{2GM(r)}{rc^2}\right]}\,, \tag{15}$$

which, together with the mass conservation equation,

$$\frac{dM(r)}{dr} = 4\pi\rho(r)\,r^2 \tag{16}$$

replace Eqs. (6) and (9). The final set of equations is then Eq. (8), (15) and (16). Processing these equations leads to a similar expression as in Eq. (10) with several additional terms which are due to general relativity. Solving for the density as a function of the radius and then integrating up to the first zero leads to the maximum mass [17]

$$M_{\max} \simeq \frac{1}{2}\frac{\hbar c^2\sqrt{a}}{(Gm)^{3/2}}\,. \tag{17}$$

2.3 Relativistic neutrons in general relativistic setting

Now we treat relativistic neutrons, for which the equation of state changes. We will no longer use the non-relativistic Gross-Pitaevskii equation (1), but start deriving the governing equations from the action of a scalar field,

$$S = \int d^4x \, \sqrt{-g} \, \mathcal{L} \tag{18}$$

with the Lagrangian density

$$\mathcal{L} = \frac{1}{2} g^{\mu\nu} \partial_\mu \phi^* \partial_\nu \phi - \frac{1}{2} \frac{m^2 c^2}{\hbar^2} |\phi|^2 - \frac{\lambda}{4} |\phi|^4 \tag{19}$$

containing a scalar field with quartic self interaction in curved spacetime [17, 18]. A variation with respect to the complex conjugate of the scalar field ϕ^* yields the Klein-Gordon equation

$$\left(\Delta_{\mathrm{LB}} - \frac{m^2 c^2}{\hbar^2} - \lambda \, |\phi|^2 \right) \phi = 0 \, , \tag{20}$$

where

$$\Delta_{\mathrm{LB}} = \frac{1}{\sqrt{-g}} \partial_\mu \sqrt{-g} g^{\mu\nu} \partial_\nu \tag{21}$$

represents the Laplace-Beltrami operator for curved spacetimes. It can be shown that with the ansatz $\phi(\mathbf{x}, t) = \exp(-imc^2 t/\hbar) \, \psi(\mathbf{x}, t)$, a spherically symmetric metric and in the non-relativistic limit the Gross-Pitaevskii equation Eq. (1) will be recovered with the identification $\lambda = 2mg/\hbar^2$.
Furthermore the energy-momentum tensor $T^{\mu\nu}$ of the scalar field follows from varying the action (18) with respect to the metric $g^{\mu\nu}$:

$$T^\mu_\nu = \frac{1}{2} g^{\mu\sigma} \left(\phi^*_{;\sigma} \phi_{;\nu} + \phi_{;\sigma} \phi^*_{;\nu} \right) - \frac{1}{2} \delta^\mu_\nu \left[g^{\kappa\sigma} \phi^*_{;\kappa} \phi_{;\sigma} + m^2 |\phi|^2 + \frac{1}{2} \lambda |\phi|^4 \right] . \tag{22}$$

Using the spherically symmetric ansatz from Eq. (12) for the metric, we end up with three equations, i.e. the Klein-Gordon equation (20), as well as the tt- and rr-components of the Einstein equations, Eqs. (9a)-(9c) in Ref. [17]. From these we obtain in analogy to above the maximum mass of the star as

$$M_{\max} \simeq 0.22 \sqrt{\frac{\lambda}{4\pi}} \frac{M_P^3}{m^2} = \frac{0.22}{\sqrt{4\pi}} \frac{\hbar c^2 \sqrt{a}}{(Gm)^{3/2}} \, , \tag{23}$$

with the Planck mass $M_P = \sqrt{\hbar c/G}$. Note that the qualitative dependence on λ has been found analytically using the Thomas-Fermi approximation, while the exact form with the coefficient 0.22 has been read off a numerical plot [17]. Investigations including thermal or quantum fluctuations have also been performed more recently in Refs. [18, 19] in a purely numerical approach.

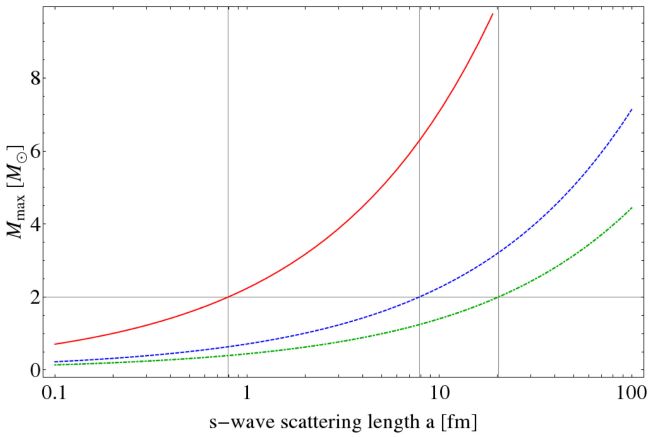

Fig. 1. Results for the predicted maximum masses of neutron stars in different treatments. Red (full line) are non-relativistic neutrons in Newtonian gravity (11), blue (dashed line) are non-relativistic neutrons in General Relativity (17), and green (dot-dashed line) are relativistic neutrons in General Relativity (23). The horizontal grid line marks the maximum observed mass of $2\,M_\odot$ [4], and the vertical grid lines denote the corresponding s-wave scattering length deduced from the respective theories.

2.4 Comparison of treatments

Even though the three models differ significantly in their physical assumptions, Fig. 1 reveals that the quantitative outcomes are rather similar and the resulting predictions all lie in the same order of magnitude. We can see that the maximum mass decreases from Newtonian to general relativistic, and from non-relativistic to relativistic treatment of neutrons. The three maximum masses are given by Eqs. (11), (17), and (23), and only differ in their numerical prefactor, which is in all three cases of the order of unity, but otherwise are proportional to $\hbar c^2\sqrt{a}/(Gm)^{3/2}$. Using the observed maximum mass of a neutron star of about $2\,M_\odot$ [4], we can infer the corresponding s-wave scattering length a of the neutrons from relations Eqs. (11), (17), and (23) and the plot in Fig. 1. The values for a are 0.8 fm, 8 fm, and 11 fm, respectively, for the three different treatments. Unfortunately astrophysical measurements do not permit the determination of the s-wave scattering length of neutrons in a neutron star, but it is surprising that the values predicted from the maximum masses are not so different from those obtained in laboratory experiments.

3 Choosing the right treatment

Some simple considerations are helpful to figure out the appropriate choice of setting for a realistic analysis. The following estimations are carried out for

the example of a neutron star. To decide whether Newtonian gravity or General Relativity is physically appropriate, it is instructive to calculate the typical Schwarzschild radius of a neutron star from observed masses, and compare it with the observed radii of neutron stars. The Schwarzschild radius of an object is defined as

$$R_S = \frac{2GM}{c^2}\,, \tag{24}$$

and with typical masses of neutron stars of about $M \simeq 1.5\,M_\odot$, this leads to a Schwarzschild radius of about $R_S \simeq 4 \cdot 10^3\,\mathrm{m}$, which is about half of the typical radius of a neutron star of $R_{\mathrm{typ}} \simeq 10^4\,\mathrm{m}$. This clearly hints at the necessity of a general relativistic treatment.

As for the choice of treatment for the neutrons, we consider the estimated temperatures in neutron stars, $T_{\mathrm{typ}} \simeq 10^{11}\,\mathrm{K}$, and equate the thermal energy of the neutrons with their kinetic energy. Assuming for now the non-relativistic energy expression, the average velocity of the particles is given by

$$v = \sqrt{\frac{2k_B T_{\mathrm{typ}}}{m}}\,, \tag{25}$$

leading to a typical velocity of neutrons in a neutron star of $v \simeq 3 \cdot 10^7\mathrm{m/s}$, which is a velocity well in the relativistic regime. For the lower temperature of about $T_{\mathrm{typ}} \simeq 10^6\,\mathrm{K}$ in the outer regions of a neutron star however, we end up with particle velocities of around $v \simeq 9 \cdot 10^4\mathrm{m/s}$, which would justify a non-relativistic treatment. Thus, the different treatments outlined above seem to be applicable for different physical scenarios. Finally, we remark that for white dwarfs in general the Newtonian treatment of non-relativistic bosons would be sufficient, as well as for dark matter in the galactic core and halo.

4 Outlook

Plenty of calculations in the field of Bose-Einstein condensates in astrophysical contexts, ranging from generic boson stars to neutron stars and white dwarfs have been performed, and all kinds of scenarios have been considered, analytically as well as within the framework of numerical simulations. However, the majority of investigations have been carried out at zero temperature, and thus have neglected thermal fluctuations around the Bose-Einstein condensated ground state. Our estimations of temperatures and conditions in the astrophysical settings in question have shown that this assumption of zero temperature is in reality not justified, and thus thermal fluctuations would have to be taken into account. This could be accomplished in a first step by extending the zero-temperature treatment of Section 2 to a Hartree-Fock theory at finite temperature. This leads to a depletion of the condensate through the presence of thermally excited bosons. Self-consistency equations for both condensate and thermal density would change predictions of measurable quantities, such as the maximum masses shown in Fig. 1, considerably. It is expected that thermal fluctuations

would destabilize compact astrophysical objects, resulting in a lower limit for the maximum mass.

Acknowledgments. C.G. is supported by the Erasmus Mundus Joint Doctorate Program by Grant Number 2010-1816 from the EACEA of the European Commission.

References

1. Tolman, R.C.: Static Solutions of Einstein's Field Equations for Spheres of Fluid. Phys. Rev. **55**, 364 (1939)
2. Oppenheimer, J.R., Volkoff, G.M.: On Massive Neutron Cores. Phys. Rev. **55**, 374 (1939)
3. Ruffini, R., Bonazzola, S.: System of self-gravitating particles in general relativity and the concept of an equation of state. Phys. Rev. **187**, 1767 (1969)
4. Demorest, P.B., et al.: A two-solar-mass neutron star measured using Shapiro delay. Nature **467**, 1081 (2010)
5. Belvedere, R., et al.: Neutron star equilibrium configurations within a fully relativistic theory with strong, weak, electromagnetic, and gravitational interactions. Nucl. Phys. A **883**, 1 (2012)
6. Page, D., et al.: Rapid cooling of the neutron star in Cassiopeia A triggered by neutron superfluidity in dense matter. Phys. Rev. Lett. **106**, 081101 (2011)
7. Eagles, D.M.: Possible Pairing without Superconductivity at Low Carrier Concentrations in Bulk and Thin-Film Superconducting Semiconductors. Phys. Rev. **186**, 456 (1969)
8. Greiner, M., Regal, C.A., Jin, D.S.: Emergence of a molecular Bose-Einstein condensate from a Fermi gas. Nature **426**, 537 (2003)
9. Kleihaus, B., et al.: Stable phases of boson stars. Phys. Rev. D **85**, 024045 (2012)
10. Benvenuto, O.G., Vito, M.A.: On the occurrence and detectability of Bose-Einstein condensation in Helium white dwarfs. J. Cosmol. Astropart. Phys. **2**, 033 (2011)
11. Nag, N., Chakrabarty, S.: Can a very low-luminosity and cold white dwarf be a self- gravitating Bose condensed system. arXiv:astro-ph/0008477v1 (2000)
12. Chavanis, P.-H.: BEC dark matter, Zeldovich approximation, and generalized Burgers equation. Phys. Rev. D **84**, 063518 (2011)
13. Harko, T.: Cosmological dynamics of dark matter Bose-Einstein condensation. Phys. Rev. D **83**, 123515 (2011)
14. Li, X.Y., et al.: Condensate dark matter stars. J. Cos. Astropart. Phys. **6**, 001 (2012)
15. Matos, T., Suarez, A.: Bose-Einstein condensate dark matter phase transition from U(1) symmetry breaking. Europhys. Lett. **96**, 56005 (2011)
16. Chavanis, P.-H., Harko, T.: Bose-Einstein condensate general relativistic stars. Phys. Rev. D **86**, 064011 (2012)
17. Colpi, M., et al.: Boson stars: gravitational equilibria of self-interacting scalar fields. Phys. Rev. Lett. **57**, 2485 (1986)
18. Bilic, N., Nicolic, H.: Self-gravitating bosons at zero temperature. Nucl. Phys. B **590**, 575 (2000)
19. Harko, T., Mocanu, G.: Cosmological evolution of finite temperature Bose-Einstein condensate dark matter. Phys. Rev. D **85**, 084012 (2012)

A Thalamacortical Feedback Model to Explain EEG During Anesthesia

Meysam Hashemi, Axel Hutt

INRIA CR Nancy - Grand Est, 54600 Villers-les-Nancy Cedex, France
{meysam.hashemi, axel.hutt}@inria.fr
http://www.loria.fr/~huttaxel

Abstract. General anaesthesia (GA) is a medical procedure which aims to achieve analgesia, amnesia, immobility and skeletal muscle relaxation. Although GA is commonly used in medical care for patients undergoing surgery, its precise underlying mechanisms and the molecular action of anaesthetic agents (AA) remain to be elucidated. A wide variety of drugs are used in modern anaesthetic practice and it has been observed that for many AAs, during the transition from consciousness to unconsciousness, the electroencephalogram shows biphasic effects in amplitude: an initial increase of the spectral power followed by a decrease at higher concentrations. Moreover during the administration of propofol, specific changes in EEG rhythms can be observed. The aim of this work is the extended discussion of a recent model by Hindriks and van Putten [8] that reproduces specific changes in EEG rhythms by the study of a neuronal population model of a single thalamocortical module. We illustrate specific features of the model, such as the physiological assumptions, the derivation of the power spectral density and the impact of the propofol concentration and of the stationary state. We show that the propofol-induced modification of the stationary state plays an important role in the understanding of the observed EEG.

Keywords: General anesthesia, Thalamocortical model, EEG, Power specrtum

1 Introduction

General anesthetics (GAs) include a large number of drugs which without them, modern medicine, especially surgery, would not have been possible. However, the mechanism underlying its anesthetic effects on human beings is not yet fully understood [1].

It has been observed that during the transition from consciousness to unconsciousness, by induction thippental, propofol, and sevoflurane, many derived EEG variables show biphasic effects, that is an initial increase of the spectral power followed by a decrease at higher concentrations [2]. Moreover, during the induction phase of propofol, enhanced oscilatory activity within several frequncy

A. Pelster and G. Wunner (eds.), *Selforganization in Complex Systems: The Past, Present, and Future of Synergetics*, Understanding Complex Systems,
DOI: 10.1007/978-3-319-27635-9_20

bands can be observed [3]. For clinically relevant concentration of propofol specific changes in EEG rhythms include an increase in alpha peak frequncy, over frontal regions, accompanied by increase in delta and theta power [4, 5].

Most of the previous studies on anesthetic phenomena have been done by considering a mean-field model to explain the biphasic behavior and describe some experimental feature of specific changes in electroencephalography (EEG) data recorded during anesthesia [6–9]. While some previous theoretical studies (Steyn-Ross 1999; Bojak and Liley et al. 2005; Hindriks and van Putten 2012) are based on the same type of continouous spatial mean-field model involving spatial partial derivatives [10], Hutt and Longtin have considered a neural populations model motivated by Wilson and Cowan [11] and Amari [12].

In this study we use a thalamocortical feedback model first developed by Rennie et al. [13] and recently extended to model general anaesthesia by Hindriks and van Putten [8] to repreduce the specific changes in EEG activity that can be observed during the propofol-induced general anesthesia. The present work reviews this latter model and points out the importance of stationary states to understand EEG power spectra during anaesthesia.

2 Methods

2.1 Model

The body of the model [8] is based on a population-level model of a single thalamo-cortical module consisting of four populations, namely an excitatory (E) and inhibitory (I) cortical population, a thalamic relay nucleus (S), and a thalamic reticular nucleus (R). The average soma membrane potential for a=E, I, S, R is modeled by

$$V_a(t) = \sum_{i=E,I,R,S} \bar{h}(t) \otimes K_{a,i}\phi_i(t - \tau_{a,i}), \tag{1}$$

where ϕ_i is the pulse firing rate of the population i (in units Hz). The constants $K_{a,b}$ are the strengths of the connections from population of type b to population of type a (in units mVs). The delay term, $\tau_{a,b}$ is zero if the both populations are in the thalamus or in the cortex. For thalamocortical or corticothalamic pathway, the delay is nonzero [14]. We point out that this model does not distinguish excitatory and inhibitory synapses in contrast to other models for general anaesthesia as [9, 6, 7].

In this model, only the axons of excitatory cortical neurons are long enough to emit propagating pulses along axons and the ϕ_E obeys the damped oscillator equation

$$D\phi_E = S(V_a), \tag{2}$$

in which the operator D is defined as

$$D = \left(\frac{1}{\gamma}\frac{\partial}{\partial t} + 1\right)^2, \tag{3}$$

where γ is the ratio of propagation velocity to mean axonal length. It is assumed that the spatial spread of activity is very fast in other populations and the activity variable can be approximated by a sigmoidal function as

$$\phi_a = S(V_a) = S_{max}[1 + \exp(-\frac{V_a - \theta}{\sigma})]^{-1}, \tag{4}$$

in which S_{max} is the maximal firing rate (in unit Hz), θ is the average activation threshold (in units mV), and σ is proportional to the standard deviation of activation thresholds over the populations (in units mV^{-1}).

In Eqs. (1), $\otimes$ denotes the convolution operator and $\bar{h}(t)$ denotes the mean synaptic responce function

$$\bar{h}(t) = \frac{\alpha\beta}{\beta - \alpha}\left(e^{-\alpha t} - e^{-\beta t}\right), \tag{5}$$

where α and β are the synaptic decay and rise rate of synaptic responce function, respectively.

External input to the system can be considered as a non-specific input to relay neurons as

$$K_{S,N}\phi_N = \langle\phi_N\rangle + \sqrt{2\kappa}\xi(t), \tag{6}$$

where $\langle\phi_N\rangle$ indicates its mean value, $\xi(t)$ is a Gaussian white noise with average zero and κ is the intensity of the driving noise. For more details of model and the nominal parameter values see [8].

2.2 Effect of propofol on populations

It has been shown that propofol increases the decay time constant of $\mathrm{GABA_A}$ synapses, and hence increases the total charge transfer in these synapses but not that of excitatory synapses [15]. Interestingly propofol has been shown to have a negligible effect on the amplitude synaptic receptors in cortical neurons [15].

To integrate physiological observations into the model, the potentiation of synaptic receptors in anaesthesia condition can be modelled by $\alpha \to \alpha/p$ with $p \geq 1$, which leads to a decrese in the decay rate constant α or equivalently, an increase in decay time constant of $\mathrm{GABA_A}$ receptors. The factor p indicates the target concentration of propofol in the neural populations. We take $p = 1$ for zero concentration i.e, baseline condition. Then we could replace the synaptic response $h(t)$ by

$$h(t) = \frac{H}{\eta(\alpha, \beta)}\bar{h}(t), \tag{7}$$

in which

$$\eta(\alpha, \beta) = \frac{\alpha\beta}{\beta - \alpha}\left[\exp\left(-\alpha\frac{\ln(\beta/\alpha)}{\beta - \alpha}\right) - \exp\left(-\beta\frac{\ln(\beta/\alpha)}{\beta - \alpha}\right)\right], \tag{8}$$

and where the constant H indicates the synaptic efficacy [8]. The maximum height of h indeed is H and hence is independent of the rate constants α and β. The baseline value chosen for α and β; α=50 Hz, β=200 Hz leads to the value $\eta(\alpha, \beta) = 31.5\mathrm{Hz}$.

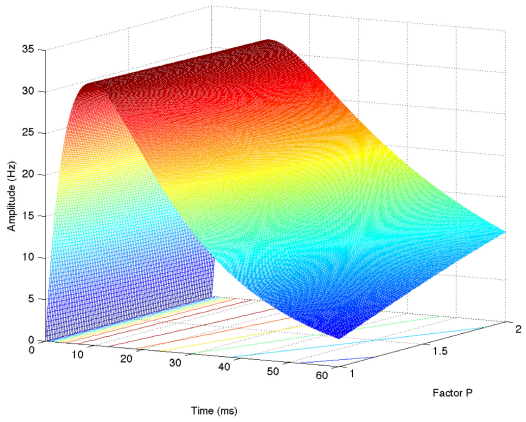

Fig. 1. The temporal synaptic response function $h(t)$ of inhibitory $GABA_A$ synapses subject to p. Parameters are set to α=50 Hz, β=200 Hz.

2.3 Theoretical power spectrum

The stationary state of Eqs. (1) obeys $dV_a(t)/dt = 0$. We could linearize the Eqs. (1) about the stationary state and write them in a general matrix form of a linear DDE as

$$\hat{\boldsymbol{L}}\left(\frac{\partial}{\partial t}\right)\boldsymbol{X}(t) = \boldsymbol{A}\boldsymbol{X}(t) + \boldsymbol{B}\boldsymbol{X}(t-\tau) + \boldsymbol{I}(t), \tag{9}$$

with matrices $\boldsymbol{A}$, $\boldsymbol{B}$, the system activity vector $\boldsymbol{X}$ and the external input $\boldsymbol{I}$. The solution of system can be written as

$$\boldsymbol{X}(t) = \int_{-\infty}^{\infty} \boldsymbol{G}(t-t')\boldsymbol{I}(t')dt', \tag{10}$$

and the Green function obeys

$$\hat{\boldsymbol{L}}\left(\frac{\partial}{\partial t}\right)\boldsymbol{G}(t) = A\boldsymbol{G}(t) + \ B\boldsymbol{G}(t-\tau) + \mathbf{1}\delta(t), \tag{11}$$

in which $\mathbf{1}$ is unitary matrix. Applying the Fourier transform

$$\boldsymbol{G}(t) = \frac{1}{\sqrt{2\pi}}\int_{-\infty}^{\infty} \tilde{\boldsymbol{G}}(\omega)e^{i\omega t}d\omega \tag{12}$$

yields

$$\tilde{\boldsymbol{G}}(\omega) = \frac{1}{\sqrt{2\pi}}[\hat{\boldsymbol{L}}(\omega) - A - Be^{-i\omega\tau}]^{-1}. \tag{13}$$

The power spectral density matrix $\mathbf{P}(\omega)$ of $\mathbf{x}$ is the Fourier transform of the auto-correlation function matrix $\langle \mathbf{X}(t)^t\mathbf{X}(t-T)\rangle$ (Wiener-Khinchine Theorem) leading to

$$\mathbf{P}(\omega) = 2\kappa\sqrt{2\pi}\tilde{\boldsymbol{G}}(\omega)\tilde{\boldsymbol{G}}^t(-\omega),$$

where the high index t denotes the transposed vector or matrix [16].

At the end, the model assumes that excitatory activity generates the EEG and by virtue of the specific choice of external input the power spectrum of the EEG depends just on one matrix component of the Greens function by

$$P_E(\omega) = 2\kappa\sqrt{2\pi}\tilde{G}_{1,3}(\omega)\tilde{G}_{1,3}(-\omega) = 2\kappa\sqrt{2\pi}\left|\tilde{G}_{1,3}(\omega)\right|^2. \tag{14}$$

The stationary state of Eqs. (1) is given by

$$\begin{aligned} V_{0E} &= K_{EE}S(V_{0E}) + p_1K_{EI}S(V_{0I}) + K_{ES}S(V_{0S}),\\ V_{0I} &= K_{IE}S(V_{0E}) + p_2K_{II}S(V_{0I}) + K_{IS}S(V_{0S}),\\ V_{0S} &= K_{SN}\langle\phi_N\rangle + p_3K_{SR}S(V_{0R}) + K_{SE}S(V_{0E}),\\ V_{0R} &= K_{RS}S(V_{0S}) + K_{RE}S(V_{0E}), \end{aligned} \tag{15}$$

where $K_{SN}\langle\phi_N\rangle = 1\text{mV}$ and we take three different impact factors for the anaesthetic effect of propofol as

$$\frac{H}{\eta_{ei}} = p_1, \frac{H}{\eta_{ii}} = p_2, \frac{H}{\eta_{sr}} = p_3,$$

in which we parametrize η_{ei}, η_{ii} and η_{sr} by

$$\eta_{ei} : \alpha \to \frac{\alpha}{p_1},\ \eta_{ii} : \alpha \to \frac{\alpha}{p_2},\ \eta_{sr} : \alpha \to \frac{\alpha}{p_3}.$$

This assumes a complete insensitivity of synaptic receptors located on cortical pyramidal neurons and reticular nucleus.

For the linearization of Eqs. (1) one obtains

$$\boldsymbol{X} = \begin{pmatrix} \phi_E \\ V_I \\ V_S \\ V_R \end{pmatrix},\ A = \begin{pmatrix} K_1 & K_2 & 0 & 0 \\ K_4 & K_5 & 0 & 0 \\ 0 & 0 & 0 & K_8 \\ 0 & 0 & K_{10} & 0 \end{pmatrix},\quad B = \begin{pmatrix} 0 & 0 & K_3 & 0 \\ 0 & 0 & K_6 & 0 \\ K_7 & 0 & 0 & 0 \\ K_9 & 0 & 0 & 0 \end{pmatrix},\ I(t) = \begin{pmatrix} 0 \\ 0 \\ \sqrt{2\kappa}\xi(t) \\ 0 \end{pmatrix},$$

with

$$\begin{aligned} K_1 = K_{EE}\ , K_2 = p_1K_{EI}\frac{\partial S[V]}{\partial V}\,|_{V=V_{0I}}\ ,\ K_3 = K_{ES}\frac{\partial S[V]}{\partial V}\,|_{V=V_{0S}},\\ K_4 = K_{IE}\ ,\ K_5 = p_2K_{II}\frac{\partial S[V]}{\partial V}\,|_{V=V_{0I}}\ ,\ K_6 = K_{IS}\frac{\partial S[V]}{\partial V}\,|_{V=V_{0S}},\\ K_7 = K_{SE}\ ,\ K_8 = p_3K_{SR}\frac{\partial S[V]}{\partial V}\,|_{V=V_{0R}}\ ,\ K_9 = K_{RE},\\ K_{10} = K_{RS}\frac{\partial S[V]}{\partial V}\,|_{V=V_{0S}}\ ,\ K_{11} = \frac{\partial S[V]}{\partial V}\,|_{V=V_{0E}}, \end{aligned}$$

and

$$\hat{\boldsymbol{L}}(\omega) - A - Be^{-i\omega\tau} = \begin{bmatrix} \tilde{L}\frac{\tilde{D}}{K_{11}} - K_1 & -K_2 & -K_3e^{-i\omega\tau} & 0 \\ -K_4 & \tilde{L} - K5 & -K_6 & 0 \\ -K_7e^{-i\omega\tau} & 0 & \tilde{L} & -K_8 \\ -K_9e^{-i\omega\tau} & 0 & -K_{10} & \tilde{L} \end{bmatrix} \tag{16}$$

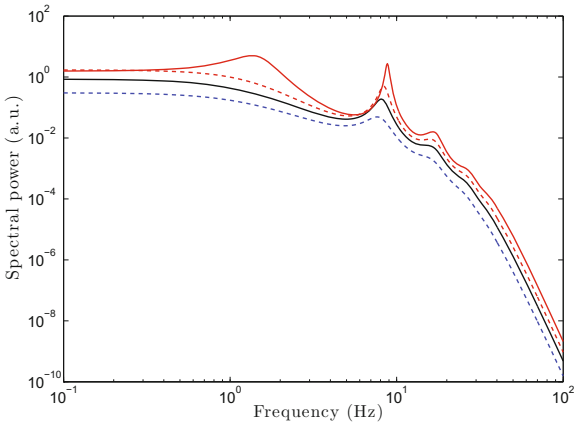

Fig. 2. Theoretical power spectrum of EEG in the baseline condition (solid black line) and three different sets of factor p in the anesthesia condition; p_1=p_3=1+0.3(p_2-1), p_2=1.05 (dashed red line), p_2=1.1 (solid red line) and p_1=p_2=p_3=1.1 (dashed blue line).

where $\tilde{L} = (1 + i\omega/\alpha)(1 + i\omega/\beta)$ and $\tilde{D} = (1 + i\omega/\gamma)^2$.
We point out that the new constants $K_i,\ i = 2, 3, 5, 6, 8, 10, 11$ are proportional to the nonlinear gain $\partial S/\partial V$ computed at the stationary state. With Eq. (13) and (16), it turns out that the stationary state and the corresponding nonlinear gain play in important role in the power spectrum.

3 Results

This section shows that the model under study repreduce the specific changes observed in EEG data during the propofol-induced anesthesia. Figure 2 shows the theoretical EEG power spectrum in the baseline condition and after the administration of propofol. The spectrum resembles well experimental observation in EEG power spectrum, i.e. increases in delta and theta power as well as more pronounced alpha oscilations with increased peak-frequency.

Figure 3 shows how the nonlinear gain and the stationary states dependent on the propofol concentration. We observe that the nonlinear gain may increase (a) or decrease (b) with increasing propofol dependent on the synapses that are modified. If the inhibitory synapses at excitatory neurons (p_1) and at relay nerons (p_3) respond identically to a change of the propofol concentration in a specific relation to the response of synapses at inhibitory neurons (p_2), then the nonlinear gain increases (Fig. 3(a)) reflecting an increased excitability and the power values increase as well (Fig. 2, red curves). In contrast, if the response of all three synapse types respond identically (as assumed in previous studies such as [9]), then the nonlinear gain decreases (Fig. 3(a)) and the decreased excitability diminishes the power spectrum values (cf. Fig. 2, blue curve).

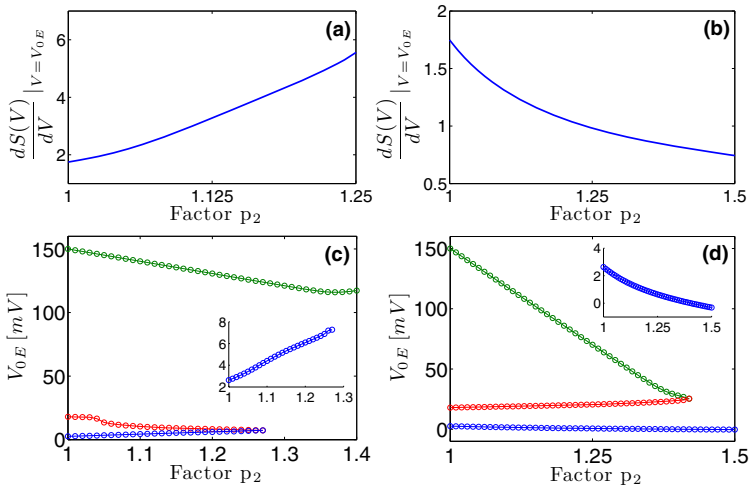

Fig. 3. The stationary states and the nonlinear gain dS/dV computed at the lowest stationary state of pyramidal neurons V_{0E} subjected to the factor p_2. **a, c)** p_1=p_3= 1+0.3(p_2-1), **b, d)** p_1=p_2= p_3. We observe three states in (c) and (d) for $p = 1$ where (c) the two lower states collide or (d) the two upper states collide. The center branch (red) is linearly unstable, whereas the other branches are linearly stable.

Moreover, the stationary states behave differently in the two cases, cf. Fig. 3(c) and (d). Increasing (decreasing) the nonlinear gain is accompanied by an increasing (decreasing) value of the corresponding stationary state, see panels (c) and (d). It is also remarkable that in (c) the two lower stationary states collide to a single state whereas in (d) the two upper states collide. This difference indicates two fundamentally different mechanisms which may yield the different dynamics obseved in the power spectrum. This link will be a research topic of future work.

4 Discussion

In the recent study of Hindriks and van Putten the authors have considered a high-dimensional mean field model to repreduce observed EEG changes during general anesthesia. The present work illustrates this work in some detail and highlights the important assumptions. We have extended the previous work by investigating the effect of the stationary state and have revealed the the increase or decrease of power seems to be strongly related the the increase or decrease of the stationary state of the system. This new finding proposes a more detailed study of the stationary state of neural population activity under anaesthesia.

Acknowledgments.

The authors acknowledge funding from the European Research Council for support under the European Union's Seventh Framework Programme (FP7/2007-2013) ERC grant agreement No.257253.

References

1. Alkire, M., Hudetz, A., Tononi, G.: Consciousness and anesthesia. Science **322**, 876–880 (2008)
2. Kuizenga, K., Wierda, J., Kalkman, C.: Biphasiceegchanges inrelation to loss of consciousness during induction with thiopental, propofol, etomidate, midazolam or sevoflurane. Br. J. Anaesth. **86**, 354–360 (2001)
3. Cimenser, A., Purdon, P.L., Pierce, E.T., Walsh, J.L., Salazar-Gomez, A.F., Harrell, P.G., et al.: Tracking brain states under general anesthesia by using global coherence analysis. Proc. Natl. Acad. Sci. U.S.A. **108**, 8832–8837 (2011)
4. Murphy, M., Bruno, M.A., Riedner, B.A., Boveroux, P., Noirhomme, Q., Landsness, E.C., et al.: Propofol anesthesia and sleep: a high-density EEG study. Sleep **34**, 283–291 (2011)
5. Ching, S., Cimenser, A., Purdon, P.L., Brown, E.N., Kopell, N.J.: Thalamocortical model for a propofol-induced rhythm associated with loss of consciousness. Proc. Natl. Acad. Sci. U.S.A. **107**, 22665–22670 (2010)
6. Bojak, I., Liley, D.: Modeling the effects of anesthesia on the electroencephalogram. Phys. Rev. E **71**, 041902 (2005)
7. Steyn-Ross, M., Steyn-Ross, D., Sleigh, J.W., Liley, D.T.J.: Theoretical electroencephalogram stationary spectrum for a white-noise-drivenvcortex: evidence for ageneral anesthetic-induced phase transition. Phys. Rev. E **60**, 7299–7311 (1999)
8. Hindriks, R., van Putten, M.J.A.M.: Mean-field modeling of propofol-induced changes in spontaneous EEG rhythms. Neuroimage **60**, 2323–2344 (2012)
9. Hutt, A., Longtin, A.: Effects of the anesthetic agent propofol on neural populations. Cogn. Neurodyn. **4**, 37–59 (2009)
10. Liley, D., Cadusch, P.J., Wright, J.J.: A continuum theory of electrocortical activity. Neurocomputing **26–27**, 795–800 (1999)
11. Wilson, H.R., Cowan, J.D.: A mathematical theory of the functional dynamics of cortical and thalamic nervous tissue. Kybernetik **13**, 55–80 (1973)
12. Amari, S.: Dynamics of pattern formation in lateral inhibition type neural fields. Biol. Cybern. **27**, 77–87 (1977)
13. Rennie, C.J., Robinson, P.A., Wright, J.J.: Unified neurophysical model of EEG spectra and evoked potentials. Biol. Cybern. **86**, 457–471 (2002)
14. Victor, J.D., Drover, J.D., Conte, M.M., Schiff, N.D.: Mean-field modeling of thalamocortical dynamics and a model-driven approach to EEG analysis. PNAS **118**, 15631–15638 (2011)
15. Kitamura, A., Marszalec, W., Yeh, J., Narahashi, T.: Effects of halothane and propofol on excita tory and inhibitory synaptic transmission in rat cortical neurons. J. Pharmacol. **304**, 162–171 (2002)
16. Hutt, A.: The anesthetic propofol shifts the frequency of maximum spectral power in EEG during general anesthesia: analytical insights from a linear model. Front. Comput. Neurosci. **7**, 2 (2013)

Paving the Royal Road for Complex Systems: On the Influence of Memory on Adaptivity

Christian Hinrichs[1], Sebastian Lehnhoff[2], and Michael Sonnenschein[1]

[1] University of Oldenburg, Germany,
christian.hinrichs@uni-oldenburg.de
sonnenschein@informatik.uni-oldenburg.de
http://www-ui.informatik.uni-oldenburg.de/1409.html
[2] OFFIS Institute for Information Technology, Oldenburg, Germany,
sebastian.lehnhoff@offis.de

Abstract. The "Royal Road" objective function was proposed by J. H. Holland in 1993 as a very hard benchmark problem for evolutionary algorithms. Generally, it belongs to the class of combinatorial optimization problems. In our work, we solve the problem in a distributed way by assigning each decision variable to an autonomous agent. The resulting multi-agent system "COHDA" forms a self-organizing complex system, where the global solution emerges from local interactions. By applying the XOR instance generator introduced by S. Yang in 2003, we are able to pertubate the system during runtime by modifying the objective function. This allows us to examine the robustness of COHDA against dynamic objectives. Here, we focus on the influence of runtime memory, which comprises the beliefs of each agent, on the adaptivity capabilities of the agents after an occured pertubation. We show that the final fitness values produced by the system do not suffer from a dynamic objective function, and are not influenced by the availability of an agents' runtime memory. The time needed by the system to adapt to such a pertubation, however, significantly increases if the agents' beliefs are being distorted. We conclude that, in terms of solution quality, COHDA is very robust against dynamic objective functions. With respect to adaptation speed, the heuristic benefits from the availability of runtime memory.

Keywords: Combinatorial Optimization, Self-Organization, Cooperation, Multi-Agent System

1 Introduction

In a general way, an optimization problem can be characterized as follows [1]: Given a set $\mathcal{S}$ of feasible solutions and an objective function $f : \mathcal{S} \to \mathbb{R}$, one tries to find those elements $s \in \mathcal{S}$ which maximize (or minimize) f. Typically, the elements in $\mathcal{S}$ are tuples comprising values for a set of decision variables $v_0 \dots v_n$. If the feasible values for these variables are discrete rather than continuous, this is called a combinatorial optimization problem. Instances of this

A. Pelster and G. Wunner (eds.), *Selforganization in Complex Systems: The Past, Present, and Future of Synergetics*, Understanding Complex Systems,
DOI: 10.1007/978-3-319-27635-9_21

family of problems are usually hard to solve, since their structure is less exploitable than in the continuous case. Even more, many of such problems are computationally intractable, so that exact solution methods are not appropriate [2]. Hence, a number of approaches have been proposed, which aim at finding a *quite good* solution in a *reasonably short* amount of time, but without guaranteeing any particular solution quality with respect to f. These approaches are called heuristics.

A special form of combinatorial optimization problem arises, if each variable $v_0 \dots v_n$ is controlled by an autonomous decision maker $a_0 \dots a_n$, respectively. Example applications for this kind of problem include distributed resource allocation, logistics and decentralized energy management. In such distributed systems, the decision makers (in the following simply denoted as agents) have to *coordinate* their decisions in order to jointly optimize the objective function f. Hence, when designing efficient solution strategies for such systems, not only computational complexity as well as memory complexity, but also communication complexity (information exchange between agents) has to be regarded.

Recently, the "COHDA" heuristic has been proposed, which utilizes a self-organization strategy in order to solve distributed combinatorial optimization problems efficiently in a completely decentralized and asynchronous way, and thus forms a nonlinear complex system, where the global solution emerges from local interactions [3, 4]. In the contribution at hand, we focus on the adaptivity capabilities of COHDA with respect to the amount of runtime memory of the underlying agents, using the example of a dynamic variant of the "Royal Road" benchmark problem.

2 The Dynamic Royal Road Benchmark Problem

The "Royal Road" objective function was proposed by J. H. Holland in 1993 as a very hard combinatorial optimization problem. The function takes a tuple $s = v_0 \dots v_{(2^k)\cdot(b+g)-1}$ of binary values as input, such that $v_i \in \{0, 1\}$, and produces a fitness value $f(s) \in \mathbb{R}$. The goal is to maximize f. The numbers k, b, g are predefined integer parameters, such that the tuple s comprises 2^k contiguous *regions*, each containing b values forming a *block*, and g values forming a *gap*. The evaluation criteria of f are designed such that each region contributes a higher fitness to the resulting global fitness value, the more 1's are contained in its block part, but only up to a certain threshold $m^* < b$. For amounts of 1's in the range $[m^* + 1, b - 1]$, a region would yield a negative fitness, and thus contribute a penalty to the global fitness value of the function. Finally, for a block full of 1's (this is then called a complete block), a region would again yield a large positive value. Furthermore, series of regions with complete blocks each would produce extra bonus values to the global fitness. In this whole fitness evaluation, the gaps do not have any influence on the resulting value. Hence, the optimal global fitness value will be reached if every block is "complete", and the worst solution (with a negative global fitness value) will be produced if every block contains exactly $b - 1$ ones.

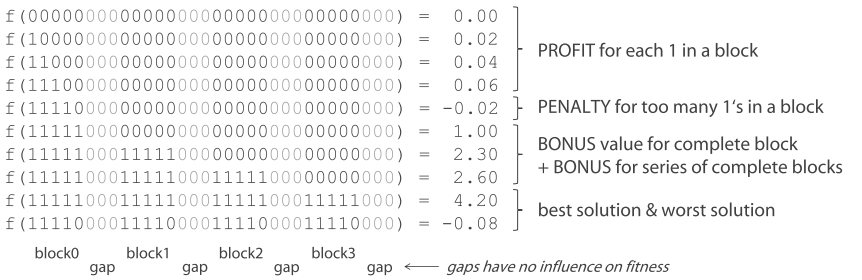

Fig. 1. Example of a "Royal Road" objective function ($k = 2$, $b = 5$, $g = 3$, $m^* = 3$).

In an iterative search process, most optimization algorithms would add more and more 1's to each block, until eventually each block comprises m^* ones. Since adding more 1's would introduce penalties and thus decrease the global fitness value, this poses a local optimum. But in order to reach the global optimum, an optimization procedure would have to pass the areas with very low fitness values in the solution landscape. Because of this property, the function is called *deceptive*. Figure 1 shows an example configuration. A more detailed description of Holland's "Royal Road" function can be found in [5].

Since the contribution at hand targets the adaptivity capabilities of the COHDA heuristic, the "Royal Road" objective function had to be converted to a dynamic variant. This can be done using the XOR instance generator introduced by S. Yang in 2003 [6]. For this purpose, a randomly chosen binary tuple T with a predefined Hamming weight $\mathrm{HW}(T)$ is chosen, and the objective function f is replaced by a function g, which is defined as $g(s) = f(s \otimes T)$. Here, the operator $\otimes$ is a component-wise XOR operation, thus changing the "meaning" of every value in s, where the corresponding value in T equals to 1. This transforms the solution landscape of the objective function without affecting its basic structure (i.e. number of optima). The Hamming weight determines the severity of the transformation: $\mathrm{sev}(T) = \frac{\mathrm{HW}(T)}{\mathrm{len}(T)}$. By applying such randomly chosen transformations at arbitrary time steps t during the optimization procedure, this allows us to analyze the behavior of the COHDA heuristic in a perturbed system.

3 COHDA

As stated in the introduction, COHDA is a heuristic for solving distributed combinatorial optimization problems. Basically, each decision variable of a given problem is controlled by an autonomous decision maker, implemented as a software agent in a multi-agent system. The agents are allowed to communicate through a communication network, whose topology forms a partially connected, undirected graph. Figure 2 shows an example of such a system. In COHDA, a global solution emerges from local interaction between agents. Each agent follows the same simple behavioral rules: 1) Upon an incoming information from

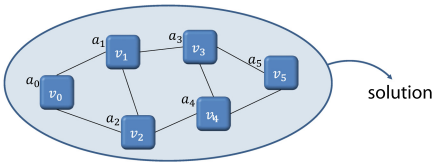

Fig. 2. Visualization of an exemplary communication topology used by COHDA.

a neighbor, the local knowledge base of the agent is updated. 2) Afterwards, the agent chooses the value for its controlled decision variable, that suites the currently believed system state the best. 3) The agent publishes its local knowledge base to the neighborhood. Following these three steps, the system will first asynchronously explore the solution space, before converging to the best solution found by an agent. More details on the heuristic can be found in [3, 4].

4 Evaluation

Our evaluation focuses on the adaptivity capabilities of COHDA in a dynamic, perturbed environment. The pertubations are modeled by a dynamic objective function as described in Sect. 2. In more detail, we analyzed the influence of an agent's runtime memory on the efficiency of the heuristic to converge after an occured pertubation. A simulation study has been performed using a royal road function with $k = 3$, $b = 5$, $g = 3$, $m^* = 3$. We compared different pertubation severities $\text{sev}(T) \in \{\text{None}, 0.0, 0.1, 0.2, 0.5\}$ against a number of configurations of runtime memory:

- **No memory.** Whenever a pertubation occured, the knowledge bases of all agents are completely erased, and each agent is re-initialized with a random value for its decision value.
- **Limited memory.** Same as above, except that the currently selected value for the decision variables are kept.
- **Full memory.** Knowledge bases are kept intact upon system pertubation.

Additionally, we included for reference an evolutionary algorithm with one parent, offspring of size 1 and adaptive mutation rate ((1+1)-ES, c.f. [7]). Each configuration was simulated 100 times, the results are summarized in Fig. 3, showing mean values and standard deviations. The upper chart presents the fitness of the solution produced by the algorithms, normalized to $[0, 1]$, whereas the lower chart depicts the number of iterations until convergence, as a measure of the time needed to converge. Concerning fitness, the COHDA heuristic produces significantly better results than the reference algorithm in all cases. Also, COHDA is unaffected by objective pertubations during runtime. With respect to the number of iterations until convergence, however, the results show that the heuristic benefits from the existence of runtime memory when a pertubation occurs, especially with low pertubation severities. Obviously, the agents make

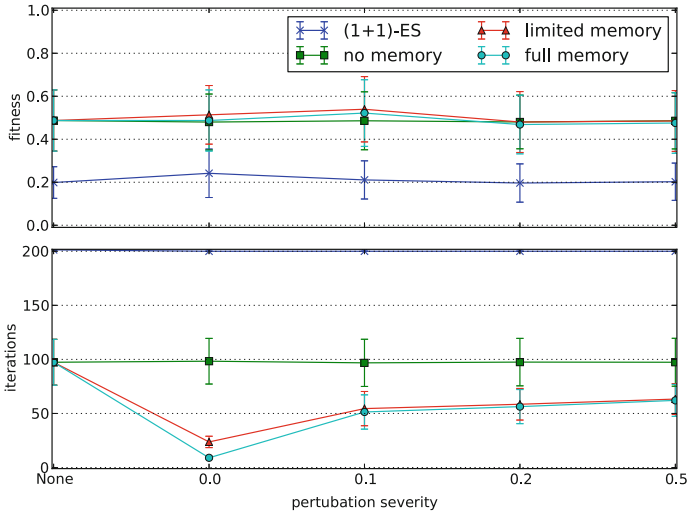

Fig. 3. Evaluation results: Pertubation severities compared against different levels of runtime memory, (1+1)-ES included for reference.

use of their existing memory in order to adapt to a changing objective function as fast as possible.

5 Application

The primary use case of the COHDA heuristic lies in the domain of decentralized energy management systems, as it is envisioned for example in the Smart Nord research project [8]. Here, coalitions of intelligent generators, loads and storages are formed in order to provide active power as well as ancillary services in the power grid. Within this research project, the goal of a coalition is to provide a *product* of either active power or ancillary services. This product can then be placed at a market (see Fig. 4). However, in the case of an active power product, the selection of an active power profile for each agent in the coalition, in order to jointly produce the desired product, forms a combinatorial optimization problem as described in the introduction. The COHDA heuristic can be used to solve this problem efficiently in a distributed way.

However, the COHDA heuristic relies on cooperative agents in principle. In our future work, we will study the influence of non-cooperative (i.e. self-interested) agents on COHDA. How many private constraints (with respect to an agent's interests) can the heuristic cope with? Up to which amount of non-cooperative agents is the heuristic still effective?

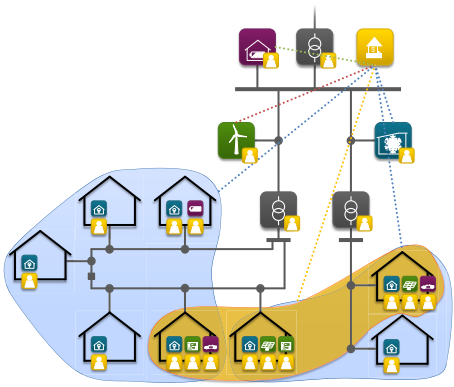

Fig. 4. Coalition Formation in the Smart Nord research project.

6 Conclusion

Our world gets more and more connected, evolving to an *internet of things*, where the interconnected entities get smarter every day. In our research, we focus on decentralized energy management systems. We believe that in such systems, self-organization is a promising way for providing coordination, and in turn to fulfill system-critical tasks. The self-organizing heuristic COHDA for solving combinatorial optimization problems is a building block in this vision.

References

1. Talbi, E.G.: Metaheuristics. John Wiley & Sons Inc., Hoboken (2009)
2. Blum, C., Roli, A.: Metaheuristics in combinatorial optimization. ACM Computing Surveys **35**, 268–308 (2003)
3. Hinrichs, C., Lehnhoff, S., Sonnenschein, M.: A decentralized heuristic for multiple-choice combinatorial optimization problems. In: Operations Research Proceedings. Springer (2012, to appear). `http://www.springer.com/series/722`
4. Hinrichs, C., Sonnenschein, M., Lehnhoff, S.: Evaluation of a self-organizing heuristic for interdependent distributed search spaces. In: Filipe, J., Fred, A.L.N. (eds) Proceedings of the 5th International Conference on Agents and Artificial Intelligence, ICAART 2013, vol. 1. SciTePress, Barcelona, February 15–18, 2013 (accepted)
5. Jones, T.: A Description of Holland's Royal Road Function. Evolutionary Computation **2**, 409–415 (1994)
6. Yang, S., Kingdom, U., Section, F.: Non-stationary problem optimization using the primal-dual genetic algorithm. In: The 2003 Congress on Evolutionary Computation, CEC 2003, vol. 3, pp. 2246–2253. IEEE Press, New York (2003)
7. Rechenberg, I.: Evolutionsstrategie - Optimierung technischer Systeme nach Prinzipien der biologischen Evolution. Fommann-Holzboog, Stuttgart (1973)
8. Smart Nord (2012). `http://www.smartnord.de`

Analysis of Noisy Spatio-Temporal Data

Oliver Kamps[1] and Joachim Peinke[2]

[1] Center for Nonlinear Science, Universität Münster, Germany
okamp@uni-muenster.de
[2] Institut für Physik & ForWind, Universität Oldenburg, Germany
peinke@uni-oldenburg.de
http://www.uni-oldenburg.de/twist

Abstract. In this article we discuss an extension of a method to extract Langevin equations from noisy time series to spatio-temporal data governed by stochastic partial differential equations (SPDEs). The reconstruction of the SPDEs from data is traced back to the estimation of multivariate conditional moments.

Keywords: Stochastic partial differential equations, data analysis

1 Introduction

The synergetic approach to complex systems, composed of many interacting subsystems, shows that the influence of the fast degrees of freedom on the order parameter dynamics can be described by dynamical noise. This leads to a mathematical description in terms of nonlinear Langevin equations of the form

$$\dot{y} = D^{(1)}(y) + \sqrt{D^{(2)}(y)}\Gamma \tag{1}$$

or a corresponding Fokker-Planck equation [1]. Here, $y(t)$ is the order parameter, $D^{(1)}(y)$, $D^{(2)}(y)$ are the drift and diffusion coefficients, respectively, and $\Gamma(t)$ describes a Gaussian distributed and δ-correlated stochastic force with zero mean. The two coefficients are defined according to

$$D^{(n)}(Y) = \lim_{\tau \to 0} \frac{1}{\tau} \frac{1}{n!} \langle [y(t+\tau) - y(t)]^n | y(t) = Y \rangle \tag{2}$$

which can for example be derived from the Kramers–Moyal expansion [2].

Pursuing the question of how to formulate an evolution equation for the velocity fluctuations on different scales in turbulent flows, Friedrich and Peinke [3] proposed to estimate these coefficients directly from experimental data by the approximation

$$D_*^{(n)}(Y) = \frac{1}{\tau_{\min}} \frac{1}{n!} \langle [y(t+\tau) - y(t)]^n | y(t) = Y \rangle \tag{3}$$

with $D^{(n)} \approx D_*^{(n)}$. In this context, $\tau_{\min}$ is the smallest available time scale which is still big enough to ensure that the stochastic dynamics can be described by a

A. Pelster and G. Wunner (eds.), *Selforganization in Complex Systems: The Past, Present, and Future of Synergetics*, Understanding Complex Systems,
DOI: 10.1007/978-3-319-27635-9_22

Markov process. In a large number of subsequent publications this method has been successfully applied to different scientific topics like turbulence research [3–5], finance [6], medicine [7–10] or engineering [11] to mention just a few. Besides applications to different scientific disciplines, research focused on technical questions connected to finite sampling times [12, 13] or measurement noise [14]. An recent overview is given in [15].

2 Outline of the Method

Many physical observables of complex systems do not only depend on time but also on space [1]. The dynamics of these systems is also influenced by dynamical noise [16]. In this contribution we want to show how the estimation of Langevin equations can be extended to spatio-temporal data governed by equations like

$$\partial_t y(\mathbf{z},t) = D^{(1)}[y(\mathbf{z},t)] + \sqrt{D^{(2)}[y(\mathbf{z},t)]}\Gamma(\mathbf{z},t) \tag{4}$$

where the drift and the diffusion coefficient depend on a spatially extended field $y(\mathbf{z},t)$. In general, the time evolution at the point $\mathbf{z}$ depends only implicitly via operators like e.g. spatial derivatives or integral expressions on the evolution at other points $\mathbf{z}'$. Due to this, we make the assumption that $D^{(1)}$ and $D^{(2)}$ are functions of the operators and $y(\mathbf{z},t)$ only and rewrite the equation as

$$\dot{y}_{\mathbf{z},t} = D^{(1)}[O_1,\ldots,O_N] + \sqrt{D^{(2)}[O_1,\ldots,O_N]}\Gamma_{\mathbf{z},t} \tag{5}$$

with $y_{\mathbf{z},t} := y(\mathbf{z},t)$ and the noise term $\Gamma_{\mathbf{z},t} := \Gamma(\mathbf{z},t)$. The stochastic force is defined according to

$$\langle \Gamma_{\mathbf{z},t}\rangle = 0\,, \quad \langle \Gamma_{\mathbf{z},t}\Gamma_{\mathbf{z}',t'}\rangle = \delta(t-t')C(|\mathbf{z}-\mathbf{z}'|) \tag{6}$$

where $C(|\mathbf{z}-\mathbf{z}'|)$ denotes the spatial correlation of the noise. The O_i represent the various operators. For example, in case of the reaction-diffusion equation

$$\partial_t y_{\mathbf{z},t} = \epsilon \Delta y_{\mathbf{z},t} + y_{\mathbf{z},t} - y^3_{\mathbf{z},t} + \sqrt{q(1+y^2_{\mathbf{z},t})}\Gamma_{\mathbf{z},t} \tag{7}$$

we would have $O_1 := y_{\mathbf{z},t}$ and $O_2 := \Delta y_{\mathbf{z},t}$. The drift and diffusion coefficients are then

$$D^{(1)}[O_1,O_2] = O_1 - O_1^3 + \epsilon O_2 \tag{8}$$

$$D^{(2)}[O_1,O_2] = q(1+O_1^2)\,. \tag{9}$$

One can show [17] that in close analogy to the normal Langevin equation (1), the drift and diffusion coefficient are defined as the multidimensional conditional averages

$$D^{(1)}[Y_1,\ldots,Y_N] = \lim_{\tau\to 0}\frac{1}{\tau}\langle y_{\mathbf{z},t+\tau} - y_{\mathbf{z},t} | O_1 = Y_1,\ldots,O_N = Y_N\rangle \tag{10}$$

$$D^{(2)}[Y_1,\ldots,Y_N] = \lim_{\tau\to 0}\frac{1}{\tau}\frac{1}{2}\langle [y_{\mathbf{z},t+\tau} - y_{\mathbf{z},t}]^2 | O_1 = Y_1,\ldots,O_N = Y_N\rangle\,. \tag{11}$$

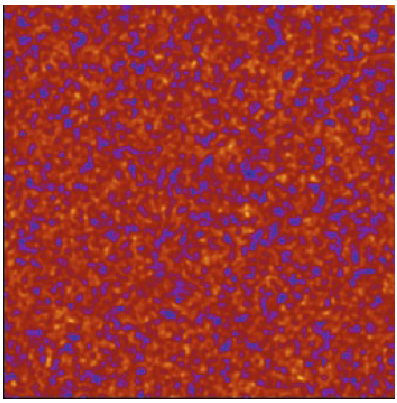

Fig. 1. Snapshot of a solution of the nonlinear SPDE (7).

It is important to note that in contrast to ordinary Langevin equations the number of conditions is not known in advance, because we do not know on how many operators the right-hand side of the SPDE depends. Therefore one has to use different combinations of operators in order to test which combination is more suitable to reproduce the data. As criterion for the correct selection of the operators, one could rearrange (4) (using the estimated coefficients $D_*^{(1,2)}$) to extract the noise, and analyze it for Gaussianity and δ-correlation. A further discussion of this question and related issues will be presented in [17].

The definitions of the drift and diffusion coefficients relate the problem of finding the structure of the SPDE to an estimation of multidimensional conditional averages or, in other words, to a multidimensional regression problem. Since kernel based methods show better convergence properties than histograms, we choose a local linear estimator [18] to determine the conditional averages.

3 Numerical Example

We now turn to a simple example illustrating the outlined procedure. By numerically integrating equation (7) we produce a time series of noisy spatial fields $y(\mathbf{z}, t)$. The data are then used to reconstruct the SPDE. The parameters used for the simulation are $\epsilon = 0.25$ and $q = 1$. The correlation function of the noise is proportional to $\exp(|\mathbf{z} - \mathbf{z}'|^2/(2l_c^2))$ with $l_c = 0.5$. The computational domain is discretized by a 256^2 grid and has a side length of $L = 100$. In Fig. 1, an example of the solution of (7) is depicted. Without noise, the equation shows moving fronts as solutions. Due to the strong noise, these structures are not visible anymore.

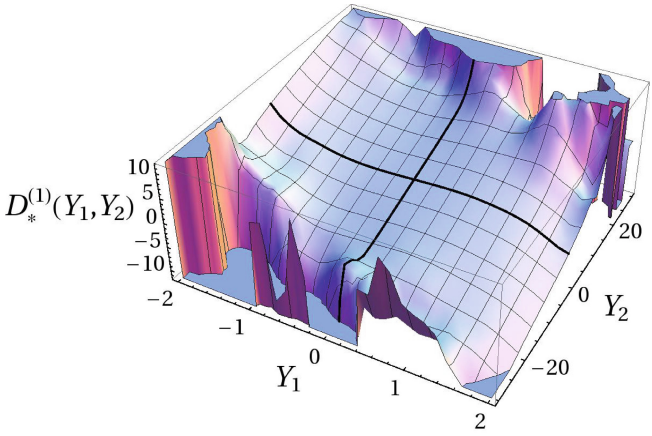

Fig. 2. Visualization of $D_*^{(1)}[Y_1, Y_2]$ estimated from the simulation data. The two thick lines highlight the cuts $Y_1 = 0$ and $Y_2 = 0$ shown in Fig. 3.

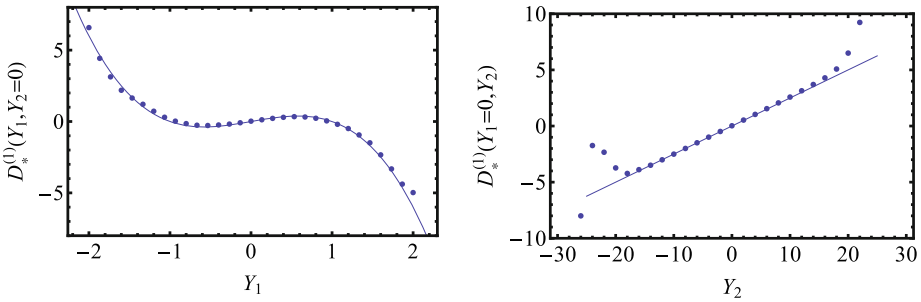

Fig. 3. The estimated drift coefficient (dots) $D_*^{(1)}[Y_1, Y_2 = 0]$ (left), $D_*^{(1)}[Y_1 = 0, Y_2]$ (right) together with the exact result (line).

Given the data from 100 time steps, the unknown coefficients are estimated via the conditional moments

$$D_*^{(1)}[Y_1, Y_2] = \frac{1}{\tau_{\min}} \langle y_{\mathbf{z},t+\tau} - y_{\mathbf{z},t} | Y_1 = y_{\mathbf{z},t}, Y_2 = \Delta y_{\mathbf{z},t} \rangle \tag{12}$$

$$D_*^{(2)}[Y_1, Y_2] = \frac{1}{\tau_{\min}} \frac{1}{2} \langle [y_{\mathbf{z},t+\tau} - y_{\mathbf{z},t}]^2 | Y_1 = y_{\mathbf{z},t}, Y_2 = \Delta y_{\mathbf{z},t} \rangle \,, \tag{13}$$

where $\tau_{\min}$ is the time difference between two subsequent time steps. In Fig. 2, a three-dimensional plot of (12) is shown. One can clearly see the cubic dependence on Y_1 and the linear dependence on Y_2, i.e. $\Delta y_{\mathbf{z}}$. At the boundaries, the estimation of $D^{(1)}$ becomes less reliable due to the small amount of data in this region, which results in larger fluctuations in the conditional moment.

For a better quantitative comparison, cuts along the Y_1-axis and the Y_2-axis are shown in Fig. 3 . In the center, the estimated conditional moment $D_*^{(1)}$

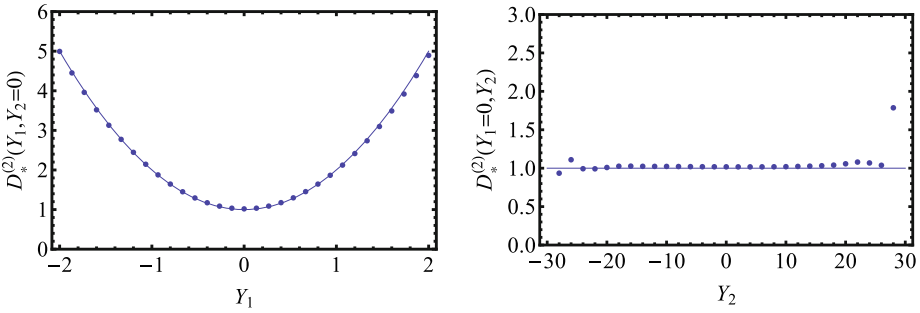

Fig. 4. The estimated diffusion coefficient (dots) $D_*^{(2)}[Y_1, Y_2 = 0]$ (left), $D_*^{(2)}[Y_1 = 0, Y_2]$ (right) together with the exact result (line).

correctly reconstructs the dependence of $D^{(1)}$ on Y_1 and Y_2. In Fig. 4, the same plot is shown for $D_*^{(2)}$: The diffusion coefficient also is estimated correctly.

4 Conlusion and Outlook

In this paper, we have shown that the method to extract drift and diffusion coefficients for Langevin equations from time-series as introduced in [3] can be extended to processes governed by SPDEs. In contrast to pure time-series, one has to estimate conditional moments depending on several conditions, each condition representing one kind of operator in the right hand side of the SPDE. Since the number and the kind of operators are not known in advance one has to test several combinations of operators, or one has to make assumptions on the general structure of the SPDE [17] to reduce the complexity of the problem. Also the methods reviewed in [15] and the extension presented here are suited to analyze experimental data, we want to point out that these methods can also be valuable tools to analyze data from large scale simulations of complex systems where a reduced description in terms of lower number of degrees of freedom is needed. An example for this approach can be found in the context of simulations of large biomolecules [19].

References

1. Haken, H.: Synergetics: Introduction and Advanced Topics. Springer (2004)
2. Risken, H.: The Fokker-Planck Equation: Methods of Solutions and Applications. Springer Series in Synergetics, 2nd edn. Springer (1996)
3. Friedrich, R., Peinke, J.: Description of a Turbulent Cascade by a Fokker-Planck Equation. Phys. Rev. Lett. **78**(5), 863–866 (1997)
4. Renner, C., Peinke, J., Friedrich, R.: Experimental indications for Markov properties of small-scale turbulence. Journal of Fluid Mechanics **433**, 383–409 (2001)
5. Renner, C., Peinke, J., Friedrich, R., Chanal, O., Chabaud, B.: Universality of small scale turbulence. Phys. Rev. Lett. **89**(12), 124502 (2002)

6. Renner, C., Peinke, J., Friedrich, R.: Evidence of Markov properties of high frequency exchange rate data. Physica A: Statistical Mechanics and its Applications **298**(3–4), 499–520 (2001)
7. Kuusela, T.: Stochastic heart-rate model can reveal pathologic cardiac dynamics. Phys. Rev. E **69**(3), 031916 (2004)
8. Prusseit, J., Lehnertz, K.: Stochastic qualifiers of epileptic brain dynamics. Phys. Rev. Lett. **98**(13), 138103 (2007)
9. Kirchner, J., Meyer, W., Elsholz, M., Hensel, B.: Nonstationary Langevin equation: Statistical properties and application to explain effects observed in cardiological time series. Phys. Rev. E **76**(2), 021110 (2007)
10. Bahraminasab, A., Ghasemi, F., Stefanovska, A., McClintock, P.V.E., Friedrich, R.: Physics of brain dynamics: Fokker-Planck analysis reveals changes in EEG $\delta-\theta$ interactions in anæsthesia. New Journal of Physics **11**(10), 12 (2009). 103051
11. Gradišek, J., Siegert, S., Friedrich, R., Grabec, I.: Analysis of time series from stochastic processes. Phys. Rev. E **62**(3), 3146–3155 (2000)
12. Kleinhans, D., Friedrich, R., Nawroth, A., Peinke, J.: An iterative procedure for the estimation of drift and diffusion coefficients of Langevin processes. Phys. Lett. A **346**(1–3), 42–46 (2005)
13. Honisch, C., Friedrich, R.: Estimation of Kramers-Moyal coefficients at low sampling rates. Phys. Rev. E **83**, 066701 (2011)
14. Böttcher, F., Peinke, J., Kleinhans, D., Friedrich, R., Lind, P.G., Haase, M.: Reconstruction of complex dynamical systems affected by strong measurement noise. Phys. Rev. Lett. **97**(9), 090603 (2006)
15. Friedrich, R., Peinke, J., Sahimi, M., Tabar, M.R.R.: Approaching complexity by stochastic methods: From biological systems to turbulence. Physics Reports **506**(5), 87–162 (2011)
16. Sagués, F., Sancho, J.M., García-Ojalvo, J.: Spatiotemporal order out of noise. Rev. Mod. Phys. **79**(3), 829–882 (2007)
17. Kamps, O., Peinke, J. (in preparation)
18. Härdle, W.K., Müller, M., Sperlich, S., Werwatz, A.: Nonparametric and Semiparametric Models. Springer (2004)
19. Hegger, R., Stock, G.: Multidimensional Langevin modeling of biomolecular dynamics. J. Chem. Phys. **130**(3), 034106 (2009)

Foam Decay with Incomparable Lorenz Curves

Katharina Knicker[1] and Peter Plath[2]

[1] Physikalische Chemie, Universität Bremen and Fritz-Haber Institut der Max-Planck Gesellschaft, Germany present address: Institute for Applied Physics, Quantum Optics, University of Bonn, Germany
knicker@iap.uni-bonn.de
[2] Fritz-Haber Institut der Max-Planck Gesellschaft, Germany
peter_plath@t-online.de

Abstract. The decay of beer foam is recorded by evaluating pictures, measuring the bubble sizes. We use Lorenz curves in order to avoid the problem of bubble size classification, which is naturally connected with the estimation of a classical distribution function. It turns out that consecutive Lorenz curves intersect which each other. The intersection of Lorenz curves is directly connected with Ruch's idea of incomparable diagrams in the lattices of partitions. This observation suggests the existence of different, incomparable structures in decaying foam.

Keywords: foam decay, intersecting Lorenz curves, incomparable structures, Ruch's partition diagram lattices

1 Introduction

Foam is of great importance for modern industrial products, cosmetics, food, and beverage industry. However, there is not much known on the creation and decay of foam up to now. We were interested in the temporal evolution of bubble size distributions during the decay of beer froth. For this reason, we used ultrasonic foaming up of beer to achieve a reproducible situation in which all bubbles are almost of the same size [1]. In this way we created an ordered structure. However, this structure is unstable because of the dependence of pressure inside the bubbles on their diameters which are slightly different by creation. Therefore the foam decays passing through very different less ordered structures. The decay was documented photographically every second using a CCD device (Fig. 1). As a result we obtained 300 pictures with 600 - 800 bubbles at the beginning and 200 bubbles per picture at the end of the measurement. The bubble size distributions right after the foaming-up are of small half-widths. They become wider in time and split up in a poly-nodal distribution function after passing the drainage phase, when Apollonian structures are formed [2]. The decrease of the number of bubbles and the formation of a poly-nodal distribution function raises the question how to characterize the different distribution functions. In economy one has a similar problem if one wishes to compare the income distribution functions of different states, or its time dependence if populations are changing

A. Pelster and G. Wunner (eds.), *Selforganization in Complex Systems: The Past, Present, and Future of Synergetics*, Understanding Complex Systems,
DOI: 10.1007/978-3-319-27635-9_23

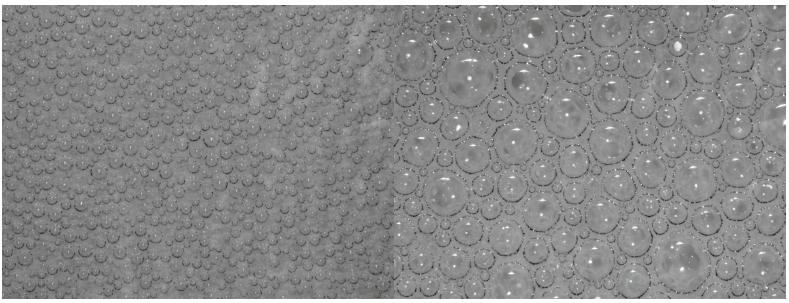

Fig. 1. Photographs of foam at the beginning (left) shows almost uniform bubble sizes while at the end of the measurement (right) large deviations of the bubble sizes can be observed.

in their magnitudes. In this context, Rothschild and Stiglitz used the methods developed by Lorenz and Gini to describe quite different social and economic situations [3, 4].

2 The Lorenz method and the Rothschild-Stiglitz statement

In order to compare the bubble size distributions we formed a vector ordered monotonously with increasing bubble size for each picture. Taking the partial sums of all components of the vector as a function of their corresponding running numbers one obtains the discrete Lorenz function, which is related to the bubble size distribution considered. This Lorenz method is well known from macroeconomics, where it is used to compare social and financial distributions. One picture results in a distribution of n bubbles. Let x_i be the diameter of bubble i, with $i = 1, \ldots, n$. Order the bubbles from small to large to obtain the vector $(x_1, \ldots, x_n)$. Now plot the points $(k/n, S_k/S_n)$, $k = 0, \ldots, n$, where $S_0 = 0$ and

$$S_k = \sum_{i=1}^{k} x_i \tag{1}$$

is the total contribution of the smallest k bubbles in the distribution. Join these points by line segments to obtain a curve connecting the origin with the point $(1, 1)$ (Fig. 2). If the bubble sizes are uniformly distributed in the foam then the Lorenz curve is a straight line – the diagonal of the doubly normalized diagram. Otherwise the curve is convex and lies under this straight line [3]. By this means one can introduce a total order on the set of all Lorenz curves, i.e. one can argue that the lower curve represents a distribution which is smaller, i.e. which has a greater inequality, than the distribution with a Lorenz curve located on top of the curve under consideration. However, if two Lorenz curves cross each other, an additional criterion has to been taken into account in order to allow

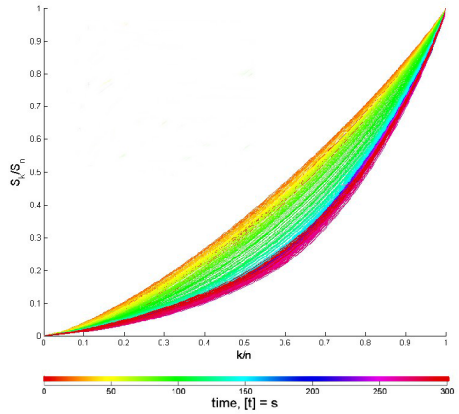

Fig. 2. Lorenz curves of bubble size distributions. Every curve belongs to one picture of the measurement. According to the pictures the number of bubbles changes over time. The rainbow sequence of colours represents the time – from red to violet.

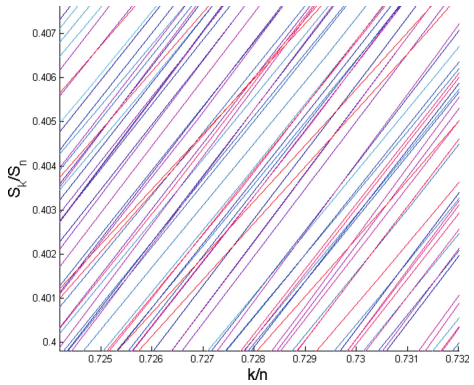

Fig. 3. A detail of Fig. 2 exemplifying the intersection of Lorenz curves. The rainbow sequence of colours represents the time.

the comparison of these distributions (theorem of Rothschild and Stiglitz [5]). From their theorem it can be concluded that if two Lorenz curves intersect, it depends on the choice of the function which of the two curves describes a greater inequality of the distribution. This statement corresponds to the idea of incomparable diagram structures developed earlier by the theoretical chemist E. Ruch [6]. Indeed, we observed crossing Lorenz curves of developing bubble size distributions which succeed each other in time (Fig. 3). One may argue that this observation is a result of the fact that we wish to compare distribution functions which originate from different numbers of bubbles. In order to examine the assumption, put the dimension n of the vector of each picture to be constant: $n = n_0$, namely the maximum number of the bubbles which have been observed

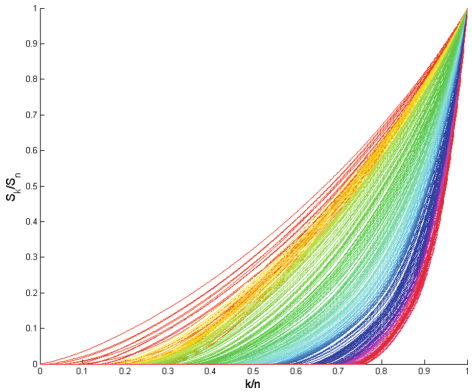

Fig. 4. Lorenz curves of bubble size distributions. Every curve belongs to one picture of the measurement. According to Ruch order [6] the number of bubbles has to be constant. Missing bubbles are represented by diameters of zero. The rainbow sequence of colours represents the time.

right at the beginning: missing or vanishing bubbles are accounted for as existing bubbles with vanishing diameter. The corresponding Lorenz functions are shown in Fig. 4. Again points of intersection of Lorenz curves can be observed (Fig. 5). It is hard to understand that red and green coloured Lorenz curves intersect because of the corresponding time intervals, but what is more, one can observe intersecting red as well as intersecting green lines which lie close to each other in time. This is indeed a very surprising result since according to the arguments of

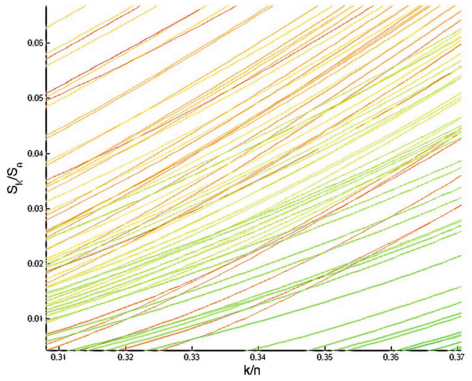

Fig. 5. A detail of Fig. 4. One can observe intersecting red coloured Lorenz curve which are temporarily neighboured as well as green crossing Lorenz curves. The rainbow sequence of colours represents the time.

Ernst Ruch incomparable states should not emanate from each other but from a common mother state.

3 Ruch's incomparable diagrams and intersecting Lorenz Curves

Partition diagrams of natural numbers $n \in \mathbb{N}$ can be represented as diagram lattices which are totally ordered if $n \leq 5$, otherwise they form lattices, which are partially ordered. In this way Ruch defined incomparable diagrams, or partitions, respectively [6]. If one takes the diagrams as representation of distribution functions, one can map one Lorenz curve to each of the diagrams. It turns out that Lorenz curves of comparable diagrams do not intersect (see Fig. 6), whereas the Lorenz curves of incomparable diagrams intersect with each other (see Fig. 7 and Fig. 8).

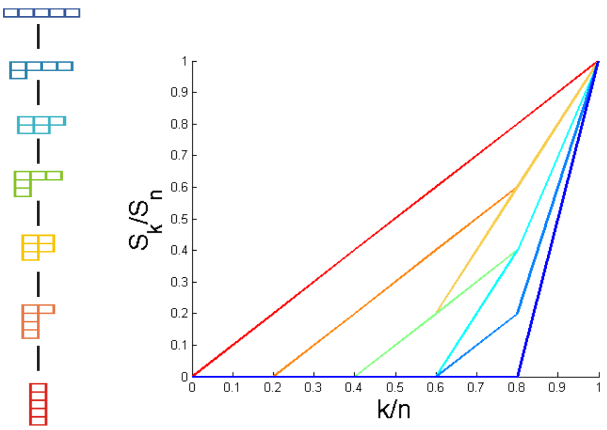

Fig. 6. Ruch's diagram lattice of the number $n = 5$ and (right) the corresponding Lorenz curves, which do not intersect with each other.

4 Concluding remarks

In earlier works (cf. [7–9]) we have used Ruch's diagrams in order to describe the temporal evolution of the different structures during decay of foam. The development of structures in the decaying foam could be described by a pathway on the diagram lattice [10]. As a consequence, the system would have to decide each time how to develop, if incomparable distributions appear in its imminent future. But this procedure was connected with the classification of bubble sizes in order to estimate bubble size distribution functions, i.e. the frequency of bubbles in the corresponding classes. In the present paper we have chosen the Lorenz method in order to avoid the problem of classification, which naturally

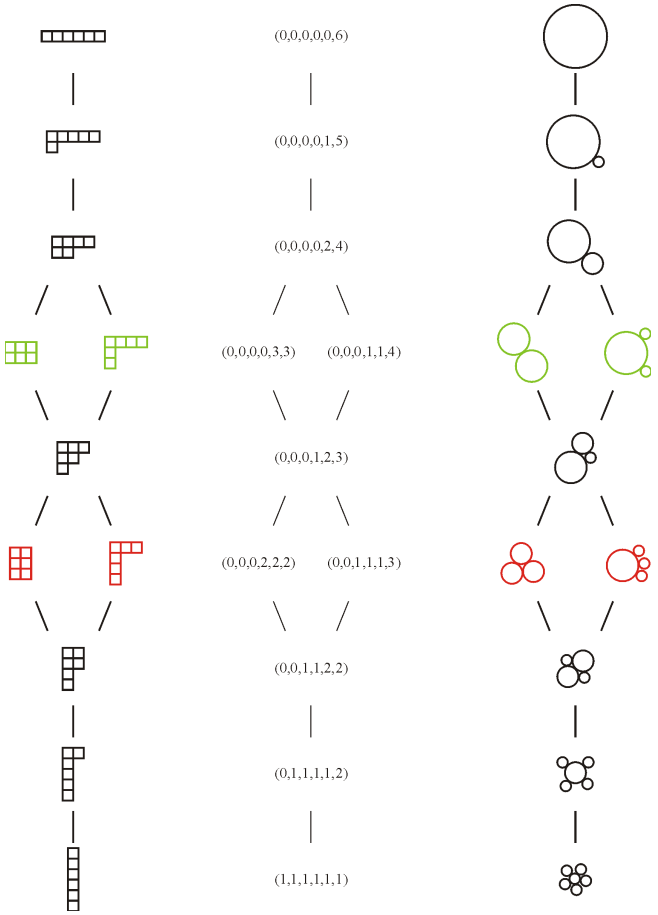

Fig. 7. Left: Ruch's diagram lattice of the number $n = 6$. The green, as well as the red marked diagrams are incomparable. Middle: Corresponding partition vectors of the number $n = 6$ ordered according to increasing number of non-zero entries. Right: A possible corresponding distribution of bubble sizes.

is connected always with some preconceptions. However, experimentally it turns out that the incomparability of distribution patterns, i.e. the intersections of Lorenz curves following each other, becomes the crucial problem again. These observations lead to our conviction that in the foam there may exist regions of incomparable structures with different histories. During our observations such regions could come to our inspection by the very fast and complex movement of bubbles in wet foam or they may by created just in the time interval of taking pictures. Nevertheless, both the methods which we used show unambiguously the simultaneous existence of incomparable distribution functions in the developing foam. As a consequence, we come to the conclusion that the foam decay has to be described by a bundle of quite different pathways in the space of the distribution functions.

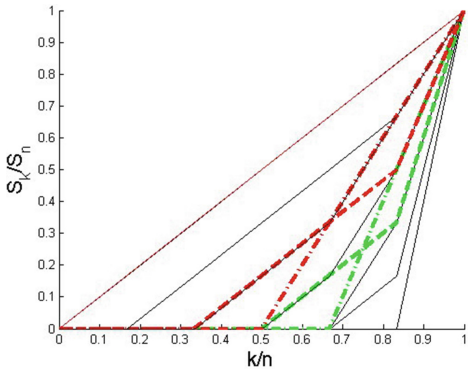

Fig. 8. Lorenz curves of Ruch diagrams for $n = 6$. The intersecting dashed Lorenz curves in boldface belong to the incomparable green and red diagrams in Fig. 7, respectively.

5 Acknowledgments

We are indebted to Dr. Sonja Sauerbrei and Dr. Ernst-Christoph Haß for fruitful discussions. We thank the Fritz Haber Institute - Abt. Physical Chemistry for offering us the opportunity to carry out the experiments.

References

1. Sauerbrei, S., Knicker, K., Sydow, U., Haß, E.-C., Plath, P.J.: An overview of the dynamics of bubble size distributions of a beer foam decay and their order structure. In: Plath, P.J., Haß, E.-C. (eds.) Vernetzte Wissenschaften, pp. 291–304. Crosslinks in Natural and Social Sciences. Logos Verlag, Berlin (2008)
2. Plath, P., Sauerbrei, S.: Apollonische Umordnung des Schaums. Brauindustrie **89**(7), 20–23 (2004). (Verlag W. Sachon)
3. Kleiber, C.: The Lorenz curve in economics and econometrics. In: Gini-Lorenz Centennial Conference, Siena, May 23–26, 2005. A publication of the Center of Business and Economics (WWZ), University of Basel, pp. 1–20 (2007). (invited paper)
4. Marshall, A., Olkin, I.: Inequalities: Theory of Majorization and its Applications. Academic Press (2009) 563, 712
5. Rothschild, M., Stiglitz, J.: Equilibrium in competitive insurance markets. Quarterly Journal of Economics **90**, 629–649 (1976)
6. Ruch, E.: The diagram lattice as structural principle. Theoret. Chim. Acta (Berl.) **38**, 167–183 (1975)
7. Sauerbrei, S., Sydow, U., Plath, P.J.: On the characterization of foam decay with diagram lattices and majorization. Z. f. Naturforschung **61a**, 153–165 (2006)
8. Sauerbrei, S., Plath, P.J.: Diffusion without constraints. Journal of Mathematical Chemistry **42**(2), 153–175 (2007)
9. Sauerbrei, S., Knicker, K., Haß, E.-C., Plath, P.J.: Weak majorization as an approach to non-equilibrium foam decay. Appl. Math. Sciences **1**(11), 527–550 (2007)
10. Patzelt, G.: Zerfall von Bierschaum - Dynamik auf Partitionsdiagrammen. Diplomarbeit Universität Bremen (2007) 40

Bubbles, Jumps, and Scaling from Properly Anticipated Prices

Felix Patzelt*, Klaus Pawelzik

Institut für Theoretische Physik, Universität Bremen
felix@neuro.uni-bremen.de
pawelzik@neuro.uni-bremen.de
http://neuro.uni-bremen.de

Abstract. Prices in financial markets exhibit extreme jumps far more often than can be accounted for by external news. Further, magnitudes of price changes are correlated over long times. These so called stylized facts are quantified by scaling laws similar to, for example, turbulent fluids. They are believed to reflect the complex interactions of heterogenous agents which give rise to irrational herding. Therefore, the stylized facts have been argued to provide evidence against the efficient market hypothesis which states that prices rapidly reflect available information and therefore are described by a martingale. Here we show, that in very simple bidding processes efficiency is not opposed to, but causative to scaling properties observed in real markets. Thereby, we link the stylized facts not only to price efficiency, but also to the economic theory of rational bubbles. We then demonstrate effects predicted from our normative model in the dynamics of groups of real human subjects playing a modified minority game. An extended version of the latter can be played online at seesaw.neuro.uni-bremen.de.

Keywords: Bubbles, Stylized Facts, Efficient Markets, Minority Games

1 Introduction

Many studies of financial datasets emphasise scaling properties [1]. Further, large jumps in price time series often cannot be attributed to external events [2]. Some claim that these findings contradict the efficient market hypothesis (EMH) [3]. However, the EMH foremost states, that no systematic profit is possible from observing previous prices p because predictable price changes are eliminated by traders exploiting them [4]. This property holds well as a stylized concept [5]. The distribution of log-returns $r(t) = \log(p_t/p_{t-1})$ would be Gaussian only if further assumptions like a fast convergence according to the central limit theorem would hold true which is not neccessarily the case. Furthermore, there are also economic models with perfectly rational traders that can exhibit "rational bubbles" where prices deviate far from fundamental values [6]. Hence, bubbles and crashes do not disprove the EMH.

* Currently supported by the Volkswagen-Foundation

A. Pelster and G. Wunner (eds.), *Selforganization in Complex Systems: The Past, Present, and Future of Synergetics*, Understanding Complex Systems,
DOI: 10.1007/978-3-319-27635-9_24

Here, we establish a systematic link between these endogenous mechanisms for bubbles and crashes on the one hand and the stylized facts on the other hand. We show, that price efficiency in a simplistic bidding process links bubbles with the most prominent stylized facts of financial price time series. While the model is rather abstract and currently tied to a specific pricing rule, many qualitative and quantitative features of real returns are captured both numerically and analytically. Our model further makes directly testable predictions, some of which were confirmed in behavioral group experiments.

2 The Model

Consider a market with N agents: N_s speculators and N_r random traders. At discrete times t each agent places a market order to either buy or sell one unit of an asset (e.g. a stock). Thereby, agents contribute to either the demand d_t or to the supply $s_t = N - d$. For simplicity we only allow market orders, that is, d_t and s_t do not depend on the price at which the orders are executed. Note, that the latter is generally not known a priori at stock-, foreign exchange-, and similar markets. We further require: 1. Increasing d_t increases the price while increasing s_t decreases the price. 2. The price p_t is invariant to the traded volume: scaling d_t and s_t by the same factor yields the same price. This allows e.g. for some not executed orders as long as the same fraction of buy and sell orders are affected. Therefore,

$$p_t = \frac{d_t}{s_t} = \frac{d_t}{N - d_t} \tag{1}$$

which naturally possesses the correct unit.

Agents make their decisions stochastically and we postulate price efficiency: the probability for a speculator to buy at each time t is chosen such that the expectation value of the new price given all previous observations

$$\langle p_t \,|\, p_{t-1}, p_{t-2}, \dots \rangle \stackrel{!}{=} p_{t-1} \tag{2}$$

is the same as the previous price. This condition may be violated only if $d_t > N_s + N_r/2$ or if $d_t < N_r/2$. In these cases, it is impossible to be price efficient in this model due to the discretization of the traded assets. However, for $N_s \gg N_r$ and $N_s \gg 1$, we consider this boundary effect acceptable.

A model time series is shown in Fig. 1 A. The distribution of log-returns is power-law tailed. The exponent in the cumulative distribution approaches $\xi = 2$ for large systems (Fig. 1 B). Finite size effects or large N_r/N_s increase ξ (not shown). Log-returns are uncorrelated while their magnitudes are correlated for long periods of time (Fig. 1 C) reflecting realistic volatility clustering.

3 Analytical Results

To obtain an explicit solution to Eq. (2), a good approximation for large N is to require efficient demands instead of efficient prices:

$$\langle d_t, \,|\, d_{t-1}, d_{t-2}, \dots \rangle \stackrel{!}{=} d_{t-1}. \tag{3}$$

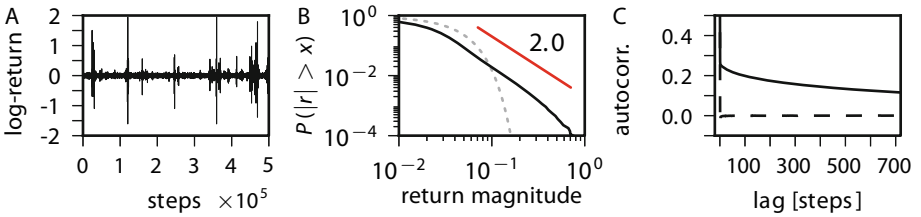

Fig. 1. Price efficient model with $N_s = 10000$ speculators and $N_r = 10$ random (coin flipping) traders. A: Time series. B: Complementary cumulative distribution of log return magnitudes (solid black line) and a Gaussian with the same variance (dashed gray line). Straight line: analytical result. C: Autocorrelation of the log returns (dashed line) and of their magnitudes (solid line).

Since agents choose stochastically, the demands generated by the speculators and random traders each are binomially distributed. Eq. (3) is fulfilled, if the probability for each speculator to buy at time t is

$$P(\text{buy} \,|\, d_{t-1}) = \frac{1}{2} + \frac{d_t - N/2}{N_s} \tag{4}$$

Fig. 2 A shows a comparison of Eq. (4) with a numerical optimization with respect to Eq. (2). For efficient prices, there is a slight drift away from the system boundaries that is not present for efficient demands. However, this difference decreases with an increased system size N.

Eq. (4) further shows why a small number of random agents is important for a finite system. For $N_r = 0$, we obtain $P(\text{buy} \,|\, d_{t-1}) = d_{t-1}/N$. Then, if by chance the system ends up in the boundary states $d = 0$ and $d = N$, it can never leave unless we allow for a violation of Eq. (2) as discussed above. An alternative to random agents would be a reset rule like $P(\text{buy} \,|\, d_{t-1} \in \{0, N\}) = 1/2$.

3.1 Stationary solution

For large N_s, we can neglect the random agents, and the difference between price- and demand efficiency. We thus consider N agents who buy at each time t with probability d_{t-1}/N. The stationary demand distribution π then satisfies

$$\pi_j = \sum_{i=0}^{N} \pi_i \, \pi_{ij}, \qquad \pi_{i,j} = \binom{N}{j} \left(\frac{i}{N}\right)^j \left(1 - \frac{i}{N}\right)^{N-j} \tag{5}$$

where the probability to move from state $i = d_{t-1}$ to state $j = d_t$ is given by the transition matrix π_{ij}. For large N, Eq. (5) is satisfied by the uniform distribution. To show this, we first divide by $\pi_i = \pi_j = \text{const}$, and obtain

$$1 = \sum_{x=0}^{1} \binom{N}{j} x^j \, (1-x)^{N-j}, \quad \text{with} \quad x = \frac{i}{N}. \tag{6}$$

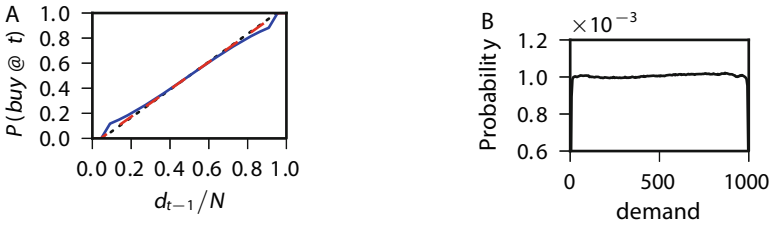

Fig. 2. A: Probability for an agent to buy at time t for different previous demands d_{t-1} normalized by the system size $N = N_s + N_r$. Fraction of random traders: $N_r/N_s = 0.1$. The demand efficient solution is given by Eq. (4) (dotted black). The price efficient solutions for $N = 22$ (solid blue) and $N = 110$ (dashed red) were obtained by numerical optimization. B: Distribution of demands in a simulation of $N_s = 1000$ speculators and $N_r = 1$ random trader for 10^8 time steps.

For large N, we can replace the sum over $x \ll 1$ with an integral. The right hand side of Eq. (6) then reads

$$\binom{N}{j} N \int_0^1 x^j (1-x)^{N-j} dx = \binom{N}{j} N \frac{\Gamma(j+1)\Gamma(N-j+1)}{\Gamma(N+2)} \tag{7}$$

$$= \frac{N}{N+1} \overset{N \gg 1}{\longrightarrow} 1 \qquad \square \tag{8}$$

Fig. 2 B shows the demand distribution for a simulation of the price efficient model. It is uniform except for the very edges where it drops sharply. For higher ratios N_r/N_s, the edges can also exhibit peaks.

3.2 Tail Exponent

The log return for two subsequent demands d and d' can be expressed as

$$r = \log\left(\frac{d'}{N-d'}\frac{N-d}{d}\right) \approx \Delta\left(\frac{1}{d} - \frac{1}{N-d}\right), \quad \text{where} \quad \Delta = d' - d. \tag{9}$$

The approximation is obtained by expanding for small Δ up to the first order. This is possible, because the standard deviation for the binomial distribution is proportional to $\sqrt{N}$ and vanishes for demands close to zero or close to N. Hence, the distribution of Δ will be very localized for large N. Fluctuations in r are then dominated by d, especially for $d \ll N$, and $N - d \ll N$. Due to the symmetry with respect to $N/2$, we now analyze only the case $d \ll N$ where $r \approx \frac{\Delta}{d}$. For the scaling of the tail of the return magnitudes, the shape of $p(\Delta)$ is negligible. The expected fluctuations in r can be expressed by

$$\langle r^2 | d \rangle \approx \left(\frac{\langle \Delta \rangle}{d}\right)^2 \approx \frac{1}{d} := \tilde{r}^2. \tag{10}$$

Using the probability integral transform, and $p(d) = \text{const.}$ yields

$$p(\tilde{r}) \propto |\tilde{r}|^{-3}, \quad \text{and therefore} \quad p(r) \overset{\propto}{\sim} |r|^{-3} \tag{11}$$

for sufficiently large N and r, and in agreement with simulations (Fig. 1 B).

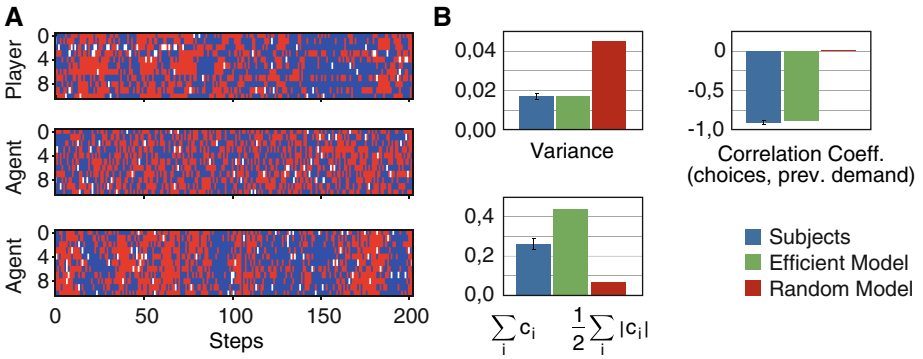

Fig. 3. A: Top: choices in an experiment with 11 Subjects. Red and blue correspond to the choices $c_i = \pm 1$, white to skipping a round. Middle: model with equal probabilities for $c_i \pm 1$. Bottom: demand efficient model. Skipping probabilities for the models were equal to the experiments. B: Variance of the outcomes, correlation coefficient of the player choices with the respective last excess demand, and the probability for a bubble. The latter is quantified by the relative number of rounds, where one choice was made by twice as many subjects (agents) as the other choice.

4 Experiments

Testing for tail exponents or stationary distributions with limited time and subjects appears impossible. However, the uniform distribution of demands implies a dynamics which spends significant amounts of time near the system boundaries, that is, in bubble phases. This testable prediction reflects that a mean reverting trend may be easily exploited and eliminated by traders. We let subjects play a game (an extension is playable online [7]) where players i in each round chose $c_{i,t} = 1$ or $c_{i,t} = -1$ before a countdown ran out. These choices correspond to the market orders in the model above. No decision was registered as $c_{i,t} = 0$. A superplayer chose $C_t = -\sum_i c_{i,t-1} = -d_{t-1}$. The players whose choices were in the minority won 1 point. Due to the superplayer, betting against the change in the other players decisions is rewarded. Note, that each new round is a nash equilibrium: If all players repeat their choices, the outcome $d_t - d_{t-1}$ (a linearized return) is zero. A single player who changes, loses. Yet, players did not stay in these equilibria.

Fig. 3 shows the subjects' choices and two models: agents chosing by flipping a coin, and agents betting demand efficient on average. The experiment and the efficient model show clusters where one choice is preferred. These bubble phases are absent for coin flipping agents. Efficient betting causes a decrease in the outcome variance, but increases the probability for a bubble phase. This effect is significant, but not as strong for the real subjects as for the efficient model. This may be due to a heterogenity of players or the use of other information which is not captured by the simple model. Nevertheless, players bet against the superplayer and therefore against mean reversion as much as the efficient model.

5 Summary

We presented an analytically tractable model which relates price efficiency to bubbles, power-law log returns and volatility clusters. The lack of mean reversion leads to a uniform demand distribution. The non-linear price causes the system to be more susceptible in bubble phases. This is analogous to, for example, many buyers betting up the price of a scarce resource. Then, in absolute terms small fluctuations in the availability of said resource may lead to large relative price changes. Another analogy would be a liquidity crisis.

We successfully tested model predictions with human subjects. Instead of a player payoff based on the excess demand like in other minority games, we use the return. This correctly compares the price at which an asset is sold by an agent not to a fundamental price, but to the price at which the agent bought said asset, and vice versa. Our game combines information efficiency as in minority games with bubbles as in majority games in a simpler way than the $-game [8] [9], and without the necessity to fine tune to a phase transition (for an overview of games, see [10]). Even if player choices were not efficient, adjusting their impact based on our payoff rule (trading success) is a learning algorithm allowing for collective efficiency with respect to the information available to the agents. [11].

References

1. Farmer, J.D.: Physicists Attempt to Scale the Ivory Towers of Finance. Computing in Science Engineering **1**, 26–39 (1999)
2. Joulin, A., Lefevre, A., Grunberg, D., Bouchaud, J.P.: Wilmott (2008)
3. Lux, T., Marchesi, M.: Scaling and criticality in a stochastic multi-agent model of a financial market. Nature **397**, 498–500 (1999)
4. Samuelson, P.A.: Proof That Properly Anticipated Prices Fluctuate Randomly. Industrial Management Review **6**, 41–49 (1965)
5. Fama, E.F.: Market efficiency, long-term returns, and behavioral finance. Journal of Financial Economics **49**, 283–306 (1998)
6. Brunnermeier, M.K.: The New Palgrave Dictionary of Economics, 2nd edn., chap. Bubbles. Palgrave Macmillan (2008)
7. seesaw.neuro.uni-bremen.de
8. Andersen, J.V., Sornette, D.: The $-game. Eur. Phys. J. B **31**, 141–145 (2003)
9. Giardina, I., Bouchaud, J.P.: Bubbles, crashes and intermittency in agent based market models. Eur. Phys. J. B **31**, 421–437 (2003)
10. Challet, D., Marsili, M., Zhang, Y.: Minority games - interacting agents in financial markets, chap. 4. Minority games as Market Models. Oxford University Press (2004)
11. Patzelt, F., Pawelzik, K.R.: Unstable Price Dynamics as a Result of Information Absorption in Speculative Markets. arXiv:1211.6695

Functional Architectures for Complex Behaviors: Analysis and Modeling of Interacting Processes in a Hierarchy of Time Scales

Dionysios Perdikis[1], Raoul Huys[2], and Viktor Jirsa[2]

[1] Max-Planck-Institute for Human Development,
Lentzealle 94, 14195, Berlin, Germany
perdikis@mpib-berlin.mpg.de
[2] Theoretical Neuroscience Group, Institut de Neurosciences des Systèmes, Inserm,
UMR1106, Aix-Marseille Université, Faculté de Médecine,
27, Boulevard Jean Moulin 13005, Marseille, France
viktor.jirsa@univ-amu.fr, raoul.huys@univ-amu.fr
http://ins.univ-amu.fr/research-teams/theoretical-neurosciences-group

Abstract. Synergetics' applications in the sciences of cognition and behavior have focused on instabilities leading to phase transitions between competing behavioral or perceptual patterns. Inspired by this scientific tradition, functional architectures are proposed as a general theoretical framework aiming at modeling the nonstationary, multiscale dynamics of complex behaviors, beyond the neighborhood of instabilities. Such architectures consist of interacting dynamical processes, operating in a hierarchy of time scales and functionally differentiated according to their mutual time scale separations. Here, the mathematical formalism of functional architectures is presented and exemplified through simulations of cursive handwriting. Then, the implications for the analysis of complex behaviors are discussed.

Keywords: functional architectures, structure flows on manifolds, hierarchies of time scales

1 Introduction

The idea that human function (be it motoric, perceptual or cognitive) is composed of elementary processes acting as functional units or "primitives" is often expressed in the biological and life sciences. Identifying such functional units implies a time scale separation between such units and the resulting composite processes. Thus, there is a relationship between time scale separation and functional differentiation of processes. Moreover, interactions among these time scales are essential for the organization of multiscale behaviors that are characterized by circular causality. For instance, serial behaviors, such as speech and handwriting, constitute a class of complex behaviors where slow processes sequentially activate functional units (elements of a sequence), modifying the

A. Pelster and G. Wunner (eds.), *Selforganization in Complex Systems: The Past, Present, and Future of Synergetics*, Understanding Complex Systems,
DOI: 10.1007/978-3-319-27635-9_25

fast dynamics of the level of units, which often results in non-stationary processes (top-down influence); at the same time, bringing functional units into meaningful relationships (here serial order) is how a complex behavior emerges (bottom-up composition). The field of nonlinear dynamics has offered descriptions of functional or behavioral units [1, 2] such as excitable point attractor systems and limit cycles to model discrete and rhythmic behaviors, respectively, as well as more complex ones (e.g. multistable or chaotic). Moreover, Synergetics [3–5] has focused on the instabilities leading to phase transitions among competing, low-dimensional, cognitive or behavioral patterns of order parameters, and the related experimentally observed phenomena, such as hysteresis, critical slowing down and fluctuations, and metastability. The present work proposes functional architectures [6–8] to account for the ensemble of interactions constituting the organization of complex human function, outside the neighborhood of instabilities as well. Functional architectures deal with a dual task: to provide a general formalism of the functional units' dynamics, and to propose dynamical mechanisms responsible for temporarily establishing a functional unit, and subsequently destabilizing it, in order to transit to another one (a role played by control parameters whose dynamics is not explicitly treated in Synergetics), for complex function to emerge.

2 Structured Flows on Manifolds modeling Functional Units

In a recent advance, 'Structured Flows on Manifolds' (SFM) [8, 9] has been proposed (in the spirit of Synergetics) to link the dynamics of large-scale brain networks interacting with bodily and environmental dynamics (high dimensional systems) to low-dimensional phenomenological descriptions of functional (or behavioral) dynamics. SFM suggest that during the engagement in a specific function, the high-dimensional network dynamics collapses (via a fast adiabatic contraction) on a functionally relevant subset of the phase (state) space, the so-called manifold. The phase flow is the structured dynamics on the manifold that evolves for the duration of a specific functional process:

$$\begin{aligned} &\tau \dot{u}_i = -g_i(\{u_i\}, \{s_k\})u_i + \mu f_i(\{u_i\}, \{s_k\}) \\ &\tau \dot{s}_k = -s_k + h_k(\{u_i\}, \{s_k\}) \\ &\{u_i\} \in \Re^N, \{s_k\} \in \Re^M, N \ll M, \mu \ll 1 \end{aligned} \tag{1}$$

where $g_i()$, $f_i()$, and $h_i(.)$ define the globally attractive manifold, the slow (due to the small value of μ) flow on it, and the fast dynamics towards the manifold, respectively. τ is the time constant of the fast contraction. The requirement for SFM is to contain an inertial manifold [10], which is a global structure used in cases of reduction of infinite dimensional dynamical systems to finite dimensional spaces. The existence and global stability of an inertial manifold has to be treated in a case-by-case manner, but it is not constrained to the neighborhood of instabilities and phase transitions. After the adiabatic elimination of

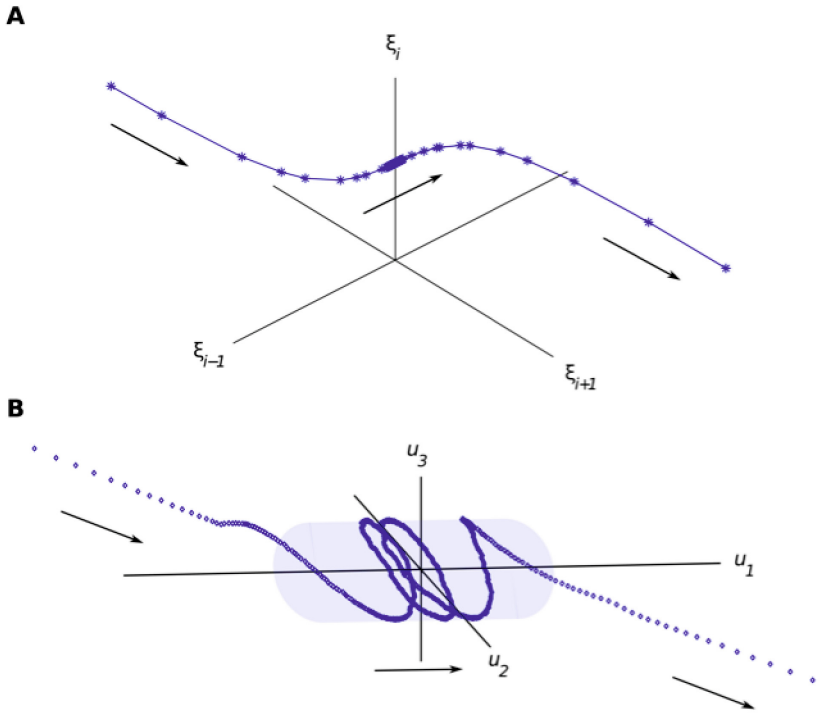

Fig. 1. Multiscale dynamics: slow operational signal and SFM emergence. Panel A: The slow operational signals $\{\xi_j\}$ converge through a fast transient to a specific ξ_j node resulting (here) in the emergence of a cylindrical manifold. Panel B: The functional dynamics $\{u_j\}$ collapses fast (also) onto the manifold where it executes a slow spiral flow. The ξ_j node's stability is sustained for the duration of the flow execution. Subsequently, the ξ_j node destabilizes, followed by the related manifold, and the dynamics moves away, again through fast transients. The density of data point is inversely proportional to the time scale of the dynamics. Figure adapted from [7].

$s_k = h(\{u_i\}, \{s_k\})$, the low-dimensional dynamics on the manifold is given by

$$\tau \dot{u}_i = F_i(\{u_i\}) = -g_i(\{u_i\})u_i + \mu f_i(\{u_i\}) \tag{2}$$

and describes (quantitatively) *functional modes*, the main building blocks of functional architectures, as autonomous, deterministic and time continuous systems. Moreover, the phase flow topology of a mode uniquely determines a system's qualitative behavior, encoding the invariant features of a dynamical process relative to quantitative variations such as robustness or stability changes due to stochastic contributions or to different contexts, thus identifying all functional possibilities within a class in a model-independent manner.

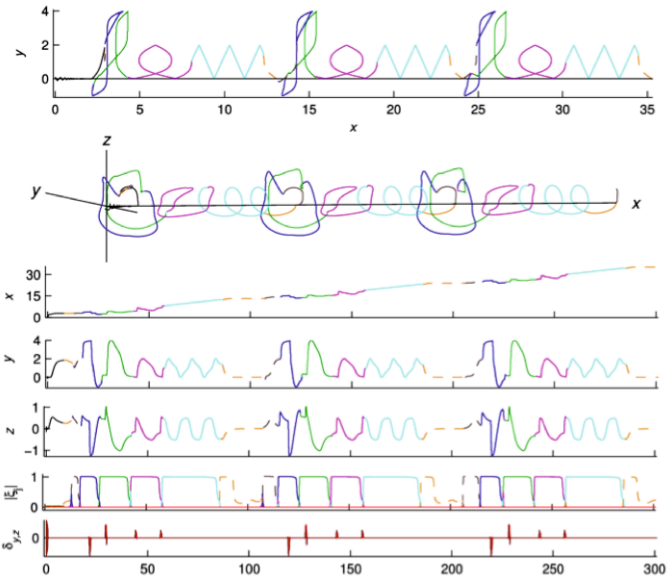

Fig. 2. The generation of the word "flow" and the operational signals involved. The word is repetitively generated after a short transient (black solid line). Four principle functional modes are used, one for each character (associated with solid blue, green, magenta and cyan lines, respectively), plus two auxiliary ones (linear point attractors) at the sequence's beginning and end (dotted dark and light brown lines, respectively). From top to bottom: three repetitions of the word in the handwriting workspace (the plane x-y), the output trajectory in the 3-dimensional functional phase space spanned by state variables x, y and z, followed by their time series, and the time series of the slow (WTA competition coefficients $|\xi_j|$) and the instantaneous ($|\delta_{x,y}|$) "kicks", light and dark red, respectively) operational signals. The mode amplitudes that do not participate in the word always have a value close to zero (red line). Figure adapted from [7].

3 Functional Architectures for Complex Behavioral Processes

In its most general formulation (first part of equation (3)), we can describe a functional architecture through its flow $\{F_i(.)\}$ in phase space, potentially subjected to additional dynamics $\{\sigma_i(t)\}$ called *operational signals* (for a detailed treatment see [6, 7]):

$$\tau \dot{u}_i = F_i(\{u_i\}, \{\sigma_i(t)\}) = \sum_j |\xi_j(t)|(F_{ij}(\{u_i\}) + \delta_i(t)) \tag{3}$$

where $\{F_{ij}(.)\}$ is the j-th functional mode that is available in an agent's dynamical repertoire and $\{\sigma_i(t)\}$ is a (generally) time-dependent operational signal.

The $\{\sigma_i(t)\}$ may operate on various time scales relative to the characteristic time scale of $\{F_{ij}(.)\}$. These time scale separations among modes and signals determine their functional differentiation and result in distinct functional architectures. The second part of equation (3) describes a more specific form of a functional architecture where, at each moment in time, the expressed phase flow $\{F_i(.)\}$ is given as a linear combination of all available modes, weighted by the operational signal $|\xi_j(t)|$. $|\xi_j(t)|$ modifies $\{F_i(.)\}$ on a slower time scale than the one of the functional modes $\{F_{ij}(.)\}$, except for the critical moments where abrupt transitions between modes take place. The operation of this slow signal upon the functional modes implements the basic mechanism of the functional architecture: slow dynamics drives the faster functional dynamics through an alternating sequence of fast and slow transients, each of the latter ones constituting a distinct function, described by a SFM (Fig. 1). Thus, elementary processes are sewed together to form a longer more complex one. The architecture also provides for the optional involvement of the operational signal $\{\delta_i(t)\}$ that leaves the flow $\{F_i(.)\}$ unaffected, because it acts instantaneously, just like a functionally meaningful perturbation (for instance, by moving the system beyond a threshold and thus initiating a significant change in the trajectory's evolution). The ensemble of subsystems ($|\xi_j(t)|$, $\{F_{ij}(.)\}$, $\{\delta_i(t)\}$) operating on distinct time scales ($\tau_\delta \ll \tau_F \ll \tau_\xi$, respectively) constitutes the functional architecture. In [7] we showed how the (($|\xi_j(t)|$, $\{F_{ij}(.)\}$, $\{\delta_i(t)\}$)) dynamics can be designed to organize functional modes so that serial order behavior emerges. Under the requirement that functional modes' activations do not overlap, we implemented a "winner-take-all competition" (WTA) for the dynamics, in the spirit of the Synergetic Computer [5]. Suitable dynamics for the parameters of the competition ("attentional parameters" in the terminology of the Synergetic Computer) had to be designed, so as to activate the functional modes taking part in the sequence one after the other and with the appropriate timing. As the different ingredients of the functional architecture were intricately coupled in various ways, the whole architecture was constituted as an autonomous multiscale dynamical system. We demonstrated the application of the functional architecture on cursive handwriting (Fig. 2), for which we designed a repertoire of functional modes implementing characters (or parts thereof) modeled as 3-dimensional SFM on cylindrical manifolds.

4 Implications for Analysis of Complex Behaviors

Functional architectures aim not only at providing the theoretician with hypotheses on the nature and mutual interactions of the dynamical components of complex behaviors, but also the experimenter with the means to identify such components. In [7] we analyzed data from several simulated trials of the handwriting architecture, assuming the time scale separations and the respective functional differentiation of functional modes and operational signals. We managed to identify and distinguish between all three kinds of dynamics (($|\xi_j(t)|$, $\{F_{ij}(.)\}$, $\{\delta_i(t)\}$) and thus, decompose the architecture's output into its dynam-

ical components and segment it into time periods where different functional modes are activated. Doing so appeared to be possible only through the calculation of the output phase flow variability (as opposed to studying the variability of the output time series), i.e. by identifying the short time periods when the expressed phase flow changed because operational signals became effective. Future work could be directed towards methods of phase flow reconstruction of stochastic systems based on Fokker-Planck equation formalisms, adjusted for nonstationary, multiscale systems [11].

References

1. Jirsa, V.K., Kelso, J.A.S.: The excitator as a minimal model for the coordination dynamics of discrete and rhythmic movement generation. Journal of Motor Behavior **37**, 35–51 (2005)
2. Huys, R., Studenka, B.E., Rheaume, N.L., Zelaznik, H.N., Jirsa, V.K.: Distinct timing mechanisms produce discrete and continuous movements. PLoS Computational Biology **4**, e1000061 (2008)
3. Haken, H.: Synergetics: Introduction and advanced topics. Springer, Berlin (1983)
4. Haken, H.: Principles of Brain Functioning: A Synergetic Approach to Brain Activity Behavior and Cognition. Springer, Berlin (1996)
5. Haken, H.: Synergetic computers and cognition: A top-down approach to neural nets. Springer, Berlin (2004)
6. Perdikis, D., Huys, R., Jirsa, V.K.: Complex Processes from Dynamical Architectures with Time-Scale Hierarchy. PLoS ONE **6**, e16589 (2011)
7. Perdikis, D., Huys, R., Jirsa, V.K.: Time scale hierarchies in the functional organization of complex behaviors. PLoS Comput. Biol. **7**, e1002198 (2011)
8. Jirsa, V.K., Huys, R., Pillai, A.S., Perdikis, D., Woodman, M.: Connectivity and dynamics of neural information processing. In: Rabinovich, M.I., Friston, K.J., Varona, P. (eds.) Principles of Brain Dynamics: Global State Interactions, pp. 209–232. MIT Press, Boston (2012)
9. Pillai, A.S.: Structured Flows on Manifolds: Distributed Functional Architectures. PhD thesis. Florida Atlantic University (2008)
10. Constantin, P., Foias, C., Nicolaenko, B., Teman, R.: Intergral manifolds and inertial manifolds for dissipative partial differential equations. Springer, Berlin (1989)
11. van Mourik, A.M., Daffertshofer, A., Beek, P.J.: Estimating KramersMoyal coefficients in short and non-stationary data sets. Physics Letters A **351**, 13–17 (2006)

Large-Scale Neural Network Model for Functional Networks of the Human Cortex

Vesna Vuksanović[1,2] and Philipp Hövel[1,2,3]

[1] Institut für Theoretische Physik, Technische Universität Berlin
Hardenbergstraße 36, 10623 Berlin, Germany
[2] Bernstein Center for Computational Neuroscience, Humboldt-Universität zu Berlin
Philippstraße 13, 10115 Berlin, Germany
[3] Center for Complex Network Research, Northeastern University, 110 Forsyth Street, Boston, USA
vesna.vuksanovic@tu-berlin.de, phoevel@physik.tu-berlin.de

Abstract. We investigate the influence of indirect connections, interregional distance and collective effects on the large-scale functional networks of the human cortex. We study topologies of empirically derived resting state networks (RSNs), extracted from fMRI data, and model dynamics on the obtained networks. The RSNs are calculated from mean time-series of blood-oxygen-level-dependent (BOLD) activity of distinct cortical regions via Pearson correlation coefficients. We compare functional-connectivity networks of simulated BOLD activity as a function of coupling strength and correlation threshold. Neural network dynamics underpinning the BOLD signal fluctuations are modelled as excitable FitzHugh-Nagumo oscillators subject to uncorrelated white Gaussian noise and time-delayed interactions to account for the finite speed of the signal propagation along the axons. We discuss the functional connectivity of simulated BOLD activity in dependence on the signal speed and correlation threshold and compare it to the empirical data.

Keywords: functional connectivity, resting state networks, time-delays

1 Introduction

Despite important progress over past few years, little is known about brain functional connectivity (FC) at rest, i.e. under no stimulation and in the absence of any overt-directed behaviour. In the studies on goal-directed mental activity, spontaneous brain activity has been considered as random enough to be averaged out across many trials [1]. However, well organized spatio-temporal low-frequency fluctuations (< 0.1 Hz) have been observed in blood-oxygen-level-dependent (BOLD) fMRI signals of a mammalian brain in the absence of any stimulation or task related behaviour [2–4]. These well organized patterns of activity, suggest existence of underlying dynamics that governs intrinsic brain processes.

Existing large-scale models of the intrinsic brain dynamics focus on the relationship between functional and anatomical connectivity. They explore the range

A. Pelster and G. Wunner (eds.), *Selforganization in Complex Systems: The Past, Present, and Future of Synergetics*, Understanding Complex Systems,
DOI: 10.1007/978-3-319-27635-9_26

of conditions under which functional networks may emerge from known anatomical connections. In particular, roles of multiple time-scales in FC networks formation [5, 6], time-delays in the signal propagation between the network nodes and system noise [7, 8], local network oscillations [9, 10] and structural disconnection [11] in the underlying dynamics have been investigated. Although RSNs reflect anatomical connectivity between brain areas comprising the networks in focus, FC cannot be understood in those terms alone [12, 13].

Here, we combine experimental and modelling approaches to investigate dynamics underlying correlated behaviour of distant cortical regions. We choose to model the local node dynamics by excitable FitzHugh-Nagumo (FHN) neurons [14, 15] and use the resulting time-series to infer the neuronal activity at the network levels and subsequently low-frequency oscillations in the BOLD data [16]. We focus on identifying how global coupling strength and different network topologies affect connectivity patterns in simulated BOLD signals.

The rest of this paper is organized as follows: In Sec. 2 we provide a detailed description of the methods used to generate the networks. In addition we introduce the model equations. This sets the stage for numerical simulations that are presented in Sec. 3. Finally we conclude with a discussion in Sec. 4.

2 Methods and Models

Subjects. We use resting state blood-oxygen-level-dependent (BOLD) fMRI signals downloaded from the *1000 Functional Connectome Project* website (`http://www.nitric.org/`). 26 functional and anatomical scans from the Berlin study are considered in the analysis. Demographic data for the subjects participated in the study along with the technical details of the signal acquisition can be found at the *Functional Connectome* website.

Data Preprocessing Steps in FSL. Image preprocessing is carried out using FSL (`http://www.fmrib.ox.ac.uk`) [17]. The preprocessing consists of the following steps: (a) temporal high-pass filtering (using Gaussian-weighted least-squares straight line fitting with sigma equals 100 s); (b) temporal low-pass filtering (using Gaussian filter with HWHM = 2.8 s); (c) slice-timing correction for interleaved acquisition (using Fourier-space time-series phase-shifting); (d) motion correction (using a six parameter affine transformation implemented in MCFLIRT); (e) spatial filtering (using Gaussian kernel of FWHM = 6 mm); (f) non-brain removal (BET brain extraction is applied to create a brain mask from the first volume in the fMRI data): (g) normalization to standard brain image (using 12 DOF linear affine transformation implemented in FLIRT each subject scan was transformed in MNI space - voxel size $2 \times 2 \times 2$ mm).

Functional Connectivity. For the connectivity analysis we extract BOLD time-series from $N = 64$ cortical regions. These regions are adapted from studies of functional segmentation of the human cortex [18, 19]. They consist of 30 pairs of the inter-hemispheric homologues and 4 additional areas chosen along the midline. The full list of the cortical areas along with their anatomical (MNI) coordinates is provided in the work by Anderson et al. in Table 1 in the Supple-

mentary material of Ref. [19]. We define the areas of interest as 5 mm spheres centered at the corresponding anatomical coordinates. For the given image resolution of $2 \times 2 \times 2$ mm voxel size (measured at $64 \times 64 \times 33$ brain sites in total), there are 81 voxel time-series within each of the spherical areas. To obtain correlation matrix, describing connections between the regions, we calculate the linear correlation coefficient between any pair of the mean signal intensity of each of the 64 regions as:

$$r(x_1, x_2) = \frac{\langle V(x_1,t)V(x_2,t)\rangle - \langle V(x_1,t)\rangle\langle V(x_2,t)\rangle}{\sigma\left(V(x_1,t)\right)\sigma\left(V(x_2,t)\right)}, \tag{1}$$

where $V(x,t)$ represents activity of the region x at time t (averaged across 81 voxels), σ is the standard deviation, and $\langle\cdot\rangle$ denotes temporal averages. The $N \times N$ correlations matrices are averaged across the ensemble of 26 subjects. The obtained correlation matrix $\{f_{ij}\}$, $i,j = 1,\ldots,N$, is used to create FC maps between the cortical regions of interest. By definition, FC between two brain regions exists if their temporal correlation exceeds some predetermined value r, regardless of their anatomical connectivity.

Thresholding: We obtain FC network topologies by thresholding the empirically derived FC matrix at different threshold values r. If $f_{ij} \geq r$, the corresponding element of the adjacency matrix is set to 1; otherwise it is set to 0. We simulate neural and BOLD activity only for $r \geq 0.26$, i.e. values for which connection density or topology cost in the brain networks is less than 0.5 [20].

Simulation of the Network Dynamics. To infer the BOLD signal in dependence on the network properties, we first simulate the underlying neural activity. We consider the neural dynamics on the network of N nodes or cortical regions, where local dynamics of the each node is represented by the homogeneous FHN neurons.

Simulation of the Neural Activity: Simulations of the neural network dynamics take into account time-delays due to finite speed of signal propagation between the nodes as well as the presence of the system noise:

$$\dot{u}_i = g(u_i, v_i) - c\sum_{j=1}^{N} f_{ij}u_j(t - \Delta t_{ij}) + n_u \tag{2}$$

$$\dot{v}_i = h(u_i, v_i) + n_v, \tag{3}$$

where c denotes global coupling parameter ($c > 0$), u_i and v_i are the activator and inhibitor variables of the i^{th} neural population, f_{ij} are the elements of the FC matrix and Δt_{ij} denote time-delays. n_u and n_v are two independent additive white Gaussian noise terms with zero mean, unity variance and noise strength D. The functions g and h describe the local neural activity according to the FHN model, where we use the notation of Refs. [7, 8]:

$$\dot{u} = g(u,v) = \tau\left(v + \gamma u - \frac{u^3}{3}\right) \tag{4}$$

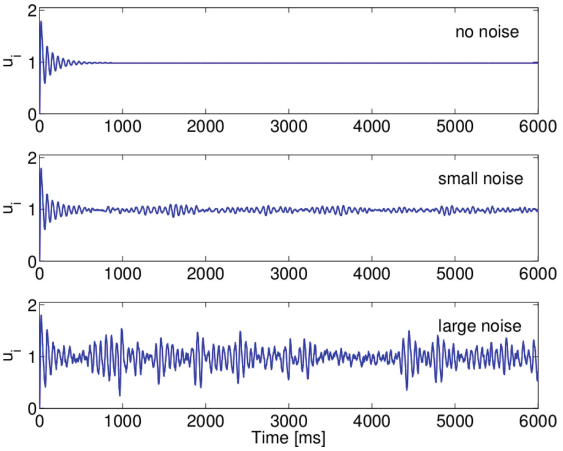

Fig. 1. Time evolution of the activator variable of the FitzHugh-Nagumo neural model for an isolated node under noise with different intensity.

$$\dot{v} = h(u, v) = -\frac{1}{\tau}\left(u - \alpha + bv - I\right), \tag{5}$$

where I is magnitude of an external stimulus, which is assumed to be 0 in our model of the resting state dynamics [7]. The system parameters are chosen as $\alpha = 0.85$, $\beta = 0.2$, $\gamma = 1.0$ and $\tau = 1.25$ to render solutions with damped oscillatory behaviour of a node dynamics, i.e. at the onset of instability, in the absence of the connectivity in the network [7, 8]. Representative time-series of the dynamics of an isolated node are shown in Fig. 1 for different noise strengths $D = 0$ (no noise), $D = 0.01$ (small noise) and $D = 0.05$ (large noise). We solve the system of coupled differential equations with time-delays and additive noise using the PYTHON-module PYDELAY [21]. The algorithm is based on the Bogacki-Sampine method [22, 23], which is also implemented in MATLAB'S DDE23. We calculate time-delays for a physiologically realistic value of the propagation velocity ($v = 7$ m/s) via $\Delta t_{ij} = d_{ij}/v$, where d_{ij} are approximated by the Euclidean distances between the centers of the spherical regions, i.e. network nodes i and j. A colour-coded representation of the d_{ij} values is shown in Fig. 2. We simulate 7.5 minutes of the real time using a time step of 1 ms. When time-delays, system noise and global coupling are taken into account, the simulated dynamics of the neural activity exhibit a behaviour that are exemplary shown in Fig. 3.

Simulation of the BOLD Activity: To infer the BOLD activity from the simulated neural activity we assume the Baloon-Windkessel hemodynamic model [16]. Simulated BOLD signals are band-passed in the frequency interval (0.01 - 0.15) Hz to match low-frequency oscillations present in the experimental BOLD data and finally down-sampled to 2.3 s to match the temporal resolution of the MRI scanner.

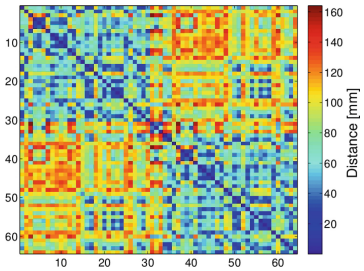

Fig. 2. Distance matrix $\{d_{ij}\}$, $i, j = 1, \ldots, N$, between cortical regions in colour code. d_{ij} are calculated as Euclidean distance between centers of spherical regions in anatomical space. Matrix is ordered in a way that corresponding contra-lateral regions are symmetrically arranged with respect to the matrix centre (right hemisphere regions, nodes 1 - 30; left hemisphere regions, nodes 35 - 64). 4 regions selected along the midline are placed in the middle of the matrix (nodes 31 - 34).

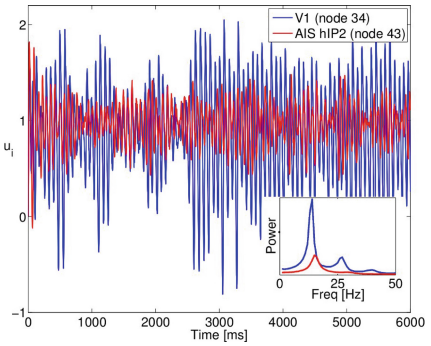

Fig. 3. Time-series of neural network nodes dynamics for one highly and one sparsely connected nodes in visual cortex (V1, blue) and anterior intraparaetal sulcus (AIS hIP2, red), respectively. Network dynamics are modelled with time-delays, large noise ($D = 0.05$) and weak coupling ($c = 0.016$). Parameters: $\alpha = 0.85$, $\beta = 0.2$, $\gamma = 1.0$ and $\tau = 1.25$. The inset shows the corresponding power spectra.

3 Results

Empirical Functional Connectivity. FC matrices obtained from fMRI data and its binarized versions for different thresholds are shown in Fig. 4 (left) and the top panels Fig. 4 (right), respectively. In the latter figure, the threshold values are chosen as $r = 0.26$, 0.38 and 0.5. $r = 0.26$ represents mean value of all correlations in the empiricaly derived FC and also the value at wich connection density (κ) of the network drops below 0.5, ($\kappa = 0.48$). Values $r = 0.38$ and 0.5 are one and two standard deviations away from the mean, respectively.

Horizontal-plane view illustrate the anatomical maps of the corresponding networks structure in the bottom panels of the Fig. 4 (right). In this representation each cortical region is treated as a network node with the connections or links to the other nodes in network if the matching correlation exceeds given threshold. FC networks show a pronounced left to right symmetry for different values of the correlation thresholds. However, distributions of the areas with most connections depend on the threshold applied. The areas showing high numbers of links for the lower threshold network differ from the areas that appear as highly connected at higher thresholds. We expect that nodes with increased connectivity play an important role in the system's dynamics.

Simulated Functional Connectivity. FC of the simulated BOLD activity are shown in Fig. 5. The data are obtained varying correlation threshold r,

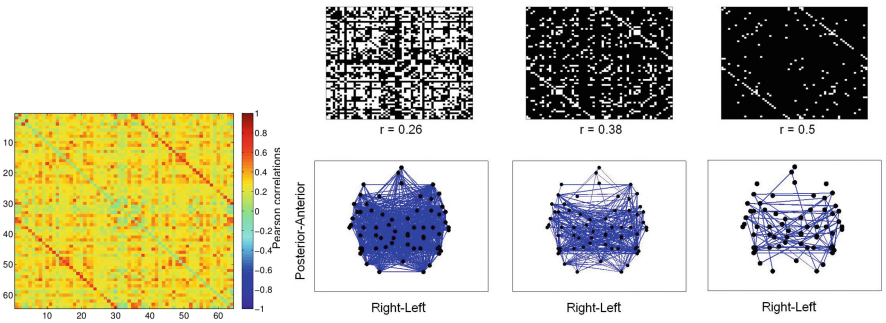

Fig. 4. (Left) Functional connectivity matrix constructed by calculating Pearson correlations on all pairwise combinations of the BOLD data from 64 cortical regions. The matrix is ordered as in the Fig. 2. The anti-diagonals reveal existing high correlations between contra-lateral regions. **(Right)** Top panels: Binarized functional-connectivity matrix at thresholds $r = 0.26$, 0.38, and 0.5. Each element is either black (if there is no significant connections between the regions) or white (if there is). Bottom Panel: Visualization of thresholded matrices in anatomical space by locating each region according to its x and y coordinates and drawing a link between significantly connected regions.

i.e. network topology and global coupling strength c while keeping other model parameters at constant values. Correlations in the brain FC networks may not necessarily originate from direct connections. Therefore, we vary the network topologies by changing the correlation threshold r in the binary filter applied to the empirically derived FC network. We use the corresponding FC matrices to study the dynamics that result in the appearance of these correlations. Furthermore we uniformly scale all connections strengths c between the network nodes. For low correlation thresholds and weak coupling strengths ($c \leq 0.05$) the simulated BOLD signals are weakly correlated as the underlying neuronal activity does not show correlated behaviour either (data not shown). Increasing the coupling strength, positive correlations among the BOLD signals emerge in the simulated data and corresponding FC networks exhibit patterns of correlated activity similar to the empirically derived FC.

4 Discussion/Conclusion

In this study we presented data obtained by combining both experimental and modelling approaches to explore dynamics underlying correlated behaviour of distant cortical regions. We showed that increasing global coupling strength between the network nodes introduces correlations into simulated BOLD activity. The spatial patterns of the correlated activity resembled those observed in corresponding experimental data. However, to get tangible measures of similarity between experimentally and theoretically derived FC networks our next step would be to apply graph-theoretical analysis to the obtained data.

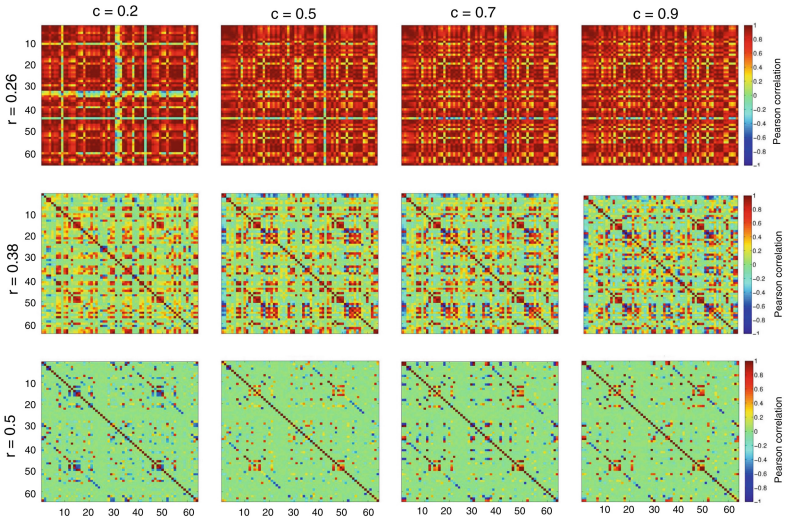

Fig. 5. Functional connectivity (FC) of simulated BOLD activity for different correlation thresholds r applied to the empirically derived FC matrix and different coupling strengths c. Other parameters as in Fig. 3.

Our results are consistent with recent findings showing that stronger structural couplings generates more globally connected and globally integrated BOLD signals [11]. Since functional connectivity implies possible role of indirect anatomical connections further studies, showing how our findings relate to known anatomical connections between cortical regions could lead to the better understanding of FC networks formation.

Acknowledgments. This work was supported by BMBF (grant no. 01Q1001B) in the framework of BCCN Berlin (Project B7). We thank John-Dylan Haynes and his group for helpful discussions concerning the data processing.

References

1. Fox, M.D., Raichle, M.E.: Spontaneous fluctuations in brain activity observed with functional magnetic resonance imaging. Nature Reviews Neuroscience **8**(9), 700–711 (2007)
2. Biswal, B., Yetkin, F.Z., Haughton, V.M., Hyde, J.S.: Functional connectivity in the motor cortex of resting human brain using echo-planar mri. Magnetic Resonance in Medicine **34**(4), 537–541 (1995)
3. Damoiseaux, J.S., Rombouts, S.A.R.B., Barkhof, F., Scheltens, P., Stam, C.J., Smith, S.M., Beckmann, C.F.: Consistent resting-state networks across healthy subjects. Proc. Natl. Acad. Sci. U.S.A. **103**(37), 13848–13853 (2006)
4. Vincent, J.L., Patel, G.H., Fox, M.D., Snyder, A.Z., Baker, J.T., Van Essen, D.C., Zempel, J.M., Snyder, L.H., Corbetta, M., Raichle, M.E.: Intrinsic functional architecture in the anaesthetized monkey brain. Nature **447**(7140), 83–86 (2007)

5. Honey, C.J., Kötter, R., Breakspear, M., Sporns, O.: Network structure of cerebral cortex shapes functional connectivity on multiple time scales. Proc. Natl. Acad. Sci. U.S.A. **104**, 10240–10245 (2007)
6. Rubinov, M., Sporns, O., Van Leeuwen, C., Breakspear, M.: Symbiotic relationship between brain structure and dynamics. BMC Neuroscience **10**(1), 55 (2009)
7. Ghosh, A., Rho, Y., McIntosh, A.R., Kötter, R., Jirsa, V.K.: Noise during rest enables the exploration of the brain's dynamic repertoire. PLoS Comput Biol **4**(10), e1000196 (2008)
8. Ghosh, A., Rho, Y., McIntosh, A.R., Kötter, R., Jirsa, V.K.: Cortical network dynamics with time delays reveals functional connectivity in the resting brain. Cogn. Neurodyn. **2**(2), 115–120 (2008)
9. Deco, G., Jirsa, V.K., McIntosh, A.R., Sporns, O., Kötter, R.: Key role of coupling, delay, and noise in resting brain fluctuations. Proc. Natl. Acad. Sci. U.S.A. **106**(25), 10302–10307 (2009)
10. Cabral, J., Hugues, E., Sporns, O., Deco, G.: Role of local network oscillations in resting-state functional connectivity. NeuroImage **57**(1), 130–139 (2011)
11. Cabral, J., Hugues, E., Kringelbach, M.L., Deco, G.: Modeling the outcome of structural disconnection on resting-state functional connectivity. NeuroImage **62**, 1342–1353 (2012)
12. Bullmore, E., Sporns, O.: Complex brain networks: graph theoretical analysis of structural and functional systems. Nature Reviews Neuroscience **10**(3), 186–198 (2009)
13. Deco, G., Jirsa, V.K.: Ongoing cortical activity at rest: criticality, multistability, and ghost attractors. The Journal of Neuroscience **32**(10), 3366–3375 (2012)
14. FitzHugh, R.: Impulses and physiological states in theoretical models of nerve membrane. Biophys. J. **1**, 445–466 (1961)
15. Nagumo, J., Arimoto, S.: Yoshizawa., S.: An active pulse transmission line simulating nerve axon. Proc. IRE **50**, 2061–2070 (1962)
16. Friston, K.J., Mechelli, A., Turner, R., Price, C.J.: Nonlinear responses in fmri: The balloon model, volterra kernels, and other hemodynamics. NeuroImage **12**(4), 466–477 (2000)
17. Jenkinson, M., Beckmann, C.F., Behrens, T.E.J., Woolrich, M.W., Smith, S.M.: Fsl. NeuroImage **62**(2), 782–790 (2012)
18. Kiviniemi, V., Starck, T., Remes, J., Long, X., Nikkinen, J., Haapea, M., Veijola, J., Moilanen, I., Isohanni, M., Zang, Y.F., Tervonen, O.: Functional segmentation of the brain cortex using high model order group pica. Hum. Brain Mapp. **30**(12), 3865–3886 (2009)
19. Anderson, J.S., Ferguson, M.A., Lopez-Larson, M., Yurgelun-Todd, D.: Reproducibility of single-subject functional connectivity measurements. Am. J. Neuroradiol. **32**(3), 548–555 (2011)
20. Bullmore, E.T., Bassett, D.S.: Brain graphs: graphical models of the human brain connectome. Annual review of clinical psychology **7**, 113–140 (2011)
21. Flunkert, V., Schöll, E.: pydelay – a python tool for solving delay differential equations. arXiv:0911.1633 [nlin.CD] (2009)
22. Bogacki, P., Shampine, L.F.: A 3(2) pair of runge - kutta formulas. Applied Mathematics Letters **2**(4), 321–325 (1989)
23. Shampine, L.F., Thompson, S.: Solving DDEs in Matlab. Appl. Num. Math. **37**(4), 441–458 (2001)

Part VI

Appendix

List of Participants

Balzer, Frank
University of Southern Denmark
Mads Clausen Institute, NanoSyd
Alsion 2
DK-6400 Sonderborg
Denmark
fbalzer@mci.sdu.dk

Bischler, Ulrike
Förderreferentin
Volkswagenstiftung
Kastanienallee 35
30519 Hannover
Germany
bischler@volkswagenstiftung.de

Borland, Lisa
Integral, San Francisco
807 Eleventh Avenue, Building 2
Sunnyvale, CA 94089
USA
lisa@evafunds.com

Caron, Christian
Springer Publishing Company
Tiergartenstr. 17
69121 Heidelberg
Germany
christian.caron@springer.com

Ciemer, Catrin
Freie Universität Berlin
Arnimallee 14
14195 Berlin
Germany
catrin.ciemer@fu-berlin.de

Clemson, Philip
Physics Department
Lancaster University
Lancaster LA1 4YB
United Kingdom
p.clemson@lancaster.ac.uk

Daffertshofer, Andreas
VU University Amsterdam
van der Boechorststraat 9
NL-1081BT Amsterdam
The Netherlands
a.daffertshofer@vu.nl

Daitche, Anton
Universität Münster
Wilhelm-Klemm-Str. 9
48149 Münster
Germany
anton.d@uni-muenster.de

Florian, Matthias
Institut für Theoretische Physik
Universität Bremen
Otto-Hahn-Allee 1
28359 Bremen
Germany
mflorian@itp.uni-bremen.de

Frank, Till
Department of Psychology
University of Connecticut
406 Babbidge Road, Unit 1020
Storrs , CT 06269
USA
till.frank@uconn.edu

Friedrich, Jan
Institut für Theoretische Physik 1
Ruhr-Universität Bochum
44780 Bochum
Germany
jaf@tp1.rub.de

Gies, Christopher
Institut für Theoretische Physik
Universität Bremen
Bremen
Germany
gies@itp.uni-bremen.de

Gießing, Carsten
Institute of Psychology
Universität Oldenburg
26111 Oldenburg
Germany
carsten.giessing@uni-oldenburg.de

Grossmann, Siegfried
Fachbereich Physik
Philipps-Universität Marburg
35032 Marburg (Lahn)
Germany
grossmann@physik.uni-marburg.de

Gruber, Christine
Fachbereich Physik
Freie Universität Berlin
Arnimallee 14
14195 Berlin
Germany
chrisigruber@physik.fu-berlin.de

Haake, Fritz
Fakultät für Physik
Universität Duisburg-Essen
Lotharstr. 1
47048 Duisburg
Germany
fritz.haake@uni-due.de

Haken, Hermann
Center of Synergetics
Universität Stuttgart
Pfaffenwaldring 57
70550 Stuttgart
hermann.haken@t-online.de

Hashemi, Meysam
INRIA Nancy
615 Rue du Jardin Botanique
54602 Villers-les-Nancy
France
meysam.hashemi@inria.fr

Hashemiyoon, Rowshanak
Department of Neuroscience
University of Pittsburgh
Pittsburgh, PA 15260
USA
row.hashemiyoon@gmail.com

Hinrichs, Christian
Fk. 2, A5 2-235
Universität Oldenburg
26111 Oldenburg
Germany
christian.hinrichs@uni-oldenburg.de

Hinrichs, Dennis
Institut für Physik
Universität Oldenburg
26111 Oldenburg
Germany
dennis.hinrichs@uni-oldenburg.de

Holthaus, Martin
Institut für Physik
Universität Oldenburg
26111 Oldenburg
Germany
martin.holthaus@uni-oldenburg.de

Hutt, Axel
INRIA Nancy
615 Rue du Jardin Botanique
54602 Villers-les-Nancy
France
axel.hutt@inria.fr

Jirsa, Viktor
Aix-Marseille Université
Faculté de Médecine
Institut de Neurociences des Systmes
27 BD Jean Moulin
13005 Marseille
France
viktor.jirsa@univ-amu.fr

Kamps, Oliver
Center for Nonlinear Science
Universität Münster
Correnstr. 2
48149 Münster
Germany
okamp@uni-muenster.de

Kittel, Achim
Institut für Physik
Universität Oldenburg
26111 Oldenburg
Germany
kittel@uni-oldenburg.de

Kleinhans, David
Department of Physics/Forwind
Universität Oldenburg
26129 Oldenburg
Germany
david.kleinhans@uni-oldenburg.de

Knicker, Katharina
Fritz-Haber-Institut der MPG
Faradayweg 4-6
14195 Berlin
Germany
kknicker@gmx.de

Koch-Pelster, Brigitte
Hanse-Wissenschaftskolleg
Lehmkuhlenbusch 4
27753 Delmenhorst
Germany
kochpelster@aol.com

Kröger, Bernd
Im Schönblick 13
72076 Tübingen
Germany
drberndkroeger@t-online.de

Lämmerzahl, Claus
Universität Bremen, ZARM
Am Fallturm
28359 Bremen
Germany
claus.laemmerzahl@zarm.uni-bremen.de

Mahler, Günter
Institut für Theoretische Physik I
Universität Stuttgart
Pfaffenwaldring 57
70469 Stuttgart
Germany
mahler@itp1.uni-stuttgart.de

Nikolić, Branko
Fachbereich Physik
Freie Universität Berlin
Arnimallee 14
14195 Berlin
Germany
branko@zedat.fu-berlin.de

Ning, Cun-Zheng
School of Electrical,
Computer, and Energy Engineering
Arizona State University
Tempe, AZ 85287
USA
cning@asu.edu

Parisi, Jürgen
Institut für Physik
Universität Oldenburg
26111 Oldenburg
Germany
parisi@ehf.uni-oldenburg.de

Patzelt, Felix
Universität Bremen
Hochschulring 18, Cognium
28359 Bremen
Germany
felix@neuro.uni-bremen.de

Pawelzik, Klaus
Institut für Theoretische Physik
Universität Bremen
Hochschulring 18, Cognium
28359 Bremen
Germany
pawelzik@neuro.uni-bremen.de

Peinke, Joachim
Department of Physics/Forwind
Universität Oldenburg
26129 Oldenburg
Germany
pawelzik@neuro.uni-bremen.de

Pelster, Axel
Hanse-Wissenschaftskolleg
Lehmkuhlenbusch 4
27753 Delmenhorst
Germany
axel.pelster@fu-berlin.de

Perdikis, Dionysos
Max Planck Institute for Human Development
Lentzeallee 94
14195 Berlin
Germany
perdikis@mpib-berlin.mpg.de

Petkoski, Spase
Physics Department
Lancaster University
Lancaster LA1 4YB
United Kingdom
s.petkoski@lancs.ac.uk

Petrovic, Cornelia
Institut für Theoretische Physik
Universität Münster
Wilhelm-Klemm-Str. 9
48149 Münster
Germany
petrovic@uni-muenster.de

Plath, Peter
Fritz-Haber-Institut der MPG
Faradayweg 4-6
14195 Berlin
Germany
peter_plath@t-online.de

Robnik, Marko
University of Maribor
CAMTP-Center Krekova 2
SI-2000 Maribor
Slovenia
robnik@uni-mb.si

Roth, Gerhard
Institut für Hirnforschung
Universität Bremen
28334 Bremen
Germany
gerhard.roth@uni-bremen.de

Schiek, Manuela
Hanse-Wissenschaftskolleg
Lehmkuhlenbusch 4
27753 Delmenhorst
Germany
manuela.schiek@uni-oldenburg.de

Schiepek, Günter
Institute of Synergetics
Paracelsus Medical University
5020 Salzburg
Austria
guenter.schiepek@ccsys.de

Schöll, Eckehard
Institut für Theoretische Physik
Technische Universität Berlin
Hardenbergstr. 36
10623 Berlin
Germany
schoell@physik.tu-berlin.de

Spiegler, Andreas
Aix-Marseille Université
Faculté de Médecine
Institut de Neurociences des Systmes
27 BD Jean Moulin
13005 Marseille
France
andreas.spiegler@univmed.fr

Stankovski, Tomislav
Physics Department
Lancaster University
Lancaster LA1 4YB
United Kingdom
t.stankovski@lancaster.ac.uk

Stefanovska, Aneta
Physics Department
Lancaster University
Lancaster LA1 4YB
United Kingdom
aneta@lancaster.ac.uk

Suprunenko, Yevhen
Physics Department
Lancaster University
Lancaster LA1 4YB
United Kingdom
y.suprunenko@lancaster.ac.uk

Tass, Peter
Forschungszentrum Jülich GmbH
INM-7, Leo-Brandt-Str.
52428 Jülich
Germany
p.tass@fz-juelich.de

Vuksanovic, Vesna
Institut for Theoretical Physics
Technische Universität Berlin
Hardenberg Str. 36
10623 Berlin
Germany
vesna.vuksanovic@bccn-berlin.de

Wächter, Matthias
Department of Physics/Forwind
Universität Oldenburg
26129 Oldenburg
Germany
matthias.waechter@uni-oldenburg.de

Wang, Tao
Department of Physics
Technische Universität Kaiserslautern
Erwin Schrödinger Str. 46
67663 Kaiserslautern
Germany
tauwaang@gmail.com

Weitz, Martin
Institute for Applied Physics
Universität Bonn
Wegelerstr. 8
53115 Bonn
Germany
martin.weitz@uni-bonn.de

Wille, Carolin
Fachbereich Physik
Freie Universität Berlin
Arnimallee 14
14195 Berlin
Germany
carolin.wille@fu-berlin.de

Woodman, Michael Marmaduke
Aix-Marseille Université
Faculté de Médecine
Institut de Neurociences des Systmes
27 BD Jean Moulin
13005 Marseille
France
michael.woodman@etu.univ-amu.fr

Wunner, Günter
Institut für Theoretische Physik I
Universität Stuttgart
Pfaffenwaldring 57
70469 Stuttgart
Germany
wunner@itp1.uni-stuttgart.de

Author Index

Subject Index